THE JOURNAL
OF
CHEMICAL PHYSICS

VOLUME 21, NUMBER 12 DECEMBER, 1953

The Temperature Dependence of the Mutual Diffusion Coefficient for Four Gaseous Systems*,†

ROGER A. STREHLOW‡
Naval Research Laboratory, Department of Chemistry, University of Wisconsin, Madison, Wisconsin
(Received March 30, 1953)

Diffusion coefficients have been measured for the systems He—A, H_2—A, H_2—nC_4H_{10}, and H_2—SF_6 over the temperature range 13°C to 150°C. The values were determined by a point concentration analysis, while diffusion proceeded at one end of a Loschmidt-type cell. The analysis was made with a hot-wire technique and utilized the large difference in thermal conductivity to indicate concentration. The generalized equations for calculating D from an experiment with a Loschmidt-type cell are given as well as an analysis of the errors involved in calculating D from these data.

The data were used to calculate binary force constants for the Lennard-Jones 6–12 potential. In the system SF_6—H_2 these are $\epsilon/k=320$°K and $(r_0)_{12}=3.25$A. The other three systems fit the theory very poorly. The middle temperature value was about 5 percent low relative to the theoretical curve through the high and low data point. The difficulties of calculating Lennard-Jones force constants from experimental viscosity or diffusion data are discussed.

INTRODUCTION

DIFFUSION coefficients of the common gases at room temperature have been known for a long time.[1] The need for accurate experimental diffusion coefficients over a large temperature range has been pointed out by the recent theoretical calculations of Hirschfelder, Bird, and Spotz[2] and Kotani and Kihara.[3] They independently evaluated the Chapman Enskog solution to the nonequilibrium Boltzman equation for the quite realistic 6–12 Lennard-Jones potential

$$V(r)=4\epsilon_0[(r_0/r)^6-(r_0/r)^{12}].$$

Where r_0=zero energy collision diameter for the molecule, ϵ_0=depth of the potential well, r=distance of separation, and $V(r)$=potential of interaction. The results are strictly valid only for spherically symmetric molecules at temperatures where classical mechanics holds and at moderate pressures where triple collisions or wall collisions are absent.

Hirschfelder, Bird, and Spotz[2,4] have tabulated Lennard-Jones force constants (obtained from viscosity data) for a large number of molecules, spherical and otherwise, and have used these to calculate the viscosities of binary mixtures of gases over a wide temperature range. Their calculated values show good agreement with experimental data which are available. At the time of their report there were no existing diffusion data over a temperature range larger than 20°C.

Since then, Hutchinson[5] has reported values for the self diffusion of argon from 194 to 362°K and Winn[6] for the self diffusion of A, Ne, N_2, O_2, CO_2, and CH_4 over approximately the same temperature range. All these values were compared by those authors to values calculated from viscosity force constants given by Hirschfelder, Bird, and Spotz. The agreement ranged from within one percent for argon to approximately six percent for methane and carbon dioxide. Amdur,

* This work was carried out under Contract NOrd 9938 with the U. S. Navy Bureau of Ordnance.
† Part of a thesis submitted in partial fulfillment of the requirement for the degree of Doctor of Philosophy in Chemistry at the University of Wisconsin.
‡ Present address: Ballistic Research Laboratories, Aberdeen Proving Ground, Maryland.
[1] Chapman and Cowling, *Mathematical Theory of Non-Uniform Gases* (Cambridge University Press, New York, 1939).
[2] Hirschfelder, Bird, and Spotz, J. Chem. Phys. **16**, 968–81 (1948); Hirschfelder, Curtiss, Bird, and Spotz, *Molecular Theory of Gases and Liquids* (John Wiley and Sons, Inc., New York, 1953).
[3] T. Kotani and M. Kihara, Proc. Phys. Math. Soc. Japan **24**, 76 (1942).
[4] Hirschfelder, Bird, and Spotz, Chem. Rev. **44**, No. 1, 205–231 (1949).
[5] Hutchinson, J. Chem. Phys. **17**, 1081 (1949).
[6] E. B. Winn, Phys. Rev. **80**, 1024 (1950).

Irvine, Mason, and Ross[7] give values for the systems CO_2-CO_2 and CO_2-N_2O. In a later paper[8] they calculated force constants from their data on these two systems which do not agree very well with either the viscosity or second virial coefficient force constants for these systems.

This paper reports some mutual diffusion coefficients over a temperature range of 285°K to 420°K taken by a point analysis method in a Loschmidt-type cell. The comparison of these values with theory to calculate binary force constants is given, and a basic limitation on the comparison between experimental transport properties and the theory is discussed.

THEORY OF THE EXPERIMENTAL METHOD AND ERROR ANALYSIS

Experimental values of D_{12} may be obtained if one can solve the diffusion equation for experimentally realizable conditions. In this report values were obtained

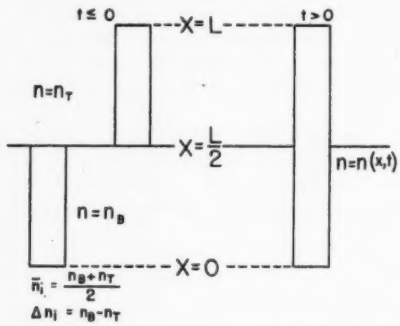

FIG. 1. Loschmidt-type diffusion cell with shear interface.

using a Loschmidt[9]-type cell with a sheer interface shown schematically in Fig. 1, where x is distance and t is time. Under these conditions the diffusion equation

$$\partial n/\partial t=\partial/\partial x[\mathrm{D}(\partial n/\partial x)] \tag{1}$$

yields a solution of the form

$$n(x,t)=\bar{n}_i+\frac{2}{\pi}\Delta n_i\sum_{m=1}^{\infty}\frac{\sin(m\pi/2)}{m}\cos\frac{m\pi x}{L}\times\exp\left(-\frac{m^2\pi^2\mathrm{D}}{L^2}t\right), \tag{2}$$

where n is mole fraction of the binary gas mixture under consideration. The assumptions in this derivation are: (1) D is constant over the entire composition range, and (2) that the gases are ideal (no pressure change on mixing).

In the case where one measures the average concentration in one-half of the cell at a time t, the solution is of the form

$$\langle n(t)_B\rangle_{Av}=2/L\int_0^{L/2}n(x,t)dx, \tag{3}$$

where $\langle n(t)_B\rangle_{Av}$ is the average concentration in the bottom of the cell at time t. If one substitutes Eq. (2) in Eq. (3) and integrates, one gets

$$\langle n(t)_B\rangle_{Av}=\bar{n}_i+\frac{4}{\pi^2}\Delta n_i\sum_{m=1}^{\infty}\frac{\sin(m\pi/2)}{m}\times\exp\left(-\frac{m^2\pi^2\mathrm{D}}{L^2}t\right). \tag{4}$$

Equations (2) and (4) may be solved explicitly for D when $\beta=\pi^2\mathrm{D}t/L^2\leq 1.0$ for Eq. (2) and ≤ 0.7 for Eq. (4), because under these conditions the second and higher terms of the series are always less than 0.2 percent of the first term. Equations (2) and (4), then, reduce to: for point analysis

$$\mathrm{D}=\frac{L^2}{\pi^2 t}\ln\left[\frac{2}{\pi}\frac{\Delta n_i}{n-\bar{n}_i}\cos\frac{\pi x}{L}\right]; \tag{5}$$

for average analysis in the bottom half

$$\mathrm{D}=\frac{L^2}{\pi^2 t}\ln\left[\frac{4}{\pi^2}\frac{\Delta n_i}{\bar{n}_B-\bar{n}_i}\right]. \tag{6}$$

If we equate Eqs. (5) and (6) we get the relation

$$\cos(\pi x/L-)=2/\pi,$$

or

$$x=0.220L. \tag{7}$$

This is the point at which a point analysis at any time yields the same concentration as an average analysis in the bottom half of the cell at that instant.

The errors to be expected in D from experimental errors inherent in measurements of x, t, and n may be calculated by using the equation for the total differential of D

$$d\mathrm{D}=(\partial\mathrm{D}/\partial\lambda)d\lambda+(\partial\mathrm{D}/\partial n)dn+(\partial\mathrm{D}/\partial t)dt,$$

where $\lambda=x/L$. It is assumed that L is accurately known and that the interface accurately divides the cell into two halves. If we replace derivatives by differences and calculate fractional errors we get

$$\frac{\Delta\mathrm{D}}{\mathrm{D}}=\left[\frac{1}{\mathrm{D}}\frac{\partial\mathrm{D}}{\partial\lambda}\right]\Delta\lambda+\left[\frac{\Delta n_i}{\mathrm{D}}\frac{\partial\mathrm{D}}{\partial n}\right]\frac{\Delta n}{\Delta n_i}+\frac{t}{\mathrm{D}}\frac{\partial\mathrm{D}}{\partial t}\frac{\Delta t}{t},$$

or substituting Eq. (2)

$$\frac{\Delta\mathrm{D}}{\mathrm{D}}=\left(\frac{\pi}{\beta}\tan\pi\lambda\right)\Delta\lambda+\frac{\Delta n_i}{\beta(n-\bar{n}_i)}\frac{\Delta n}{\Delta n_i}+\frac{\Delta t}{t}$$

$$=\lambda_f\Delta\lambda+n_f\frac{\Delta n}{\Delta n_i}+\frac{\Delta t}{t}, \tag{8}$$

where since $\Delta L=0$ we have $\Delta\lambda=\Delta x/L$.

[7] Amdur, Irvine, Mason, and Ross, J. Chem. Phys. **20**, 436–443 (1952).
[8] Amdur, Ross, and Mason, J. Chem. Phys. **20**, 1620–23 (1952).
[9] J. Loschmidt, Akad. Wiss. Wein **61**, 367 and **62**, 468 (1870).

Plots of λ_f and n_f as functions of λ and β are given in Figs. 2 and 3. In Fig. 3 the concentration at the bottom of the cell is also shown as a function of β.

Equation (8) allows one to explicitly evaluate the experimental errors inherent in measured diffusion coefficients and the errors in the measured variables x, n, and t, for a point analysis method. In combination with Eq. (7), it allows one to evaluate the relative accuracy of the two possible methods of measuring D with a Loschmidt cell from a knowledge of existing experimental errors. Explicitly for an average concentration analysis in one-half the cell, $\lambda_f \Delta\lambda$ in Eq. (8) disappears and the equation reduces to

$$\Delta D/D = n_f(\Delta n/\Delta n_i) + \Delta t/t$$

with the added condition that n_f must be evaluated along the line $\lambda = 0.220$ in Fig. 3.

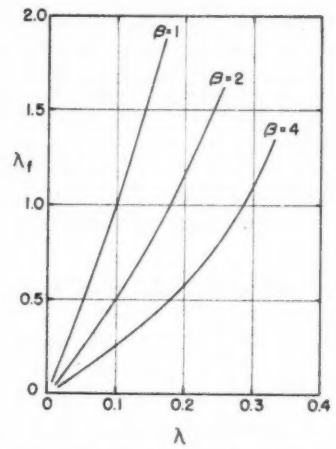

FIG. 2. Coefficient for position errors in Loschmidt-type diffusion cell.

EXPERIMENTAL

The diffusion cell shown in Fig. 4 is made of stainless steel and the cylinders are 1.523-in. internal diameter with an over-all length of 40.826 cm. The shear interface is 20.416 cm on the bottom. The cell was immersed in a large (30-gallon) oil bath with a temperature cycle of 0.02°C. Temperatures were read with National Bureau of Standards calibrated mercury in glass thermometers.

A concentration analysis at a point 0.50 cm from the bottom of the cell was used to calculate the diffusion coefficient. Concentration was determined by using the thermal conductivity of the gas as the indicating variable. A fine (diameter 0.00031 in.) tungsten wire $\frac{1}{2}$ inch long was heated with a constant current of 60 milliamperes, and the voltage across the wire was read 0.01 second after it was turned on. This was done by photographing a single 100-cycle sweep of a 304 H Du Mont oscilloscope which was triggered by the voltage pulse. One hundredth of a second was chosen as the optimum time because the wire approaches its equilibrium voltage in this time, and schlieren photographs showed that the top of the hot gas bubble is then only 0.7 cm from the wire. Since this gas comes from around and below the wire, the position used for calculating D was 0.25 cm from the bottom. An error of 0.25 cm in the analysis point at this position in a 40-cm cell causes an error of less than 0.1 percent in D. The oscilloscope was found to have very good short time stability and linearity; and therefore, a three volt standard deflection photograph was taken on each film immediately before each determination. The wire voltages were calibrated at the temperature of the run with gas mixtures made in an independently thermostated bulb which was specially constructed to allow one to measure the pressure of one gas and then measure the total pressure of the completely mixed mixture at constant

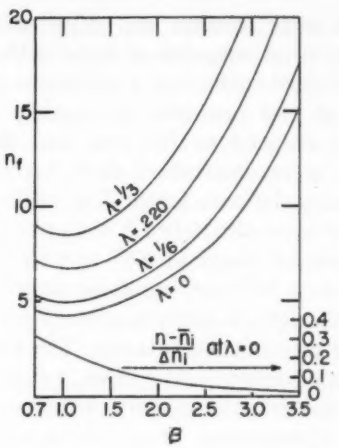

FIG. 3. Coefficient for concentration errors and concentration at the bottom of the cell ($\lambda = 0$) for Loschmidt-type diffusion cell.

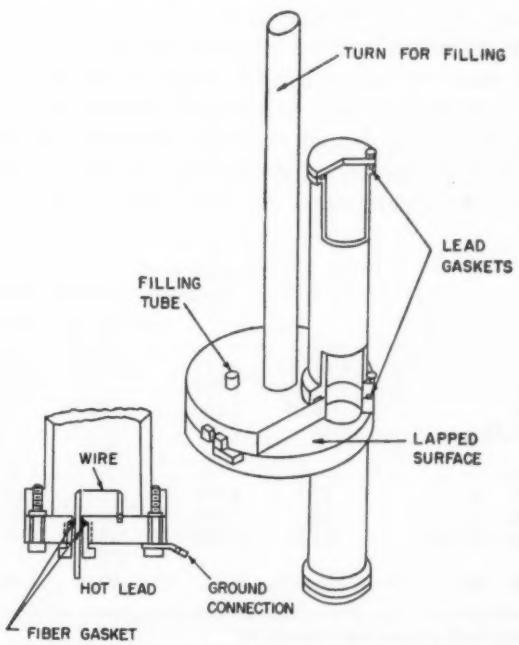

FIG. 4. The diffusion cell.

volume. The mole fraction was calculated using this data and the virial equation of state with a Lennard-Jones second virial coefficient. Calibration photographs were taken at two pressures bracketing 760 mm of mercury and reduced to 760 mm and the unknown compositions were determined from voltages reduced to 760 mm using the same factor. The calibration curves had a slope of approximately 2.5 volts per mole fraction unit in the useable range of 0.65 to 0.80 mole fraction unit. Calibration voltages could be reproduced to 0.5 percent which yields a relative error of less than 0.003 mole fraction unit in concentration. The error in D due to concentration errors is, therefore, 1.5 percent.

The time was recorded directly on data film by open flash spark illumination of a calibrated 0.01-second stopwatch. Zero time was determined by the position of a microswitch on the cell. The correct position of this switch on the cell was calculated on the assumption that the cell was closed at a constant angular velocity. The microswitch flashed the lamp on the already moving stopwatch for zero time measurement. Diffusion times range from 90 to 600 seconds. The uncertainty in time due to reading errors was less than 0.04 second. A systematic zero time error is estimated to be 0.05 second or less, and therefore errors in D due to time measurement error are less than 0.1 percent.

Only one data point could be taken on each filling of the cell, and five to nine runs were made for each determination. Pressures were equalized externally just before closing the cell. A value of D_{12} was calculated for each run, and the resulting values were averaged after correction to 760 mm of Hg pressure. Tank gases were used with no further purification. A stated manufacturer's purity of the gases was: H_2—99.9 percent, He—99.99 percent, A—99.99 percent, nC_4H_{10}—99.0 percent, and SF_6—99.0 percent.

The individual values for each determination were made over the largest feasible range of concentration, that is, from about 0.65 to 0.80 mole fraction of the gas at the bottom of the cell. Over this concentration range the method showed no dependence on concentration within the experimental accuracy. The range of the determinations was limited by two factors: the first and most important is that the measured wire voltage varied most rapidly in the concentration range from 0.65 to 1 percent light gas; secondly, Eq. (6) is not valid above concentrations of 0.80 at the bottom of the cell, and the error coefficient starts to get large after the bottom concentration reaches 0.65-mole fraction unit.

The above mentioned theoretical calculation errors add up to an experimental error of about 1.7 percent in D, for an individual determination. This compares favorably with the errors listed in Tables II through V, which are the calculated probable errors of the five to nine determinations made for each run.

TABLE I. Force constants.

Gas or system	Viscosity		Second virial coefficient	
	ϵ/k(°K)	r_0(A)	ϵ/k(°K)	r_0(A)
H_2	33.3	2.968	37.0	2.92
He	6.03	2.70	6.03	2.73
nC_4H_{10}	410	4.997	379[a]	—
			320[b]	—
SF_6	—	—	239[c]	4.85[c]
He—A	27.3	3.059	26.9	3.07
H_2—A	64.3	3.193	66.5	3.125
H_2—nC_4H_{10}	116.8	3.982	118.3	—
			108.7	—
H_2—SF_6	—	—	94.0	3.88

[a] From boiling point (see reference 4).
[b] From critical temperature (see reference 4).
[c] From critical temperature and volume (see references 4 and 11).

RESULTS

Table I lists force constants obtained by Hirschfelder, Bird, and Spotz[2,4] from experimental equation of state data and viscosities of pure substances. It also gives binary force constants for the four systems under consideration which were determined by the usual averaging method $(\epsilon/k)_{12}=[(\epsilon/k)_1\cdot(\epsilon/k)_2]^{\frac{1}{2}}$ and $(r_0)_{12}=\frac{1}{2}[(r_0)_1+(r_0)_2]$

An attempt was made to fit the experimental diffusion data to the Hirschfelder, Bird, and Spotz equation for diffusion derived from the Lennard-Jones 6-12 potential

$$D_{12}=\frac{.00092916T^{\frac{1}{2}}(m_1+m_2/m_1m_2)^{\frac{1}{2}}}{P(r_0)_{12}^2W^{(1)}[1;(kT/\epsilon)_{12}]}, \tag{9}$$

where T is temperature in °K, m is molecular weight, P is pressure in atmospheres, $(r_0)_{12}$ is the zero energy binary collision radius, $W^{(1)}[1;(kT/\epsilon)_{12}]$ is the effective reduced cross section tabulated by Hirschfelder, Bird, and Spotz[2,4] and subscript 1 and 2 refer to the two molecules in question.

Two methods were used to fit the data. One method is a modified form of Buckingham's method[10] for obtaining potential energy information from second virial coefficients. For this method Eq. (9) is rewritten

$$X=\log_{10}(r_0)_{12}^2=\log_{10}\frac{.00092916T^{\frac{1}{2}}(m_1+m_2/m_1m_2)^{\frac{1}{2}}}{PD_{12}W^{(1)}[1;(kT/\epsilon)]},$$

and a series of X's are calculated using the temperature and diffusion coefficients of one data point plus a series of ϵ/k values. One then plots the resulting X against $\log_{10}\epsilon/k$ to obtain a curve for each data point. This process is repeated for every data point and the intersections of the curves yield a range of values of ϵ/k and $(r_0)_{12}$, which conform to the data. The closer the intersections are to each other, the closer the theoretical fit. The other method has been suggested by Amdur,

[10] R. A. Buckingham, Proc. Roy. Soc. (London) A168, 264 (1938).

TABLE II. D_{12} for He—A
D_{12} cm²/sec.

Temperature °K	Theory Viscosity	Theory Eq. of state	Experiment D_{12}	Experiment Prob. error	n
287.9	0.689	0.685	0.697	±0.0026	7
354.2	0.965	0.961	0.979	±0.0072	7
418.0	1.269	1.263	1.398	±0.0063	6

TABLE III. D_{12} for H_2—A
D_{12} cm²/sec.

Temperature °K	Theory Viscosity	Theory Eq. of state	Experiment D_{12}	Experiment Prob. error	n
287.9	0.747	0.773	0.828	±0.0037	5
354.2	1.063	1.099	1.111	±0.0033	6
418.0	1.402	1.456	1.714	±0.0091	8

TABLE IV. D_{12} for H_2—nC_4H_{10}
D_{12} cm²/sec.

Temperature °K	Theory Viscosity	Theory Boiling temp.	Theory Critical temp.	Experiment D_{12}	Experiment Prob. error	n
287.9	0.408	0.406	0.417	0.361	±0.0016	8
354.2	0.591	0.589	0.602	0.507	±0.0018	9
430.0	0.829	0.827	0.843	0.763	[a]	3

[a] Average of only three determinations.

Ross, and Mason.[8] Equation (9) is rewritten to yield

$$\log_{10}\left[\frac{0.00092916T^{\frac{1}{2}}(m_1+m_2/m_1m_2)^{\frac{1}{2}}}{PD_{12}}\right] = \log_{10}W^{(1)}[1;(kT/\epsilon)_{12}]+2\log_{10}(r_0)_{12}.$$

One may also write the identity

$$\log_{10}T=\log_{10}(kT/\epsilon)+\log_{10}(\epsilon/k).$$

A plot of the experimental quantities

$$\log_{10}\left[\frac{0.00092916T^{\frac{1}{2}}(m_1+m_2/m_1m_2)^{\frac{1}{2}}}{PD_{12}}\right]$$

against $\log_{10}T$ for each data point will produce points which should lie somewhere on the curve $\log_{10}W^{(1)}[1;(kT/\epsilon)]$ plotted against $\log_{10}(kT/\epsilon)$. The amount of translation parallel to the axes to superimpose the points and the curve determines the value of ϵ/k and r_0.

Of the four systems used for diffusion measurements only the system SF_6—H_2 was useable for calculating force constants. Only three data points were taken in the other three systems, and because of the poor comparison with theory, no binary force constants were calculated. From attempts to fit these data using the second method listed above it appeared that the middle temperature diffusion coefficient was approximately 3–5 percent too low to be consistent with the theoretical curve and the upper and lower experimental points. This error is outside the estimated experimental error of one percent and seems to be a systematic error. The data have been recently rechecked, but no reason for a systematic error appeared. Because of this, the data for these three systems are compared in Tables II to IV to diffusion coefficients calculated from the force constants listed in Table I.[11]

The data on SF_6—H_2 was used to calculate force constants by both methods listed above. Method one yielded ϵ/k values ranging from 195 to 420°K while method two yielded $\epsilon/k=320$°K and $r_0=3.25$A. These values should be compared with $\epsilon/k=94$°K and $r_0=3.88$ from Table I. Table IV[12] lists the experimental and calculated diffusion coefficients for this system.

APPENDIX: DISCUSSION OF A LIMITATION TO THE CALCULATION OF FORCE CONSTANTS FROM EXPERIMENTAL TRANSPORT COEFFICIENTS

Whalley and Schneider[13] have recently made the statement that the 6–12 model fits viscosity data very well over the range of kT/ϵ of 1.2 to 3 and that outside this range it is frequently impossible to choose any values of the parameters which will fit viscosity data satisfactorily.

That this is true for diffusion as well as viscosity may be shown quite easily. Any of the processes for comparing experiment with a Lennard-Jones 6–12 model for the force field return, in the final analysis, to a comparison of the experimental data points at two temperatures to the theoretical curve of $W^{(1)}[n;(kT/\epsilon)]$ against kT/ϵ. For diffusion this comparison may be written analytically by rewriting Eq. (9) for two different temperatures T_1 and $T_2>T_1$ and dividing

$$\frac{D_1T_2^{\frac{1}{2}}}{D_2T_1^{\frac{1}{2}}}=\frac{W^{(1)}[1;(kT_2/\epsilon)]}{W^{(1)}[1;(kT_1/\epsilon)]},$$

where $D_1T_2^{\frac{1}{2}}/D_2T_1^{\frac{1}{2}}=\beta$ is an experimentally determined constant for any particular temperature ratio $T_2/T_1=\alpha$. The temperature ratio α however directly

TABLE V. D_{12} for H_2—SF_6
D_{12} cm²/sec.

Temperature °K	Theory Eq. of state	Theory Diffusion[a]	Experiment Present work D_{12}	Experiment Present work Prob. error	n	Reference 12
286.2	0.448	0.3970	0.396	±0.00072	7	
293.2	0.468	0.4165				0.418
306.9	0.507	0.4563	0.458	±0.0017	6	
370.8	0.705	0.6639	0.647	±0.0017	5	
418.0	0.866	0.8390	0.838	±0.0043	6	

[a] $(\epsilon/k)_{12}=320$°K $(r_0)_{12}=3.88$Å as determined in this paper.

[11] R. Wentorf and C. Boyd, University of Wisconsin CM724 (May 1952).
[12] Boyd, Stein, Steingrimsson, and Rumpel, J. Chem. Phys. **19**, 548–553 (1951).
[13] Whalley and Schneider, J. Chem. Phys. **20**, 657–661 (1952).

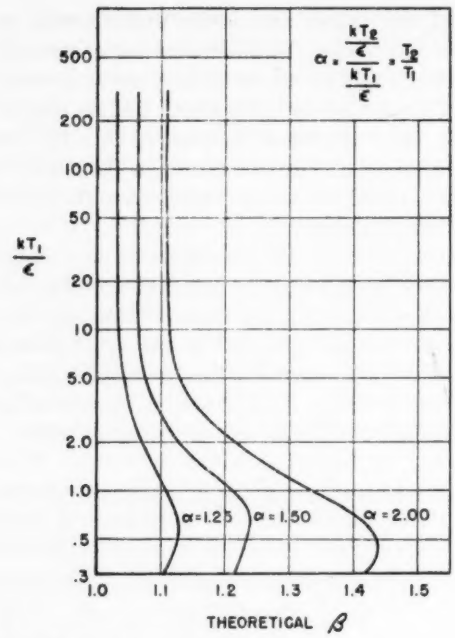

FIG. 5. Diffusion: the value of

$$\beta = W^{(1)}(1; kT_2/\epsilon)/W^{(1)}(1; kT_1/\epsilon)$$

as a function of kT_1/ϵ for three values of $\alpha = T_2/T_1$.

controls the theoretically allowable range for β. Figure 5 shows how the theoretical β range varies with kT_1/ϵ for various α's.

These curves show that to get any accuracy in ϵ/k from experimental data one must necessarily have the experimental values in a temperature range such that kT_1/ϵ lies between 1 and 3. This then sets a range of temperatures for any system which will yield clearly determined force constants for that system. Outside this temperature range the experimental errors would have to be extremely small to allow one to calculate force constants with any accuracy. Since for most systems of practical interest the Lennard-Jones 6–12 potential is only a first approximation to the true potential field the calculation of force constants is virtually impossible except in this narrow range of kT_1/ϵ. The reverse is not necessarily true. That is, the above statement places no restrictions on the range of kT/ϵ over which the experimental data will fit the theory with reasonable accuracy. This range can only be determined by experiment.

In the case of viscosity the experimental ratio $\gamma = \eta_1 T_2^{\frac{1}{2}}/\eta_2 T_1^{\frac{1}{2}}$ is related to theory by the equation

$$\frac{\eta_1 T_2^{\frac{1}{2}}}{\eta_2 T_1^{\frac{1}{2}}} = \frac{W^{(2)}[2; (kT_2/\epsilon)]}{W^{(2)}[2; (kT_1/\epsilon)]}.$$

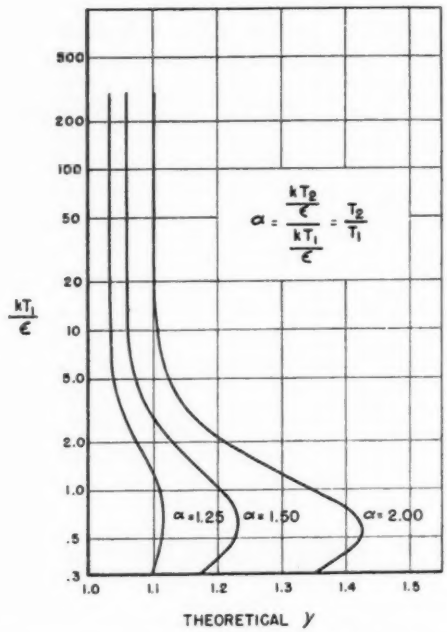

FIG. 6. Viscosity: the value of $\gamma = W^{(2)}(2; kT_2/\epsilon)/W^{(2)}(2; kT_1/\epsilon)$ as a function of kT_1/ϵ for three values of $\alpha = T_2/T_1$.

Figure 6 shows how the theoretical γ range varies with kT_1/ϵ for various α's.

ACKNOWLEDGMENTS

The author would like to thank Professor J. O. Hirschfelder and Dr. C. A. Boyd for their helpful discussions and suggestions during the course of this work. He would also like to acknowledge the work of Mr. Lloyd E. Lincoln who constructed the diffusion cell and large thermostat bath.

THE JOURNAL OF CHEMICAL PHYSICS VOLUME 21, NUMBER 12 DECEMBER, 1953

Theory of Intermolecular Potential and Second Virial Coefficient of Hydrogen at Low Temperature

MASATAKA MIZUSHIMA
Department of Physics, Duke University, Durham, North Carolina

AND

KIMIO OHNO AND AKIKO OHNO
Department of Physics, Faculty of Science, University of Tokyo, Tokyo, Japan

(Received April 20, 1953)

The intermolecular potential between hydrogen molecules is calculated taking into account its dependence on the relative orientation of the molecules. Assuming that the rotational quantum number of each molecule is a good quantum number throughout collision at low temperature, the matrix elements of the repulsive short-range intermolecular potential and the London potential are calculated. If the intermolecular potential depends on the relative orientation of colliding molecules, the resulting matrix element depends on the rotational quantum number. Thus it is pointed out that the second virial coefficient of ordinary hydrogen (which is, at low temperature, a mixture of 75 percent of $J=1$ molecule and 25 percent of $J=0$ molecules, where J is the rotational quantum number), and pure *para* hydrogen (which consists of only $J=0$ molecules at low temperature) must be different, even if there were no statistical effect. The virial coefficient is calculated for very low temperature by solving the Schrödinger equation numerically.

I. INTRODUCTION

MUCH theoretical work has been done on the second virial coefficient since the day of Lennard-Jones,[1] and a large amount of information on the intermolecular forces is obtained therefrom.[2] Theories are also presented taking into account the quantum mechanical effect, and the dependence of intermolecular potential on the relative orientation of molecules. No theory has been presented, however, which pointed out the combined effect of quantum property and the directionality of the intermolecular potential.

De Boer[3] and Margenau[4] independently have calculated the short range repulsive force between two hydrogen molecules, and shown that it depends not only on the intermolecular distance but also on the relative orientation of these molecules. On the long-range attractive London force some discussion on the same property was made by de Boer[3] and one of the present authors.[5] The effect of this property on the second virial coefficient, however, has been treated classically, in which case only the average value of intermolecular potential over relative orientation can be observed. This situation does not hold in the low-temperature region where the quantum effect appears.

The quantum mechanical theory of the second virial coefficient was presented by Gropper,[6] Uhlenbeck, and Beth,[7] and the numerical calculation was done by de Boer *et al.*[8] for the He atom and by Miyako[9] for the H_2 molecule. However, in these papers they neglected the internal degrees of freedom such as vibration and rotation. In the case of a molecule we must consider the effect of quantization of these internal degrees of freedoms. Especially in the case of the hydrogen molecule, where the characteristic temperature of rotation is 85.33°K, the states with rotational quantum number larger than 2 will have a very small population at temperature below 250°K. Thus, in this case, the quantum effect of rotation is very large and one cannot treat it classically.

II. HAMILTONIAN OF TWO-MOLECULAR SYSTEM

In order to calculate the second virial coefficient we must first solve the collision problem of two molecules, which is given by the Hamiltonian of two-molecular system. Since the characteristic temperature of vibration of a hydrogen molecule is 6100°K, we can neglect the vibrational degrees of freedom at low temperature. We shall treat the molecule as a rigid body in this paper.

Take the mass center of a two-molecular system as the origin and designate this point as O. Fix a coordinate system $OXYZ$ in space. The inclination of the line which connects the two mass centers of the individual molecules can be described by the Eulerian angle Θ and Φ relative to $OXYZ$ in space. The distance between the mass centers of individual molecules is denoted by R. The Eulerian angles which describe the inclination of the molecular axis of the first molecule relative to the R axis are denoted by θ_1, φ_1, and in the same manner we adopt θ_2, φ_2 for the second molecule. These seven

[1] J. Lennard-Jones, Proc. Roy. Soc. (London) **A106**, 463 (1924).
[2] R. H. Fowler and E. A. Guggenheim. *Statistical Thermodynamics* (The University Press, Cambridge, England, 1939), Chap. VII.
[3] J. de Boer, Physica **9**, 363 (1942).
[4] H. Margenau, Phys. Rev. **64**, 131 (1943).
[5] M. Mizushima, Research in Chem. Phys. **5**, 25 (1947).
[6] L. Gropper, Phys. Rev. **50**, 963 (1936).
[7] G. E. Uhlenbeck and E. Bethard, Physica **3**, 729 (1936).
[8] J. de Boer and A. Michels, Physica **6**, 409 (1939); de Boer, van Krannendonk, and Compaan, Physica **16**, 545 (1950).
[9] R. Miyako, Proc. Phys.-Math. Soc. Japan **24**, 852 (1942).

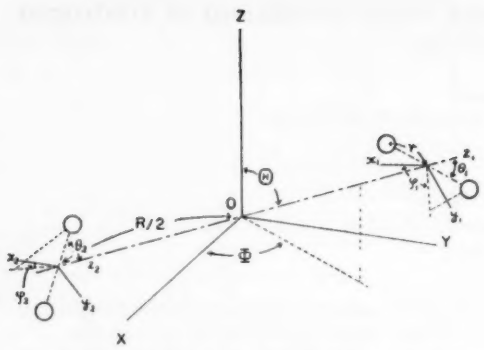

FIG. 1. Coordinates in the two molecular system.

quantities Θ, Φ, R, θ_1, φ_1, θ_2, and φ_2 are just enough to describe the relstive motion of the two molecules.

Let us denote the internuclear distance of the hydrogen molecules as $2r$ and proton mass as m. Then the kinetic energy of our system can be expressed as

$$\mathfrak{T}=T_1+T_2, \tag{1}$$

$$\begin{aligned}T/m=&\tfrac{1}{8}\dot{R}^2+\tfrac{1}{4}R^2(\partial\Theta/\partial t)^2+\tfrac{1}{4}R^2\sin^2\Theta(\partial\Phi/\partial t)^2\\&+\gamma^2\theta^2+\gamma^2\sin^2\theta\dot{\varphi}^2+[\gamma^2(\sin^2\theta\cos^2\varphi\\&+\cos^2\theta)(\partial\Theta/\partial t)^2+\gamma^2\{(\cos\Theta\sin\theta\cos\varphi\\&+\sin\Theta\cos\theta)^2+\sin^2\theta\sin^2\varphi\}(\partial\Phi/\partial t)^2\\&+2\gamma^2\sin\theta\sin\varphi(\sin\Theta\sin\theta\cos\varphi\\&-\cos\Theta\cos\theta)(\partial\Theta/\partial t)(\partial\Phi/\partial t)+2\gamma^2\cos\varphi(\partial\Theta/\partial t)\dot{\theta}\\&-2\gamma^2\sin\theta\cos\theta\sin\varphi(\partial\Theta/\partial t)\dot{\varphi}\\&+2\gamma^2(\sin\Theta\sin\varphi(\partial\Phi/\partial t)\dot{\theta}+2\gamma^2\sin\theta(\cos\Theta\sin\theta\\&+\sin\Theta\cos\theta\cos\varphi)(\partial\Phi/\partial t)\dot{\varphi},\end{aligned} \tag{2}$$

where T_1 and T_2 come from first and second molecule, respectively. Thus, in Eq. (2), θ, φ means θ_1, φ_1 in T_1 and θ_2, φ_2, in T_2.

If the classical kinetic energy is expressed by a matrix $\mathbf{g}$ and a vector $\mathbf{q}$ as

$$T=(\partial\mathbf{q}/\partial t)^{-1}\mathbf{g}(\partial\mathbf{q}/\partial t), \tag{3}$$

then it is known that the corresponding quantum mechanical operator is

$$T=-\frac{\hbar^2}{(|\mathbf{g}|)^{\frac{1}{2}}}\frac{\partial}{\partial\mathbf{q}}(|\mathbf{g}|)^{\frac{1}{2}}\mathbf{g}^{-1}\frac{\partial}{\partial\mathbf{q}}. \tag{4}$$

According to this formula we obtain the quantum mechanical kinetic energy operator for our system from Eqs. (1) and (2) as

$$\begin{aligned}\mathfrak{T}=-\frac{\hbar^2}{2m}\Bigg[&\Bigg\{\frac{4}{R^2}\frac{\partial}{\partial R}R^2\frac{\partial}{\partial R}+\frac{2}{R^2\sin\Theta}\frac{\partial}{\partial\Theta}\sin\Theta\frac{\partial}{\partial\Theta}\\&+\frac{2}{R^2\sin^2\Theta}\frac{\partial^2}{\partial\Phi^2}+\frac{1}{\gamma^2\sin\theta_1}\frac{\partial}{\partial\theta_1}\sin\theta_1\frac{\partial}{\partial\theta_1}+\frac{1}{\gamma^2\sin^2\theta_1}\frac{\partial^2}{\partial\varphi_1^2}\\&+\frac{1}{\gamma^2\sin\theta_2}\frac{\partial}{\partial\theta_2}\sin\theta_2\frac{\partial}{\partial\theta_2}+\frac{1}{\gamma^2\sin^2\theta_2}\frac{\partial^2}{\partial\varphi_2^2}\Bigg\}\\&+\frac{2}{R^2}\Bigg\{\frac{2}{\sin\theta_1}\frac{\partial}{\partial\theta_1}\sin\theta_1\frac{\partial}{\partial\theta_1}+(\cot^2\Theta+\cot^2\theta_1)\frac{\partial^2}{\partial\varphi_1^2}\\&+\cot\Theta\cot\theta_1\frac{\partial}{\partial\varphi_1}\cos\varphi_1\frac{\partial}{\partial\varphi_1}\\&+\cot\Theta\left(\frac{\sin\varphi_1}{\sin\theta_1}\frac{\partial}{\partial\theta_1}\sin\theta_1\frac{\partial}{\partial\varphi_1}+\frac{\partial}{\partial\varphi_1}\sin\varphi_1\frac{\partial}{\partial\theta_1}\right)\\&-\frac{\sin\varphi_1}{\sin\Theta}\left(\frac{1}{\sin\theta_1}\frac{\partial}{\partial\theta_1}\sin\theta_1\frac{\partial}{\partial\Phi}+\frac{\partial^2}{\partial\Phi\partial\theta_1}\right)\\&-\cos\varphi_1\left(\frac{1}{\sin\theta_1}\frac{\partial}{\partial\theta_1}\sin\theta_1\frac{\partial}{\partial\Theta}+\frac{1}{\sin\Theta}\frac{\partial}{\partial\Theta}\sin\Theta\frac{\partial}{\partial\theta_1}\right)\\&-\frac{2\cos\Theta}{\sin^2\Theta}\frac{\partial^2}{\partial\varphi_1\partial\Phi}-\frac{\cot\theta_1}{\sin\Theta}\left(\frac{\partial}{\partial\varphi_1}\cos\varphi_1\frac{\partial}{\partial\Phi}\right.\\&\left.+\cos\varphi_1\frac{\partial^2}{\partial\Phi\partial\varphi_1}\right)+\cot\theta_1\left(\frac{\partial}{\partial\varphi_1}\sin\varphi_1\frac{\partial}{\partial\Theta}\right.\\&\left.+\frac{\sin\varphi_1}{\sin\Theta}\frac{\partial}{\partial\Theta}\sin\Theta\frac{\partial}{\partial\varphi_1}\right)+\cos(\varphi_1-\varphi_2)\frac{1}{\sin\theta_1}\frac{\partial}{\partial\theta_1}\\&\times\sin\theta_1\frac{\partial}{\partial\theta_2}+\cot\theta_1\cot\theta_2\frac{\partial}{\partial\varphi_1}\cos(\varphi_1-\varphi_2)\frac{\partial}{\partial\varphi_2}\\&+\cot^2\Theta\frac{\partial^2}{\partial\varphi_1\partial\varphi_2}+2\cot\Theta\frac{\sin\theta_1\cos\theta_1}{\sin^2\theta_2}\frac{\partial}{\partial\varphi_1}\\&\times\cos\varphi_1\frac{\partial}{\partial\varphi_2}-\cot\theta_1\frac{\partial}{\partial\varphi_1}\sin(\varphi_2-\varphi_1)\frac{\partial}{\partial\theta_2}\\&-\cot\theta_1\sin(\varphi_2-\varphi_1)\frac{1}{\sin\theta_2}\frac{\partial}{\partial\theta_2}\sin\theta_2\frac{\partial}{\partial\varphi_1}\\&-\cot\Theta\sin\varphi_2\left(\frac{\partial^2}{\partial\varphi_1\partial\theta_2}+\frac{1}{\sin\theta_2}\frac{\partial}{\partial\theta_2}\sin\theta_2\frac{\partial}{\partial\varphi_1}\right)\\&+(\text{corresponding terms obtained by exchanging subscripts 1 and 2})\Bigg\}\Bigg].\end{aligned} \tag{5}$$

De Boer,[3] Margenau,[4] and Nagamiya and Kishi[10] have calculated the repulsive potential between hydrogen molecules, but unfortunately they could not obtain a reliable numerical result. Thus in our paper we shall assume the repulsive potential to have a form like

$$V_r=v_r(1,3)+v_r(1,4)+v_r(2,3)+v_r(2,4), \tag{6}$$

where $v_r(i,j)$ is the repulsive potential between i and j atoms (1, 2 atoms are the members of the first molecule

[10] T. Nagamiya and H. Kishi, Research Chem. Phys. 39, 64 (1951).

and 3, 4 those of the second molecule). When the Heitler-London method is adopted we shall obtain the repulsive potential of the form.[3,4]

Slater[11] has shown for He atom that v_r can be approximated by $A\exp(-l/\rho)$, where l is the internuclear distance and A, ρ are adjustable parameters. Thus we may assume

$$V_r=A\{\exp(-l_{13}/\rho)+\exp(-l_{14}/\rho)+\exp(-l_{23}/\rho)+\exp(-l_{24}/\rho)\}, \quad (7)$$

and determine A and ρ by fitting with experiment. Formula (7) can be approximated when the intermolecular distance is greater than $2r$, by

$$V_r=4A\exp(-R/\rho)\cosh(\gamma\cos\theta_1/\rho)\cosh(\gamma\cos\theta_2/\rho). \quad (8)$$

When discussing the phenomena at low temperatures this approximate formula is sufficient.

London[12] has obtained the attractive long-range intermolecular potential by the second-order pertubation calculation using the perturbation term of

$$h=(\mu_1\mu_2/R^3)\{2\cos\theta_1\cos\theta_2-\sin\theta_1\sin\theta_2\cos(\varphi_1-\varphi_2)\}. \quad (9)$$

The result depends on R as R^{-6}, but the higher order contributions will give terms which are proportional to R^{-8}, R^{-10}, etc., respectively. In this paper we shall adopt the R^{-6} term only and treat the theory phenomenologically, hoping to include the effect of higher order terms effectively.

Thus our Hamiltonian is

$$H=T+V_r+h, \quad (10)$$

where T is given by Eq. (5), V_r by (8), and h by (9).

TABLE I. Matrix elements of attractive intermolecular potential (London force).

$(0000|V_a|)\equiv(J_1=M_1=J_2=M_2=0$ in formula (15)$)=6\alpha^2 f$
$(0010|V_a|)=(6\alpha^2+(4/5)\alpha\gamma)f$
$(0011|V_a|)=(001-1|V_a|)=(6\alpha^2-(2/5)\alpha\gamma)f$
$(1010|V_a|)=(6\alpha^2+(8/5)\alpha\gamma+(8/25)\gamma^2)f$
$(1011|V_a|)=(6\alpha^2+(2/5)\alpha\gamma-(4/25)\gamma^2)f$
$(1111|V_a|)=(111-1|V_a|)=(1-1\ \ 1-1|V_a|)$
$=(6\alpha^2-(4/5)\alpha\gamma+(2/25)\gamma^2)f$
$f=-E/8R^6$ E: average excitation energy
$\alpha\equiv(\alpha_{11}+2\alpha_\perp)/3=0.7894\text{A}^3=5.328$ A.U.[14]
$\alpha\equiv\alpha_{11}-\alpha_\perp=0.2778\text{A}^3=1.875$ A.U.[14]

When the above values of α and γ are used

$(0000|V_a|)\equiv c$
$(0010|V_a|)=1.05c$
$(0011|V_a|)=0.98c$
$(1010|V_a|)=1.10c$
$(1011|V_a|)=1.02c$
$(1111|V_a|)=0.95c$

[11] J. C. Slater, Phys. Rev. **32**, 349 (1928).
[12] F. London, Trans. Faraday Soc. **32**, 8 (1936).

TABLE II. Matrix elements of repulsive intermolecular potential.

$(0000|V_r|)\equiv(J_1=0,\ M_1=0,\ J_2=0,\ M_2=0,\ |V_r|J_1=0,\ M_1=0,\ J_2=0,\ M_2=0)=4A\eta^{-2}\sinh^2\eta\exp(-R/\rho)$.
$(0010|V_r|)=12A\eta^{-2}\sinh\eta P(\eta)\exp(-R/\rho)$
$(0011|V_r|)=(001-1|V_r|)=12A\eta^{-3}\sinh\eta Q(\eta)\exp(-R/\rho)$
$(1010|V_r|)=36A\eta^{-2}\{P(\eta)\}^2\exp(-R/\rho)$
$(1011|V_r|)=(101-1|V_r|)=36A\eta^{-3}P(\eta)Q(\eta)\exp(-R/\rho)$
$(1111|V_r|)=(111-1|V_r|)=(1-1\ \ 1-1|V_r|)$
$=36A\eta^{-4}\{Q(\eta)\}^2\exp(-R/\rho)$
$\eta\equiv r/\rho$, $P(\eta)=(1+2\eta^{-2})\sinh\eta-2\eta^{-1}\cosh\eta$,
$Q(\eta)=\cosh\eta-\eta^{-1}\sinh\eta$.

When
$\rho=0.2564$A, $2r=0.74$A,
$(0000|V_r|)=7.67A\exp(-R/\rho)\equiv d$
$(0010|V_r|)=9.45A\exp(-R/\rho)=1.23d$
$(0011|V_r|)=6.78A\exp(-R/\rho)=0.88d$
$(1010|V_r|)=11.65A\exp(-R/\rho)=1.52d$
$(1011|V_r|)=8.36A\exp(-R/\rho)=1.09d$
$(1111|V_r|)=6.00A\exp(-R/\rho)=0.78d$

III. WAVE FUNCTION AND MATRIX ELEMENT OF INTERMOLECULAR POTENTIAL

In the two-molecular system, only the total angular momentum which is the sum of the angular momenta of the individual molecules and that of the relative motion, is exactly conserved. But in the case of hydrogen, the energy difference between rotational states being very large ($J=0$ and 1 states are separated by about 180°K), we may be able to assume that the rotational quantum number J of each molecule is conserved throughout collision in the low-temperature region (<150°K).[13] We further assume that the magnetic quantum number M relative to the intermolecular axis is also conserved. When the terms in the second parenthesis { } of Eq. (5) are neglected in comparison with the intermolecular potential this assumption will hold. If we adopt the values of adjustable parameters which we shall find in Section 4, we find this is the case in the region where the repulsive potential is large. In the outer region where the attractive potential is large, we shall find in Table I that the potential is nearly spherical in which case it does not matter how we choose the M axis.

Thus, we may assume the wave function of our system to be

$$\Psi=R(R)\theta_j{}^m(\Theta,\Phi)\theta_{J_1}{}^{M_1}(\theta_1,\varphi_1)\theta_{J_2}{}^{M_2}(\theta_2,\varphi_2), \quad (11)$$

where θ is the usual rotational wave function, and R can be obtained by solving the wave equation

$$\left\{-\frac{\hbar^2}{2m}\frac{4}{R^2}\frac{\partial}{\partial R}R^2\frac{\partial}{\partial R}+(J_1M_1J_2M_2|V_r+h|J_1M_1J_2M_2)+\frac{j(j+1)}{R^2}\right\}R=E_tR, \quad (12)$$

[13] The exachange effect of the rotational quantum number is neglected. Takayanagi (Progr. Theoret. Phys. **8**, 497 (1952)) showed the exchange of rotational and translational energy is extremely small.

TABLE III. Population of each rotational state when *para*:*ortho*=1:3.[a]

J \ T°K	300	223	173	123	90
0	0.129	0.166	0.199	0.232	0.246
1	0.659	0.714	0.738	0.748	0.750
2	0.117	0.083	0.051	0.018	0.004
3	0.089	0.036	0.012	0.002	
4	0.004	0.001			
5	0.001				

[a] Moment of inertia is $4.718\cdot10^{-41}$ g cm² (characteristic temperature is 85.33°K).

where E_t is the translational energy, and the matrix element of intermolecular potential will be shown below.

In Table II, the matrix element of V_r which is given by Eq. (8) is shown for $J_1, J_2=0, 1$. In this table numerical values of the matrix elements, which are given by the constants obtained in the next section, are also shown. The dependence of the matrix elements on rotational quantum number is rather remarkable, and this fact makes M conservative. There are no matrix elements between different M states.

Using Racah's notation,[14] Eq. (9) can be written as

$$h=(\mu_1\mu_2/R^3)\{2C_0^{(1)}(1)C_0^{(1)}(2)+C_1^{(1)}(1)C_{-1}^{(1)}(2) -C_{-1}^{(1)}(1)C_1^{(1)}(2)\}\equiv(\mu_1\mu_2/R^3)h'. \quad (13)$$

If we designate the electronic state by α, the second order perturbation of h is expressed as

$$\sum_{\alpha_1' J_1' M_1'}\sum_{\alpha_2' J_2' M_2'}\frac{(\alpha_1 J_1 M_1\alpha_2 J_2 M_2|h|\alpha_1' J_1' M_1'\alpha_2' J_2' M_2')^2}{E_1+E_2-E_{1'}-E_{2'}}. \quad (14)$$

The energy difference which appears in the denominator of Eq. (14), being the difference between different electronic states, may be assumed to be independent of J_1, J_2. Then it is reduced to

$$\frac{1}{R^6}\sum_{\alpha_1'}\sum_{\alpha_2'}\frac{(\alpha_1|\mu_1|\alpha_1')^2(\alpha_2|\mu_2|\alpha_2')^2}{E_{\alpha_1}+E_{\alpha_2}-E_{\alpha_1'}-E_{\alpha_2'}}\sum_{J_1' M_1'}\sum_{J_2' M_2'}\times(J_1 M_2 J_2 M_2|h'|J_1' M_1' J_2' M_2')^2. \quad (15)$$

According to Racah,[14]

$$(lm|C_{m-m'}^{(1)}|l'm')=(-1)^{g+m}\times[\tfrac{1}{2}(2l+1)(2l'+1)C_{l'l'}]^{\frac{1}{2}}V(ll'1;-mm'm-m'), \quad (16)$$

where

$$2g=l+l'+1,$$

and V is defined in Racah's paper. It easily can be seen that (16) is zero unless $l'=l\pm1$. Thus the sum of the matrix elements of h which appears in Eq. (15) can be expressed for the case, for example, that μ_1 and μ_2 are parallel to the molecular axis as

$$(J_1+1)(J_2+1)f(J_1+1, J_2+1) +J_1(J_2+1)f(J_1-1, J_2+1) +(J_1+1)J_2f(J_1+1, J_2-1) +J_1J_2f(J_1-1, J_2-1),$$

where

$$f(J_1\pm1, J_2\pm1)=4V(J_1J_1\pm11;-M_1M_10)^2\times V(J_2J_2\pm11;-M_2M_20)^2. \quad (17)$$

In this case the sum over α_1', α_2' can be expressed as $(9/4)\,\alpha_{11}\alpha_{11}E$, where α_{11} is the polarizability in the direction parallel to the molecular axis and E is a certain average value of the excitation energy and is near to the ionization energy. In the other terms where $\alpha_\perp\alpha_{11}$ or $\alpha_\perp\alpha_\perp$ appear ($\alpha_\perp$ is the perpendicular polarizability) the factor corresponding to (17) can be obtained easily and the results for all cases of interest are shown in Table I. The value of the polarizability is obtained by Ishiguro *et al.*[15] from which the numerical values of the matrix element are also calculated in Table I.

In contrast to the case of the repulsive potential, the matrix element of the attractive potential is nearly independent of J and M. It is shown by one of the present authors[5] that if the matrix element is averaged over M_1 and M_2, it will be $3\alpha^2E/4R^6$ which is independent of J_1 and J_2.

IV. DETERMINATION OF PARAMETERS OF INTERMOLECULAR POTENTIAL

As is well known, there are two kinds of hydrogen molecules; *ortho* and *para* hydrogen. Under usual conditions the transition between these two can hardly occur. Thus when the temperature of hydrogen gas which has long been at room temperature is made very low, the

TABLE IV. Value of parameters (ρ=0.2564A).

	(0000|V|)	(0010|V|)	(0011|V|)	(1010|V|)	(1011|V|)	(1111|V|)
$b\times10^9$ erg	1.39	1.71	1.22	2.11	1.52	1.08
$\mu\times10^{12}$ erg A^6	10.23	10.74	10.03	11.25	10.43	9.72
$\epsilon\times10^{15}$ erg	4.35	4.07	4.55	3.86	4.23	4.78
R_0 A	3.28	3.37	3.23	3.46	3.32	3.17

[14] G. Racah, Phys. Rev. **62**, 438 (1942).
[15] Ishiguro, Arai, Kotani, and Mizushima, Proc. Phys. Soc. (London) **A65**, 178 (1952).

gas will be a mixture of $J=0$ state molecules and $J=1$ state molecule, the ratio of the population being about 1 to 3.

The population of each rotational state at various temperatures is calculated in Table III under the assumption that the ratio of *ortho* to *para* molecules is 3:1.

We may assume that the molecules with rotational quantum number larger than 2 can be neglected at temperatures lower than 223°K. The quantum effect of the translational motion cannot be neglected in the region $T<200$°K, but this can be taken into account by the second term in the expansion

$$B(T)=B_{cl}(T)+h^2B_1(T)+\cdots, \tag{18}$$

neglecting higher order terms.[16]

Thus, the calculation is made assuming hydrogen gas to be a mixture of same portion of four types of molecules with $J=0$ and $J=1$ with $M=1$, 0, and -1, respectively, and adopting a semiclassical formula $B(T)=B_{cl}(T)+h^2B_1(T)$. We choose parameters in the formula for the intermolecular potential so as to fit the experimental values of $B(T)$ in the $170°K\leq T\leq 223°K$ region.

The calculation was performed using Buckingham-Corner's table.[17] In their paper, the intermolecular potential is assumed to be expressed as

$$V=b\exp(-R/\rho)-\mu R^{-6}\exp\{-4(R_0/R-1)^3\}, \quad \text{for } R<R_0 \tag{19a}$$

and

$$V=b\exp(-R/\rho)-\mu R^{-6}, \quad \text{for } R>R_0, \tag{19b}$$

and $B_{cl}(T)$ and $B_1(T)$ are tabulated for several values of $\alpha\equiv R_0/\rho$ and $x\equiv\epsilon/\kappa T$ where R_0 is the intermolecular distance where the potential is a minimum and $\epsilon\equiv -V(R_0)$. The exponential factor of the second term in Eq. (19a) makes the contribution of the R^{-6} term small in the region $R\ll R_0$. Since this is consistent with our assumption that the R^{-6} term comes from the London force, we accept their expression (19).

Assuming a value of ρ we calculate the ratios of b from Table I. The ratios of μ are already known from Table II. Thus, taking a potential in a collision as

$$V=b\exp(-R/\rho)-\mu R^{-6}, \quad \alpha\equiv R_0/\rho, \tag{20}$$

the others can be expressed as

$$V'=\lambda b\exp(-R/\rho)-\nu\mu R^{-6}, \quad \alpha'\equiv R/\rho_0', \tag{21}$$

where the relation

$$\alpha' 7\ln\alpha'=\ln\lambda-\ln\nu+(\alpha-7\ln\alpha) \tag{22}$$

holds. Also $\epsilon=\mu(\alpha-6)\alpha^{-7}\rho^{-6}$. Thus, assuming certain values for α and μ we obtain $B_{cl}(T)$ and $B_1(T)$ for all kinds of collision by interpolating Buckingham-Corner's table. Then averaging them over all kinds of collisions we obtain the theoretical value of $B(T)$ which is to be compared with observation. After trial and error we obtained the values shown in Table IV. Since there are only two experimental data in our temperature range, there remains an ambiguity in the intermolecular potential thus obtained.

It might be better to fix ν in Eq. (21) to be 1 for all collisions, since as is pointed out in Section III, the terms in the second parenthesis { } in Eq. (5) make the potential spherical in the outer region, however, this does not change our result essentially.

[16] $h^2B_1(T)/B_{cl}(T)$ is about 0.2 at 173°K, and 0.1 at 223°K.

[17] A. Buckingham and J. Corner, Proc. Roy. Soc. (London) A189, 118 (1947).

TABLE V. Value of $(B_{cl}+h^2B_1)/N$ for the cases *para*:*ortho*=1:3 and 1:0 (Å³).

T°K	223	173	123	90	65.1
$p:o=1:3$	19.37	15.60	8.09	−2.17	−17.06
$p:o=1:0$	19.69	15.95	8.52	−1.59	−16.28

V. DETECTION OF NONSPHERICITY OF INTERMOLECULAR POTENTIAL IN SECOND VIRIAL COEFFICIENT

Although the usual hydrogen is a mixture of $J=0$ and $J=1$ state molecules with fixed proportion, we can obtain a gas in which the population of these molecules is given by the Maxwell distribution law by using some catalyst.

Since we have seen that the effective intermolecular potential depends on the rotational state of colliding molecules, it may easily be understood that the second virial coefficient is different for these two kinds of gas which have a different population in the rotational states.[18]

The result of calculations using the values of parameters obtained in Table IV is shown in Table V. The difference shown in this table seems to be detectable experimentally. In fact Schäfer[19] tried this kind of experiment at very low temperature without anticipating the difference caused by our mechanism. In his experiment, which is shown in Table VI, $B(T)$ for pure *para* hydrogen seems to be a little larger than that of ordinary hydrogen. Although our theory in this section cannot be applied to such a low-temperature region, we may assume, extrapolating the values in Table V, that $B(T)$ for pure *para* hydrogen will be larger by about

TABLE VI. Second virial coefficient at $T<25$°K (Å³).

T(°K)	$B_{00}^{(a)}/N$ (this paper)	$B^{(a)}/N$ Miyako[a]	T(°K)	B_{exp}/N[16] (pure *para*)	T(°K)	B_{exp}/N[16] ($p:o=1:3$)
5	−695					
10	−355		20.41	−240.8	20.37	−242.8
15	−223		22.62	−203.1	22.08	−212.1
20	−155	−149	25.25	−176.5	25.23	−177.0
25	−115	−141	28.39	−149.3	27.91	−153.3

[a] See reference 9.

[18] Of course, there is also the difference due to the statistical effect.

[19] K. Schäfer, Z. physik Chem. **36**, 85 (1937); **38**, 187 (1938).

TABLE VII. $(2j+1)\eta_j(k^*)$.

k^* \ j	0	2	4	6	8	10	12	14	16	18	20	22	24	26	28	30	32	$\sum_j (2j+1)\eta_j(k^*)$
0	3.14																	3.14
0.2	2.76																	2.76
0.4	2.39	0.02																2.41
0.6	2.04	0.16	0.01															2.21
0.8	1.70	0.59	0.02															2.31
1.0	1.39	1.73	0.04	0.01														3.17
1.2	1.10	4.08	0.08	0.02	0.01													5.29
1.4	0.83	6.44	0.15	0.03	0.01													7.46
1.6	0.57	7.51	0.25	0.05	0.02	0.01												8.41
1.8	0.32	7.75	0.41	0.08	0.03	0.01	0.01											8.61
2.0	0.09	7.59	0.62	0.12	0.04	0.02	0.01											8.49
2.4	-0.35	6.76	1.64	0.26	0.08	0.03	0.02	0.01	0.01									8.46
2.8	-0.77	5.61	3.26	0.47	0.15	0.06	0.03	0.02	0.01	0.01								8.85
3.2	-1.16	4.32	5.45	0.80	0.26	0.11	0.05	0.03	0.02	0.01	0.01	0.01						9.91
3.6	-1.54	2.97	7.35	1.27	0.42	0.18	0.09	0.05	0.03	0.02	0.01	0.01	0.01					10.87
4.0	-1.90	1.57	8.28	2.28	0.64	0.27	0.13	0.07	0.04	0.03	0.02	0.02	0.01	0.01				11.47
5.0	-2.77	-1.98	7.17	5.64	1.55	0.65	0.32	0.18	0.10	0.07	0.04	0.03	0.02	0.02	0.01	0.01	0.01	11.07
6.0	-3.59	-5.53	3.72	8.71	3.60	1.35	0.67	0.36	0.22	0.14	0.09	0.06	0.04	0.03	0.02	0.02	0.01	9.92
7.0	-4.37	-9.06	-0.68	8.63	6.54	2.82	1.23	0.68	0.40	0.25	0.17	0.11	0.08	0.06	0.04	0.03	0.03	6.96
8.0	-5.13	-12.54	-5.52	5.82	8.95	4.59	2.11	1.15	0.68	0.43	0.29	0.20	0.14	0.10	0.08	0.06	0.04	1.45

$1\sim 2A^3$ than that for ordinary hydrogen, which is the case in Schäfer's experiment.

VI. SECOND VIRIAL COEFFICIENT IN REGION $T=25°K$

Since the quantum effect is very large in this region, we must solve the wave equation.

Assuming the intermolecular potential

$$(J_1M_1J_2M_2|V|J_1M_1J_2M_2)$$

to have the form given in Eq. (19), the problem is reduced to that of a spherical potential.

Solving wave Eq. (12) we obtain the phase shift $\eta_j(k)$ at large R then the second virial coefficient for Bose-Einstein statistics and Fermi-Dirac statistics is given by

$$B^{(s)}=B_{\text{con}}(j=\text{even})+B_{\text{disc}}(j=\text{even}) -(N/16)(h^2/\pi m\kappa T)^{\frac{3}{2}}, \quad (23a)$$

$$B^{(as)}=B_{\text{con}}(j=\text{odd})+B_{\text{disc}}(j=\text{odd}) +(N/16)(h^2/\pi m\kappa T)^{\frac{3}{2}}, \quad (23b)$$

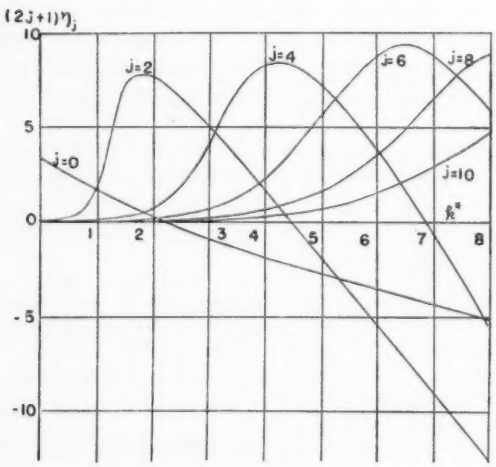

FIG. 2. $(2j+1)\eta_j(k^*)$.

where

$$B_{\text{con}}=-N\left(\frac{h^2}{\pi m\kappa T}\right)^{\frac{3}{2}}\frac{1}{2\pi^2}\int_0^\infty \exp\left(-\frac{h^2k^2}{m\kappa T}\right) \times\sum_j (2j+1)k\eta_j(k)dk,$$

$$B_{\text{disc}}=-N\left(\frac{h^2}{\pi m\kappa T}\right)^{\frac{3}{2}}\sum_{n,j}(2j+1)\{\exp(-E_{jn}/\kappa T)-1\},$$

where N is the total number of molecules, and the translational energy is expressed by h^2k^2/m. E_{jn} is an energy of a discrete energy state which is identified by j and n.

When the ratio of *para* to *ortho* molecules is $1:t$, the observable coefficient is given by

$$B=\frac{5}{9}\left(\frac{t}{t+1}\right)^2 B_{1,1}{}^{(s)}+\frac{t}{(1+t)^2}B_{1,0}{}^{(s)}+\frac{1}{(1+t)^2}B_{0,0}{}^{(s)} +\frac{4}{9}\left(\frac{t}{1+t}\right)^2 B_{1,1}{}^{(as)}+\frac{t}{(1+t)^2}B_{1,0}{}^{(as)}, \quad (24)$$

where $B_{i,j}$ is the second virial coefficient corresponding to the collision of molecules in states $J=i$ and $J=j$.

Since the numerical calculation is very laborious, we limited our calculation to the case of $t=0$, that is $B=B_{0,0}{}^{(s)}$.

The wave equation to be integrated is

$$\frac{d^2(R\psi)}{dR^2}+\left\{k^2-\frac{j(j+1)}{R^2} -(b\exp(-R/\rho)-\mu R^{-6})\right\}R\psi=0, \quad \text{for } R>R_0, \quad (25a)$$

$$\frac{d^2(R\psi)}{dR^2}+\left[k^2-\frac{j(j+1)}{R^2}-(b\exp(-R/\rho)-\mu R^{-6} \times\exp\{-4(R_0/R-1)^3\})\right]R\psi=0, \quad \text{for } R<R_0. \quad (25b)$$

Transforming by $R^*=R/\tau$, $k^*=k\tau$ (where τ is arbitrarily taken to be $3.4963\cdot10^{-8}$ cm), we obtain

$$\frac{d^2(R^*\psi)}{dR^{*2}}+\left\{k^{*2}-\frac{j(j+1)}{R^{*2}}-(b^*\exp(-R^*/\rho^*)-\mu^*R^{*-6})\right\}R^*\psi=0, \quad \text{for} \quad R^*>R_0^*, \quad (26a)$$

$$\frac{d^2(R^*\psi)}{dR^{*2}}+\left[k^{*2}-\frac{j(j+1)}{R^{*2}}-(b^*\exp(-R^*/\rho^*)-\mu^*R^{*-6}\exp\{-4(R_0^*/R^*-1)^3\})\right]R^*\psi=0,$$

$$\text{for} \quad R^*<R_0^*, \quad (26b)$$

where $b^*=\tau^2mb\hbar^{-2}$, $\mu^*=\tau^{-4}m\mu\hbar^{-2}$.

The boundary condition is $R^*\psi\to0$ when $R^*\to0$.

After trying several methods we found it best to give a small value for $R^*\psi$ and its derivative at $R^*=0.5$ and perform numerical integration towards larger R.[20]

When R^* is large enough to give

$$|b^*\exp(-R^*/\rho^*)-\mu^*R^{*-6}|\ll|k^{*2}-j(j+1)R^{*-2}|,$$

the solution must be approximated by

$$R^*\psi=AR^{*\frac{1}{2}}J_{j+\frac{1}{2}}(k^*R^*)+BR^{*\frac{1}{2}}J_{-(j+\frac{1}{2})}(k^*R^*), \quad (27)$$

thus the phase shift is given by

$$\eta_j(k^*)=(-1)^j\tan^{-1}(B/A). \quad (28)$$

The numerical integration was performed to $R^*=6$, and it was seen that we reached the region where Eq. (27) holds as a good approximation.

When $\eta_j(k^*)$ is smaller than 0.1, the Born approximation can be applied, which gives

$$\sin\eta_j\doteqdot-(\pi m/2\hbar^2)\int_0^\infty V(R)J_{j+\frac{1}{2}}{}^2(kR)RdR. \quad (29)$$

In our case it gives

$$\eta_j(k^*)\doteqdot-(\pi/2)(b^*I_1-\mu^*I_2), \quad (30)$$

where

$$I_1=\int_0^\infty\exp(-R^*/\rho^*)J_{j+\frac{1}{2}}{}^2(k^*R^*)R^*dR^*, \quad (30a)$$

$$I_2=\int_0^\infty R^{*-5}J_{j+\frac{1}{2}}{}^2(k^*R^*)dR^*, \quad (30b)$$

which can be expressed as

$$I_1=-(\pi\rho^*k^{*3})^{-1}dQ_j(x)/dx, \quad x=1+(2k^*\rho^{*2})^{-1}, \quad (31a)$$

$$I_2=(k^*/2)^4\,3\Gamma(j-3/2)/\Gamma(j+7/2), \quad j>3/2. \quad (31b)$$

[20] We used the values $R^*\psi=1.10^{-4}$, $dR^*\psi/dR^*=3.10^{-4}$ at $R^*=0.5$.

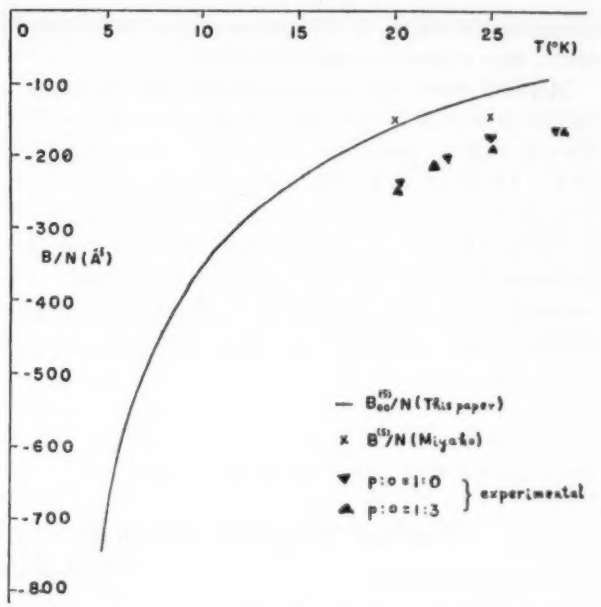

FIG. 3. The second virial coefficient in the region $T<25$°K.

Numerical values of those functions which appear in Eqs. (31) can be found in many places.[21]

In calculating by the Born approximation, we neglected the exponential factor in the second term of Eq. (19a), but the effect is negligible.

The phase shifts thus obtained are shown in Table VII and Fig. 2. In Table VII, the figures shown on the left side of the dotted line are obtained by numerical integration and those on the right are obtained by the Born approximation.

Since the wave function of the $j=0$, $k^*=0$ state has only one node and those for $j>0$ have no node, it is clear that there is only one discrete energy level which has $j=0$. The energy value is obtained by the *WKB* method as

$$E_{0,1}=4.1296\cdot10^{-16}\text{ erg} \quad (32)$$

which is about 10 percent of the depth of potential.

The numerical values of $B_{00}{}^{(o)}(T)$ thus obtained are shown in Table VI and Fig. 3. They are somewhat larger than the experimental value for pure *para* hydrogen. This may be due to the fact that, as is pointed out in Section IV, we could not fix uniquely the value of the parameters in the intermolecular potential. The result in Table VI shows the adopted value was not the best possible.

Miyako[9] has performed similar calculations, but his result shows a different dependence on temperature than ours and the experimental result. Since the dependence on temperature does not change much by

[21] H. Ataka and M. Moji, *Tables of Bessel Functions* (Complex variable) (Maruzen, Tokyo, Japan, 1948). *Tables of Associated Legendre Functions* (Columbia University Press, New York, 1945), *Tables of Spherical Bessel Functions* (Columbia University Press, New York, 1947), Vol. I.

changing the value of the intermolecular potential, his result may contain a numerical error.

Miyako[9] used the same potential for all kinds of collisions as in $B_{00}^{(s)}(T)$, and obtains the value of $B(T)$ for the case of *para*:*ortho*=1:3. As $-114A^3$ at 25°K and $-128A^3$ at 20°K this is larger than the result for pure *para* hydrogen, while the experimental data shown in Table VI seem to indicate that $B(T)$ of pure *para* hydrogen is larger than that of ordinary hydrogen. This contradiction will be improved, if the dependence of the intermolecular potential on the rotational quantum number is taken into account as pointed out in Section V.[22]

ACKNOWLEDGMENTS

The authors wish to thank Professor M. Kotani and the members of his laboratory for their useful suggestions and economical help. They also wish to thank Misses N. Mizushima and N. Sugawara for performing numerical calculations, and Mr. Grayson for assistance with English.

[22] In the theory of viscosity also, the effect of statistics is known to have the wrong sign (E. W. Becker and V. Stell, Phys. Rev. 87, 525 (1952)).

THE JOURNAL OF CHEMICAL PHYSICS VOLUME 21, NUMBER 12 DECEMBER, 1953

Nuclear Magnetic Resonance in Metals. II. Temperature Dependence of the Resonance Shifts*

B. R. McGarvey† and H. S. Gutowsky
Noyes Chemical Laboratory, University of Illinois, Urbana, Illinois

(Received July 16, 1953)

The temperature dependence of the nuclear resonance shift in metals has been investigated in lithium, sodium, rubidium, cesium, and gallium. The resonance shifts were found to change by no more than 5 to 6 percent over temperature ranges of 200°, including the melting point. For sodium, the observed temperature dependence of the resonance shift is correlated directly with the volume dependence predicted theoretically for the mass magnetic susceptibility due to the conduction electrons. In the other metals, effects appear which are related apparently to the volume dependence of the wave functions for electrons at the top of the conduction band. The room temperature resonance shifts of Sn^{117} and Sn^{119} and the temperature dependence of the Rb^{87} line width are also reported for the metals. The resonance shift of tin is 0.705×10^{-2}. The estimation of activation energies for self-diffusion from the temperature dependence of the line widths is discussed.

INTRODUCTION

A PREVIOUS paper[1] was concerned primarily with the magnetic resonance absorption line shapes and widths and their temperature dependence in several metals. In most of the metals the resonance line was broadened significantly by the interaction of the nuclear spins with the conduction electrons, the interaction also determining the short spin-lattice relaxation time. In the case of lithium and sodium, magnetic dipolar broadening was important in the solid at temperatures below about 250°K, with self-diffusion narrowing the resonance line at higher temperatures.

The main part of this paper reports measurements of the temperature dependence of the resonance shifts in lithium, sodium, rubidium, cesium, and gallium. The resonance shifts in metals were first observed by Knight[2] and have been attributed[3] to the magnetic interaction between the nuclei and the conduction electrons. The resonance shifts have been expressed by Townes, Herring, and Knight as

$$\frac{\Delta H}{H_c}=\frac{8\pi}{3}M\chi_m\langle|\psi_k(0)|^2\rangle_F, \tag{1}$$

where $\Delta H=H_c-H$; H_c, the higher field, is the resonance field, at a given frequency, for a compound of the metal and H is the resonance field for the metal; M is the weight in grams of an atom of the metal; χ_m is the contribution of the conduction electron spins to the mass susceptibility of the metal, and $\langle|\psi_k(0)|^2\rangle_F$ is the value for the square of the conduction electrons' wave functions at the nucleus, averaged over the top of the Fermi band. The resonance shifts have been measured for quite a few metals[1-6] at room temperature, but, except for a preliminary report[7] on Na^{23}, no investigation of the effect of temperature upon the resonance shifts seems to have been published.

In principle, the effect of temperature upon the resonance shifts may be obtained by considering in Eq. (1) the two terms which are responsible for the shift and

* Supported in part by the U. S. Office of Naval Research.
† U. S. Atomic Energy Commission Predoctoral Fellow. Present address: Department of Chemistry and Chemical Engineering, University of California, Berkeley 4, California.
[1] H. S. Gutowsky and B. R. McGarvey, J. Chem. Phys. **20**, 1472 (1952).
[2] W. D. Knight, Phys. Rev. **76**, 1259 (1949).
[3] Townes, Herring, and Knight, Phys. Rev. **77**, 852 (1950).
[4] D. F. Abell and W. D. Knight, Phys. Rev. **85**, 762(A) (1952).
[5] W. D. Knight, Phys. Rev. **85**, 762(A) (1952).
[6] H. E. Walchli and H. W. Morgan, Phys. Rev. **87**, 541 (1952).
[7] H. S. Gutowsky, Phys. Rev. **83**, 1073 (1951).

its magnitude. To a first approximation, both χ_m and $\langle|\psi_k(0)|^2\rangle_F$ are independent of temperature. There is possible a slight dependence upon atomic volume of each of these terms, which could give rise to an indirect dependence of the shift upon temperature. The small changes observed in the shift with temperature are evidently the net result of the volume dependence. The interpretation is complicated by there being two terms, neither of which is known independently.

In addition to the temperature dependence of the resonance shifts in several metals, we report the resonance line widths and shifts observed for Sn^{117} and Sn^{119} at room temperature, as well as the temperature dependence of the Rb^{87} line width. The line widths in tin are of interest in regard to possible mechanisms for the broadening of the resonance lines in metals. All of the other metals observed have nuclear spins greater than $\frac{1}{2}$ so that quadrupole coupling of some sort might contribute to the line widths. But the spins of Sn^{117} and Sn^{119} are $\frac{1}{2}$ and quadrupole effects cannot exist. Nonetheless, the observed line widths in tin exceed the predicted dipolar broadening, proving the importance of other than quadrupole effects.

EXPERIMENTAL

Most of the apparatus and procedures have been described.[1,8] All of the measurements were made with the larger of our permanent magnets, at a field of 6365 ± 2 gauss. The sample of tin was a fine powder with an oxide coating providing sufficient insulation for use without further treatment. The other metal samples were those used in I.

The room temperature line widths and resonance shifts in tin and the temperature dependence of the Rb^{87} line width were measured with a super-regenerative spectrometer.[8] This system can be operated at high rf levels with a decent noise figure and is useful for samples such as the metals which have a short spin-lattice relaxation time T_1. The two tin isotopes with magnetic moments are of low abundance (Sn^{117}—7.54 percent, Sn^{119}—8.62 percent) and their resonances could not be detected in either the metal or salt with any of our apparatus other than the super-regenerative spectrometer.

The resonance shifts for Sn^{117} and Sn^{119} were obtained by measuring the resonance frequencies, at constant magnetic field, of the metal and the salt. The metal and the salt samples were placed alternately in the same rf coil and the oscillator tuned to give a maximum output from the narrow-band amplifier.[8] The system detects the dispersion rather than the absorption observed with most setups, so the maximum in the derivative of the resonance line is its center. The resonance frequencies were then measured with a BC-221 Signal Corps frequency meter set by reference to WWV. Care was exercised to insure that the carrier frequency was measured and not one of the side bands.

In I, the line width δH was taken to be the separation of the two peaks of the derivative of the resonance absorption line. However for rubidium the absorption line became too weak for accurate measurement below room temperature, because the line broadened. So the derivative of the Rb^{87} resonance dispersion was plotted several times at each temperature with the super-regenerative spectrometer, and the width of the center peak at half-maximum intensity was determined. In the next section these values are related to the customary absorption line widths. The Rb^{85} resonance was not observed because its low resonance frequency offsets its high isotopic abundance to give a weaker signal than Rb^{87}. The constructional details have been given elsewhere[8] for the cryostat used in these line-width measurements and in the temperature dependence of the resonance shifts.

The temperature dependence of the resonance shifts was observed with a dual rf bridge system activated by the same signal generator. Two identical metal samples were used; one was placed in an rf probe at room temperature while the other was in the cryostat, the two samples as close together as possible in the magnet gap. A switch enabled the output of either bridge to be connected to the detection system. The resonances from the cryostat and the reference were observed alternately and the difference in applied field required for each was measured as a function of temperature. For lithium, sodium, and gallium the absorption lines were displayed on an oscilloscope, while for rubidium and cesium the derivative of the absorption line was observed with the narrow-band amplifier and the line center taken as the point midway between the minimum and maximum. The measurements are reported in terms of the quantity $\delta(\Delta H/H)$ which is defined as follows:

$$\delta\left(\frac{\Delta H}{H}\right)=\frac{H_{25°C}-H_T}{H_{25°C}}, \tag{2}$$

where $H_{25°C}$ is the applied field for the resonance in the sample at 25°C and H_T is the resonance field for the sample at temperature T, the radio-frequency remaining constant. The temperature of the sample in the cryostat was measured with a copper constantan thermocouple immersed directly in the sample.

RESULTS AND DISCUSSION

Line Width and Resonance Shift in Tin

The resonance shift was measured at room temperature with respect to a saturated aqueous solution of $SnCl_2$, which was 0.2 molar in $MnCl_2$. The paramagnetic Mn^{+2} ions were added to reduce T_1 so the super-regenerative system would not saturate the resonance. The resonance in the solution required the narrow-band amplifier for detection even though the line was narrow.

[8] Gutowsky, Meyer, and McClure, Rev. Sci. Instr. **24**, 644 (1953).

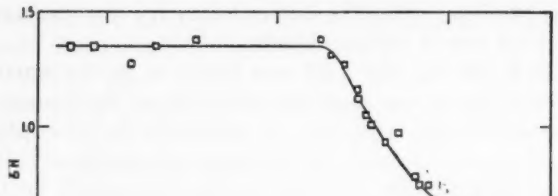

FIG. 1. Temperature dependence of the magnetic resonance absorption line width for Rb^{87} in the metal. δH is given in gauss. The points plotted as squares were obtained from the resonance dispersion, as described in the text.

The results are: for Sn^{117}, $(\Delta H/H_c)=0.701\times10^{-2}$, and for Sn^{119}, $(\Delta H/H_c)=0.709\times10^{-2}$. The error is estimated to be ±1 percent of the measured value, and within this error the resonance shifts are the same for the two isotopes. The metal sample was the β form, i.e., white tin, as confirmed by x-ray analysis.[9]

The derivative of the resonance *dispersion* in the metal was plotted for both isotopes at room temperature, giving curves similar in general appearance to that shown elsewhere[8] for Cu^{63}. However, the discussion in I is based on the second moment and width of the resonance *absorption*. When the dipolar broadening is small, the absorption has the Lorentzian shape

$$f(\Delta H)=4T_1[1+16\pi^2T_1^2(\Delta H)^2]^{-1}, \qquad (3)$$

where ΔH is the magnetic field separation from the line center. The absorption and dispersion are related by the expression[10]

$$f^1(\Delta H^1)=\frac{1}{\pi}\int_{-\infty}^{+\infty}\frac{f(\Delta H)d(\Delta H)}{\Delta H-\Delta H^1}, \qquad (4)$$

where $f^1(\Delta H^1)$ is the dispersion shape function. The width of the dispersion derivative at half-maximum, $\delta H_{\frac{1}{2}\max}$, is given via Eqs. (3) and (4) in terms of the width of the absorption derivative δH by the expression

$$\delta H=1.188\delta H_{\frac{1}{2}\max}. \qquad (5)$$

The theoretical dipolar second moments ΔH_2^2 of the absorption lines for both Sn^{117} and Sn^{119} are about 0.06 gauss.[2] The experimental δH values for Sn^{117} and Sn^{119} obtained through Eq. (5) are 2.5 and 3.0 gauss with uncertainties of ±0.5 gauss. The relation between δH and ΔH_2^2 depends upon line shape; in the extreme case of a rectangular shape, $\delta H=2\sqrt{3}\Delta H_2$ so the maximum δH possible in tin from dipolar broadening is 0.9 gauss, with 0.5 gauss a more likely value. Even allowing for the error introduced by assuming a Lorentzian shape in computing δH from the observed $\delta H_{\frac{1}{2}\max}$, the resulting values are nearly double the maximum dipolar width. T_1 values based[1] upon the observed resonance shift are 1.4×10^{-4} and 1.3×10^{-4} sec. If only T_1 broadening were present, the line widths computed from the equation[1] $T_1=1/2\sqrt{3}\pi\delta H$ would be 0.4 and 0.5 gauss. In the other metals the observed nondipolar broadening of the resonance exceeds that predicted from the resonance shift by a factor of about two. Adding the T_1 and dipolar broadening, the line widths should be in the range of 1 to 2 gauss, which, in view of the indirect procedure used, agrees reasonably well with experiment. Moreover, white tin is tetragonal and anisotropy in the resonance shift with crystal orientation might also contribute to the line width.

Temperature Dependence of the Rb^{87} Line Width

Absorption line widths of Rb^{87} were measured at several temperatures above 300°K and the results reported in I. The dispersion line widths have since been measured at lower temperatures with the super-regenerative spectrometer. The absorption lines were nearly Lorentzian in shape,[1] so δH values can be estimated with Eq. (5) from the observed $\delta H_{\frac{1}{2}\max}$ data. Both sets of data are given in Fig. 1; the δH values computed from the dispersion curves are indicated by squares while the directly observed δH values are plotted as circles. The data join very well, indicating the general validity of the procedure.

The rubidium resonance line is broad in the liquid like that of cesium[1] and is similar to lithium[1] and sodium[7] in having a transition below the melting point. But at lower temperatures it does not decrease like cesium. The width at the higher temperatures and in the liquid state is due mainly to the short spin-lattice relaxation time T_1 as is the case in cesium, while the greater width at the lower temperatures must be due to the contribution of both dipolar and T_1 broadening. The dipolar contribution to the line width should be

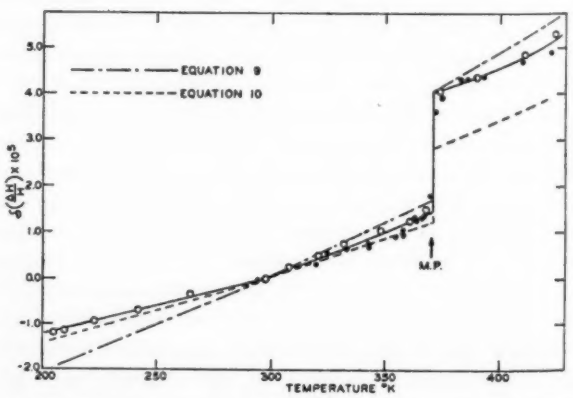

FIG. 2. Temperature dependence of the resonance shift for Na^{23}. The broken lines represent the theoretical predictions of Eqs. (9) and (10) for this metal. The solid circles are data reported previously in reference 7.

[9] We are indebted to Walter E. Thatcher of the department's x-ray laboratory for the analysis.

[10] G. E. Pake and E. M. Purcell, Phys. Rev. 74, 1184 (1948).

approximately 0.5 gauss in the rigid lattice, and this is about the magnitude of the change in line width during the transition which occurs below the melting point. Therefore, this transition is evidently associated with self-diffusion of the metal atoms as in sodium and lithium. The small discontinuous change at the melting point[11] may be the effect upon the dipolar broadening or upon T_1 of a cooperative change in the self-diffusion rate. The T_1 broadening should decrease at low temperatures as it did in cesium because of the increase in T_1; however, any line narrowing of this sort in rubidium occurs below the 90°K limit of our observations.

The combination of dipolar and T_1 broadening in rubidium prevents any very good estimate from the line-width transition of the activation energy for self-diffusion such as made for lithium[1] and sodium.[7] The T_1 broadening is negligible for the latter two metals but is significant in the heavier elements. Moreover, it seems likely that self-diffusion would produce time-dependent field gradients in the metals. If the self-diffusion were fast enough, the gradients would average substantially to zero, but at slower rates there might be some broadening of the resonance line by quadrupole interactions, which could also contribute to T_1. Seymour[12] has reported a line-width transition in aluminum, centered at 330°C, but did not obtain very reasonable values for the diffusion processes. The T_1, and perhaps quadrupole effects as well, may cause the discrepancies.

Overhauser[13] has suggested that the method described by Wert and Marx[14] could be used to estimate activation energies for self-diffusion from the temperature T_M, at which the resonance line begins to narrow, rather than from its change with temperature. The method assumes a constant factor ν_0 in the equation $\nu=\nu_0 e^{-E_a/RT}$

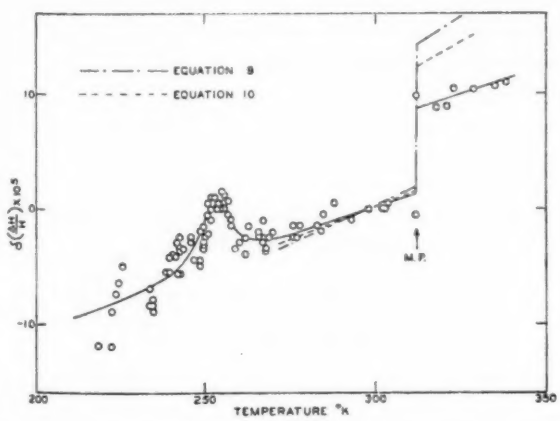

FIG. 3. Temperature dependence of the resonance shift for Rb^{87}. The broken lines represent the theoretical predictions of Eqs. (9) and (10) for this metal.

[11] The resonance shift *increases* upon melting so the line width change cannot result from an increase in T_1 as suggested in I.

[12] E. F. W. Seymour, Proc. Phys. Soc. (London) **A66**, 85 (1953).

[13] A. L. Overhauser, private communication. We wish to thank Dr. Overhauser for reading the manuscript of our paper and discussing it with us.

[14] C. Wert and J. Marx, Acta Metallurgica **1**, 113 (1953).

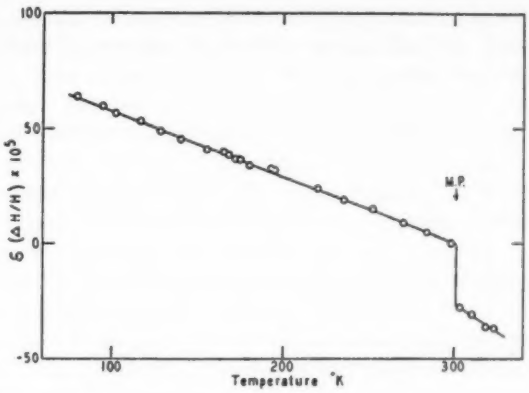

FIG. 4. Temperature dependence of the resonance shift for Cs^{133} in the metal.

and also requires in this case that there be the same critical frequency of self-diffusion when the resonance line starts narrowing in the different metals. Under these conditions we have $E_a=AT_M$, where A can be evaluated from a known E_a and T_M.

Using Nachtrieb's directly measured[15] E_a of 10.5 kcal for sodium and the line width[7] T_M of 160°K, A is 65.5 cal deg^{-1}. Differences in the critical diffusion frequency are corrected by adding the term $RT_M \ln(\nu_{Na}/\nu_M)$ to AT_M; ν_{Na} and ν_M are the frequency widths of the resonance lines in sodium and in the metal, at T_M. In this way, activation energies of self-diffusion of 10.3, 13.9, 14.8, and 29.8 kcal are estimated for Cs^{133}, Li^7, Rb^{87}, and Al^{27}, respectively, from data in this article and in I. The 13.9 kcal for lithium is to be compared with the 9.8-kcal value found in I from the change in line width with temperature. The 29.8 kcal for aluminum is in better agreement with the expected value[12] of 33 kcal than is the 21-kcal value obtained by Seymour.

Temperature Dependence of the Resonance Shifts

The observed resonance shifts are given as a function of temperature in Figs. 2, 3, 4, and 5 for sodium, rubid-

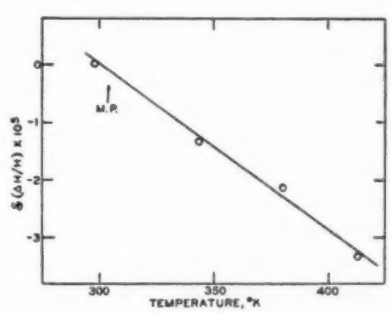

FIG. 5. Temperature dependence of the resonance shift for Ga^{71} in the metal. These data were obtained with the setup described in reference 7. The point at 298°K was obtained in the supercooled liquid; the resonance has not been detected in the solid.

[15] Nachtrieb, Catalano, and Weil, J. Chem. Phys. **20**, 1185 (1952).

ium, cesium, and gallium, respectively. In the case of lithium, no measurable difference was found between room temperature and 200°C, outside the experimental error of $\pm 2\times 10^{-6}$, and this includes any possible change occurring at 186°C, the melting point. Each point on the sodium, cesium, and gallium plots is the average of several separate measurements, while for rubidium each measurement is plotted. The rubidium data are given in this manner to demonstrate more graphically the apparent realness of the peak in the curve in the region of 254°K. The broadness of the rubidium resonance below 220°K and of the sodium resonance[7] below 200°K precluded measurements of significant accuracy; however, an observation of rubidium at 80°K showed that its resonance shift below 220°K follows the general trend indicated by the solid line in Fig. 3. The gallium resonance could not be found in the solid below the melting point, 303°K, probably because of quadrupole broadening in the tetragonal lattice.

The earlier measurements for sodium above room temperature are plotted as solid circles in Fig. 2, and they agree well with the present data. The previous results at lower temperatures[7] were inaccurate because of an incomplete correction for changes in the field at the sample caused by the materials of the cryostat itself. The proton resonance in hexane was used to determine the correction; however, possible differences in the glass sample containers were overlooked. In these experiments the latter were found to be important below room temperature. The corrections are a significant fraction of the observed effects only for the sodium measurements below room temperature.

From the data given, the resonance shifts are seen to depend only slightly upon the temperature; the maximum change over the temperature ranges investigated is about 5 or 6 percent of the total shift. The smallness of the temperature dependence accounts for the apparent absence of an effect in lithium; in it the resonance shift is so small that the expected change with temperature is within the experimental error. It was pointed out in the Introduction that the observed temperature effects express the net influence of the atomic volume upon the two terms, χ_m and $\langle|\psi_k(0)|^2\rangle_F$, in Eq. (1). Of the theoretical work on metals, none seems to give any firm indication of how the latter term varies as the lattice constant is varied. Fortunately, more can be said concerning the possible volume dependence of the spin paramagnetic susceptibility χ_m.

One would expect χ_m to increase with an increase in volume. As the volume in which the conduction electrons are confined increases, the separation of the different energy levels decreases; this increases the energy-level density and gives a corresponding increase in χ_m. In this manner the Pauli theory[16] for the paramagnetic susceptibility of metals predicts that χ_m should be proportional to $V^{\frac{1}{3}}$. In the preliminary account[7] of temperature effects for Na^{23}, the Pauli theory was found to predict a rather smaller change in resonance shift than that observed. It was suggested that chemical shifts of the resonance in different compounds of the metal could introduce some uncertainty in the *actual* value of the conduction electron shift, which might account for part of the discrepancy.

Another pertinent factor, which has been noted independently by Overhauser,[13] is that the Pauli theory assumes the conduction electrons are free and noninteracting. Sampson and Seitz[17] have refined the Pauli theory for the alkali metals by taking into account the exchange and correlation energies of the electrons. For χ_m they obtain the expression

$$\chi_m = M\mu_0^2/2\alpha, \tag{6}$$

where μ_0 is the Bohr magneton and

$$\alpha = (h^2/6m^*)(9/32\pi^2)^{\frac{1}{3}}\frac{1}{r_s^2} - \frac{2.32\times 10^{-20}}{r_s} + 1.46\times 10^{-20} r_s \frac{(2r_s+6.75\times 10^{-8})}{(r_s+2.70\times 10^{-8})^2}. \tag{7}$$

m^* is the effective electron mass for the metal, and r_s is the radius of the atomic sphere for the metal and is found from the equation

$$r_s = \left(\frac{3V}{4\pi N}\right)^{\frac{1}{3}}, \tag{8}$$

where V is the volume of the metal and N is the number of atoms contained in that volume.

If the term $\langle|\psi_k(0)|^2\rangle_F$ were *independent* of volume, the change in resonance shift would be given from the Sampson-Seitz theory by the expression

$$\delta\left(\frac{\Delta H}{H}\right) = \left(\frac{\Delta H}{H}\right)_{25°C}\left\{\left(\frac{\alpha_{25°C}}{\alpha}\right)-1\right\}. \tag{9}$$

This function is plotted for Na^{23} in Fig. 2 and for Rb^{87} in Fig. 3. For comparison the expression

$$\delta\left(\frac{\Delta H}{H}\right) = \left(\frac{\Delta H}{H}\right)_{25°C}\left\{\left(\frac{V}{V_{25°C}}\right)^{\frac{1}{3}}-1\right\}, \tag{10}$$

which is what the simple Pauli theory would predict, is also plotted for both Na^{23} and Rb^{87}. Similar plots are not given for Cs^{133} and Ga^{71} since it is apparent from Figs. 4 and 5 that neither Eq. (9) or Eq. (10) would give a temperature dependence for the shift which agrees with experiment.

As can be seen in Fig. 2, Eq. (9) gives quite well the observed temperature dependence of the Na^{23} resonance shift. In making this plot, the coefficients of volume

[16] W. Pauli, Z. Physik **41**, 81 (1927).

[17] J. B. Sampson and F. Seitz, Phys. Rev. **58**, 633 (1940).

expansion used were Hackspill's[18] for temperatures above 0°C and were Dewar's[19] for temperatures below 0°C. The value used for the percentage volume change at the melting point was that of Losana.[20] There appears to be a great deal of uncertainty about the latter quantity, with reported values[18,20–23] varying between the 1.5 percent of Hackspill[18] and the 2.53 percent of Endo.[22] For all of the various values, Eq. (9) agrees somewhat better with experiment than Eq. (10), but Losana's value of 2.17 percent gives with Eq. 9 almost the exact change at the melting point. The divergence between experiment and Eq. (9) at lower temperatures could be due to Dewar's data[19] being somewhat inaccurate. For the other metals the situation is more complex. The Rb^{87} shift increases with temperature but not nearly as much as predicted by either Eq. (9) or (10), while the Cs^{133} and Ga^{71} shifts actually decrease with increasing temperature. The thermal expansion data used in plotting Eqs. (9) and (10) for Rb^{87} were those reported by Hackspill,[18] and the volume change at the melting point was that reported by Losana,[20] which agrees well with that of other observers.[19,22,23]

The theory of Sampson and Seitz for χ_m should be particularly good for sodium, so that agreement between Eq. (9) and the experimental data furnishes good evidence that in this metal the term $\langle|\psi_k(0)|^2\rangle_F$ is independent of volume. Or alternately, as we shall see later, there is an indirect argument that Eq. (9) is a better representation for χ_m of sodium than is the free electron theory. The exact volume dependence of χ_m for the other metals will probably not be given by either Eq. (9) or (10), but it is very unlikely that χ_m would decrease with increasing volume. Thus it is clear for cesium and gallium that the decrease in resonance shift with increasing temperature must come about from a decrease in $\langle|\psi_k(0)|^2\rangle_F$.

The dependence of the latter term upon the volume is a rather difficult question. For one thing, those wave functions which have been computed for metals are poorest in the region of interest to us, that is, at the top of the conduction band. If an electron were perfectly free, the square of its wave function at every point would be inversely proportional to the volume, from the normalization condition. But the effect of normalization on the volume dependence of the wave function at a nucleus is not necessarily the same. An increase in the volume over which the wave function is normalized will always trend to decrease the value of the wave function at most points, but since the nature of the wave function may also change with volume, the change in value of the wave function at a specific point is uncertain.

Assuming a free election model, we have the V^1 dependence of χ_m from the Pauli theory and the V^{-1} effect of normalization upon $\langle|\psi_k(0)|^2\rangle_F$. These combine to give a net $V^{-\frac{1}{3}}$ equation for the resonance shift. This agrees qualitatively with the experimental results for Ga^{71} and Cs^{133}; however, the predicted decrease in the resonance shift with increasing temperature is about half that actually observed for these two metals. The behavior of the rubidium shift suggests a decrease in $\langle|\psi_k(0)|^2\rangle_F$ with increasing volume but not nearly a V^{-1} dependence, since the experimental data do not fall too far below the curves plotted from Eqs. (9) and (10).

To summarize, it appears that $\langle|\psi_k(0)|^2\rangle_F$ decreases relatively little for sodium, if at all, with increasing volume, more for rubidium, and so much for cesium that the increase in χ_m is overcompensated and a net decrease in the resonance shift results. The systematic trend with nuclear charge is probably significant. At least it suggests that any change in $\langle|\psi_k(0)|^2\rangle_F$ with increasing volume for sodium is probably a decrease rather than an increase. Therefore, the better fit of the data by Eq. (9) implies that the Sampson and Seitz theory is really a better expression for χ_m than is the free-electron theory.

At present no explanation can be given the peak in the rubidium resonance shift occurring at 254°K. No transitions have been reported at this temperature for any of the other properties of rubidium metal, such as structure, heat capacity, or electrical resistance.

ACKNOWLEDGMENT

The continuing interest of Dr. C. P. Slichter in our research on metals has been very helpful to us. The direct observation of nuclear relaxation phenomena in metals by his research group has been valuable in our choice of experiments and in the interpretation of our results. Also, we wish to thank Mr. R. E. McClure for his assistance with the measurements on Ga^{71}.

[18] L. Hackspill, Ann. Chim. **28**, 633 (1913).
[19] J. Dewar, Proc. Roy. Soc. (London) **A70**, 237 (1902).
[20] L. Losana, Gazz. Chim. Ital. **65**, 851 (1935).
[21] A. Bernini and C. Cantoni, Nuovo Chimento **8**, 241 (1914).
[22] H. Endo, J. Inst. Metals **30**, 121 (1923).
[23] E. Hagen, Ann. Physik **19**, 537 (1883).

Fractionation of the Carbon Isotopes in Decarboxylation Reactions. VI. Comparison of the Intermolecular Isotope Effects of a Pair of Isotopic Isomers*

JACOB BIGELEISEN AND MAX WOLFSBERG
Chemistry Department, Brookhaven National Laboratory, Upton, Long Island, New York
(Received June 15, 1953)

Theoretical considerations show that malonic acid $-2C^{14}$ should decarboxylate precisely twice as fast as the isotopic isomer malonic acid $-1C^{14}$ liberates $C^{14}O_2$. The calculations are supported by the experimental data of Ropp and Raaen. It is shown that these experiments are consistent with a C^{14} isotope effect twice that of the C^{13} one.

THE decarboxylation of both mono- and di-basic acids have been examined for isotopic fractionation of the carboxyl carbon atom. Two types of processes have been considered to date: (1) the relative rates of reaction of an all C^{12} acid and one containing C^{13} or C^{14} in the carboxyl group, intermolecular isotope effect, and (2) the relative rates of production of $C^{12}O_2$ and $C^{13}O_2$ or $C^{14}O_2$ from a carboxyl singly labeled dibasic acid, unsymmetric only because of isotopic composition, intramolecular isotope effect. Comparison between theory and experiment shows good agreement in all cases for C^{13} while a few cases for C^{14} exist where there is poor agreement between theory and experiment and between different experimental investigations.[1] In general the C^{14} experiments do not have the precision of the C^{13} experiments. The most extensively studied system is the decarboxylation of malonic acid, which was first investigated with C^{14} by Yankwich and Calvin.[2]

Recently Yankwich and co-workers[3–5] have reinvestigated the inter- and intramolecular isotope effects of malonic acid with C^{13} and the intramolecular isotope effect with C^{14}. Their results in the case of C^{13} confirm previous experimental investigations,[6–7] which were in quantitative agreement with theoretical predictions.[1,6,9] Their C^{14} results are not in agreement with theory,[9] and support the previous results of Yankwich and Calvin[2] on malonic acid, but present a more reasonable value in the case of bromo malonic acid. Some preliminary measurements by Yankwich and Stivers[4] indicate little difference between the inter- and intramolecular isotope effects with C^{14} in the carboxyl group. It is a consequence of the theory[1,9] that a difference between these should exist and this difference has been verified with C^{13}.[4–8]

Ropp and Raaen[10] have determined a combination of the intra- and intermolecular isotope effects in the decarboxylation of malonic acid containing tracer amounts of malonic acid $-1C^{14}$. They have also investigated the intermolecular isotope effect in the decarboxylation of malonic acid containing the other isotopic isomer of C^{14} malonic acid, i.e., malonic acid $-2C^{14}$. This reaction has not as yet been studied with C^{13}. The reactions and rate constants are defined by the equations[6]

$$C^{12}H_2(C^{12}OOH)_2 \xrightarrow{k_1} C^{12}O_2 + C^{12}H_3C^{12}OOH \quad (1)$$

$$C^{14}H_2(C^{12}OOH)_2 \xrightarrow{k_2} C^{12}O_2 + C^{14}H_3C^{12}OOH \quad (2)$$

$$C^{12}H_2 \begin{cases} C^{14}OOH \\ C^{12}OOH \end{cases} \xrightarrow{k_3} C^{14}O_2 + C^{12}H_3C^{12}OOH \quad (3)$$

$$\xrightarrow{k_4} C^{12}O_2 + C^{12}H_3C^{14}OOH. \quad (4)$$

An evaluation of the data of Ropp and Raaen[10] leads to the results

$$k_1/k_2 = 1.076 \pm 0.006 \text{ at } 154°C, \quad (5)$$

$$k_1/2k_3 = 0.5178 \pm 0.0015(1+k_4/k_3) \text{ also at } 154°C^{11}. \quad (6)$$

It is clear from Eq. (6) that an *a priori* knowledge of k_4/k_3, intramolecular isotope effect, is necessary to calculate the intermolecular isotope effect with the carboxyl C^{14} isomer, $k_1/2k_3$, from Ropp and Raaen's data. Three values of this ratio are available and $k_1/2k_3$ is calculated for these values in Table I. If one accepts the restriction that $k_1 \geq 2k_4$ because of the zero-point energy

TABLE I. Intermolecular isotope effect in malonic acid $-1C^{14}$.

k_4/k_3	$k_1/2k_3 \pm 0.003$
1.038[9] (Theor)	1.055
1.06[12] (Exp)	1.067
1.10[4] (Exp)	1.087

* Research carried out under the auspices of the U. S. Atomic Energy Commission.

[1] J. Bigeleisen, J. Phys. Chem. **56**, 823 (1952).
[2] P. E. Yankwich and M. Calvin, J. Chem. Phys. **17**, 109 (1949).
[3] Yankwich, Stivers, and Nystrom, J. Chem. Phys. **20**, 344 (1952).
[4] P. E. Yankwich and E. C. Stivers, J. Chem. Phys. **21**, 61 (1953).
[5] Yankwich, Belford, and Fraenkel, J. Am. Chem. Soc. **75**, 832 (1953).
[6] J. Bigeleisen and L. Friedman, J. Chem. Phys. **17**, 998 (1949).
[7] Lindsay, Bourns, and Thode, Can. J. Chem. **29**, 192 (1951).
[8] Lindsay, Bourns, and Thode, Can. J. Chem. **30**, 163 (1952).
[9] J. Bigeleisen, J. Chem. Phys. **17**, 425 (1949).
[10] G. A. Ropp and V. F. Raaen, J. Am. Chem. Soc. **74**, 4992 (1952).
[11] The experimental errors are estimated from the precision of the activity and half time measurements. The latter introduce the major part of the estimated errors in these experiments.

effect, then the data of Ropp and Raaen Eq. (6) lead to the result that $k_4/k_3<1.074$. This is consistent with the measurements of Roe and Hellman[12] and with theoretical calculations,[9] but not with those measurements which purport this ratio to be much higher.[2-4] The similar magnitude of k_2 and $2k_3$ determined by Ropp and Raaen indicates that lack of equilibrium in the transition state, attention to which has been directed by Pitzer,[13] cannot introduce any serious corrections to the ratio $k_1/2k_4$.[14]

It is unfortunate that an unambiguous value for the ratio $k_2/2k_3$ cannot be obtained from Ropp and Raaen's data, since the latter would be of considerable theoretical interest. In the theoretical evaluation of the intermolecular isotope effect the zero-point energy effect has been approximated by considering only those bonds ruptured (or formed) by the reaction in question.[1] Thus, the intercomparison of k_2 and $2k_3$ would test the role of the zero-point energies of the other vibrations.

In the case of the decarboxylation of malonic acid $-2C^{14}$ the formation of the C—H bond, either in the transition state or at some prior or subsequent time, may have an effect both on the reduced mass factor and the zero-point energy terms. In the model proposed for the estimation of the zero point energy effect,[1,9] the formation of a C—H bond is of no consequence in determining the ratios $k_1/2k_3$ or k_4/k_3, i.e., in dealing with isotopic substitution in the carboxyl group. We have recently carried out calculations on the effect of the formation of a C—H bond simultaneous with C—C bond rupture on the reduced mass factor for the substitution of isotopic carbon.[15] If a C—H motion is important in the transition state, it will reduce the value of the mass term, $(m^{1*}/m^*)^{\frac{1}{2}}$. The magnitude of the effect of the hydrogen motion on this ratio depends on which carbon atom is being substituted isotopically and the relative amounts of C—H to C—C motion in the transition state (cf. curves 1 and 4 of reference 15). In the case of isotopic substitution in the carboxyl group a comparison of the theoretical calculations with the C^{13} data shows that there is no motion of the methyl forming hydrogen in the reaction coordinate. The reduced mass terms are, therefore, identical for the $-1C^{14}$ and $-2C^{14}$ isomers. Any difference in the rate constants k_2 and $2k_3$ must therefore arise from the zero-point energy effects. According to the model, the zero-point energy terms, $\sum^{3n-6} G(u_i)\Delta u_i - \sum^{3n-6} G(u_i^{\ddagger})\Delta u_i^{\ddagger}$, are replaced by $G(u_1)\Delta u_1$, where $G(u)$ is the free energy function derived by Bigeleisen and Mayer,[16] u_1 is the C—C stretching frequency multiplied by hc/kT, and Δ refers to the change in the latter on isotopic substitution.

Thus, according to the model, there should be no difference between k_2 and $2k_3$. This seems to be borne out by the experiments of Ropp and Raaen. The theoretical value for k_1/k_2 at 154°C is 1.064. This value is calculated with the reduced mass factor of 1.038 discussed previously[9] and a C—C stretching frequency of 900 cm^{-1}. The theoretical value for k_1/k_2 is a little low, but not more than twice the estimated experimental error. Intercomparison of this theoretical value for $k_1/2k_3$ with the Ropp and Raaen data supports an experimental value for k_4/k_3 between 1.04 and 1.07. The theory applied to malonic acid is, therefore, supported by the experimental data on C^{13} for k_4/k_3 and $k_1/2k_3$ at all temperatures,[1,4] and for C^{14} by the data of Ropp and Raaen on k_1/k_2. The only disagreement between theory and experiment is in the case of k_4/k_3 when C^{14} is substituted for C^{12} in the carboxyl group. The present analysis of the data of Ropp and Raaen indicate that the contention of Yankwich and Stivers that $[(k_4/k_3)C^{14}-1]>2[(k_4/k_3)C^{13}-1]$ is not well founded.

[12] A. Roe and M. Hellman, J. Chem. Phys. **19**, 660 (1951).
[13] K. S. Pitzer, J. Chem. Phys. **17**, 1341 (1949).
[14] For additional discussion of this question see A. A. Bothner-By and J. Bigeleisen, J. Chem. Phys. **19**, 755 (1951).
[15] J. Bigeleisen and Max Wolfsberg (submitted for publication in J. Chem. Phys.).
[16] J. Bigeleisen and M. G. Mayer, J. Chem. Phys. **15**, 261 (1947).

The Proton Magnetic Resonance in Natural Rubber*

H. S. GUTOWSKY AND L. H. MEYER†
Noyes Chemical Laboratory, University of Illinois, Urbana, Illinois
(Received July 16, 1953)

The proton magnetic resonance has been observed in natural rubber from liquid nitrogen temperature to room temperature. The absorption line widths show two regions of change. With rising temperature, the first change in width starts at about 155°K, and we assign it to the onset of CH_3 group rotation. The second, larger change to a narrow line, starts at about 225°K and is assigned to the onset of segmental motions. The latter change coincides with the second-order transitions observed in various physical properties and provides a direct confirmation of the cause of the transition. Samples cured 30, 60, and 90 minutes were investigated, and it was found that curing has a larger effect on the line width changes at lower temperature than at higher temperature. The inferred greater effect of curing upon CH_3 group motions than upon segmental motions suggests that cross linking is not the primary mechanism of vulcanization. Rubber stretched 70 percent was found to have the same resonance absorption as unstretched samples.

INTRODUCTION

SEVERAL methods based upon the various characteristics of nuclear magnetic resonance have been developed[1] for investigating the structure of solids, particularly the presence and nature of nuclear motions. The extension of these methods from simple ionic or molecular crystals to polymers was first made in some detail by Guth and coworkers,[2,3] while less extensive observations were reported earlier by Alpert[4] and by Newman.[5] In Guth's work the proton resonance absorption line widths were observed over a temperature range in a number of synthetic polymers, and the results were associated qualitatively with the hindrance to internal motions and the effects thereon of various processing. Newman gave a similar, more quantitative discussion of polyethylene. This report is concerned with the nature of the rotational processes in natural rubber. The analysis is based upon the temperature dependence observed for the proton magnetic resonance absorption and the results bear upon the nature of the curing process.

EXPERIMENTAL

Apparatus

The general type of experimental arrangement for observing the temperature dependence of the broad, resonance line widths and shapes has been described elsewhere.[6] The experiments were performed at fixed frequency with a variable applied magnetic field about 6365 gauss. A regenerative oscillator, 30-cycle modulation system, and a narrow band amplifier were used to observe the derivative of the proton absorption line, with respect to magnetic field, as a function of applied field. The line shapes were plotted manually[7] from the observed output of the narrow band amplifier. A complete plot of the line was made only at temperatures of particular interest. Otherwise the line width δH was measured by observing the field difference between points of maximum and minimum output of the narrow band amplifier. Satisfactory temperature control was obtained with an earlier version of the cryostat described.[6]

Samples

Three natural rubbers were used, differing only in the length of cure time which was 30, 60, and 90 minutes. Each was cured at a temperature of 280°F. The samples were very kindly furnished by F. T. Wall of this department, who obtained them from the University of Akron. The samples were initially in narrow strips approximately $10\times0.7\times0.2$ cm. For our measurements four strips, $2.5\times0.7\times0.2$ cm, were laminated through the rf coil in the cryostat. A small hole was drilled in each end of the strips, and 3/32-in. brass rods were threaded through the holes to mount the samples in the probe. Brass washers, outside the rf coil, were used as spacers between each strip. Provision was made to vary the separation of the brass mounting rods so the samples could be stretched and any effects of stretching investigated. The temperature of the sample was measured with a copper-constantan thermocouple, one junction of which was placed between two adjacent strips of the sample.

RESULTS AND DISCUSSION

Figure 1 is a typical plot of the derivative of the proton absorption in the rubber samples. This particular curve was obtained at 86°K in the 30-minute cure sample. In some of the samples, at various tempera-

* Supported in part by the U. S. Office of Naval Research.
† U. S. Atomic Energy Commission Predoctoral Fellow. Present address: U. S. Atomic Energy Division, E. I. du Pont de Nemours and Company, Augusta, Georgia.
[1] G. E. Pake, Am. J. Phys. **18**, 438, 473 (1950) summarizes work prior to 1950.
[2] Holroyd, Codrington, Mrowca, and Guth, J. Appl. Phys. **22**, 696 (1951).
[3] Holroyd, Mrowca, and Guth, Phys. Rev. **79**, 1026 (1950).
[4] N. L. Alpert, Phys. Rev. **75**, 398 (1949).
[5] R. Newman, J. Chem. Phys. **18**, 1303 (1950).
[6] Gutowsky, Meyer, and McClure, Rev. Sci. Instr. **24**, 644 (1953).
[7] This research was done before completion of the automatic recording system reported in reference 6.

tures there were more pronounced outer shoulders on the derivative curve, but no inflection points; the integrated lines in all cases are simple bell-shaped curves. The observed line widths are listed in Table I for temperatures between that of liquid nitrogen and room temperature, and the data are plotted in Figs. 2–4.

Interpretation of the Line Width Changes

The temperature dependence of the line widths seems to be of the general form observed for other polymers.[2,3,5] In all three of the natural rubbers the lines are narrow, about 0.15 gauss wide, at room temperature, but definitely broader than field inhomogeneities. There is a very gradual increase in line width upon cooling, until a temperature of about 263°K is reached. At this temperature the line widths begin to increase more rapidly. However, there is a decrease in the slope of the line width *versus* temperature curves at about 220°K for the 30-minute cure rubber and at about 228°K for the 60- and 90-minute cure rubbers. On further cooling the line widths in the three samples increase until the same limiting value of about 9.5 gauss is reached, at temperatures of 143°K, 163°K, and 173°K for the 30-, 60-, and 90-minute rubbers respectively. In other words, all three rubbers show two different transition regions in the line width *versus* temperature curves, and a basic question in this research is the identification of these two transitions with the types of nuclear motions possible in the sample.

A semiquantitative analysis has been given of the dependence of line width upon the nature and frequency of nuclear motions.[8] In general, a magnetic dipolar broadened resonance line will start to narrow when the atomic configuration about the observed nuclei changes "significantly" with a frequency the order of the frequency width of the broadened line, that is about 50 kc per sec in these experiments. The monomer of natural rubber is the isoprene molecule $CH_2=CCH_3-CH=CH_2$. Powles,[9] in recent research on some simple compounds containing methyl groups, found that the CH_3 groups move about their C_3 symmetry axis fast enough to narrow the proton resonance at temperatures around 125°K. Motions involving the carbon skeleton of the same compounds ordinarily required temperatures 50° higher, or more, to become effective. This, then, gives a qualitative argument for assigning the low-temperature line width change in the rubbers to CH_3 group "rotation" and the change at higher temperatures to motion of the chain segments.

Confirmation of this model can be obtained by considering the second moment[10] of the resonance line. The experimental second moment, ΔH_2^2, was 18.3,

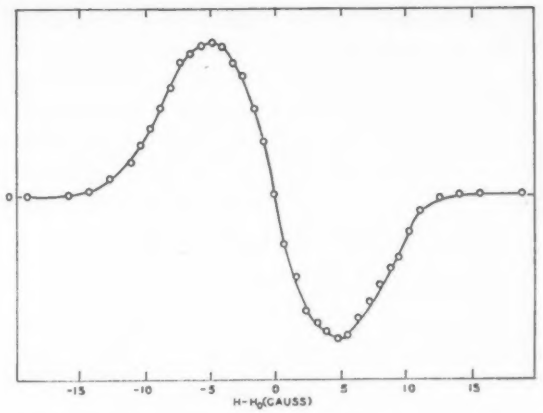

FIG. 1. Derivative of the proton magnetic resonance absorption line in natural rubber, 30-minute cure, at 86°K. The absorption intensity is given in arbitrary units.

TABLE I. Proton magnetic resonance absorption line widths in natural rubber at different temperatures.

30 min cure[a]		60 min cure[a]		90 min cure[a]	
T(°K)	δH (gauss)	T(°K)	δH (gauss)	T(°K)	δH (gauss)
86	9.45	89	9.45	89	9.45
104	9.45	109	9.45	104	9.45
116	9.45	128	9.45	124	9.45
131	9.45	160	9.45	135	9.45
141	9.45	192	8.65	141	9.45
161	8.80	205	8.50	152	9.45
175	8.20	214	8.35	162	9.45
188	7.55	229	7.85	168	9.45
202	7.10	237	5.20	175	9.45
220	6.30	250	1.60	185	9.15
222	6.00	255	0.90	201	8.85
235	4.25	259	0.45	211	8.65
241	2.70	267	0.25	221	8.50
249	1.10	297	0.15	227	8.05
255	0.50			235	5.05
264	0.25			238	4.25
276	0.15			243	3.15
295	0.13			253	1.10
				263	0.40
				273	0.20
				295	0.15

[a] The samples were cured at 280°F.

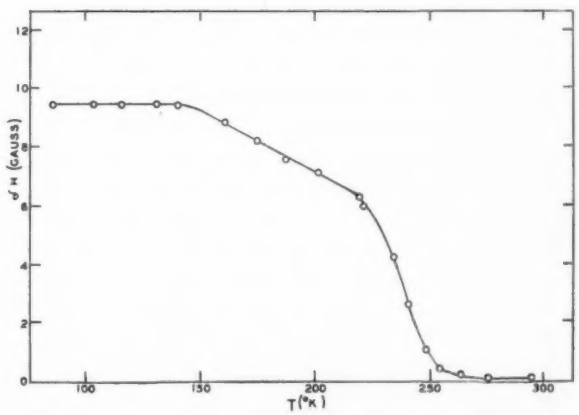

FIG. 2. Temperature dependence of the proton resonance line width in natural rubber; 30-minute cure.

[8] H. S. Gutowsky and G. E. Pake, J. Chem. Phys. **18**, 162 (1950); the analysis is an extension of earlier work cited there.

[9] J. G. Powles and H. S. Gutowsky, J. Chem. Phys. **21**, 1704, (1953).

[10] J. H. Van Vleck, Phys. Rev. **74**, 1168 (1948).

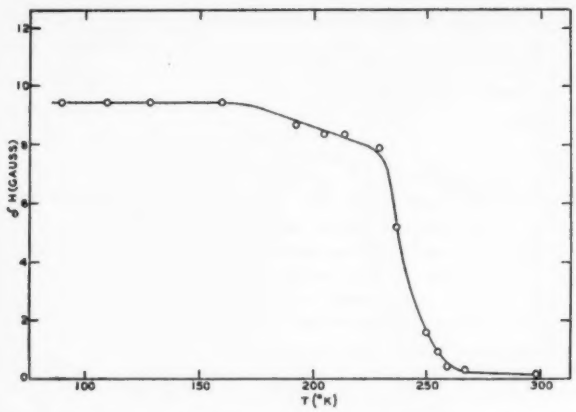

FIG. 3. Temperature dependence of the proton resonance line width in natural rubber; 60-minute cure.

18.9, and 18.4 gauss^2 for the 30-, 60-, and 90-minute cure, respectively, at liquid nitrogen temperature. These values are the same within experimental error. A good estimate of the second moment expected in the rubber for a rigid lattice can be obtained by adding up the contributions of each of the various structural groups to the total absorption. The CH_3 group contains 3/8 of the protons; its rigid lattice second moment is[9] 21.8 gauss^2 plus about 2 gauss^2 of broadening external to the CH_3 group itself. The CH_2 groups contain 1/2 of the protons, and here we use the value of 18.2 gauss^2 observed[11] in CH_2Cl-CH_2Cl. The CH contributes 1/8 of the absorption, and with no near magnetic neighbors its second moment should be the order of inter-CH_3 group broadening,[9] say 3 gauss^2. We have then a predicted rigid lattice second moment for natural rubber of

$$\Delta H_2^2 = (3/8)24 + (1/2)18.2 + (1/8)3 = 18.5 \text{ gauss}^2.$$

The approximations in the analysis are not serious so, the identity of the predicted and experimental second moments confirms a rigid lattice in the rubbers at temperatures below 140°K. The observed line shape also agrees with that predicted by adding the absorption of the various groups, each assumed to be rigid.

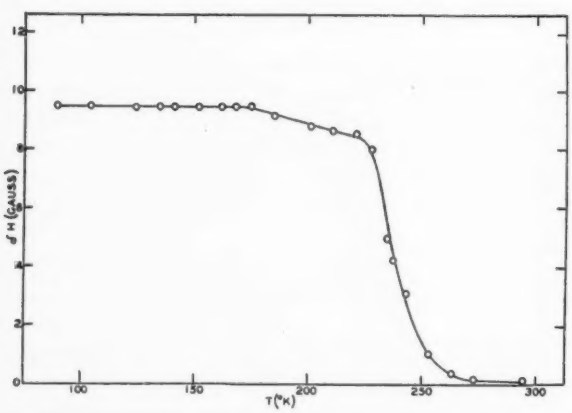

FIG. 4. Temperature dependence of the proton resonance line width in natural rubber; 90-minute cure.

[11] Gutowsky, Kistiakowsky, Pake, and Purcell, J. Chem. Phys. 17, 972 (1949).

If the only motion fast enough in the rubber to average out the dipolar broadening were rotation of the CH_3 groups about their C_3 axes, the contribution of the methyl groups to the second moment would be reduced[8,9] by a factor of 1/4. In this case we find

$$\Delta H_2^2 = (3/8)(1/4)24 + (1/2)18.2 + (1/8)3 = 11.8 \text{ gauss}^2.$$

The second moment observed at temperatures about 225°K, at the beginning of the more rapid change in line width at higher temperature, was 12.9, 14.4, and 13.0 gauss^2 for the 30-, 60-, and 90-minute cure, respectively. Motion of the chain segments could start before the CH_3 rotational motion was completely effective,[9] so although the agreement is not remarkable, it is nonetheless good evidence that CH_3 group rotation is associated with the change in line width at the lower temperatures. Moreover, motion of the chain segments would also carry the CH_3 groups along and give a much larger change in second moment than that observed in the lower temperature region, but compatible with that at higher temperatures.

Many of the physical properties of rubber when plotted against temperature have a change in slope at a temperature characteristic of the sample, and it has been proposed that these second-order transitions are associated with the freezing-out of segmental motion.[12] The change in the rate of increase of line width with decreasing temperature occurs at temperatures in the range of the second-order transitions. So our conclusion that this change is associated with the segmental motion provides a direct confirmation of the nature of the second order transition. The second order transition temperature in unvulcanized natural rubber has been reported to be −73°C.[12] Bekkedahl, reported in reference 12, and Ueberreiter[13] have shown however that the second-order transition temperature increases with the amount of combined sulfur and hence with the degree of vulcanization. We find a transition temperature of −53°C in the 30-minute cure rubber and of about −45°C in the 60- and 90-minute cures. Bekkedahl's results are in terms of combined sulfur and, when compared with our transition temperatures, suggest 4–5 percent and 6–7 percent combined sulfur for the two transition temperatures, respectively. Unfortunately, the combined sulfur content of the rubbers we investigated is not known for direct comparison, but the values do not seem unreasonable.

The Influence of Cure Time

The dependence of the line width changes upon cure time has some interesting aspects. It was remarked

[12] R. F. Boyer and R. S. Spencer, Advances in Colloid Sci. 2, 1 (1946).

[13] K. Ueberreiter, Z. physik. Chem. **B45**, 361 (1940).

above that narrowing from the rigid lattice line widths upon warming starts at temperatures of 143°K, 163°K, and 173°K for the 30-, 60-, and 90-minute cured samples, respectively. These changes mark the onset of effective CH_3 group rotation. On the other hand, the transitions marking the onset of segmental motion occur at 220°K, 228°K, and 228°K. So it seems that curing has a relatively greater effect upon CH_3 group motions than upon segmental motions.

The mechanism by which vulcanization affects the internal structure of rubber has been a somewhat controversial question for a number of years.[14] The original hypothesis involved a simple cross linking of the rubber molecules with sulfur bridges, a thioether type linkage as shown below.

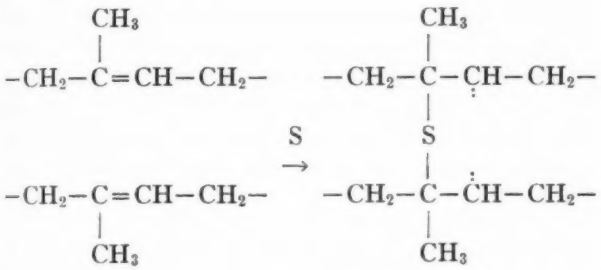

However, Farmer and Shipley[15] have found experimental evidence suggesting that the physical properties imparted to natural rubber by vulcanization are due only in small part to cross linking of the type illustrated above. Instead they state that the effects of vulcanization are due largely to the formation of sulfur containing rings within single rubber molecules. Such rings would probably be of the structure shown below.

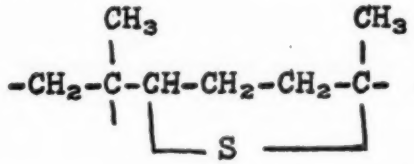

The improvement in the physical properties is then ascribable to steric hindrance of the ring to the free slippage of chains. Still another theory, advanced by Stiehler and Wakelin,[16] proposes that the sulfur reacts with the rubber molecule at the α-methylene group or the double bond and then becomes a center of polarity. According to this method, electric dipolar interaction accounts for the change in physical properties.

The fact that the CH_3 group rotation is affected more by the curing than is the segmented motion, suggests that cross linking is not the primary mechanism of vulcanization. An appreciable amount of cross linking, particularly of the simple dimolecular type, would almost certainly produce a greater effect on the segmental motion than on the CH_3 group rotation.

A semiquantitative analysis of the effect of cure time upon the two types of motions can be based upon the approximate relations[8] between line width, correlation frequency, and temperature.

$$(\delta\nu)^2 = A^2(2/\pi)\tan^{-1}(\alpha\delta\nu/\nu_c), \quad (1)$$

$$\nu_c = \nu_0 e^{-V/RT}. \quad (2)$$

$\delta\nu$ is the observed frequency width of the resonance line, A is the rigid lattice line width, ν_c is a correlation frequency giving the average rate of change in structural configuration, and α is a line shape parameter which we assume to be 1. Equation (2) expresses the assumption that the motions are thermally activated; ν_0 is a frequency factor and V is an activation energy or potential barrier for the motions reducing the line width.

Equation (1) can be modified to cover two regions of change in the line width, when each is associated with a particular restricted type of motion of the observed nuclei. In this case

$$(\delta\nu)^2 = B^2 + C^2(2/\pi)\tan^{-1}(\alpha\delta\nu/\nu_{c1}), \quad (3a)$$

$$(\delta\nu)^2 = B^2(2/\pi)\tan^{-1}(\alpha\delta\nu/\nu_{c2}). \quad (3b)$$

Here $(B^2+C^2)^{\frac{1}{2}}$ is the rigid lattice line width, and B is the intermediate line width. Equation (3a) covers the change in line width at lower temperatures and Eq. (3b) that at higher; ν_{c1} and ν_{c2} are the correlation frequencies of the two different motions; they are assumed to have the temperature dependence of Eq. (2). The logarithms of the correlation frequencies determined by Eqs. (3a) and (3b) from the temperature dependence of the line width in the 30-minute rubber are plotted against the corresponding values of $1/T$ in Fig. 5. The data for the center of each temperature range fall upon a good straight line. If we apply Eq. (1) to the straight line sections we obtain values of the potential barriers and frequency factors for the two motions. These values are tabulated in Table II for the three cure times.

TABLE II. The influence of cure time upon the frequency factors and potential barriers estimated for the two types of molecular motion observed in natural rubber.

Cure time	Low temp. motion ν_{01}	V_1	High temp. motion ν_{02}	V_2
30 min	7.3×10^7 sec^{-1}	2.7 kcal	1.5×10^{16} sec^{-1}	12.8
60	1.3×10^9	4.1	2.4×10^{16}	13.0
90	3.2×10^9	4.5	6.0×10^{16}	13.3

The values for the low-temperature barriers are in accord with what might be expected for methyl group rotation. The relatively large values for the high-temperature barriers are reasonable for a rotary motion of the chain segments about the chain axes. The effect of cure time on the values for segmental motion is small.

[14] See for example L. F. Fieser and M. Fieser, *Organic Chemistry* (D. C. Heath and Company, Boston, 1944), pp. 329–334.
[15] E. H. Farmer and F. W. Shipley, Rubber Chem. and Technol. **20**, 341 (1947).
[16] R. D. Stiehler and J. H. Wakelin, Rubber Chem. and Technol. **21**, 325 (1948).

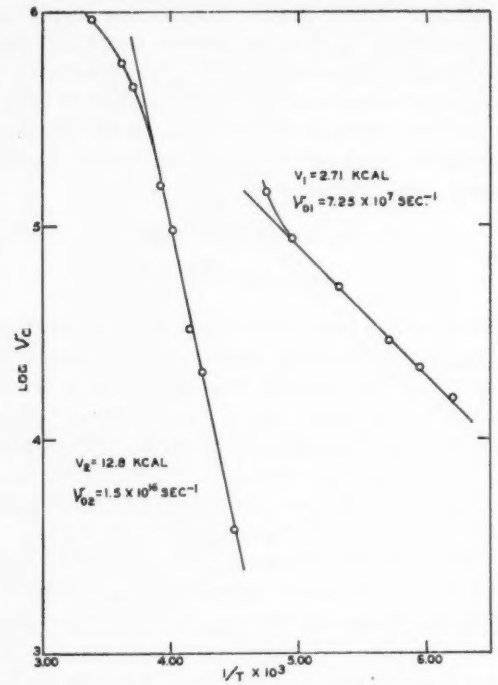

FIG. 5. Log ν_c, determined from the line width, plotted against $1/T$ for the 30-minute cure rubber.

On the other hand, there is an appreciable effect on the values for the methyl group rotation. These results provide additional support of the view that cross linkage is not the primary process in vulcanization.

There are too many approximations[17] in applying this type of model and analysis to polymers to put much physical reliance on the particular values given in Table II. Yet the fit of the experimental data by this simple approach is good, as may be seen in Fig. 5. Still it is to be noted that Eq. (3) really applies to one type of structure experiencing two types of motion, while in rubber there are two types of structures, CH_3 groups and chain segments, whose motions are partially coupled.

[17] A detailed discussion of the factors governing line width changes will be submitted to this journal shortly.

Preliminary Results on Stretched Samples

It has long been known that stretching produces crystallization in polymers.[18] The results given above suggest that nuclear magnetic resonance should provide a means of examining the effects of stretching on the actual rotational processes in rubber. For this reason the same general experiments were performed on the 30- and 60-minute cure rubbers at extensions of about 70 percent. No effects on either the line shapes or the line width-temperature dependence were detected, even though the resonance lines were examined at several orientations of the direction of stretch with respect to the applied field. The negative results agree with the observations of Witte and Anthony[19] who found no observable effect of stretching on the second-order transition temperature of a cured natural rubber up to 150 percent elongation. Recently, effects of stretching on the temperature dependence of the proton spin-spin relaxation times in a natural rubber have been reported[20] above about 70 percent elongation. The effects of stretching on the second-order transition are more readily detected[19] in other polymers than natural rubber. So rather than modify our apparatus for greater elongation of the rubber, we investigated cold drawn polyethylene. In it the proton magnetic resonance exhibits pronounced and complex anisotropy, which we hope to present later.

[18] L. A. Wood, Advances in Colloid Sci. **2**, 57 (1946).
[19] R. S. Witte and R. L. Anthony, J. Appl. Phys. **22**, 689 (1951).
[20] A. Cohen-Hadria and R. Gabillard, Compt. Rend. **234**, 1877 (1952).

Temperature Jump and Velocity of Slip at the Boundary of a Gas*

HERBERT PAYNE
Flight Research Laboratory, Wright-Patterson Air Force Base, Ohio
(Received March 20, 1953)

Approximate expressions are derived from the kinetic theory for the temperature jump and the velocity of slip occurring at an infinite plane solid surface of constant temperature bounding a gas whose state remains invariant throughout all planes parallel to the surface. These derivations differ from earlier ones in the elimination of an assumption, for which an argument is presented as to its untenability, regarding the distribution of the velocities of the molecules striking the surface. Instead, from the mathematical theory of non-uniform gases are derived conditions on this distribution sufficient to confine possible values of the temperature jump and slip velocity to within fairly close limits.

I. INTRODUCTION

CONSIDERING an infinite plane solid surface of constant temperature T_W bounding a gas whose state remains invariant throughout all planes parallel to the surface, one may depict the temperature jump, occurring at the boundary when the gas is conducting heat perpendicularly thereto, as the quantity $T_K - T_W$ in Fig. 1(a). Here, T_K represents the temperature the gas would assume at the wall if the linearity of the temperature profile prevailing at some distance [$z=\zeta$ in Fig. 1(a)] from the wall were maintained in its vicinity.

Analogously, the velocity of slip, occurring when the gas is flowing parallel to the surface, may be depicted by v_K (the wall velocity being zero) in Fig. 1(b).

Approximate theoretical expressions have been developed from the kinetic theory of gases by Maxwell[1] for the slip and by Smoluchowski[2] by two separate methods for the temperature jump. In his first paper Smoluchowski employs the basic simplifying assumptions of Clausius, which, he points out, are open to question in several respects. His second, and probably more realistic, approach follows that of Maxwell, who made two assumptions regarding the properties of the gas at the wall.

The first assumption, as to the molecular reflection characteristic of the wall, requires that of the molecules striking the wall a fraction β, randomly selected, be momentarily adsorbed later to return to the gas conforming to a Maxwellian velocity distribution appropriate for a gas at rest with the temperature of the wall. The portion $1-\beta$ is specularly reflected. This model, while considered crude in the light of more recent experimental and theoretical investigations, has yet to be replaced as perhaps the best one for the analysis of a gas near its boundary and will be used for the calculations of this paper. For the temperature jump problem β becomes the thermal accommodation coefficient.

The second assumption relates to the distribution of the velocities of the molecules striking the wall. It was assumed that this distribution is the same, except corresponding to the temperature T_K or the mass velocity v_K as the case may be, as that governing the velocities of those molecules striking the plane $z=\zeta$ of Fig. 1 in the direction of the wall. Maxwell described this supposition as "liable to important corrections" since there exists an "essential discontinuity in the conditions of the gas at the surface."

It is the purpose of this paper to develop approximate expressions for the slip and the temperature jump without this second assumption. Instead, from Boltzmann's equation and the boundary conditions implicit

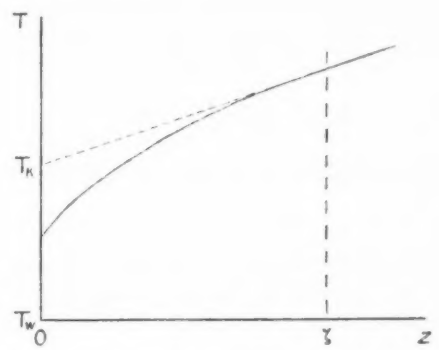

FIG. 1(a). The variation of the gas temperature T with distance z from the wall.

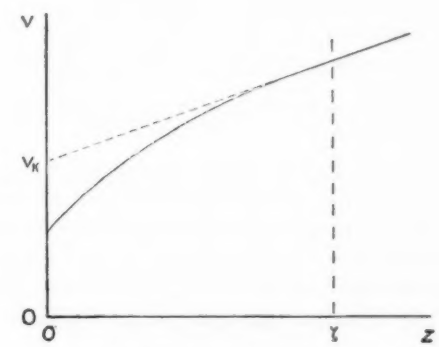

FIG. 1(b). The variation of the mass velocity v of the gas with distance z from the wall.

* Portions of this manuscript comprise a dissertation presented in partial fulfillment of the requirements for the degree Doctor of Philosophy in the Graduate School of The Ohio State University.

[1] J. C. Maxwell, *Scientific Papers* (Librairie Scientifique, J. Hermann, Paris, 1890), Vol. 2, pp. 681–712.

[2] M. v. Smoluchowski, Sitzber. Akad. Wiss. Wien (Ab. 2a) **107**, 304 (1898); **108**, 5 (1899).

in the first assumption and the given macroscopic properties of the gas are derived conditions on the molecular velocity distribution in the immediate vicinity of the wall sufficient to confine possible values of these two quantities to within fairly close limits—for the case of a gas of Maxwellian molecules the limit of error amounting to 14 percent of the mean value for the temperature jump and 12 percent of the mean value for the slip. The limits for these quantities having the lower absolute values agree exactly with the results of the methods of Maxwell and of Smoluchowski in his second paper. However, it is shown that Maxwell's second assumption fails to satisfy the derived conditions.

Consideration will be limited to gases of monatomic molecules, in accordance with the present state of development of the kinetic theory.

In connection with these quantities it should be noted that Herzfeld[3] has investigated the possibility of their derivation by applying a modification of Chapman and Enskog's solution of Boltzmann's equation to that portion of the gas adjacent to the wall. Also, Hilbert[4] has solved the problem for a known molecular velocity distribution at the wall.

II. THE MOLECULAR VELOCITY DISTRIBUTION FUNCTION

Let the molecular velocity distribution function, which specifies the density of gas molecules in the six dimensional space of velocity and position, be represented by

$$f(\mathbf{C}, z)=f^0[1+\psi(\mathbf{C}, z)],$$

where

$$\mathbf{C}=\mathbf{c}-\mathbf{c}_0=(U, V, W)$$

with $\mathbf{c}$ representing the molecular velocity and

$$\mathbf{c}_0=(0, v_0, 0),$$

a reference velocity parallel to the mass velocity of the gas. The component W is chosen perpendicular to the wall, a positive value indicating motion away. Also,

$$f^0=n_0(m/2\pi kT_0)^{\frac{3}{2}}\exp(-\mathfrak{C}^2),$$

the Maxwellian distribution for a density n_0, temperature T_0, and mass velocity $\mathbf{c}_0$—parameters to be specified for the moment merely as invariant with z. Here, m indicates the molecular mass; k Boltzmann's constant; and

$$\mathfrak{C}^2=(m/2kT_0)C^2, \quad \mathfrak{U}=(m/2kT_0)^{\frac{1}{2}}U, \quad \text{etc.}$$

If it is required of ψ that it be essentially small in comparison with unity—which will be realized when the temperature jump is small in comparison with the absolute temperature of the wall and v_K is small in comparison with the velocity of sound in the gas—the values of the density, temperature, and mass velocity of the gas, with $|\int f^0\psi d\mathbf{C}|\ll\int f^0 d\mathbf{C}$, may be written

$$n(z)=n_0\left[1+(1/n_0)\int f^0\psi(\mathbf{C}, z)d\mathbf{C}\right], \tag{1a}$$

$$T(z)=T_0\left[1-(1/n_0)\int(1-2\mathfrak{C}^2/3)f^0\psi(\mathbf{C}, z)d\mathbf{C}\right], \tag{1b}$$

$$v(z)=v_0+(1/n_0)\int Vf^0\psi(\mathbf{C}, z)d\mathbf{C}, \tag{1c}$$

where

$$\int F(\mathbf{C})d\mathbf{C}=\int_{-\infty}^{+\infty}dU\int_{-\infty}^{+\infty}dV\int_{-\infty}^{+\infty}F(U, V, W)dW.$$

Three conditions imposed on ψ are

$$\int Wf^0\psi(\mathbf{C}, z)d\mathbf{C}=0, \tag{2a}$$

i.e., the mass velocity of the gas perpendicular to the wall is zero;

$$(m/2)\int WC^2f^0\psi(\mathbf{C}, z)d\mathbf{C}=q, \tag{2b}$$

the rate of heat transfer per unit area from wall to gas; and

$$m\int VWf^0\psi(\mathbf{C}, z)d\mathbf{C}=p_{23}, \tag{2c}$$

the invariant stress component arising from the mass velocity gradient of the gas.

III. BOLTZMANN'S EQUATION

Boltzmann's equation as it pertains to this problem may be written[5]

$$W\partial f/\partial z=Wf^0\partial\psi/\partial z=S(\psi), \tag{3}$$

where S represents an integral expression, which with the assumed smallness of ψ becomes linear in ψ.

IV. THE QUANTITY $\psi(\mathbf{C}, \zeta)$

Now $f(\mathbf{C}, \zeta)$ may be readily determined by the method of Chapman and Enskog.[5] A solution to Eq. (3) complying with the requirements of invariant gradients of density, temperature, and mass velocity of the gas is of the form:

$$\psi(\mathbf{C}, \zeta)=a_1(\zeta)+a_2(\zeta)\mathfrak{C}^2+2a_3(\zeta)\mathfrak{V}+\Phi(\mathbf{C}) \tag{4}$$

with

$$a_i(\zeta)=\alpha_i+\mu_i\zeta \quad i=1, 2, 3.$$

The function $\Phi(\mathbf{C})$ may be expressed as

$$\Phi(\mathbf{C})=\tau_2\mathfrak{W}A_2(\mathfrak{C}^2)+\tau_3\mathfrak{U}\mathfrak{W}A_3(\mathfrak{C}^2), \tag{5}$$

[3] K. F. Herzfeld, Ann. Physik **23**, 476 (1935).

[4] D. Hilbert, *Theorie der linearen Integralgleichungen* (Teubner, Leipzig, 1912), p. 277.

[5] S. Chapman and T. G. Cowling, *Mathematical Theory of Non-Uniform Gases* (Cambridge University Press, Cambridge, 1952), Chap. 7.

where

$$\tau_2=(\pi m/2k^3n_0^2T_0^3)^{\frac{1}{2}}q$$
$$\tau_3=(\pi^{\frac{1}{2}}/kn_0T_0)p_{23},$$

and, as required by Eqs. (2) and (4),

$$\int Wf^0\Phi d\mathbf{C}=0$$

$$(m/2)\int WC^2f^0\Phi d\mathbf{C}=q \qquad (6a, b, c)$$

$$m\int VWf^0\Phi d\mathbf{C}=p_{23}.$$

From Eqs. (1), (4), and (5)

$$n(\zeta)=n_0[1+a_1(\zeta)+(3/2)a_2(\zeta)]$$
$$T(\zeta)=T_0[1+a_2(\zeta)]$$
$$v(\zeta)=v_0+(2kT_0/m)^{\frac{1}{2}}a_3(\zeta).$$

Consequently,

$$T_K=T_0[1+a_2(0)]=T_0(1+\alpha_2) \qquad (7a)$$
$$v_K=v_0+(2kT_0/m)^{\frac{1}{2}}a_3(0)=v_0+(2kT_0/m)^{\frac{1}{2}}\alpha_3. \qquad (7b)$$

Also, it can be shown that

$$S[\psi(\mathbf{C},\zeta)]=S(\Phi),$$

so that applying Eq. (4) to Eq. (3) gives the integral equation satisfied by Φ,

$$Wf^0(\mu_1+\mu_2\mathcal{C}^2+2\mu_3\mathcal{U})=S(\Phi). \qquad (8)$$

V. SEPARATION OF COMPONENTS OF $\psi(\mathbf{C}, z)$

In considering ψ for the whole range of z set

$$\psi(\mathbf{C},z)=\theta(\mathbf{C},z)+\mu_1z+\mu_2z\mathcal{C}^2+2\mu_3z\mathcal{U}+\Phi(\mathbf{C}). \qquad (9)$$

Then, in view of Eq. (3)'s linearity in ψ and its satisfaction by the last four terms on the right in Eq. (9),

$$Wf^0\partial\theta/\partial z=S(\theta). \qquad (10)$$

From Eqs. (2), (6), and (9) one deduces that

$$\int\chi_i(\mathbf{C})f^0\theta(\mathbf{C},z)d\mathbf{C}=0 \quad i=1, 2, 3, \qquad (11)$$

where

$$\chi_1=\mathcal{W} \quad \chi_2=\mathcal{W}\mathcal{C}^2 \quad \chi_3=\mathcal{U}\mathcal{W}.$$

From Eqs. (4) and (9)

$$\theta(\mathbf{C},\zeta)=\alpha_1+\alpha_2\mathcal{C}^2+2\alpha_3\mathcal{U} \qquad (12a)$$
$$\theta(\mathbf{C},0)=\psi(\mathbf{C},0)-\Phi(\mathbf{C}). \qquad (12b)$$

It is evident that

$$\int\mathcal{W}f^0\theta(\mathbf{C},\zeta)^2d\mathbf{C}=0, \qquad (13a)$$

and, by virtue of Eqs. (6),

$$\int\mathcal{W}\Phi(\mathbf{C})f^0\theta(\mathbf{C},\zeta)d\mathbf{C}=(\tau_2\alpha_2+\tau_3\alpha_3)n_0/\pi^{\frac{1}{2}}. \qquad (13b)$$

VI. THE QUANTITY $\theta(\mathbf{C}, 0)$

Let

$$\left.\begin{aligned}\psi_+(\mathbf{C})&=\psi(\mathbf{C},0)\\ \theta_+(\mathbf{C})&=\theta(\mathbf{C},0)\end{aligned}\right\}\text{ for } W>0$$

$$\left.\begin{aligned}\psi_-(\mathbf{C})&=\psi(\mathbf{C},0)\\ \theta_-(\mathbf{C})&=\theta(\mathbf{C},0)\end{aligned}\right\}\text{ for } W<0.$$

Then Maxwell's theory concerning the reflection of the gas molecules from the wall requires

$$\begin{aligned}&f^0[1+\psi_+(U,V,W)]\\ &=\beta n_W(m/2\pi kT_W)^{\frac{1}{2}}\exp\{-m[U^2+(V+v_0)^2\\ &\quad+W^2]/2kT_W\}+(1-\beta)f^0[1+\psi_-(U,V,-W)]\\ &=f^0[1+\beta(b_1+b_2\mathcal{C}^2+b_3\mathcal{U})\\ &\qquad+(1-\beta)\psi_-(U,V,-W)], \qquad (14)\end{aligned}$$

where

$$b_1=(n_W-n_0)/n_0-3(T_W-T_0)/2T_0$$
$$b_2=(T_W-T_0)/T_0$$
$$b_3=-2(m/2kT_0)^{\frac{1}{2}}v_0,$$

with disregard of terms containing cross-products and higher powers of $(n_W-n_0)/n_0$, $(T_W-T_0)/T_0$, and $(m/2kT_0)^{\frac{1}{2}}v_0$.

From Eqs. (5), (12b), and (14)

$$\begin{aligned}\theta_+(U,V,W)&=\beta(b_1+b_2\mathcal{C}^2+b_3\mathcal{U})\\ &\quad+(1-\beta)\theta_-(U,V,-W)-(2-\beta)\Phi(U,V,W). \qquad (15)\end{aligned}$$

The quantities n_0, T_0, and v_0 are now to be so chosen as to impart such values to b_1, b_2, and b_3 for given values of n_W (which is dependent on the gas pressure) and T_W that

$$\int_{W>0}\chi_i[\beta(b_1+b_2\mathcal{C}^2+b_3\mathcal{U})-(2-\beta)\Phi]f^0d\mathbf{C}=0 \quad i=1, 2, 3, \qquad (16)$$

where

$$\int_{W>0}F(\mathbf{C})d\mathbf{C}=\int_{-\infty}^{+\infty}dU\int_{-\infty}^{+\infty}dV\int_0^{+\infty}F(U,V,W)dW$$

$$\int_{W<0}F(\mathbf{C})d\mathbf{C}=\int_{-\infty}^{+\infty}dU\int_{-\infty}^{+\infty}dV\int_{-\infty}^{0}F(U,V,W)dW.$$

These values, determined with the aid of Eqs. (6), are

$$\begin{aligned}b_1&=-(2-\beta)\tau_2/\beta\\ b_2&=(2-\beta)\tau_2/2\beta \qquad (17a, b, c)\\ b_3&=(2-\beta)\tau_3/\beta.\end{aligned}$$

Therefore,

$$\theta_+(U,V,W)=-(2-\beta)[\tau_2(1-\mathcal{C}^2/2)-\tau_3\mathcal{U}+\Phi(U,V,W)]+(1-\beta)\theta_-(U,V,-W) \quad (18)$$

$$T_W=T_0[1+(2-\beta)\tau_2/2\beta] \quad (19a)$$

$$v_0=-(2kT_0/m)^{\frac{1}{2}}(2-\beta)\tau_3/2\beta. \quad (19b)$$

VII. DERIVATION OF CONDITIONS ON θ_-

From Eqs. (11), (15), and (16)

$$K_i=\int_{W<0}\chi_i f^0\theta_- d\mathbf{C}=0 \quad i=1,2,3. \quad (20)$$

It may be readily shown that[6]

$$\int gS(h)d\mathbf{C}=\int hS(g)d\mathbf{C},\ \int gS(g)d\mathbf{C}\leq 0 \quad (21a,b)$$

for arbitrary $g(\mathbf{C})$ and $h(\mathbf{C})$.

With Eq. (10) and expression (21b) one may write

$$(1/2)(\partial/\partial z)\int Wf^0\theta^2 d\mathbf{C}=\int\theta Wf^0(\partial\theta/\partial z)d\mathbf{C}=\int\theta S(\theta)d\mathbf{C}\leq 0.$$

Then, as a consequence of Eq. (13a)

$$-\int_{W<0}\mathcal{W}f^0\theta_-^2 d\mathbf{C}=s\int_{W>0}\mathcal{W}f^0\theta_+^2 d\mathbf{C} \quad 0\leq s\leq 1. \quad (22)$$

Let

$$J=\int_{W>0}\mathcal{W}[\tau_2(1-\mathcal{C}^2/2)-\tau_3\mathcal{U}+\Phi]^2 f^0 d\mathbf{C}=-\int_{W<0}\mathcal{W}[\tau_2(1-\mathcal{C}^2/2)-\tau_3\mathcal{U}-\Phi]^2 f^0 d\mathbf{C}=\tau_2^2 j_2+\tau_3^2 j_3, \quad (23)$$

from Eq. (5) with

$$j_2=\int_{W>0}\mathcal{W}[1-\mathcal{C}^2/2+\mathcal{W}A_2(\mathcal{C}^2)]^2 f^0 d\mathbf{C}, \quad (24a)$$

$$j_3=\int_{W>0}\mathcal{W}[\mathcal{U}-\mathcal{U}\mathcal{W}A_3(\mathcal{C}^2)]^2 f^0 d\mathbf{C}. \quad (24b)$$

From Eqs. (18), (22), (20), and (23)

$$K_4=-r\int_{W<0}\mathcal{W}f^0\theta_-^2 d\mathbf{C}+2(1-\beta)\int_{W<0}\mathcal{W}\Phi f^0\theta_- d\mathbf{C}=(2-\beta)J, \quad (25)$$

where

$$r=[1-s(1-\beta)^2]/s(2-\beta),$$

and, as required by the limitations on s,

$$r\geq\beta.$$

Now, from Eqs. (10), (21a), (8), and (11)

$$(\partial/\partial z)\int W\Phi f^0\theta d\mathbf{C}=\int\Phi S(\theta)d\mathbf{C}=\int\theta S(\Phi)d\mathbf{C}=\int W(\mu_1+\mu_2\mathcal{C}^2+2\mu_3\mathcal{U})f^0\theta d\mathbf{C}=0.$$

Then, with Eqs. (13b), (18), (23), (16), and (17) one obtains

$$I=\int_{W<0}\mathcal{W}\Phi f^0\theta_- d\mathbf{C}=[n_0/\pi^{\frac{1}{2}}(2-\beta)](\tau_2\alpha_2+\tau_3\alpha_3)+J. \quad (26)$$

Thus, the unknown function θ_- must satisfy conditions (20) and (25) and is related to the as yet undetermined constants α_2 and α_3 through Eq. (26).

VIII. CALCULATION OF LIMITS ON THE TEMPERATURE JUMP AND THE SLIP

Of all possible expressions for θ_- satisfying Eqs. (20) and (25) for a particular value of r let that one which renders a maximum (or minimum) value to I be designated θ_-^m. To determine θ_-^m write

$$I=\int_{W<0}M(\mathbf{C},\theta_-)d\mathbf{C} \quad K_i=\int_{W<0}N_i(\mathbf{C},\theta_-)d\mathbf{C} \quad i=1,2,3,4.$$

Then, from the calculus of variations a necessary condition for a maximum or minimum value of I subject to particular values of K_i is

$$(\partial M/\partial\theta_-)+\sum_{i=1}^{4}\lambda_i(\partial N_i/\partial\theta_-)=0,$$

where λ_i is the Lagrange multiplier. With λ_1, λ_2, and λ_3 determined so that conditions (20) are satisfied one obtains

$$\theta_-^m=\lambda_4'[\tau_2(1-\mathcal{C}^2/2)-\tau_3\mathcal{U}-\Phi],$$

with condition (25) requiring

$$\lambda_4'=-(1/r)\{(1-\beta)\pm[1+(r-\beta)(2-\beta)]^{\frac{1}{2}}\}. \quad (27)$$

Accordingly,

$$I^m=\int_{W<0}M(\mathbf{C},\theta_-^m)d\mathbf{C}=\lambda_4' J.$$

[6] Reference 5, p. 67.

To establish that this represents the maximum and minimum values of I, consider

$$\theta_- = \theta_-^m + \epsilon(\mathbf{C}).$$

From Eqs. (20), (25), (26), and (27) one obtains

$$rI = -(1-\beta)J \pm \left\{ [1+(r-\beta)(2-\beta)]^{\frac{1}{2}} J + (r^2/2)[1+(r-\beta)(2-\beta)]^{-\frac{1}{2}} \int_{W<0} \mathfrak{W} f^0 \epsilon^2 d\mathbf{C} \right\}.$$

Since

$$\int_{W<0} \mathfrak{W} f^0 \epsilon^2 d\mathbf{C} \leq 0$$

and $J \geq 0$ and as a result of the limitation on r,

$$-(2-\beta)J/\beta \leq I \leq J.$$

Therefore, invoking Eqs. (26), (7), (19), and (23) and setting $\tau_3 = 0$ and $\tau_2 = 0$ in turn give as limiting values

$$T_K - T_W = -[(2-\beta)/2\beta]\tau_2 T_0 (1+\delta_2 \pm \delta_2) \quad (28a)$$

$$v_K = -[(2-\beta)/2\beta]\tau_3 (2kT_0/m)^{\frac{1}{2}} (1+\delta_3 \pm \delta_3), \quad (28b)$$

where

$$\delta_i = (2\pi^{\frac{1}{2}}/n_0) j_i \quad i = 2, 3. \quad (29)$$

On the basis of the original supposition that

$$|T_K - T_W| \ll T_W$$

one may infer from Eqs. (19a) and (28a) that

$$T_W \approx T_0$$

and, accordingly, may substitute T_W for T_0 in Eq. (28a).

IX. THE CASE OF MAXWELLIAN MOLECULES

As an example consider a gas composed of Maxwellian molecules (for which the intermolecular force varies inversely with the fifth power of the intermolecular distance). In this case[7]

$$A_2(\mathfrak{C}^2) = -(2/\pi^{\frac{1}{2}})(1-2\mathfrak{C}^2/5) \quad A_3(\mathfrak{C}^2) = 2/\pi^{\frac{1}{2}}.$$

[7] Reference 5, pp. 173–177.

Then, from Eqs. (24) and (29)

$$\delta_2 = 0.162 \quad \delta_3 = 0.137.$$

It follows that the limits of error resulting from the use of mean values from Eqs. (28) amount to 14 percent and 12 percent of the mean values for the temperature jump and the slip, respectively.

X. MAXWELL'S SECOND ASSUMPTION

Maxwell's assumption regarding the distribution of the velocities of the molecules striking the wall is equivalent to setting

$$\theta_-(\mathbf{C}) = \theta(\mathbf{C}, \zeta) = \alpha_1 + \alpha_2 \mathfrak{C}^2 + 2\alpha_3 \mathfrak{V}.$$

Conditions (20) then demand that

$$\alpha_i = 0 \quad i = 1, 2, 3, \quad \text{or} \quad \theta_- = 0.$$

Then, from Eqs. (7) and (19)

$$T_K - T_W = -[(2-\beta)/2\beta]\tau_2 T_0$$
$$v_K = -[(2-\beta)/2\beta]\tau_3 (2kT_0/m)^{\frac{1}{2}}.$$

Thus, the absolute values of the temperature jump and the slip determined by the methods of Smoluchowski and Maxwell equal the lower limits of the ranges of possible absolute values of these quantities as determined from Eqs. (28).

It follows from Eq. (25) that this assumption requires

$$J = 0.$$

However, a perusal of the form of the integrands of Eqs. (24) reveals that j_2, $j_3 > 0$. Therefore, Eq. (23) requires

$$J \neq 0 \quad \text{for} \quad \tau_2 \neq 0 \quad \text{or} \quad \tau_3 \neq 0.$$

Thus, Maxwell's second assumption fails to simultaneously satisfy conditions (20) and (25).

XI. ACKNOWLEDGMENT

The author is indebted to Professor John G. Daunt for critically reading that portion of this manuscript concerned with the temperature jump.

Note on the Interaction of Methane and Water Vapor in the Hydrogen-Oxygen Reaction

ARTHUR LEVY
Battelle Memorial Institute, Columbus, Ohio
(Received July 28, 1953)

The influence of methane on the hydrogen-oxygen reaction was studied in the region of the second-explosion limit. The experimental data show that there exists a critical concentration of methane, below which both methane and water vapor produce an identical reduction of the explosion limit. Observations on the course of the slow reaction also show that the accelerating effects of these additives on the rate of combination of hydrogen and oxygen are directly related to one another. It is postulated, on the basis of both the explosion and slow reaction rate data, that methane and water vapor influence the kinetics of the hydrogen-oxygen reaction by similar processes.

THE inhibiting effect of hydrocarbons on the combustion of hydrogen has been well established.[1,2] Furthermore, if one uses the LeChatelier rule to predict the flame-propagation limits of a mixed hydrogen-hydrocarbon fuel, the observed upper limits are almost invariably less than the calculated values.

As part of a study of the combustion of mixed fuels, the kinetics of the reaction of hydrogen with oxygen in the presence of methane has been studied in greater detail. Lewis and Von Elbe[3] have shown that the mechanism for the second explosion limit must include a chain-breaking step in the gas phase,

$$H+O_2+M\rightarrow HO_2+M, \quad (1)$$

and two chain-branching steps,

$$H+O_2\rightarrow OH+O, \quad (2)$$

$$O+H_2\rightarrow OH+H. \quad (3)$$

When methane is present and participates in the reaction, another step is possible, which may be expressed as

$$CH_4+X=CH_3+HX,^4 \quad (4)$$

where X is one of the atoms or radicals H, O, OH, or HO_2 produced in Reactions 1, 2, or 3. This is followed by the rapid reaction

$$CH_3+O_2=HCHO+OH=CHO+H_2O. \quad (5)$$

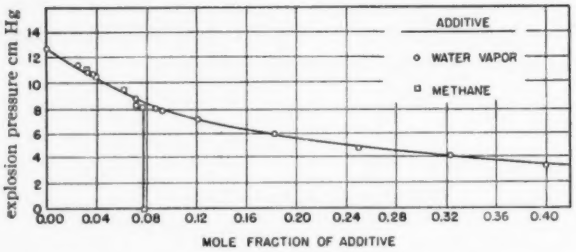

FIG. 1. The reduction of the second explosion limit of 2:1 hydrogen-oxygen mixtures by methane and water vapor. $T=560$ C.

It has been shown by the author[5] that the activation energy at the second explosion limit is reduced from 22.6 kcal/mole for methane-free hydrogen-oxygen explosions to 15.6 kcal/mole for the reduced explosion limits of hydrogen-oxygen mixtures containing a fixed methane concentration. On the basis of these facts, it has been postulated that the second explosion limit of hydrogen and oxygen is reduced in the presence of methane because of the rapid formation of water vapor and of formaldehyde in reactions preceding the explosion.

Figure 1 shows the progressive reduction of the pressure at the second explosion limit in a system at constant temperature containing a stoichiometric H_2-O_2 mixture, as the amount of methane or water vapor present is progressively increased. The pressure at the limit does not decrease continuously to zero with increasing methane concentrations, but drops abruptly to zero at a critical methane concentration. This abrupt total inhibition of explosion is believed caused by formation of a critical formaldehyde concentration, produced via reactions 4 and 5. It is interesting to note that up to this critical point, the water vapor and the methane curves are coincident.

It has been shown by several investigators[6] that water vapor accelerates the oxidation of hydrocarbons and of hydrogen in the nonexplosive, slow reactions. Some data of the author show a similar acceleration occurring with the addition of methane to hydrogen-oxygen mixtures.

Figure 2 shows rate curves at 560 C and 420-mm Hg initial pressure for 2:1 hydrogen-oxygen mixtures with methane added. The initial rate of reaction increases with increasing methane concentration. The maximum rate for 2:1 H_2-O_2 mixtures is reduced, however, because some of the oxygen is consumed by the methane. In H_2-O_2 mixtures with a higher proportion of oxygen, the maximum rate, as well as the initial rate, increases with the addition of methane.

[1] E. Jones, J. Appl. Chem. **1**, 411 (1951).
[2] L. Seig, Angew. Chem. **63**, 143 (1951).
[3] B. Lewis and G. von Elbe, *Combustion, Flames and Explosions of Gases* (Academic Press, New York, 1951), Chap. 2.
[4] When $X=O$ atom, reaction 4 is $CH_4+O=CH_2+H_2O$. See E. W. R. Steacie, *Atomic and Free Radical Reactions* (Reinhold Publishing Corp., New York, 1946), page 359.
[5] A. Levy, Battelle Memorial Institute, Technical Report No. 15036-6 Contract AF 33(038)-12656 to Wright Air Development Center, July 1952; presented at the 122nd National Meeting of the American Chemical Society, Atlantic City, New Jersey, September 1952.

To compare the effect of water vapor and of methane on the combination of hydrogen and oxygen, a series of $H_2-O_2-H_2O$ and $H_2-O_2-CH_4$ mixtures was tested. The results of these studies are shown in Table I.

If, as postulated in the explosion-inhibition studies, the methane accelerates the initial rate of water formation, it would be expected that, as the water vapor formed in a $H_2-O_2-CH_4$ system reaches a concentration equivalent to the initial concentration in a $H_2-O_2-H_2O$ system, the rates in these two systems would be equal, with perhaps slight variations because of differences in partial pressures of the reactants in the two systems.

Table II shows that this prediction is confirmed within experimental error.

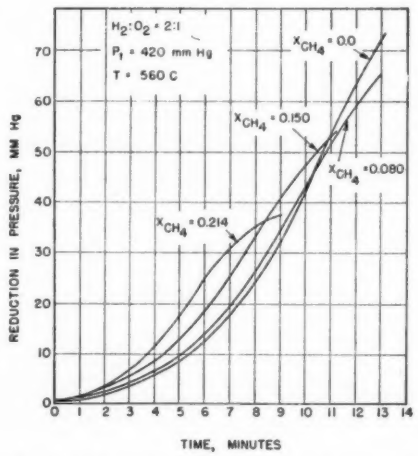

FIG. 2. The effect of methane on the slow reaction of hydrogen-oxygen mixtures.

It would appear from the explosion data in Fig. 1 and the rate data in Table II that the effects of water vapor and of methane on the combination of hydrogen and oxygen should be explainable by similar mechanisms. This similarity of effects may be represented by the following steps.

$$CH_4+HO_2=CH_3+H_2O_2,$$

$$CH_3+O_2=HCHO+OH=CHO+H_2O,$$

and

$$H_2O+HO_2 \xrightarrow{\text{wall}} OH+H_2O_2.$$

One mole of water vapor is formed for each mole of methane added, which conforms with the observed equivalent reduction in explosion pressure by methane and by water vapor. Both methane and water vapor react with the HO_2 radical to form the peroxide, and each reaction increases the OH radical concentration, thus increasing the rate of reaction. As pointed out by Voevodskii,[6] this last step also accounts for the *S*-shaped-pressure-time curves in these reactions, where the water vapor accelerates the reaction after a latent period during which the HO_2 and H_2O concentrations are negligible.

TABLE 1. The effect of water vapor or methane on the rate of combination of hydrogen and oxygen. $T=560$ C, $P=420$-mm Hg, KCl-coated Pyrex vessel.

Partial pressures, mm Hg				Max rate, $\frac{dP}{dt}$, mm/min	Time to max, min
H_2	O_2	CH_4	H_2O		
272	136	12	···	10.0	8.5
276	138	6	···	11.0	9.0
280	140	0	···	12.0	9.0
280	140	0	···	12.0	9.0
260	130	···	30	17.0	2.5
272	136	···	12	15.5	4.0
276	138	···	6	14.0	5.3
280	140	···	0	12.0	9.0

TABLE II. A comparison of instantaneous reaction rates with equivalent concentrations of water vapor in the $H_2-O_2-CH_4$, $H_2-O_2-H_2O$, and H_2-O_2 systems. $T=560$ C, $P=420$-mm Hg, KCl-coated Pyrex vessel.

Partial pressures, mm Hg				Time to form 12 mm H_2O, min	Rate at $t_{12\,mm}$, mm/min
H_2	O_2	CH_4	H_2O		
272	136	···	12	0.0	3.8
276	138	···	6	1.2	4.0
272	136	12	···	3.0	3.5
276	138	6	···	3.1	3.7
280	140	0	···	3.2	3.6
				Time to form 6 mm H_2O, min	Rate at t_6 mm
276	138	···	6	0	2.0
272	136	12	···	1.9	2.2
276	138	6	···	2.2	2.4
280	140	0	···	2.2	2.3

A more detailed and more complete report and discussion of these studies is planned for the future. This investigation was sponsored by the Flight Research Laboratory, Wright Air Development Center, Dayton, Ohio. Permission to publish these results is gratefully acknowledged.

[6] See reference 3, p. 62; N. Chirkov, Acta Physicochim. U.R.S.S. **6**, 915 (1937); Doklady Akad. Nauk. S.S.S.R. **45**, 244 (1944); M. Vanpee, Ann. mines Belg. **48**, 44 (1949); V. V. Voevodskii, J. Phys. Chem. (U.S.S.R.) **22**, 457 (1948).

The Application of Jacobians to Statistical Thermodynamics

HARVEY EINBINDER*
Pupin Physics Laboratory, Columbia University, New York, New York
(Received November 18, 1952)

Shaw's Jacobian method for calculating thermodynamic derivatives is extended so that any partial second derivative can be expressed in terms of two sets of reference derivatives based on the independent variables (V, T) and (P, T), respectively. A simplified and enlarged table of second-order Jacobians is given in terms of these reference sets. Methods are developed for obtaining the reference J's explicitly in the cases of greatest importance in statistical thermodynamics, i.e., from A, E, the partition function and the caloric equation $PV=sE$, permitting any first or second partial derivative to be found as an explicit function of (V, T). These J's are given for the polyatomic ideal and van der Waals gases, black-body radiation, the general (relativistic and nonrelativistic) quantum gas, and the general degenerate Bose-Einstein and Fermi-Dirac gases. Their great usefulness is illustrated, and the possible application of reference Jacobians in evaluating semi-empirical theories of liquids and gases is noted. Finally, the classical theory of thermodynamic fluctuations is extended using Jacobians. General formulas are derived which give explicitly the total variance, partial variance, and covariance of the fluctuation of any thermodynamic variable from its equilibrium value.

1. INTRODUCTION

FOR the usual one-component system, any thermodynamic function can be expressed in terms of two independent variables. An important thermodynamic problem is to find any partial derivative as an explicit function of the independent variable of such a system, usually (V, T) or (P, T), given its complete function, i.e., one from which all other thermodynamic functions can be found. Shaw has developed a very powerful and systematic method for deriving thermodynamic relations using Jacobians. A detailed and lucid discussion of its theory and application is given in his original paper;[1] briefer treatments are to be found elsewhere.[2] A simplified version has been given recently[3] and it has also been extended to multicomponent systems with n independent variables.[4] Shaw limited the discussion of this particular problem to first derivatives and used the equation of state and the specific heat as the complete function, one useful only in calculations based on experimental data. Here the treatment will be extended to include second derivatives and the use of the most important complete functions of statistical thermodynamics.

Shaw's method employs five reference Jacobians:

$$\mathbf{a}=J(V,T),\quad \mathbf{b}=J(P,V)=J(T,S),\quad \mathbf{c}=J(P,S),\quad \mathbf{l}=J(P,T),\quad \mathbf{n}=J(V,S), \tag{1.1}$$

where by definition

$$J(x,y)=\partial(x,y)/\partial(r,s), \tag{1.2}$$

r and s being any pair of thermodynamic variables. These reference J's are connected by the constraining relation

$$\mathbf{ac}=\mathbf{ln}-\mathbf{b}^2. \tag{1.3}$$

In statistical thermodynamics where the natural independent variables are (V, T), calculations are simplified if $r=V$, $s=T$, so that $\mathbf{a}=1$ and Eq. (1.3) becomes

$$\mathbf{c}=\mathbf{ln}-\mathbf{b}^2. \tag{1.4}$$

From the properties of the Jacobian,

$$(\partial y/\partial x)_z=\partial(y,z)/\partial(x,z)=J(y,z)/J(x,z), \tag{1.5}$$

so using Eq. (1.5) and Table I, any partial first derivative can be expressed in terms of four independent reference J's.

2. EXTENSION TO SECOND DERIVATIVES

The Jacobian treatment can be directly extended to include partial second derivatives. Applying Eq. (1.5),

$$\left[\frac{\partial}{\partial w}\left(\frac{\partial x}{\partial y}\right)_z\right]_r=\frac{J[J(x,z)/J(y,z),r]}{J(w,z)}=\frac{J(y,z)J[J(x,z),r]-J(x,z)J[J(y,z),r]}{J(w,r)J^2(y,z)}, \tag{2.1}$$

since from Eq. (2.6) $J(x/y,z)=[yJ(x,z)-xJ(y,z)]/y^2$. Setting

$$\theta=J(x,z),\quad \mu=J(y,z),\quad \nu=J(w,r), \tag{2.2}$$

then

$$[\partial/\partial w(\partial x/\partial y)_z]_r=[\mu J(\theta,r)-\theta J(\mu,r)]/\nu\mu^2. \tag{2.3}$$

If $w=y$ and $r=z$, then $\nu=\mu$;

$$(\partial^2 x/\partial y^2)_z=[\mu J(\theta,z)-\theta J(\mu,z)]/\mu^3. \tag{2.4}$$

If $w=z$ and $r=y$, then $\nu=-\mu$;

$$\partial^2 x/\partial y\partial z=-[\mu J(\theta,y)-\theta J(\mu,y)]/\mu^3. \tag{2.5}$$

In general, any second derivative can be expressed in terms of four second-order Jacobians of the type

* Present address: 550 Fifth Avenue, New York 36, New York.
[1] A. N. Shaw, Trans. Roy. Soc. (London) A234, 299 (1935).
[2] H. Margenau and G. M. Murphy, *The Mathematics of Physics and Chemistry* (D. Van Nostrand Company, Inc., New York, 1943), p. 17; T. K. Sherwood and C. E. Reed, *Applied Mathematics in Chemical Engineering* (McGraw-Hill Book Company, Inc., New York, 1939), p. 172.
[3] P. H. Crawford, Am. J. Phys. 17, 1, 450 (1949).
[4] F. H. Crawford, Proc. Am. Acad. Arts Sci. 78, 165 (1950).

TABLE I. First-order Jacobians.

$J(x,y)$ $y\rightarrow$ / $x\downarrow$	P	V	T	S	E	H	A	G	Q	W
P	0	$\mathbf{b}$	$\mathbf{l}$	$\mathbf{c}$	$T\mathbf{c}-P\mathbf{b}$	$T\mathbf{c}$	$-P\mathbf{b}-S\mathbf{l}$	$-S\mathbf{l}$	$T\mathbf{c}$	$P\mathbf{b}$
V	$-\mathbf{b}$	0	1 (unity)	$\mathbf{n}$	$T\mathbf{n}$	$T\mathbf{n}-V\mathbf{b}$	$-S$	$-S-V\mathbf{b}$	$T\mathbf{n}$	0
T	$-\mathbf{l}$	-1 (unity)	0	$\mathbf{b}$	$P+T\mathbf{b}$	$T\mathbf{b}-V\mathbf{l}$	P	$-V\mathbf{l}$	$T\mathbf{b}$	$-P$
S	$-\mathbf{c}$	$-\mathbf{n}$	$-\mathbf{b}$	0	$P\mathbf{n}$	$-V\mathbf{c}$	$S\mathbf{b}+P\mathbf{n}$	$S\mathbf{b}-V\mathbf{c}$	0	$-P\mathbf{n}$
E	$P\mathbf{b}-T\mathbf{c}$	$-T\mathbf{n}$	$-P-T\mathbf{b}$	$-P\mathbf{n}$	0	$P(V\mathbf{b}-T\mathbf{n})$ $-VT\mathbf{c}$	$S(P+T\mathbf{b})$ $+PT\mathbf{n}$	$S(P+T\mathbf{b})$ $+V(P\mathbf{b}-T\mathbf{c})$	$-PT\mathbf{n}$	$-PT\mathbf{n}$
H	$-T\mathbf{c}$	$V\mathbf{b}-T\mathbf{n}$	$V\mathbf{l}-T\mathbf{b}$	$V\mathbf{c}$	$P(T\mathbf{n}-V\mathbf{b})$ $+VT\mathbf{c}$	0	$S(T\mathbf{b}-V\mathbf{l})$ $+P(T\mathbf{n}-V\mathbf{b})$	$S(T\mathbf{b}-V\mathbf{l})$ $-VT\mathbf{c}$	$VT\mathbf{c}$	$P(V\mathbf{b}-T\mathbf{n})$
A	$P\mathbf{b}+S\mathbf{l}$	S	$-P$	$-S\mathbf{b}-P\mathbf{n}$	$-S(P+T\mathbf{b})$ $-PT\mathbf{n}$	$S(V\mathbf{l}-T\mathbf{b})$ $+P(V\mathbf{b}-T\mathbf{n})$	0	$S(P+V\mathbf{l})$ $+PV\mathbf{b}$	$-T(S\mathbf{b}+P\mathbf{n})$	PS
G	$S\mathbf{l}$	$S+V\mathbf{b}$	$V\mathbf{l}$	$V\mathbf{c}-S\mathbf{b}$	$V(T\mathbf{c}-P\mathbf{b})$ $-S(P+T\mathbf{b})$	$VT\mathbf{c}$ $+S(V\mathbf{l}-T\mathbf{b})$	$-S(P+V\mathbf{l})$ $-PV\mathbf{b}$	0	$T(V\mathbf{c}-S\mathbf{b})$	$P(S+V\mathbf{b})$
Q	$-T\mathbf{c}$	$-T\mathbf{n}$	$-T\mathbf{b}$	0	$PT\mathbf{n}$	$-VT\mathbf{c}$	$T(S\mathbf{b}+P\mathbf{n})$	$T(S\mathbf{b}-V\mathbf{c})$	0	$-PT\mathbf{n}$
W	$-P\mathbf{b}$	0	P	$P\mathbf{n}$	$PT\mathbf{n}$	$P(T\mathbf{n}-V\mathbf{b})$	$-PS$	$-P(S+V\mathbf{b})$	$PT\mathbf{n}$	0

$(\mathbf{a}=1;\ \mathbf{c}=\mathbf{ln}-\mathbf{b}^2)$

$J[J(x,y),z]$ and three first-order ones of the type $J(x,y)$. In choosing the second-order J's it is convenient to use a different set for each combination of independent variables. Since the most important sets of independent variables are (V,T) and (P,T), only these two cases will be considered here. To apply the method, a table of the corresponding second-order J's must be constructed, which can be expressed in its simplest form when (r,s) is taken as (V,T) and (P,T), respectively. With this simplification Table II is obtained using results largely implicit in Table IV of Shaw's article.[1] His table contains the second-order J's only with respect to P, V, T, and S; but if $w=w(x,y)$, then

$$J(w,z)J=(x,z)(\partial w/\partial x)_y+J(y,z)(\partial w/\partial y)_x, \quad (2.6)$$

$$J(w,z)=[J(x,z)J(w,y)-J(y,z)J(w,x)]/J(x,y). \quad (2.7)$$

By setting (x,y) equal to (V,T) and (P,T) and letting w successively equal E, H, A and G, the table is extended to include these variables. $J[J(x,y),Q]$ and $J[J(x,y),W]$ have not been tabulated because they have only a formal meaning. It should be remembered that opposite entries in the two columns of Table II must not be equated since they correspond to different (r,s), i.e., (V,T) and (P,T).

From (2.6) two very useful equations may be derived:

$$J(x+y,z)J=(x,z)+J(y,z), \quad (2.8)$$

$$J(xy,z)=yJ(x,z)+xJ(y,z). \quad (2.9)$$

With the aid of Tables I and II and Eqs. (1.4)–(2.9), any partial second derivative can be expressed in terms of the reference J's, i.e., a set of reference derivatives, which may be considered explicit functions of (V,T) or (P,T), as the case may be. The second derivatives of auxiliary functions, such as the fugacity, can be readily found by using Eq. (2.6), regarding $w=w(x,y)$ as the definition of the auxiliary function in terms of standard thermodynamic variables. Note that in Table I, $\mathbf{a}=1$ since in the applications to be made here the independent variables are (V,T), but if they were (P,T), as is the case in engineering applications, then $\mathbf{l}$ rather than $\mathbf{a}$ should be set equal to unity.

As an illustration consider $(\partial^2S/\partial V^2)_E$ which arises in the theory of fluctuations.[5] Here $\theta=P\mathbf{n}$ and $\mu=T\mathbf{n}$, so using Eqs. (2.4) and (2.8),

$$(\partial^2S/\partial V^2)_E=[TJ(P,E)-PJ(T,E)]/T^3\mathbf{n}$$
$$=(T^2\mathbf{c}-2PT\mathbf{b}-P^2)/T^3\mathbf{n}. \quad (2.10)$$

Transforming the J's into derivatives,

$$(\partial^2S/\partial V^2)_E$$
$$=[T(\partial P/\partial V)_S-2P(\partial T/\partial V)_S-P^2/C_v]/T^2. \quad (2.11)$$

No second-order reference J's appear because $(\partial S/\partial V)_E=P/T$.

A major problem considered in the rest of this paper is the calculation of the reference J's as explicit functions of (V,T) from the most important complete functions of statistical thermodynamics.

[5] P. S. Epstein, *Textbook of Thermodynamics* (John Wiley and Sons, Inc., New York, 1937), p. 390.

TABLE II. Second-order Jacobians.

	In terms of the A's $\begin{matrix}\mathbf{a}=1\\ r=V\quad s=T\end{matrix}$	In terms of the L's $\begin{matrix}\mathbf{l}=1\\ r=P\quad s=T\end{matrix}$
$J(\mathbf{a}, P)$	0	$-\mathbf{L}_2$
$J(\mathbf{a}, V)$	0	$\mathbf{b}\mathbf{L}_1-\mathbf{a}\mathbf{L}_2$
$J(\mathbf{a}, T)$	0	$\mathbf{L}_1$
$J(\mathbf{a}, S)$	0	$\mathbf{c}\mathbf{L}_1+\mathbf{b}\mathbf{L}_2$
$J(\mathbf{a}, E)$	0	$(T\mathbf{c}-P\mathbf{b})\mathbf{L}_1+(P\mathbf{a}+T\mathbf{b})\mathbf{L}_2$
$J(\mathbf{a}, H)$	0	$T\mathbf{c}\mathbf{L}_1+(T\mathbf{b}-V)\mathbf{L}_2$
$J(\mathbf{a}, A)$	0	$-(S+P\mathbf{b})\mathbf{L}_1+P\mathbf{a}\mathbf{L}_2$
$J(\mathbf{a}, G)$	0	$-S\mathbf{L}_1-V\mathbf{L}_2$
$J(\mathbf{b}, P)$	$\mathbf{l}\mathbf{A}_1-\mathbf{b}\mathbf{A}_2$	$\mathbf{L}_3$
$J(\mathbf{b}, V)$	$\mathbf{A}_1$	$\mathbf{b}\mathbf{L}_2+\mathbf{a}\mathbf{L}_3$
$J(\mathbf{b}, T)$	$\mathbf{A}_2$	$\mathbf{L}_2$
$J(\mathbf{b}, S)$	$-\mathbf{b}\mathbf{A}_1+\mathbf{n}\mathbf{A}_2$	$\mathbf{c}\mathbf{L}_2-\mathbf{b}\mathbf{L}_3$
$J(\mathbf{b}, E)$	$-(P+T\mathbf{b})\mathbf{A}_1+T\mathbf{n}\mathbf{A}_2$	$(T\mathbf{c}-P\mathbf{b})\mathbf{L}_2-(P\mathbf{a}+T\mathbf{b})\mathbf{L}_3$
$J(\mathbf{b}, H)$	$(V\mathbf{l}-T\mathbf{b})\mathbf{A}_1+(T\mathbf{n}-V\mathbf{b})\mathbf{A}_2$	$T\mathbf{c}\mathbf{L}_2+(V-T\mathbf{b})\mathbf{L}_3$
$J(\mathbf{b}, A)$	$-P\mathbf{A}_1-S\mathbf{A}_2$	$-(S+P\mathbf{b})\mathbf{L}_2-P\mathbf{a}\mathbf{L}_3$
$J(\mathbf{b}, G)$	$-V\mathbf{l}\mathbf{A}_1-(S+V\mathbf{b})\mathbf{A}_2$	$-S\mathbf{L}_2+V\mathbf{L}_3$
$J(\mathbf{c}, P)$	$-3\mathbf{b}\mathbf{l}\mathbf{A}_1+(3\mathbf{b}^2+\mathbf{c})\mathbf{A}_2-\mathbf{b}\mathbf{n}\mathbf{A}_3+\mathbf{l}^2\mathbf{A}_4$	$\mathbf{L}_4$
$J(\mathbf{c}, V)$	$-2\mathbf{b}\mathbf{A}_1+\mathbf{n}\mathbf{A}_2+\mathbf{l}\mathbf{A}_4$	$\mathbf{b}\mathbf{L}_3+\mathbf{a}\mathbf{L}_4$
$J(\mathbf{c}, T)$	$\mathbf{l}\mathbf{A}_1-2\mathbf{b}\mathbf{A}_2+\mathbf{n}\mathbf{A}_3$	$\mathbf{L}_3$
$J(\mathbf{c}, S)$	$(3\mathbf{b}^2+\mathbf{c})\mathbf{A}_1-3\mathbf{b}\mathbf{n}\mathbf{A}_2+\mathbf{n}^2\mathbf{A}_3-\mathbf{b}\mathbf{l}\mathbf{A}_4$	$\mathbf{c}\mathbf{L}_3-\mathbf{b}\mathbf{L}_4$
$J(\mathbf{c}, E)$	$-(P+T\mathbf{b})J(\mathbf{c}, V)+T\mathbf{n}J(\mathbf{c}, T)$	$(T\mathbf{c}-P\mathbf{b})\mathbf{L}_3-(P\mathbf{a}+T\mathbf{b})\mathbf{L}_4$
$J(\mathbf{c}, H)$	$(V\mathbf{l}-T\mathbf{b})J(\mathbf{c}, V)+(T\mathbf{n}-V\mathbf{b})J(\mathbf{c}, T)$	$T\mathbf{c}\mathbf{L}_3+(V-T\mathbf{b})\mathbf{L}_4$
$J(\mathbf{c}, A)$	$-PJ(\mathbf{c}, V)-SJ(\mathbf{c}, T)$	$-(S+P\mathbf{b})\mathbf{L}_3-P\mathbf{a}\mathbf{L}_4$
$J(\mathbf{c}, G)$	$-V\mathbf{l}J(\mathbf{c}, V)-(S+V\mathbf{b})J(\mathbf{c}, T)$	$-S\mathbf{L}_3+V\mathbf{L}_4$
$J(\mathbf{l}, P)$	$\mathbf{l}\mathbf{A}_2-\mathbf{b}\mathbf{A}_3$	0
$J(\mathbf{l}, V)$	$\mathbf{A}_2$	0
$J(\mathbf{l}, T)$	$\mathbf{A}_3$	0
$J(\mathbf{l}, S)$	$-\mathbf{b}\mathbf{A}_2+\mathbf{n}\mathbf{A}_3$	0
$J(\mathbf{l}, E)$	$-(P+T\mathbf{b})\mathbf{A}_2+T\mathbf{n}\mathbf{A}_3$	0
$J(\mathbf{l}, H)$	$(V\mathbf{l}-T\mathbf{b})\mathbf{A}_2+(T\mathbf{n}-V\mathbf{b})\mathbf{A}_3$	0
$J(\mathbf{l}, A)$	$-P\mathbf{A}_2-S\mathbf{A}_3$	0
$J(\mathbf{l}, G)$	$-V\mathbf{l}\mathbf{A}_2-(S+V\mathbf{b})\mathbf{A}_3$	0
$J(\mathbf{n}, P)$	$-\mathbf{b}\mathbf{A}_1+\mathbf{l}\mathbf{A}_4$	$-\mathbf{c}\mathbf{L}_2+2\mathbf{b}\mathbf{L}_3+\mathbf{a}\mathbf{L}_4$
$J(\mathbf{n}, V)$	$\mathbf{A}_4$	$\mathbf{b}\mathbf{c}\mathbf{L}_1+(3\mathbf{b}^2-\mathbf{n})\mathbf{L}_2+3\mathbf{a}\mathbf{b}\mathbf{L}_3+\mathbf{a}^2\mathbf{L}_4$
$J(\mathbf{n}, T)$	$\mathbf{A}_1$	$\mathbf{c}\mathbf{L}_1+2\mathbf{b}\mathbf{L}_2+\mathbf{a}\mathbf{L}_3$
$J(\mathbf{n}, S)$	$\mathbf{n}\mathbf{A}_1-\mathbf{b}\mathbf{A}_4$	$\mathbf{c}^2\mathbf{L}_1+3\mathbf{b}\mathbf{c}\mathbf{L}_2+(\mathbf{n}-3\mathbf{b}^2)\mathbf{L}_3-\mathbf{a}\mathbf{b}\mathbf{L}_4$
$J(\mathbf{n}, E)$	$T\mathbf{n}\mathbf{A}_1-(P+T\mathbf{b})\mathbf{A}_4$	$-(P\mathbf{a}+T\mathbf{b})J(\mathbf{n}, P)+(T\mathbf{c}-P\mathbf{b})J(\mathbf{n}, T)$
$J(\mathbf{n}, H)$	$(T\mathbf{n}-V\mathbf{b})\mathbf{A}_1+(V\mathbf{l}-T\mathbf{b})\mathbf{A}_4$	$(V-T\mathbf{b})J(\mathbf{n}, P)+T\mathbf{c}J(\mathbf{n}, T)$
$J(\mathbf{n}, A)$	$-S\mathbf{A}_1-P\mathbf{A}_4$	$-P\mathbf{a}J(\mathbf{n}, P)-(S+P\mathbf{b})J(\mathbf{n}, T)$
$J(\mathbf{n}, G)$	$-(S+V\mathbf{b})\mathbf{A}_1-V\mathbf{l}\mathbf{A}_4$	$VJ(\mathbf{n}, P)-SJ(\mathbf{n}, T)$
$\mathbf{a}=J(V, T)$	$\mathbf{A}_1=(\partial^2P/\partial T^2)_V=-(\partial\mathbf{b}/\partial T)_V$	$\mathbf{L}_1=(\partial^2V/\partial P^2)_T=(\partial\mathbf{a}/\partial P)_T$
$\mathbf{b}=J(P, V)$	$=\partial^2S/\partial T\partial V=(\partial\mathbf{n}/\partial V)_T$	$\mathbf{L}_2=\partial^2V/\partial P\partial T=(\partial\mathbf{a}/\partial T)_P$
$=J(T, S)$	$\mathbf{A}_2=-(\partial^2S/\partial V^2)_T=(\partial\mathbf{b}/\partial V)_T$	$=(\partial^2S/\partial P^2)_T=(\partial\mathbf{b}/\partial P)_T$
$\mathbf{c}=J(P, S)$	$=-\partial^2P/\partial V\partial T=-(\partial\mathbf{l}/\partial T)_V$	$\mathbf{L}_3=-(\partial^2V/\partial T^2)_P=-(\partial\mathbf{b}/\partial T)_P$
$\mathbf{l}=J(P, T)$	$\mathbf{A}_3=(\partial^2P/\partial V^2)_T=(\partial\mathbf{l}/\partial V)_T$	$=\partial^2S/\partial T\partial P=(\partial\mathbf{c}/\partial P)_T$
$\mathbf{n}=J(V, S)$	$\mathbf{A}_4=-(\partial^2S/\partial T^2)_V=-(\partial\mathbf{n}/\partial T)_V$	$\mathbf{L}_4=-(\partial^2S/\partial T^2)_P=-(\partial\mathbf{c}/\partial T)_P$

3. GIVEN THE HELMHOLTZ FUNCTION $A=A(V,T)$

As $A=E-TS$ and $dA=-PdV-SdT$, so

$$P=-(\partial A/\partial V)_T, \tag{3.1}$$

$$S=-(\partial A/\partial T)_V, \tag{3.2}$$

$$E=A-T(\partial A/\partial T)_V, \tag{3.3}$$

Whence with the definitions of the J's, (III, 2) is obtained.[6] These results are very simple because $(r, s)=(V, T)$ are the natural independent variables for the Helmholtz function,[7] i.e., for constant V and T, dA vanishes; or alternately $A(V, T)$ is a characteristic function from which all other thermodynamic functions can be derived.[8]

4. GIVEN THE INTERNAL ENERGY $E=E(V,T)$

One of the commonest procedures in statistical mechanics is the calculation of the internal energy of a

[6] (III, 2) stands for Table III, column 2. Similar abbreviations will be used in the rest of this paper, for references to Tables III and IV.

[7] J. W. Gibbs, *Collected Works* (Longmans, Green and Company, New York, 1928), Vol. 1, p. 86.

[8] M. Planck, *Treatise on Thermodynamics* (Dover Publications, New York, 1945), p. 121.

system. Equation (3.3) can be written as

$$[(\partial/\partial T)(A/T)]_V = -E/T^2. \tag{4.1}$$

Integrating

$$A = -T\int_0^T (E/T^2)dT - T\phi(V), \tag{4.2}$$

and using Eq. (3.2),

$$S = E/T + \int_0^T (E/T^2)dT + \phi(V). \tag{4.3}$$

According to the third law $S=0$ at $T=0$. If it is obeyed $\phi(V)\equiv 0$, so

$$A = -T\int_0^T (E/T^2)dT. \tag{4.4}$$

Since for S to exist for all T, $\mathrm{Lim}_{T=0}(E/T)=0$, integrating Eq. (4.3) by parts yields

$$S = \int_0^T (\partial E/\partial T)_V dT/T. \tag{4.5}$$

Using Eqs. (4.4) and (4.5), (III, 3) is obtained.

For application to engineering thermodynamics, where $H(P, T)$ is a known function, the same analysis can be carried out using the Gibbs-Helmholtz relation between G and H analogous to Eq. (4.1).

Instead of applying these formulas in which E is used directly, as a rule it is much simpler to calculate A by Eq. (4.4), and then successively differentiate A to obtain the reference J's from (III, 2). An illustration is blackbody radiation whose energy density is given by the Stefan-Boltzmann law,

$$E/V = \kappa T^4, \tag{4.6}$$

TABLE III. Explicit expressions for the reference Jacobians.

J	$A(V, T)$	[a]$E(V, T)$	$PV = sE(V, T)$	$Q(V, T)$	$Q = Q_V(V)\cdot Q_T(T)$
b	$\dfrac{\partial^2 A}{\partial V \partial T}$	$\displaystyle\int_0^T \frac{E_\delta}{T}dT$	$-\dfrac{sE_\beta}{V}$	$\dfrac{Nk}{Q}\left(\dfrac{TQ_\alpha Q_\beta}{Q} - Q_\alpha - TQ_\delta\right)$	$-NkQ_{V\alpha}/Q_V$
c	$\mathbf{l}\mathbf{n} - \mathbf{b}^2$	$\mathbf{l}\mathbf{n} - \mathbf{b}^2$	$-\mathbf{b}(\mathbf{b} + V\mathbf{l}/sT)$	$\mathbf{l}\mathbf{n} - \mathbf{b}^2$	$\mathbf{l}\mathbf{n} - \mathbf{b}^2$
l	$-\dfrac{\partial^2 A}{\partial V^2}$	$T\displaystyle\int_0^T \frac{E_\gamma}{T}dT$	$s\dfrac{\partial}{\partial V}\left(\dfrac{E}{V}\right)$	$\dfrac{NkT}{Q}\left(Q_\gamma - \dfrac{Q_\alpha^2}{Q}\right)$	$\dfrac{NkT}{Q_V}\left(Q_{V\gamma} - \dfrac{Q_{V\alpha}^2}{Q_V}\right)$
n	$-\dfrac{\partial^2 A}{\partial T^2}$	$\dfrac{E_\beta}{T}$	$\dfrac{E_\beta}{T}$	$-\dfrac{Nk}{Q}\left(TQ_\epsilon + 2Q_\beta - T\dfrac{Q_\beta^2}{Q}\right)$	$\dfrac{Nk}{Q_T}\left(TQ_{T\epsilon} + 2Q_{T\beta} - T\dfrac{Q_{T\beta}^2}{Q_T}\right)$
Λ_1	$-\dfrac{\partial^3 A}{\partial V \partial T^2}$	$\dfrac{E_\delta}{T}$	$\dfrac{sE_\epsilon}{V} = \dfrac{E_\delta}{T}$	$-\dfrac{\partial \mathbf{b}}{\partial T} = \dfrac{\partial \mathbf{n}}{\partial V}$	0
Λ_2	$\dfrac{\partial^3 A}{\partial V^2 \partial T}$	$-E_\gamma - \dfrac{\mathbf{l}}{T}$	$-\dfrac{s\partial}{\partial V}\left(\dfrac{E_\beta}{V}\right)$	$-\dfrac{\partial \mathbf{l}}{\partial T} = \dfrac{\partial \mathbf{b}}{\partial V}$	$-\dfrac{\mathbf{l}}{T}$
Λ_3	$-\dfrac{\partial^3 A}{\partial V^3}$	$\dfrac{\partial \mathbf{l}}{\partial V}$	$\dfrac{\partial \mathbf{l}}{\partial V}$	$\dfrac{\partial \mathbf{l}}{\partial V}$	$\dfrac{\partial \mathbf{l}}{\partial V}$
Λ_4	$\dfrac{\partial^3 A}{\partial T^3}$	$-\dfrac{\partial}{\partial T}\left(\dfrac{E_\beta}{T}\right)$	$-\dfrac{\partial}{\partial T}\left(\dfrac{E_\beta}{T}\right)$	$-\dfrac{\partial \mathbf{n}}{\partial T}$	$-\dfrac{\partial \mathbf{n}}{\partial T}$
P	$-\dfrac{\partial A}{\partial V}$	$T\displaystyle\int_0^T \frac{E_\alpha}{T^2}dT$	$\dfrac{sE}{V}$	$NkTQ_\alpha/Q$	$NkTQ_{V\alpha}/Q_V$
S	$-\dfrac{\partial A}{\partial T}$	$\displaystyle\int_0^T \frac{E_\beta}{T}dT$	[a]$\displaystyle\int_0^T \frac{E_\beta}{T}dT$	$Nk\left(\log\dfrac{Q}{N} + T\dfrac{Q_\beta}{Q} + 1\right)$	$Nk\left(\log\dfrac{Q}{N} + T\dfrac{Q_{T\beta}}{Q_T} + 1\right)$
E	$A - T\dfrac{\partial A}{\partial T}$	E	E	$NkTQ_\beta/Q$	$NkTQ_{T\beta}/Q_T$
A	A	$-T\displaystyle\int_0^T \frac{E}{T^2}dT$	[a]$-T\displaystyle\int_0^T \frac{E}{T^2}dT$	$-NkT\left(\log\dfrac{Q}{N} + 1\right)$	$-NkT\left(\log\dfrac{Q}{N} + 1\right)$

$X_\alpha = \partial X/\partial V$; $X_\beta = \partial X/\partial T$; $X_\gamma = \partial^2 X/\partial V^2$; $X_\delta = \partial^2 X/\partial V \partial T$; $X_\epsilon = \partial^2 X/\partial T^2$

[a] The system must obey the third law.

TABLE IV. Reference Jacobians for special systems.[a]

J	Black-body radiation	Polyatomic ideal gas	Polyatomic van der Waals gas	Degenerate Bose-Einstein gas	Degenerate Fermi-Dirac gas
b	$\frac{4}{3}\kappa T^3$	$\frac{Nk}{V}$	$\frac{k}{v-b}$	$(s+1)KT^\sigma$	$\frac{2Nky}{(\sigma+1)V}\{c_1-2c_2y^2\}$
c	$\frac{16}{9}\kappa^2T^6$	$\left(\frac{f}{2}+1\right)\left(\frac{Nk}{V}\right)^2$	$k^2\left\{\frac{f/2+1}{(v-b)^2}-\frac{fa}{kTv^3}\right\}$	$[(s+1)KT^\sigma]^2$	$\frac{2}{\sigma+1}\left(\frac{Nk}{V}\right)^2\{c_1+(c_1^2-2c_2)y^2-3c_1c_2y^4\}$
l	0	$\frac{NkT}{V^2}$	$\frac{1}{N}\left\{\frac{kT}{(v-b)^2}-\frac{2a}{v^3}\right\}$	0	$\frac{NkT}{(\sigma+1)V^2y}\{(s+1)-(s-1)c_1y^2+(3s-1)c_2y^4\}$
n	$4\kappa VT^2$	$\frac{f}{2}\frac{Nk}{T}$	$\frac{f}{2}\frac{Nk}{T}$	$(\sigma+1)KVT^{(\sigma-1)}$	$\frac{2Nky}{(s+1)T}\{c_1-2c_2y^2\}$
$\mathbf{A}_1$	$4\kappa T^3$	0	0	$-(\sigma+1)KT^{(\sigma-1)}$	$\frac{-2Nky}{(\sigma+1)VT}\{c_1-6c_2y^2\}$
$\mathbf{A}_2$	0	$\frac{Nk}{V^2}$	$\frac{k}{N(v-b)^2}$	0	$\frac{-2Nky}{(\sigma+1)V^2}\{(s-1)c_1-2(3s-1)c_2y^2\}$
$\mathbf{A}_3$	0	$\frac{2NkT}{V^3}$	$\frac{1}{N^2}\left\{\frac{2kT}{(v-b)^3}-\frac{6a}{v^4}\right\}$	0	$\frac{NkT}{(s+1)V^2y}\left\{\begin{array}{c}(s+1)(s+2)+(s-1)(s-2)c_1y^2\\-(3s-1)(3s-2)c_2y^4\end{array}\right\}$
$\mathbf{A}_4$	$-8\kappa VT$	$\frac{f}{2}\frac{Nk}{T^2}$	$\frac{f}{2}\frac{Nk}{T^2}$	$(1-\sigma^2)KT^{(\sigma-2)}$	$\frac{8Nkc_2y^3}{(s+1)T^2}$
P	$\frac{\kappa}{3}T^4$	$\frac{NkT}{V}$	$\frac{kT}{v-b}-\frac{a}{v^2}$	$sKT^{(\sigma+1)}$	$\frac{NkT}{(\sigma+1)Vy}\{1+c_1y^2-c_2y^4\}$
S	$\frac{4}{3}\kappa VT^3$	$kN\left\{\log\left(\frac{2\pi mkT}{h^2}\right)^{f/2}\frac{V}{N}+f/2+1\right\}$	$kN\left\{\log\left(\frac{2\pi mkT}{h^2}\right)^{f/2}(v-b)+f/2+1\right\}$	$(s+1)KVT^\sigma$	$\frac{2Nky}{s+1}\{c_1-\frac{2}{3}c_2y^2\}$
E	κVT^4	$\frac{f}{2}NkT$	$\frac{f}{2}NkT-\frac{Na}{v}$	$KVT^{(\sigma+1)}$	$\frac{NkT}{(s+1)y}\{1+c_1y-c_2y^2\}$

[a] $\{\kappa=8\pi^5k^4/15h^3c^3;\quad K=\zeta(\sigma+1)\Gamma(\sigma+1)Ck^{\sigma+1};\quad y=[\Gamma(\sigma+1)x]^{-s},\quad \beta=1\}$
$\{c_1=(\sigma+1)\pi^2/6,\quad c_2=(\sigma+1)(\sigma-1)(9-2\sigma)\pi^4/120;$ cf. §6$\}$.

whence

$$A=-(1/3)\kappa VT^4, \tag{4.7}$$

giving a complete thermodynamic description of the system, (IV, 2). Note that using the third law, P can be derived directly from E without an analysis of the pressure due to isotropic radiation.[9]

5. GIVEN THE PARTITION FUNCTION

(A) General Case, $Q=Q(V,T)$

A standard procedure in statistical mechanics is to derive a partition function Q for the system studied.[10] The thermodynamic functions and derivatives that are of primary interest can be found by expressing the reference J's in terms of Q and its derivatives. By definition, referred to a single particle,

$$A=-kT\log Q, \tag{5.1}$$

and for N particles ($N\gg1$),

$$A=-kT\log Q_N=-kT\log(Q^N/N!)$$
$$=-NkT\,(\log Q/N+1). \tag{5.2}$$

Applying (III, 2) yields (III, 5).

While the partition function is customarily defined only for classical statistics, an analogous function Z is sometimes used in quantum statistics.[11] With only slight changes the formulas derived for Q can be applied to Z.

[9] F. K. Richtmeyer and E. H. Kennard, *Introduction to Modern Physics* (McGraw-Hill Book Company, Inc., New York, 1942), p. 164.

[10] J. E. Mayer and M. G. Mayer, *Statistical Mechanics* (John Wiley and Sons, Inc., New York, 1940), p. 125; S. Glasstone, *Theoretical Chemistry* (D. Van Nostrand Company, Inc., New York, 1944), p. 355.

[11] E. C. Stoner, Phil. Mag. **28**, 257 (1936).

(B) Completely Separable, $Q=Q_V(V)Q_T(T)$

It is often possible to factor Q into volume and temperature dependent parts, thus effecting a marked simplification in the expressions for the reference J's (III, 6) because now $A=-kT\,(\ln Q_V+\ln Q_T)$, i.e., $E=E(T)$ and $P=T\psi(V)$. Since $(\partial E/\partial V)_T=0$, the partition function for a classical system of non-interacting particles is completely separable. An illustration is a gas of close-packed rigid spheres,[12] where

$$Q=(2\pi mkT/h^2)^{\frac{1}{2}}\kappa V[1-(V_0/V)^{\frac{1}{3}}]^3. \tag{5.3}$$

The most important example of this case is the ideal polyatomic gas with f degrees of freedom, where

$$Q=(2\pi mkT/h^2)^{f/2}V, \tag{5.4}$$

whose reference J's are given in (IV, 3).

(C) Partially Separable, $Q=Q_V(V)Q_T(T)Q'(V,T)$

In this frequent case, the thermodynamic functions and the J's are the sum of contributions from each of the product terms of Q, so Q' and Q_VQ_T can be treated separately using (III, 5) and (III, 6), respectively. When $Q'(V, T)$ is an exponential function, the simplest procedure is to transform it to the corresponding $A'(V, T)$ by either Eq. (5.1) or (5.2), as the case may be. Thus, for blackbody radiation,[13] where $Q=\exp(\kappa VT^3/3k)$, $A=-(1/3)\kappa VT^4$ agreeing with Eq. (4.7). An example of this case is the polyatomic van der Waals gas with f degrees of freedom, for which referred to a single particle

$$Q=(2\pi mkT/h^2)^{f/2}(v-b)\exp(a/kTv), \tag{5.5}$$

where $v=V/N$, leading to (IV, 4). For the Bertholet gas, a must be replaced by a'/T in Eq. (5.5).

6. GIVEN THE CALORIC EQUATION $(PV=sE(V,T))$

For a monatomic gas of non-interacting particles in equilibrium in an n dimensional space obeying classical or quantum mechanics,[14]

$$PV=sE(V, T), \tag{6.1}$$

where $s=2/n$ for a nonrelativistic gas ($E\ll mc^2$) and $s=1/n$ for a completely relativistic one ($E\gg mc^2$). From this equation a number of important consequences can be deduced; notably the behavior of the gas at absolute zero (the $\aleph$ (*Aleph*) theorem)[15] and that $G(V, T)$, which is directly related to the normalization constant of the distribution, is a complete function from which all other thermodynamic functions can be derived.[16] Using Eq. (6.1), (III, 4) is derived and, as might be expected, it is simpler than (III, 3) based on the general $E(V, T)$. Since (III, 4) does not require the third law, it can be applied to the ordinary ideal gas. It is especially suited for quantum gases where the energy is expressed as an infinite series, but is valid for gases obeying any type of ideal statistics, e.g., intermediate statistics.[17] Thus, the J's for the general (nonrelativistic and relativistic) degenerate Bose-Einstein[18] and Fermi-Dirac[19] gases given in (IV, 5) and (IV, 6), respectively, have been derived from their $E(V, T)$. Likewise for the general nondegenerate quantum gas,[20]

$$E=\sigma NkT[1+a_1\beta x-a_2(\beta x)^2+a_3(\beta x)^3-\cdots], \tag{6.2}$$

$$S=Nk[(\sigma+1)-\ln x+(\sigma-1)a_1\beta x-(\sigma-\tfrac{1}{2})a_2(\beta x)^2+(\sigma-1/3)a_3(\beta x)^3-\cdots], \tag{6.3}$$

where

$$\begin{aligned} a_1&=1/2^{\sigma+1},\\ a_2&=2/3^{\sigma+1}-1/4^{\sigma},\\ a_3&=3/4^{\sigma+1}-5/2^{3\sigma+1}-3/6^{\sigma}, \end{aligned} \tag{6.4}$$

$$x=\frac{\Gamma(n/2)}{\Gamma(\sigma)}\left(\frac{h^2}{\pi}\right)^{n-2}\frac{N}{CgV(kT)^{\sigma}}, \tag{6.5}$$

$$\text{nonrelativistic: } C=(2m)^{n/2},\quad \sigma=1/s=n/2; \tag{6.6}$$

$$\text{relativistic: } C=c^{-n},\quad \sigma=1/s=n; \tag{6.6}$$

$$\text{Fermi-Dirac: } \beta=1;\quad \text{Bose-Einstein: } \beta=-1; \tag{6.7}$$

$$\mathbf{b}=-(Nk/V)[1-(\sigma-1)a_1\beta x+(2\sigma-1)a_2(\beta x)^2-(3\sigma-1)a_3(\beta x)^3], \tag{6.8}$$

$$\mathbf{c}=-(\sigma+1)(Nk/V)^2[1-(\sigma-2)a_1\beta x+(\sigma-1)(2a_2-a_1^2)(\beta x)^2-(3\sigma-2)(a_3-a_1a_2)(\beta x)^3], \tag{6.9}$$

$$\mathbf{l}=-(NkT/V^2)[1+2a_1\beta x-3a_2(\beta x)^2+4a_3(\beta x)^3], \tag{6.10}$$

$$\mathbf{n}=(\sigma Nk/T)[1-(\sigma-1)a_1\beta x+(2\sigma-1)a_2(\beta x)^2-(3\sigma-1)a_3(\beta x)^3], \tag{6.11}$$

$$\mathbf{A}_1=(\sigma Nk/VT)[(\sigma-1)a_1\beta x-2(2\sigma-1)a_2(\beta x)^2+3(3\sigma-1)a_3(\beta x)^3], \tag{6.12}$$

$$\mathbf{A}_2=(Nk/V^2)[1-2(\sigma-1)a_1\beta x+3(2\sigma-1)a_2(\beta x)-4(3\sigma-1)a_3(\beta x)^3], \tag{6.13}$$

$$\mathbf{A}_3=(2NkT/V^3)[1+3a_1\beta x-6a_2(\beta x)^2+10a_3(\beta x)^3], \tag{6.14}$$

$$\mathbf{A}_4=(Nk/T^2)[\sigma-(\sigma^2-1)a_1\beta x+(4\sigma^2-1)a_2(\beta x)^2-(9\sigma^2-1)a_3(\beta x)^3]. \tag{6.15}$$

[12] O. K. Rice, J. Chem. Phys. **10**, 653 (1942); **12**, 1 (1944).
[13] R. H. Fowler and E. A. Gugenheim, *Statistical Thermodynamics* (Cambridge University Press, Cambridge, 1939), p. 128.
[14] H. Einbinder, Phys. Rev. **74**, 803 (1948).
[15] H. Einbinder, Phys. Rev. **74**, 805 (1948).
[16] H. Einbinder, Phys. Rev. **76**, 410 (1949).
[17] G. Gentile, Ricera Sci. **12**, 1020 (1941); A. Sommerfeld, Ber. deut. chem. Ges, **75B**, 1988 (1942).
[18] B. N. Singh, Indian J. Phys. **14**, 459 (1940); D. S. Kothari and B. N. Singh, Proc. Roy. Soc. (London) **A178**, 135 (1941).
[19] B. N. Singh, Indian J. Phys. **15**, 73 (1941); D. S. Kothari and B. N. Singh, Proc. Roy. Soc. (London) **A180**, 414 (1942).
[20] D. S. Kothari, Proc. Natl. Inst. Sci. (India) **4**, 69 (1938); B. N. Srivastava, Proc. Natl. Inst. Sci. (India) **4**, 75 (1938); D. Gogate, Phil. Mag. **25**, 694 (1938); **26**, 166 (1938).

7. APPLICATIONS

With the traditional methods, the explicit calculation of $(\partial x/\partial y)_z$ is simple if two of the variables are V and T; it is much more involved if only one is V or T, and extremely lengthy if none are V or T. Using Jacobians, all three cases are equally straightforward and their advantage for second derivatives is even more pronounced. Thus, for the van der Waals gas whose J's are given by (IV, 4), using Eqs. (1.5) and (2.5),

$$\mu=(\partial T/\partial P]_H=J(T,H)/J(P,H)$$
$$=(T\mathbf{b}-V\mathbf{l})/T\mathbf{c}\approx(2a/kT+b)/k(f/2+1), \quad (7.1)$$

$$C_p=(\partial Q/\partial T)_P=J(Q,P)/J(T,P)$$
$$=T\mathbf{c}/\mathbf{l}\approx Nk[(f/2+1)+2a/kTv], \quad (7.2)$$

$$(\partial C_p/\partial P)_T=[\partial/\partial P(\partial Q/\partial T)_P]_T$$
$$=T[\mathbf{l}J(\mathbf{c},T)-\mathbf{c}J(\mathbf{l},T)]/\mathbf{l}^3.$$
$$=T(\mathbf{l}^2\mathbf{A}_1-2\mathbf{blA}_2+\mathbf{b}^2\mathbf{A}_3)/\mathbf{l}^3\approx 2Na/kT^2. \quad (7.3)$$

In calculating second derivatives of Q and W using Eq. (2.3), the order in which the derivatives are taken must be preserved because $\int dQ$ and $\int dW$ are not independent of the path,[19a] which is necessary for $\partial^2X/\partial Y\partial Z=\partial^2X/\partial Z\partial Y$. In particular,

$$\left[\frac{\partial}{\partial P}\left(\frac{\partial Q}{\partial T}\right)_P\right]_T=\left[\frac{\partial}{\partial T}\left(\frac{\partial Q}{\partial P}\right)_T\right]_P+\left(\frac{\partial V}{\partial T}\right)_P. \quad (7.4)$$

Another illustration is the Joule-Kelvin effect for a quantum gas which has been treated quite extensively.[20,21] The problem is given $P(V,T)$ and $E(V,T)$, find explicitly $\mu=(\partial T/\partial P)_H$. Singh, who treats the general case to third order in βx using standard methods, is forced to employ four thermodynamic relations obtaining μ only after lengthy calculation. Using Eq. (7.1) and the J's of Sec. 6 gives μ directly as the ratio of two power series,

$$\mu=-\left(\frac{V}{Nk}\right)\frac{a_1\beta x-2a_2(\beta x)^2+3a_3(\beta x)^3}{1-(\sigma-2)a_1\beta x+(\sigma-1)(2a_2-a_1^2)(\beta x)^2}. \quad (7.5)$$

Expanding the denominator yields

$$\mu=-(V/Nk)\{a_1\beta x-[(\sigma+2)a_1^2-2a_2](\beta x)^2$$
$$+[3a_3-(4\sigma-6)a_1^2a_2-(\sigma^2-3\sigma+3)a_1^3](\beta x)^3\}, \quad (7.6)$$

which except for a typographical error agrees with Singh's result. This demonstration of the utility of Jacobians becomes even more convincing when a large number of difficult derivatives must be calculated.

Jacobians provide a systematic method for testing alternate theories of liquids and gases, especially semi-empirical treatments[22] which depend on one or more parameters whose values must be determined from experimental data. An example is the important semi-empirical theory of the gas-liquid region near the critical point advanced by Lennard-Jones and Devonshire.[23] Their simplest cage model leads to the partition function, referred to a single particle, of

$$Q=(2\pi mkT/h^2)^{\frac{3}{2}}v\exp[-\psi(v)/kT], \quad (7.7)$$

where the atoms are taken as point masses and the cellar potential $\psi(v)$ is only a function of the cellular volume, $v=V/N$. In their most general formulation,

$$Q=(2\pi mkT/h^2)^{\frac{3}{2}}\kappa v[1-(v_0/v)^{\frac{1}{3}}]^3\exp-\phi(v,T)/kT, \quad (7.8)$$

where each atom has a volume v_0. The problem is to find a suitable $\psi(v)$ or $\phi(v,T)$, which best represents the experimental data.[24] Lennard-Jones and Devonshire choose

$$\phi(v)=Av^{-m}-Bv^{-n}, \quad (7.9)$$

with $m=4$ and $n=2$, which is found to hold for some inert gases[25] and fit A and B using the experimental values of the critical volume and the Kamerlingh Onnes constant, $K=kT_c/P_cv_c$. Such a treatment based on only two points is hardly satisfactory, since they aim to fit entire curves. A more systematic approach would fit three independent reference J's to the experimental data, thus assuring the best over-all thermodynamic description of the system. In this way, instead of singling out a few special properties, the entire problem is treated en bloc.

8. THE GENERAL THEORY OF THERMODYNAMIC FLUCTUATIONS

A final application will be the theory of thermodynamic fluctuations which was inaugurated by Smoluchowski[26] and later applied by Einstein[27] to the scattering of light by liquids, providing an elegant explanation of the opalescence observed at the critical point. Since then a large number of individual fluctuations have been calculated.[28] Kar[29] has attempted to derive formulas connecting these different fluctuations, but his work is vitiated by numerous errors and a lack of rigor.[30] The theory has been summarized in a number of places.[31]

To maintain the symmetry of the relations to be derived, **a** is not set equal to unity in this section.

The thermodynamic probability $\mathcal{P}$ of a given state for a system obeying classical statistics is

$$\mathcal{P}=C_1e^{\Delta S/k}=C_2e^{-\Delta E/kT}=C_3e^{-\Delta A/kT}=C_4e^{-\Delta G/kT}, \quad (8.1)$$
$$(\Delta V=\Delta T=0)\ (\Delta V=\Delta S=0)\quad (\Delta V=\Delta T=0)\quad (\Delta P=\Delta T=0)$$

[19a] J. C. Slater, *Introduction to Chemical Physics* (McGraw-Hill Book Company, Inc., New York, 1939), p. 8.
[21] B. N. Singh, Indian J. Phys. **14**, 459 (1940).
[22] J. Kincaid and H. Eyring, J. Chem. Phys. **5**, 587 (1937).
[23] J. F. Lennard-Jones and A. F. Devonshire, Proc. Roy. Soc. (London) **A163**, 53 (1937); **A165**, 1 (1937).
[24] T. L. Hill, J. Phys. Colloid Chem. **51**, 1219 (1947).
[25] J. F. Lennard-Jones, Physica **4**, 941 (1937).
[26] M. Smoluchowski, Ann. Physik **25**, 205 (1908).
[27] A. Einstein, Ann. Physik **33**, 1275 (1910); K. Bai, Proc. Indian Acad. Sci. **A15**, 338 (1942); **A18**, 190 (1943); B. Zimm, J. Chem. Phys. **13**, 141 (1945).
[28] F. Hauer, Ann. Physik **47**, 365 (1915); M. Laue, Physik. Z. **18**, 542 (1917); R. Furth, Physik. Z. **20**, 350 (1919).
[29] K. Kar, Phys. Rev. **21**, 672 (1923); Physik. Z. **24**, 429 (1923); **25**, 397 (1924).
[30] R. Furth, Physik. Z. **25**, 111 (1924).
[31] R. Furth, *Swankungserscheinugen in der Physik* (Viewig, Braunschweig, 1920); L. Landau and E. Lifshitz, *Statistical Physics* (Oxford University Press, London, 1938), p. 110.

where ΔX is the deviation from the equilibrium state $X-X_0$ and the deviations of the variables in parenthesis must be constant for the total system. The form in ΔS is due to Boltzmann, while that in ΔE is associated with Gibbs and that in ΔA with Einstein. The thermodynamic system is now divided into two parts, one very small and the other so large that it can be treated as a reservoir, i.e., a system with huge thermal capacity and invariable intensity factors. A virtual variation from equilibrium is considered between the two systems subject to the constraining conditions. The resulting deviations in the exponentials are then expanded in a Taylor series in the variables in parentheses up to square terms, leading to a bivariate normal distribution for the deviations.[32] All the equivalent forms lead to the same result, since[33]

$$-T(dS)_{V,S}=(dE)_{V,S}=(dA)_{V,T}=(dG)_{P,T}. \quad (8.2)$$

Thus expanding ΔA,

$$\Delta A=\left(\frac{\partial A}{\partial T}\right)_V\Delta T+\left(\frac{\partial A}{\partial V}\right)_T\Delta V+\frac{1}{2}\left[\left(\frac{\partial^2 A}{\partial T^2}\right)_V(\Delta T)^2+2\frac{\partial^2 A}{\partial T\partial V}\Delta T\Delta V+\left(\frac{\partial^2 A}{\partial V^2}\right)_T(\Delta V)^2\right], \quad (8.3)$$

where the derivatives refer to the reservoir. But $\Delta V=\Delta T=0$, and $(\partial^2 A/\partial V^2)_T=-(\partial P/\partial V)_T$, $(\partial^2 A/\partial V^2)_T=(\partial S/\partial T)_V=C_v/T$, so

$$\Delta A=\tfrac{1}{2}[(C_v/T)(\Delta T)^2-(\partial P/\partial V)_T(\Delta V)^2], \quad (8.4)$$

or using reference J's

$$\Delta A=\tfrac{1}{2}[\mathbf{n}(\Delta T)^2-\mathbf{l}(\Delta V)^2]/\mathbf{a}. \quad (8.5)$$

Therefore,

$$\mathcal{P}=C_3\exp-\tfrac{1}{2}[\mathbf{n}(\Delta T)^2-\mathbf{l}(\Delta V)^2]/kT\mathbf{a}. \quad (8.6)$$

Now

$$\Delta T=\left(\frac{\partial T}{\partial S}\right)_P\Delta S+\left(\frac{\partial T}{\partial P}\right)_S\Delta P=(\mathbf{l}\Delta S+\mathbf{b}\Delta P)/\mathbf{c}, \quad (8.7)$$

$$\Delta V=\left(\frac{\partial V}{\partial S}\right)_P\Delta S+\left(\frac{\partial V}{\partial P}\right)_S\Delta P=(\mathbf{b}\Delta S+\mathbf{n}\Delta P)/\mathbf{c}. \quad (8.8)$$

Substituting in Eq. (8.5) yields

$$\Delta A=\tfrac{1}{2}(\mathbf{ln}-\mathbf{b}^2)[\mathbf{l}(\Delta S)^2-\mathbf{n}(\Delta P)^2]/\mathbf{ac}^2. \quad (8.9)$$

Since $\mathbf{ac}=\mathbf{ln}-\mathbf{b}^2$,

$$\mathcal{P}=C_3\exp-\tfrac{1}{2}[\mathbf{l}(\Delta S)^2-\mathbf{n}(\Delta P)^2]/kT\mathbf{c}. \quad (8.10)$$

The normal distribution for two statistically independent variables is[34]

$$\mathcal{P}=C\exp-\tfrac{1}{2}[X_1^2/\sigma X_1^2+X_2^2/\sigma X_2^2]. \quad (8.11)$$

[32] R. F. Green and H. B. Callen, Phys. Rev. **83**, 1231 (1951).
[33] Reference 10, p. 110.
[34] H. Cramèr, *Mathematical Methods of Statistics* (Princeton University Press, Princeton, 1946), p. 287.

Whence it follows from Eqs. (8.6) and (8.10) that ΔT and ΔV, and ΔS and ΔP are independent and normally distributed variates, whose variances equal

$$\sigma_{\Delta T}^2=kT\mathbf{a}/\mathbf{n}, \quad (8.12) \qquad \sigma_{\Delta V}^2=-kT\mathbf{a}/\mathbf{l}, \quad (8.13)$$

$$\sigma_{\Delta S}^2=kT\mathbf{c}/\mathbf{l}, \quad (8.14) \qquad \sigma_{\Delta P}^2=-kT\mathbf{c}/\mathbf{n}. \quad (8.15)$$

Since any thermodynamic fluctuation can be expressed as a linear combination of two others, all fluctuation moments can be derived from the distribution functions (8.6) or (8.9). Thus

$$\Delta Y_1=[J(Y_1,X_2)\Delta X_1-J(Y_1,X_1)\Delta X_2]/J(X_1,X_2), \quad (8.16)$$

$$\Delta Y_2=[J(Y_2,X_2)\Delta X_1-J(Y_1,X_1)\Delta X_2]/J(X_1,X_2). \quad (8.17)$$

Multiplying ΔY_1 by ΔY_2 and taking the mathematical expectation[35] $\mathcal{E}$ of the resulting equation yields

$$\mu_{\Delta Y_1\Delta Y_2}=\{J(Y_1,X_2)J(Y_2,X_2)\sigma_{\Delta X_1}^2-[J(Y_1,X_1)J(Y_2,X_2)+J(Y_1,X_2)J(Y_2,X_1)]\mu_{\Delta X_1\Delta X_2}+J(Y_1,X_1)J(Y_2,X_1)\sigma_{\Delta X_2}^2\}/J^2(X_1,X_2), \quad (8.18)$$

since $\mathcal{E}(X_i,X_j)=\mu_{X_iX_j}$ and $\mu_{X_iX_i}=\sigma_{X_i}^2$, where $\mu_{X_iX_j}$ is the mean value of the product X_iX_j. When ΔX_1 and ΔX_2 are independent, their covariance $\mu_{\Delta X_1\Delta X_2}$ vanishes. If $\Delta X_1=\Delta T$ and $\Delta X_2=\Delta V$, then using Eqs. (8.12) and (8.13),

$$\mu_{\Delta Y_1\Delta Y_2}=kT[J(Y_1,V)J(Y_2,V)/\mathbf{n}-J(Y_1,T)J(Y_2,T)/\mathbf{l}]/\mathbf{a}, \quad (8.19)$$

or if $\Delta X_1=\Delta S$ and $\Delta X_2=\Delta P$, then

$$\mu_{\Delta Y_1\Delta Y_2}=kT[J(Y_1,P)J(Y_2,P)/\mathbf{l}-J(Y_1,S)J(Y_2,S)/\mathbf{n}]/\mathbf{c}. \quad (8.20)$$

From either (8.19) or (8.20) the variance and covariance of any thermodynamic fluctuation can be readily calculated, e.g.,

$$\mu_{\Delta T\Delta S}=kT, \quad (8.21) \qquad \mu_{\Delta T\Delta P}=-kT\mathbf{b}/\mathbf{n}, \quad (8.22)$$

$$\mu_{\Delta V\Delta S}=kT\mathbf{b}/\mathbf{l}, \quad (8.23) \qquad \mu_{\Delta V\Delta P}=-kT, \quad (8.24)$$

$$\sigma_E^2=-kT(P^2\mathbf{a}+2PT\mathbf{b}-T^2\mathbf{c})/\mathbf{l}. \quad (8.25)$$

The index of correlation $\rho_{X_1X_2}$ between X_1 and X_2 is defined as[36]

$$\rho_{X_1X_2}=\mu^2{}_{X_1X_2}/\sigma^2{}_{X_1}\sigma^2{}_{X_2}. \quad (8.26)$$

Using Eqs. (8.12)–(8.15) and (8.21)–(8.24), then

$$\rho^2{}_{\Delta T\Delta S}=\rho^2{}_{\Delta V\Delta P}=\mathbf{nl}/\mathbf{ac}, \quad (8.27)$$

$$\rho^2{}_{\Delta T\Delta P}=\rho^2{}_{\Delta V\Delta S}=-\mathbf{b}^2/\mathbf{ac}. \quad (8.28)$$

Now

$$\rho^2{}_{\Delta Y\Delta X_1}+\rho^2{}_{\Delta Y\Delta X_2}=[\mu^2{}_{\Delta Y\Delta X_1}/\sigma^2{}_{\Delta X_1}+\mu^2{}_{\Delta Y\Delta X_2}/\sigma^2{}_{\Delta X_2}]/\sigma^2{}_{\Delta Y}. \quad (8.29)$$

[35] Reference 34, p. 170.
[36] Reference 34, p. 277.

TABLE V. Conditional variances.

$(\sigma X^2)_Y$	$Y\rightarrow$ ΔV	ΔT	ΔP	ΔS
X ↓				
ΔV	0	$-kT\mathbf{a}/\mathbf{l}$	$kT\mathbf{b}^2/\mathbf{cl}$	$-kT\mathbf{n}/\mathbf{c}$
ΔT	$kT\mathbf{a}/\mathbf{n}$	0	$kT\mathbf{l}/\mathbf{c}$	$-kT\mathbf{b}^2/\mathbf{cn}$
ΔP	$kT\mathbf{b}^2/\mathbf{an}$	$-kT\mathbf{l}/\mathbf{a}$	0	$-kT\mathbf{c}/\mathbf{n}$
ΔS	$kT\mathbf{n}/\mathbf{a}$	$-kT\mathbf{b}^2/\mathbf{al}$	$kT\mathbf{c}/\mathbf{l}$	0
ΔX	$kTJ^2(X, V)/\mathbf{an}$	$-kTJ^2(X, T)/\mathbf{al}$	$kTJ^2(X, P)/\mathbf{cl}$	$-kTJ^2(X, S)/\mathbf{cn}$

If ΔX_1 and ΔX_2 are independent ($\mu_{\Delta X_1 \Delta X_2}=0$), it follows from Eq. (8.18) that

$$\frac{\mu^2_{\Delta V \Delta X_1}}{\sigma^2_{\Delta X_1}}+\frac{\mu^2_{\Delta V \Delta X_2}}{\sigma^2_{\Delta X_2}} = \frac{[J^2(Y_1, X_2)\sigma^2_{\Delta X_1}+J^2(Y, X_1)\sigma^2_{\Delta X_2}]}{J^2(X_1, X_2)}=\sigma^2_{\Delta V}, \quad (8.30)$$

so

$$\rho^2_{\Delta V \Delta X_1}+\rho^2_{\Delta V \Delta X_2}=1. \quad (8.31)$$

From the properties of the correlation coefficient,[36] this means that any thermodynamic fluctuation ΔV can be predicted with null error from the values of the independent fluctuations ΔX_1 and ΔX_2, i.e., from either $(\Delta T, \Delta V)$ or $(\Delta S, \Delta P)$. In agreement with this equation, $\rho^2_{\Delta T \Delta S}+\rho^2_{\Delta T \Delta P}=\rho^2_{\Delta V \Delta P}+\rho^2_{\Delta V \Delta S}=1$.

The conditional variance $(\sigma {X_1}^2)_{X_2}$ is defined as the variance of X_1 when X_2 is held constant. Obviously, if X_1 and X_2 are statistically independent, the conditional variance $(\sigma {X_1}^2)_{X_2}$ is identical with the total variance $\sigma {X_1}^2$. For the general bivariate normal distribution,

$$\mathcal{P}=C \exp -\tfrac{1}{2}(a_{11}{X_1}^2-2a_{12}X_1X_2+a_{22}{X_2}^2), \quad (8.32)$$

the conditional variance is[37]

$$(\sigma {X_1}^2)_{X_2}=1/a_{11}. \quad (8.33)$$

Setting $\Delta Y_1=\Delta T$ and $\Delta Y_2=\Delta V$ in Eqs. (8.16) and (8.17), and substituting for $(\Delta T)^2$ and $(\Delta V)^2$ in the normal distribution (8.6), leads to a bivariate distribution in ΔX_1 and ΔX_2 of the form (8.26). Therefore, from Eq. (8.27),

$$(\sigma^2_{\Delta X_1})_{X_2}=\frac{kT\mathbf{a}J^2(X_1, X_2)}{\mathbf{n}J^2(X_2, T)-\mathbf{l}J^2(X_2, V)}. \quad (8.34)$$

Similarly, substituting for $(\Delta S)^2$ and $(\Delta P)^2$ in the distribution (8.10) yields an alternate expression for the conditional variance,

$$(\sigma^2_{\Delta X_1})_{\Delta X_2}=\frac{kT\mathbf{c}J^2(X_1, X_2)}{\mathbf{l}J^2(X_2, S)-\mathbf{n}J^2(X_2, P)}. \quad (8.35)$$

From these two equations, Table V has been constructed which gives explicitly the conditional variance for various combinations of ΔT, ΔV, ΔP, and ΔS. Note that

$$(\sigma_{\Delta E^2})_{\Delta V}=kT^2\mathbf{n}/\mathbf{a}, \quad (8.36)$$

so $\sigma_{\Delta E^2} \neq (\sigma_{\Delta E^2})_{\Delta V}$, which is to be expected since ΔE and ΔV are not independent fluctuations.

The formulas derived for the fluctuation moments expressed in reference J's can be written in terms of partial derivatives using Table I or explicitly calculated for the systems given in Table IV.

The dimensionless partial variance is defined as

$$(\delta {X_1}^2)_{X_2}=(\delta {X_1}^2)_{X_2}/{X_1}^2. \quad (8.37)$$

Using Tables V and (IV, 3) it follows that for a polyatomic gas composed of N molecules, each with f degrees of freedom,

$$(\delta_{\Delta T^2})_{\Delta V}=(\delta_{\Delta P^2})_{\Delta V}=2/fN, \quad (8.38)$$

$$(\delta_{\Delta V^2})_{\Delta T}=(\delta_{\Delta P^2})_{\Delta T}=1/N, \quad (8.39)$$

$$(\delta_{\Delta V^2})_{\Delta P}=(\delta_{\Delta T^2})_{\Delta P}=2/(f+2)N, \quad (8.40)$$

$$(\delta_{\Delta P^2})_{\Delta S}=(f+2)/fN, \quad (8.41)$$

$$(\delta_{\Delta V^2})_{\Delta S}=f/(f+2)N, \quad (8.42)$$

$$(\delta_{\Delta T^2})_{\Delta S}=4/f(f+2)N. \quad (8.43)$$

Since $E=\frac{1}{2}fkT$,

$$(\delta_{\Delta E^2})_{\Delta X}=(\delta_{\Delta T^2})_{\Delta X}. \quad (8.44)$$

$$(\delta_{\Delta X^2})_{\Delta E}=(\delta_{\Delta X^2})_{\Delta T}. \quad (8.45)$$

These general results include all the special cases derived by earlier workers.[28]

Finally, it should be noted that the distribution functions (8.6) and (8.10) are only valid for systems obeying classical statistics, but the general method developed here for connecting different fluctuation moments can be applied to systems obeying quantum statistics.[38] Furthermore, these distributions break down at the critical point where $(\partial P/\partial V)_T=(\partial T/\partial S)_P=0$. Smoluchowski[26] attempted to circumvent this difficulty by including higher powers of ΔV and ΔS in the Taylor expansion of ΔA, so that ΔV and ΔS are no longer normally distributed. However, these more advanced developments[39] will not be pursued further here.

[37] Reference 34, p. 289.

[38] M. Ghosh, Phil. Mag. **19**, 694 (1935).

[39] M. J. Klein and L. Tisza, Phys. Rev. **76**, 1861 (1949).

The Molar Activity Coefficients of Electrolytes Predicted from Conductivity Data†

HENRY P. MARSHALL AND ERNEST GRUNWALD
Chemistry Department, Florida State University, Tallahassee, Florida
(Received February 9, 1953)

The molar activity coefficients of uni-univalent electrolytes may be predicted on the basis of conductivity data with an accuracy of at least 1 percent up to concentrations of the order of 0.01 M in solvents of dielectric constant as low as 10. The method is based on Bjerrum's theory of ion association,[1] with the ion pair dissociation constant evaluated from conductivity data.[4–6] The success of the method depends on the use of expressions for y', the quasi-activity coefficient of the dissociated fraction, and for Λ, the equivalent conductivity, which go beyond the limiting law approximations of the interionic attraction theory. Equations (6), (8), (10), (12), and (13) have been developed for this purpose. In solvents of dielectric constant 10–40 the prediction involves no adjustable parameters characteristic of the electrolyte. The equations have been tested by comparing the conductivity-predicted y values for hydrochloric acid with those determined from emf measurements. To insure the significance of this comparison, new emf data for the cell Pt-$H_2(g)$/HCl AgCl-Ag have been obtained for 82.00 wt percent dioxane ($D=10.56$) in the concentration range 0.0001 -0.01 M.

ABOUT 30 years ago Bjerrum showed that, because of the interionic attraction effects, completely ionized electrolytes need not be completely dissociated at moderate concentration even in aqueous solution.[1] Incomplete dissociation of the electrolyte affects the molar activity coefficient y, as shown for symmetrical electrolytes by the equation

$$y=\alpha y', \tag{1}$$

where α is the degree of dissociation and y' is the quasi-activity coefficient[2] of the dissociated fraction. Bjerrum developed expressions[1] for α and y' as functions of the temperature T, of the electrolyte concentration c, of the dielectric constant D, of the ionic valency Z, and of the quasi-dissociation constant[2] of the ion pairs,

$$K=\frac{\alpha^2 y'^2 c}{(1-\alpha)}, \tag{2}$$

which he treated as an adjustable parameter.

More recently Fuoss[4] gave a rigorous treatment of Bjerrum's theory of ion association which he, Kraus, and others applied with considerable success to the conductivity of a number of incompletely dissociated electrolytes.[5,6] According to the theory, the conductometric ion pair dissociation constant for completely ionized electrolytes is identical with Bjerrum's K. This means that K is experimentally accessible and therefore that y may be predicted without adjustable parameters, at least in principle.

It is the purpose of the present paper to show that y may in fact be obtained from conductivity data with an accuracy often exceeding 1–2 percent. The discussion, will be limited to solutions containing a single uni-univalent electrolyte under conditions where association into higher ion aggregates, namely triple or multiple ions, is negligible. The paper will consist of the following parts:

(*A*) *The Dependence of y' and of the Equivalent Conductivity Λ on the Ionic Strength $\mu=\alpha c$.* In order to evaluate K and y with sufficient accuracy, it is necessary to carry the approximations for y' and Λ beyond the limiting laws of the interionic attraction theory.

(*B*) *Comparison of Predicted and Observed Activity Coefficients for Hydrochloric Acid.* Values predicted from conductivity data are compared with those based on the emf of the cell

$$\text{Pt}-\text{H}_2(1\text{ atmos})/\text{HCl}(c)/\text{AgCl}-\text{Ag}, \tag{3}$$

in a number of hydroxylic solvents where the electrolyte is only partly dissociated, ranging in dielectric constant from 40 to 10.

(*C*) *Experimental Part.* New emf measurements will be reported for the cell (3) in 82.00 percent (by weight) aqueous dioxane ($D=10.56$) at 25.0° in the concentration range 0.01 to 0.001 M.

DEPENDENCE OF y' AND Λ ON IONIC STRENGTH

General Remarks

The calculation of y' and Λ from the interionic attraction theory requires a precise definition of ion association. The ion pair distribution function $G(r)$, as derived by Fuoss[4] and illustrated in Fig. 1(a), has a shallow minimum near the interionic distance $r=q=|Z_1Z_2|\epsilon^2/2DkT$, where ϵ is the unit of ionic charge

† Supported by the Office of Ordinance Research, U. S. Army.

[1] N. Bjerrum, Kgl. Danske Videnskab. Selskab, Math-fys. Medd. 7, No. 9 (1926).

[2] The prefix *quasi* is used to indicate that ion association, as described by Bjerrum, is not a typical chemical equilibrium. This is because the two ionized fractions involved are parts of a single chemical species. Nevertheless the quantitative description of this phenomenon by means of Eqs. (1) and (2) is formally analogous to that of a typical chemical dissociation equilibrium such as the ionization of a weak acid in water (see reference 3).

[3] R. H. Fowler and E. A. Guggenheim, *Statistical Thermodynamics* (Cambridge University Press, New York, 1949), pp. 409–415.

[4] R. M. Fuoss, Trans. Faraday Soc. 30, 967 (1934).

[5] R. M. Fuoss and C. A. Kraus, J. Am. Chem. Soc. 55, 476 (1933).

[6] R. M. Fuoss, J. Am. Chem. Soc. 57, 488 (1935).

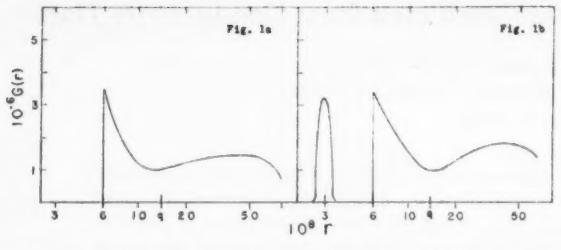

FIG. 1. Ion pair distribution as a function, $G(r)$, of interionic distance for uni-univalent electrolytes at 25°. (a) The Fuoss function; $D=20$, $c=0.001$ M, $s=6.00$A°. Electrolyte is completely ionized. (b) $G(r)$ for incomplete ionization; $D=20$, $c=0.001$ M, $s=6.00$A°, $a=3.00$A°. The scale of the abscissas is logarithmic.

and k is Boltzmann's constant. This distance q is chosen[1,4] as the basis for defining ion association: an ion pair is considered associated if $r/q<1$, and is dissociated if $r/q>1$. On the basis of this definition Bjerrum[1] has obtained the expression for K,

$$K=1000/32\pi Nq^3Q(b), \tag{4}$$

where N is Avogadro's number, $b=2q/s$, s is the effective distance of closest approach of the two ions [see Fig. 1(a)], and $Q(b)$ is a function the values of which have been tabulated.[1,7a] In support of this somewhat arbitrary definition of ion association, there is considerable evidence that ion pairs with $r/q<1$ do not contribute appreciably to the measured conductivity. For example, the conductometric values of K for completely ionized electrolytes such as tetra-isoamylammonium nitrate vary with solvent in accordance with Eq. (4), the value of s being quite constant and of a reasonable magnitude.[7b]

The definition of ion association on the basis of $r/q<1$ remains valid even if part of the nonconducting fraction is unionized. Figure 1(b) shows $G(r)$ for a case, such as the ionization of a weak in a medium of low dielectric constant, which may be represented by the equilibria

$$C-A=C^+A^-=C^++A^-.$$

Equation (1) still applies in this case, with α derived from the conductometric dissociation constant which is now smaller than expected from Bjerrum's equation (4). Similarly Eq. (1) still applies, with α derived conductometrically, even if the mutual potential energy of the ion pairs is not strictly coulombic as assumed in Bjerrum's theory (i.e., if $V\neq Z_1Z_2\epsilon^2/Dr$), provided that the deviations occur at $r/q<1$. Such deviations are to be expected in varying degrees for all electrolytes caused by such factors as desolvation, decrease of the effective dielectric constant below the macroscopic value, and deformation of the ions,[8-10] but the magnitudes of these deviations should decrease rapidly with distance and should in many cases be negligible for $r>q$. Thus the method for predicting y on the basis of Eq. (1) is particularly fortunate, since the theoretically troublesome and highly specific short-range interionic effects are taken care of by direct measurement of K, whereas the interionic attraction theory is used only at the longer distances where it is likely to be valid.

Figure 1 shows $G(r)$ for a medium of $D=20$ and $q>s$. As D increases, q decreases, and since s remains approximately constant, eventually $q<s$. When this occurs, the effective distance of closest approach of the conducting portion of the electrolyte is s rather than q.

Expressions for y' for Uni-univalent Electrolytes

In order to obtain an accuracy of at least 1–2 percent in y for uni-univalent electrolytes up to concentrations of the order of 0.01 M, it is necessary to use a better approximation than the Debye-Hückel limiting law for y'. For the case $s>q$, it is sufficient to use Debye's first approximation,[7c]

$$\log y'=(-S\sqrt{\mu})/(1+As\sqrt{\mu}), \tag{5}$$

where S, the limiting slope, is equal[11] to $1.825\times10^6/D^{\frac{3}{2}}T^{\frac{3}{2}}$, and $A=50.30\times10^8/D^{\frac{1}{2}}T^{\frac{1}{2}}$.

For calculating $\log y'$ when $q>s$, we recognize two different models which *a priori* are both reasonable. The first of these assumes that the degree of association of the electrolyte and the effective distance of closest approach of two free ions remain constant during the reversible charging, the latter being equal to q. The resultant expression[1] for y' is analogous to Eq. (5) with q substituted for s, namely

$$\log y'=(-S\sqrt{\mu}/(1+Aq\sqrt{\mu})$$
$$=(-S\sqrt{\mu})/(1+2.303\,S\sqrt{\mu}). \tag{6}$$

The second model assumes that during the reversible charging the degree of association and the effective distance of closest approach of the free ions may vary. At each stage in the reversible charging, the state of the electrolyte is still described by Bjerrum's equations, but one now uses the instantaneous fractional charges of the ions rather than their final full charges. The application of this model is convenient

[7] H. S. Harned and B. B. Owen, *The Physical Chemistry of Electrolytic Solutions* (Reinhold Publishing Corporation, New York, 1950), second edition: (a) pp. 122–124; (b) pp. 190–193; (c) pp. 37–39; (d) p. 32; (e) p. 537; (f) pp. 379–383; (g) Chap. 4; (h) Chap. 10.

[8] P. Debye and L. Pauling, J. Am. Chem. Soc. **47**, 2129 (1925).
[9] H. S. Frank, J. Am. Chem. Soc. **63**, 1789 (1941).
[10] For many completely ionized electrolytes, $G(r)$ may well resemble Fig. 1(b). The distance s then corresponds to separation of the ions by an approximately monomolecular layer of solvent molecules. [See, for example, Spedding, Porter, and Wright, J. Am. Chem. Soc. **74**, 2781 (1952).] To pierce this layer and to bring the ions into direct contact at a in many cases requires considerable activation energy. [See, for example, Hawdon, Hughes, and Ingold, J. Chem. Soc. 2499 (1952).] Thus $G(r)\approx0$ between s and a, as in Fig. 1(b).
[11] Numerical values of S, A, and B are based on the compilation of universal constants by J. W. M. DuMond and E. R. Cohen, Am. Scientist **40**, 447 (1952).

only for the Güntelberg charging process,[12] and is especially simple in the case $q \gg s$, as follows.

Consider the charging of a given univalent cation at the instant when its fractional charge is $\lambda\epsilon$. According to Bjerrum's definition,[1] this ion is "free" or unassociated if the distance to the nearest free neighbor ion is at least $\lambda\epsilon^2 2DkT=\lambda q$. In order to get the maximum reduction in the charging-work due to the ionic atmosphere, it is therefore necessary to set the instantaneous distance of closest approach equal to λq. Thus,

$$-\ln y' = \frac{1}{kT}\int_0^1 \frac{\lambda\epsilon^2\kappa d\lambda}{D(1+\kappa\lambda q)} = \frac{\epsilon^2[\kappa q - \ln(1+\kappa q)]}{\kappa q^2 DkT}, \quad (7)$$

where $1/\kappa$, the effective thickness of the ionic atmosphere, is defined as usual.[1,7d] Since the expression (7) is not very convenient for calculation, we have in actual practice obtained y' from the equation

$$\log y' = \frac{-S\sqrt{\mu}}{(1+2.303\,S\sqrt{\mu})^{\frac{1}{2}}}, \quad (8)$$

which can be shown to be a good approximation to Eq. (7).

We have tried to confirm the validity of Eq. (8) by use of the integral charging method of Debye and Hückel.[13] At a given stage in the charging process, when the ions bear the charge $\lambda Z\epsilon$, the effective distance of closest approach of the free ions is $\lambda^2\epsilon^2/2DkT=\lambda^2 q$. Exact calculation of the charging work is difficult because the free ion concentration is now a function of λ, varying from c at $\lambda=0$ to αc at $\lambda=1$. However, it is possible to estimate the upper and lower limits to the value of $\log y'$ by assuming the free ion concentration as constant at either αc or c. The corresponding limits can be shown to be given approximately by

$$\frac{-S(\alpha c)^{\frac{1}{2}}}{[1+2.303\,S(\alpha c)^{\frac{1}{2}}]^{\frac{1}{2}}} > \log y' > \frac{-S\sqrt{c}}{(1+2.303\,S\sqrt{c})^{\frac{1}{2}}},$$

with the correct value of $\log y'$ closer to the upper limit than to the lower limit.

When s is not very much less than q, expression (8) becomes inaccurate. In the charging of a given "free" ion by the Güntelberg method, the effective distance of closest approach to the nearest ion neighbor is equal to λq only when $\lambda > s/q$, and it is equal to s when $\lambda < s/q$. Hence,

$$-\ln y' = \frac{1}{kT}\int_0^{s/q} \frac{\lambda\epsilon^2\kappa d\lambda}{D(1+\kappa s)} + \int_{s/q}^1 \frac{\lambda\epsilon^2\kappa d\lambda}{D(1+\kappa\lambda q)}. \quad (9)$$

A convenient and good approximation to the exact solution of Eq. (9) is the expression

$$\log y' = -\frac{S\sqrt{\mu}}{(1+2.303\,S\sqrt{\mu})^{\frac{1}{2}}} + \frac{Bs^3\mu}{(1+As\sqrt{\mu})^{\frac{1}{2}}}, \quad (10)$$

where $B=43.84\times10^{20}$ if s is expressed[11] in cm. Finally, when $s\approx q$, the two models for calculating y' become indistinguishable, and $\log y'$ is given by Eq. (6).

As is clear from Eqs. (6), (8), and (10), the values of y' calculated from the two models are different when $s<q$. In these cases we prefer to use Eqs. (8) and (10), partly because the charging process leading to Eq. (6) does not seem to us to be truly reversible in the thermodynamic sense, and partly because (8) and (10) lead to y values in better agreement with observations.

Expressions for Λ and Calculation of K

K may be calculated from conductivity data by well-known methods[5,6,14] when y' and Λ have been expressed as functions of the ionic strength. For example, in the method described by Fuoss and Kraus[5] y' was calculated from Eq. (5) and Λ from the limiting law of Onsager,[7g]

$$\Lambda/\alpha = \Lambda_0 - S_\Lambda(\alpha c)^{\frac{1}{2}}. \quad (11)$$

In a later improvement of this method,[6] Eq. (11) was retained for Λ but, for the sake of consistency, y' was calculated from the Debye-Hückel limiting law. In this form the method has been widely used and the fit of the experimental conductivity data has generally been good.

We have found that the method based on Eqs. (1) and (2) and on the limiting laws (LL) for y' and Λ usually fails to fit the observed y values with sufficient accuracy in solvents where ion association is appreciable. The situation is not improved significantly when Eqs. (5), (6), or (8) are used instead of the limiting law for y'. In order to predict y on the basis of conductivity data it therefore seemed to us to be necessary also to carry the expression for Λ beyond the limiting approximation.

The expressions for Λ which we finally adopted are as follows:

When $s>q$, $\Lambda/\alpha=\Lambda_0-S_\Lambda(\alpha c)^{\frac{1}{2}}[1+As(\alpha c)^{\frac{1}{2}}]$. (12)

When $q>s$, $\Lambda/\alpha=\Lambda_0-S_\Lambda(\alpha c)^{\frac{1}{2}}/[1+2.303\,S(\alpha c)^{\frac{1}{2}}]$. (13)

These expressions are obtained from Eq. (11) by dividing the term $S_\Lambda(\alpha c)^{\frac{1}{2}}$, which corrects for the interionic effects at limiting concentrations, by the divisors $(1+\kappa s)$ or $(1+\kappa q)$, respectively. The expressions may be justified in part on the basis of theory: the electrophoretic term in Onsager's equation is now given correctly to the first approximation, and the equally important term due to force transfer is changed at least in the right direction. More convincing perhaps is the justification on the basis of empirical evidence. Equation (12) is practically equivalent to Shedlovsky's very successful empirical equation[15] for the equivalent conductance of strong electrolytes in water, with the

[12] N. Bjerrum, Z. physik. Chem. **119**, 145 (1926).
[13] P. Debye and E. Hückel, Physik. Z. **24**, 185, 305 (1923).
[14] C. A. Kraus and W. C. Bray, J. Am. Chem. Soc. **35**, 1315 (1913).
[15] T. Shedlovsky, J. Am. Chem. Soc. **54**, 1405 (1932).

TABLE I. Equivalent conductances of some electrolytes in Aqueous Solution at 25°C.

Electrolyte	$10^3\,c(M)$	Λ(obs)[a]	Λ(Eq. 11)[b]	Λ(Eq. 12)[b]
HCl	0	—	426.16	426.03
	0.5	422.75	422.63	422.61
	1	421.36	421.17	421.25
$s=4.25$A°	5	415.80	415.01	451.86
	10	412.00	410.39	412.15
	20	407.24	403.85	407.33
	50	399.09	390.89	399.01
KCl	0	—	149.86	149.75
	0.5	147.81	147.75	147.70
$s=3.94$A°	1	146.95	146.87	146.88
	5	143.55	143.18	143.62
	10	141.27	140.41	141.36
	20	138.34	136.50	138.42
	50	133.37	128.73	133.28

[a] Data taken from the compilation by Harned and Owen.[7e]
[b] Assume $\alpha=1.0000$.

additional requirement that the adjustable parameter is equal to As. Since this same quantity can be determined independently from activity coefficients on the basis of Eq. (5), a direct test of Eq. (12) is possible.

Some relevant data for hydrochloric acid and potassium chloride are shown in Table I. It is seen that Eq. (12) will fit the observed equivalent conductances over the entire range of concentration, up to at least $0.05M$, within ±0.03 percent for HCl and ±0.07 percent for KCl, whereas the limiting law (11) fails to fit accurately above $c=0.001$. Moreover, the conductometric values of the parameter s, 4.25A° for HCl and 3.94A° for KCl, are in quite satisfactory agreement with the corresponding values based on activity coefficients, 4.3A° and 3.8A° calculated from Hückel's extended equation,[7f,16] or 4.47A° and 3.63A° using the theory of Stokes and Robinson.[17] This is significant evidence in favor of Eq. (12) and also, by inference, of Eq. (13).

TABLE II. The calculation of K and Λ_0 from conductivity data.

Electrolyte	Temp., °C	Equations for Λ and y'	Percent error of fit	Λ_0	10^3K	Ref.
HCl, 45 percent dioxane	25.0	*LL*	0.02	179.98	962	a
		13,6	0.02	180.02	226	
HCl, 70 percent dioxane	25.0	*LL*	0.21	92.72	8.01	a
		13,6	0.34	92.34	7.37	
		13,8	0.25	92.63	6.67	
HCl, 82 percent dioxane	25.0	*LL*	0.66	56.59	0.234	a
		13,6	0.46	54.67	0.291	
		13,8	0.52	55.49	0.259	
HCl, ethanol	25.0	*LL*	0.07	84.27	11.3	b
		13,8	0.07	84.31	9.15	
KCl, ammonia	−34.0	*LL*	0.08	345.3	0.729	c
		13,8	0.15	346.4	0.891	

[a] See reference 19.
[b] See reference 20.
[c] V. F. Hnizda and C. A. Kraus, J. Am. Chem. Soc. **71**, 1565 (1949). The dielectric constant of ammonia at −34.00° was taken as 23.45 by interpolation from values at −33.35° [G. S. Hooper and C. A. Kraus, J. Am. Chem. Soc. **56**, 2265 (1934)] and at −36.00° [J. Sedlet and T. DeVries, J. Am. Chem. Soc. **73**, 5808 (1951)].

[16] E. Hückel, Physik. Z. **26**, 93 (1925).
[17] R. H. Stokes and R. A. Robinson, J. Am. Chem. Soc. **70**, 1870 (1948).

Calculation of K (and of Λ_0) from a set of conductivity data ξ on the basis of Eq. (13) is done by successive approximations similar to those described by Fuoss and Kraus.[5] Starting with a reasonable first estimate Λ_0^I, one calculates for each point the value of

$$\alpha=\frac{1000\xi[1+2.303\,S(\alpha c)^{\frac{1}{2}}]}{c\Lambda_0^I\{1+2.303\,S(\alpha c)^{\frac{1}{2}}-[S_\Lambda(\alpha c)^{\frac{1}{2}}/\Lambda_0^I]\}}$$

and of y' from the appropriate expression (5), (6), (8), or (10). For $c<3\times10^{-7}\,D^3$, the plot of $1/\alpha\Lambda_0^I$ *vs* cy'^2 is expected[6] to be linear, with intercept equal to $1/\Lambda_0^{II}$ and slope equal to $1/K(\Lambda_0^{II})^2$. If Λ_0^{II} is much different from Λ_0^I, the procedure is repeated until the successive approximations for Λ_0 converge. In practice the convergence is as rapid as that with the equations of Fuoss and Kraus.[5]

In Table II we are comparing three methods of treating conductivity data: A.—The *LL* method of Fuoss[6]; B.—The method using Eq. (13) for Λ and (6) for log y', as required by the first of the alternative models for y'; C.—The method using Eq. (13) for Λ and either (6), (8), or (10), for log y', depending on the relative magnitudes of q and s, in accordance with the second model for calculating y'. The probable percent errors of fit are quite comparable for the three methods and do not differentiate between them.[18] Similarly, the various values of Λ_0 are not very different, the discrepancy among them exceeding 1 percent in only one case. On the other hand, the K values are quite sensitive to the method of calculation. The discrepancies are usually at least 10 percent and often much greater. Since the predicted values of y depend very much on the numerical value of K in solvents where association is appreciable, the correct choice of the method of calculation is important for our purpose. When the choice cannot be made uniquely on the basis of theory alone, one of the theoretical alternatives may be elected on the basis of superior agreement with experiment. In the present case the y values predicted using method *C* (which we prefer also on theoretical grounds) agree better with experiment than those based on method *B*, as will be shown in a later section.

COMPARISON OF PREDICTED AND OBSERVED ACTIVITY COEFFICIENTS FOR HYDROCHLORIC ACID

The available data for hydrochloric acid furnish good experimental material for the testing of Eqs. (1)-(13). The conductivity has been measured in a number of solvents,[19–24] and many of the early measurements

[18] The expectedly linear plots of $F(Z)/\Lambda$ *vs* $c\Lambda y'^2/F(Z)$ in method A and their analogs in method B and C often have slight curvature.
[19] B. B. Owen and G. W. Waters, J. Am. Chem. Soc. **60**, 2371 (1938); dielectric constants taken from Critchfield, Gibson, and Hall, J. Am. Chem. Soc. **75**, 1991 (1953).
[20] I. I. Bezman and F. H. Verhoek, J. Am. Chem. Soc. **67**, 1330 (1945).

TABLE III. Predicted values of $E°$ for hydrochloric acid,[a,b] 25.0°.

Concentration Range (M)	82 percent dioxane $E°$(mv)[c]	70 percent dioxane $E°$(mv)[c]	45 percent dioxane $E°$(mv)[c]	45 percent dioxane $E°$(mv)[d]	Ethanol $E°$(mv)[c]	Methanol $E°$(mv)[d]
0.0001–0.0002	−48.6	——	——	——	——	——
0.0002–0.0003	−48.4	——	——	——	−88.0	——
0.0003–0.0006	−48.3	——	——	——	−88.2	——
0.0006–0.001	−48.5	66.1	——	——	−88.9	−22.1
0.001–0.002	−48.5	66.2	——	——	−88.8	−22.1
0.002–0.003	−48.4	66.8	——	——	−89.3	−22.2
0.003–0.006	−48.9	66.4	165.74	165.50	−88.5	−22.3
0.006–0.01	−49.1	65.8	165.84	165.47	−88.2	−22.9
0.01–0.02	——	——	165.83	165.35	−88.8	−23.7
0.02–0.05	——	63.6	165.65	164.76	−90.1	−24.3
0.05–0.1	——	60.1	——	——	−91.1	——

[a] The difference between molar and rational activity coefficients has been neglected in these calculations in all solvents except 45 percent dioxane, where it amounts to less than 0.06 mv at the highest concentration.
[b] The calculations for the dioxane-water mixtures are based on the recent dielectric constant values of Critchfield, Gibson, and Hall (see reference 19). At the time these were published we had already completed a set of calculations using the dielectric constants of Akerlof and Short [J. Am. Chem. Soc. 58, 1241 (1936)]. The fit was almost as good as with the more accurate recent values.
[c] y' from Eq. (8).
[d] y' from Eq. (10).
[e] y' from Eq. (6).

have in recent years been checked on the Jones bridge. The emf values for the cell,

$$\mathrm{Pt-H_2}(g,\ 1\ \mathrm{atmos})/\mathrm{HCl}(c)/\mathrm{AgCl-Ag}, \qquad (14)$$

are available down to 0.001 M concentration in many solvents,[25–28] and by means of the Nernst equation the values generate sets of numbers strictly proportional to y.

In order to predict y from conductivity data in a given solvent, we found the following procedure convenient. First we calculated K from the available conductivity data, using the method of least squares to evaluate the slope and intercept of the required linear plot of $1/\alpha\Lambda_0{}^I$ *vs* $cy'^2\alpha\Lambda_0{}^I$ described in the previous section. Then we calculated the values of y', $(1-\alpha)c$, c, and y for a set of conveniently spaced αc values. Next we plotted y *vs* c on 50-cm precision graph paper and interpolated at the concentrations at which the emf values have been determined. Finally we substituted the predicted values of y in the Nernst equation[7h]

$$E+(2RT\ \ln cy)/F=E° \qquad (15)$$

and calculated $E°$. If the calculated values of $E°$ remained constant within their experimental error as c was varied, y was assumed to be correct.

It is difficult to estimate the experimental error of the emf data because at low concentrations there are several sources of determinate error. These include adsorption of hydrochloric acid on the cell surface[29]; introduction of acidic or basic substances from the glass walls of the cell and volumetric ware[30] (this effect is less serious in partly organic media than in water); irreversible formation of hydrochloric acid according to

$$\mathrm{AgCl}+\tfrac{1}{2}\mathrm{H_2}=\mathrm{HCl}+\mathrm{Ag} \qquad (16)$$

which occurs at an appreciable rate in the cell[29,31]; and poisoning of the electrodes, notably of the Ag-AgCl, caused by reducing impurities in the organic solvent.[26] These errors may be eliminated by suitable experimental precautions, and have been largely eliminated in this work. In our judgment the accuracy of the emf values at concentrations below 0.005 M is of the order of 0.5–1.0 mv. This is the order of internal consistency of near-duplicates whereas the precision of the measuring apparatus is often much better.

Since an error of 0.5 mv in emf corresponds to an uncertainty of about 1 percent in y, it is necessary to cover a very wide range of all variables in order to clearly demonstrate the predictability of y from conductivity data. Thus it is necessary to cover a wide range of solvents and in each solvent to cover a sufficient range of concentrations so that possible statistically significant trends in the calculated $E°$ values might be detected. For this reason we felt it was necessary to add to the existing data at least one extensive study in a solvent of rather low dielectric constant. We have therefore reinvestigated the emf of hydrochloric acid solutions in 82 percent dioxane ($D=10.56$ at 25°), covering the range from 0.01 to 0.0001 M with over 30 experimental

[21] H. Goldschmidt and P. Dahll, Z. physik. Chem. **A114**, 1 (1925).
[22] D. M. Murray-Rust and H. Hartley, Proc. Roy. Soc. (London) **A126**, 84 (1929).
[23] W. F. K. Wynne-Jones, J. Phys. Chem. **31**, 1647 (1927).
[24] L. Thomas and E. Marum, Z. physik. Chem. **A143**, 191 (1929).
[25] (a) H. S. Harned and J. O. Morrison, J. Am. Chem. Soc. **58**, 1908 (1936); (b) H. S. Harned, J. Am. Chem. Soc. **60**, 336 (1938); (c) H. S. Harned and C. Calmon, J. Am. Chem. Soc. **60**, 2130 (1938); (d) Harned, Walker, and Calmon, J. Am. Chem. Soc. **61**, 44 (1939); (e) Harned, Morrison, Walker, Donelson, and Calmon J. Am. Chem. Soc. **61**, 49 (1939).
[26] J. W. Woolcock and H. Hartley, Phil. Mag., No. (7) **5**, 1133 (1928).
[27] G. Nonhebel and H. Hartley, Phil. Mag., No. (6) **50**, 729 (1925).
[28] B. E. Conway, *Electrochemical Data* (Elsevier Publishing Company, Inc., Houston, 1952), pp. 97, 301.
[29] N. J. Anderson, Ph.D. dissertation, University of Chicago, Chicago, Illinois, 1934.
[30] C. A. Kraus and H. C. Parker, J. Am. Chem. Soc. **44**, 2429 (1922).
[31] E. F. Sieckmann, M. S. dissertation, Florida State University, Tallahassee, Florida, 1952.

points. In order to circumvent many of the problems of the Pt—H_2 electrode we have used a glass electrode which gave sufficiently stable readings in this solvent. The accuracy of these readings was tested by comparing the new emf's with those obtained previously with the Pt—H_2 electrode[25d] in the range from 0.01 to 0.001 M where the two series overlap. Details of the new measments are described in the experimental section. The measurements are accurate to about 0.3 mv.

The pertinent results are summarized in Table III. In order to save space, the data for each solvent have been grouped in convenient concentration ranges varying from 0.0001 to 0.1 M. The values of $E°$ listed in Table III for a given concentration range are the means of the individual $E°$ values calculated for each of the experimental points in the range. The data for the individual solvents are as follows.

82 Percent Dioxane ($D=10.56$; $q=26.53$A°)

This solvent has the lowest dielectric constant of the solvents listed in the Table and hence affords the most critical test of the theory. The calculations are based on Eqs. (8) and (13). K is given in Table II. The emf data are our own and are given in Table VII. Below 0.003 M, the $E°$ values are constant at −48.5 mv, the deviations of the individual values from this figure being random. Above 0.003 M the $E°$ values drift downward slightly but significantly. Yet at the highest concentration, 0.01 M, the observed value of y is still only 1.4 percent greater than the predicted value even though over 70 percent of the electrolyte is associated.

In order to show more clearly that the agreement between the predicted and observed values of y is really excellent over the entire range of c and α, we are presenting some relevant data at rounded concentrations in Table IV. As is shown in this Table, the mean deviation between the two sets of y values is only 0.0014, or 0.5 percent. For comparison, the fit of methods A and B is not nearly so good, as is shown in Table V.

TABLE IV. Data for hydrochloric acid in 82 percent dioxane, 25°.

$10^4\,c(M)$	y(observed)[a]	y(predicted)[b]	α(predicted)
1.5	0.624	0.623	0.776
2	0.580	0.581	0.740
3	0.521	0.519	0.688
4	0.475	0.476	0.649
5	0.440	0.444	0.619
6	0.417	0.419	0.594
8	0.379	0.379	0.556
10	0.349	0.350	0.527
20	0.269	0.269	0.442
30	0.228	0.228	0.395
40	0.204	0.202_5	0.365
50	0.185_5	0.184_2	0.344
60	0.172_3	0.1703	0.327
80	0.152_5	0.1506	0.302
100	0.137_9	0.1360	0.284

[a] $E°=-48.5$ mv.
[b] $K=2.59\times10^{-4}$.

TABLE V. Values of $E°$ for cell (3) in 82.00 percent dioxane calculated by various methods, 25.0°.

	$-E°$(mv), Method[a]			
$10^4\,c(M)$	A	B	C	D
1.5	50.7	47.0	48.5	44.8
3	51.5	46.5	48.7	44.5
6	52.2	45.7	48.3	44.3
10	53.1	45.5	48.3	44.6
20	54.5	45.0	48.4	44.2
30	55.7	44.8	48.5	43.3
40	57.4	44.9	48.9	42.3
60	60.2	45.3	49.1	—
100	67.7	45.0	49.2	—

[a] Description of methods: A—LL; B—Eqs. (6), (13); C—Eqs. (8), (13); D—Extended terms solution of Gronwall, La Mer, and Sandved (see reference 33), $s=5.70$A°.

70 Percent Dioxane ($D=19.07$; $q=14.69$A°)

The calculations are based on the emf data of Harned, Morrison, and Calmon[25a,c] and on the conductivity data of Owen and Waters.[19] $K=0.00667$ as given in Table II, and y' is obtained from Eq. (8). As is shown in Table III, the calculated values of $E°$ remain satisfactorily constant at 66.4±0.2 mv up to $c=0.006$ M. Above this concentration the values drift significantly downward. At 0.01 M the predicted value of y is still within 2 percent of the observed value, but at higher concentrations the error increases rapidly.

45 Percent Dioxane ($D=40.25$; $q=6.96$A°)

The calculations are based on the emf data of Harned and Morrison and the conductivity data of Owen and Waters[19] (Table II). Two sets of calculations are presented. In the first set, where y' is obtained from Eq. (6), $E°$ is seen to remain constant at 165.8 mv up to 0.02 M concentration. In the second set y' is obtained from Eq. (10) with $s=5.4$A° as calculated from K by means of Eq. (4). $E°$ is now constant at 165.5 mv up to 0.01 M concentration. Unfortunately the emf data do not extend to sufficiently low concentrations to define the limiting values of $E°$ at infinite dilution. Calculations based on the extended terms theory of Gronwall, La Mer, and Sandved[7,32] lead to $E°=165.5$ mv with s adjusted to 5.4A°, thus favoring the second set.

Ethanol ($D=24.3$; $q=11.53$A°)

The emf data are those of Woolcock and Hartley.[26] There are several sets of conductivity data. The recent data of Bezman and Verhoek[20] give 0.00913 for K, which is the value we have used. (See Table II.) In addition there are the closely agreeing values of 0.00885 (Wynne-Jones),[23] 0.00870 (Murray-Rust and Hartley),[23] and the somewhat discrepant value of 0.0148 (Goldschmidt and Dahll).[21] The values of y' have been calculated from Eq. (8). As is seen in Table III, the

[32] Gronwall, La Mer, and Sandved, Physik. Z. 29, 358 (1929).

fit of the predicted y values is good. The calculated values of $E°$ vary at random about an average value of -88.6 mv up to concentrations of the order of 0.02 M. At still higher concentrations there is a slight but significant downward drift. Thus at 0.1 M, the predicted value of y is in error by about 5 percent.

Methanol ($D=32.5$; $q=8.62$A°)

The emf data are those of Austin, Hunt, Johnson, and Parton.[28] The conductometric K values are 0.068 (Murray-Rust and Hartley),[22] 0.056 (Wynne-Jones),[23] and 0.041 (Goldschmidt and Dahll).[21] Although the rather large discrepancies between these three values are troublesome, a highly accurate estimate of K is fortunately not required when K is large, the resultant errors in α and y being much less than the original error in K. The $E°$ values in Table III have been calculated using Eq. (10) for y' with s estimated as 5.0A°, and using the value 0.06 for K. It is clear from Table III that the predicted y values fit as well as can be expected, being in error by about 2 percent at 0.01 M concentration. The best estimate of $E°$ at infinite dilution is -22.1 mv on the basis of this treatment.

COMPARISONS OF VARIOUS METHODS FOR CALCULATING THE MOLAR ACTIVITY COEFFICIENTS OF ELECTROLYTES

In the preceding section we have shown that method C of treating conductivity data leads to predicted y values that are remarkably consistent with experimental emf data for cell (3) over a wide range of solvents and at concentrations ranging from 0.0001 to 0.01 M. The constancy of the predicted $E°$ values in a given solvent proves that the y values are accurate, at least up to a proportionality constant. The latter is probably near unity but cannot be evaluated with certainty because extrapolation of $E°$ to infinite dilution cannot be done with perfect confidence even from the lowest concentrations. In order to define more closely the range of uncertainty of $E°$, it is instructive to compare the present results with those obtained by other methods.

One such comparison has already been made for 45 percent dioxane. As has been shown, three different methods have led to almost equal estimates of $E°$, 165.6±0.2 mv, which makes it highly probable that the true value at infinite dilution is thus defined. Another comparison for 82 percent dioxane is shown in Table V. In this Table, methods A, B, and C employ conductivity data and do not involve any adjustable parameters. Method D uses the extended terms solution of the Debye-Hückel equations due to Gronwall, La Mer, and Sandved.[32] It predicts y without recourse to conductivity data but treats s as an adjustable parameter.

Method A employs the limiting laws for y' and Λ. The fit to the emf data is poor. $E°$ varies considerably with concentration and is in all cases below -50 mv. Method B employs Eqs. (6) and (13). $E°$ is quite constant at -45.0 mv between 0.01 and 0.002 M but decreases steadily and significantly below 0.002 M. The limit at infinite dilution appears to be about -48 mv. Method C has already been discussed. It employs Eqs. (8) and (13), and $E°$ is constant at -48.5 mv up to 0.003 M. In method D, when s is adjusted to 5.70A°, $E°$ is constant at -44.4 mv up to 0.002 M concentration. The numerical value of s, 5.70A°, is in good agreement with the value 5.68A° calculated from the conductometric K on the basis of Eq. (4). (See Table VI.) Unfortunately the convergence of the extended terms is poor in this solvent, the highest tabulated term[7,33] still being of the same order as the next lower one. It is therefore difficult to decide on the validity of this calculation.

The data in Table V establish method C as the most satisfactory of the methods tried. Furthermore, they make it seem unlikely that the true value of $E°$ at infinite dilution will deviate from -48.5 mv by more than 5 mv, thus suggesting an outer limit to the accuracy of method C.

$E°$ Values for Cell (3) in the System Dioxane Water at Various Temperatures

Method C is successful also in fitting the observed emf data[25] at temperatures other than 25.0°. The relevant data are collected in Table VI. The dielectric constants are based on the work of Critchfield, Gibson, and Hall,[19] the values at 45° being obtained by extrapolation from the data at lower temperatures. The K values are calculated in the same way as before. The $E°$ values in 70 percent dioxane are based on data[25] at $c<0.004$ M and are constant within the mean deviation indicated. The values in 82 percent dioxane are based on data[25] in the concentration range 0.001 to 0.01 M where our estimates of y at 25° were somewhat in error. (See Table IV.) They have been calculated on

TABLE VI. Values of K, $E°$, and s for hydrochloric acid in the system dioxane-water.[a]

Solvent (wt percent dioxane)	Temperature °C	D	10^3K	Apparent[d] s, A°	$E°$(mv)[e]
82.00[b]	15.0	11.11	0.296	5.71	−24.4±0.3
	25.0	10.56	0.259	5.68	−48.5±0.3
	35.0	10.04	0.212	5.58	−75.1±0.7
	45.0	9.54	0.148	5.30	−105.6±0.6
70.00[b]	15.0	20.33	8.20	6.03	84.8±0.3
	25.0	19.07	6.67	5.73	66.4±0.2
	35.0	18.07	5.84	5.61	47.6±0.4
	45.0	17.10	5.26	5.65	29.0±0.5
45.00[c]	15.0	42.66	194	4.9	—
	25.0	40.25	226	5.4	165.6
	35.0	38.03	223	5.6	—

[a] Calculations based on data given in references 19 and 25.
[b] Eqs. (8) and (13).
[c] Eqs. (6) and (13).
[d] Eq. (4).
[e] Parameters in Eq. (17): 82 percent dioxane, $a=-2.55_8$, $b=-0.0143$; 70 percent dioxane, $a=-1.86$, $b=-0.0008$.

the assumption that the percent error of the predicted y values at a given concentration is independent of the temperature, and by evaluating this error from the data at 25°. The variation with temperature is represented satisfactorily by the empirical equation

$$E_t°(\text{mv}) = E_{25}° + a(t-25) + b(t-25)^2, \qquad (17)$$

where t is in °C. Values of a and b are included in Table VI.

Table VI also contains s values calculated by means of Eq. (4). It is seen that the s values are quite independent of temperature and solvent, as one would expect if Eq. (4) were strictly applicable. Since this cannot be guaranteed, it is perhaps more significant that the s values resemble in their magnitude (5−6A°) and small sensitivity to temperature change the presumably equal quantities based on the emf of cell (3) in systems where Eq. (5) is directly applicable.[33] These facts further strengthen the evidence in favor of method C for calculating K. By comparison, the results of method B are not so satisfactory though still compatible with predictions based on the use of Eq. (5), and the results of method A, which have been tabulated in detail elsewhere,[19] seem to us sufficiently incompatible to argue strongly against the use of this method for obtaining K.

EXPERIMENTAL PART

The emf Values for Cell (3) in 82.00 Percent Dioxane

The emf values were obtained in the concentration range 0.01 to 0.0001 from data for the two cells

$$\text{Pt}-\text{H}_2(g, 1 \text{ atmos})/\text{HCl}(c)/\text{Glass Electrode}; \qquad (18)$$

$$\text{Glass Electrode}/\text{HCl}(c)/\text{AgCl}-\text{Ag}. \qquad (19)$$

This procedure was adopted because the direct use of cell (3) is impractical at $c<0.001$ M due to the appreciable error resulting in weakly buffered solutions from the occurrence of reaction (16).[29,31] Cells (18) and (19) are not troubled by this source of error since reaction (16) does not occur when either silver chloride or hydrogen is absent. If the glass electrode measures the activity of hydrogen ion in conformance with the Nernst equation, the emf of cell (18) is independent of c, and the additional labor due to the use of two cells instead of one is small.

TABLE VII. Emf values for cell (3) in 82.00 wt percent dioxane at 25.00°.

$10^4c(M)$	E(mv)	$10^4c(M)$	E(mv)	$10^4c(M)$	E(mv)
1.123	439.6	5.389	381.3	22.49	334.8
1.265	435.0	5.773	378.9	22.99	333.6
1.448	429.6	6.555	374.5	26.32	330.2
1.703	423.3	7.589	369.4	30.77	325.0
2.063	416.1	9.009	364.0	36.90	319.4
2.190	412.9	9.958	360.4	46.25	312.6
2.473	409.0	10.93	357.4	47.80	311.7
2.618	407.7	11.15	356.8	53.13	308.2
2.842	403.7	12.77	352.4	60.17	304.6
3.389	397.4	14.93	347.4	69.59	300.5
4.157	390.4	17.97	341.4	81.64	295.6
5.177	383.2	20.54	337.6	99.79	290.0

This is in fact the case. The difference between our emf values for cell (19) and the previously determined[25(d)] values for cell (3) was constant to well within the combined experimental errors over the entire concentration range, $0.01>c>0.001$, covered by the data for cell (3). The emf of cell (18) was thus determined as 281.1 mv and 236.2 mv, respectively, for two different glass electrodes. If these two glass electrodes had not conformed to the Nernst equation, the deviations would almost certainly have been greatest for the most acid solutions by analogy with the behavior of typical glass electrodes in aqueous acid.[34] We therefore felt safe in using the same emf values for cell (18) also at concentrations below 0.001.

One seemingly unavoidable source of error characteristic of glass electrodes is a slow drift of the emf readings in solvents containing a high percentage of an organic component. The drift may be detected by leaving the electrodes immersed over a period of time in a given test solution, and its rate varies considerably from electrode to electrode. The resulting error may be minimized by careful selection of the glass electrodes, and in the present instance the drifts were measured to be less than +0.4 mv and +0.5 mv, respectively, for the two electrodes used in cell (19), *over the entire period of experimentation*. Therefore the errors of our emf values due to electrode drift are not likely to exceed 0.3 mv.

Our new emf values for cell (3) in 82.00 wt percent dioxane at 25.00° are summarized in Table VII. Each value is the average of two determinations involving two different glass electrodes and is precise to ±0.2 mv. The new emf values are compared in Table VIII at rounded concentrations with those previously available in the range $0.01>c>0.001$. Except at the very lowest concentration where the experimental difficulties inherent in the direct measurement of cell (3) are at a maximum, the agreement of the two sets of values is satisfactory.

We believe that the data listed in Table VII afford an accurate measure (within 1 percent) of the hydrochloric acid activity even at the very lowest concentrations, for the following reasons.

The solubility of silver chloride in 82 percent dioxane is too low to have a measurable effect on the emf values. The solubility product was determined using cell (19) which now contained nitric acid and silver nitrate instead of hydrochloric acid. Molar activity coefficients were set equal to those for hydrochloric

[33] H. D. Crockford, "Proceedings of the NBS Semicentennial Symposium on Electrochemical Constants," Natl. Bur. Standards Circ. 524, No. 16, August 14, 1953.

[34] The pH of 0.01 M hydrochloric acid in 82 percent dioxane is about −1.0. [Gutbezahl, Marshall, and Grunwald, unpublished results. See also J. Am. Chem. Soc. 75, 565 (1953).]

acid at the same total electrolyte concentration which was varied from 0.0019 to 0.0025. Three separate experiments gave $K_{sp}=(1.13\pm0.01)\times10^{-15}(M^2)$.

In order to prevent errors due to the adsorption of hydrochloric acid on the surfaces of the glass vessels used in the experiments,[29] every single piece of apparatus was first pre-rinsed with a separate hydrochloric acid solution of the same concentration (within 2 percent) as that to be studied.

In order to detect possible acid or chloride impurities in the solvent which would cause the emf values to be erroneous, we measured the emf of an extremely dilute solution which we had made up to be 2.379×10^{-5} M. For this solution the emf of cell (3) is predicted to be 507.3 mv. The actual observed value was 509 ± 2 mv. Although at this very low concentration the measurement is much less satisfactory than at the higher concentrations reported in Table VII, the observed value is of the correct magnitude and indicates that the concentration of interfering impurities is insignificant.

Details of the Experiments

Materials

The best available commerical grade of 1, 4-dioxane was further purified by the method of Kraus and Vingee.[35] The purified material was finally redistilled from sodium through a 20-plate bubble cap column immediately before use. The mp was 11.78°, water content below 0.03 percent by Karl Fischer titration, and purity better than 99.90 mole percent by freezing-curve analysis. Water was redistilled from alkaline permanganate through an all-glass still. Constant-boiling hydrochloric acid was prepared from reagent grade acid by the method of Foulk and Hollingsworth.[36] The acid was analyzed for chloride by Volhard titration against reagent grade silver nitrate, and for acid by comparison with Bureau of Standards potassium acid phthalate. The two analyses agreed within 0.05 percent among themselves and with the value reported by Foulk and Hollingsworth.

Electrodes

The glass electrodes were type 1190-42 of the National Technical Laboratories and satisfied the criteria for accuracy and reversibility worked out by Gutbezahl in this laboratory.[37] They came to equilibrium within 10 minutes. The silver-silver chloride electrode consisted of a platinum spiral coated with thermally deposited silver (Harned's type 2)[38] and was prepared by the method of Anderson.[29,31]

[35] C. A. Kraus and R. A. Vingee, J. Am. Chem. Soc. **56**, 511 (1934).
[36] C. W. Foulk and M. Hollingsworth, J. Am. Chem. Soc. **45**, 1220 (1923).
[37] B. Gutbezahl and E. Grunwald, J. Am. Chem. Soc. **75**, 559 (1953).
[38] H. S. Harned, J. Am. Chem. Soc. **51**, 416 (1929).

TABLE VIII. Comparison of emf values for cell (3) in 82.00 wt percent dioxane at 25.00°.

m[a]	E(mv) Reference 26d	E(mv) Present Work
0.001	360.9	359.4
0.0015	346.8	346.3
0.002	337.3	337.4
0.003	324.7	324.8
0.005	309.1	309.1
0.007	298.9	299.2
0.01	288.4	(288.9)[b]

[a] Moles of acid/kg of solvent.
[b] Result of a short extrapolation.

The thermostat was a table model maintaining the temperature at $25.00\pm0.05°$ and was mounted above a Mag-Mix stirring assembly as previously described.[37]

The potentiometer was a Beckmann Model G pH meter. The pH scale of this instrument was calibrated at the graduation points at 0.1 unit interval against a type K potentiometer. The sensitivity of the null-indicating galvonometer was about 5.0 scale divisions/0.1 pH unit, and emf readings were obtained with maximum accuracy by linear interpolation on the galvanometer scale between adjacent calibration points rather than by direct reading of the pH scale. On the basis of many comparisons with the type K potentiometer, the standard error of a single reading was 0.003 pH unit (0.2 mv).

The cell was a 180 ml Pyrex electrolytic beaker. It was stoppered with a rubber stopper which supported the silver-silver chloride electrode and two glass electrodes and which had a hole for the insertion of the tip of a calibrated 50 ml buret.

A typical experiment was as follows: The primary standard for all solutions was a 0.009979 N solution of hydrogen chloride in 82.00 wt percent dioxane which had been prepared gravimetrically from constant-boiling hydrochloric acid, water, and dioxane. A sample of this solution was diluted with 82.00 wt percent dioxane to the desired concentration and was used to pre-rinse all glass apparatus and the electrodes. A second dilution of the same concentration (within 2 percent) was then prepared gravimetrically, about 50 ml placed in the cell, and the emf was measured at 2 minute intervals until electrode equilibrium had been established. This solution was then diluted further by adding 82.00 wt percent dioxane to the cell from a calibrated 50-ml buret, 10 ml at a time, stirring the cell contents with a magnetic stirrer[37] after each addition, and the emf was again measured after each addition until electrode equilibrium had been re-established.

The values of the densities required for the calculation of the molar concentrations were taken from the compilations of Harned and Owen.[7]

We wish to thank Professor J. B. Ramsey and Dr. M. D. Cohen for helpful suggestions during the preparation of this manuscript.

Electronic Properties of Carbons and of Their Interstitial Bisulfate Compounds*

E. A. KMETKO†
Department of Physics, University of Buffalo, Buffalo, New York
(Received April 27, 1953)

The conductivity of graphite increases when it is oxidized into graphite bisulfate, this being the result of the expulsion of resonance electrons by the negative ions and the resulting creation of excess holes in the π-band. This study concerns the electronic properties of the bisulfate compounds formed by the oxidation of carbons in sulfuric acid, the range of heat-treatment of carbons extending from 1400°C (baked carbons) to 3000°C (polycrystalline graphite). The resistivities of all samples thus treated decrease with increase in the degree of oxidation. The rate of decrease in resistance depends upon the heat-treatment, the rate being increasingly greater for samples treated to higher temperatures. The curve of the Hall constant of unoxidized carbons *versus* the heat-treatment temperature H has a sharp positive peak at about $H=2000$°C. The curve rapidly drops on either side of the peak, the coefficient becoming negative and exhibiting a minimum around $H=1400$°C.

The thermoelectric power of all samples studied becomes more positive with oxidation, with maxima appearing for lamellar compounds. The rate of the initial rise is greater for higher heat-treatment temperatures. The temperature coefficient of resistance depends strongly upon the ion concentration, changing from negative to positive for carbons heat-treated above 2000°C. On the other hand, the coefficients remain negative and are remarkably independent of ion concentration for carbons treated to temperatures below 2000°C.

The results are in general consistent with the electronic model for carbons proposed by Mrozowski whereby the Fermi level is initially depressed during devolatilization of the hydrocarbon material by the formation of a large number of excess holes (heat-treatments below 1400°C) and later steadily rises with the growth of the crystallites towards the top of the π band, the growth of the crystal planes resulting also in a steady decrease of the energy gap between the π and conduction bands. The negative Hall coefficient for baked carbons indicates the π band to be so depleted that the Fermi level drops at least partially below the inflection curve. At room temperature the conduction is therefore semi-metallic in nature for carbons treated to $H<2000$°C in contrast with cases for which $H>2000$°C where the number of excess holes is relatively small and the current is carried mainly by the holes and electrons thermally activated into the conduction band.

INTRODUCTION

CHANGES in the electrical properties of graphite occurring when foreign ions are introduced between the aromatic lattice planes have been extensively studied.[1–3] The substance designated as graphite bisulfate is perhaps the most thoroughly investigated, both experimentally and theoretically, of these so-called graphite compounds.[4] It is formed by reacting graphite with sulfuric acid by either electrolysis or use of a chemical oxidizing agent such as nitric acid. In the formation of the compound, the negatively charged ions enter preferentially into the spaces between the lattice planes so as to progressively fill every nth layer where n becomes smaller as more ions are introduced into the crystal.[5] This is presumably the result of the strong electrostatic repulsion between the ions, as well as of the spreading of the layers. The electrical resistivity decreases rapidly, and the Hall constant changes from negative to positive as the concentration of ions increases. The ordered, so-called lamellar compounds can be reduced by reversing the process of formation. However, reduction is not complete, and relatively large numbers of ions remain trapped in the graphite, presumably at lattice imperfections.[1] In spite of the disordered nature of this residual bisulfate compound, its resistance is about the same as that of a lamellar compound having the same ratio of bisulfate ions to carbon atoms. This fact seems remarkable, especially since the Hall coefficients differ considerably; an explanation will be suggested in a later section.

The expulsion of electrons from the otherwise full π band of graphite by the invading ions, and the formation thereby of conducting holes is believed to be mainly responsible for the larger conductivity as well as the change in sign of the Hall coefficient.[1] The contribution to the conduction by the ions themselves is negligible. The scattering of the conduction electrons by the intercalated ions is also small; this follows, according to Hennig, from the similarity of the electronic properties of different types of graphite compounds (similarity of the curves for the Hall constant *versus* relative resistance in particular).[2] This conclusion also evolves directly from a consideration of differences in the dependence of relative resistance on temperature for natural and polycrystalline graphites.[4]

The depth to which a band can be probed by forming compounds is severely limited, since the expansion of the crystallites by the invading ions induces stresses and causes disintegration of the samples for oxidations exceeding about 5×10^{-3} equivalents, i.e., when only about 5 π electrons per thousand have been removed.

It was of interest to investigate the possible differences in the effects of chemical oxidation upon the electrical properties of carbons. These substances are intermediates in the process of converting organic materials into graphite and differ from graphite in crystal size, the crystals being smaller as a result of limiting the maximum treatment temperature, and in having disordered orientation of their layer planes. In order to explain in a

* Supported in part by the U. S. Office of Naval Research.
† Now at Physics Laboratories, Sylvania Electric Products, Inc., Bayside, New York.
[1] G. R. Hennig, J. Chem. Phys. **19**, 9122 (1951).
[2] G. R. Hennig, J. Chem. Phys. **20**, 1443 (1952).
[3] McDonnell, Pink, and Ubbelohde, J. Chem. Soc. **1951**, 191.
[4] S. Mrozowski, J. Chem. Phys. **21**, 492 (1953).
[5] W. Rudorf and U. Hoffman, Z. anorg. u. allgem Chem. **238**, 1 (1938).

consistent way the temperature dependence of the electrical resistivity for the entire class of solids ranging from condensed aromatics to graphite, it is necessary to assume (1) the existence of an energy gap between the valence and conduction bands which varies inversely with crystallite size and (2) the presence of surface traps on the crystal boundaries, these surface traps being the result of the free carbon valencies left after the removal of hydrogen and hydrocarbon groups during devolatilization.[6] It seems, therefore, that there is a mechanism present whereby the carbon atoms themselves supply holes to the resonance band and depress the Fermi level by amounts which can exceed greatly those obtainable by the chemical treatment of graphite. According to this picture, the dependence of the electrical properties of carbons upon oxidation should differ appreciably from those observed in graphite.

EXPERIMENTS AND RESULTS

Materials

The graphite and carbons used primarily in this study were prepared by heat-treating a baked pitch-bonded petroleum coke stock manufactured by the National Carbon Company. Portions of this carbon were heated while in a purified dry nitrogen atmosphere to temperatures ranging from 1400°C to 3000°C in a resistance furnace with a graphite tube element. The lowest temperature of 1400°C was selected to insure similar treatment for both the coke particles and the binder coke matrix since normally coke is calcined to temperatures in excess of 1000°C, the baking temperature. A diffuse value for the treatment temperature of 1000–1200°C was assigned, for plotting purposes, to the stock as obtained commercially. Where treatment temperatures below this are indicated, the carbon used was a laboratory prepared stock made from petroleum coke calcined to 500°C, extruded with a compatible binder and then baked to the indicated temperature.

Electrical Resistance

Samples of carbon and graphite to be oxidized were cut into rods of square cross-section 2×2×40 mm. Platinum current and potential leads were inserted into small holes drilled near the ends of the rods. All wires were sealed in glass tubing, and their exposed lengths were kept as short as possible. These leads also acted as supports for the sample. The cell in which the reaction took place consisted of two test tubes connected together near their midpoints by a filter tube containing a very fine sintered glass disk. The cathode consisted of several square centimeters of pure platinum foil. Oxidizing currents for all samples were maintained near 2 ma. Resistances were determined as a function of oxidation state by measuring the potential drop across the sample

[6] S. Mrozowski, Phys. Rev. 85, 609 (1952) and Errata, Phys. Rev. 86, 1056 (1952).

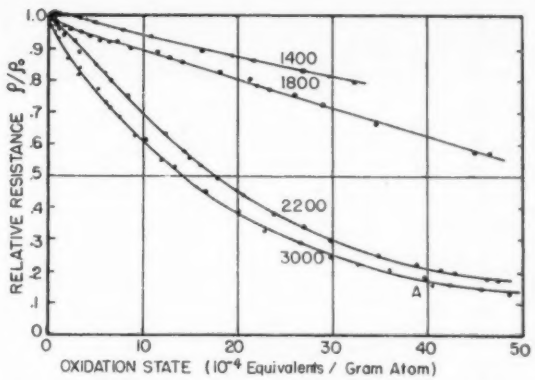

FIG. 1. Variations of the relative electrical resistances of carbons with degree of oxidation in sulfuric acid. Heat-treatment temperatures of carbon samples are indicated in °C. Termination of the curve for 1400°C carbon is due to disintegration of samples.

and comparing it with that measured on a Leeds and Northrup standard resistance of 0.01 ohm. The rapidly decaying potential observed after switching off the current was subtracted from the readings; this was a relatively small correction, however. Essentially the procedure followed was that described by Hennig.[1]

Whenever the sample was oxidized to a point below which internal stresses created by the ions caused disintegration or bending, it was reduced by reversing the electrode polarity. The residue compound thus formed was washed for at least two days in running water and dried thoroughly. The gain in weight in each case showed that the efficiency of the reaction was the same as for polycrystalline graphite (carbon treated to 3000°C). This efficiency is known from the work of Hennig to be very close to unity.[1]

The ratio of the resistance at a given oxidation state to that of the unoxidized sample is plotted in Fig. 1 for carbons prepared at various temperatures. The data shown are for lamellar bisulfates only, since there is, as previously mentioned, no noticeable difference between resistances of the ordered and disordered compounds at the same ion concentration. Each curve represents data obtained for at least two samples. It is evident in the figure that the influence of oxidation strongly depends upon the maximum temperature of heat-treatment of the carbon especially when the temperature is below 2200°C.

Hall Effect

It seemed desirable to study the Hall constants for the full range of substances as a function of oxidation state. However, because of the unavailability of a magnet for the lengthy periods required, it was decided to investigate the thermoelectric effect instead. Hall measurements were, however, performed on chemically untreated samples because of the absolute nature of the information derived. The results are important by themselves for any discussion of the phenomena associated with the carbon and graphite compounds.

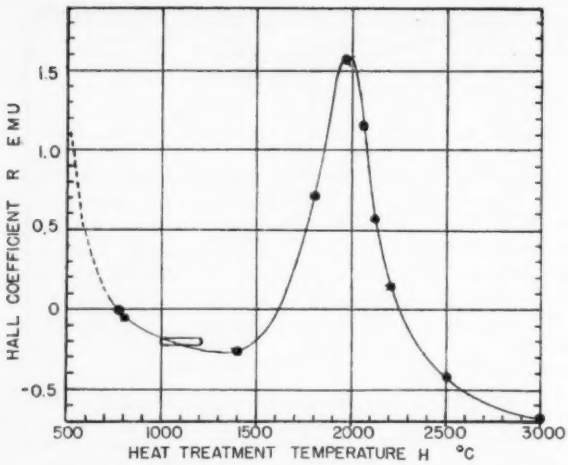

FIG. 2. The Hall constants for unoxidized carbons as a function of heat-treatment temperature of the carbon. Dashed curve for temperatures below 800°C represents an extrapolation based on the known behavior of the thermoelectric power.

Hall coefficients were determined for carbons heat-treated to temperatures ranging from 800°C to 3000°C. Measurements were precluded for heat-treatments below 800°C because of the high resistance of samples. The samples were cut from slabs ca 1 mm thick and were 5 mm wide and 3 cm long. Fine platinum leads were firmly fixed in holes drilled at the ends of arms 1 mm wide extending 5 mm from the sample. These served to minimize the Ettinghausen potentials.[1] Current contacts at the ends of the specimen were made by dead soft platinum held firmly by small brass "*C*" clamps. The sample with its leads and supports was surrounded by a glass tube which acted as a necessary shield against air currents, since air currents were the cause of large fluctuations in measured potential.

A Weiss-type magnet with pole faces of 7.5 cm diameter was calibrated using a Sensitive Research fluxmeter and a search coil of a total effective area of 25.05 cm.[2] Hall potentials were measured with a type *K* potentiometer. Field strengths were in the neighborhood of 13 000 Oersteds. Both field and current directions were reversed several times for each determination.

Figure 2 gives the Hall coefficient found as a function of treatment temperature. It shows the same general behavior as does the thermoelectric power.[7] The existence of the peak around 2000°C in the Hall effect has been reported[8] but thus far no measurements for carbon heat-treated below 1400°C were performed. Both the Hall and thermoelectric effect are closely related, and it is considered quite likely that, for treatment temperature below 800°C, the Hall coefficient continues to rise and becomes positive as indicated by the dotted portion of the curve in Fig. 2.

[7] E. E. Loebner, Phys. Rev. **84**, 153 (1951) and Errata, Phys. Rev. **86**, 1056 (1952).

[8] J. J. Donoghue and W. P. Eatherly, Rev. Sci. Instr. **22**, 513 (1951).

Thermoelectric Power

The thermoelectric power of carbons and graphite was studied as a function of ion concentration. Thermal emf's were measured relative to pure platinum while the samples were immersed in the electrolyte. This was necessary since the compounds are unstable outside of the concentrated acid. The apparatus designed for the purpose is depicted in Fig. 3. The thermal as well as electrical contacts to the ends of the specimen rods (same size and shape as used in the measurement of resistance) were made by platinum electrodes. The cold contact consisted of a platinum disk, *F*, sealed into the lower end of the specimen compartment. The upper electrode, *C*, was machined from graphite. Its lower end was grooved to receive the specimen while its upper portion was deeply threaded to give good thermal contact to the atmosphere. Thermocouples and potentiometric leads were brought into the apparatus through holes bored into the assembly. In order to protect the electrode from the acid, the entire lower portion was covered with platinum foil and thickly coated with paraffin. A small area in the groove was then cleared of paraffin to act as contact surface. The lower end of the specimen made connection to an ice bath via the platinum disk and the graphite rod, *G*, upon which the specimen compartment rested.

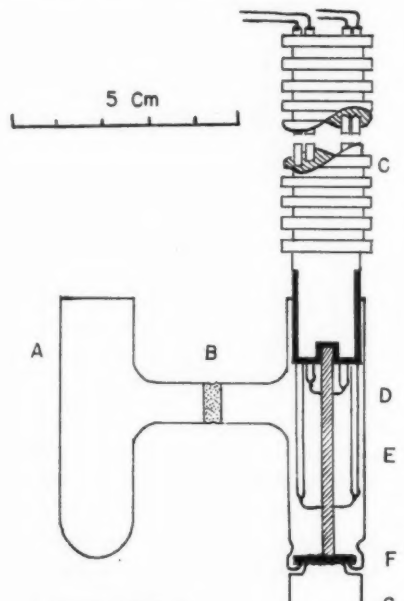

FIG. 3. Schematic view of apparatus used to determine thermoelectric power of carbons as a function of bisulfate ion concentration. The tube assembly is of Pyrex glass: *A*, cathode compartment; *B*, sintered glass disk (very fine); *C*, upper thermal and electrical contact assembly, showing glass lead-in tubes for electrodes and thermocouples; *D*, specimen compartment showing specimen, *E*, in place with attached electrodes; *F*, platinum disk; and *G*, graphite rod. *F* and *G* together constitute the lower thermal and electrical contact assembly.

By varying the level of the ice bath in which the lower portion of the graphite rod, *G*, was immersed, the temperature drop along the specimen could be adjusted to any desired value. Temperature differences of 8° to 10°C were used in this study. The time required to achieve thermal equilibrium was of the order of several minutes. Platinum *versus* platinum-10 percent rhodium thermocouple leads placed in holes drilled one-half centimeter from the ends were sealed over with soft paraffin. Potentiometer leads entered small holes drilled at points exactly opposite the thermocouple wells. Since there existed a danger of thermocouple breakage, separate leads were used for measuring thermal emf's in order to keep the same platinum reference through the whole series of experiments.

Values of the thermoelectric power obtained before and after the specimen was immersed in the acid did not differ noticeably. The procedure adopted was simply to oxidize the sample by running the current for a certain period of time after which temperature drop, thermal emf, potential drops across both sample and standard resistance were measured. The direction of the oxidizing current was then reversed to convert the lamellar compound into a residue compound and measurements repeated. After that the sample was further oxidized, new measurements performed, and so forth.

The dependence of the thermoelectric power on the concentration of ions is strongly influenced by temperature of heat-treatment in a manner paralleling that of the resistance. Figures 4 and 5 show this for the lamellar and residue compounds, respectively. The relative resistance ρ/ρ_0 was used to obtain the corresponding oxidation state from data obtained in the study of the resistance. Comparison of the two sets of curves shows that the thermoelectric power of a residue compound is greater than that of the corresponding lamellar compound (similar to relation indicated by Hennig's study of the Hall effect in graphite bisulfate).[1]

Temperature Dependence of Resistance

Samples of carbon heat-treated to various temperatures were mounted for resistance measurement and oxidized by immersion in concentrated sulfuric acid to which a few drops of nitric acid had been added. The sample was withdrawn after being treated to various oxidation levels, dipped into liquid nitrogen, and its resistance measured. It was then transferred to a dry ice-petroleum ether bath and the measurement repeated. After rinsing in concentrated acid, it was again placed in the oxidizing bath and the resistance continually measured to check progress of the oxidation. The temperature coefficient of resistance calculated from data for several samples are presented in Fig. 6 where, in addition, a curve derived from Hennig's data for polycrystalline graphite is also plotted.

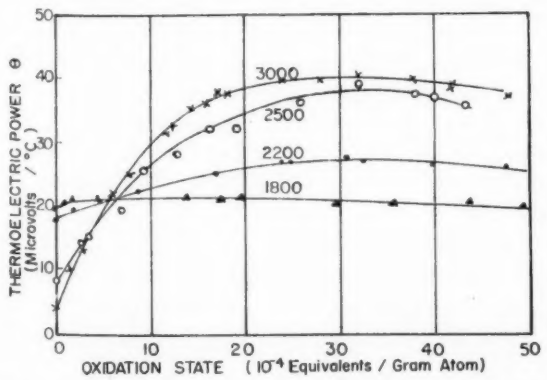

FIG. 4. The thermoelectric power of lamellar bisulfates of carbons as a function of degree of oxidation. Heat-treatment temperatures of carbon samples are indicated in °C.

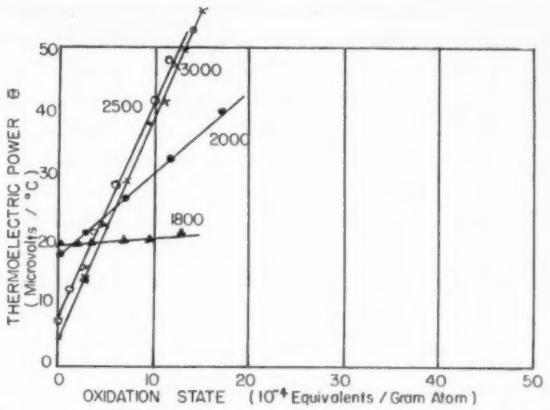

FIG. 5. The thermoelectric power of residual bisulfates of carbons as a function of degree of oxidation. Heat-treatment temperatures of carbon samples are indicated in °C. *Note added in proof:*—The heat-treatment temperature indicated as 2000°C, should read 2200°C.

DISCUSSION

As carbons are heat-treated to higher temperatures, their electrical resistivities become increasingly sensitive to the addition of acceptor impurities (Fig. 1). This behavior is in accord with the electronic model for aromatics mentioned in the introduction wherein the free carbon valencies on the crystallite edges act as electron traps, thus creating holes in the π band.[6] As the result of crystal growth, the number of carbon atoms in peripheral sites, and of the concomitant excess holes, continually diminishes with increasing treatment temperature H. For baked carbons comparatively large numbers of holes exist prior to oxidation. Thus, in these substances, the relative increase in the number of carriers for a given oxidation increment is smaller than in the case of the graphite. The system of curves in Fig. 1 is a fine illustration of a statement made concerning the relative influence of impurities on the electronic properties of baked carbons and polycrystalline graphite (see reference 6, p. 618.)

The near coincidence of the ρ/ρ_0 curves for the carbons heated to 2200°C and 3000°C is largely fortuitous, the result of an inappropriate selection of the value for ρ_0.[4] Two corrections are required to bring about the proper representation of the variation for the carbon treated to

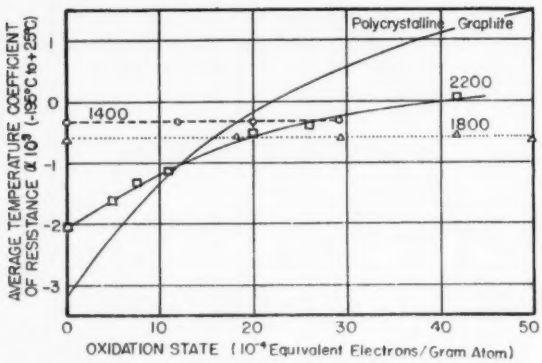

FIG. 6. Variation of the temperature coefficient of resistance with degree of oxidation in sulfuric acid. Heat-treatment temperatures of carbon samples are indicated in °C.

the lower temperature. One of these accounts for the existence of an energy of activation into the conduction band whereby the value of ρ_0 is obtained by extrapolating to room temperature the linear portion of the ρ *vs* T curve for this substance.[4] With the proper correction, the ρ/ρ_0 plot begins at a value greater than unity, quickly descends and joins the curve for natural graphite when the Fermi level is depressed by an amount greater than kT. The second correction consists of a horizontal shift equal to the excess hole concentration. In this instance the shift is relatively small (of the order 5×10^{-4}). It just so happens that the two corrections about counteract each other for carbons heat-treated to 2200°C or higher. When, however, we consider baked carbon, the horizontal shift may be considerable, the starting point of the plot being at a point such as A in Fig. 1. Since the number of excess holes in baked carbon is large, the Fermi level is located considerably below the top of the band and no correction for activation into the conduction band is necessary. Since ρ at A is taken as ρ_0, the slope of the resulting curve decreases as A moves toward higher oxidation values.

The Hall constant R of unoxidized carbons shows an interesting variation with respect to treatment temperature (Fig. 2). For the purpose of discussion, the temperature range has been divided into two regions: region I for $H>2000$°C and region II for $H<2000$°C. In region I, a steady change of R occurs in the positive direction as H decreases. In order to find the meaning of this variation, it is necessary to consider the formula for R. This is:

$$R=\frac{3\pi}{8n_he}\frac{c^2-n_e/n_h}{(c+n_e/n_h)^2}, \qquad (1)$$

where n_e and n_h are the numbers of electrons and holes, respectively, and c is the ratio of the mobility of the holes to that of the electrons. For very large graphite crystals, $n_e/n_h=1$, thus c, as indicated by the experimental value of R, is less than unity, i.e., the electrons have a higher mobility than the holes. Since the crystallite structure remains essentially the same through at least the whole of the region I, even though the crystallite size varies over a rather wide range[9] it seems impossible to attribute all, or even most of the change in R, to a variation in the mobility ratio c. It even seems quite reasonable to expect that in the crystals themselves this ratio will not change very much throughout the entire range from aromatic molecules up through graphite, and that the observed c will rather decrease as we go toward samples with smaller crystallites, due to an increasing contribution from intercrystalline barriers.

Thus, in order to explain the increase of R with decreasing crystal size in region I, it is necessary to assume an actual increase in the relative number of positive carriers. This is supported by the fact that when holes are introduced into graphite by oxidation, the Hall constant changes in the same direction.[1] Taking the total number of carriers in graphite to be 2×10^{-4} per atom[6] and $R=-0.70$ a mobility ratio c of about 0.85 is obtained. It is necessary to keep in mind that Eq. (1) from which c has been calculated is derived under the assumption of a parabolic E *vs* k relationship.

The knowledge of the mobility ratio c and of the experimental values of R is insufficient, however, to calculate the two unknowns n_h and n_e/n_h from Eq. (1) for carbons heated to various temperatures. The excess holes are provided by the peripheral carbon traps and the total number of holes and electrons are determined furthermore, by the thermal activation of electrons into the conduction band, with a steadily increasing energy of activation as one goes to lower heat-treatment temperatures (energy of activation is equal to the energy gap between the bands plus depression of the Fermi level).

In region II, the energy of activation is so large that $n_e=0$ and the Hall curve reflects the changes in n_h directly. The large drop occurring for the thermoelectric power Θ and presumably for the Hall effect R as well at low values of H (Fig. 2) is due to devolatilization of the hydrocarbon material and the resulting abundance of excess holes. The minimum at $H=1400$°C is caused by the completion of the process of removal of peripheral hydrogen and the subsequent diminution in the number of peripheral atomic sites due to crystallite growth above $H=1400$°C. Although the energy of activation decreases with increasing H, the Hall coefficient at first continues to rise because of the diminishing concentration of excess holes. As greater numbers of electrons are excited into the conduction band, its trend reverses and gives rise to the sharp peak at $H=2000$°C.

It is extremely interesting that the Hall coefficient is negative for baked carbons, for by crossing the axis it indicates a change in sign of the predominant carriers. Since the Brillouin zone possesses hexagonal symmetry

[9] For the changes occurring with heat-treatment in crystallite sizes and in their perfection see: R. E. Franklin, Proc. Roy. Soc. (London) **209**, 196 (1951) and H. T. Pinnick, J. Chem. Phys. **20**, 756 (1952).

and the energy momentum relationship is quasi-linear at its corners, the inflection curve, i.e., the curve on which $\partial^2 E/\partial k^2 = 0$ lies close to the zone boundaries. Evidently the depletion of the π band by the surface traps is sufficient to depress the Fermi level at least partly below the inflection curve. As a result, the sign of the predominant carriers and consequently of the Hall coefficient changes. In view of the complicated energy relationships existing around the inflection curve, the number of carriers cannot be estimated from Eq. (1) assuming $n_e = 0$, but a more general formula such as given by Wilson[10] should be used. Unfortunately, the exact form of the energy surface in graphite is not known and consequently no estimate of the number of holes or of the position of the Fermi level can be made at present from the experimental data.

It must be admitted that a difficulty is encountered in the foregoing interpretation. Baked carbons with negative Hall constants should exhibit, according to such a model, an increase in resistance when electrons are removed. This is because the Fermi level presumably lies partially below the inflection curve where the removal of electrons corresponds to a decrease in the effective number of carriers. Since no steady rise in ρ is obtained, (only a slight transient one at oxidation states of less than 10^{-4} equivalent electron per gram atom has been observed) it seems probable that the bisulfate ions mask the effect by contributing in some way to the conduction. It seems possible that ions lodged between crystallites might lower the intercrystalline barriers. Thus, the picture may not be so simple as originally supposed.[1]

Because of the simple relationship between the Hall and the thermoelectric effects, the same arguments used in discussing the variation of the former with heat-treatment may be employed in the case of the latter, since the factors in Eq. (1) also affect in a similar way the thermoelectric power. The temperature range again breaks up into two regions on either side of the maximum. In region *II* (1400°C < *H* < 2000°C), the number of holes, because of the peripheral traps, continually decreases with the increase of *H*; the diminishing activation energy provides, however, increasing numbers of electrons in the conduction band to allow electronic conduction eventually to predominate, giving rise to a maximum in Θ at a point only slightly displaced from that found in the Hall effect.

The amount of change occurring in the thermoelectric power of carbons with respect to electron removal depends strongly upon the heat-treatment. (Figures 4 and 5.) Thus, for carbons heat-treated to the lower temperatures the changes are much smaller for a given degree of oxidation than observed in well-graphitized carbons. The steady variation in the way the oxidation influences Θ emphasizes the fortuitous character of the similarity of ρ/ρ_0 curves for carbons treated to 2200°C and 3000°C (Fig. 1). Since Θ is a function of relative carrier concentrations, as well as the mobility ratio, these results show such quantities to vary less for those carbons having the greater hole concentrations. For such carbons which possess smaller crystallites, the Fermi level lies farther below the top of the band, and the shift of this level, accompanying removal of a given number of electrons, is smaller the greater the depth of the Fermi level. The initial rise in thermoelectric power with oxidation for carbons treated to 1800°C is somewhat puzzling. The results for 1400°C carbons were irregular and are therefore omitted.

The dependence of the temperature coefficient of resistance on oxidation for baked carbons differs from that exhibited by polycrystalline graphite, for which the slope of the ρ *vs* T curve changes from its rather large negative value, typical for a semiconductor, eventually becoming positive.[1] This is due to lowering the Fermi level sufficiently far so that electrons are no longer excited in great numbers into the upper band, the conduction then being due almost entirely to excess holes and having thus a metallic character (positive temperature coefficient).[4] Baked carbons, however, do not show any change over the widest ranges of oxidation obtainable. This difference reveals most lucidly the basic distinction between the conduction mechanisms operative in these substances in the untreated states. Thus, in baked carbon the number of carriers does not depend upon temperature, the resistance being due almost entirely to scattering by the intercrystalline barriers (negative temperature coefficient).[11] The conduction in baked carbons is definitely of the semi-metallic type and this is entirely the result of the large number of excess holes formed by the peripheral traps.

The fact that carbons treated to 1400°C and 1800°C, though they have Hall constants of opposite sign, still behave similarly in a number of other respects lends support to the view that the difference in the Hall sign is only the result of the position of the Fermi level relative to the inflection curve.

A simple interpretation of the result that the resistivities of corresponding lamellar and residual bisulfate compounds are not noticeably different can also be given. A graphite crystallite consists of stacked conducting planes which are essentially insulated from each other. The equivalent circuit is, therefore, a parallel resistance network for which the conductivities are additive. Thus, the conduction of a crystallite is an invariant with respect to the arrangement of the ions, depending simply upon the total number of carriers. The Hall coefficient and thermoelectric power on the other hand are not simply additive for a parallel network; thus, different systems of curves result for the two types of compounds.

For well-graphitized carbons a slight increase in ρ/ρ_0 is expected at low oxidation levels, since the more mobile

[10] A. H. Wilson, *The Theory of Metals* (Cambridge University Press, Cambridge, 1936), p. 164.

[11] A discussion of the scattering mechanisms in carbons is contained in reference 6, page 612.

electrons give way in numbers to less mobile holes as oxidation proceeds. The slightly apparent inflection in the curve for carbon treated to 2200°C (Fig. 1) at low oxidation levels is perhaps a manifestation of this trend which is, however, probably in most cases largely obliterated by the stepwise character of the ionic invasions.

CONCLUSION

The influence of chemical oxidation upon the resistivity and thermoelectric power of solid carbons depends upon the crystallite size, being increasingly greater for carbons composed of larger crystals. A fairly consistent picture of the relationships is provided by considering that for carbons heat-treated to above 1400°C the Fermi level rises continually toward the top of the band, accompanied by a decrease in the size of the energy gap as the crystallites grow, the initial depression of the Fermi level for carbons below 1400°C being caused by surface traps formed in great profusion during devolatilization. The negative Hall constants for unoxidized carbons indicate the π band in baked carbons to be so depleted that the Fermi level lies at least partly below the inflection curve. The semi-metallic character of the conduction in baked carbons is furthermore emphasized by the fact that the temperature coefficient of resistance is independent of the oxidation level.

The author is grateful to Professor S. Mrozowski for his encouragement, guidance, and criticism. He also wishes to express appreciation to members of the Department of Physics for valued assistance.

THE JOURNAL OF CHEMICAL PHYSICS VOLUME 21, NUMBER 12 DECEMBER, 1953

Diffusional Processes in the Growth of Aerosol Particles. II*

H. L. Frisch† and F. C. Collins
Department of Chemistry, Polytechnic Institute of Brooklyn, Brooklyn, New York
(Received March 27, 1953)

The effect of the moving boundary of the growing aerosol particle upon the diffusional processes previously investigated for the special case of sinks with stationary boundaries is now discussed in detail. The zeroth-order approximation for the flux rate, valid for aerosol and most colloid systems, is found to be of the same analytic form as that for the stationary boundary case. A growth equation is derived for particles growing in the presence of a plurality of competing sinks which deplete the supersaturation. The growth equation here derived is found to be in satisfactory agreement with experiment in the case of barium sulfate crystals growing in aqueous solution. It is further shown that self-nucleated sols tend to monodispersity with growth. The effects of additional molecules becoming available for diffusion and of variability of the absorption probability are also discussed and evaluated for the special case of a single particle in the diffusion field.

INTRODUCTION

In an earlier paper,[1] approximate equations have been derived for the flux into sinks with stationary boundaries where the radius sink is small compared to the mean free path of the diffusing molecules, not every molecule colliding with the sink is absorbed, more than one sink exists within the diffusion field, and additional molecules become available during the diffusion process. In the present paper, the effect of the moving boundary of the growing spherical particle upon the flux and consequent growth rate of a particle subject to the above enumerated conditions is discussed. Suitable approximate equations are derived for the growth of aerosol particles and the relative magnitudes of the various factors affecting growth are evaluated.

Previous investigations of the effect of the three-dimensional moving boundary have restricted themselves to the special case of the Nernst boundary condition,[2,3] or to the steady state and a special form of the Nernst condition, the Smoluchowski boundary condition, which assumes that every molecule arriving at the sink is absorbed.[4–8] This paper will discuss an application of the perturbation method developed by one of us[9] to the spherically symmetric moving boundary problem where the boundary condition at the surface of the colloid particle is the previously derived "limiting" boundary condition,[1] which accounts for partial reflection of the diffusing species at this boundary. The solutions obtained will then be combined with the solution

* The research reported in this paper has been sponsored by the Geophysics Research Division of the Air Force Cambridge Research Center under Contract No. AF 19(122)–412.

† Present address: Department of Physics, Syracuse University, Syracuse, New York.

[1] H. L. Frisch and F. C. Collins, J. Chem. Phys. **20**, 1797 (1952).

[2] R. Rieck, thesis, Göttingen, 1924.

[3] F. C. Frank, Proc. Roy. Soc. (London) **A201**, 586 (1950).

[4] H. G. Houghton, Physics **2**, 467 (1932).

[5] N. Fuchs, Physik. Z. Sowjetunion **6**, 224 (1934).

[6] H. Reiss and V. K. La Mer, J. Chem. Phys. **18**, 1 (1950).

[7] H. Reiss, J. Chem. Phys. **19**, 482 (1951).

[8] H. Fujita and A. Kishimoto, J. Phys. Soc. Japan **6**, 408 (1951); Textile Research J. **22**, 94 (1952).

[9] H. L. Frisch, Z. Elektrochem. **56**, 324 (1952).

for the case of a plurality of sinks found in the previous paper,[1] in a derivation of an approximate equation describing the growth behavior of erosols.

THE MOVING BOUNDARY

The velocity of the moving boundary, $v(t)=dR/dt$, where $R(t)$ is the radius of the spherical sink and t is the time, is determined by applying the principle of conservation of mass. The quantity of vapor condensing per second at the surface of the growing aerosol droplet is given by the effective flux to the sink

$$\Phi(t)=4\pi R^2(t)D\left(\frac{\partial c}{\partial r}\right)_{R(t)}, \tag{1}$$

where c is the concentration in excess of the equilibrium concentration and D is the diffusion constant. This flux is proportional to the rate of increase of volume of the growing droplet as follows:

$$k\Phi(t)=\frac{dV}{dt}=4\pi R^2(t)\frac{dR}{dt}=4\pi R^2(t)v(t), \tag{2}$$

where $V(t)$ is the volume of the droplet and k is a proportionality constant depending on the choice of units for concentration and length.

Let us now investigate the effect of $v(t)$ on the diffusion to a single droplet located in an infinite region. Using the notation of the previous paper[1] we have

$$D\left(\frac{\partial^2 c}{\partial r^2}+\frac{2}{r}\frac{\partial c}{\partial r}\right)=\frac{\partial c}{\partial t}; \quad R(t)<r<\infty, \quad t>0 \tag{3}$$

$$\begin{aligned} &c(r,t)\to a \quad \text{as} \quad t\to 0; \quad r>R_0 \\ &c(r,t)\to a \quad \text{as} \quad r\to\infty; \quad t>0 \\ &\gamma(\partial c/\partial r)=c(R,t); \quad t>0, \end{aligned} \tag{3a}$$

where R_0 is the initial radius of the droplet and

$$\gamma=\rho/\alpha\epsilon. \tag{3b}$$

ρ is a length of the order of the mean free path; α, the absorption probability; and ϵ, a correction factor of the order of unity arising from the fact that the mean free path may be long compared with the sink radius. In the previous paper,[9] the concentration and velocity of the moving boundary in the one-dimensional case were expressed as series in a perturbation parameter, $ak=\lambda$. It was shown that, for $\lambda\ll 1$, only the first term of the series for the concentration and boundary velocity need be retained. This condition will always be fulfilled in the case of aerosols and will usually be fulfilled in the case of hydrosols. The term retained turns out to be the solution of the analog of Eq. (3) with fixed boundary.

Following the general method of the previous paper,[9] a moving reference system is introduced into Eqs. (1) to (3) by means of the relations

$$\xi=r-R(t), \quad t=t, \quad u(\xi,t)=c(r,t)/a. \tag{4}$$

Equation (3) becomes

$$D\left(\frac{\partial^2 u}{\partial\xi^2}+\frac{2}{\xi+R}\frac{\partial u}{\partial\xi}\right)+v(t)\frac{\partial u}{\partial\xi}=\frac{\partial u}{\partial t}, \quad 0<\xi<\infty, \quad t>0 \tag{5}$$

$$\begin{aligned} &u(\xi,t)\to 1 \quad \text{as} \quad t\to 0, \quad \xi>0 \\ &u(\xi,t)\to 1 \quad \text{as} \quad \xi\to\infty, \quad t>0 \\ &\gamma(\partial u/\partial\xi)_0=u(0,t), \quad t>0, \end{aligned}$$

and the velocity of the moving boundary is now

$$v(t)=kD(\partial u/\partial\xi)_0. \tag{6}$$

Expanding u and v in perturbation series,

$$\begin{aligned} u&=u_0+\lambda u_1+\lambda^2 u_2+\cdots \\ v&=\lambda v_1+\lambda^2 v_2+\cdots, \end{aligned}$$

one finds for $\lambda\ll 1$, the following solution for the zeroth-order term:[10]

$$c_0(r,t)=a-\frac{a(R-\beta)}{r}\left[\operatorname{erfc}\frac{r-R}{2(Dt)^{\frac{1}{2}}}-\exp\left(\frac{Dt}{\beta}+\frac{r-R}{\beta}\right)\operatorname{erfc}\left(\frac{r-R}{2(Dt)^{\frac{1}{2}}}+\frac{(Dt)^{\frac{1}{2}}}{\beta}\right)\right], \tag{7}$$

where $\beta=\gamma R/(R+\gamma)$. It is of interest to note that Eq. (7), corresponding to the zeroth-order terms of the perturbation series, is identical in form with the stationary boundary solution, Eq. (28), of the previous paper.[1]

The differential equation for the moving boundary can be obtained by use of Eqs. (1) and (2) on Eq. (7):

$$\frac{dR}{dt}=\frac{kD}{\gamma}\left\{\frac{a\beta}{R}\left[1-\exp\left(\frac{Dt}{\beta^2}\right)\operatorname{erfc}\left(\frac{(Dt)^{\frac{1}{2}}}{\beta}\right)\right]\right\}, \tag{8}$$

which for $(Dt)^{\frac{1}{2}}/\beta\gg 1$ can be written

$$\frac{dR}{dt}=\frac{kDa}{R+\gamma}\left[1+\frac{R^2}{(R+\gamma)^2(\pi Dt)^{\frac{1}{2}}}+\cdots\right]. \tag{9}$$

In the present physical case, γ will be much larger than R for small values of the time. Hence, except for a very short initial period, the rate of advance of the boundary is given with sufficient accuracy by the leading term of Eq. (7). Integration then gives

$$\gamma[R(t)-R_0]+\tfrac{1}{2}[R^2(t)-R_0]=akDt. \tag{10}$$

It is of interest to note that Eq. (10) predicts that the radius R of the growing aerosol particle initially has a linear dependence on the time before R becomes sufficiently large for Eq. (10) to assume, as a limiting form, the well-known parabolic growth law.[4] During this ini-

[10] F. C. Collins and H. L. Frisch, Report No. 2, July 31, 1952, Contract No. AF 19(122)-412, Air Force Cambridge Research Center.

tial growth period, the linear rate of growth is proportional to the absorption coefficient α as might be expected. However, when the growth equation assumes the limiting square form, the growth rate becomes independent of α, no matter how small α is. A small value of α, however, leads to a prolongation of the period during which the radius depends linearly on the time. The probability α is known[11] to be near unity for liquid mercury; it may be substantially smaller for associated liquids such as water.

When γ is set equal to zero, Eq. (10) agrees with the exact solution of the diffusion problem with the boundary condition,

$$c(R, t)=0. \tag{11}$$

It has been previously shown[3] that the exact form of $R(t)$ is (taking $R_0\simeq 0$)

$$R^2(t)=S^2Dt, \tag{12}$$

where

$$\lambda=ak=-\tfrac{1}{2}S^3\exp(S^2/4)\{(\pi)^{\frac{1}{2}}/2[1-\operatorname{erf}(S/2)] -S^{-1}\exp(-S^2/4)\}. \tag{13}$$

For $\lambda<1$ (S small), the right-hand side of Eq. (19) may be expanded in a power series in S, and thus one finds

$$S^2=2\lambda \tag{14}$$

in partial agreement with Eq. (7),

$$R^2(t)=2\lambda Dt=2akDt. \tag{15}$$

PRECISION OF THE APPROXIMATE MOVING BOUNDARY SOLUTION

It is now necessary to determine the error involved in the neglect of the higher-order terms in the perturbation series in the derivation of Eq. (7). This requires that Eq. (10) be derived by a somewhat more elaborate method. Corresponding to the neglect of higher-order terms in Eq. (9), the diffusion process will be considered in the "quasi-steady" state in which $\partial u/\partial t=0$. This is to be distinguished from the true "steady" state characterized by the vanishing of $\partial u/\partial t-v\partial u/\partial\xi$. Upon setting $\partial u/\partial t=0$ in Eq. (5), one obtains

$$D\left(\frac{\partial^2 u}{\partial\xi^2}+\frac{2}{\xi+R(t)}\frac{\partial u}{\partial\xi}\right)+v\frac{\partial u}{\partial\xi}=0. \tag{16}$$

Let $p(\xi)=\partial u/\partial\xi$; then

$$1/p(\partial p/\partial\xi)=-[2/(\xi+R)]-(v/D).$$

Integrating this equation once, one finds for

$$p(\xi)=\frac{\partial u}{\partial\xi}=A\exp\left(-\frac{v}{D}\xi\right)\Big/(\xi+R)^2, \tag{17}$$

where A is a constant of integration. Equation (17) is integrated from ξ to ∞, using the boundary condition at infinity, giving

$$u(\xi, t)=1-\frac{A\exp\left(-\frac{v}{D}\xi\right)}{\xi+R}+\frac{Av}{D}\int_{\xi+R}^{\infty}\frac{\exp\left[-\frac{v}{D}(x-R)\right]}{x}dx. \tag{18}$$

The constant of integration A can be evaluated from the boundary condition at $\xi=0$. One finds

$$A=R^2\Big/\left[\gamma+R-\frac{vR^2}{D}M\left(\frac{v}{D}R\right)\right], \tag{19}$$

where

$$M\left(\frac{v}{D}R\right)=\exp\left(\frac{vR}{D}\right)\left[1-\int_0^{vR/D}\frac{\exp(-x)}{x}dx\right].$$

Substituting Eq. (19) into Eq. (17), since

$$v=kD(\partial u/\partial\xi)_0,$$

we have

$$v=\left(\frac{\lambda D}{\gamma+R}\right)\left\{1\Big/\left[1-\frac{v}{D}\left(\frac{R^2}{\gamma+R}\right)M\left(\frac{v}{D}R\right)\right]\right\}. \tag{20}$$

Since

$$\frac{v}{D}\left(\frac{R^2}{\gamma+R}\right)M\left(\frac{v}{D}R\right)\ll 1$$

for all values of the physical variables, we may expand the last term of Eq. (20),

$$v=v_0\left[1+\frac{v}{D}\left(\frac{R^2}{\gamma+R}\right)M\left(\frac{v}{D}R\right)+\frac{v^2}{D^2}\left(\frac{R^2}{\gamma+R}\right)^2M^2\left(\frac{v}{D}R\right)+\cdots\right], \tag{21}$$

where

$$v_0=\lambda D/(\gamma+R).$$

The solution of this transcendental series for v may be approximated by iteration,

$$v=\lim_{n\to\infty}v_n=\lim_{n\to\infty}v_0\left[1+\frac{v_{n-1}}{D}\left(\frac{R^2}{\gamma+R}\right)\times M\left(\frac{v_{n-1}R}{D}\right)+\cdots\right];\quad n=1, 2, \cdots. \tag{22}$$

Hence

$$v=v_0\left[1+\lambda\left(\frac{R}{\gamma+R}\right)^2M\left(\frac{\lambda R}{\gamma+R}\right)+O(\lambda^2)\right]. \tag{23}$$

[11] M. Knudsen, Ann. Physik **47**, 697 (1915).

TABLE I. Magnitude of ϵ' vs η and R/γ.

p/p_0	10 001	1001	101	11
η	10^{-2}	10^{-3}	10^{-4}	10^{-5}
R/γ				
10^{-3}	10^{-8}	10^{-9}	10^{-10}	10^{-11}
10^{-2}	10^{-6}	10^{-7}	10^{-8}	10^{-9}
10^{-1}	8×10^{-4}	8×10^{-5}	8×10^{-6}	8×10^{-7}
1	2.5×10^{-3}	2.5×10^{-4}	2.5×10^{-5}	2.5×10^{-6}
10	8×10^{-3}	8×10^{-4}	8×10^{-5}	8×10^{-6}
10^2	10^{-2}	10^{-3}	10^{-4}	10^{-5}
∞	10^{-2}	10^{-3}	10^{-4}	10^{-5}

For values of $\lambda=ak\ll1$, Eq. (23) reduces to

$$v\simeq akD/(\gamma+R). \tag{24}$$

Upon integrating Eq. (24) with respect to time from zero to t, one obtains again Eq. (10).

The error ϵ' to terms in λ^2, committed in using Eq. (24) [and (10)], is found from Eq. (23) to be

$$\lambda\left(\frac{R}{\gamma+R}\right)^2 M\left(\frac{akR}{\gamma+R}\right)\leqslant\lambda\left(\frac{R}{\gamma+R}\right)^2=\epsilon'. \tag{25}$$

In Table I the magnitude of the error ϵ' is given as a function of the principal physical variables of the system corresponding to normal erosol growth problems. These are, at constant temperature, R/γ and λ which is related to the relative supersaturation p/p_0 of the diffusing substance. For example, for $R(t)=10^{-4}$ cm, $\gamma=10^{-4}$ cm, $\lambda=10^{-4}(p/p_0\simeq10^2)$, the error committed in using Eq. (24) for v is of the order of 2.5×10^{-3} percent.

GROWTH OF A SINGLE PARTICLE WITH A VARIABLE ABSORPTION PROBABILITY AND A SOURCE FUNCTION

The limiting boundary condition for droplets whose radius is smaller than the mean free diffusional jump length is, upon combining Eqs. (1), (3a), and (3b),

$$\Phi(t)=(4\pi R^2D\alpha\epsilon/\rho)c(R,t), \tag{26}$$

and as $\alpha\rightarrow1$, $\Phi(t)$ must approach $\Phi_T(t)$, the total flux of vapor molecules impinging on the droplet.

As the droplet grows, the assumption that the absorption probability α is constant will fail as a result of at least two causes: (a) the increase of the radius of the droplet may affect such parameters as the surface tension[12] of the droplet, which in turn would change the value of α; and (b) the higher temperature $T_s(t)$ of the transition zone between the liquid droplet and the vapor phase, due to the heat liberated on condensation of vapor molecules, which increases their fugacity in the interface and in turn decreases α. Under these conditions Eq. (3′) must be replaced by

$$(\partial c/\partial r)_R=(\epsilon\alpha(t)/\rho)c(R,t), \tag{27}$$

where $\alpha(t)$ is now a given function of the time. Unfortunately, the solution of diffusion equations with Eq. (27) as a boundary condition offers considerable mathematical difficulties. These can be circumvented by the following method: The flux of vapor molecules reflected by the droplet $\Phi_R(t)=\Phi_T(t)-\Phi(t)$ will lead to an increase in the concentration of vapor molecules in the interface separating the droplet from the vapor, above that which exists when all molecules impinging on the droplet are absorbed. This excess concentration will be denoted by $b(t)$. Its value is given by

$$b(t)=\rho\Phi_R(t)/4\pi R^2D\epsilon, \tag{28}$$

since the concentration gradient in the interface due only to the reflected vapor molecules is $b(t)\epsilon/\rho$. Substituting Eqs. (28) and (27) into the definition of α,

$$\alpha(t)=\frac{\Phi(t)}{\Phi_T(t)}=\frac{\Phi_T(t)-\Phi_R(t)}{\Phi_T(t)}=1-\frac{b(t)}{c(R,t)}. \tag{29}$$

The "limiting" boundary condition at the surface of the droplet $r=R$ is, instead of Eq. (27),

$$(\partial c/\partial r)_R=\epsilon/\rho[c(R,t)-b(t)]. \tag{30}$$

The boundary condition, Eq. (30), is the diffusion analog of Newton's law of cooling in heat conduction theory.[13]

Let us now consider the case where the excess concentration $c(R,t)$ is uniformly changing with time throughout the diffusion field. This change may be brought about by cooling of the medium, homogeneous chemical reaction, etc. It may be represented by introducing the source function $Q(t)$ into Eq. (3), which then becomes

$$D\left(\frac{\partial^2c}{\partial r^2}+\frac{2}{r}\frac{\partial c}{\partial r}\right)+Q(t)=\frac{\partial c}{\partial t} \tag{31}$$

in $R<r<\infty$, $t>0$, where $Q(t)$ is a homogeneous source function and

$$\begin{aligned} &c(r,0)=a, \quad r>R \\ &c(\infty,t)=a+\int_0^t Q(\tau)d\tau. \end{aligned} \tag{31a}$$

The solution of Eq. (31) with the boundary conditions (31a) can be found by means of Laplace transforms to be

$$\begin{aligned} c(r,t)=a&+\int_0^t Q(\tau)d\tau-\frac{aR^2}{r(\gamma+R)}F_1(r-R,t;\beta) \\ &-\frac{R^2}{r(\gamma+R)}\int_0^t Q(\tau)F_1(r-R,t-\tau;\beta)d\tau \\ &+\frac{R^2}{r(\gamma+R)}\int_0^t b(\tau)F_2(r-R,t-\tau;\beta)d\tau, \end{aligned} \tag{32}$$

[12] F. P. Buff, J. Chem. Phys. **19**, 1591 (1951).

[13] H. S. Carslaw and J. C. Jaeger, *Conduction of Heat in Solids* (Oxford University Press, New York, 1947), p. 13 ff.

where

$$F_1(r-R,\,t,\,\beta)=\operatorname{erfc}\left[\frac{r-R}{2(Dt)^{\frac{1}{2}}}\right]-\exp\left[\frac{r-R}{\beta}+\frac{Dt}{\beta^2}\right]\operatorname{erfc}\left[\frac{r-R}{2(Dt)^{\frac{1}{2}}}+\frac{(Dt)^{\frac{1}{2}}}{\beta}\right]$$

and

$$F_2(r-R,\,t;\beta)=\frac{1}{\beta}\left(\frac{1}{\pi Dt}\right)^{\frac{1}{2}}\exp\left[\frac{r-R}{2(Dt)^{\frac{1}{2}}}\right]^2-\frac{1}{\beta^2}\exp\left[\frac{r-R}{\beta}+\frac{Dt}{\beta^2}\right]\operatorname{erfc}\left[\frac{r-R}{2(Dt)^{\frac{1}{2}}}+\frac{(Dt)^{\frac{1}{2}}}{\beta}\right].$$

It may be noted that F_1 is the integral of F_2,

$$\int_0^t F_2(r-R,\,\tau;\beta)d\tau=F_1(r-R,\,\tau;\beta). \tag{33}$$

As the time increases, $c(r,\,t)$, given by Eq. (32) can be approximated by the steady-state solution $c(r,\,t)$ satisfying the criterion

$$(\partial c/\partial t)=Q(\tau).$$

This solution, which can be found either directly or from inspection of Eq. (32), is

$$c(r,\,t)=a+\int_0^t Q(\tau)d\tau-\frac{R^2}{r(\gamma+R)}\left[a+\int_0^t Q(\tau)d\tau-b(t)\right]. \tag{34}$$

The gradient at $r=R$ is

$$(\partial c/\partial r)_R=\left[a+\int_0^t Q(\tau)d\tau-b(t)\right]/(\gamma+R). \tag{35}$$

In the case of aerosol growth where $ak\ll 1$, the velocity of the moving boundary is given to a good approximation by substituting the steady-state gradient, Eq. (35), into Eqs. (1) and (2),

$$v(t)=(dR/dt)=kD\left[a+\int_0^t Q(\tau)d\tau-b(t)\right]\Big/(\gamma+R). \tag{36}$$

Integrating Eq. (36) from 0 to t, one obtains the radius of a growing single aerosol particle for which the boundary condition, Eq. (31), holds in the presence of the source function $Q(t)$,

$$\gamma[R(t)-R_0]+\tfrac{1}{2}[R^2(t)-R_0^2]=kD\left[at+\int_0^t\int_0^\tau Q(s)ds\,d\tau-\int_0^t b(\tau)d\tau\right]. \tag{37}$$

THE GROWTH OF AN AEROSOL PARTICLE SURROUNDED BY A PLURALITY OF COMPETING AEROSOL PARTICLES

The preceding formulas for the radius and volume of a growing aerosol particle may be strictly applied if, and only if, a single particle is present in the diffusion field. This is an idealization which in practice is almost never attained. Due to the plurality of aerosol particles competing for vapor molecules, the flux of vapor molecules to any given particle Φ is smaller than the flux Φ_0 without the competing particles. In consequence, the volume $V(t)$ of a given particle will be smaller than $V_0(t)$ in the absence of the competing sinks. The fluxes and volumes are related as before by

$$(dV/dt)=k\Phi(t);\quad (dV_0/dt)=k\Phi_0(t). \tag{38}$$

Let us consider that the particle which we wish to study is surrounded by a concentration of m competing monodisperse aerosol particles, homogeneously and randomly distributed in the very large volume V containing the system. We have shown[14] that the flux in the presence of competition is given by

$$\Phi=\Phi_0\exp\left[-\frac{m}{a}\int_0^t\Phi_0(\tau)d\tau\right], \tag{39}$$

where $\Phi_0(t)$ is the flux to the central droplet in the absence of other competing droplets. Equation (39) describes the diminution of the flux to the exhaustion of the supersaturation. The steady-state form of the flux Φ_0 is obtained by combining Eq. (2) with the leading term of Eq. (9). Thus the flux Φ, taking into account the competition effect but neglecting the short initial period when the steady-state form of Eq. (9) is not valid, is

$$\Phi(t)=\frac{4\pi R^2Da}{\gamma+R}\exp\left[-\frac{m}{a}\int_0^t\frac{4\pi R^2Da}{\gamma+R}d\tau\right]. \tag{40}$$

The time dependence of the radius R is obtained from Eq. (40) by the use of Eq. (2) and is

$$\frac{4\pi R^2}{k}\frac{dR}{dt}=\frac{4\pi R^2Da}{\gamma+R}\exp\left[-\frac{m}{a}\int_0^t\frac{4\pi R^2Da}{\gamma+R}d\tau\right]. \tag{41}$$

The last equation can be put into the form

$$4\pi R^2dR/k=(a/m)e^{-s}ds, \tag{42}$$

where

$$s=\frac{m}{a}\int_0^t\frac{4\pi R^2Da}{\gamma+R}d\tau. \tag{43}$$

Upon integration Eq. (42) becomes

$$(4\pi/3)(R^3-R_0^3)=(ak/m)(1-e^{-s}). \tag{44}$$

Rearranging Eq. (44) and taking the logarithms of

[14] F. C. Collins and H. L. Frisch, J. Chem. Phys. **21**, 1116 (1953).

both sides gives

$$-s=\ln[1-(4\pi/3)(m/ak)(R^3-R_0^3)], \quad (45)$$

which, upon reintroducing Eq. (43) and differentiating, yields

$$\left(\frac{m}{a}\right)\frac{4\pi R^2 Da}{\gamma+R}=\frac{4\pi(m/ak)R^2(dR/dt)}{[1-(4\pi/3)(m/ak)(R^3-R_0^3)]}. \quad (46)$$

By separating variables and integrating, we finally obtain

$$\left(\frac{4\pi}{3}\frac{m}{a}\right)^{\frac{1}{3}}k^{\frac{1}{3}}Dat$$

$$=\frac{\gamma}{3A^2}\left[\tfrac{1}{2}\ln\frac{(A^2+Ax+x^2)}{(A-x)^2}\frac{(A-x_0)^2}{(A^2+Ax_0+x_0^2)}\right.$$

$$+\sqrt{3}\tan^{-1}\left(\frac{2x+A}{A\sqrt{3}}\right)-\sqrt{3}\tan^{-1}$$

$$\left.\times\left(\frac{2x_0+A}{A\sqrt{3}}\right)\right]+\frac{[(3/4\pi)(ak/m)]^{\frac{1}{3}}}{3A}$$

$$\times\left[\tfrac{1}{2}\ln\frac{(A^2+Ax+x^2)}{(A-x)^2}\frac{(A-x_0)^2}{(A^2+Ax_0+x_0^2)}\right.$$

$$\left.+\sqrt{3}\tan^{-1}\left(\frac{2x+A}{A\sqrt{3}}\right)-\sqrt{3}\tan^{-1}\left(\frac{2x_0+A}{A\sqrt{3}}\right)\right], \quad (47)$$

where

$$x=[(4\pi/3)(m/ak)]^{\frac{1}{3}}R; \quad x_0=[(4\pi/3)(m/ak)]^{\frac{1}{3}}R_0,$$

$$A=1+(4\pi/3)(m/ak)R_0^3.$$

Equation (47) can be considerably simplified. By combining Eqs. (38) and (39)

$$dV=dV_0\exp\left[-\frac{m}{ak}\int_0^t\frac{dV_0}{d\tau}d\tau\right]$$

$$=dV_0\exp\left\{-\frac{m}{ak}[V_0(t)-V_0(0)]\right\}. \quad (48)$$

Equation (48) is easily integrated to give

$$V(t)-V(0)=(ak/m)$$
$$\times\{1-\exp[-(m/ak)(V_0(t)-V_0(0))]\}. \quad (49)$$

The initial volume is the same with or without competition, $V(0)=V_0(0)=V_0$, so that the final limiting volume V_∞ is then

$$V_\infty=V_0+(ak/m), \quad (50)$$

which is the value expected from *a priori* considerations. Now the initial volume will be ordinarily small compared to the final limiting volume so that

$$x_0=R_0/R_\infty\simeq 0, \quad A\simeq 1,$$

where

$$R_\infty\simeq[(3/4\pi)(ak/m)]^{\frac{1}{3}}.$$

Thus Eq. (47) can be written

$$kDat/R_\infty=\tfrac{1}{6}(\gamma+R_\infty)\ln\frac{R_\infty^2+R_\infty R+R^2}{(R_\infty-R)^2}$$

$$+\frac{\sqrt{3}}{3}(\gamma-R_\infty)\left[\tan^{-1}\frac{2R+R_0}{R_\infty\sqrt{3}}-\tan^{-1}\frac{1}{\sqrt{3}}\right]. \quad (51)$$

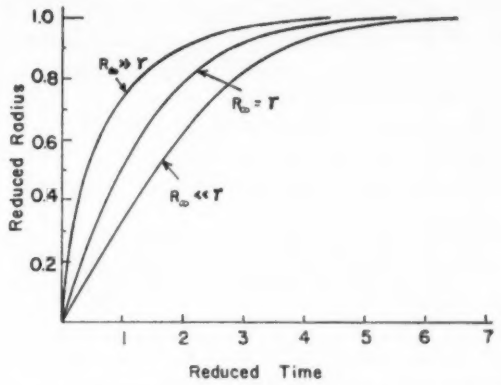

FIG. 1. The reduced radius $R(t)/R_\infty$ as a function of the reduced time $kDat/R_\infty(\gamma+R_\infty)$.

It will be seen from Eq. (51) that the form of the dependence of the radius $R(t)$ upon the time depends on the relative magnitudes of γ and R_∞. The γ and R_∞ terms on the right-hand side of Eq. (51) express the contributions of the "boundary condition" control and "pure diffusion" control to the particle growth. The larger the constant, $\gamma=\rho/\alpha\epsilon$, the more nearly linear the growth behavior will be. In the cloud-droplet growth problem, the absorption probability α and the correction factor ϵ introduced by the long mean free path both appear to be near unity, so that the radius as a function of the time depends on the ratio of the limiting radius of the droplet and the mean free path of the vapor molecules.

In Fig. 1, the dimensionless ratio $R(t)/R_\infty$ is plotted against the time-dependent dimensionless ratio $kDat/R_\infty(\gamma+R_\infty)$ for the limiting cases

$$R_\infty\ll\gamma, \quad R_\infty=\gamma, \quad \text{and} \quad R_\infty\gg\gamma.$$

In Fig. 2, the ratio of the volumes $V(t)/V_\infty$ is plotted against the same dimensionless ratio for the same limiting cases. It will be seen that a family of curves similar to those of Figs. 1 and 2 may be plotted for any specified values of the ratio R_∞/γ, thus enabling prediction of the growth behavior for any values of the initial supersaturation a, the diffusion constant D, and the mean free path. If experimental data for the growth as a function of time are available, the fit of the data on one

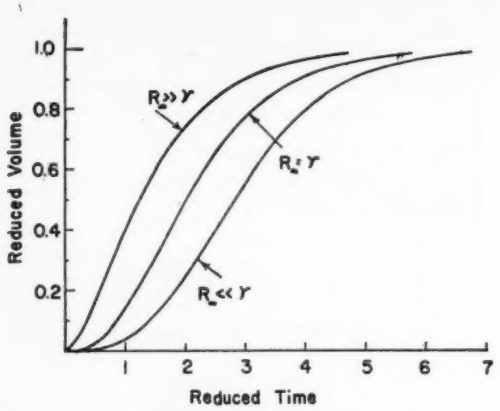

FIG. 2. The reduced volume $V(t)/V_\infty$ as a function of the reduced time $kDat/R_\infty(\gamma+R_\infty)$.

of the family of curves, as in Figs. 1 or 2, enables approximate determination of the constant γ. The value of the absorption coefficient α can then be immediately calculated using a value of the mean free path obtained from the kinetic theory of gases.

Equation (51) is also applicable to hydrosols. Data for the growth of barium sulfate crystals in supersaturated aqueous solution have been recently obtained by Leineweber[15] and David Turnbull[16] using conductivity measurements. The method of measurement enables precise determination of the fraction of the supersaturated solute precipitated at any given time. The sols were prepared by Turnbull by direct mixing of solutions while Leineweber used the La Mer-Dinegar[17] method of introducing the sulfate ion by homogeneous chemical reaction. Figure 3 compares data from a typical determination of Leineweber with a curve calculated from the theoretical Eq. (51). The data were adjusted so that the effect of the continued slow production of sulfate ion by the chemical reaction could be ignored. The chemical reaction rate is very slow compared to the growth process, so that the corresponding adjustment of the experimental points is small. The obtaining of the theoretical curve required the arbitrary choice of a zero on the time scale and also of the proportionality factor $kDa/R_\infty(\gamma+R_\infty)$. It will be seen that the resulting agreement between the theoretical curve and the experimental points is close.

EFFECT OF POLYDISPERITY OF THE NUCLEI

It is implicit in the above treatment that the droplets of which the system is composed all have the same initial radius R_0 at the starting point in time. However, in any actual system, the sizes of the droplets at any arbitrarily selected starting time will be somewhat polydisperse because of small differences in the times of their nucleation. It is, therefore, important to ascertain whether these differences in droplet radius become accentuated as growth proceeds or whether the system tends toward monodispersivity with growth.

Let us assume at some arbitrarily chosen starting time very shortly after the end of the nucleation period (which is abruptly terminated by the small decrease in the supersaturation which takes place as a consequence of the nucleation process itself) there exists a distribution $m(\rho_0)$ of droplet radii ρ_0. It will be further assumed that while $0<\rho_0<\infty$, $m(\rho_0)$ approaches zero sharply at values of ρ_0 not greatly larger than the radius of the critical nucleus.

The sink function expressing the effect of the competition between droplets is then

$$f=\frac{c(r,t)\int_0^\infty m(\rho_0)\Phi(t;\rho_0)d\rho_0}{a-\int_0^t\int_0^\infty m(\rho_0)\Phi(\tau;\rho_0)d\rho_0 d\tau}, \tag{52}$$

to be substituted in Eq. (43) in the earlier paper[1] in place of Eq. (37′) of the erratum.[14] We may then obtain in analogy with Eq. (41′) of the erratum

$$\Phi(t;R_0)=\Phi_0(t;R_0)\exp\left\{-\int_0^\infty\int_0^{\Theta_p(t)}\times\frac{m(\rho_0)d\Theta_p'd\rho_0}{a-\int_0^\infty m(\rho_0')\Theta_p'(\tau,\rho_0')d\rho_0}\right\}, \tag{53}$$

where

$$\Theta_p(t)=\int_0^t\Phi(\tau;\rho_0)d\tau,$$

$$d\Theta_p=\Phi(\tau;\rho_0).$$

Multiplying Eq. (53) by $m(\rho_0)$ and integrating, we ob-

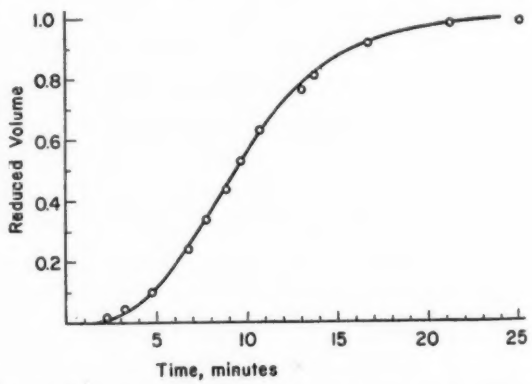

FIG. 3. Comparison of experimental data (0) obtained by J. P. Leineweber for the growth of barium sulfate crystals in water with the theoretical curve from Eq. (51) for the case of $\gamma \gg R_\infty$.

[15] J. P. Leineweber, American Cyanamid Company (private communication).

[16] David Turnbull, General Electric Research Laboratory, advance copy of manuscript submitted to *Acta Metallurgica*.

[17] V. K. La Mer and R. H. Dinegar, J. Am. Chem. Soc. **73**, 380 (1951).

tain by a derivation similar to that presented in the earlier paper[1]

$$\int_0^\infty m(\rho_0)\Phi(t;\rho_0)d\rho_0=\int_0^\infty m(\rho_0)\Phi(t;\rho_0)$$

$$\times\exp\left[-\frac{1}{a}\int_0^\infty\int_0^t m(\rho_0')\Phi(\tau;\rho_0')d\tau d\rho_0'\right], \quad (54)$$

so that for all those droplets with the radius R_0 at the starting point in time, the flux rate is

$$\Phi(t;R_0)=\Phi_0(t,R_0)$$

$$\times\exp\left[-\frac{1}{a}\int_0^t\int_0^\infty m(\rho_0')\Phi_0(\tau,\rho_0')d\rho_0'd\tau\right]$$

$$=\Phi(t,R_0)\exp\left[-\frac{m}{a}\int_0^t\langle\Phi_0(\tau)\rangle d\tau\right], \quad (55)$$

where $\langle\Phi(\tau)\rangle$ represents the mean flux averaged over all droplet sizes. Equation (55) is analogous to Eq. (39) of the present paper for the monodisperse system except that the exponential term is a function of the mean flux instead of the flux to the central reference droplet. The form of Eq. (55) is such that the dependence of the radius of the selected droplet cannot be readily obtained even should the function $m(\rho_0)$ be known. However, it is possible to draw certain conclusions concerning the relative rates of growth of the various droplet sizes without solving Eq. (55). Because the exponential decay factor is common to all droplet sizes, the rate of growth of a given droplet relative to those of other sizes will depend only on the *a priori* flux $\Phi_0(t,R_0)$. Thus, making use of Eq. (24),

$$\frac{dR'/dt}{dR/dt}=\frac{kDa/(\gamma+R')}{kDa/(\gamma+R)}=\frac{\gamma+R}{\gamma+R'}. \quad (56)$$

Here R and R' are the radii of droplets which had the radii R_0 and R_0', respectively, at the starting point in time. Thus the relative rates of growth are equal in the region $\gamma\gg R$ and inversely proportional to the ratio of the radii in the region where $\gamma\ll R$, thus tending to suppress differences in relative radius with growth. However, even should γ be greater than R throughout the growth period, initial differences in droplet radius become insignificant as the droplets approach their limiting sizes because $R_\infty\gg R_0$. Hence it may be concluded that in the case of self-nucleation, the resulting aerosol will tend to be monodisperse. It may be further concluded that no serious error is introduced by the use of Eq. (51) which was derived assuming monodispersivity for the actually occurring case where the initial radius of the droplets may not be strictly uniform.

THE EFFECT OF THE VARIABLE VAPOR PRESSURE OF THE DROPLET ON ITS GROWTH IN THE PRESENCE OF COMPETING DROPLETS

To take account of the combined effect of variable vapor pressure of the droplet and of competition, it is necessary to introduce Eq. (35) into Eqs. (2) and (39) in place of Eq. (9). However, the resulting expression cannot be readily integrated to yield a growth law comparable to Eq. (47). However, numerical analysis of the growth of water droplets[18] reveals that the change of vapor pressure due to superheating of the droplet by the condensation process and the variation of surface tension with droplet radius contributes a lowering of the flux rate by less than 10 percent. Hence, Eq. (51) can be used in conjunction with Eq. (36) to compute the actual growth behavior by obvious perturbation and graphical methods. The correction is, however, of the order of the uncertainties of the experimental measurements and detailed calculations will not be presented here.

CONCLUSION

A growth law of relatively simple form has been obtained for aerosol and other colloid particles growing in supersaturated media. The effects of the moving boundary of the particle and the depletion of the supersaturation by the growth process are taken account of in the growth law. The contributions of secondary effects, such as variable absorption probability at the particle boundary and additional molecules becoming available for diffusion during the growth process, must be calculated by perturbation methods. Fortunately these latter contributions are small.

An experimental study of the growth of self-nucleated hydrosols is in progress for further comparison of theory with experiment. The results of the investigation will be presented elsewhere.

---

[18] F. C. Collins, Final Report, Contract No. AF19(122)–412, Air Force Cambridge Research Center.

Note on a Nitrogen Molecule Calculation*

MAX WOLFSBERG
Chemistry Department, Brookhaven National Laboratory, Upton, Long Island, New York
(Received June 19, 1953)

Recent calculations of the binding energy of the nitrogen molecule carried out by Kopineck are examined by means of molecular orbital calculations. The Hellmann-Kopineck procedure of omitting certain permutations in a valence bond procedure is investigated. It is concluded that the Kopineck calculation should not be used as an argument favoring the 9.8 ev value for the binding energy (D_0^0) of the nitrogen molecule.

I. INTRODUCTION

NONEMPIRICAL quantum mechanical calculations of binding energies of molecules have been largely restricted to molecules containing only s bonds. Recently H-J. Kopineck[1] has, however, attempted to calculate a potential energy curve for the $^1\Sigma_g^+$ ground state of the nitrogen molecule. His calculations were made possible by his compilation of tables of integrals[2] which are necessary for such computations and which previously were not available in the literature. For reasons of greater ease of calculation, Kopineck first treated the nitrogen molecule as a six electron problem (omitting both the $1s$ and $2s$ electrons) and later as a ten electron problem (omitting only the $1s$ electrons). He employed a valence bond approach as outlined by Hellmann.[3] The calculations were carried out with the use of hydrogenic $2p$ atomic orbitals and nodeless hydrogenic $2s$ atomic orbitals. The effective Z's of the $2s$ and $2p$ orbitals were assumed to be the same and were fixed by a variational procedure. Prior to the appearance of Kopineck's first paper on nitrogen, the author had carried out calculations on the lowest lying $^1\Sigma_g^+$ state of the C_2 molecule[4] (treated as an eight electron problem) employing a molecular orbital approach. At one stage in the calculations a variational approach was employed to calculate the effective Z values to be used in the atomic orbitals. It was found, as it was also found by Kopineck, that the effective Z's thus obtained are quite different from the Slater Z values for the free atoms[5] (because of the fact that the nodeless $2s$ orbitals were used in these molecular calculations, see reference 1) and the author was, therefore, not greatly disturbed that the binding energy obtained by this procedure was much too large. It was, therefore, rather surprising when Kopineck, using a similar variational approach, was able to construct a potential curve for the nitrogen molecule (when treated as a ten electron problem) in quite good agreement, in the vicinity of the equilibrium internuclear distance, with the experimental one favored by Gaydon. It appeared worthwhile, therefore, to reinvestigate Kopineck's calculation, especially since Kopineck concluded that his calculation points towards the correctness of the 9.8 ev value for the dissociation energy (D_0^0) of nitrogen and since he also concluded that the treatment employed was probably of general applicability to other molecular systems.

II. MOLECULAR ORBITAL PROCEDURE

Computations were carried out on the N_2 molecule using the LCAO molecular orbital method. The atomic orbitals employed were of the same form as those employed by Kopineck with effective Z values found, as by Kopineck, by means of a variational procedure. One calculates the energy for different values of a parameter $\alpha=(Z/2)(R/a_0)$, where R is the internuclear distance and a_0 is the Bohr radius. The expression for the energy takes the form $E=A(\alpha)Z^2+B(\alpha)Z$. In calculating a potential energy curve, employing a variational procedure to fix Z as Kopineck did, one must then take into account the fact that A and B depend on Z implicitly. Since there was no interest in actually constructing a potential energy curve in carrying out the calculations reported in this note, the Z corresponding to each α was simply calculated by $Z=-B/2A$. In practice the Z's calculated in this way differ but little from those calculated by the more exact procedure. The important thing, of course, is that an energy calculated in this way must always be either equal to or larger than the energy corresponding to the potential minimum calculated by the full variational procedure.

The following single configuration molecular orbital wave functions were employed:

treated as a six electron problem,

$$\Psi=(\pi_u 2p)^4(\sigma_g 2p)^2; \tag{1}$$

treated as a ten electron problem,

$$\Psi=(\sigma_g 2s)^2(\sigma_u 2s)^2(\pi_u 2p)^4(\sigma_g\omega)^2. \tag{2}$$

These wave functions were properly antisymmetrized. The molecular orbital designation is the usual one with

$$\sigma_g\omega=\xi(\sigma_g 2s)+\eta(\sigma_g 2p), \tag{3}$$

* Research carried out under the auspices of the U. S. Atomic Energy Commission.

[1] H-J. Kopineck, Z. Naturforsch. **7a**, 22 (1952); **7a**, 314 (1952).

[2] H-J. Kopineck, Z. Naturforsch. (a) **5a**, 420 (1950); (b) **6a**, 177 (1951); also (c) **7a**, 785 (1952) for correction of previous integrals and some new integrals not used in the calculation here discussed.

[3] H. Hellmann, *Einfuhrung in die Quantenchemie* (Franz Deuticke, Leipzig and Wien, 1937).

[4] M. Wolfsberg (to be published).

[5] J. C. Slater, Phys. Rev. **36**, 57 (1930).

where ξ and η are determined by the conditions that $\sigma_g\omega$ is to be orthogonal to $\sigma_g 2s$ and also normalized. Thus only forced hybridization[6] is included in this calculation and no attempt is made to minimize the energy with respect to a hybridization parameter as was done by Kopineck. The Hamiltonians used in these computations were the same as those used in Kopineck's computation with effective nuclear charges of 3 for the six electron calculation and 5 for the ten electron calculation. The results of the six and ten electron calculations are listed in Tables I and II[7] in terms of the difference between the separated atoms energy $[E(S^4+{}^4S)]$ (which has the same value in our calculation as in Kopineck's calculation) and the molecular energy calculated at a given value of α. This energy difference is called the binding energy and is compared with Kopineck's maximum value of this difference. It is seen that the binding energies here calculated tend to be larger than Kopineck's. The binding energies may still be further increased by introducing configuration interaction. Thus it was found for $\alpha=5.5$ in the ten electron calculation that configuration interaction of the ${}^1\sum_g{}^+$ molecular orbital configuration (2) with four other ${}^1\sum_g{}^+$ molecular orbital states,[8] not especially chosen for having large matrix elements with the configuration (2), raised the binding energy from 7.00 ev to 13.03 ev. Now a variational procedure does not guarantee a binding energy equal to or less than the true binding energy in a case where, in the first place, the energy of the separated atoms is not the true energy of the separated atoms and where, secondly, not all the electrons are included in the calculation. One concludes then that Kopineck's excellent results are quantum mechanically fortuitous and that, if he had introduced resonance with other valence bond structure, he would have calculated much larger binding energies[9] since, of course, any molecular orbital function may be expressed as a linear combination of valence bond functions.

In order to test the molecular orbital computations, it was decided to construct a linear combination of molecular orbital wave functions equivalent to the valence bond function employed by Kopineck and then to evaluate the energy matrix element of this function. In the process of attempting to do this, it was found that the transformation properties of the wave functions employed by Kopineck both in the treatment of the molecule as a six electron problem and as a ten electron problem are not those of ${}^1\sum_g{}^+$ functions. In fact the functions were found not to transform according to any irreducible representation of $D_{\infty h}$. This problem was investigated further for the six electron problem because of the greater ease of handling this problem. It was found here that the Kopineck function could be expressed as a linear combination of ${}^1\sum_g{}^+$ and ${}^1\Gamma_g$ molecular orbital wave functions. The six electron Kopineck function is

$$\Psi=\sum_P (1-T_{cd})(1-T_{ef})(1-T_{gh}) \times P\varphi\delta_P(1+T_{cd})(1+T_{ef})(1+T_{gh})P\psi^{10}, \quad (4)$$

where P is the permutation operator

$\delta_P=\pm 1$, depending on whether the permutation is even or odd

$\varphi=[cd][ef][gh]$

and

$$\psi=\psi_c(1)\psi_d(2)\psi_e(3)\psi_f(4)\psi_g(5)\psi_h(6) =a_\sigma(1)b_\sigma(2)a_{\pi y}(3)b_{\pi y}(4)a_{\pi z}(5)b_{\pi z}(6). \quad (5)$$

Here the bracket symbol $[cd]$ is the Weyl spin invariant

$$[cd]=\alpha_c\beta_d-\alpha_d\beta_c, \quad (6)$$

where α and β have their usual spin connotation. a_σ stands for the p_σ atomic orbital on atom a and b_σ stands for the corresponding orbital on atom b, and the T's are transposition operators. When the function (4) is expanded, one finds, using usual notation,[11] that it is

TABLE I. Six electron molecular orbital calculations. (Maximum binding energy found by Kopineck, 7.55 ev, at $R=1.196$A, $Z=2.43$).

$\frac{Z}{2}\frac{R}{a_0}$	Z	Binding energy (ev)
3.5	2.54	7.5
3.0	2.53	11.3
2.5	2.49	14.1

TABLE II. Ten electron molecular orbital calculations. (Maximum binding energy found by Kopineck, 9.261 ev, at $R=1.108$A, $Z=5.2$).

$\frac{Z}{2}\frac{R}{a_0}$	Z	Binding energy (ev)
5.5	5.23	7.0
5.0	5.25	11.6
4.5	5.24	13.7
4.0	5.18	11.3

[6] R. S. Mulliken, J. Chem. Phys. **19**, 912 (1951).

[7] The results listed here were obtained using the integrals listed in Kopineck's tables in references 2(a) and 2(b). Some of the binding energies were recalculated using the corrections listed in reference 2(c) and using more accurate one center and one electron integrals. The binding energies obtained in this way differed from the original ones by only a few tenths of an electron volt.

[8] These four states were: three states resulting from the configuration $\ldots(\pi_u 2p)^2(\pi_g 2p)^2\ldots$ and one state resulting from the configuration $\ldots(\pi_g 2p)^4\ldots$

[9] Actually, it will be seen in the next section that Kopineck's low binding energies have also another cause.

[10] The summation has here been extended over all permutations P rather than only over the permutations P' (see next section) for reasons of convenience. Summation only over P' is of course equivalent to summation over P.

[11] See for instance Eyring, Walter, and Kimball, *Quantum Chemistry* (John Wiley and Sons, Inc., New York, 1947), p. 144.

equal to

$$\Psi=\tfrac{1}{4}\sum_P(-1)^P P_P(a_\sigma b_\sigma a_{\pi x} b_{\pi x} a_{\pi y} b_{\pi y}+a_\sigma b_\sigma a_{\pi x} b_{\pi x} b_{\pi y} a_{\pi y}+a_\sigma b_\sigma b_{\pi x} a_{\pi x} a_{\pi y} b_{\pi y}+a_\sigma b_\sigma b_{\pi x} a_{\pi x} b_{\pi y} a_{\pi y}+\text{all these terms with } a \text{ replaced by } b \text{ and vice versa}+\text{all previous terms with } x\leftrightarrow y-\text{all previous terms with spins interchanged}), \quad (7)$$

where

$$a_\sigma b_\sigma a_{\pi x} b_{\pi x} a_{\pi y} b_{\pi y} = a_\sigma(1)\alpha(1) b_\sigma(2)\beta(2) a_{\pi x}(3)\alpha(3) b_{\pi x}(4)\beta(4) \times a_{\pi y}(5)\alpha(5) b_{\pi y}(6)\beta(6). \quad (8)$$

The function (7) may then be expressed in terms of molecular orbital functions. Define, therefore, the following molecular orbital functions

$$A=j\bar{j}k\bar{k}=$$

$$B=\tfrac{1}{2}(j\bar{j}c\bar{c}+j\bar{j}d\bar{d}+k\bar{k}c\bar{c}+k\bar{k}d\bar{d})=$$

$$D=\frac{1}{2\sqrt{2}}(jk\bar{c}\bar{d}+jk\bar{d}\bar{c}+k\bar{j}c\bar{d}+k\bar{j}d\bar{c}+j\bar{j}c\bar{c}+k\bar{k}d\bar{d}-j\bar{j}d\bar{d}-k\bar{k}c\bar{c})= \quad (9)$$

$$E=c\bar{c}d\bar{d}=$$

$$T=\frac{1}{2\sqrt{2}}(jk\bar{c}\bar{d}+jk\bar{d}\bar{c}+k\bar{j}c\bar{d}+k\bar{j}d\bar{c}-j\bar{j}c\bar{c}-k\bar{k}d\bar{d}+j\bar{j}d\bar{d}+k\bar{k}c\bar{c})=$$

and further define

$$A_f=\sum_P(-1)^P P_P j\bar{j}k\bar{k}f\bar{f}= \quad (10)$$

$$A_h=\sum_P(-1)^P P_P j\bar{j}k\bar{k}h\bar{h}=$$

etc.

where $j, k, c, \cdots$ are normalized molecular orbitals

$$j=(a_{\pi x}+b_{\pi x})N \qquad k=(a_{\pi y}+b_{\pi y})N$$
$$c=(a_{\pi x}-b_{\pi x})N' \qquad d=(a_{\pi y}-b_{\pi y})N' \quad (11)$$
$$f=(a_\sigma+b_\sigma)N_P \qquad h=(a_\sigma-b_\sigma)N_P'.$$

One finds then that function (7) may be expressed in the following form

$$\Psi=M[2N^{-4}N_P^{-2}A_f-2N^{-4}N_P'^{-2}A_h+2N'^{-4}N_P^{-2}E_f-2N'^{-4}N_P'^{-2}E_h+N^{-2}N'^{-2}N_P^{-2}(\sqrt{2}D_f-\sqrt{2}T_f-2B_f)+N^{-2}N'^{-2}N_P'^{-2}(-\sqrt{2}D_h+\sqrt{2}T_h+2B_h)], \quad (12)$$

where M is a normalizing factor. All of the molecular orbital expressions are ${}^1\sum_g{}^+$ functions except T_f and T_h which are ${}^1\Gamma_g$ functions. Computing energies with the function (12), one finds at $\alpha=2.5$, with $Z=2.52$, a binding energy of 8.8 ev and at $\alpha=3.0$,[12] with $Z=2.50$, a binding energy of 9.1 ev. Both of these binding energies are lower than the corresponding binding energies computed with the single molecular orbital configuration, but are still larger than those computed by Kopineck using the Hellmann valence bond procedure. It was therefore decided to investigate the procedure employed by Kopineck.

[12] The normalized wave function (12), becomes at $\alpha=3.0$,

$$\Psi=0.716A_f-0.519A_h+0.094E_f-0.068E_h+0.183D_f-0.183T_f-0.259B_f-0.133D_h+0.133T_h+0.188B_h.$$

By comparison, the single configuration molecular orbital function (1) is just A_f.

III. VALENCE BOND PROCEDURE

The Hellmann procedure of calculating valence bond energies leads to the following equation

$$\sum_{P'}[(1-T_{cd})(1-T_{ef})(1-T_{gh})P'\varphi]\delta_{P'} \times[\psi|H-E|(1+T_{cd})(1+T_{ef})(1+T_{gh})P'\psi]=0, \quad (13)$$

where P' stands for all those permutations which satisfy the requirement that none of the $(1+T_{cd})(1+T_{ef})\times(1+T_{gh})P'\psi$'s are identically equal to each other.

Now, following Hellmann, Kopineck first restricted P' to the following:

$$P'=1, T_{ce}, T_{cg}, T_{df}, T_{dh}, T_{eg}, T_{fh}, T_{cf}, T_{ch}, T_{de}, T_{dg}, T_{eh}, T_{fg}, \quad \text{for } (\psi|H|\cdots P'\psi), \quad (14)$$

and

$$P'=1, \quad \text{for } (\psi|E|\cdots P'\psi). \quad (15)$$

Following Hellmann, Kopineck then also omits all terms involving products of transpositions. The binding energies calculated in this way were found to be ten times as high as the expected magnitude of the binding energy (D_0^0) of the N_2 molecule. In the next higher approximation, Kopineck does not restrict the P' for $(\psi|E|\cdots P'\psi)$ to 1 but uses the same P''s that are used for $(\psi|H|\cdots P'\psi)$. This is the approximation by which the results given in his paper were calculated.

It was now decided to make a completely rigorous calculation using the Hellmann formula (13). There are 720 permutations of six electrons. It was found, on account of orthogonality relationships existing between the atomic orbitals employed, that only 104 of these permutations give non-zero values of $(\psi|H|P\psi)$. It was moreover found that these 104 permutations are all the permutations obtained by multiplying 1, T_{cd}, T_{ef}, T_{gh}, $T_{cd}T_{ef}$, $T_{cd}T_{gh}$, $T_{ef}T_{gh}$, $T_{cd}T_{ef}T_{gh}$ by all the P' permutations given in (14). Taking into account the fact that

$$(1-T_{cd})(1-T_{ef})(1-T_{gh})1\varphi=2^3\varphi$$
$$(1-T_{cd})(1-T_{ef})(1-T_{gh})(-T_{ce})\varphi=(1-T_{cd})(1-T_{ef})(1-T_{gh})(-T_{cg})\varphi=\cdots=-2^2\varphi, \quad (16)$$

one obtains from (13)

$$[\psi|H-E|(1+T_{cd})(1+T_{ef})(1+T_{gh})(1-\tfrac{1}{2}T_{ce}-\tfrac{1}{2}T_{cg}-\tfrac{1}{2}T_{df}-\tfrac{1}{2}T_{dh}-\cdots)\psi]=0. \quad (17)$$

The energy was calculated in this way for $\alpha=2.5$ and $\alpha=3.0$. A complete check was obtained with the mo-

lecular orbital calculation using the function (12) presented in the last section. This is a very good check on the internal consistency of the calculation here presented.

To justify his approximation, Kopineck calculated in some cases the added contribution to the energy gotten by including up to three and four electron permutations in the $(\psi|H|P\psi)$ integrals but only including two electron permutations in the $(\psi|E|P\psi)$ integrals. We found that the binding energies calculated in this particular way at $\alpha=2.5$ and $\alpha=3.0$ are of the order of two to three times the binding energies calculated by (13), (14), (15). This result appears to be at variance with that obtained by Kopineck, who found that the inclusion of the higher permutations in the $(\psi|H|P\psi)$'s changed the final results only negligibly.

CONCLUSIONS

It has been shown very specifically how the discrepancy between the single configuration molecular orbital calculation and the valence bond calculation arises in the six electron case. It appears reasonable to assume that for the ten electron calculation the discrepancy is again attributable to a basic difference in the wave function and to the errors arising from Kopineck's approximation in dealing with permutations.

A number of conclusions may be reached from these calculations. Firstly, one may say that at the present time no quantum theoretical calculation exists which favors any one of the proposed binding energies (D_0^0) of the nitrogen molecule. Secondly, the procedure employed by Kopineck is certainly of no general applicability; if it should give reasonable binding energies for other molecular systems its use could be justified only empirically, but not quantum mechanically without carrying out further calculations. From a more general view the calculations presented here show the danger involved in making calculations with only one single configuration, be it of the valence bond or of the molecular orbital type. Lastly, as far as the question of the kinds of permutations which must be retained in carrying out valence bond calculations is concerned, it has been shown in the particular case here treated that the Hellmann-Kopineck approximation of only using transpositions certainly appears unjustified.

THE JOURNAL OF CHEMICAL PHYSICS VOLUME 21, NUMBER 12 DECEMBER, 1953

Applications of the Free Volume Theory of Binary Mixtures*

ZEVI W. SALSBURG† AND JOHN G. KIRKWOOD
Sterling Chemistry Laboratory, Yale University, New Haven, Connecticut

(Received June 11, 1953)

Detailed calculations for the free volume theory of binary mixtures are presented and compared with experimental results. It is found that this theory predicts heats of mixing and volumes of mixing larger in magnitude than the observed values and excess entropies of mixing which are smaller than the experimental results. The theory, however, does predict a volume contraction, a negative excess entropy of mixing and a positive heat of mixing for solutions of carbon tetrachloride and neopentane in qualitative agreement with recent observations.

THE free volume theory[1–3] has provided a useful description of the thermodynamic properties of dense gases and liquids. To facilitate the application of this theory Wentorf, Buehler, Hirschfelder, and Curtiss[4] prepared tables of all the pertinent thermodynamic properties over a wide range of temperatures and densities. Comparison with experimental results shows that the theoretical calculations are unsatisfactory in the critical region but improve at high densities. These calculations have been applied only to spherical nonpolar molecules where the energy of interaction between a pair of molecules, i and j, can be represented satisfactorily by the Lennard-Jones type potential,

$$V_{ij}(R)=4\epsilon_{ij}\left[\left(\frac{a_{ij}}{R}\right)^{12}-\left(\frac{a_{ij}}{R}\right)^{6}\right]. \quad (1)$$

In view of these results and the simplicity of the numerical calculations, it seemed advisable to extend this theory to liquid mixtures in order to try to calculate the excess thermodynamic properties of simple liquid nonelectrolyte solutions. By combining the Lennard-Jones and Devonshire cell method[2] with the order-

* This work was carried out with support from the U. S. Office of Naval Research under Contract with Yale University.

† National Science Foundation Fellow, 1952–1953. Material herein presented is contained in the thesis of Zevi W. Salsburg presented for the degree of Doctor of Philosophy in Yale University. Present address: University of Amsterdam, Amsterdam, Holland.

[1] H. J. Eyring and J. O. Hirschfelder, J. Chem. Phys. 4, 250 (1937).

[2] J. E. Lennard-Jones and A. F. Devonshire, Proc. Roy. Soc. (London) **A163**, 53 (1937); **A165**, 1 (1938).

[3] J. G. Kirkwood, J. Chem. Phys. **18**, 380 (1950).

[4] Wentorf, Buehler, Hirschfelder, and Curtiss, J. Chem. Phys. 18, 1484 (1950).

disorder theory of the crystalline state, we[5] have recently derived expressions for the excess thermodynamic properties of fluid mixtures. The purpose of this article is to present in detail the numerical calculations based upon this theory and to give a comparison with experimental results. In general this theory predicts heats of mixing larger than the experimental values and excess entropies of mixing which are smaller than the experimental results.

The simple theory of nonpolar mixtures developed by Hildebrand[6] and his co-workers states that it is the square of the difference between the square roots of the cohesive energy densities of the components which determines the deviations from ideality. However, the treatment of nearly ideal solutions makes too drastic a demand on this simple theory since it requires a small difference between large numbers. One finds that the quantitative calculations based on Hildebrand's theory give only about a fifth of the measured values for the heats of mixing (e.g., see reference 22). The model considered in this semi-empirical approach neglects deviations from a random distribution of molecules in the neighborhood of a given molecule and also neglects effects that give rise to volume changes on mixing. In addition, the interpretation of this theory in terms of statistical mechanics is obscure.

Using the cell method of Lennard-Jones and Devonshire, Prigogine and his co-workers[7–10] have recently formulated a solution theory which is closely related to our development. In addition to the random mixing hypothesis they have assumed that the Lennard-Jones potential parameters a_{ij} [see Eq. (1)] for all the components are equal. While the cells in the free volume theory are all equal in size, the relative sizes of the molecules are not nearly as severely limited. We shall see that small variations in the relative sizes of the components have an appreciable effect on the mixing properties of the solutions. The simplified model considered by Prigogine *et al.*, however, does show that the effects related to a change of volume on mixing at constant pressure can give rise to important entropy and heat changes.

In mixture theories in which the intermolecular potential is assumed to be a sum of pair potentials there arises the problem of determining the parameters which describe the interaction between unlike pairs of molecules. The analysis of the dispersion forces by London indicates that, for the energy parameter ϵ_{ij}, the geometric mean approximation

$$\epsilon_{ij}=(\epsilon_{ii}\epsilon_{jj})^{\frac{1}{2}} \tag{2}$$

may be used for similar type molecules. The experimental work on the measurement of second virial coefficients for gaseous mixtures[11] supports this assumption and moreover indicates that a suitable approximation to a_{ij} is given by

$$a_{ij}=(a_{ii}+a_{jj})/2. \tag{3}$$

The article by Prigogine and Mathot[8] considers the qualitative effects due to deviations of ϵ_{ij} from the value given by Eq. (2). This problem has also been treated in a recent article by Rowlinson[12] who, in the same manner as Prigogine, assumes that all a_{ij} are equal. The errors introduced by this assumption are of the same order of magnitude as those effects which Prigogine and Rowlinson attribute to deviations from the geometric mean approximation. In fact, the numerical calculations will show that small changes in the relative value of $a_{ii}-a_{jj}$ in certain cases can change the sign of the predicted volumes and excess entropies of mixing.

I. EQUATIONS FOR THE THERMODYNAMIC FUNCTIONS

In a recent article[5] we have extended the free volume theory to multicomponent fluid mixtures. The expressions for the thermodynamic functions on which our numerical calculations are based were obtained under the following approximations.

(a) The communal free energy, $RT\ln\sigma$ [see Eq. (5) or reference 5], which contains the corrections due to multiple occupancy of the cells is approximated by its low density value, $\sigma=e$. This approximation is identical to that originally made by Eyring and Hirschfelder.[1] However, there is reason to believe that for common liquids the high density value of $\sigma=1$ would be more appropriate. In any case, if one approximates σ by a constant the excess entropy of mixing is independent of this constant.

(b) Under the restriction of single occupancy for each cell, the relative probability density in configuration space $P^{(1)}$ is approximated by a product of distribution functions for the individual cells. That is

$$P^{(1)}=\prod_{s=1}^{N}\varphi_s,$$

where φ_s depends only on the position of the molecule in cell s and on the given distribution of molecules in the neighboring cells. By minimizing the Helmholtz free energy at constant temperature and volume one obtains a set of simultaneous integral equations for the cell distribution functions.

(c) An approximate solution to this set of integral equations which is identical in form with the Lennard-Jones and Devonshire[2] cell distribution function is used.

[5] Z. W. Salsburg and J. G. Kirkwood, J. Chem. Phys. **20**, 1538 (1952).
[6] J. H. Hildebrand and R. L. Scott, *The Solubility of Nonelectrolytes* (Reinhold Publishing Corporation, New York, 1950), third edition.
[7] I. Prigogine and V. Mathot, J. Chem. Phys. **20**, 49 (1950).
[8] I. Prigogine and G. Garikian, Physica **16**, 236 (1950).
[9] I. Sarolea, J. Chem. Phys. **21**, 182 (1953).
[10] J. Nasielski, J. Chem. Phys. **21**, 184 (1953).
[11] R. H. Fowler and E. A. Guggenheim, *Statistical Thermodynamics* (Cambridge University Press, Cambridge, 1939), pp. 296–300.
[12] J. S. Rowlinson, Proc. Roy. Soc. (London) **A214**, 192 (1952).

Mayer and Careri[13] have recently given an alternative approximation to this function which may prove to give better quantitative results.

(d) The method of moments[14,15] is used to solve the order disorder problem for the distribution of molecules among cells. For our approximate calculations we have only retained the first moment. This is equivalent to the random mixing assumption made by Prigogine *et al.*[7,8] For the case of a quasi-lattice model, the problem of nonrandom mixing has been studied by Kirkwood,[15] Rushbrooke,[16] and Guggenheim.[17] These results indicate that the corrections due to nonrandomness are small compared to the free volume corrections. This numerical comparison can be seen in Table VIII. A recent analysis by Sarolea,[9] who used the theory developed by Prigogine, supports the view that these corrections are small.

The results of our treatment are identical in form with the Lennard-Jones and Devonshire theory for a pure liquid in which the potential constants (or parameters) are given by certain averages of the constants for the individual components. For a system containing N_1 molecules of type 1, N_2 of type 2, $\cdots$, N_r of type r, the free energy can be written in the form

$$A_{N_1,\cdots,N_r}=NkT\sum_{i=1}^{r}x_i\ln x_i + A^*_{N_1,\cdots,N_r}+A^E_{N_1,\cdots,N_r}, \quad (4)$$

where

$$A^*_{N_1,\cdots,N_r}=-kT\sum_{i=1}^{r}N_i\ln\left\{ev\left(\frac{2\pi m_i kT}{h^2}\right)^{\frac{3}{2}}\right\}, \quad (4a)$$

$$A^E_{N_1,\cdots,N_r}=-NkT\ln\frac{2\pi\sqrt{2}G}{N}+\frac{N}{2}E_0(N_1,\cdots,N_r). \quad (4b)$$

T is the thermodynamic temperature, k the Boltzmann constant, m_i the mass of a molecule of species i, and v is the volume of the system. x_i is the mole fraction of species i.

$$E_0=12\bar{\epsilon}\left\{1.0109\left(\frac{\bar{v}^0}{v}\right)^4-2.4090\left(\frac{\bar{v}^0}{v}\right)^2\right\}, \quad (5)$$

$$G=\int_0^{0.030544}y^{\frac{1}{2}}\exp[-\beta w_0(y)]dy, \quad (6)$$

where

$$\beta=1/kT,$$

$$w_0(y)=12\bar{\epsilon}\left\{\left(\frac{\bar{v}^0}{v}\right)^4L(y)-2\left(\frac{\bar{v}^0}{v}\right)^2M(y)\right\}$$

and

$$L(y)=l(y)+\frac{1}{128}l\left(\frac{y}{2}\right)+\frac{2}{729}l\left(\frac{y}{3}\right),$$

$$M(y)=m(y)+\frac{1}{16}m\left(\frac{y}{2}\right)+\frac{2}{27}m\left(\frac{y}{3}\right),$$

$$l(y)=(1+12y+25.2y^2+12y^3+y^4)(1-y)^{-10}-1,$$

$$m(y)=(1+y)(1-y)^{-4}-1.$$

The average constants $\bar{\epsilon}$ and $\bar{v}^0$ are functions of the Lennard-Jones constants for the individual types of molecular pairs and the mole fractions of the components,

$$\bar{v}^0=\left\{\frac{\sum_{i,l=1}^{r}x_ix_l\epsilon_{il}v_{il}{}^{0^4}}{\sum_{i,l=1}^{r}x_ix_l\epsilon_{il}v_{il}{}^{0^2}}\right\}^{\frac{1}{2}}, \quad (7)$$

$$\bar{\epsilon}=\frac{\left\{\sum_{i,l=1}^{r}x_ix_l\epsilon_{il}v_{il}{}^{0^2}\right\}^2}{\sum_{i,l=1}^{r}x_ix_l\epsilon_{il}v_{il}{}^{0^4}}, \quad (8)$$

where

$$v_{il}{}^0=Na_{il}{}^3,$$

$$N=\sum_{i=1}^{r}N_i.$$

The equation of state is given by the relation

$$\frac{pv}{NkT}=1-\frac{12\bar{\epsilon}}{kT}\left[2.4090\left(\frac{\bar{v}^0}{v}\right)^2-2.0219\left(\frac{\bar{v}^0}{v}\right)^4\right]-\frac{48\bar{\epsilon}}{kT}\left[\left(\frac{\bar{v}^0}{v}\right)^2\left(\frac{g_M}{G}\right)-\left(\frac{\bar{v}^0}{v}\right)^4\left(\frac{g_L}{G}\right)\right], \quad (9)$$

where

$$g_M=\int_0^{0.30544}y^{\frac{1}{2}}M(y)\exp[-\beta w_0(y)]dy$$

$$g_L=\int_0^{0.30544}y^{\frac{1}{2}}L(y)\exp[-\beta w_0(y)]dy.$$

The internal energy of gas imperfection per mole takes the form

$$E^E=\frac{N}{2}E_0+12N\bar{\epsilon}\left[\left(\frac{\bar{v}^0}{v}\right)^4\frac{g_L}{G}-2\left(\frac{\bar{v}^0}{v}\right)^2\frac{g_M}{G}\right]. \quad (10)$$

The excess entropy, S^E, is defined in such a way that it is zero in the limit of large volume. From Eq. (4) we

[13] J. E. Mayer and G. Careri, J. Chem. Phys. **20**, 1001 (1952).
[14] J. G. Kirkwood, J. Chem. Phys. **6**, 70 (1938).
[15] J. G. Kirkwood, J. Phys. Chem. **43**, 97 (1939).
[16] G. S. Rushbrooke, Proc. Roy. Soc. (London) **A166**, 296 (1938).
[17] E. A. Guggenheim, Proc. Roy. Soc. (London) **A148**, 304 (1935).

obtain

$$S^E = Nk \ln \frac{G}{G_\infty} + \frac{N}{T} 12\bar{\epsilon}\left[\left(\frac{\bar{v}^0}{v}\right)^4 \frac{g_L}{G} - 2\left(\frac{\bar{v}^0}{v}\right)^2 \frac{g_M}{G}\right] \quad (11)$$

$$G_\infty = \lim_{v\to\infty} G = (2\pi\sqrt{2})^{-1}.$$

The chemical potential μ_i of component i can be obtained from Eq. (4) and the thermodynamic relation

$$\mu_i = (\partial A/\partial N_i)_{T,\, v,\, N_j}.$$

The result is

$$\mu_i = \mu_i^* + kT \ln x_i + \mu_i^E \quad (12)$$

where

$$\mu_i^* = -kT \ln v\left\{\left(\frac{2\pi m_i kT}{h^2}\right)^{\frac{3}{2}}\right\}.$$

μ_i^E is the excess chemical potential referred to the ideal gas as a standard state.

$$\mu_i^E = -kT \ln \frac{2\pi\sqrt{2}G}{N} - 12\bar{\epsilon}\left\{1.2045\left(\frac{\bar{v}^0}{v}\right)^2 - \left(1.51635 + \frac{2g_L}{G}\right)\left(\frac{\bar{v}^0}{v}\right)^4\right\}$$

$$-\sum_{l=1}^{r} x_l 12\epsilon_{li}\left\{\left(2.4090 + \frac{4g_M}{G}\right)\left(\frac{v_{li}^0}{v}\right)^2 - \left(1.0109 + \frac{2g_L}{G}\right)\left(\frac{v_{li}^0}{v}\right)^4\right\}.$$

In the simple theory proposed by Hildebrand[6] the cohesive energy density plays a central role. This quantity can be obtained by means of the relation

$$\frac{v}{NkT}\left(\frac{\partial E^E}{\partial v}\right)_T = 1 - \frac{pv}{NkT} - 4\left(\frac{12\bar{\epsilon}}{kT}\right)^2\left(\frac{\bar{v}^0}{v}\right)^4 B, \quad (13)$$

where

$$B = \left(\frac{\bar{v}^0}{v}\right)^4\left[\left(\frac{g_L}{G}\right)^2 - \frac{g_{LL}}{G}\right] + 3\left(\frac{\bar{v}^0}{v}\right)^2\left[\frac{g_{ML}}{G} - \frac{g_M}{G}\frac{g_L}{G}\right] + 2\left[\left(\frac{g_M}{G}\right)^2 - \frac{g_{MM}}{G}\right]$$

and

$$g_{LL} = \int_0^{0.30544} y^{\frac{1}{2}}[L(y)]^2 \exp[-\beta w_0(y)]dy,$$

$$g_{ML} = \int_0^{0.30544} y^{\frac{1}{2}} L(y) M(y) \exp[-\beta w_0(y)]dy,$$

$$g_{MM} = \int_0^{0.30544} y^{\frac{1}{2}}[M(y)]^2 \exp[-\beta w_0(y)]dy.$$

The excess heat capacity at constant volume, C_v^E, can be computed from the relation

$$\frac{C_v^E}{Nk} = \left(\frac{12\bar{\epsilon}}{kT}\right)^2\left(\frac{\bar{v}_0}{v}\right)^4\left\{\left(\frac{\bar{v}^0}{v}\right)^4\left[\frac{g_{LL}}{G} - \left(\frac{g_L}{G}\right)^2\right] + 4\left(\frac{\bar{v}^0}{v}\right)^2\left[\frac{g_L}{G}\frac{g_M}{G} - \frac{g_{ML}}{G}\right] + 4\left[\frac{g_{MM}}{G} - \left(\frac{g_M}{G}\right)^2\right]\right\}. \quad (14)$$

Equations (4) and (9) through (14) enable one to calculate all the pertinent thermodynamic functions of the system. The enthalpy of the system can be obtained from Eqs. (9) and (10) together with the thermodynamic definition $H = E + pv$. The excess internal energy and entropy of mixing per mole of solution are defined by

$$\Delta E^E = E^E - \sum_{i=1}^{r} x_i E_i^E, \quad (15)$$

$$\Delta S^E = S^E - \sum_{i=1}^{r} x_i S_i^E, \quad (16)$$

where E_i^E and S_i^E are the molal internal energy and entropy of gas imperfection for pure component i.

II. CALCULATION OF THE THERMODYNAMIC FUNCTIONS

It is convenient to express the volume, temperature, and pressure in the reduced forms,

$$q = \frac{v}{\bar{v}^0} \quad (17)$$

$$\theta = \frac{kT}{\bar{\epsilon}} \quad (18)$$

$$p^* = \frac{p}{p_1} = \left(\frac{pv}{NkT}\right)\left(\frac{kT}{\bar{\epsilon}}\right)\left(\frac{\bar{v}^0}{v}\right) \quad (19)$$

Here p_1 is the characteristic pressure of the substance defined as

$$p_1 = 136.23\left(\frac{\bar{\epsilon}}{k}\right)\frac{1}{\bar{a}^3}\text{ atmos.}; \quad \bar{a} = (\bar{v}^0/N)^{\frac{1}{3}},$$

where $\bar{\epsilon}/k$ is given in degrees Kelvin and $\bar{a}$ is given in Angströms.

The magnitudes of the excess mixing properties of the simple solutions we wish to treat are very small in comparison with the total thermodynamic quantities. Therefore, unless the calculations are carried out with extreme accuracy the error in the calculation will be greater than the mixing property itself. Although Wentorf, Buehler, Hirschfelder, and Curtiss[4] have compiled extensive tables of the free volume thermodynamic functions, the accuracy of these tables does not permit the calculation of the excess mixing properties of solu-

TABLE I. Integrals.[a]

q	θ	G	ε_L/G	ε_M/G	ε_{LL}/G	ε_{MM}/G	ε_{LM}/G
0.94	0.15	1.80198(−5)	2.45168(−2)	5.78886(−3)	2.34147(−4)	5.50469(−5)	9.96033(−4)
0.94	0.16	1.98287(−5)	2.60955(−2)	6.15693(−3)	2.65860(−4)	6.24343(−5)	1.13218(−3)
0.94	0.17	2.16375(−5)	2.76741(−2)	6.52500(−3)	2.97572(−4)	6.98217(−5)	1.26832(−3)
0.94	0.19	2.54453(−5)	3.08077(−2)	7.25357(−3)	3.67852(−4)	8.61471(−5)	1.57090(−3)
0.94	0.20	2.74158(−5)	3.23657(−2)	7.61509(−3)	4.05500(−4)	9.48743(−5)	1.73333(−3)
0.95	0.25	4.11491(−5)	4.23101(−2)	9.91102(−3)	6.87426(−4)	1.59887(−4)	2.95609(−3)
0.95	0.26	4.35368(−5)	4.39150(−2)	1.02797(−2)	7.39664(−4)	1.71875(−4)	3.18377(−3)
0.95	0.27	4.59614(−5)	4.55142(−2)	1.06466(−2)	7.93557(−4)	1.84225(−4)	3.41898(−3)
0.95	0.30	5.34458(−5)	5.02778(−2)	1.17365(−2)	9.64945(−4)	2.23395(−4)	4.16906(−3)
0.96	0.30	5.80065(−5)	5.30378(−2)	1.23661(−2)	1.07122(−3)	2.47611(−4)	4.63558(−3)
0.96	0.31	6.07780(−5)	5.46948(−2)	1.27434(−2)	1.13784(−3)	2.62761(−4)	4.92860(−3)
0.96	0.32	6.35833(−5)	5.63458(−2)	1.31187(−2)	1.20614(−3)	2.78272(−4)	5.22947(−3)
0.96	0.34	6.92917(−5)	5.96303(−2)	1.38639(−2)	1.34773(−3)	3.10358(−4)	5.85440(−3)
0.97	0.36	8.16214(−5)	6.69336(−2)	1.55072(−2)	1.71499(−3)	3.92771(−4)	7.49188(−3)
0.97	0.37	8.46323(−5)	6.79788(−2)	1.57493(−2)	1.74066(−3)	3.98990(−4)	7.59705(−3)
0.97	0.38	8.78604(−5)	6.96747(−2)	1.61307(−2)	1.82649(−3)	4.18272(−4)	7.97930(−3)
0.97	0.40	9.44046(−5)	7.30485(−2)	1.68879(−2)	2.00313(−3)	4.57870(−4)	8.76752(−3)
0.98	0.40	1.02234(−4)	7.69190(−2)	1.77544(−2)	2.21419(−3)	5.05068(−4)	9.71180(−3)
0.98	0.42	1.09411(−4)	8.04291(−2)	1.85376(−2)	2.41532(−3)	5.49901(−4)	1.06146(−2)
0.98	0.43	1.13042(−4)	8.21747(−2)	1.89263(−2)	2.51845(−3)	5.72841(−4)	1.10784(−2)
0.98	0.44	1.16700(−4)	8.39141(−2)	1.93131(−2)	2.62325(−3)	5.96122(−4)	1.15504(−2)
0.98	0.45	1.20385(−4)	8.56473(−2)	1.96980(−2)	2.73970(−3)	6.19738(−4)	1.20305(−2)
0.99	0.48	1.42283(−4)	9.55052(−2)	2.18778(−2)	3.37126(−3)	7.61460(−4)	1.49366(−2)
0.99	0.49	1.46355(−4)	0.72932(−2)	2.22714(−2)	3.49481(−3)	7.88627(−4)	1.54988(−2)
0.99	0.50	1.50451(−4)	9.90749(−2)	2.26630(−2)	3.62001(−3)	8.16123(−4)	1.60693(−2)
1.00	0.50	1.62553(−4)	1.04134(−1)	2.37726(−2)	3.98429(−3)	8.94962(−4)	1.77327(−2)
1.00	0.52	1.71433(−4)	1.07838(−1)	2.45819(−2)	4.26324(−3)	9.56872(−4)	1.90112(−2)
1.00	0.53	1.75909(−4)	1.09679(−1)	2.49836(−2)	4.40529(−3)	9.87826(−4)	1.96635(−2)
1.00	0.54	1.80408(−4)	1.11515(−1)	2.53832(−2)	4.54902(−3)	1.01910(−3)	2.03246(−2)
1.00	0.55	1.84929(−4)	1.13344(−1)	2.57810(−2)	4.69442(−3)	1.05070(−3)	2.09942(−2)
1.01	0.57	2.09337(−4)	1.22820(−1)	2.78340(−2)	5.47818(−3)	1.22041(−3)	2.46172(−2)
1.01	0.58	2.14254(−4)	1.24709(−1)	2.82413(−2)	5.64187(−3)	1.25570(−3)	2.53772(−2)
1.01	0.60	2.24151(−4)	1.28467(−1)	2.90501(−2)	5.97430(−3)	1.32721(−3)	2.69239(−2)
1.02	0.60	2.41605(−4)	1.34781(−1)	3.04052(−2)	6.54796(−3)	1.45030(−3)	2.96004(−2)
1.02	0.62	2.52286(−4)	1.38670(−1)	3.12326(−2)	6.91648(−3)	1.52903(−3)	3.13272(−2)
1.02	0.63	2.57657(−4)	1.40605(−1)	3.16483(−2)	7.10329(−3)	1.56886(−3)	3.22044(−2)
1.04	0.70	3.42112(−4)	1.68941(−1)	3.76303(−2)	1.00867(−2)	2.19869(−3)	4.63555(−2)
1.04	0.71	3.48390(−4)	1.70978(−1)	3.80556(−2)	1.03208(−2)	2.24760(−3)	4.74774(−2)
1.04	0.72	3.54682(−4)	1.73008(−1)	3.84788(−2)	1.05566(−2)	2.29679(−3)	4.86080(−2)
1.04	0.75	3.73649(−4)	1.79058(−1)	3.97366(−2)	1.12737(−2)	2.44605(−3)	5.20603(−2)
1.06	0.76	4.37885(−4)	1.98116(−1)	4.36719(−2)	1.36496(−2)	2.93715(−3)	6.35728(−2)
1.06	0.77	4.45198(−4)	2.00554(−1)	4.41615(−2)	1.40165(−2)	3.01006(−3)	6.54288(−2)
1.06	0.78	4.52319(−4)	2.02411(−1)	4.45507(−2)	1.42191(−2)	3.05388(−3)	6.63567(−2)
1.08	0.82	5.52485(−4)	2.30142(−1)	5.01750(−2)	1.81154(−2)	3.84562(−3)	8.55693(−2)
1.08	0.83	5.60685(−4)	2.32405(−1)	5.06291(−2)	1.84550(−2)	3.91395(−3)	8.72611(−2)
1.08	0.84	5.68895(−4)	2.34661(−1)	5.10809(−2)	1.87964(−2)	3.98254(−3)	8.89639(−2)
1.08	0.85	5.77112(−4)	2.36909(−1)	5.15307(−2)	1.91395(−2)	4.05138(−3)	9.06776(−2)
1.08	0.87	5.93572(−4)	2.41382(−1)	5.24237(−2)	1.98307(−2)	4.18978(−3)	9.41372(−2)
1.10	0.87	6.78814(−4)	2.62710(−1)	5.66589(−2)	2.32288(−2)	4.86658(−3)	1.11238(−1)
1.10	0.88	6.88048(−4)	2.65092(−1)	5.71272(−2)	2.36287(−2)	4.94533(−3)	1.13268(−1)
1.10	0.89	6.97288(−4)	2.67465(−1)	5.75933(−2)	2.40302(−2)	5.02471(−3)	1.15310(−1)
1.10	0.90	7.06532(−4)	2.69830(−1)	5.80571(−2)	2.44336(−2)	5.10412(−3)	1.17364(−1)
1.10	0.91	7.15780(−4)	2.72188(−1)	5.85187(−2)	2.48386(−2)	5.18376(−3)	1.19428(−1)
1.12	0.90	8.05431(−4)	2.93018(−1)	6.25838(−2)	2.84815(−2)	5.89754(−3)	1.38070(−1)
1.12	0.93	8.36377(−4)	3.00538(−1)	6.40344(−2)	2.98751(−2)	6.16776(−3)	1.45277(−1)
1.12	0.94	8.46693(−4)	3.03028(−1)	6.45133(−2)	3.03431(−2)	6.25826(−3)	1.47705(−1)
1.12	0.95	8.57010(−4)	3.05510(−1)	6.49898(−2)	3.08129(−2)	6.34896(−3)	1.50133(−1)
1.14	0.95	9.73295(−4)	3.30938(−1)	6.98526(−2)	3.57253(−2)	7.29335(−3)	1.75773(−1)
1.14	0.96	9.84738(−4)	3.33570(−1)	7.03504(−2)	3.62609(−2)	7.39528(−3)	1.78596(−1)
1.14	0.97	9.96178(−4)	3.36192(−1)	7.08450(−2)	3.67983(−2)	7.49839(−3)	1.81433(−1)
1.14	1.00	1.03047(−3)	3.44006(−1)	7.23157(−2)	3.84209(−2)	7.80485(−3)	1.90023(−1)
1.16	0.97	1.12800(−3)	3.63444(−1)	7.59690(−2)	4.24813(−2)	8.57284(−3)	2.11562(−1)
1.16	0.99	1.15326(−3)	3.68982(−1)	7.69967(−2)	4.37026(−2)	8.80127(−3)	2.18113(−1)
1.16	1.00	1.16587(−3)	3.71770(−1)	7.75069(−2)	4.43159(−2)	8.91573(−3)	2.21410(−1)
1.18	1.02	1.34356(−3)	4.06829(−1)	8.39656(−2)	5.23174(−2)	1.04002(−2)	2.64694(−1)
1.18	1.03	1.35738(−3)	4.09716(−1)	8.44895(−2)	5.30133(−2)	1.05277(−2)	2.68506(−1)
1.18	1.05	1.38498(−3)	4.15462(−1)	8.55296(−2)	5.44104(−2)	1.07831(−2)	2.76176(−1)

[a] Note.—The number in parentheses is the power of 10 by which the corresponding entry is to be multiplied.

tions. In addition these tables omit calculations for $\theta<0.70$ since this represents the experimental triple point for simple monatomic solids (argon, neon, etc.). In view of these considerations we have undertaken the numerical program of calculating the thermodynamic properties in the region of interest.

TABLE II. Thermodynamic functions.[a]

q	θ	p^*	pv/NkT	E^E/N	S^E/Nk
0.94	0.15	−3.14400(−1)	−1.97024(0)	−8.36897	−6.27571
0.94	0.16	−2.23784(−1)	−1.92911(−1)	−8.35471	−7.18237
0.94	0.17	−1.29167(−1)	−7.14220(−2)	−8.34044	−7.09714
0.94	0.19	5.49524(−2)	5.49524(−2)	−8.31207	−6.93932
0.94	0.20	1.73333(−1)	6.89030(−1)	−8.29794	−6.86684
0.95	0.25	−2.62737(−2)	−9.98400(−2)	−8.20821	−6.47479
0.95	0.26	6.31745(−2)	2.30830(−1)	−8.19437	−6.42051
0.95	0.27	1.52362(−1)	5.36090(−1)	−8.18057	−6.36842
0.95	0.30	4.18421(−1)	1.32500(0)	−8.13937	−6.22372
0.96	0.30	−1.52141(−1)	−4.86850(−1)	−8.11426	−6.14615
0.96	0.31	−6.46447(−2)	−2.00190(−1)	−8.10068	−6.10159
0.96	0.32	2.26000(−2)	6.78000(−2)	−8.08713	−6.05857
0.96	0.34	1.96356(−1)	5.54416(−1)	−8.06013	−5.97673
0.97	0.36	−1.21557(−1)	−3.27528(−1)	−7.99813	−5.80752
0.97	0.37	−6.55609(−2)	−1.71876(−1)	−7.99014	−5.78821
0.97	0.38	1.94819(−2)	4.97300(−2)	−7.97688	−5.75274
0.97	0.40	1.88859(−1)	4.57982(−1)	−7.95047	−5.69499
0.98	0.40	−2.83935(−1)	−6.95640(−1)	−7.91633	−5.61121
0.98	0.42	−1.17080(−1)	−2.73186(−1)	−7.89024	−5.54757
0.98	0.43	−3.40033(−2)	−7.74960(−2)	−7.87724	−5.51697
0.98	0.44	4.88391(−2)	1.08778(−1)	−7.86428	−5.48696
0.98	0.45	1.31456(−1)	2.86282(−1)	−7.85134	−5.45808
0.99	0.48	−5.53484(−2)	−1.14156(−1)	−7.77524	−5.30378
0.99	0.49	2.55295(−2)	5.15800(−2)	−7.76254	−5.27747
0.99	0.50	1.06189(−1)	2.10254(−1)	−7.74987	−5.25258
1.00	0.50	−2.86667(−1)	−5.73334(−1)	−7.70888	−5.24551
1.00	0.52	−1.27733(−1)	−2.45640(−1)	−7.68386	−5.13255
1.00	0.53	−4.85946(−2)	−9.16880(−2)	−7.67139	−5.10910
1.00	0.54	3.03275(−2)	5.61620(−2)	−7.65896	−5.08588
1.00	0.55	1.09034(−1)	1.98244(−1)	−7.64655	−5.06283
1.01	0.57	−9.45805(−2)	−1.67590(−1)	−7.57835	−4.95116
1.01	0.58	−1.73966(−2)	−3.02940(−2)	−7.56615	−4.92995
1.01	0.60	1.36352(−1)	2.29526(−1)	−7.54184	−4.88878
1.02	0.60	−1.91406(−1)	−3.25390(−1)	−7.49581	−4.82234
1.02	0.62	−4.02988(−2)	−6.62980(−2)	−7.47186	−4.78308
1.02	0.63	3.49539(−2)	5.65920(−2)	−7.45993	−4.76396
1.04	0.70	−2.33760(−2)	−3.47300(−2)	−7.28029	−4.51314
1.04	0.71	4.84568(−2)	7.09790(−2)	−7.26883	−4.49693
1.04	0.72	1.20099(−1)	1.73477(−1)	−7.25740	−4.48088
1.04	0.75	3.33939(−1)	4.63062(−1)	−7.22325	−4.43447
1.06	0.76	−7.71816(−2)	−1.07648(−1)	−7.10882	−4.29880
1.06	0.77	−5.01226(−5)	−6.90000(−5)	−7.09611	−4.28198
1.06	0.78	6.03095(−2)	8.19590(−2)	−7.08677	−4.27011
1.08	0.82	−6.87335(−2)	−9.05270(−2)	−6.93570	−4.10015
1.08	0.83	−2.84198(−3)	−3.69800(−3)	−6.92508	−4.08726
1.08	0.84	6.28802(−2)	8.08460(−2)	−6.91448	−4.07455
1.08	0.85	1.28438(−1)	1.63192(−1)	−6.90391	−4.06204
1.08	0.87	2.59065(−1)	3.21598(−1)	−6.88283	−4.03756
1.10	0.87	−7.54543(−2)	−9.54020(−2)	−6.77283	−3.92752
1.10	0.88	−1.22768(−2)	−1.53460(−2)	−6.76260	−3.91584
1.10	0.89	5.07405(−2)	6.27130(−2)	−6.75240	−3.90429
1.10	0.90	1.13600(−1)	1.38845(−1)	−6.74221	−3.89292
1.10	0.91	1.76305(−1)	2.13116(−1)	−6.73205	−3.88163
1.12	0.90	−1.61915(−1)	−2.01494(−1)	−6.63031	−3.78726
1.12	0.93	2.01362(−2)	2.42500(−2)	−6.60071	−3.75491
1.12	0.94	8.05186(−2)	9.59370(−2)	−6.59088	−3.74417
1.12	0.95	1.40751(−1)	1.65938(−1)	−6.58108	−3.73396
1.14	0.95	−8.96850(−2)	−1.07622(−1)	−6.46895	−3.63316
1.14	0.96	−3.14307(−2)	−3.73240(−2)	−6.45944	−3.62324
1.14	0.97	2.66801(−2)	3.13560(−2)	−6.44995	−3.61341
1.14	1.00	2.00160(−1)	2.28182(−1)	−6.42159	−3.58462
1.16	0.97	−1.61715(−1)	−1.93391(−1)	−6.33768	−3.51656
1.16	0.99	−4.95051(−2)	−5.80060(−2)	−6.31930	−3.49783
1.16	1.00	6.39310(−3)	7.41600(−3)	−6.31014	−3.48832
1.18	1.02	−4.10567(−2)	−4.74970(−2)	−6.18102	−3.37822
1.18	1.03	1.26934(−2)	1.45420(−2)	−6.17218	−3.36963
1.18	1.05	1.19806(−1)	1.34639(−1)	−6.15455	−3.35258

[a] Note.—The number in parentheses is the power of 10 by which the corresponding entry is to be multiplied.

The integrals were computed using the sixteen-point Gauss integration formula.[18] The upper limit of integration was adjusted to neglect values of the independent variable corresponding to negligible values of the integrand. If one uses y as a variable of integration some difficulty in the integration often occurs near $y=0$ for the integrand of G varies here as $y^{\frac{1}{2}}$. This difficulty can be avoided if one chooses $y^{\frac{1}{2}}$ as the variable of integration. In this manner, our calculations procedure differs from previous ones.[4] Eight significant digits were carried in each operation and we believe that the results are good to five significant figures. As an aid to computation we present six digits in our tables. The values of the integrals are presented in Table I and the corresponding thermodynamic functions are given in Table II.

Experimental measurements are almost invariably carried out under conditions of constant pressure (about 1 atmos). For this reason we have limited our calculations to the region around 1-atmos pressure. The corresponding values of p^* for a typical range of $\bar{\epsilon}$ and $\bar{a}$ are given in Table III.

For convenience in calculation we will consider the properties of the mixture at $p^*=0$. With this approximation we are neglecting the small variation of the mixing properties with pressure. Although this approximation does not affect the general conclusions given in this article an accurate study of a given mixture can be readily obtained from Tables I and II and should be carried out when necessary.

TABLE III. p^* as a function of $\bar{\epsilon}/k$ and $\bar{a}$ at one-atmosphere pressure.

$\bar{\epsilon}/k$ °K	$\bar{a}$ Å	p^*
300	4.50	2.23×10^{-3}
400	5.00	2.29×10^{-3}
500	6.00	3.17×10^{-3}

The values of the thermodynamic variables at $p^*=0$ were computed by inverse interpolation using a table of three-point and four-point Lagrangian interpolation coefficients[19] and are given in Table IV.

III. CALCULATION OF THE EXCESS MIXING PROPERTIES OF BINARY MIXTURES AND COMPARISON WITH EXPERIMENT

By using Eqs. (15) and (16) together with Table IV the excess internal energy and enthalpy, together with the excess entropy of mixing, at $p^*=0$ can be computed. At $p^*=0$ the internal energy and enthalpy of mixing are exactly equal and since the change in volume on mixing is very small (or the order of 1 or 2 cc per mole), they can be set equal to within the error of the calculation for pressures around one atmosphere.

[18] W. E. Milne, *Numerical Calculus* (Princeton University Press, Princeton, 1949), pp. 285–289.

[19] L. J. Briggs and A. N. Lowan, *Tables of Lagrangian Interpolation Coefficients* (Math. Tables Project, W. P. A., 1944).

The major problem in calculating the thermodynamic functions is the determination of the individual Lennard-Jones parameters. Ideally, these parameters can be determined from second virial coefficient measurements, but little has been done with substances of experimental interest in solutions. As a result we are forced to adopt an approximation for the mixed parameters (e.g., see Eqs. (2) and (3)) and to determine the parameters for the pure components by some empirical means. In this article we will first use Eqs. (2) and (3) to determine $\tilde{\epsilon}$ and $\tilde{v}^0$ indirectly. In connection with the use of these equations we will consider two empirical methods of determining the Lennard-Jones constants for the pure substances. The first method uses the experimentally determined critical temperature and pressure; the second method will use the experimental values of the heat of vaporization and molal volume at a given temperature.

TABLE IV. Thermodynamic functions at $p^*=0$.

q	θ	E^E/N	S^E/N
0.94	0.1840	−8.3200	−6.9870
0.95	0.2530	−8.2039	−6.4590
0.96	0.3175	−8.0910	−6.0704
0.97	0.3741	−7.9795	−5.7638
0.98	0.4340	−7.8719	−5.5042
0.99	0.4858	−7.7664	−5.2850
1.00	0.5315	−7.6635	−5.0950
1.01	0.5804	−7.5643	−4.9252
1.02	0.6250	−7.4661	−4.7723
1.04	0.7031	−7.2764	−4.5075
1.06	0.7700	−7.0961	−4.2820
1.08	0.8304	−6.9240	−4.0871
1.10	0.8819	−6.7612	−3.9133
1.12	0.9261	−6.6035	−3.7634
1.14	0.9652	−6.4539	−3.6179
1.16	0.9989	−6.3111	−3.4893

(A) Use of Critical Constant Data

The problem of obtaining a semi-empirical method for the determination of the potential-energy curve has been examined by Hill.[20] He remarks that the law of corresponding states requires that the Lennard-Jones parameters be related to the critical point by the equations

$$a=c_5(T_c/p_c)^{\frac{1}{3}},\qquad \epsilon/k=c_4T_c. \tag{20}$$

The constants c_4 and c_5 are determined empirically by Hill from the measured properties of neon, argon, nitrogen, and methane. Using a geometric mean to determine an average c_4 and an arithmetic mean to determine c_5, Hill obtains

$$a(\text{A})=2.633\left[\frac{T_c(^\circ\text{K})}{p_c(\text{atmos.})}\right]^{\frac{1}{3}},\qquad \epsilon/k(^\circ\text{K})=0.780T_c(^\circ\text{K}). \tag{21}$$

[20] T. L. Hill, J. Chem. Phys. **16**, 399 (1948).

TABLE V. Empirical relation between critical constants and Lennard-Jones potential parameters (see Sec. II-A).[a]

Substance	T_c[b] °K	p_c[b] atms	a A	ϵ/k °K	c_5	c_4
CCl_4	556.3	45.0	5.411	485.7	2.340	0.873
C_6H_{12}	554.2	40.4	5.624	485.7	2.349	0.876
C_6H_6	561.7	47.7	5.260	493.6	2.312	0.879
$SnCl_4$	591.9	37.0	5.818	582.6	2.309	0.984
n-hexane	508.0	29.5	5.964	462.1	2.309	0.910
CS_2	546.2	76.0	4.580	413.7	2.373	0.757
n-octane	569.2	24.6	6.500	604.6	2.281	1.062
n-heptane	540.0	26.8	6.241	538.1	2.294	0.996

[a] The Lennard-Jones parameters were computed from the experimental heats of vaporization and molal volumes using the free volume expressions for the thermodynamic functions.
[b] *Handbook of Chemistry and Physics* (1947), thirtieth edition, p. 1807.

If we anticipate section B of this discussion which determines the values of the Lennard-Jones parameters from the experimental heat of vaporization and molal volume of the liquid, we can compute empirical values for c_4 and c_5 for various common nonpolar substances. These results are given in Table V. Although the error introduced by the free volume equation of state for the liquid may be large, the relative discrepancies among the values indicate, roughly, the failure of the law of corresponding states, which reflects the use of the two parameter Lennard-Jones potential to represent the interaction between a pair of molecules. This potential is at best a rough approximation and from a qualitative examination of Table V we expect the calculations for mixtures of carbon tetrachloride, benzene, and cyclohexane to be more reliable than for several other mixtures we will consider.

Returning to Eq. (21) which is based upon second virial coefficient measurements, we use Eqs. (2) and (3), determine $\tilde{\epsilon}$ and $\tilde{v}^0$ and then calculate the mixing properties of various solutions. A brief summary of the results together with the experimental values is given in Table VI. The experimental values were obtained from the various references given in the table. The agreement between the calculated and the experimental values is very poor. However, a detailed examination of the calculations reveals that the mixing properties are very sensitive to small variations in the Lennard-Jones parameters (this will be discussed in more detail in a

TABLE VI. Excess thermodynamic properties of equimolal mixtures $T=298.2^\circ$K (see Sec. II-A).[a]

Mixture	$\tilde{\epsilon}/k$ °K	$\tilde{v}^0$ cc	$100\Delta v/v_0^0$ calc	$100\Delta v/v_0^0$ exp	ΔH^E cal/mole calc	ΔH^E cal/mole exp	$\Delta S^E/R$ calc	$\Delta S^E/R$ exp
$CCl_4-C_6H_6$	430.8	143.8	0.37	0.003	40	30	0.010	0.018
$CCl_4-C_6H_{12}$	435.5	132.9	0.11	0.16	10	34	0.004	0.030
$C_6H_6-C_6H_{12}$	430.2	141.0	0.75	0.65	97	176	0.024	0.171
CCl_4-SnCl_4	433.4	159.0	2.60	0.40	257	···	0.073	···

$v_0^0=x_1v_1+x_2v_2$

[a] The Lennard-Jones parameters for the pure components were computed from the experimental critical constants of the pure liquids. The experimental values of the mixing properties were taken from reference (6) and from Scatchard, Wood, and Mochel, J. Am. Chem. Soc. **62**, 712 (1940).

TABLE VII. Excess thermodynamic properties of equimolal mixtures [see Sec. II(B)].[a]

Mixture	T °K	$\bar{\epsilon}/k$ °K	$\bar{v}^0$ cc	$100\Delta v/v_0$ calc	$100\Delta v/v_0$ exp	ΔH^E cal/mole calc	ΔH^E cal/mole exp	$\Delta S^E/R$ calc	$\Delta S^E/R$ exp	$\Delta S^E/R$ non-random[b]
$CCl_4-C_6H_6$	298.2	487.9	91.74	0.25	0.003	30	30	0.007	0.018	−0.0003
$CCl_4-C_6H_{12}$	298.2	482.4	101.70	0.46	0.16	52	34	0.013	0.030	−0.0002
$C_6H_6-C_6H_{12}$	298.2	479.9	98.43	1.32	0.65	171	176	0.042	0.171	−0.0061
CCl_4-SnCl_4	298.2	521.0	108.90	3.00	0.40	233	···	0.042	···	
CCl_4-SiCl_4	298.2	462.0	104.3	0.66	0.02	101	32	0.024	0.020	
$C_6H_{12}-n$-hexane	293.2	466.7	118.3	0.90	···	129	48	0.034	0.055	
$C_6H_{12}-$dioxane	293.2	509.1	96.70	−0.88	···	174	280	0.032	0.081	
CCl_4-CS_2	293.2	401.7	82.20	9.60	···	857	76	0.25	···	
$CCl_4-C(CH_3)_4$	293.2	405.9	103.34	−2.96	···	16	···	−0.174	···	

[a] The Lennard-Jones parameters for the pure components were obtained from the experimental heats of vaporization and molal volumes of the pure liquids. The experimental values listed in this table were taken from reference (6) and from the following: Scatchard, Wood, and Mochel, J. Am. Chem. Soc. **62**, 712 (1940). V. W. Schulze, Z. anorg. Chem. **261**, 297 (1950). J. H. Simons and J. B. Hickman, J. Phys. Chem. **56**, 420 (1952). R. D. Vold, J. Am. Chem. Soc. **59**, 1515 (1937). Anna-Luise Vierk, Z. anorg. Chem. **261**, 283 (1950). J. H. Hildebrand and J. M. Carter, J. Am. Chem. Soc. **59**, 1510 (1937). I. Prigogine and V. Mathot, J. Chem. Phys. **18**, 765 (1950).

[b] Contribution to the excess entropy of mixing as calculated from the Kirkwood (reference 4) quasi-lattice theory.

later section). For this reason the results given in Table VI may be regarded as tentative until accurate second virial coefficient measurements on the vapors have been performed.

(B) Use of Heats of Vaporization and Molal Volumes of the Pure Liquids

Using the energy of vaporization and the molal volume of a liquid at 25°C or 20°C, the free volume expressions for the excess internal energy and the equation of state at $p^*=0$ can be solved to give ϵ and v^0. In practice these equations were solved graphically and the results can be found in Table V. The thermodynamic properties of equimolar mixtures calculated on this empirical basis are summarized in Table VII together with the experimental results. As mentioned earlier we have included a few examples of the contribution due to nonrandom mixing as calculated[21] from the Kirkwood[14] quasi-lattice theory of solutions.

(C) Empirical Use of the Heats and Volumes of Mixing

The average Lennard-Jones constants $\bar{\epsilon}/k$ and $\bar{v}^0$ can be computed empirically from the knowledge of the heat of mixing and volume of mixing of the solution in the same manner in which one obtains ϵ/k and v^0 for a pure liquid using the energy of vaporization and the molal volume. The results of this calculation for several equimolar mixtures are summarized in Table VIII.

It is possible to empirically attribute the discrepancies between the experimental and theoretical values for the heats of mixing and volumes of mixing to the failure of the approximation given by Eq. (2). If we let

$$\epsilon_{12}=(\epsilon_{11}\epsilon_{22})^{\frac{1}{2}}+\delta, \tag{22}$$

then δ can be determined by means of the equation

$$\delta=\frac{\bar{\epsilon}_e\bar{v}_e^{0^2}-\bar{\epsilon}\bar{v}^{0^2}}{2x_1x_2v_{12}^{0^2}}, \tag{23}$$

where $\bar{\epsilon}_e$ and $\bar{v}_e^0$ are the values determined from the experimental properties of the mixture (see Table VIII) and $\bar{\epsilon}$ and $\bar{v}^0$ are computed using Eqs. (2) and (3) and the experimental properties of the pure components. Several values of δ are given in Table VIII.

TABLE VIII. Excess thermodynamic properties of equimolal mixtures $T=298.2$°K (see Sec. II-C).[a]

Mixture	$\bar{\epsilon}/k$ °K	$\bar{v}^0$ cc	$\Delta S^E/R$	δ/k
$CCl_4-C_6H_6$	487.90	91.52	0.007	−0.008
$CCl_4-C_6H_{12}$	483.62	101.38	0.009	−0.006
$C_6H_6-C_6H_{12}$	478.10	97.77	0.043	−0.034
CCl_4-SiCl_4	469.38	101.03	0.0018	−0.094

[a] The average potential parameters, $\bar{\epsilon}/k$ and $\bar{v}^0$ for the mixture were computed empirically from the measured heats and volumes of mixing.

III. COMMENTS

The calculated volumes, heats, and entropies of mixing given in this paper are only correct to two significant

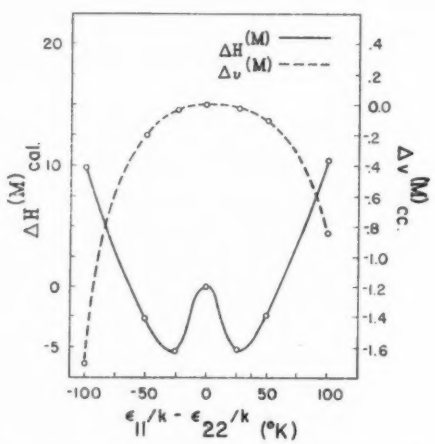

FIG. 1. Typical variation of $\Delta H^{(M)}$ and $\Delta v^{(M)}$ with $\epsilon_{11}/k-\epsilon_{22}/k$.

[21] Scatchard, Wood, and Mochel, J. Am. Chem. Soc. **62**, 712 (1940).

digits. We have not fully exploited the accuracy which can be obtained from the functions given in Tables I and II, for the agreement with the experimental results permits one to draw only qualitative conclusions about the theory. As a general feature, with only one or two exceptions, we find that the predicted volumes and heats of mixing are too large, and the calculated entropies of mixing are always too small. It is possible to explain the discrepancies in terms of the small deviations from the mixture approximation given in Eqs. (2) and (3). However, this is purely an empirical assignment and is misleading in view of the sensitivity of the mixing properties to variations in the Lennard-Jones parameters. In order to illustrate the dependence upon these potential parameters we have prepared Figs. 1 and 2 which give the behavior of the heat of mixing and volume of mixing for a typical case.

The entropy of mixing is consistently too low. Scatchard[21] *et al.* have remarked that the experimental evidence, in the case of C_6H_6, CCl_4 and C_6H_{12} solutions, indicates that the relatively large excess entropies of mixing are not caused by preferential orientation in the pure liquids. A possible improvement in the predicted entropy might be expected by using a simple extension of the present theory, namely the introduction of vacant cells or "holes." However, the fraction of vacant cells, x_0, which is obtained by minimizing the free energy at constant temperature and volume is extremely small. The hole fraction, x_0, in the region of interest and at $p^*=0$ is given in Table IX. The largest correction due to

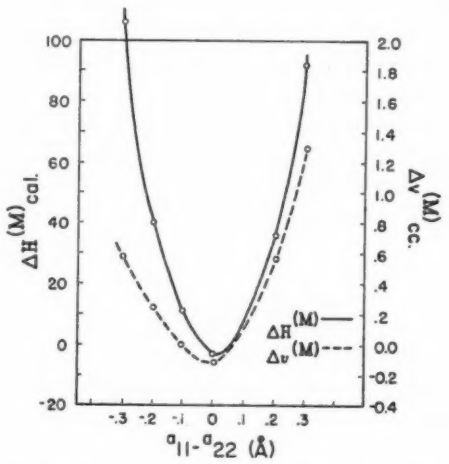

FIG. 2. Typical variation of $\Delta H^{(M)}$ and $\Delta v^{(M)}$ with $a_{11}-a_{22}$.

TABLE IX. "Hole" fraction at $p^*=0$.

q	θ	x_0
1.00	0.5315	3.352(−9)[a]
1.01	0.5804	1.568(−8)
1.02	0.6250	5.416(−8)
1.04	0.7031	3.532(−7)
1.06	0.7700	1.374(−6)
1.08	0.8304	4.017(−6)
1.10	0.8819	9.358(−6)
1.12	0.9261	1.852(−5)
1.14	0.9652	3.337(−5)
1.16	0.9989	5.489(−5)

[a] Note.—The number in parentheses is the power of 10 by which the corresponding entry is to be multiplied.

holes comes from a term which corresponds to the ideal entropy of mixing of holes and molecules. When x_0 is very small this term is given by

$$\frac{\Delta S_0^E}{R}=x_1x_0^{(1)}\ln x_0^{(1)}+x_2x_0^{(2)}\ln x_0^{(2)}-x_0\ln x_0, \quad (24)$$

where $x_0^{(1)}$, $x_0^{(2)}$ and x_0 are the fractions of vacant cells in pure liquid 1, pure liquid 2, and the solution, respectively. For an equimolar mixture of benzene and carbon tetrachloride this term increases the excess entropy of mixing by 2.9×10^{-8} units in $\Delta S/R$, which is a negligible contribution.

As a final comment we would like to point to the lack of experimental data on simple solutions to which one might expect this theory to apply. The wide class of tetrahalides might be considered as approaching the symmetrical requirements although there is some doubt as to whether the forces between molecules are of the central type. In the absence of experimental techniques which can treat mixtures of liquid argon, neon, methane, etc. a careful experimental study of some group of symmetrical molecules would be appropriate to the present state of the theory of solutions.

Since repulsive forces play an important role at the densities under consideration, a better approximation for the effectively spherical nonpolar molecules can be obtained by considering the three-parameter intermolecular potential

$$V(R)=-\frac{\mu}{R^6}+P\exp\left[-\frac{R}{\rho}\right]. \quad (25)$$

This extension of the theory is possible with modern calculating facilities, but the unknown errors inherent in the cell method itself places some doubt on the value of such a program.

The Infrared Spectrum and Molecular Constants of Sulfur Dioxide*,†

R. D. SHELTON,‡ A. H. NIELSEN, *Department of Physics*

AND

W. H. FLETCHER, *Department of Chemistry, The University of Tennessee, Knoxville, Tennessee*

(Received June 11, 1953)

By means of an infrared prism-grating spectrometer equipped with a multiple-path cell, seventeen vibration-rotation absorption bands of SO_2 have been observed and recorded. Seven bands exhibiting rotational structure were analyzed for the rotational constants of the upper and lower vibrational states. Harmonic and anharmonic constants in the vibrational energy expression have been calculated, and suitable values for the force constants in a four-constant potential function have been obtained. No bands ascribable to $S^{34}O_2^{16}$ were found.

I. INTRODUCTION

THE sulfur dioxide molecule belongs to the bent XY_2 or C_{2V} symmetry group. Recent microwave investigations[1–3] have established an O–S–O angle of 119.53° and an O–S distance of 1.432A. Bailey, Cassie, and Angus[4,5] observed six vibration-rotation absorption bands of SO_2—namely, ν_1, ν_2, ν_3, $\nu_2+\nu_3$, $2\nu_1$, and $\nu_1+\nu_3$. These authors performed a vibrational analysis which yielded a reasonable O–S–O angle and O–S distance, but as the bands appeared as unresolved envelopes with doublet and triplet structure with no rotational structure in evidence, there remained some question as to the accuracy of the values. Barker,[6] using a grating instrument, resolved ν_1 and ν_2 sufficiently to permit the application of combination relations which yielded the rotational constants for the upper and lower vibrational states. The ν_3 band was also observed, but no rotational structure was evident. There appears to have been no published infrared investigations of the SO_2 molecule since the work of Barker.

A review of the previous investigations of the SO_2 molecule indicated that further investigation in the infrared with a grating spectrometer equipped with a multiple-path cell would be of value. The observation of additional vibration-rotation bands would make possible the calculation of the harmonic and anharmonic constants in the vibrational energy expression. From the harmonic frequencies, suitable force constants could be calculated. Bands exhibiting rotational structure would yield rotational constants for the upper and lower vibrational states. The possibility of observing isotope bands was also of interest.

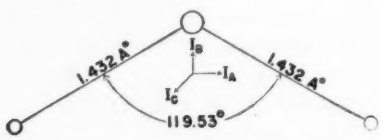

FIG. 1. The SO_2 molecule. The principal moments of inertia, I_A, I_B, and I_C, are, respectively (reference 3), $13.8046\cdot10^{-40}$, $81.3067\cdot10^{-40}$, and $95.3376\cdot10^{-40}$ g cm². $\kappa\equiv(2B-A-C)/(A-C)=-0.9416$, where $A=h/(8\pi^2 I_A C)$, etc.

II. THEORETICAL BAND STRUCTURE

A model of the SO_2 molecule is shown in Fig. 1. As the two large moments of inertia are roughly equal, the SO_2 molecule is almost a prolate symmetric top and the vibration-rotation bands, therefore, should resemble those of a prolate symmetric top.

Following the convenient notation of King, Hainer, and Cross,[7] the rotational energy levels and the corresponding eigenfunctions are identified by three numbers, J, K_{-1}, and K_1, where J is the total angular momentum

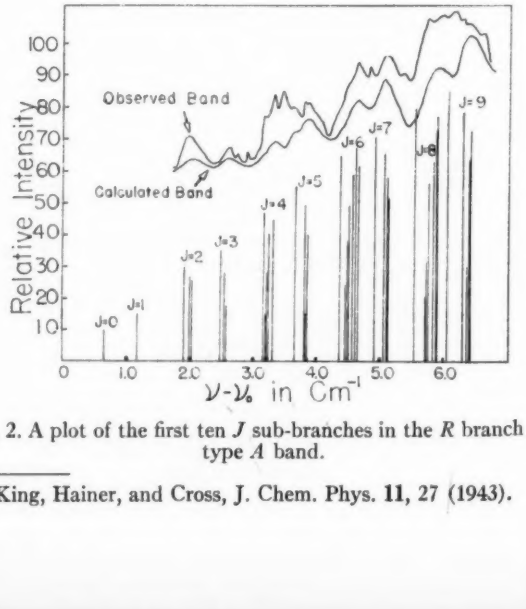

FIG. 2. A plot of the first ten J sub-branches in the R branch of a type A band.

* This work was supported in part by the Office of Ordnance Research.

† This paper is based on a thesis submitted by R. D. Shelton in partial fulfillment of the requirements for the degree of Ph.D. in physics. The material of this paper was presented at the Durham, North Carolina meeting of the American Physical Society, Phys. Rev. **91**, 235A (1953); and at the Réunion Internationale de Spectroscopie Moléculaire, held in Paris, France June 29–July 3, 1953. An abbreviated version of the present paper will appear in a forthcoming special edition of the Journal de Physique as a part of the complete proceedings of the symposium.

‡ Present address, Nuclear Engineering Division, Convair Aircraft, Fort Worth, Texas.

[1] Dailey, Golden, and Wilson, Jr., Phys. Rev. **72**, 871 (1947).
[2] G. F. Crable and W. V. Smith, J. Chem. Phys. **19**, 502 (1951).
[3] M. H. Sirvetz, J. Chem. Phys. **19**, 938 (1951).
[4] Bailey, Cassie, and Angus, Proc. Roy. Soc. (London) **A130**, 142 (1930).
[5] C. R. Bailey and A. B. D. Cassie, Proc. Roy. Soc. (London) **A140**, 605 (1933).
[6] E. F. Barker, Revs. Modern Phys. **14**, 198 (1942).
[7] King, Hainer, and Cross, J. Chem. Phys. **11**, 27 (1943).

quantum number, and K_{-1} and K_1, respectively, are the quantum numbers associated with the projection of the angular momentum on the unique axis in the limiting case of the prolate and oblate symmetric top.

The SO_2 vibration-rotation absorption spectrum contains two types of bands. In the type A bands, the oscillating dipole moment lies along the axis of the least moment of inertia, and the selection rules for J, K_{-1} and K_1 are[8] $\Delta J=0, \pm1$; $J=0\leftrightarrow J=0$; $\Delta K_{-1}=0, \pm2, \pm4, \cdots$; $\Delta K_1=\pm1, \pm3, \cdots$. In the type B bands, the oscillating dipole moment lies along the axis of the intermediate moment of inertia, and the selection rules are $\Delta J=0, \pm1$; $J=0\leftrightarrow J=0$; $\Delta K_{-1}=\pm1, \pm3, \cdots$; $\Delta K_1=\pm1, \pm3, \cdots$. Individual transitions may be identified in the manner of Cross, Hainer, and King.[8] For example, $R_{25}(J, K_{-1}, K_1)$ denotes a transition for which $\Delta J=+1$, $\Delta K_{-1}=2$, and $\Delta K_1=-3$.

Using the microwave data, the above selection rules, and the tables of King, Hainer, and Cross,[7,8] it was possible to calculate the theoretical band structure as shown in Figs. 2 and 3. The type A band is characterized

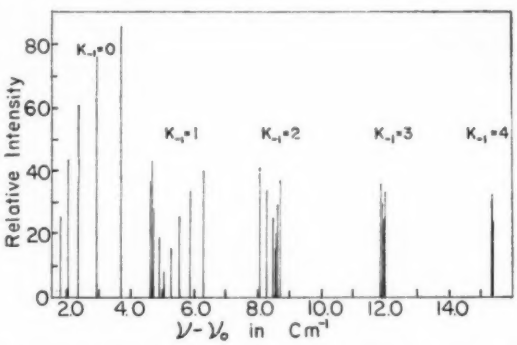

FIG. 3. A partial plot of the first five $Q_{1\bar{1}}$ branches of a type B band.

by a strong central Q branch and J sub-branches spaced approximately 0.62 cm^{-1} apart. The sub-branches may be identified by the value of J associated with the initial states for the transitions comprising the sub-branch. The pairing of the J sub-branches and the irregularity of the line structure are a result of the asymmetry.

The type B band, on the other hand, is characterized by Q branches spaced approximately 3.4 cm^{-1} apart. As suggested by Fig. 3, the Q branches follow very closely a symmetric top approximation for $K_{-1}>3$. The splitting of the Q branches for small values of K_{-1} is a result of the asymmetry.

III. EXPERIMENTAL DETAILS

The vibration-rotation bands of SO_2 were observed with the aid of an automatically-recording prism-grating spectrometer designed by A. H. Nielsen.[9] The optics of the instrument appear to be precise enough to permit the resolution of lines separated by 0.3 cm^{-1}, but unfavorable energy and detector conditions in several

[8] Cross, Hainer, and King, J. Chem. Phys. 12, 210 (1944).
[9] A. H. Nielsen, J. Tenn. Acad. Sci. 22, 241 (1947).

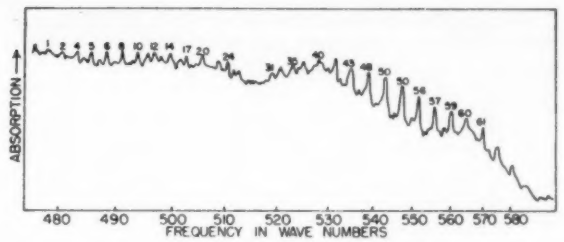

FIG. 4. The ν_2 vibration-rotation band. The numbers above the absorption peaks are the ordinal numbers of Table I (the sixth number from the right above the peaks should be 54 instead of 50).

spectral regions necessitated the use of slits ranging from 0.30 to 2.00 cm^{-1}. A set of echelette gratings, having 1200, 1800, 3600, 7200, and 15 000 lines per inch, was available for the work. From 450 to 3400 cm^{-1}, a Golay pneumatic cell, manufactured by Eppley Laboratories, was employed as the detector. Above 3400 cm^{-1}, a PbS photoconductive cell manufactured by the Continental Electric Company, Inc., was used.

A two-foot, multiple-path cell based on a design by White[10] provided a usable absorption path length of twenty meters. Since the cell windows were attached to the cell by a mixture of beeswax and rosin, pressures greater than one atmosphere were avoided. The sample of SO_2 was obtained from the Matheson Company,

TABLE I. Observed line frequencies in cm^{-1} for ν_2.

Ordinal No.	ν	Identification K_{-1}	Ordinal No.	ν	Identification K_{-1}
1	478.61	14	34	523.21	1
2	481.01	13	35	524.47	2
3	481.72		36	525.81	
4	483.44	12	37	526.98	2
5	486.02	11	38	528.21	
6	488.58	10	39	529.22	3
7	490.22		40	530.19	3
8	491.35	9	41	533.82	4
9	493.05		42	534.72	
10	494.17	8	43	537.72	5
11	495.99		44	538.44	
12	497.07	7	45	539.06	
13	499.02		46	539.72	
14	500.05	6	47	540.40	
15	501.48		48	541.62	6
16	502.15		49	542.38	
17	503.09	5	50	545.58	7
18	504.88		51	546.75	
19	505.42		52	547.41	
20	506.19	4	53	548.10	
21	507.75		54	549.58	8
22	508.33	3	55	552.02	
23	509.30	3	56	553.67	9
24	511.08		57	557.77	10
25	512.38	2	58	560.31	
26	513.41	2	59	561.90	11
27	514.29		60	566.08	12
28	515.43		61	570.34	13
29	517.86		62	574.56	14
30	518.55		63	578.90	15
31	520.11		64	583.28	16
32	521.37		65	584.50	
33	522.26	1	66	587.69	

[10] J. U. White, J. Opt. Soc. Am. 32, 285 (1942).

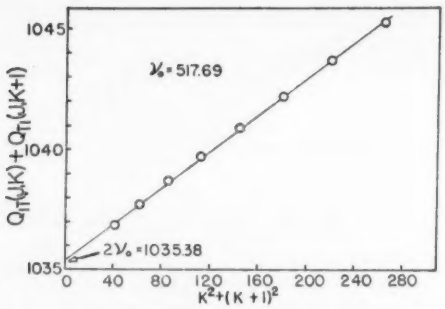

FIG. 5. Band center plot for ν_2.

Inc., of East Rutherford, New Jersey. The quoted purity was 99.988 percent. No absorptions attributable to impurities other than H_2O and CO_2 were observed.

IV. EXPERIMENTAL RESULTS

Type *B* Bands

The ν_2 vibration-rotation band, which is of type *B*, is exhibited in Fig. 4. The clearly defined absorption peaks are *Q* branches, the frequencies of which are given in Table I. The numbers listed above the absorption peaks in Fig. 4 are the ordinal numbers of the line frequencies

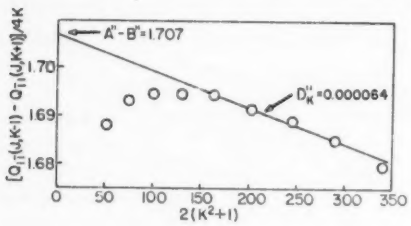

FIG. 6. $A''-B''$ plot for ν_2.

of Table I. Each *Q* branch is identified by the K_{-1} value associated with the initial states of the transitions comprising the branch. Each *Q* branch has associated with it a *P* and an *R* branch, and these *P* and *R* branches give rise to numerous weak absorptions which overlap to form some of the background absorption between the *Q* branches.

Assuming the SO_2 molecule to be a prolate symmetric top, combination relations were formed among the *Q* branches of the type *B* bands. Figures 5–7 show typical combination relation plots for the type *B* bands. Similar plots were obtained for ν_1, $2\nu_1$, and $2\nu_3$, which also exhibited rotational structure. Since K_{-1} is the K value in the limiting case of the prolate symmetric top, the subscript will be dropped here for the sake of brevity.

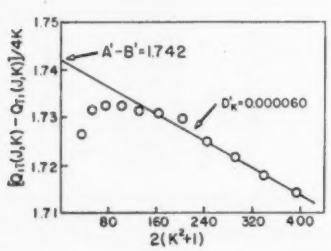

FIG. 7. $A'-B'$ plot for ν_2.

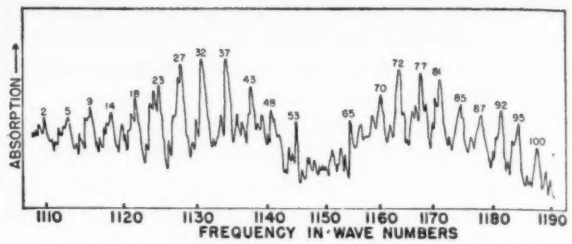

FIG. 8. The ν_1 vibration-rotation band.

K_1, which is the K value in the limiting case of the oblate symmetric top, does not enter into the energy expression for the prolate top approximation. However, it is a convenient symmetry index and useful for the formulation of selection rules. Figures 8–10, respectively, are tracings of ν_1, $2\nu_1$, and $2\nu_3$. Tables II–IV give the measured frequencies of the absorption peaks of these bands.

Type *A* Bands

The type *A* bands of SO_2 are strongly influenced by the slight asymmetry. In the type *B* bands, energy levels associated with the most intense transitions follow very closely the symmetric top approximation, whereas,

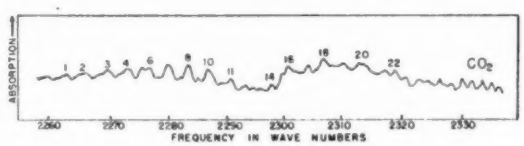

FIG. 9. The $2\nu_1$ vibration-rotation band.

in the type *A* bands, the energy levels associated with the most intense transitions of a given *J* sub-branch in general deviate most from a symmetric top approximation. Figures 11–13, respectively, show ν_3, $\nu_2+\nu_3$, and $\nu_1+\nu_3$, while Tables V–VII give the frequencies of the absorption peaks of these bands.

The irregularity of the rotational structure of these bands, together with the fact that several of the *J* sub-branches were obscured by the strong central *Q* branches, rendered the application of combination relations difficult and doubtful. Therefore, least squares formulas were fitted to the *J* sub-branches. For example, the rotational constants of ν_3 were obtained by fitting the equation,

$$R_{01}(JK)=\nu_0+2(J+1)B'+J(J+1)\Delta B,$$

to the first seven *J* sub-branches of the *R* branch. The constant B' is associated with the upper vibrational

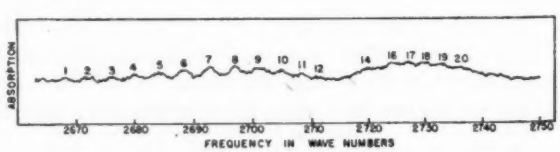

FIG. 10. The $2\nu_3$ vibration-rotation band.

TABLE II. Observed line frequencies in cm^{-1} for ν_1.

Ordinal No.	ν	Identification K_{-1}	Ordinal No.	ν	Identification K_{-1}	Ordinal No.	ν	Identification K_{-1}
1	1108.47		39	1136.95		77	1166.71	4
2	1109.04	13	40	1137.48		78	1167.46	
3	1110.34		41	1138.38		79	1168.63	
4	1111.05		42	1139.16		80	1169.23	
5	1112.31	12	43	1139.58	4	81	1170.14	5
6	1113.60		44	1140.70		82	1171.57	
7	1114.32		45	1141.44		83	1172.15	
8	1115.01		46	1142.42		84	1172.68	
9	1115.62	11	47	1143.09	3	85	1173.52	6
10	1116.37		48	1143.51		86	1174.90	
11	1117.09		49	1144.56	3	87	1176.61	7
12	1117.72		50	1145.17		88	1177.29	
13	1118.41		51	1145.80	2	89	1177.87	
14	1119.03	10	52	1146.31		90	1178.46	
15	1120.33		53	1147.01	2	91	1179.53	
16	1121.15		54	1147.64		92	1180.19	8
17	1121.54		55	1147.96		93	1181.34	
18	1122.42	9	56	1148.74		94	1182.01	
19	1122.98		57	1149.22		95	1183.53	9
20	1123.66		58	1149.83		96	1184.15	
21	1124.41		59	1150.71		97	1184.90	
22	1125.01		60	1151.46		98	1185.26	
23	1125.76	8	61	1152.26		99	1185.84	
24	1126.41		62	1152.57		100	1186.40	
25	1127.44		63	1154.01		101	1187.00	10
26	1128.44		64	1154.87		102	1188.11	
27	1129.15	7	65	1155.73	1	103	1188.86	
28	1129.73		66	1156.44		104	1189.40	
29	1130.50		67	1157.42		105	1190.08	11
30	1131.15		68	1158.94	1	106	1191.05	
31	1131.86		69	1159.23	2	107	1191.58	
32	1132.47	6	70	1160.35	2	108	1192.18	
33	1133.33		71	1161.80		109	1192.78	
34	1133.65		72	1163.25	3	110	1193.37	
35	1133.90		73	1164.04		111	1193.85	
36	1135.12		74	1164.61		112	1194.87	
37	1136.01	5	75	1165.19		113	1195.60	
38	1136.52		76	1165.79				

state, B'' is associated with the lower vibrational state, and $\Delta B = B' - B''$. Centrifugal terms were not included because only small values of J were involved.

The remaining ten observed bands of SO_2 are not exhibited here because they evinced no rotational fine structure, either because of the necessity for wide spectrometer slits or because of vibration-rotation interaction, or both. Table VIII summarizes the vibrational experimental data, and Table IX contains the

TABLE III. Observed line frequencies in cm^{-1} for $2\nu_1$.

Ordinal No.	ν	Identification K_{-1}	Ordinal No.	ν	Identification K_{-1}
1	2263.07	10	12	2293.23	1
2	2266.15	9	13	2294.69	1
3	2269.67	8	14	2297.97	0
4	2272.93	7	15	2299.58	0
5	2275.05		16	2300.74	1
6	2276.44	6	17	2304.18	2
7	2279.66	5	18	2306.94	3
8	2283.40	4	19	2310.51	4
9	2285.35		20	2313.05	5
10	2287.06	3	21	2317.09	CO_2
11	2290.88	2	22	2318.96	CO_2

TABLE IV. Observed line frequencies in cm^{-1} for $2\nu_3$.

Ordinal No.	ν	Identification K_{-1}	Ordinal No.	ν	Identification K_{-1}
1	2668.16	12	11	2708.44	2
2	2672.23	11	12	2710.89	1
3	2676.77	10	13	2714.22	0
4	2680.78	9	14	2719.23	1
5	2684.86	8	15	2721.70	2
6	2688.87	7	16	2724.31	3
7	2692.95	6	17	2727.12	4
8	2696.98	5	18	2730.12	5
9	2701.13	4	19	2732.68	6
10	2705.07	3	20	2736.10	7

results of the rotational analyses of bands exhibiting rotational structure.

V. THE VIBRATIONAL PROBLEM

Assuming the vibrational energy in cm^{-1}, $G(v_1, v_2, v_3)$, to be given by

$$G(v_1, v_2, v_3) = (v_1+\tfrac{1}{2})\omega_1 + (v_2+\tfrac{1}{2})\omega_2 + (v_3+\tfrac{1}{2})\omega_3 + (v_1+\tfrac{1}{2})^2 X_{11} + (v_2+\tfrac{1}{2})^2 X_{22} + (v_3+\tfrac{1}{2})^2 X_{33} + (v_1+\tfrac{1}{2})(v_2+\tfrac{1}{2})X_{12} + (v_1+\tfrac{1}{2})(v_3+\tfrac{1}{2})X_{13} + (v_2+\tfrac{1}{2})(v_3+\tfrac{1}{2})X_{23};$$

the band centers, $\nu(v_1, v_2, v_3)$ of bands arising from the ground state are given by

$$\nu(v_1, v_2, v_3) = v_1\omega_1{}^0 + v_2\omega_2{}^0 + v_3\omega_3{}^0 + v_1{}^2X_{11} + v_2{}^2X_{22} + v_3{}^2X_{33} + v_1v_2X_{12} + v_1v_3X_{13} + v_2v_3X_{23},$$

where

$$\omega_1{}^0 = \omega_1 + X_{11} + \tfrac{1}{2}X_{12} + \tfrac{1}{2}X_{13}, \text{ etc.},$$

and v_1, v_2, and v_3, respectively, are the vibrational quantum numbers associated with ν_1, ν_2, and ν_3. The ω_i are the zero-order harmonic frequencies, and the X_{ij} are

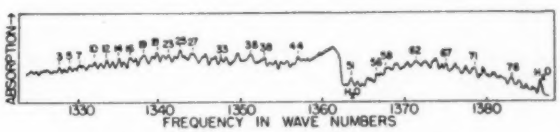

FIG. 11. The ν_3 vibration-rotation band.

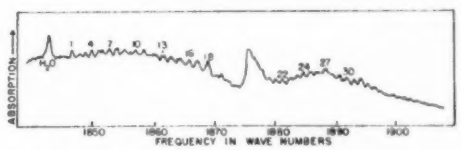

FIG. 12. The $\nu_2+\nu_3$ vibration-rotation band.

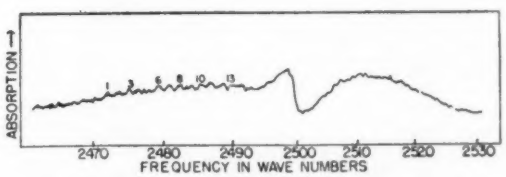

FIG. 13. The $\nu_1+\nu_3$ vibration-rotation band.

TABLE V. Observed line frequencies in cm^{-1} for ν_3.

Ordinal No.	ν	Identification J	Ordinal No.	ν	Identification J	Ordinal No.	ν	Identification J
1	1325.95		28	1344.18		55	1365.49	5
2	1326.62		29	1344.95		56	1366.23	6
3	1327.33		30	1345.44		57	1366.76	7
4	1328.09		31	1346.23		58	1367.48	
5	1328.79		32	1346.83		59	1368.94	
6	1329.48		33	1347.55		60	1369.79	
7	1330.20		34	1348.18		61	1370.30	
8	1330.83		35	1349.49		62	1371.37	
9	1331.49		36	1351.07		63	1372.65	
10	1332.09		37	1351.88		64	1373.44	
11	1332.82		38	1352.43		65	1373.93	
12	1333.53		39	1353.16	13	66	1374.55	
13	1334.20		40	1353.75	12	67	1375.04	
14	1334.91		41	1354.43	11	68	1376.04	
15	1335.54		42	1355.07	10	69	1376.57	
16	1336.30		43	1355.83	9	70	1377.46	
17	1336.87		44	1356.52	8	71	1378.51	
18	1337.65		45	1357.22	7	72	1379.65	
19	1338.09		46	1357.69	6	73	1380.81	
20	1338.95		47	1359.30		74	1382.10	
21	1339.53		48	1361.76		75	1382.40	
22	1340.33		49	1362.02		76	1383.15	
23	1340.93		50	1362.50	0	77	1384.18	
24	1341.69		51	1363.07	1, H_2O	78	1385.21	
25	1342.34		52	1363.77	2	79	1386.15	
26	1342.84		53	1364.32	3	80	1386.61	
27	1343.87		54	1365.01	4			

TABLE VI. Observed frequencies in cm^{-1} for $\nu_2+\nu_3$.

Ordinal No.	ν	Ordinal No.	ν
1	1844.06	17	1867.70
2	1846.29	18	1869.14
3	1847.75	19	1875.55
4	1849.21	20	1880.28
5	1850.70	21	1881.53
6	1852.15	22	1882.89
7	1853.58	23	1884.16
8	1855.02	24	1885.30
9	1856.52	25	1886.56
10	1857.83	26	1887.75
11	1859.28	27	1889.07
12	1860.70	28	1890.21
13	1862.15	29	1891.42
14	1863.52	30	1892.48
15	1864.81	31	1893.84
16	1866.38	32	1894.93

TABLE VII. Observed line frequencies in cm^{-1} for $\nu_1+\nu_3$.

Ordinal No.	ν
1	2470.45
2	2472.40
3	2473.97
4	2475.58
5	2477.18
6	2479.02
7	2480.61
8	2482.07
9	2483.79
10	2485.29
11	2486.83
12	2488.28
13	2489.77
14	2491.26
15	2499.50

TABLE VIII. Summary of experimental data for observed bands.

No.	Band	ν_0 (cm^{-1})	Slits (cm^{-1})	Path length (atmometers)	Grating	Relative intensity
1	ν_2	517.69	0.3	0.0052	1800	455
2	$\nu_3-\nu_2$	844.93	1.0	20.0	1800	0.55
3	ν_1	1151.38	0.33	0.012	3600	565
4	ν_3	1361.76	0.34	0.0008	3600	1000
5	$3\nu_2$	1535.06	1.02	20.0	3600	0.1
6	$\nu_1+\nu_2$	1665.07	1.02	20.0	7200	0.1
7	$\nu_2+\nu_3$	1875.55	0.30	1.6	7200	6.0
8	$2\nu_1$	2295.88	0.46	2.0	7200	5.5
9	$\nu_1+\nu_3$	2499.55	0.48	4.8	7200	20.0
10	$2\nu_3$	2715.46	0.84	4.8	7200	0.2
11	$2\nu_1+\nu_2$	2808.32	0.84	20.0	7200	0.8
12	$\nu_1+\nu_2+\nu_3$	3011.25	1.48	20.0	7200	0.02
13	$3\nu_1$	3431.19	2.00	20.0	7200	0.01
14	$2\nu_1+\nu_3$	3629.61	2.00	20.0	15 000	0.8
15	$3\nu_3$	4054.26	1.00	6.0	15 000	0.03
16	$3\nu_1+\nu_3$	4751.23	1.10	20.0	15 000	0.006
17	$\nu_1+3\nu_3$	5165.64	1.10	20.0	15 000	0.020

anharmonic and interaction terms. Fitting the above equation for the band centers to the observed band centers, the following values for the harmonic and anharmonic constants in the vibrational energy expression were obtained: $\omega_1=1167.60$, $\omega_2=526.27$, $\omega_3=1380.91$, $X_{11}=-3.99$, $X_{22}=-3.00$, $X_{33}=-5.17$, $X_{12}=-2.05$, $X_{13}=-13.71$, and $X_{23}=0.390$ cm^{-1}. A comparison of the observed band centers with the band centers calculated from the above constants is found in Table X.

Vibrational Potential Function for the SO_2 Molecule

The most general quadratic potential function controlling the fundamental vibrations of bent XY_2 molecules may be written in the form[11]

$$2V=f_1(\Delta l_1^2+\Delta l_1^2)+l_1l_2f\theta\Delta\theta^2 +2f_{12}\Delta l_1\Delta l_2+2l_1g_c(\Delta l_1+\Delta l_2)\Delta\theta$$

where the l_i are the O−S bond distances and θ is the O−S−O angle. A calculation of the normal vibrations expected from such a potential function yields three equations containing the four force constants in the above equation, the zero-order frequencies, the O−S−O angle, and the atomic masses. Inserting the zero-order frequencies calculated from the infrared investigations, the O−S−O angle calculated from the microwave

TABLE IX. Summary of rotational constants,[a] constants in cm^{-1}.

Band	B''	ΔB	$A''-B''$	$\Delta(A-B)$	D_K''	ΔD_K
ν_1			1.713	−0.013	0.000090	−0.00008
ν_2			1.707	0.039	0.000060	−0.000012
ν_3	0.3232	−0.0038				
$2\nu_1$			1.704	−0.0367		
$2\nu_3$			1.712	−0.0627		
$\nu_1+\nu_3$	0.3247	−0.0014				
$\nu_2+\nu_3$	0.3264	−0.0029				
Average	0.3244		1.7091			
Microwave	0.3188		1.7085			

[a] Barker (see reference 6) gave $A''-B''=1.70$, $A'-B'=1.74$ for ν_2, and $A'-B'=1.698$ for ν_1.

[11] J. Duchesne, Mem. Soc. Roy. Sci. Liège II, 429 (1943).

investigations, and the atomic masses given by mass spectrometry, the following three equations containing the four force constants are obtained:

$$12.328 \cdot 10^5 = f_1' + 2.7867 f_\theta - 1.3854 g_c,$$

$$8.739 \cdot 10^{10} = f_1' f_\theta - 2 g_c^2,$$

$$10.286 \cdot 10^5 = f_1'',$$

where $f_1' = f_1 + f_{12}$ and $f_1'' = f_1 - f_{12}$.

As these three equations contain four constants, and as only the three harmonic frequencies of $S^{32}O_2^{16}$ are known, it is impossible to determine the constants unambiguously. Following a method suggested by a number of authors[11,12] a set of values of the constant g_c was substituted into the equations and corresponding sets of values of f_1, f_{12}, and f_θ were calculated. Plots of the several constants as functions of the others were made in order to establish limits for their magnitudes. From the nature of the electronic structure of SO_2 it appears reasonable to suppose that both g_c and f_{12} are positive. This assumption imposes the limits $0.2\times10^5 < g_c < 2.45\times10^5$ dynes/cm and $0 < f_{12} < 0.5\times10^5$ dynes/cm. From the foregoing third equation, among the force constants, it is evident that $f_1 = 10.3 + f_{12}$, and from the limits on f_{12} it is clear that the limits on f_1 are $10.3\times10^5 < f_1 < 10.8\times10^5$ dynes/cm. With these limits on g_c, f_{12}, and f_1 it may also be seen that $0.8\times10^5 < f_\theta < 1.15\times10^5$ dynes/cm. Following Glockler and Tung[12] in choosing a singular set of force constants using the condition that $df_{12}/dg_c = 0$ the force constants for $S^{32}O_2^{16}$ take on the values $f_1 = 10.75\times10^5$ dynes/cm, $f_{12} = 0.461\times10^5$ dynes/cm, $f_\theta = 1.10\times10^5$ dynes/cm and $g_c = 1.41\times10^5$ dynes/cm. These constants are somewhat different from those given by Glockler and Tung because the present zero-order frequencies are larger than the band centers used in their work.

Using the present force constants the zero-order frequencies for $S^{34}O_2^{16}$ were calculated as $\omega_1' = 1165.2$ cm^{-1}, $\omega_2' = 519.3$ cm^{-1}, and $\omega_3' = 1363.4$ cm^{-1}. As the sulfur isotope S^{34} comprises 4.2 percent of naturally occurring sulfur it was thought likely that the isotopic bands could be observed. This would have permitted the unique determination of the force constants. However, the intensity of the $S^{32}O_2^{16}$ transitions evidently obscured the isotopic bands and not even the Q branch of ν_3' with a shift of about 17.5 cm^{-1} was observed.

TABLE X. Observed and calculated band centers for SO_2.

Band	Observed frequency	Calculated frequency	$\Delta\nu$	Previous observations
ν_1	1151.38	1151.74	−0.36	1151.38[6], 1152[5]
$2\nu_1$	2295.88	2295.51	0.37	2305[5]
$3\nu_1$	3431.19	3431.31	−0.12	
ν_3	1361.76	1361.76	0	1361.50[6], 1361[5]
$2\nu_3$	2715.46	2713.18	2.28	
$3\nu_3$	4054.26	4054.26	0	
ν_2	517.69	517.69	0	517.84[6], 524[5]
$3\nu_2$	1535.06	1535.06	0	
$\nu_1+\nu_2$	1665.07	1667.39	−2.32	
$2\nu_1+\nu_2$	2808.32	2808.10	0.22	
$\nu_1+\nu_3$	2499.55	2499.79	−0.24	2499[5]
$2\nu_1+\nu_3$	3629.61	3629.85	−0.24	
$\nu_1+3\nu_3$	5165.64	5164.87	0.77	
$3\nu_1+\nu_3$	4751.23	4751.94	−0.71	
$\nu_1+\nu_2+\nu_3$	3011.25	3011.53	−0.28	
$\nu_2+\nu_3$	1875.55	1875.55	0	1871[5]
$\nu_3-\nu_2$	844.93	844.07	0.86	

[12] J. Duchesne, Physica **9**, 249 (1942); G. Glockler and J. Y. Tung, J. Chem. Phys. **13**, 388 (1945); P. Torkington, J. Chem. Phys. **17**, 357 (1949); J. Duchesne and L. Burnelle, J. Chem. Phys. **19**, 1191 (1951).

Diffusion and Thermal Diffusion of Isotopic Gases

EUGENE M. HOLLERAN
St. John's University, Brooklyn 6, New York
(Received September 15, 1953)

The thermal diffusion ratio, R_T, for argon and neon isotopes is known to be a linear function of $\ln T$ over a considerable temperature range. It is shown that $d\ln D/d\ln T$ must also be approximately linear in $\ln T$, and that the diffusion coefficient, D, should therefore obey an empirical equation of the form

$$D=\alpha T^{(\beta+\gamma\ln T)},$$

where α, β, γ are constants. Considerable latitude is possible in the values of these constants which can reproduce the diffusion data available at the present time. Satisfactory values of β and γ can be found from thermal diffusion data. Except for the factor α, $D(T)$ can thus be calculated from $R_T(T)$. It is also possible to calculate the thermal diffusion ratio as a function of temperature from measurements of the diffusion coefficient, but completely reliable results require more extensive diffusion data than is now available.

INTRODUCTION

THE following relation has been shown theoretically to represent the temperature dependence of the thermal diffusion ratio, R_T, for an isotopic mixture of gases composed of spherically symmetrical molecules,[1]

$$R_T=z(2-n), \tag{1}$$

where n is the derivative with respect to $\ln T$ of the natural logarithm of the self-diffusion coefficient, D, of either isotope, and

$$z=\frac{8.43(A+1)}{A[10A+16-n(5-n)-q]} \tag{2}$$

in which $q=dn/d\ln T$, and

$$A=\frac{MD}{246\eta T}, \tag{3}$$

where M is the molecular weight of the isotope in question, and η is its viscosity coefficient.

R_T for a mixture of isotopes is thus a function of the coefficients of viscosity and self-diffusion of either pure isotope. However, due mainly to the approximate constancy of A (see Table I), it turns out that the factor z is nearly independent of the temperature. Under this condition, Eq. (1) shows that the temperature variation of R_T depends only on the temperature variation of D, and vice versa. In other words, assuming that the value of z is known from D and η or can otherwise be estimated, R_T as a function of T can be found from measurements of D. And, as seen from the integral of Eq. (1),

$$\ln(D/\alpha)=2\ln T-\frac{1}{z}\int R_T d\ln T \tag{4}$$

where $\ln\alpha$ is the integration constant, the coefficient of diffusion, except for the constant factor α, can be found as a function of T from the thermal diffusion ratio if the temperature dependence of the latter is known.

D/α FROM R_T

As has recently been verified,[2] experimental measurements of the thermal diffusion ratio for argon and neon isotopes can be fitted over a large range of temperature by empirical equations of the form given by Stier,[3]

$$R_T=a\ln\frac{T}{b}, \tag{5}$$

where a and b are constants. Combination of Eqs. (1) and (5) gives

$$n=\beta+2\gamma\ln T, \tag{6}$$

where

$$\beta=2(1-\gamma\ln b);\quad \gamma=-a/2z. \tag{7}$$

Again taking z constant, β and γ are constants. Differentiation of Eq. (6) then gives q constant with the value 2γ, and integration of Eq. (6) gives Eq. (4) in the form

$$\ln D=\ln\alpha+\beta\ln T+\gamma(\ln T)^2. \tag{8}$$

Thus, when z is known, D/α as a function of temperature can be found very simply from the constants of Eq. (5) over the temperature range for which this equation is valid. An upper limit on this range of validity is expected if R_T *vs* T eventually levels off at high temperatures as it does for noble gas mixtures.[4] A lower limit must also exist if the theoretically expected[5] minimum in R_T is to be found. Nevertheless, Eq. (5) holds[2] for neon over the entire temperature range (132° to 713°K) that has been investigated experimentally,[3] and for argon from about 150°K to at least 729°K. Equation (5) also appears to hold for other gases over the much shorter temperature ranges that have been investigated. Therefore, still assuming a negligible temperature variation for z, Eq. (8) and the

[1] E. M. Holleran and H. M. Hulburt, J. Phys. Chem. **56**, 1034 (1952).

[2] E. M. Holleran, J. Chem. Phys. **21**, 1901(L) (1953).
[3] L. G. Stier, Phys. Rev. **62**, 548 (1942).
[4] K. E. Grew, Proc. Phys. Soc. (London) **62A**, 655 (1949).
[5] E. R. S. Winters, Trans. Faraday Soc. **46**, 81 (1950).

TABLE I. The dependence of A on temperature.[a]

T(°K)	$\eta\times10^5$	A (rough)	A (smooth)
	Argon		
77.7	6.71	0.418	0.415
90.2	7.64	0.425	0.427
194.7	15.55	0.446	0.444
273.2	21.01	0.442	0.441
295.2	22.40	0.438	0.441
353.2	25.8	0.444	0.443
	Neon		
77.7	11.69	0.440	0.440
194.7	23.31	0.457	0.454
273.2	29.68	0.453	0.453
298.2	31.59	0.445	0.452
353.2	35.3	0.458	0.454

[a] A (rough) was found from the experimental values of D (Table II, col. 2). A (smooth) was found from the smoothed values of D (Table II, col. 4). The values of η were interpolated from the results of Johnston, Grilly, and McCloskey (see references 8 and 9) except for the values at 353.2°K, which were interpolated from the results of Trautz and co-workers. [Landolt-Bornstein, *Physical Chemical Tables* (Julius Springer, Berlin, 1935), fifth edition, Vol. 1.]

equivalent empirical equation for the coefficient of diffusion

$$D=\alpha T^{(\beta+\gamma\ln T)} \tag{9}$$

may be valid for many gases over considerable ranges of temperature.

COMPARISON WITH EXPERIMENT

It is not surprising that Eq. (9) with three arbitrary constants can represent fairly well the most extensive diffusion data available, due to Winn,[6] which consists of from four to six experimental values for each gas at temperatures between 77.7°K and 353.2°K. The data are not nearly extensive enough to determine the constants unambiguously. This is apparent in Table II in which rather different sets of constants are seen to give very similar results.

In order to determine the values of α, β, and γ for neon and argon that result from the known temperature variation of their thermal diffusion ratios, suitable values for the factor z are required. Theoretically, according to the Lennard-Jones 12,6 intermolecular potential,[7] the quantity A is practically constant over a very wide range of temperature. Experimentally, the limited data seem to confirm this. In Table I, column 3, are given the values of A calculated from Eq. (2) at Winn's experimental temperatures from his values of D and from viscosity values (column 2) mostly interpolated from the graphically smoothed data given by Johnston, Grilly, and McCloskey.[8,9] These values of A are rather erratic. That they are random variations about approximately constant values for the four highest temperatures in each case seems pretty well established by the values of A given in column 4. These were found by using values of D (Table II, column 4) calculated from Eq. (8) with constants found from a least-squares fit of the diffusion data. Further calculations at intermediate temperatures show that for argon $A=0.442\pm0.002$ down to about 120°K, and for neon $A=0.452\pm0.002$ down to about 150°K.

Judging from Stier's R_T data and Eq. (1) with z about two, n varies roughly from 1.7 to 2.0 for argon and from 1.6 to 1.9 for neon in the approximate temperature range of 125° to 725°K. Using these extremes in Eq. (2) along with the values of A given above and with $q=-0.1$, z is found to be 1.87 ± 0.03 for argon, and 1.81 ± 0.03 for neon. Variations of this magnitude will be seen to be unimportant for the present purpose.

The thermal diffusion ratio for argon obeys Eq. (5) above about 150°K with $a=0.257$ and $b=91.0$°K. For neon, $a=0.259$ and $b=29.7$°K.[2] Equations (7) now lead to $\beta=2.620$ and $\gamma=-0.0687$ for argon, and $\beta=2.485$ and $\gamma=-0.715$ for neon. The values of α, 5.582×10^{-7} for argon and 3.795×10^{-6} for neon, were found by the method of least squares from the observed D values and D/α found using the above values of β and γ in Eq. (8). Table II, column 3, shows that Eq. (8) or (9) with these values of the constants reproduces the experimental diffusion data fairly well. The calculated values of D for neon differ from the observed values by somewhat more than the reported most

TABLE II. Observed and calculated values of D.[a]

T(°K)	D(obs.)	$D(R_T)$	D(L.S.)
	Argon		
77.7	0.0134±0.0002	0.0136	0.0133
90.2	0.0180±0.0003	0.0184	0.0181
194.7	0.0830±0.0011	0.0824	0.0826
273.2	0.156 ±0.002	0.1554	0.1557
295.2	0.178 ±0.003	0.1792	0.1795
353.2	0.249 ±0.003	0.2487	0.2483
	a	0.257	0.340
	b	91.0	113.
	$\alpha\cdot10^7$	5.582	2.924
	β	2.620	2.8604
	γ	−0.0687	−0.09094
	Neon		
77.7	0.0492±0.0004	0.0488	0.0492
194.7	0.255 ±0.004	0.2543	0.2532
273.2	0.452 ±0.003	0.4535	0.4523
298.2	0.516 ±0.005	0.5252	0.5242
353.2	0.703 ±0.005	0.6953	0.6958
	a	0.259	0.205
	b	29.7	18.0
	$\alpha\cdot10^6$	3.795	5.742
	β	2.485	2.3271
	γ	−0.0715	−0.056561

[a] D(obs.) are the experimental values of Winn (reference 6). $D(R_T)$ were calculated from R_T via Eqs. (7) and (8). D(L.S.) were calculated from a least-squares fit of Eq. (8) to the experimental data. The constants for Eqs. (8) and (5) are given in the corresponding columns.

[6] E. B. Winn, Phys. Rev. **80**, 1024 (1950).
[7] Hirschfelder, Bird, and Spotz, J. Chem. Phys. **16**, 968 (1948).
[8] H. L. Johnston and K. E. McCloskey, J. Phys. Chem. **44**, 1038 (1940).
[9] H. L. Johnston and E. R. Grilly, J. Phys. Chem. **46**, 948 (1942).

probable experimental error at the two highest temperatures. The seriousness of this discrepancy seems lessened, however, by the fact that the least-squares fit of Eq. (8) to the data experiences similar difficulty at these temperatures (column 4). The agreement between calculated and smoothed values (columns 3 and 4) is quite good. For argon the agreement between calculated and observed values is well within the experimental error at the four highest temperatures. For both gases the agreement continues to be good down to the lowest temperatures which are below the range in which A is constant and in which Eq. (5) is known to hold.

From the foregoing it may be concluded that satisfactory values of β, γ, and D/α can be found from thermal diffusion data. More extensive diffusion data would provide a more conclusive test.

Equation (5) with $a=0.30$ and $b=39°$K gives R_T for neon 5 percent high at the highest experimental temperature, 713°K, and 5 percent low at the lowest, 132°K. With $a=0.22$ and $b=19$, R_T is 5 percent low at 713° and 5 percent high at 132°. These sets of values may thus be taken as the limits of acceptability for reproducing R_T in this temperature range within the reported most probable experimental error of ± 5 percent. Corresponding sets for argon between the temperatures 163° and 729°K are $a=0.28$, $b=99$, $a=0.23$, $b=83$.

Use of these values in Eqs. (7) results in calculated values of D (using appropriate α's) which differ very little from those calculated using the "best" values of a and b. This insensitivity of calculated D to such changes in a and b indicates that, until more extensive diffusion data necessitate refinement, the same value of z can be used for many, if not all, gases. The average of the limiting constant values of A for the gases used by Winn (A, Ne, CH_4, N_2, O_2, CO_2) is about 0.46, so that 1.8 is a good value for z. D/α may then be estimated from thermal diffusion data only.

R_T FROM D

The impossibility of determining unambiguously the constants of Eq. (8) from present diffusion data, and the insensitivity of calculated D values to changes in a and b indicate that no set of these constants now determinable can be relied upon to give a very good reproduction of thermal diffusion data. As it turns out, least-squares fits of Eq. (8) to the diffusion data for neon and argon (Table II, column 4) lead to values of a and b of 0.205 and 18°K for neon and 0.340 and 113°K for argon. These values are not within the limits mentioned above for reproducing R_T within 5 percent over the temperature range in which Eq. (5) is valid. However, since the diffusion data from which a and b were determined do not extend beyond 353°K, and since there is no assurance that A and z remain constant above this temperature (R_T is more sensitive than D to changes in z), comparison of calculated and observed values of R_T at higher temperatures is not particularly significant. A lower limit of about 150°K is also imposed by the facts that below this temperature z for neon begins to vary appreciably, and R_T for argon appears to deviate from Eq. (5). With these restrictions on the range of temperature, Table III shows that the agreement between observed and calculated values of R_T is not so bad, being, in fact, within experimental error for the case of neon.

TABLE III. Observed and calculated values of R_T.[a]

	Argon		Neon	
T(°K)	R_T(obs.)	R_T(calc.)	R_T(Obs.)	R_T(calc.)
150	0.13	0.10	0.42	0.43
200	0.20	0.19	0.49	0.49
250	0.26	0.27	0.55	0.54
300	0.31	0.33	0.60	0.58
350	0.35	0.38	0.64	0.61

[a] All values were calculated from Eq. (5). The constants, a and b, were found from a least-squares fit of the R_T data of Stier (see reference 3) to obtain R_T(obs.). For R_T(calc.) the constants were determined by a least-squares fit of Eq. (8) to the diffusion data of Winn (see reference 6).

Holleran and Hulburt[1] obtained somewhat better agreement for argon in this range from a least-squares fit of the experimental $\ln D$ to a cubic in $\ln T$,

$$\ln D = -12.660 + 1.5864 \ln T + 0.13371 (\ln T)^2 - 0.013089 (\ln T)^3. \quad (10)$$

Although the cubic for $\ln D$ is inappropriate to the temperature range in which R_T and n are linear in $\ln T$, Table IV shows that values of n found from the derivative of Eq. (10) agree very well in the temperature range of the diffusion data (77.7° to 353.2°K) with those found from Eq. (6) using β and γ from thermal diffusion. The error in R_T calculated from $n(10)$ is about $1.87\Delta n$. The differences are fortunately arranged (column 4), so that the best straight line fit of n from Eq. (10) *vs* $\ln T$ in this range would give a and b capable of reproducing R_T excellently even at higher temperatures. Equation (10) itself is useless outside the T range of the diffusion data.

TABLE IV. Values of n for argon.[a]

$\ln T$	$n(10)$	$n(R_T)$	Δn
4.35	2.007	2.022	0.015
4.4	2.003	2.015	0.012
4.6	1.986	1.988	0.002
4.8	1.965	1.961	−0.004
5.0	1.942	1.933	−0.009
5.2	1.915	1.906	−0.009
5.4	1.886	1.878	−0.008
5.6	1.853	1.851	−0.002
5.8	1.817	1.823	0.006
5.87	1.803	1.814	0.011

[a] $n(10)$ were found from Eq. (10). $n(R_T)$ are from Eq. (6) with constants found from thermal diffusion.

The comparison made in reference 1 between n predicted for argon by the Lennard-Jones 12,6 potential and "observed" n from Eq. (10) might more reasonably be made with "observed" n found from R_T via Eq. (6), at least above 150°K. Discrepancies of about the same magnitude as before still exist. The uncertainty of experimental n at low temperatures now makes it clear that no reliable prediction of the thermal diffusion inversion temperature can be made at the present time.

It should be noted that in fitting Eq. (8) to the diffusion data the low temperature points were included even though these lie below the range of known validity of Eq. (5) and of constant A and z. Although Eq. (8) then fits these points reasonably well, their inclusion for the purpose of calculating R_T is questionable. Nevertheless, their omission is at present impractical, since that would leave only four experimental values in each case, and the method of least squares permits such contortions in fitting so few points that values of n so determined would be completely untrustworthy. Again the need is felt for experimental measurements at higher temperatures.

However, when D is known more extensively, and R_T more accurately, it will probably be advisable in calculating R_T to find z more exactly as a function of T from D and η, and to employ a modification of Eq. (1), given in reference 1, which can affect R_T by one unit in the second decimal place.

The author would like to express his thanks to St. John's University for a summer research grant.

A Sum Rule for the Vibrational Frequencies of Homologs*

H. J. BERNSTEIN AND A. D. E. PULLIN†
Division of Chemistry, National Research Council, Ottawa, Ontario, Canada
(Received June 2, 1953)

It is shown empirically that the zero-point energy in substituted methanes may be treated as a constitutive property when account is taken of the interaction between nonbonded atoms. Thus, the sum of the vibration frequencies ($\Sigma\nu$) of the halogenated methanes is found to have the predicted quadratic dependence on the number of substituents. This reduces to a linear dependence in the case of isotopically substituted homologs, compared to the linear dependence for $\Sigma\nu^2$ found theoretically by Decius and Wilson, and Sverdlov. Both $\Sigma\nu$ and $\Sigma\nu^2$ give good agreement between observed and calculated results. Various applications are given for the $\Sigma\nu$ rule and it is shown further that $\Sigma\nu$, $\Sigma\nu^2$, $\Sigma 1/\nu$, $\Sigma 1/\nu^2$ are all approximately constitutive properties of the halogenated methanes.

BECAUSE of the systematization of thermochemical data,[1] it has been necessary to extend the simple additivity treatment[2] for heats of atomization by including the contributions made from nonbonded atoms.[3] Thus, the constitutive property P_n of the substituted methane $CX_{4-n}Y_n$ is shown to be[3] a parabolic function of n, *viz.*,

$$P_n = P_0 + an + bn^2, \tag{1}$$

where

$$a = \frac{P_4 - P_0}{4} - 4b$$

and $b = \frac{1}{2}$ (the contribution to P_n made by the interaction of two X atoms plus the contribution to P_n made by the interaction of two Y atoms minus twice the contribution to P_n made by the interaction of an X and Y atom). Indeed, the heat of formation in kcal per mole[1] of the chloro- and bromo-methanes may be expressed respectively as $\Delta H_f^0 = -17.8 - 1.62n - 0.086n^2$ and $\Delta H_f^0 = -17.8 + 9.51n - 0.521n^2$ quite accurately. In these equations $n = 0$ for CH_4 and is 4 for the tetra-substituted methane. The experimental heats of formation yield values for the heat of atomization for the ground state. It seems reasonable to inquire here whether the zero-point energies and, therefore, the heats of atomization for the equilibrium configuration may be considered as constitutive properties. More explicitly, do the zero-point energies of the substituted methanes, for example, obey a relation of the type given in Eq. (1)? In order to answer this question the vibrational assignments given by Plyler and Benedict[4] for some 18 fluoro-chloro-bromo-methanes may be used. The zero-point energy is defined as $\frac{1}{2}\sum_{i=1}^{m} d_i\omega_i$ where ω_i is the zero-order frequency of the ith fundamental and d_i is the corresponding degree of degeneracy of this mode, and the sum is taken over all m fundamentals. Since zero-order frequencies are not available for most molecules and even gas-phase data are not available for most of the observed fundamentals $\frac{1}{2}\sum_{i=1}^{m} d_i\nu_i$ will be taken as a measure of the zero-point energy. Here ν_i is the observed

TABLE I. The substituted methanes $CX_{4-m-n}Y_nZ_m$ with $m = 0, 1, 2, 3, 4$ and $n = 0, 1, 2, \cdots 4-m$.

	X	Y	Z	P_{CX_4}	α	β	γ	Δ_{XY}	Δ_{XZ}
1.	Br	H	Cl	3075	4656	261.3	4664	456.3	−7.31
2.	F	H	Cl	7473	3516	−860.9	3547	424.8	−20.9
3.	Br	Cl	F	3082	250.7	988.5	279.2	−15.34	−77.74
4.	Br	H	F	3074	4649	996.1	4672	449.0	−69.98

TABLE II. $\Sigma\nu$ in cm^{-1} for the fluoro-bromo-chloro-methanes.

Molecule	Obs[a]	Calc	Obs-calc	Molecule	Obs[a]	Calc	Obs-calc
CBr_4	3069	3077	−8	CH_2F_2	14 077	14 079	−2
CBr_3H	7731	7727	+4	CH_3F	16 783	16 743	40
CBr_2H_2	11 929	11 927	+2	CF_3Cl	6618	6614	−4
$CBrH_3$	15 680[b]	15 674	6	CF_2Cl_2	5777	5770	7
CH_4	18 953	18 976	−23	$CFCl_3$	4962	4954	8
CBr_3Cl	3351	3335	16	CF_2HCl	10 166	10 159	7
CBr_2Cl_2	3600	3602	−2	CFH_2Cl	13 315	13 281	34
$CBrCl_3$	3890	3880	10	$CFHCl_2$	9296	9329	−33
CCl_4	4170	4165	5	CBr_3F	4083[c]	4070	13
CBr_2HCl	7987	7999	−12	CBr_2F_2	5142[c]	5136	6
$CBrH_2Cl$	12 216	12 207	9	$CBrF_3$	6303[d]	6276	+27
CH_3Cl	16 031[b]	15 968	+63	CH_2BrF	12 974[c]	12 966	8
$CBrHCl_2$	8267	8276	−9	$CHBrF_2$		9831	
$CHCl_3$	8537	8560	−23	$CHFBr_2$	8695[c]	8742	−47
CH_2Cl_2	12 510	12 500	10	CBr_2ClF	4330[c]	4350	−20
CF_4	7499	7485	14	$CBrCl_2F$	4619[c]	4644	−25
CHF_3	10 943	10 989	−44	$CBrClF_2$		5366	

[a] All data from Plyler and Benedict (reference 4) except where otherwise indicated.
[b] Taken from data compiled in *Ramanspektren* (reference 17).
[c] These data are from M. L. Delwaulle and F. Francois, J. phys. **7**, 15 (1946).
[d] S. R. Polo and M. K. Wilson, J. Chem. Phys. **20**, 1183 (1952).

* Presented at the Symposium on Molecular Structure held at Columbus, Ohio, 1952.

† National Research Laboratories Post-doctorate Research Fellow 1950–52.

[1] *Selected Values of Properties of Hydrocarbons*, Natl. Bur. Standards Circ. 461 (Government Printing Office, Washington, D. C., 1947). *Selected Values of Chemical Thermodynamic Properties*, Natl. Bur. Standards, Circ. 500 (Government Printing Office, Washington, D. C., 1952).

[2] See L. Pauling, *Nature of Chemical Bond* (Cornell University Press, Ithaca, 1942). Y. Syrkin, Zhur. Fiz. Khim. **17**, 347 (1943) and others.

[3] H. J. Bernstein, J. Chem. Phys. **20**, 263 (1952). It is emphasized here that the physical picture may be one of interaction between charge distributions in bonds and/or interactions between nonbonded atoms and still yield the same algebraic relations between the constitutive properties of molecules in homologous series.

[4] E. K. Plyler and W. S. Benedict, J. Research Natl. Bur. Standards **47**, 202 (1951). Their values are quoted sometimes for the gas phase and others are for the liquid or solution.

TABLE III. Linear $\Sigma\nu$ rule for isotopic homologues.

	C_6H_6	C_6H_5D	1:4-$C_6H_4D_2$	1:3:5-$C_6H_3D_3$	1:2:4:5-$C_6H_2D_4$	C_6HD_5	C_6D_6
obs[a]	42 773[b]	41 348[c]	40 033[c]	38 724[d]	37 307[d]		34 576[e]
calc		41 407	40 040	38 675	37 309	35 943	
	CH_4	CH_3D	CH_2D_2	CHD_3	CD_4		
obs[e]	18 946	17 819	16 484	15 343	13 954		
calc		17 698	16 450	15 202			
			$C_2H_2D_2$				
	C_2H_4	C_2H_3D	*cis*	*trans*	1,1	C_2HD_3	C_2D_4
obs[f]	21 564	20 347	19 062[g]	19 036[h]	19 086[i]	17 675	16 490
calc		20 297	19 028	19 028	19 028	17 759	
		C_2H_2	C_2HD	C_2D_2			
obs[e]		9975	8972	7934			
calc.			8955				

[a] The frequencies used here are from Ingold *et al.*, J. Chem. Soc. **1946**, 332, 222 and following.
[b] This sum includes R. D. Mair and D. F. Hornig's [J. Chem. Phys. **17**, 1236 (1949)] value for ν_{14} and ν_{18}.
[c] These sums include a value for ν_{14} obtained by Mair and Hornig, reference b, from a re-interpretation of Raman overtones by Ingold *et al.*, reference a.
[d] These sums include values of ν_{14} obtained by Teller-Redlich product rule calculations.
[e] Data used by J. C. Decius and Bright Wilson, Jr. (reference 6) for their $\Sigma\nu^2$ rule.
[f] From R. H. Arnett and B. L. Crawford, Jr., J. Chem. Phys. **18**, 118 (1950).
[g] This sum contains one frequency calculated from the Teller-Redlich product rule and two calculated from the force constants of reference f.
[h] This sum contains one frequency calculated from the Teller-Redlich product rule.
[i] This sum contains one frequency calculated from the Teller-Redlich product rule and one from the force constants of reference f.

frequency of the fundamental mode. In what follows we shall, for convenience, write $\Sigma\nu$ for the sum of the fundamentals, where it is understood that proper account of the degree of degeneracy has been taken.

It has been shown in Table III of reference 3 that the constitutive property of the fifteen methanes with X, Y, and Z as substituents may be related in terms of six parameters. In Table I the least-squares values of these parameters for evaluating $\Sigma\nu$ are given for the substituted methanes with Br, Cl, and F, as substituents. The values of $\Sigma\nu$ calculated with these values are compared with those observed for $\Sigma\nu$ in Table II. Since the least-squares solutions were obtained for groups of 15 molecules, there will be more than one calculated value for some molecules. These would be equal for perfect internal consistency, just as Δ_{XY} in row 1 should be equal to Δ_{XY} of row 4 in Table I, etc. The calculated values given in Table II are the average values calculated from the parameters of Table I.

It is apparent that for the molecule CHF_2Br, for example, the values of the parameters given in the 4th row of Table I are to be used in the relation for this molecule obtained from Table III of reference 3, *viz.*,

$$\Sigma\nu_{CHF_2Br}=\Sigma\nu_{CXYZ_2}=P_{CX_4}-\alpha+2\beta+2\gamma-\Delta_{XZ}.$$

The agreement between observed and calculated values of $\Sigma\nu$ is much better than could have been anticipated being about ± 50 cm^{-1} which is equivalent to ± 0.07 kcal per mole in zero-point energy. Thus, it seems pretty well established for the substituted methanes that the zero-point energy is a constitutive property. This is equivalent to a constitutive relationship between the sums of the frequencies, i.e., a sum rule for vibrational frequencies in this homologous series.

It is apparent that all 24 values for the parameters given in Table I are not independent. In fact there are 14 relations among these 24 leaving 10 independent parameters in terms of which the constitutive properties of all the substituted chloro-bromo-fluoro-methanes except the molecule CFBrClH may be expressed. Since it is much more practical to solve the actual problem in terms of 6 parameters for 15 substituted methanes of the series $CX_{4-m-n}Y_nZ_m$ [$m=0, 1, 2, 3, 4$ and $n=0, 1, 2, \cdots(4-m)$] than in terms of the 11 parameters for the 35 methanes of the series $CH_{(4-m-n-p)}Br_nCl_mF_p$ [$p=0, 1, 2, 3, 4$, $m=0, 1, 2, \cdots(4-p)$, $n=0, 1, \cdots(4-\{m+p\})$], the relations between the 24 values given in Table I will not be presented here.

TABLE IV. Deuterium substituted acetylenes.

		C_2H_2	C_2HD	C_2D_2
Σ^+ type vibration	(obs)	8635	7770	6890
	(calc)		7762	
π-type vibration	(obs)	1341	1202	1044
	(calc)		1192	

ISOTOPIC HOMOLOGOUS SERIES

Suppose the substituted methane series under consideration is the one in which deuterium atoms are being substituted, i.e., $X=H$ and $Y=D$, it is not unreasonable to assume then that b is very nearly zero.‡ Thus, an approximately linear relation between $\Sigma\nu$ and the number of deuterium atoms is indicated for the deuterated methanes.[5] Similarly, in Table VII of reference 3 for the

‡ $b=\frac{1}{2}$ (The contribution made to the zero-point energy by interaction of two nonbonded H atoms+that due to the interaction of two nonbonded D atoms−twice that due to the interaction of an H and D atom).

[5] In the extreme case of linear interpolation for $\Sigma\nu$ in bonded atoms such as H_2, HD, and D_2 an error of 1.5 percent is made in the calculated value of the HD frequency. It seems reasonable to expect, therefore, that the absolute error introduced for interactions between nonbonded atoms will be small.

ethylenes, $a-c=a-d=a-b\approx 0$ so $a=b=c=d$ and Table VII of reference 3 reduces to a linear relation between the number of D atoms and the constitutive property of the D substituted ethylenes. In a similar manner it can be shown for all the homologous series discussed in reference 3 that the relations for the value of the constitutive property reduce to approximately linear ones in the number of isotopes substituted. This is indeed verified in Table III, where the comparison has been made between the value of $\Sigma\nu$ in cm^{-1} obtained by linear interpolation between the end members of the series and the values observed for deuterium substituted benzenes, methanes, ethylenes, and acetylenes.

At this point it is instructive to consider the sum rule derived recently by Decius and Wilson[6] and indepenently by Sverdlov[7] for isotopically substituted homologous series. This sum rule, which is derived rigorously for zero-order frequencies from small vibration theory, shows that a linear relation exists between $\Sigma\nu^2$ and the number of isotopes substituted and that this relation is valid for symmetry types which are common to all members of the series.

Since the relation betwen $\Sigma\nu$ and the number of substituents has been shown to be linear from zero-point energy consideration and $\Sigma\nu^2$ has been shown to be a linear function of the number of substituents from vibration theory, it would seem that the same types of relations are valid for $\Sigma\nu$ as are indicated by vibration theory for $\Sigma\nu^2$. Thus, it is not entirely unexpected that the $\Sigma\nu$ rule is valid for least common symmetry types in a homologous series. That this is indeed so may be seen from Tables IV, V, and VI where the summations have been made also for common symmetry types.

The linear $\Sigma\nu$ rule for deuterium compounds has been verified further by the results[8] on PH_3, PH_2D, PHD_2 and PD_3 and NH_3,[9] NH_2D,[10] and ND_3,[9] and more recently, also, by the results for the deuterated vinyl bromides.[11]

It is indeed surprising that there should be linear relations for both $\Sigma\nu$ and $\Sigma\nu^2$, and it suggests that the functional dependence of the sum of the frequencies raised to the xth power, $\Sigma\nu^x$, is not very sensitive to the number of substituents in the isotopically substituted series. As a matter of general interest we have made corresponding calculations for $\Sigma\nu^{\frac{1}{2}}$ and $\Sigma\nu^3$ and find them also to give reasonably good linear relations. The calculations are made by linear interpolation between the end members of the series and are given also with $\Sigma\nu$ and $\Sigma\nu^2$ for comparison, in Table VII. It is apparent that the agreement is best for the $\Sigma\nu$ rule and gets progressively worse as we proceed to higher powers of the frequency.

It seems certain that the only rule which may be established rigorously on a theoretical basis is that involving $\Sigma\nu^2$ but, since $\Sigma\nu^x$ is not sensitive to the functional dependence on the number of substituents, we have additivity relations valid for $\Sigma\nu$. Thus, the zero-point energy may be regarded as a constitutive property. Similarly for nonisotopic series, it should be possible to show from vibration theory that $\Sigma\nu^2$ is very nearly a parabolic function of the number of substituents but, because $\Sigma\nu^x$ is insensitive to the number of substituents, the $\Sigma\nu$ rule will again be valid. Numerically it is possible

TABLE V. Deuterium substituted ethylenes.

			All modes	In-plane	Out-of-plane	$\nu_1+\nu_2+\nu_3+\nu_9+\nu_{10}$[a]	$\nu_5+\nu_6+\nu_{11}+\nu_{12}$	$\nu_4+\nu_8$	ν_7	$\nu_1+\nu_2+\nu_3+\nu_5+\nu_6$	$\nu_9+\nu_{10}+\nu_{11}+\nu_{12}$	$\nu_4+\nu_7$	ν_8	$\nu_1+\nu_2+\nu_3+\nu_4+\nu_{11}+\nu_{12}$	$\nu_5+\nu_6+\nu_9+\nu_{10}$	$\nu_7+\nu_8$	ν_4
C_2H_4	D_{2h}	obs[b]	21 564	18 645	2919	9900	8745	1970	949	10 295	8350	1976	943	10 418	8227	1892	1027
		calc															
C_2H_3D	C_s	obs	20 347	17 595	2752												
		calc	20 297	17 549	2745												
cis-$C_2H_2D_2$	C_{2v}	obs	19 062[c]	16 481[d]	2581[e]	8786	7695[d]	1738[e]	843								
		calc	19 028	16 454	2572	8788	7666	1738	835								
trans-$C_2H_2D_2$	C_{2h}	obs	19 036[d]	16 457[d]	2579					9161	7296[d]	1715	864				
		calc	19 028	16 454	2572					9176	7273	1711	862				
a-$C_2H_2D_2$	C_{2v}	obs	19 086[f]	16 501[d]	2585[g]									9245	7256[d]	1696	889[g]
		calc	19 028	16 454	2572									9222	7233	1696	877
C_2HD_3	C_s	obs	17 675	15 267	2408												
		calc	17 759	15 359	2399												
C_2D_4	D_{2h}	obs	16 490	14 264	2226	7676	6588	1506	720	8057	6207	1446	780	8025	6239	1500	726
		calc															

[a] The numbering of the fundamentals is that of R. H. Arnett and B. L. Crawford, Jr. (reference f, Table III).
[b] All data from the paper by Crawford, Lancaster, and Inskeep, J. Chem. Phys. **21**, 678 (1953).
[c] This sum contains one frequency calculated from the Teller-Redlich product rule and two calculated from force constants of Arnett and Crawford.
[d] This sum contains one frequency calculated from the Teller-Redlich product rule.
[e] This sum contains two frequencies calculated from force constants of Arnett and Crawford.
[f] This sum contains one frequency calculated from the Teller-Redlich product rule and one calculated from force constants of Arnett and Crawford.
[g] This sum contains one frequency calculated from force constants of Arnett and Crawford.

[6] J. C. Decius and E. B. Wilson, Jr., J. Chem. Phys. **19**, 1409 (1951).
[7] L. M. Sverdlov, Doklady Akad. Nauk. S. S. S. R. **78**, 1115–19 (1951).
[8] R. E. Weston, Jr., and M. H. Sirvetz, J. Chem. Phys. **20**, 1820 (1952).
[9] See (a) G. Herzberg, *Infrared and Raman Spectra* (D. Van Nostrand Company, Inc., New York, 1945); (b) J. S. Burgess, Phys. Rev. **76**, 1267 (1949).
[10] Perlman, Bigeleisen, and Elliott, J. Chem. Phys. **21**, 70 (1953).
[11] J. Charette and M. de Hemptinne, Acad. roy. Belg. Bull. classe sci. **38**, 934 (1952).

TABLE VI.[a] Deuterium substituted benzenes.

		All fundamentals	In-plane	Out-of-plane	$\nu_1+\nu_2$ $+\nu_{12}+\nu_{13}$[b]	$2(\nu_6+\nu_7+\nu_8$ $+\nu_9+\nu_{18}$ $+\nu_{19}+\nu_{20})$	$\nu_3+\nu_{14}$ $+\nu_{15}$	$\nu_4+\nu_5$ $+\nu_{11}$	$2(\nu_{10}+\nu_{16}$ $+\nu_{17})$	$\nu_1+\nu_2+\nu_3$ $+\nu_{6a}+\nu_{6b}$ $+\nu_{7a}+\nu_{7b}$ $+\nu_{8a}+\nu_{8b}$ $+\nu_{9a}+\nu_{9b}$	$\nu_{12}+\nu_{13}+\nu_{14}$ $+\nu_{15}+\nu_{18a}$ $+\nu_{18b}+\nu_{19a}$ $+\nu_{19b}+\nu_{20a}$ $+\nu_{20b}$	$\nu_{11}+\nu_{16a}$ $+\nu_{16b}$ $+\nu_{17a}+\nu_{17b}$	$\nu_4+\nu_5$ $+\nu_{10a}$ $+\nu_{10b}$
C_6H_6	obs	42 773[c]	35 966[d]	6807	8124	24 057	3786[c]	2359	4448	18 323	17 734[c]	3421	3386
	calc												
C_6H_5D	obs	41 348[d]	34 742[d]	6606									
	calc	41 407	34 811	6596									
1:4-$C_6H_4D_2$	obs	40 033[d]	33 633[d]	6401						17 100	16 533[d]	3215	3186
	calc	40 040	33 657	6384						17 087	16 570	3210	3174
1:3:5-$C_6H_3D_3$	obs	38 724[e]	32 525[e]	6199	7294	21 769	3462[e]	2134	4060				
	calc	38 675	32 502	6173	7306	21 730	3467	2142	4031				
1:2:4:5-$C_6H_2D_4$	obs	37 307[e]	31 331[e]	5976						15 945	15 386[e]	3001	2975
	calc	37 309	31 348	5961						15 941	15 407	2998	2963
C_6D_6	obs	34 576[d]	29 038	5538	6489	19 402	3147	1925	3613	14 795	14 243	2787	2751
	calc												

[a] The frequencies used to construct this table, except in the cases noted below, have been taken from the assignments of Ingold and his co-workers (reference a of Table III). These assignments contain a number of frequencies calculated from product rule relations. The number of isotopic molecules studied enabled systematic anharmonicity corrections to be made in these calculations. The frequencies are mixed vapor and liquid values. Comparison of the Raman and infrared values of the frequencies of doubly appearing fundamentals in C_6H_5D and 1:3:5-$C_6H_3D_3$ (*ibid*, p. 258, 303) shows that the liquid-vapor frequency shift is very small. The conclusions of Mair and Hornig (reference b of Table III) based on the infrared spectrum of crystalline C_6H_6 have been adopted for ν_{14} and ν_{15}.

[b] Numbering of frequencies after E. Bright Wilson, Phys. Rev. **45**, 706 (1934).

[c] These frequency sums include Mair and Hornig's value for ν_{14} and ν_{15}.

[d] These frequency sums include a value for ν_{14}, obtained by Mair and Hornig from a reinterpretation of Raman overtones observed by Ingold *et al.*

[e] These sums include values of ν_{14} obtained by product rule calculation.

to fit the observed and calculated values of $\Sigma\nu^2$ for the molecules of Table II with the least-squares values of the parameters given in Table VIII. The values of $\Sigma\nu^2$ calculated with these parameters are compared with the observed values in the same table. The agreement is slightly better for $\Sigma\nu$ than for $\Sigma\nu^2$, and it is suggested that in all cases $\Sigma\nu$ be used instead of $\Sigma\nu^2$ for observed fundamentals because of simplification in arithmetic. In the same table (VIII) the calculated and observed values of $\Sigma 1/\nu$ and $\Sigma 1/\nu^2$ are given (due account of degeneracy being taken). As can be seen from this table, $\Sigma\nu^x$ with $x=1$, 2, -1, and -2 are all constitutive properties of these molecules, although the agreement between observed and calculated results is best for $x=1$ and progressively worse for $x=2$, -1, -2. For the purposes of assigning vibrational spectra the simplest and, therefore, most useful rule will, of course, be the one involving $\Sigma\nu$. In forthcoming publications it will be shown that the vibrational contribution to the gaseous heat capacity, entropy, and free energy is a constitutive property because $\Sigma\nu$, $\Sigma\nu^2$, $\Sigma 1/\nu$, and $\Sigma 1/\nu^2$ are all very nearly constitutive properties.

TABLE VII.

$$\%\ \text{deviation} = 100\times\left[\frac{(\Sigma\nu^x)_{\text{calc}}-(\Sigma\nu^x)_{\text{obs}}}{(\Sigma\nu^x)_{\text{obs}}}\right]$$

Homologous series	$x=1$	$x=3/2$	$x=2$	$x=3$
1. $C_2H_2\rightarrow C_2D_2$				
C_2HD Σ^+ type	−0.1	−0.2	−0.2	−0.3
π type	−0.8	−1.1	−1.4	−1.6
2. $CH_4\rightarrow CD_4$				
CH_3D all vib.	−0.7	−0.9	−1.1	−1.4
CH_2D_2 all vib.	−0.2	−0.4	−0.2	+0.5
CHD_3 all vib.	−0.9	−1.5	−1.0	−0.9
3. $C_6H_6\rightarrow C_6D_6$				
C_6H_5D in-plane	+0.2	+0.3	+0.4	+0.4
out-of-plane	−0.2	−0.3	−0.5	−0.8
1:3:5-$C_6H_3D_3$ A_1' type	+0.2	+0.3	+0.5	+0.8
A_2' type	+0.2	+0.3	+0.6	+1.1
E' type	−0.2	−0.4	−0.7	−1.4
A_2'' type	+0.2	+0.2	+0.3	+0.7
E'' type	−0.7	−1.4	−2.1	−2.6
1:4-$C_6H_4D_2$ Ag type	−0.1	−0.1	0	+0.1
Au type	−0.2	−0.2	−0.3	−0.2
Bg type	−0.4	−0.4	−0.8	−1.4
Bu type	+0.2	+0.4	+0.5	+0.7
1:2:4:5-$C_6H_2D_4$ Ag	0	−0.2	−0.2	0
Au	−0.1	−0.1	0	+0.2
Bg	−0.4	−0.7	−1.0	−1.7
Bu	0.1	0.2	0.3	0.4

APPLICATION OF $\Sigma\nu$ RULE TO CHLOROETHYLENES

If the problem of fitting the values of $\Sigma\nu$ for the chloroethylenes to the observed data were approached solely in a formal way, the correct functional form of $\Sigma\nu$ as a function of the number of chlorine atoms would be difficult to determine. Consideration of the zero-point energy as a constitutive property suggests that a treatment similar to that already used for substituted ethylenes,[3] which included contributions from all nonbonded interactions, would be suitable. The relations between $\Sigma\nu$ for the chloroethylenes would then be given in terms of the 5 parameters of Table VII of reference 3. In Table X, $\Sigma\nu$ for all the modes, and also for the in-plane and out-of-plane modes is evaluated from the ob-

TABLE VIII. Sum rules for fluoro-bromo-chloro-methanes.

Molecule	$\Sigma\nu^2\times10^{-6}$ Obs	Calc	$\Sigma 1/\nu\times10^3$ Obs	Calc	$\Sigma 1/\nu^2\times10^6$ Obs	Calc
CBr_4	1.545	1.562	40.885	40.661	242.52	238.79
CBr_3H	13.132	13.118	24.416	24.612	114.178	118.81
CBr_2H_2	24.291	24.278	13.404	13.310	42.45	39.777
$CBrH_3$	35.178	35.166	6.971	6.756	6.984	1.43
CH_4	45.669	45.653	4.943	4.428	3.063	3.497
CBr_3Cl	1.756	1.750	35.52	36.00	181.33	187.55
CBr_2Cl_2	1.963	1.956	32.26	31.79	150.6	144.3
$CBrCl_3$	2.191	2.178	27.97	28.02	108.2	108.2
CCl_4	2.404	2.399	24.64	24.68	81.35	81.54
CBr_2HCl	13.387	13.406	21.19	21.39	81.89	85.40
$CBrH_2Cl$	24.704	24.707	11.70	11.59	27.75	24.82
CH_3Cl	35.793	35.68	6.487	6.589	5.743	5.535
$CBrHCl_2$	13.736	13.714	18.60	18.69	59.41	60.85
$CHCl_3$	14.048	14.04	16.49	16.46	43.89	44.42
CH_2Cl_2	25.101	25.14	10.40	10.43	19.38	19.14
CF_4	7.282	7.281	12.79	12.81	21.09	21.12
CF_3H	17.932	17.91	9.767	9.743	13.26	13.62
CF_2H_2	27.792	27.85	7.376	7.404	7.717	8.261
CFH_3	37.031	37.10	5.671	5.789	4.030	4.767
CF_3Cl	5.878	5.892	15.13	15.17	30.44	30.20
CF_2Cl_2	4.612	4.618	17.95	17.92	44.14	43.71
$CFCl_3$	3.465	3.452	21.06	21.09	60.25	60.65
CF_2HCl	16.624	16.537	11.61	11.59	20.25	20.20
CFH_2Cl	26.637	26.464	8.736	8.727	12.23	11.79
CBr_3F	2.685	2.658	30.60	30.79	142.1	145.5
CBr_2F_2	3.986	3.978	22.95	22.85	80.36	77.22
$CBrF_3$	5.574	5.522	17.13	16.87	41.43	36.75
$CBrH_2F$	26.128	25.97	9.706	9.452	16.61	12.13
CBr_2HF	14.395	14.494	17.91	17.79	59.90	59.07
$CBrHF_2$		16.09		12.82		68.85
CBr_2ClF	2.871	2.901	27.04	27.10	107.7	108.8
$CBrCl_2F$	3.125	3.164	23.86	23.87	80.30	80.66
$CBrClF_2$		4.279		21.14		56.41

Parameters for calculating $\Sigma\nu^2$

X	Y	Z	P_{CX_4}	α	β	γ	Δ_{XY}	Δ_{XZ}
Br	H	F	1.567	11.561	1.091	11.836	0.3592	−0.2272
Br	Cl	F	1.561	0.1844	1.099	0.2419	−0.0203	−0.2215
Br	H	Cl	1.557	11.551	0.1982	11.651	0.3497	−0.00999
F	H	Cl	7.2639	10.650	−1.358	10.631	0.7038	−0.0897

Parameters for calculating $\Sigma 1/\nu$

Br	H	F	40.668	−15.990	−9.840	−13.038	−4.699	−1.916
Br	Cl	F	40.660	−4.643	−9.909	−3.656	−0.4334	−1.966
Br	H	Cl	40.656	−16.109	−4.670	−14.598	−4.795	−0.4576
F	H	Cl	12.804	−3.0808	2.3761	−3.5936	−0.7340	−0.3884

Parameters for calculating $\Sigma 1/\nu^2$

Br	H	F	238.43	−118.82	−92.388	−86.968	−40.022	−25.313
Br	Cl	F	239.30	−51.514	−94.181	−36.280	−8.102	−26.518
Br	H	Cl	238.64	−120.62	−51.324	−101.92	−41.343	−8.0808
F	H	Cl	20.919	−7.625	9.7765	−10.499	−2.095	−3.486

served fundamentals (see Table IX) and compared with the values calculated by means of Table VII of reference 3. From reference 3 we see that the constitutive properties of the substituted ethylenes are given in terms of the 5 parameters $P_{C_2X_4}$ a, b, c, and d. Using the data for ethylene, monochloroethylene, the three isomeric dichloroethylenes, and trichloroethylene, we have 6 equations to determine the 5 parameters. Average values of the parameters were calculated by solving all sets of equations. These calculations were repeated to find the corresponding values of the parameters for the in-plane vibrations. Those for the out-of-plane vibrations are obtained from the relations

$$a_{\text{for all modes}} = a_{\text{in-plane}} + a_{\text{out-of-plane}}$$

and similarly for b, c, and d. The values of the parameters used in obtaining the calculated values in Table X are:

	$P_{C_2X_4}$	a	b	c	d
All modes	21 765	−3648	−3772	−3796	−3622
In-plane	18 835	−3175	−3351	−3202	−3162
Out-of-plane	2930	−473	−421	−594	−460.

For C_2Cl_4 there is one major difference in assignment proposed by Torkington,[12] namely, that there is no

[12] P. Torkington, see reference h, Table IX.

TABLE IX. Chloro-ethylenes.

				Planar			
C_2H_4[a]	C_2H_3Cl[b]	*cis*[c]	*trans*[c]	1,1[d]	Tri[e]	Tetra[f]	Tetra[g]
3020	3030	3077	3071	3035	3082	1571	1571
1623	3080	1587	1576	1616	1586	447	447
1342	3130	1179	1270	1391	1242	237	237
3272	395	711	844	601	933[h]	1000	512
1236	1280	173	349	299	842	347	347
3106	1030	3072	3080	3130	628	782	913
810	1370	1294	1200	1088	381	194	332
2990	1620	848	817	788	274	913	782
1443	724	571	265	375	165	318	387
				Out-of-plane			
1027	622	406	192	686	212	114[i]	135[j]
949	897	876	895	458	452[h]	288	185
943	940	697	758	874	783	512	215

[a] See reference f, Table III.
[b] H. W. Thompson and P. Torkington, Proc. Roy. Soc. (London) **A184**, 21 (1945).
[c] H. J. Bernstein and D. A. Ramsay, J. Chem. Phys. **17**, 556 (1949).
[d] P. Joyner and G. Glockler, J. Chem. Phys. **20**, 302 (1952).
[e] H. J. Bernstein, Can. J. Research **B28**, 132 (1950).
[f] H. J. Bernstein, J. Chem. Phys. **18**, 478 (1950).
[g] P. Torkington, Trans. Faraday Soc. **45**, 445 (1949); Proc. Phys. Soc. (London) **A63**, 804 (1950).
[h] These frequencies have been interchanged here whereas the band at 933 cm^{-1} was considered to be associated with an out-of-plane vibration in reference e.
[i] Estimated from the torsion frequency in ethylene at 1027 cm^{-1}, see reference a.
[j] Estimated in reference g.

fundamental at 1000 cm^{-1}. Other investigators[13] prefer to regard this frequency as that of a fundamental. For this molecule the calculations are given in Table X for both assignments of C_2Cl_4, and it is clear that the $\Sigma\nu$ rule does not support Torkington's assignment with regard to this frequency. The data used for Table X are listed in Table IX.

It seems probable that the $\Sigma\nu$ rule would apply equally well for other homologous series, and it is suggested that the relations to be used for any series such as the substituted ethanes, benzenes, and the aliphatic acyclic hydrocarbons are those given in Tables V, IX, and XI of reference 3.

APPLICATION TO THE SERIES $CH_{4-n}X_n$, $CD_{4-n}X_n$, AND $C_2H_{4-n}X_n$, AND $C_2D_{4-n}X_n$

Let us consider the constitutive property P_n of the substituted methane $CH_{4-n}X_n$ to be the sum of the fundamentals $\Sigma\nu$. From Eq. (1), we have

$$\Sigma\nu_{CH_{4-n}X_n}=\Sigma\nu_{CH_4}+an+bn^2,$$

where

$$a=\frac{\Sigma\nu_{CX_4}-\Sigma\nu_{CH_4}}{4}-4b$$

and $b=\frac{1}{2}$ (the contribution to $\Sigma\nu$ from interaction of two H atoms plus that from two X atoms minus twice the contribution to $\Sigma\nu$ from interaction between H and X). Correspondingly for the deuterium substituted series $CD_{4-n}X_n$, we have

$$\Sigma\nu_{CD_{4-n}X_n}=\Sigma\nu_{CD_4}+a'n+b'n^2$$

where

$$a'=\frac{\Sigma\nu_{CX_4}-\Sigma\nu_{CD_4}}{4}-4b'$$

and $b'=\frac{1}{2}$ (the contribution to $\Sigma\nu$ from interaction of two D atoms plus that from two X atoms minus twice that from interaction of D with X).

Since deuterium substitution does not change the force field appreciably, $b\approx b'$ if zero-point energy differences for the nonbonded interactions are small,[6] and so

$$\Sigma\nu_{CH_{4-n}X_n}-\Sigma\nu_{CD_{4-n}X_n}\approx(\Sigma\nu_{CH_4}-\Sigma\nu_{CD_4})(1-n/4),$$

where $n=0, 1, 2, 3, 4$. Thus the left-hand side must be independent of the substituent X. That this relation is very nearly true may be seen from Fig. 1 in which $[\Sigma\nu_{CH_{4-n}X_n}-\Sigma\nu_{CD_{4-n}X_n}]$ has been plotted against n for X=chlorine and X=bromine. The data used for this figure and the one following are listed in reference 15.

For the ethylenes $C_2H_{4-n}X_n$ and $C_2D_{4-n}X_n$, we make

TABLE X. Chloro-ethylenes.[a]

	$\Sigma\nu$ cm^{-1}					
	All modes		In-plane		Out-of-plane	
Molecule	Obs	Calc	Obs	Calc	Obs	Calc
C_2H_4	21 761[a]	21 765	18 842[a]	18 835	2919[a]	2930
C_2H_3Cl	18 118[b]	18 117	15 659[b]	15 660	2459[b]	2457
$C_2H_2Cl_2$						
cis	14 491[c]	14 495	12 512[c]	12 498	1979[c]	1997
trans	14 317[c]	14 324	12 472[c]	12 458	1845[c]	1863
1−1	14 341[d]	14 345	12 323[d]	12 309	2018[d]	2036
C_2HCl_3	10 580[e]	10 575	9133[h]	9120	1447[h]	1455
C_2Cl_4	6723[f]	6681	5809[f]	5755	914[i]	926
	6063[g]		5528[g]		535[j]	

[a] All footnotes are the same as in Table IX.

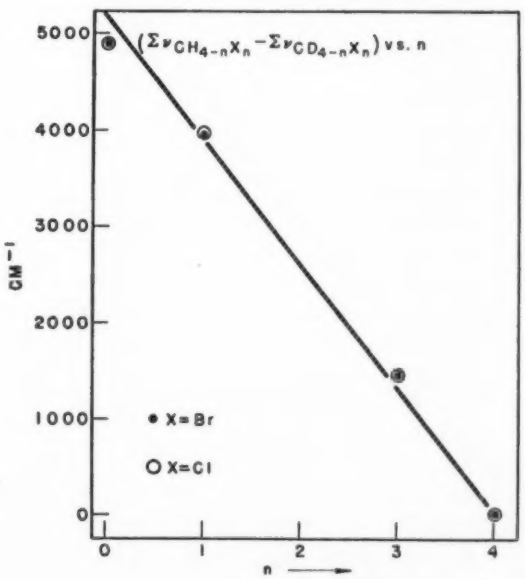

FIG. 1.

[13] H. J. Bernstein, footnote g, Table IX and references therein.

the corresponding assumptions, namely, that

$$a-c=a'-c'$$
$$a-d=a'-d'$$
$$a-b=a'-b' \quad \text{(see Table VII of reference 3)},$$

where the primes are for the deuterium analogs and the $a-c$, $a-d$, $a-b$ have been defined on p. 266 of reference 3.

Thus $a-a'=b-b'=c-c'=d-d'$, and $\Sigma\nu_{C_2H_{4-n}X_n}-\Sigma\nu_{C_2D_{4-n}X_n}=(1-n/4)(\Sigma\nu_{C_2H_4}-\Sigma\nu_{C_2D_4})$ with $n=0, 1, 2, 3, 4$. This equation is valid also for the deuterium substituted di-chloro-ethylenes.[14]

In Fig. 2, $\Sigma\nu_{C_2H_{4-n}X_n}-\Sigma\nu_{C_2D_{4-n}X_n}$ has been plotted against n for $X=Cl$, and it is evident that such a linear relation is very nearly true.

Yet another test of whether $b-b'\approx 0$ or not is obtained for CH_3Br, CH_2DBr, CHD_2Br, and CD_3Br and the analogous iodides. If $b-b'=0$, then it is easily seen that the following relations also are valid:

$$\Sigma\nu_{CH_3Br}-\Sigma\nu_{CD_3Br}=\Sigma\nu_{CH_3D}-\Sigma\nu_{CD_4}=3865$$

and

$$\Sigma\nu_{CH_3Br}-\Sigma\nu_{CH_2DBr}=\Sigma\nu_{CH_2DBr}-\Sigma\nu_{CHD_2Br}=\Sigma\nu_{CHD_2Br}-\Sigma\nu_{CD_2Br}$$

and also equal to the first differences in the corresponding iodide. Thus, all the sums of these homologs may be calculated from the difference 3865 cm^{-1} observed for the methanes and the value of any one sum from the homologous series. Since the values of $\Sigma\nu_{CH_3Br}$ and $\Sigma\nu_{CH_3I}$ are fairly well established,[4,15] we have used them to calculate the values in Table XI. The lack of agreement between observed and calculated values is of the order of 1 percent.

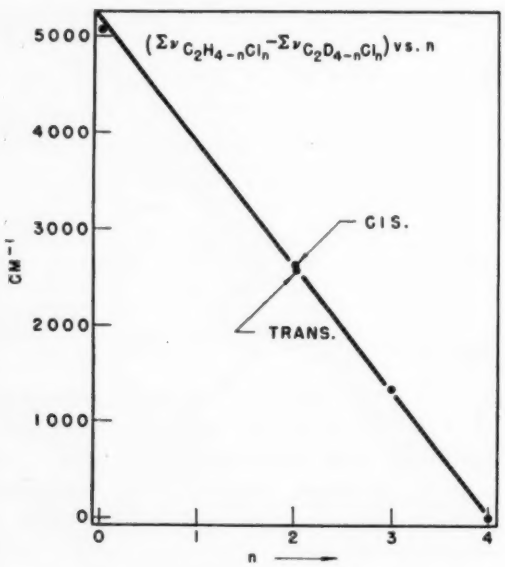

FIG. 2.

TABLE XI.

	$\Sigma\nu$ calc	$\Sigma\nu$ obs[a]	(obs-calc)	% diff
CH_3Br	15 824	15 824[b]		
CH_2DBr	14 534	14 428	106	0.74
CHD_2Br	13 244	13 126	118	0.90
CD_3Br	11 954	11 856	148	1.25
CH_3I	15 526	15 526[b]		
CH_2DI	14 236	14 194	42	0.30
CHD_2I	12 946	12 852	94	0.73
CD_3I	11 656	11 592	64	0.55

[a] M. de Hemptinne, *Rapport et Discussion sur les Isotopes* (Condenberg Bruxelles, 1948), R. Stoops, 76–78, p. 161.
[b] These values have been used along with $\Sigma\nu_{CH_3D}-\Sigma\nu_{CD_4}=3865$ to calculate all others.

AN APPROXIMATE SUM RULE FOR SKELETAL FREQUENCIES AND CONSEQUENTLY A SUM RULE FOR HYDROGEN VIBRATIONS

a. Isotopic Homologous Series

It can be shown from small vibration theory[16] that the frequency of each skeletal mode varies linearly with the number of isotopes substituted.

Thus, for hydrocarbons in which D atoms are being substituted for H, we should expect both a linear skeletal sum rule and a linear sum rule for hydrogen vibrations to be valid. That this is nearly so may be verified for the carbon vibration of the deuterium substituted benzenes (see Table XII). The data used in Table VI are used here for Table XII.

TABLE XII. Skeletal carbon vibrations in benzenes.

Wilson notation[a]	C_6H_6	d_1	1:4-d_2	1:3:5-d_3	1:2:4:5-d_4	d_6
ν_1	992	980	978	956	961	948
ν_{12}	1010	1007	992	1004	977	963
ν_4	703	698	634	691	615	601
ν_{14}	1310	1295	1292	1300	1291	1285
ν_{6a}	606	603	601	593	586	577
ν_{6b}	606	601	597	593	589	577
ν_{8a}	1596	1574	1569	1573	1564	1552
ν_b	1596	1591	1587	1573	1572	1552
ν_{16a}	405	380	367	373	383	352
ν_{16b}	405	405	405	373	352	352
ν_{19a}	849	778	736	710	767	662
ν_{19b}	849	849	849	710	663	662
$\Sigma\nu$ obs	10 927	10 761	10 607	10 449	10 319	10 083
$\Sigma\nu$ calc	10 927	10 783	10 639	10 495	10 351	10 083
Obs-calc		−22	−32	−46	−32	

[a] See reference b of Table VI.

[14] H. J. Bernstein and A. D. E. Pullin, Can. J. Chem. **30**, 963 (1952).
[15] CCl_4, see reference 4. $CHCl_3$, $CDCl_3$, see reference 9(a). CH_2Cl, CD_2Cl, M. de Hemptinne, Trans. Faraday Soc. **42**, 5, (1946); see also reference 9(a). CH_4, CD_4, see reference 9(a) $CHBr_3$, $CDBr_3$, Redlich and Strucks, Monatsch. Chem. **67**, 203 (1936); Sitzber. Akad. Wiss. Wien. Abt. IIb, **145**, 192 (1936). CH_3Br, CD_3Br, see reference 9(a); also for CH_3I and CD_3I. C_2H_4, C_2D_4, see reference b to Table V. C_2HCl_3, C_2DCl_3, reference (f) to Table IX. *Cis* and *trans* $C_2H_2Cl_2$, $C_2D_2Cl_2$, reference c to Table IX.
[16] E. Teller, *Handbuch und Jahrbuch der Chemischen Physik* (Leipzig 1934) **IX**, 2; H. J. Bernstein, Can. J. Chem. **29**, 284 (1951).

Since $\Sigma\nu$ has been shown to be linear in the number of D atoms for all vibrations (Table IV, column 2) and in Table XII, $\Sigma\nu$ is shown to be linear in the number of D atoms for the carbon vibrations, it follows that $\Sigma\nu$ for the hydrogen vibrations is a linear function of the number of deuterium substituents.

b. Nonisotopic Homologous Series

Arguing by analogy we might expect here that the sum of the skeletal modes and that of the hydrogen frequencies are approximately a parabolic function of the number of substituents for the substituted methanes. Inspection of the previous data on substituted methanes does indeed show this to be verified very approximately (±10 percent). For the alkanes we should expect a relationship of the type $\Sigma\nu = an + bn^2$ for the series ethane, propane, isobutane, and neopentane, with $n = 1, 2, 3, 4$, respectively, (since there are no skeletal modes for $n = 0$ which would be methane). Also, more approximately, we might expect that $\Sigma\nu^2 \approx a'n$ i.e., $\Sigma\nu^2/n = \text{constant}$. This is identical with the "sum rule" proposed for hydrocarbons by Kohlrausch and Barnes.[17]

Skeletal sum rules can be expected to be obeyed only very approximately and, in cases where interactions are great, are not to be trusted at all. The purpose of the above paragraphs is to indicate only why very approximate rules of this kind are not unexpected.

[17] K. W. F. Kohlrausch *Ramanspektren* (J. W. Edwards, Ann Arbor, Michigan, 1945), p. 206 and following.

THE JOURNAL OF CHEMICAL PHYSICS VOLUME 21, NUMBER 12 DECEMBER, 1953

The Assignments of the Raman and Infrared Frequencies of 1,2-Dichloroethane Observed in the Gaseous, Liquid, and Solid States

ICHIRO NAKAGAWA AND SAN-ICHIRO MIZUSHIMA
Chemical Laboratory, Faculty of Science, Tokyo University, Tokyo, Japan

(Received July 22, 1953)

Based on the normal vibration calculation of the *trans* and the *gauche* molecules of 1,2-dichloroethane as an eight-body problem, the assignments of the Raman and infrared frequencies of this substance observed in the gaseous, liquid, and solid states have been made. The vibrational modes of these frequencies have been discussed.

A LARGE number of experimental data have now been accumulated concerning the molecular structure of 1,2-dichloroethane, as described in our previous papers and in those of other authors. They have been obtained from measurements of the Raman and infrared spectra in the gaseous, liquid, and solid states and in solutions,[1] as well as from dipole moments in the gaseous states and in solutions,[1] electron diffraction in the gaseous state,[2] x-ray diffraction in the solid state,[3] nuclear magnetic resonance,[4] and some thermal properties.[5] All these data have been explained quite satisfactorily from the view that the molecules exist in the *trans* (C_{2h}) and the *gauche* (C_2) forms in the gaseous and the liquid states and in solutions, and only in the *trans* form in the solid state. However, we have made the partial assignments of the vibrational frequencies, since, so far, we have calculated only the skeletal frequencies.[6]

Recently one of us has calculated the normal vibrations of 1,2-dichloroethane as an eight-body problem, using a potential function of the Urey-Bradley type.[7] Based on this result we shall make complete assignments of the observed vibrational frequencies of 1,2-dichloroethane and clarify the points that have been subject to uncertainty in the previous investigations.

In Table I are shown the calculated frequencies together with those observed in the Raman effect and in infrared absorption. The assignments have been made according to the following procedure. First of all we apply the experimental technique of observing the spectral difference between the liquid and solid states, by which we can pick out separate spectra for the *trans* and the *gauche* forms. There remain some uncertainties because of overlapping, etc. We then apply the sum rule derived in our previous paper[8] in order to remove

[1] Mizushima, *et al.*, Sci. Pap. Inst. Phys. Chem. Research (Tokyo) **25**, 159 (1934); **26**, 1 (1934); **29**, 63, 111, 188 (1936); **37**, 205 (1940); **38**, 437 (1941); **39**, 387, 396, 401, **40**, 87, 100 (1942); **42**, 51 (1944); J. Chem. Phys. **17**, 591, 663 (1949); **18**, 1420, 1516 (1950); Reilly Lectures, University of Notre Dame, Vol. 5 (1952). The references to the papers of other authors are given in these papers.

[2] Yamaguchi, Morino, Watanabe, and Mizushima, Sci. Pap. Inst. Phys. Chem. Research (Tokyo) **40**, 417 (1943); J. Ainthworth and J. Karle, J. Chem. Phys. **20**, 425 (1952).

[3] M. E. Milberg and W. N. Libscomb, Acta Cryst. **4**, 369 (1951).

[4] H. S. Gutowsky and G. E. Pake, J. Chem. Phys. **18**, 162 (1950).

[5] Morino, Watanabe, and Mizushima, Sci. Pap. Inst. Phys. Chem. Research (Tokyo) **40**, 100 (1942); Odan, Mizushima, and Morino, *ibid.* **42**, 27 (1944); W. G. Gwinn and K. S. Pitzer, J. Chem. Phys. **16**, 303 (1948).

[6] S. Mizushima and Y. Morino, Sci. Pap. Inst. Phys. Chem. Research (Tokyo) **26**, 1 (1934); Mizushima, Morino, and Shimanouchi, *ibid.* **40**, 87 (1942).

[7] I. Nakagawa, J. Chem. Soc. Japan **74**, 848 (1953).

[8] Mizushima, Shimanouchi, Nakagawa, and Miyake, J. Chem. Phys. **21**, 215 (1953).

such uncertainties as far as possible. According to this rule, the sum of all the squared frequencies ($\Sigma\nu_i^2$) should remain constant for the stable configurations of rotational isomers. From the observed frequencies shown in Table I, we have

$$\Sigma\nu_i^2\ (trans)=4.970\times10^7$$

and

$$\Sigma\nu_i^2\ (gauche)=4.962\times10^7.$$

Therefore, the assignments of the observed frequencies to the *trans* and the *gauche* forms shown in Table I are quite satisfactory.

After we have picked out separate spectra for the *trans* and the *gauche* forms, we have to assign each observed frequency to the corresponding normal vibration of one of these two stable forms. Evidently the first step is to consult the selection rule for the Raman and the infrared spectra, which is shown in Table II for each symmetry class. The state of polarization observed for each Raman line also helps us in making assignments, if the line is isolated and sufficiently intense. However, many lines of interest do not fall in this category. Moreover, a Raman line reported as depolarized may belong to a polarized class, because the depolarization ratio of a totally symmetric vibration may have any value up to the limiting one expected for a depolarized line.

Taking these points into consideration as well as the calculated values of normal frequencies, we can assign the observed frequencies as shown in Table I. It is not necessary to describe the actual procedure of assignments for all the Raman lines and the absorption peaks, but it is desirable to explain some of these assignments which do not seem to be straightforward.

A very weak Raman line observed in our laboratory at 223 cm^{-1} was assigned to the C−C−Cl bending frequency belonging to class B_u of the *trans* form.* This assignment apparently seems a violation of the selection rule, since class B_u contains the normal vibrations antisymmetric to the center of symmetry which are forbidden in the Raman effect. However, this weak line can be explained as arising from molecules distorted in the liquid state by the influence of the neighboring molecules. The corresponding frequencies in 1-chloro, 2-bromoethane and 1-chloro, 2-iodoethane become Raman active, since there is no center of symmetry for the *trans* form of these molecules.[9] It can be shown that the extrapolation from these observed frequencies yields a value of the 1,2-dichloroethane frequency close to 223 cm^{-1}. The calculated frequency shown in Table I is also close enough to the observed.†

TABLE I. The calculated and the observed frequencies of 1,2-dichloroethane in cm^{-1}.

	Trans form: C_{2h}				*Gauche* form: C_2		
Class	Mode	Calc	Obs	Class	Mode	Calc	Obs
A_g	ν_1: C−H stretching	2929	2957	A	ν_1'	2931	2957
	ν_2: CH_2 bending	1457	1445		ν_2'	1454	1429
	ν_3: CH_2 wagging	1294	1304		ν_3'	1285	1264
	ν_4: C−C stretching	1017	1052		ν_4'	1019	1031
	ν_5: C−Cl stretching	797	754		ν_5'	671	651
	ν_6: C−C−Cl bending	279	300		ν_6'	224	265
A_u	ν_7: C−H stretching	2967	3005		ν_7'	2960	3005
	ν_8: CH_2 twisting	1112	1124		ν_8'	1098	1207
	ν_9: CH_2 rocking	742	768		ν_9'	917	943
	ν_{10}: torsional	...	...		ν_{10}'	...	125
B_g	ν_{11}: C−H stretching	2957	3005		ν_{11}'	2965	3005
	ν_{12}: CH_2 twisting	1093	1264		ν_{12}'	1108	1145
	ν_{13}: CH_2 rocking	937	989		ν_{13}'	862	881
B_u	ν_{14}: C−H stretching	2946	2957	B	ν_{14}'	2943	2957
	ν_{15}: CH_2 bending	1454	1450		ν_{15}'	1456	1429
	ν_{16}: CH_2 wagging	1300	1230		ν_{16}'	1318	1304
	ν_{17}: C−Cl stretching	737	709		ν_{17}'	691	677
	ν_{18}: C−C−Cl bending	235	223		ν_{18}'	396	411

The Raman line at 125 cm^{-1} must be assigned to a vibration of the *gauche* form, since it has been observed only in the liquid state. For this frequency no calculation was made,‡ but this frequency undoubtedly corresponds to the torsional motion about the C−C axis. In the first place, this frequency lies far below all other frequencies calculated for this molecule, and secondly it accounts for the entropy value contributed by the torsional motion. As stated in a previous paper,[5] this is obtained by subtracting from the calorimetric entropy the entropy calculated by taking into account all other degrees of freedom. The torsional frequency of the *trans* form is inactive in the Raman effect and is too low to be observed by ordinary infrared apparatus.

A note may be added on the coupling of the torsional motion with the C−C−Cl bending frequency. In the *trans* form there is no coupling between them, since the former (ν_{10}) belongs to class A_u, while the latter (ν_6) to class A_g. In the *gauche* molecule these two frequencies belong to the same class A, and accordingly there is a

TABLE II. Number of normal vibrations belonging to each symmetry class.

	Trans form (C_{2h})				*Gauche* form (C_2)		
Class	Number of vibrations	Activity Raman	Activity Infrared	Class	Number of vibrations	Activity Raman	Activity Infrared
A_g	6	+	−	A	10	+	+
A_u	4	−	+				
B_g	3	+	−	B	8	+	+
B_u	5	−	+				

* See the second paper of reference 6.

[9] Mizushima, Morino, Miyahara, Tomura, and Okamoto, Sci. Pap. Inst. Phys. Chem. Research (Tokyo) **39**, 387 (1942).

† This frequency is infrared active but lies outside the region measurable by an ordinary prism spectrometer. After completing this manuscript, we have noticed a paper by Bohn, Freeman, Gwinn, Hollenberg, and Pitzer, J. Chem. Phys. **21**, 719 (1953), in which these authors reported an absorption band at 222 cm^{-1} observed by a grating spectrometer. This value is in excellent agreement with ours. A similar result was obtained by J. K. O'Loane, J. Chem. Phys. **21**, 669 (1953) by the method of residual rays.

‡ In the potential function of ClH_2C-CH_2Cl we have not included azimuthal angle as an internal coordinate and have neglected the interaction between the two movable groups (see references 6 and 7). Therefore, the torsional frequency has not been calculated.

coupling between them. This means that the pure torsional motion has a frequency higher than the observed (125 cm^{-1}) and that the pure C−C−Cl bending frequency ν_6' of the *gauche* form has a frequency lower than the observed (265 cm^{-1}).

A similar coupling occurs between the C−Cl stretching (ν_5, ν_5') and the CH_2 rocking frequencies (ν_9, ν_9'). In the *trans* form for which ν_5 belongs to class A_g and ν_9 belongs to A_u, there is no coupling, while in the *gauche* form for which both ν_5' and ν_9' belong to the same class A, there is a coupling between the two frequencies. The fact that ν_5' of the *gauche* form (654 cm^{-1}) is lower than ν_5 of the *trans* form (754 cm^{-1}), while ν_9' (943 cm^{-1}) is much higher than ν_9 (768 cm^{-1}) is considered to be partly due to this situation.§

In order to discuss such a problem more rigorously, we have to calculate the relative amplitude for each of the internal coordinates (e.g., the change of bond lengths or bond angles) or internal symmetry coordinates in a given normal mode of vibration. This is done in the following way.

The internal coordinates R or the internal symmetry coordinates S are related linearly to the normal coordinates Q through the matrix expressions

$$R=LQ$$

and

$$S=L'Q.$$

If, therefore, we calculate the elements of the L matrix or of the L' matrix for a given normal vibration, we can at once determine the relative amplitude for each internal coordinate or for each internal symmetry coordinate. Such calculations have been made for all the normal vibrations of 1,2-dichloroethane, and the result is shown in the second column of Table I as C−H stretching, CH_2 bending, etc. We must, however, realize, that these are very rough characterizations, since none of the vibrations is restricted to a single internal coordinate or to a single internal symmetry coordinate, as these terms might suggest. The detailed account of the L matrix or of the L' matrix will be published elsewhere.

We have stated above that the observed frequency 754 cm^{-1} can be assigned to the symmetric C−Cl stretching vibration of the *trans* form which is not coupled with CH_2 rocking. By the calculation of the L matrix we can also show that other kinds of hydrogen vibrations belonging to the same class play no significant part in this C−Cl vibration. However, we see from the same calculation that there is a large contribution of the C−C−Cl bending vibration, and, accordingly, we conclude that in this vibration there is a conspicuous change not only in the C−Cl bond length but also in the C−C−Cl bond angle, although we designate it as the C−Cl stretching vibration. In any event, as the coupling in this vibration takes place only among the motions of heavier atoms, the calculation of the skeletal vibration is a good approximation to the solution of the problem of normal vibrations.

By contrast the calculation of the L matrix for the corresponding vibration of the *gauche* form (ν_5') shows that the contribution of motions of hydrogen atoms is considerable in this case, as has been expected. This is due to the fact that the hydrogen deformation vibrations belong to the same symmetry class A as ν_5'. Among these hydrogen deformation vibrations, ν_9' (CH_2 rocking vibration) is very tightly coupled with ν_5' as stated above. Similarly, there is a strong coupling between the antisymmetric C−Cl stretching vibration of the *gauche* form (ν_{17}') and the CH_2 rocking vibration. Therefore, in such normal vibrations, the calculation of the skeletal vibrations, in which CH_2 group is treated as a mass point, cannot be considered a good approximation.||

In connection with these problems we want to add a remark on the assignment of the C−C stretching frequency (ν_4) of the *trans* form. This frequency was first assigned by Mizushima and Morino[10] to the Raman line at 1052 cm^{-1}, but afterwards some investigators preferred the 989 cm^{-1} line.[11] The same problem has arisen as to the assignment of the C−C stretching frequency of 1,2-dibromoethane which was first assigned by Mizushima and Morino[10] to the 1053 cm^{-1} line, but some investigators[11] preferred the 933 cm^{-1} line because the 1053 cm^{-1} line was reported depolarized, which would not be the case of a line belonging to class A_g containing only the totally symmetric vibrations. However, the assignment of a depolarized Raman line is uncertain, as mentioned above, so that the reported depolarization of the 1053 cm^{-1} line is not in direct contradiction to the assignment of this line to the C−C stretching frequency. Neu and Gwinn who made a thorough investigation of the vibrational spectrum of 1,2-dibromoethane also assigned the 1053 cm^{-1} line to the C−C stretching frequency.[12] With regard to the polarization of the 1052 cm^{-1} line of 1,2-dichloroethane there is no question, since Neu, Ottenberg, and Gwinn reported this line to be polarized.[13] The calculation of the L matrix for ν_4, the computed frequency of which is close enough to the observed (1052 cm^{-1}), settles this problem definitely. This calculation shows that we can

§ We cannot attribute the whole difference between ν_5 and ν_5' or between ν_9 and ν_9' to the coupling effect. A part of this difference is due to the change of molecular configuration with the change of azimuthal angle of internal rotation.

|| We would like to note that the contribution of the hydrogen vibrations is small in the case of the C−C−Cl bending vibrations of both the *trans* and the *gauche* forms. Therefore, the calculations of the skeletal deformation vibrations reported in our previous paper can be considered to be a good approximation. (See reference 8).

[10] S. Mizushima and Y. Morino, Sci. Pap. Inst. Phys. Chem. Research (Tokyo) **29**, 188 (1936).

[11] T. Y. Wu, *Vibrational Spectra and the Structure of Polyatomic Molecules* (J. W. Edwards Brothers, Inc., Ann Arbor, Michigan, 1946), p. 306; K. W. F. Kohlrausch and H. Wittek, Z. phys. Chem. **B47**, 55 (1940).

[12] J. T. Neu and W. D. Gwinn, J. Chem. Phys. **18**, 1642 (1950).

[13] Neu, Ottenberg, and Gwinn, J. Chem. Phys. **16**, 1004 (1948).

properly designate ν_4 as essentially a C—C stretching frequency. The line observed at 989 cm^{-1} is close to the calculated frequency ν_{13} of the CH_2 rocking motion.

In the discussions given above we have dealt with the frequencies which are lower than the C—C stretching frequencies. The frequencies higher than these are all assigned to hydrogen vibrations, either stretching or deformation. Of these hydrogen vibrations, the C—H stretching vibrations are expected to be simple in character because these frequencies appear in a region (about 3000 cm^{-1}) far from those of the other frequencies, so that the coupling problem does not come into question. Actually, the calculation of the L matrix for the C—H stretching frequencies $\nu_1(A_g)$, $\nu_7(A_u)$, $\nu_{11}(B_g)$ and $\nu_{14}(B_u)$ shows that vibrations of large amplitude take place only along the C—H bonds. The other group of hydrogen vibrations appears in the frequency region below 1500 cm^{-1} and consists of CH_2 bending, CH_2 wagging, CH_2 twisting, and CH_2 rocking vibrations. Their vibrational modes are shown in Fig. 1.

The calculated values of the CH_2 deformation frequencies are in agreement with those observed except for ν_{12} (see Table I).¶ On the basis of this calculation we can assign the CH_2 rocking frequencies 943 and 881 cm^{-1} of the *gauche* form which have so far remained uncertain. As each of these two frequencies belongs to a different symmetry class (A and B), the correct assignment is very desirable in the application of the product rule of rotational isomers to different symmetry classes. (In a previous paper[8] we determined the azimuthal angle of the *gauche* form by the application of the product rule.) The calculation of the L matrices for these frequencies shows that they are quite pure frequencies; in other words, the actual modes of these normal vibrations are expressed fairly accurately by the displacement vectors shown in Fig. 1. One might expect a fairly strong coupling of the C—C stretching frequency with some of these hydrogen deformation frequencies, but as stated above, the calculation of the L matrices for these hydrogen frequencies shows that such is not actually the case. We have already shown that ν_4 is also a fairly pure C—C stretching.

The assignments explained above all refer to fundamental frequencies. Besides these, there have been observed (especially in the infrared spectra) some overtones and combination tones.

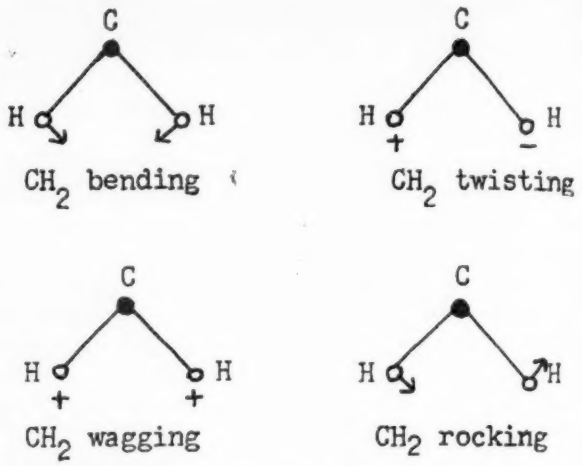

FIG. 1. The modes of the CH_2 bending, CH_2 wagging, CH_2 twisting, and CH_2 rocking vibrations. (+ and − signs indicate motions perpendicular to the plane of the paper.)

In the spectra observed in the solid state, there appear low-frequency Raman lines, which can be assigned neither to the fundamentals nor to the overtones of intramolecular vibrations, since their frequencies are too low to be accounted for as such (53 and 74 cm^{-1} at −140°C and 66 cm^{-1} at −40°C). As explained in a previous paper, these lines can be assigned to rotatory vibrations of a molecule as a whole in the crystal lattice.[14] The molecules of 1,2-dichloroethane take only the *trans* form in the crystalline state, and of the three Raman active rotatory vibrations one about the molecular axis would escape detection owing to the small change of polarizability. Therefore, the two frequencies 53 and 74 cm^{-1} should be assigned to the rotatory vibrations about the axes, both perpendicular to the molecular axis. Instead of these two lines only one line was observed at higher temperatures. This is because above the transition point the free rotation about the molecular axis sets in** and there is no more any difference between the two rotatory vibrations mentioned above.

¶ The discrepancy between the calculated and the observed frequencies in the case of ν_{12} seems to be the result of the same origin as in the case of a frequency belonging to B_{2g} of long chain paraffin molecules. See T. Shimanouchi and S. Mizushima, J. Chem. Phys. **17**, 1102 (1949).

[14] I. Ichishima and S. Mizushima, J. Chem. Phys. **18**, 1420 (1950).

** Evidently this is the rotation of the molecule as a whole, and should not be confused with the internal rotation about the C—C axis.

A Calculation of the Diamagnetic and Paramagnetic Susceptibility of N_2 by the Statistical Method

J. V. BONET* AND A. V. BUSHKOVITCH
St. Louis University, St. Louis, Missouri

(Received July 10, 1953)

The diamagnetic and the paramagnetic term in the susceptibility of N_2 are calculated using the statistical method of Thomas and Fermi corrected for exchange and correlation effects. A statistical electron density of N_2, corrected for exchange and correlation, is used in the evaluation of the integral $\int \rho r^2 dv$, which defines the mean square position of the electronic charge of the molecule appearing in the diamagnetic term. A statistical distribution function of the square electronic angular momentum of the molecule is derived, and the mean square electronic angular momentum of the molecule, appearing in the paramagnetic term, is defined in terms of the distribution function. This procedure leads to a result which, although approximately two times larger than the observed value, still is fully as good as similar calculations for atoms.

I. INTRODUCTION

THE complete expression[1] for the molar magnetic susceptibility of a diatomic gas is

$$\chi = -A\langle r^2\rangle + B \sum_{n' \neq n} \frac{|P(n';n)|^2}{\nu(n;n')}, \qquad (1)$$

where $A = Le^2/6mc^2$, $\langle r^2\rangle$ stands for $\sum_i \langle r_i^2\rangle$, the sum of the mean squares of the distances of each electron from the center of gravity of the molecule, $B = Le^2/6m^2c^2h$ (L is Avogadro's number, e the electronic charge, m the electronic mass, c the velocity of light, and h Planck's constant), $|P(n';n)|^2$ is the matrix element of the total electronic angular momentum of the molecule, and $\nu(n;n')$ is the transition frequency from the ground state n to the excited state n'. The first term on the right of (1) is known as the diamagnetic term and the second, as the paramagnetic term.

A rigorous quantum mechanical calculation of this quantity would require a knowledge of the wave functions for the ground and excited states of the molecule. Since wave functions of only the simplest electronic systems have been obtained so far, it is not surprising to find that the only rigorous calculation of magnetic susceptibilities of diatomic molecules so far published are those of H_2, by Wang,[2] Van Vleck and Frank,[3] and Witmer,[4] and that of D_2, by Witmer.[5] Even then the complications arising from the paramagnetic term are considerable. This paper is an attempt at calculating both the diamagnetic and the paramagnetic term in the susceptibility of N_2.

The large number (14) of electrons in the N_2 molecule is a serious obstacle to a rigorous calculation. Nakamura and Hijikata[6] have reported some progress in their molecular orbital calculations of the ground state of N_2. But numerical calculations involving molecular orbitals are in general so complex that, as a first attempt at calculating both terms in the magnetic susceptibility of a diatomic molecule more complicated than H_2, it seems advisable to try other less laborious, even if less rigorous, methods.

Both the diamagnetic and the paramagnetic term of the susceptibility are dependent on the electron density of the molecule. The statistical model, originated by Thomas[7] and Fermi,[8] and developed by Dirac[9] and others,[10] provides electron densities of atoms, molecules, and crystals in a fairly simple form. It has been applied by Sommerfeld and others,[11] to the calculation of magnetic susceptibilities of atoms with some success. Therefore, it appears promising to use this method in the molecular case also.

An objection might be raised to the use of the statistical method for a system with a comparatively low number of electrons. The objection is reasonable; in fact, better results might be expected from a statistical calculation, if it were concerned with heavier molecules such as I_2 or Br_2. However, the statistical theory of molecules is still in an undeveloped stage, although valuable contributions have been made by Hund,[12] March,[13] Glazer and Reiss,[14] and others.[15] In fact, the only statistical electron density of a diatomic homonuclear molecule so far found in the literature is that calculated by Hund[12] who, by means of the Ritz varia-

* Now at St. Xavier's College, University of Bombay, Bombay, India.

[1] J. H. Van Vleck, *The Theory of Electric and Magnetic Susceptibilities* (Oxford University Press, London, 1932), p. 275.
[2] S. C. Wang, Proc. Natl. Acad. Sci. U. S. **13**, 798 (1927).
[3] J. H. Van Vleck and A. Frank, Proc. Natl. Acad. Sci. U. S. **15**, 539 (1929).
[4] E. E. Witmer, Phys. Rev. **48**, 380 (1935); **51**, 383 (1937).
[5] E. E. Witmer, Phys. Rev. **58**, 202 (1940).
[6] N. Nakamura and T. Hijikata, University of Tokyo Progress Report, No. 1, p. 9.
[7] L. H. Thomas, Proc. Cambridge Phil. Soc. **23**, 542 (1927).
[8] E. Fermi, Z. Physik **48**, 73 (1928).
[9] P. A. M. Dirac, Proc. Cambridge Phil. Soc. **26**, 376 (1930).
[10] See for instance, A. Sommerfeld, Z. Physik **78**, 283 (1932); Jensen, Meyer-Gossler, and Rohde, Z. Physik **110**, 277 (1938); Feynman, Metropolis, and Teller, Phys. Rev. **75**, 1561 (1949).
[11] See P. Gombás, *Die statistische Theorie des Atoms*, (Springer, Vienna, 1949), p. 233.
[12] F. Hund, Z. Physik **77**, 12 (1932); see also J. Lopuszanski, Acta Phys. Polon. **10**, 213 (1951).
[13] N. H. March, Proc. Cambridge Phil. Soc. **48**, 665 (1952).
[14] H. Glazer and H. Reiss, J. Chem. Phys. **21**, 903 (1953).
[15] See, for instance, H. Jensen, Z. Physik **77**, 722 (1932).

tion method, obtained an approximate solution to the Thomas-Fermi equations for N_2 and F_2. It was decided, therefore, to make use of Hund's calculations. If the values of the magnetic susceptibility of N_2 obtained in this manner are found to be in reasonable agreement with experiment, then similar calculations for heavier molecules may be expected to yield substantially better results.

II. CORRECTION OF HUND'S ELECTRON DENSITY OF N_2

The electron density of N_2 obtained by Hund[12] does not take into account exchange and correlation effects. Yet the inclusion of these effects can be shown[11] to be of importance in calculations of magnetic susceptibilities.

Although a differential equation describing the behavior of the statistical electron density of N_2 and including exchange and correlation effects can be written down, solutions to such a partial, nonlinear differential equation are not available as yet.[16] The proper way of accounting for these effects would be to solve the corresponding equation. Instead of doing this, a short-cut method is suggested which might prove useful when high accuracy is not demanded and when no electronic computer is available.

The statistical model, corrected for exchange and correlation effects, of a free atom has a finite radius, and the electron density at any point over its bounding spherical surface can be shown[17] to be equal to $0.003074/a_0^3$ for all atoms, ($a_0=0.529\times10^{-8}$ cm). The authors have generalized this theorem to diatomic homonuclear molecules in the following manner. The starting point is an expression for the total energy of a degenerate electron gas containing additional exchange and correlation terms and written in prolate spheroidal coordinates. This expression is simplified by making use of the axial symmetry properties of the molecule and is shown to be a function of one coordinate only (the one corresponding to the sum of r_1 and r_2). Then it is minimized with respect to this coordinate. After considerable algebraic manipulation and assuming that the total molecular charge is bounded at a finite distance from the nuclei by a prolate spheroidal surface over which the electron density is constant, it is shown that the boundary electron density for homonuclear diatomic molecules is equal to $0.003074/a_0^3$, the same value as the boundary electron density for atoms.

When the radial electron density of statistical atomic models, with and without exchange and correlation effects, is plotted *versus* the distance r from the nucleus, it can be seen[18] that the inclusion of these effects does not affect too much the general shape of the corresponding curves, but results mainly in a closer packing of the electrons within the atom. The curve corresponding to the Thomas-Fermi model approaches the r-axis asymptotically. The curve of the Thomas-Fermi-Dirac model drops to zero discontinuously at the point where the electron density reaches the boundary value predicted by the same model. The curve of the Thomas-Fermi-Dirac-Gombás[19] model drops to zero at the point where the electron density reaches the boundary value predicted by this model.

Similarly, the behavior of the electron density of the Thomas-Fermi-Dirac-Gombás model of N_2 is assumed to differ little from the simple Thomas-Fermi electron density which Hune calculated, except for the fact that the former is assumed to drop to zero where it reaches the boundary value previously deduced.

Thus Hund's function will be used up to the point where it reaches the boundary value previously deduced. Moreover, in order to ensure that the integral of the electron density of N_2 throughout the space occupied by the molecular electrons equals 14, Hund's function is multiplied by an appropriate constant factor.

This corrected version of Hund's function is taken to represent approximately the Thomas-Fermi-Dirac-Gombás electron density of N_2.

III. CALCULATION OF THE DIAMAGNETIC TERM

According to the statistical method $\langle r^2\rangle$ is given[20] by the integral

$$\langle r^2\rangle=\int\rho\langle r^2\rangle dv, \tag{2}$$

where ρ is the statistical electron density of the molecule and dv is the volume element. The integral is taken throughout the configuration space occupied by the molecule.

Hund's expression for the electron density of N_2 can be written as follows

$$\rho=11.2\times10^{24}\times u^3, \tag{3}$$

$$u=\frac{1}{r_1}\phi[\kappa r_1 f(r_1)]+\frac{1}{r_2}\phi[\kappa r_2 f(r_2)], \tag{4}$$

where u is a linear combination of the Thomas-Fermi functions for the free nitrogen atom; r_1, r_2 are the distances from any point in the field to the two nuclei of the molecule; κ is a constant and f an interpolation function.

After expressing ρ, r^2 and dv in terms of prolate spheroidal coordinates, the integral of Eq. (2) is com-

[16] Dr. J. W. Sheldon, of International Business Machines Corporation, New York, has informed us, in a private communication, that he is preparing, for publication, data on the electron density of the Thomas-Fermi-Dirac model of N_2 obtained with an electronic computer.

[17] See reference 11, p. 99.

[18] See reference 11, p. 107, Fig. 12.

[19] The statistical model of atoms and molecules, corrected for exchange and correlation effects, will be referred to as the Thomas-Fermi-Dirac-Gombás model since it was Gombás who first introduced a correction accounting for correlation effects into the Thomas-Fermi-Dirac model. See P. Gombás, Z. Physik 121, 523 (1943).

[20] See reference 11, p. 229.

TABLE I. Comparison of calculated and observed molar magnetic susceptibilities. The values for the monatomic gases, Ne, Kr, and Xe, are those of previous investigators and have been taken from Gombás.[a] The calculated value for N_2 represents the chief result of the present calculation. The values given in the table should be multiplied by -1×10^{-6}.

	Ne	Kr	Xe	N_2
Thomas-Fermi calculation	67.0	102.0	117.0	...
Thomas-Fermi-Dirac-Gombás calculation	12.9	35.8	47.3	24.6
Observed values	6.8	28.0	42.2	13.3

[a] See reference 11 (p. 233, Table 29).

puted numerically,[21] keeping in mind the modifications imposed upon Hund's expression for ρ in the previous section. When this is done, the calculated value of the diamagnetic term is -33.7×10^{-6}.

IV. CALCULATION OF THE PARAMAGNETIC TERM

Van Vleck and Frank[2] in their determination of the paramagnetic susceptibility of H_2 introduced a useful simplification which can also be applied to N_2. First, the variable denominator $\nu(n;n')$ is replaced by a mean value ν' and taken out of the summation sign. Then the restriction $n\neq n'$ is no longer necessary since the average angular momentum of the normal state of N_2 is zero, and it can be verified, in virtue of the hermiticity of the matrices, that

$$(B/\nu')\textstyle\sum_{n'}|P(n';n)|^2=(B/\nu')\langle P^2\rangle, \tag{5}$$

where $\langle P^2\rangle$ is the mean square of the total angular momentum of N_2.

In the calculation of ν' use is made of the procedure described by Van Vleck and Frank[2] in their calculation. Applying their method to N_2, ν' is found to be equal to 2.74×10^{15} sec^{-1}.

$\langle P^2\rangle$ is determined by a statistical method according to the following steps: (1) A statistical distribution function of the electronic angular momentum of N_2 is obtained by means of a straightforward generalization to diatomic molecules of a procedure developed by Fermi[7] for atoms in order to predict certain features of the periodic system of the elements. (2) The distribution function of the angular momentum is transformed into a distribution function $R(P^2)$ of the square angular momentum of the molecule according to well-known rules of mathematical statistics.[22] (3) The mean square angular momentum is defined in terms of the distribution function as follows:

$$\langle P^2\rangle=\frac{\int P^2R(P^2)dP^2}{\int R(P^2)dP^2}. \tag{6}$$

In prolate spheroidal coordinates $R(P^2)$ takes the form

$$R(P^2)=\int_1^{\xi_0}\int_0^1\left[(C\rho)^{\frac{1}{2}}-\frac{P^2}{a^2(\xi^2+\eta^2-1)}\right]^{\frac{1}{2}}\times\frac{(\xi^2-\eta^2)}{(\xi^2+\eta^2-1)}d\xi d\eta, \tag{7}$$

where C is equal to $(3h^2/8\pi)$ and a is the internuclear distance of N_2.

By integrating numerically over ξ and η for several appropriate values of P^2 (values of P^2 for which the integrand becomes imaginary are excluded) a table of values of $R(P^2)$ is obtained from which, with the help of Simpson's rule, $\langle P^2\rangle$ is easily determined. The calculated value obtained in this manner for the paramagnetic term is 9.1×10^{-6}.

V. DISCUSSION OF RESULTS

Addition of the diamagnetic and the paramagnetic terms results in the value -24.6×10^{-6} for the complete molar magnetic susceptibility of N_2.

The observed molar susceptibility of nitrogen gas is found to be -13.3×10^{-6}; this value is actually a mean of various observations[23] which range from -11 to -14×10^{-6}. Thus the calculated value is nearly twice as large as the observed value.

Table I indicates that the order of agreement with experiment that has been achieved is just about the right one to expect in statistical calculations of magnetic susceptibilities of electronic systems roughly of the size of the nitrogen molecule (14 electrons). As is clear from the table, the Thomas-Fermi calculated magnetic susceptibility of neon gas (10 electrons) is about ten times larger than the corresponding observed value, and the calculated value corrected for exchange and correlation is still about twice as large as the observed value. The fact that the calculated values for Kr and Xe are in appreciably closer agreement with experiment, leads one to believe that statistical calculations of the magnetic susceptibility of diatomic gases heavier than N_2, such as Cl_2, Br_2, and I_2, will yield results in much closer agreement with experiment.

[21] Some care should be exercised in the numerical integration in the neighborhood of the nuclei, where ρ becomes infinite although the integrals involving ρ do not.

[22] See P. G. Hoel, *Introduction to Mathematical Statistics* (John Wiley and Sons, Inc., New York, 1947), p. 132.

[23] L. Hector, Phys. Rev. **24**, 229 (1924); V. I. Vaidyanathan, Phil. Mag. **5**, 380 (1928); F. Bitter, Phys. Rev. **35**, 1648 (1930).

Kinetics of the Fast Reaction between Nitrogen Dioxide and Fluorine*

RICHARD L. PERRINE AND HAROLD S. JOHNSTON
Department of Chemistry, Stanford University, Stanford, California

(Received May 6, 1953)

The rate of the reaction between nitrogen dioxide and fluorine to form nitryl fluoride has been measured at 27.7, 50.4, and 70.2°. Light absorption by nitrogen dioxide was used to follow the reaction. By using a 22-liter Pyrex flask and by going to low concentrations of reactants, between 0.5 and 20×10^{-8} moles cc^{-1}, the rate of this fast reaction was reduced to a convenient value. The rate was found to be first order in each reactant, and it showed no dependence on nitryl fluoride. The proposed mechanism is

$$NO_2+F_2 \xrightarrow{k_1} NO_2F+F \text{ (slow)},$$

$$NO_2+F+M \xrightarrow{k_2} NO_2F+M \text{ (fast)}.$$

The empirical second order rate constant is k_1, that of an elementary bimolecular reaction. If the rate constant is written as $Ae^{-E/RT}$ then A is 1.6×10^{12} cc moles^{-1} sec^{-1} and E is 10.5 kcal.

THE preparation of nitryl fluoride from nitrogen dioxide and fluorine was reported in 1932 by Ruff, Menzel, and Neumann.[1] These authors established the stoichiometry and completeness of the gas-phase reaction, and determined the physical properties of nitryl fluoride. These properties were confirmed by the work of Faloon and Kenna,[2] who obtained nitryl fluoride from gaseous fluorine and liquid nitrogen dioxide. The object of the present investigation was to study the kinetics of the reaction between nitrogen dioxide and fluorine in the gas phase.

EXPERIMENTAL

Fluorine was generated by the electrolysis of a fused potassium fluoride-hydrogen fluoride mixture in the approximate mole ratio $KF\cdot2HF$ at 98°C, employing a carbon anode. The electrolytic cell design* was a composite of what were considered desirable features of other cells[3] with substantial modification. The result was a cell which operated on four to five amperes of current at eight to ten volts, continuously or for short intervals as desired, and delivered about two liters at S.T.P. of fluorine per hour while requiring a minimum of attention. Fluorine from the generator, after removal of hydrogen fluoride in an adsorber packed with trays containing sodium fluoride, was diluted with dry helium. This mixture passed through a dry-ice acetone-cooled trap, then through a trap cooled by liquid nitrogen in which the fluorine was collected. The product was purified by fractionation from the liquid under its own vapor pressure at liquid nitrogen temperature in a stainless-steel column packed with stainless-steel helices, and stored in stainless-steel bulbs. Cylinder nitrogen dioxide was purified before use, and stored at dry ice temperature in a glass trap protected from moisture by phosphorus pentoxide.

The reaction was followed in a 34-liter stainless-steel tank and in a 22-liter Pyrex flask. In the stainless-steel apparatus the reaction was fast, irreproducible, and obviously heterogeneous. Also nitrogen dioxide adsorbed to a considerable extent on the fluorinated metal surface. None of the results of this work is included in this article, and the apparatus will not be described here, except with respect to the windows, Fig. 1, which were developed. These windows are apparently unaffected by prolonged exposure to fluorine, are vacuum tight, can withstand high pressure (200 psi or more), and are useful at moderately high temperature (200°C or more, if the protruding soft-solder connection is wrapped in a copper cooling coil). The window is quartz with a three-quarter wavelength coating of magnesium fluoride. A layer of silver about 0.05 mm thick was deposited on the quartz tube. The stainless-steel window holder was tapered down to a tube whose inside diameter was 0.2 mm greater than the quartz tube, and its walls were about 0.04 mm thick. This metal tube was tinned on the inside with soft solder and bored out until it just slipped over the unsilvered portion of the quartz tube. The window holder was heated just to the melting point of solder, and the silvered quartz tube was quickly

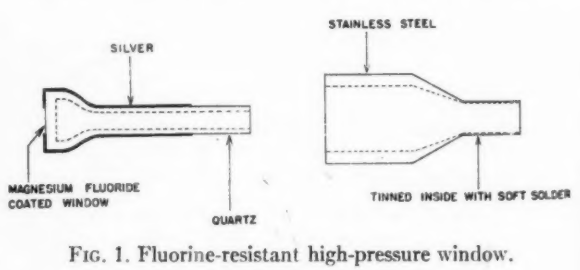

FIG. 1. Fluorine-resistant high-pressure window.

* Abstracted from a dissertation submitted by Richard L. Perrine in partial fulfillment of the requirements for the degree of Doctor of Philosophy at Stanford University, 1953, microfilm copies of which are available from University Microfilms, Ann Arbor, Michigan, on remittance of $1.00.

[1] Ruff, Menzel, and Neumann, Z. anorg. Chem. **208**, 293 (1932).

[2] Albert V. Faloon and William B. Kenna, J. Am. Chem. Soc. **73**, 2937–2938 (1951).

[3] John T. Pinkston Jr., Ind. Eng. Chem. **39**, 255–258 (1947). Schumb, Young, and Radimer, Ind. Eng. Chem. **39**, 244–254 (1947). Downing, Benning, Downing, McHarness, Richards, and Tomkowitt, **39**, 259–262 (1947). J. F. Gall and H. C. Miller, Ind. Eng. Chem. **39**, 262–266 (1947).

inserted into the metal holder. The metal holder was silver soldered to the rest of the apparatus.

The successful runs were followed in an apparatus previously described.[4] Calibrations and corrections for nitrogen tetroxide were carried out as previously. A pipet system with known relative volumes, 0.01 and 0.001 that of the flask, was used to inject the reactants into a 22-liter Pyrex flask contained in an air thermostat. A 1700-cc stainless-steel storage bulb containing fluorine was attached by a Kovar-to-glass seal to the pipet system of the apparatus. Nitrogen dioxide was followed optically by means of the 436 mμ line of an AH4 mercury arc. At the concentrations used, nitryl fluoride and fluorine absorb this radiation to an undetectable extent. "Halocarbon" stopcock grease, Halocarbon Products Company, North Bergen, New Jersey, which was unaffected at least by short exposure to fluorine, was used.

After recording an initial (evacuated cell) light-intensity reading, a suitable concentration of nitrogen dioxide was injected from the pipet system into the flask and the initial concentration of nitrogen dioxide determined absorptiometrically. While the pipet system was quickly evacuated, the temperature of the flask was recorded. Fluorine was injected from the stainless-steel storage bulb into the pipet system and rapidly released into the reaction flask with the start of the run. With practice, the overall time required for this last procedure could be reduced to about 10 seconds, thus minimizing the extent of the slow reaction at room temperature of dry fluorine with glass, or with the Halocarbon stopcock grease. No evidence of such reaction was discernible at the end of this work. Light intensity readings, timed by a stopwatch, were recorded at intervals of 5 seconds or more and the corresponding concentrations of nitrogen dioxide calculated by using the measured extinction coefficient. Clock time was also recorded so that any drift of initial intensity, as shown by a second value obtained when the cell was again evacuated, would be noted. No drift sufficient to require correction during a run was observed.

Pressure of fluorine in its storage bulb was found by filling a Bourdon gage with air at a pressure less than expected for the fluorine and then balancing. By repeating several times in succession the pressure could be known fairly well in this way. This method was uncertain because some of the pressure observed could be due to silicon tetrafluoride. This method was used only to get the initial pressure in the fluorine storage bulb and to provide a check on the stoichiometry. During the rate measurements, the concentration of fluorine was determined by the difference between the initial and final nitrogen dioxide and the stoichiometry of the reaction. This method was used because it was found that the optical analysis had much better precision than pressure measurements with fluorine. Also, this technique permitted rapid injection into the bulb, thus minimizing contamination of the fluorine by prolonged exposure to glass. In the reaction flask the reactant pressures were of the order of a few tenths of a millimeter and up to a few millimeters. By injecting nitrogen dioxide into the flask containing air, it was established that mixing and thermal equilibrium was attained in less than 5 seconds under the least favorable conditions.

[4] H. S. Johnston and R. L. Perrine, J. Am. Chem. Soc. 73, 4782 (1951).

RESULTS

The stoichiometry of the reaction has been established by Ruff, Menzel, and Neumann,[1] and Faloon and Kenma[2]

$$2NO_2+F_2=2NO_2F.$$

This relation was confirmed under the conditions of reaction reported here, although the accuracy with which the concentration of fluorine was known was probably no better than 10 percent. The ratio of nitrogen dioxide consumed to fluorine added was accurately (2 percent) the same over the range of pressures encountered; this fact was established by alternating runs from the large and small pipets and from a knowledge of relative volumes of pipets and bulb containing fluorine. That the reaction is complete is indicated by the absence of measurable quantities of nitrogen dioxide after reaction with excess fluorine, and taking full consideration of the errors involved, one can set a minimum of 99 percent completion under all conditions studied. The 22-liter flask with surface-volume ratio of 0.17 cm^{-1} was used to ensure homogeneity, but aside from internal consistency of the data the absence of heterogeneity was not proven.

A series of runs was made in which the initial quantity of fluorine was varied, and the initial nitrogen dioxide concentrations were constant. For the initial rate a first order dependence on fluorine was indicated. Next, a series of runs was made in which the initial fluorine was held constant and nitrogen dioxide concentration was varied, and the initial rate indicated a first order dependence on nitrogen dioxide. The empirical second-order rate constant k is defined by

$$\text{Rate}=-\frac{d[F_2]}{dt}=-\frac{1}{2}\frac{d[NO_2]}{dt}=k[NO_2][F_2].$$

The integrated rate expression is

$$\ln\frac{[F_2]_0[NO_2]}{[NO_2]_0[F_2]}=k[NO_2]_\infty t.$$

The data for all runs were plotted according to this expression, and the points follow the second order integrated expression, Fig. 2. Deviations (some positive and some negative) from a straight line observed at the very end of some runs were readily accounted for by the known errors in the absorptiometric method of measurement.

The effect of nitryl fluoride on the rate was examined by adding further quantities of reactants to the products of the previous run without evacuating the flask. Thus, the ratio of initial concentration of nitryl fluoride to that of nitrogen dioxide was progressively increased from zero to eight. No significant effect of nitryl fluoride on the rate was observed.

A number of rate measurements was made at each of three temperatures: 27.7°, 50.4, and 70.2°. Temperature dependence was determined by least-squares fit of the 44 rate constants to the Arrhenius equation to give

$$k=1.59\times10^{12}e^{-10470/RT}\text{ cc mole}^{-1}\text{ sec}^{-1}.$$

This equation and the data it represents are plotted in Fig. 3. Since, if the individual rate constants were plotted, most would superimpose and be indistinguishable, only the arithmetic mean value at each temperature is presented. In the logarithmic form of the equation the intercept and its standard deviation are 12.20 ± 0.12, the energy of activation and standard deviation are 10.47 ± 0.18 kcal, and the standard deviation from the mean of the logarithm of a single empirical constant is ±0.044.[5]

MECHANISM

Having established first-order dependence of the rate on both reactants, one can immediately eliminate the elementary termolecular reaction

$$2NO_2+F_2\rightarrow2NO_2F,$$

and also the sequence of steps

$$2NO_2\rightleftarrows N_2O_4,$$

$$N_2O_4+F_2\rightarrow2NO_2F.$$

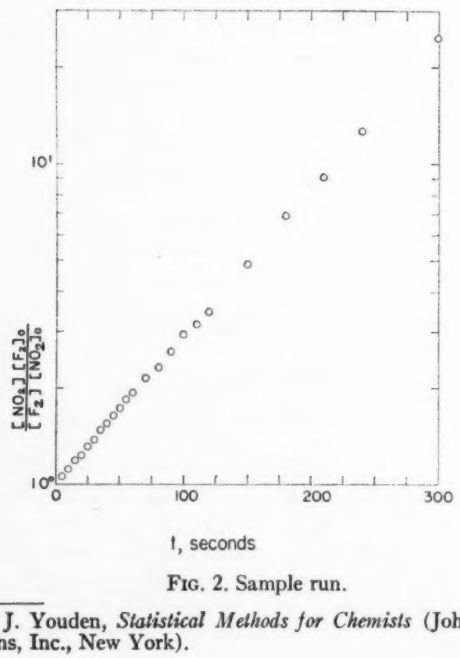

FIG. 2. Sample run.

[5] W. J. Youden, *Statistical Methods for Chemists* (John Wiley and Sons, Inc., New York).

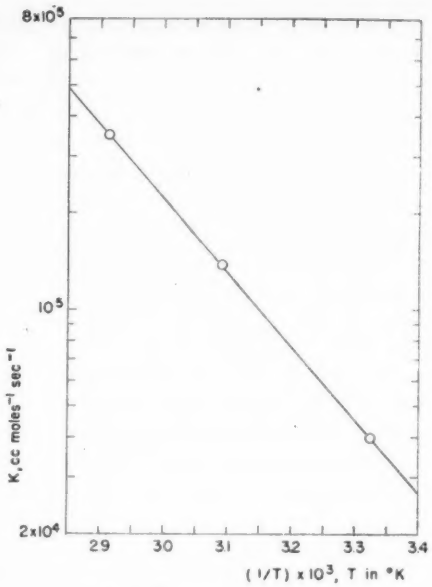

FIG. 3. Temperature dependence.

The alternative is initiation of reaction by a bimolecular step involving nitrogen dioxide and fluorine, for which the following seems the most reasonable

$$NO_2+F_2\xrightarrow{k_1}NO_2F+F. \quad (1)$$

Fluorine atoms produced in this manner must be consumed by one or more of the following steps

$$F+NO_2+M\xrightarrow{k_2}NO_2F+M, \quad (2)$$

$$F+F+M\xrightarrow{k_3}F_2+M, \quad (3)$$

$$F+NO_2F\xrightarrow{k_4}NO_2+F_2, \quad (4)$$

$$F+\text{walls}\rightarrow\text{products such as } SiF_4. \quad (5)$$

in which M represents a molecule of any one of the species present. The third body M is necessary for atom recombinations such as (3) to prevent the product from flying apart with the first vibration. Step (2) is a bimolecular association reaction, the reverse of the unimolecular dissociation of nitryl fluoride into nitrogen dioxide and a fluorine atom. As such, a more detailed mechanism for (2) is

$$F+NO_2\xrightarrow{d}NO_2F^*,$$

$$NO_2F^*\xrightarrow{c}NO_2+F, \quad (6)$$

$$NO_2F^*+M\xrightarrow{b}NO_2F+M,$$

in which NO_2F^* represents a molecule of nitryl fluoride with sufficient energy to dissociate. The result is a

pressure dependence like that for a unimolecular dissociation

$$k_2=\frac{db[\mathrm{M}]}{b[\mathrm{M}]+c}.$$

Thus, with appropriate values of total concentration [M], (2) can be second order with constant d, third order with constant $db[\mathrm{M}]/c$, or intermediate between these limits. Recent work in this laboratory on the closely analogous reactions[6,7]

$$HNO_3\rightarrow HO+NO_2,$$

$$NO_2Cl\rightarrow Cl+NO_2,$$

show that at low pressures such as those used in this study these reactions are definitely in the second order region of the unimolecular decomposition and, therefore, the third order region of the bimolecular association. Thus by analogy with these two cases, (2) must be assumed to be third order as written.

Any combination of (1), (2), (3), and (4) leads to the observed stoichiometry. However, (5) reduces the ratio of nitrogen dioxide to fluorine which reacts, and in the present system the effect of (5) appears to be negligible on the basis of stoichiometry.

Should one choose as a mechanism any one of: (1), (2), (3), (4); (1), (2), (3); or (1), (3), (4), the result is a very complicated algebraic expression for the rate not in agreement with the data. If (1), (2), and (4) are included, the rate is expressed by

$$\text{rate}=k_1[NO_2][F_2]\frac{k_2[NO_2][M]}{k_2[NO_2][M]+k_4[NO_2F]}. \quad (7)$$

No inhibition by nitryl fluoride was observed, and thus (7) cannot fit the data unless $k_2[NO_2][M]\gg k_4[NO_2F]$, and then the result is identical with that obtained from (1) and (2) alone

$$\text{rate}=k_1[NO_2][F_2].$$

If only (1) and (3) constitute the mechanism, the rate equation is

$$\text{rate}=\tfrac{1}{2}k_1[NO_2][F_2].$$

These two mechanisms lead to the same rate expression except for the factor of $\frac{1}{2}$ in the constant term. Thus, these mechanisms consisting of (1) and (2) or (1) and (3) are indistinguishable so far as kinetic measurements are concerned. However, by making several reasonable assumptions and by carrying out an order-of-magnitude calculation, it is possible to make a fairly clear-cut decision between (2) and (3).

[6] Johnston, Herschbach, and White. Meeting of the American Chemical Society in Los Angeles, March 1953.

[7] Herman Cordes (unpublished research).

The ratio of rate (2) to rate (3) is $k_2[\mathrm{M}][\mathrm{F}][NO_2]/k_3[\mathrm{M}][\mathrm{F}]^2$. Whereas one might expect k_2 to be one or two orders of magnitude larger than k_3 (since k_2 is for the association of a polyatomic molecule and k_3 is for the association of a diatomic molecule), it is not unreasonable for the purposes of this calculation to assume that k_2 is about equal to k_3. In a detailed examination one might expect the effects of [M] to be different for these two cases, but here one makes the rough approximation of cancelling out [M] in the expression above. In this way, the ratio of rate (2) to rate (3) reduces approximately to $[NO_2]/[\mathrm{F}]$. If k_2 and k_3 are assumed to have about the order of magnitude of the constants for the recombination of bromine or iodine atoms,[8–10] the concentration of nitrogen dioxide exceeds that of fluorine atoms by at least two orders of magnitude for the most unfavorable case. Thus it is reasonable to assume that (3) is negligible compared to (2) and the proposed mechanism is

$$NO_2+F_2=NO_2F+F, \quad (1)$$

$$NO_2+F+M=NO_2F+M, \quad (2)$$

and the observed rate constant from

$$-\frac{d[F_2]}{dt}=k[NO_2][F_2],$$

is identically k_1, that of the elementary bimolecular reaction (1).

ACKNOWLEDGMENT

This investigation was conducted under the sponsorship of U. S. Office of Naval Research contract.

[8] E. Rabinowitch and W. C. Wood, Trans. Faraday Soc. 32, 547 (1936); J. Chem. Phys. 4, 497 (1936).

[9] Davidson, Marshall, Larsh, and Carrington, J. Chem. Phys. 19, 1311 (1951).

[10] Having made this estimate of k_2 one can use the previous conclusion

$$k_2[NO_2]\,M]\gg k_4[NO_2F]$$

to set limits on several quantities not directly observed. At the lowest concentrations of nitrogen dioxide the condition of at least 99 percent completion gives $k_4\approx 10^6$ or 10^7 cc mole^{-1} sec^{-1} as a maximum. The equilibrium constant k_1/k_4 may be calculated from partition functions

$$K=\frac{k_1}{k_4}=\frac{Q_{NO_2F}Q_{Fe}^{-\Delta E/RT}}{Q_{NO_2}Q_{F_2}}.$$

The product of partition functions was evaluated (0.07) from the harmonic-oscillator rigid-rotator approximation, the assumption that nitryl fluoride is a planar equilateral triangle of 1.2A bond distance, and the assumption that the oscillator frequencies of nitryl fluoride are no lower than those in nitrogen dioxide. Combining this value with observed value of k_1, one estimates $k_4=2.2\times 10^{13}e^{-E_4/RT}$ cc mole^{-1} sec^{-1}. The limit set on k_4 gives $E_4\approx 9$ or 10 kcal. Thus (1) appears to be very nearly thermoneutral, nitryl fluoride is stable by at least 10 or 11 kcal, and (2) is exothermic by 37 or more kcal. We are grateful to the referee for suggesting these calculations.

The Entropy of Aqueous Oxy-Anions

ROBERT E. CONNICK AND RICHARD E. POWELL
Department of Chemistry and Chemical Engineering, University of California, Berkeley, California
(Received June 26, 1953)

The entropies of oxy-anions of the formula XO_n^{-z} are well represented by the equation $\bar{S}_2^0 = 43.5 - 46.5\,(Z - 0.28n)$. Species containing hydroxyl groups are included by disregarding the hydroxyl groups in counting the number of oxygens n. The form of the equation is partially justified on the basis of a model. Binuclear ions are treated by calculating for the two halves separately and making a correction for the entropy of dimerization.

TO a good approximation, the entropies of monatomic ions in aqueous solution are determined by their charges and radii.[1] One might expect that the entropies of the oxy-anions also would be controlled by their charges and charge distributions. Examination of the standard entropies[2] of the oxy-anions does in fact reveal such regularities. The entropies are approximately the same for ions of the same charge and the same number of oxygen atoms, e.g., ClO_3^- and NO_3^-, or SO_4^{--} and CrO_4^{--}. Moreover, the entropy becomes about 46.5 eu more negative for each additional negative charge, and about 13.0 eu more positive for each additional oxygen atom surrounding the central atom. Consequently, the entropy of an ion XO_n^{-z} can be estimated fairly well from the empirical relation

$$\bar{S}_2^0 = 43.5 - 46.5\,(Z - 0.28n). \qquad (1)$$

The agreement between calculated and experimental values can be judged from Fig. 1. For the 22 ions (including several which have hydroxyl groups, vide infra), the average discrepancy is ± 3.7 eu. A number of the experimental entropy values, e.g., that of phosphate ion, are not known to within this accuracy.

The entropies of oxy-anions having hydroxyl groups can also be estimated by Eq. (1), and these ions have been included in the comparison on Fig. 1. In counting the number of charge-bearing oxygens, n, the hydroxyl groups are to be disregarded; thus the bicarbonate ion, $HOCO_2^-$, and the dihydrogen phosphate ion, $(HO)_2PO_2^-$, are regarded as ions of the type XO_2^-. It is probable that the hydroxyl group carries very little of the net charge of the ion, and any entropy decrease arising from its hydrogen bonding appears to be approximately cancelled by its contribution to the internal entropy of the ion. The observation that the hydroxyl group makes a net contribution of approximately zero to the entropy of these ions may lead one to conjecture that it will do the same for other ions, such as the hydroxyl-complex ions $M(OH)_m^{+z}$. There are very few entropy data for such ions, but one pair for which the comparison is possible is Fe^{++} ($\bar{S}^0 = -27$) and $FeOH^{++}$ ($\bar{S}^0 = -23$).

In the earlier treatment of the monatomic ions,[1] it was found that the entropies of cations and anions could be obtained from a single equation. However, for two ions of the same crystal radius, the effective radius of the cation had to be taken larger than that of the anion. Otherwise stated, the entropy of a cation is somewhat more positive than that of an anion of the same crystal radius. If the same behavior is found in the oxy-cations, then one expects that the entropy of an ion MO_n^{+z} will be a few entropy units more positive than would be calculated from Eq. (1) for an ion XO_n^{-z}. Reliable entropies for the oxy-cations are largely nonexistent; the value for uranyl ion, UO_2^{++} ($\bar{S}^0 = -17$), can be compared with the value $\bar{S}^0 = -23.5$ calculated for an ion XO_2^{--}.

Though Eq. (1) is not intended to apply to oxy-anions whose oxygen atoms are grouped around two separate central atoms, the entropies of such ions can be estimated by treating each end of the ion independently, and then subtracting a reasonable number of entropy units for the dimerization process. This

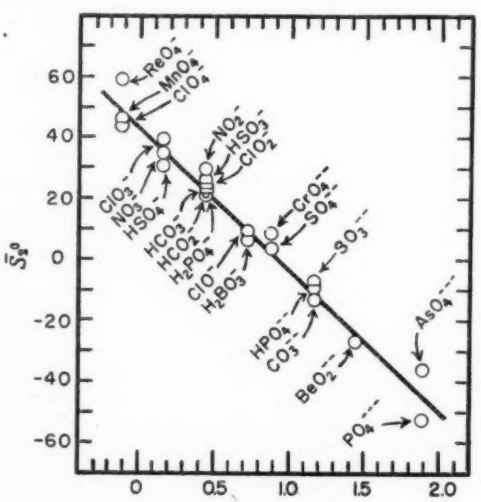

FIG. 1. The entropy of some oxy-anions XO_n^{-z}.

[1] R. E. Powell and W. M. Latimer, J. Chem. Phys. **19**, 1139 (1951).

[2] Tabulated in W. M. Latimer, *Oxidation Potentials* (Prentice-Hall, Inc., New York, second edition, 1952); also in U. S. National Bureau of Standards, *Selected Values of Chemical Thermodynamic Properties* (U. S. Government Printing Office, Washington, D. C., 1952). Recorded entropy values which are merely estimates or are highly uncertain have been omitted from the comparison. The value for perrhenate ion is from unpublished data of J. W. Cobble, W. T. Smith, Jr., and G. D. Oliver.

TABLE I. Entropies of some binuclear ions.

Ion	Estimated entropy	Experimental entropy
$^{-}O_3Cr-O-CrO_3^{-}$	+54	+51
$^{-}O_3S-SO_3^{-}$	+28	+28
$^{-}O_2C-CH_2-CH_2-CO_2^{-}$	+28	+24
$^{-}ON=NO^{-}$	+2	+6

procedure cannot be valid unless the charged groups are sufficiently far apart, and the ionic hydration forces are sufficiently short range, so that the effective hydration shells of the two groups do not overlap greatly. To illustrate the calculation, let us take dichromate ion: Since the structure of the ion is $^{-}O_3Cr-O-CrO_3^{-}$, each end is of the type XO_3^{-}, for which the entropy computed from Eq. (1) would be +36 eu. For the two ends the entropy would be +72 eu, and the subtraction of 18 eu for dimerization (the number was arbitrarily chosen, but it is of reasonable magnitude) leads to an estimated entropy of +54 eu for dichromate. The results of several such calculations are collected in Table I. The entropy of the oxalate ion, $^{-}O_2C-CO_2^{-}$, is tabulated as +10.6 eu, whereas the estimated entropy would be +2.5 eu if it were regarded as a mononuclear ion, or +28 eu as a binuclear ion. This apparent discrepancy with the binuclear model perhaps can be explained by the strong tendency of oxalate ion to be planar.[3] In such a configuration, the oxygens on each side of the molecule lie very close together—even closer than in nitrate ion, sulfate ion, etc. The overlapping of the hydration spheres would lower the entropy.

Because Eq. (1) is linear in Z, the dependence on total charge can be interpreted as arising from the sum of the effects of any arbitrarily chosen distribution of charge in the ion. For example, the equation can be recast in terms of formal charges:

$$\bar{S}_2^0=43.5-46.5(0.72n-f_x),$$

where f_x is the formal charge on the central ion. Therefore, no unique interpretation of charge distribution can be made.

The form of the equation can be partly justified by the following model: (1). The charge is distributed equally on the oxide oxygens. (2). At constant charge per oxygen, i.e. Z/n constant, the entropy is a linear function of the number of oxygens, n. (3). At constant number of oxygens the entropy is a linear function of the charge per oxygen (or of the total charge), which is the result for monatomic ions.[1] It can be shown that this model results in an equation of the general form:

$$\bar{S}^0=a+bZ+cn+(dZ/n).$$

Therefore Eq. (1) is a special case of the above model in which the coefficient of the Z/n term is zero.

Cobble[4] has recently proposed an equation for correlating entropies of oxygenated ions:

$$\bar{S}_2^0=3/2R\ln M+66-(81Z/\rho),$$

where R is the gas constant, M the mass of the ion, Z the charge, and ρ an "effective" radius. The latter is defined as

$$\rho=r_{12}/f,$$

where r_{12} is the oxygen central atom interatomic distance and f is a structural factor dependent on the geometry and charge of the ion. Using 11 arbitrary constants he fits the entropies of 21 of the ions treated by us with an average deviation of 3.1 eu. Our equation with three parameters fits the same data with an average deviation of 3.7 eu.

[3] S. B. Hendricks and M. E. Jefferson, J. Chem. Phys. 4, 102 (1936).

[4] J. W. Cobble, J. Chem. Phys. 21, 1443 (1953).

Molal Volumes and Compressibilities of the System NaCl−H_2O above the Critical Temperature of Water*

SIDNEY W. BENSON, CHARLES S. COPELAND, AND DAVID PEARSON†
Chemistry Department, University of Southern California, Los Angeles, California

(Received July 1, 1953)

From quantitative P, T, V, x data on the system NaCl−H_2O in the supercritical region it has been possible to calculate apparent molal volumes, partial molal volumes, and compressibilities with accuracies of about 10 percent, 25 percent, and 15 percent, respectively.

The apparent molal and partial molal volumes of NaCl show similar, remarkable, and quite anomalous behavior. Above the critical temperature of the particular solution studied and at low NaCl compositions, the molal volumes are very large and negative, being of the order of magnitude of liters/mole. As the densities decrease, the values become more negative, pass through a minimum, and then rise again.

These minima decrease in absolute magnitude with increasing temperature, but seem to occur (for 0.2 percent solutions) at densities not very different from the critical density of water. When the partial molal volumes at constant temperature are plotted against partial densities of water, the results seem to fall on a smooth curve independent of the concentration of NaCl.

The compressibilities show a behavior which resembles that of the pure solvent and whose significance has heretofore escaped any detailed attention. They go through maxima at densities near the density at the critical temperature.

These observations can be accounted for qualitatively if it is assumed that above the critical temperature all fluids are capable of undergoing continuous, short-range condensation over a narrow range of densities near the critical density of the fluid.

The particular behavior of the NaCl−H_2O systems emphasizes quantitatively the enormous effect of small amounts of solutes (capable of associating strongly with the solvent) on the behavior of the solvent near its critical temperature.

INTRODUCTION

MEASUREMENTS of pressure and temperature on a series of both homogeneous and two-phase solutions of NaCl in H_2O at known densities and compositions above the critical temperature of water have made possible the construction of many of the interesting regions of the phase diagram NaCl−H_2O.[1] It was also shown that the partial molal volume of NaCl in steam can be negative and very large. For example, at 390°C in a 1.00 percent by weight solution of NaCl, the partial molal volumes of NaCl are, approximately, −1 liter/mole at a solution density of 0.476 g/cc (280 atm) and −1.8 liters/mole at 0.429 g/cc (265 atm). Such large negative values show that the role of sodium chloride in the fluid solution is to compress the water molecules into a much denser structure. This then suggests that the magnitude of the partial molal volume must be closely related to the compressibility of the steam. The fact that the compressibility of steam at supercritical temperatures goes through a maximum at densities close to the critical density (as shown in Fig. 1) suggests that in this density region the apparent and partial molal volumes of NaCl might have minimum values. To determine this, it was decided to study a solution of NaCl in steam of sufficiently low composition so that the density of the solution could be reduced below the critical density of water without separation of a liquid phase, a condition not met by any of the solutions first used.

EXPERIMENTAL

Examination of our previously obtained density composition data indicated that a 0.2 percent by weight solution of NaCl would, in the desired temperature range, remain a vapor solution at the required densities. Accordingly, pressure, density, and temperature data were obtained for this system by the method already described.[1] To insure internal consistency, similar data were obtained for pure steam. These latter data were compared with steam table data.[2] It was found, for our observed pressures and densities, that our observed temperatures were up to 2°C lower than the steam table values in the range 380–400°C, or, that for our observed temperature and densities, our observed pressures were up to 2 percent higher than the steam table values. The steam results were corrected to bring them into line with the steam table values and the same correction was applied to the salt solution results to obtain the final pressure-density temperature values given in Table I. The pressure-density isotherms for steam and the solutions are shown in Fig. 2.

TABLE I. The pressures of steam and 0.2 percent by weight solution of NaCl in steam at several densities and temperatures.

Steam				0.2 percent NaCl in steam			
	P (atmos)				P (atmos)		
ρ (g/cc)	385°C	390°	396°	ρ (g/cc)	385°C	390°	396°
0.195	234	242.5	253	0.221	236	246.5	258
0.246	241.5	252.5	265.5	0.251	239.5	251	264
0.298	246	259.0	274.5	0.297	241.5	255	271
0.349	249.5	263.5	282	0.351	244.5	259.5	278
0.404	256.5	273	293	0.422	255.5	273	294.5

* This work was done under Contract No. N6onr238-11 between the U. S. Office of Naval Research and the University of Southern California. Reported at the September Meeting of the American Chemical Society, Chicago, 1953.

† Graduate Student Research Assistant under U. S. Office of Naval Research Contract No. N6onr238-11.

[1] Copeland, Silverman, and Benson, J. Chem. Phys. **21**, 12 (1953).

[2] J. H. Keenan and F. G. Keyes, *Thermodynamic Properties of Steam* (John Wiley and Sons, Inc., New York, 1936).

RESULTS

The apparent molal volumes of NaCl in the 0.2-percent solutions, based on densities obtained from the curves of Fig. 2, are given in Table II. Figure 3 shows the variation of the apparent molal volume with solution density. The indicated spreads in the apparent molal volumes are based on a ±1-percent error in densities. As anticipated, the apparent molal volume shows a minimum in the expected density range. The increasing depth of the minimum with decreasing temperature is consistent with the change in the compressibility of steam with temperature (Fig. 1). The pronounced effect of a small quantity of NaCl is perhaps even better indicated in Fig. 4, which compares the coefficients of compressibility of pure steam and the 0.2-percent solution (6.17×10^{-4} mole ratio, NaCl to H_2O).

At the higher densities, the pressures of the NaCl solutions overlap the pressures previously found[1] for solutions of higher composition. At these pressures it is possible to estimate the partial molal volumes of NaCl over the range of composition 0.2 percent to 6.74 percent NaCl. The results are shown in Fig. 5, which is a plot of the partial molal volume of NaCl *vs* the partial density of steam.[3] The partial molal volumes were calculated from the slopes of the curves obtained by plotting the volume of solution containing one mole of steam against the square root of the mole ratio of salt to steam. The conventional method of plotting the apparent molal volume against the square root of the molality was not considered satisfactory because of the unknown trend of the apparent molal volume at compositions below the lowest composition employed and also because of the very great rate of change of this volume with composition between 1 and 0.2 percent salt. The curves used have a constraint on them, namely, that they must reach the zero composition axis with zero slope if the partial molal volume is not to become infinite. For any plausible variation of volume with composition below 0.2 percent salt this limiting slope is not approached very quickly. This behavior of the curve was taken into consideration in obtaining the partial molal volumes shown in Fig. 5 and we feel that the results are probably good to about 25 percent.

In the region of low densities and compositions (e.g.,

TABLE II. The apparent molal volumes ϕ_v, of NaCl in 0.2 percent by weight solutions.

385°C			390°			396°		
P (atmos)	ρ (g/cc)	$-\phi_v$ (liters/mole)	P	ρ	$-\phi_v$	P	ρ	$-\phi_v$
241.5	0.292	18	247	0.225	6	260	0.229	5
242	0.314	22.5	250	0.245	6.5	265	0.255	5.5
243	0.333	24	255	0.297	11.5	270	0.289	6.5
243.5	0.341	23.5	257	0.324	13	275	0.330	7.5
244	0.348	22.5	258	0.335	13	278	0.350	7
245	0.360	20.5	260	0.354	11.5	280	0.365	6.5
247	0.379	15	265	0.389	6.5	285	0.390	4.5
250	0.399	9	270	0.412	4	290	0.410	3
255	0.421	4.5	273	0.422	3	293	0.419	2.5

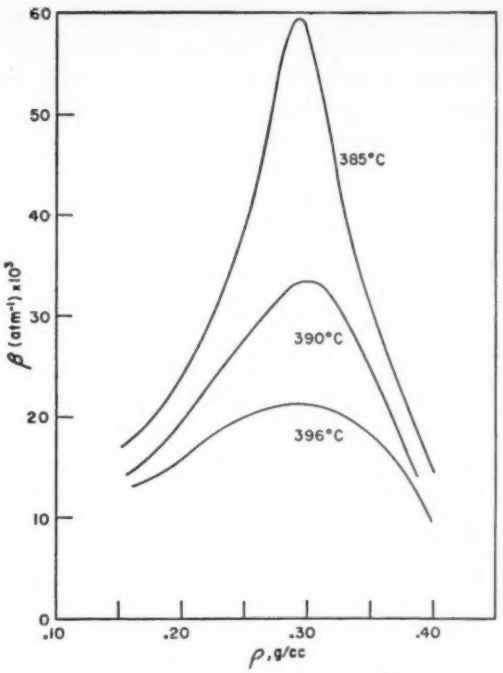

FIG. 1. The coefficient of compressibility, β, of steam as a function of density, ρ. Based on steam table data (reference 2).

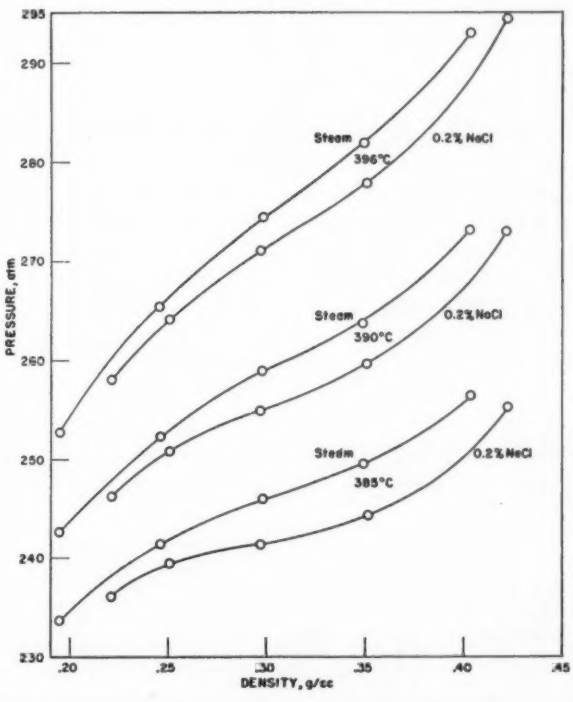

FIG. 2. Pressure-density isotherms for steam and a 0.2 percent by weight solution of NaCl in steam.

[3] Defined as the weight of steam divided by the total volume of the system. This rather unusual variable is employed because of the evidence which indicates that the cooperative phenomena in this system are determined principally by the concentration of water molecules, the latter being of course proportional to the "partial density" or weight concentration.

far below the critical point), it is possible to draw conclusions about the sign and limiting values of the partial molal volume of NaCl in steam from a consideration of the pressure-composition co-existence isotherms. The slope of the vapor isotherm is given by

$$\left(\frac{dP}{dX_2'}\right)_T = \frac{\left(\frac{X_2'}{X_1'} - \frac{X_2''}{X_1''}\right)\cdot\left(\frac{\partial\mu_2'}{\partial X_2'}\right)}{\left[(\bar{V}_1' - \bar{V}_1'') + \frac{X_2''}{X_1''}\cdot(\bar{V}_2' - \bar{V}_2'')\right]}, \quad (1)$$

where X is mole fraction, superscripts $'$ and $''$ refer to the vapor and liquid phases, respectively, subscripts 1 and 2

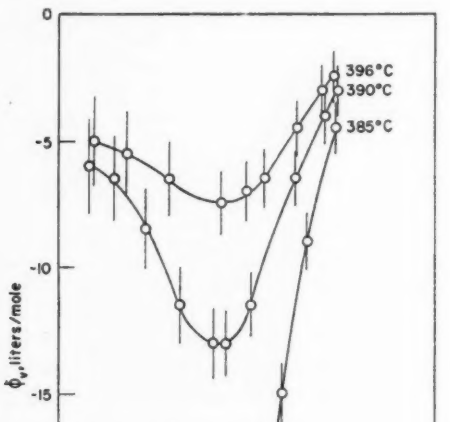

FIG. 3. The apparent molal volume ϕ_v of NaCl in 0.2 percent by weight solution in steam as a function of the solution density ρ.

refer to H_2O and NaCl, respectively, and μ is the chemical potential.[4]

Since

$$\bar{V}_1 = \frac{V}{n_1} - \frac{X_2}{X_1}\bar{V}_2, \quad (2)$$

where V/n_1 is the total volume of the phase containing n_1 moles of H_2O, Eq. (1) becomes, on substituting Eq. (2),

$$\left(\frac{dP}{dX_2'}\right)_T = \frac{\left(\frac{X_2'}{X_1'} - \frac{X_2''}{X_1''}\right)\cdot\left(\frac{\partial\mu_2'}{\partial X_2'}\right)}{\left[\left(\frac{V'}{n_1'} - \frac{V''}{n_1''}\right) + \left(\frac{X_2''}{X_1''} - \frac{X_2'}{X_1'}\right)\bar{V}_2'\right]}. \quad (3)$$

[4] This equation is readily derived from the relations: $d\mu_1' = d\mu_1''$; $d\mu_2' = d\mu_2''$; and $X_1 d\mu_1 + X_2 d\mu_2 = 0$, T and P constant.

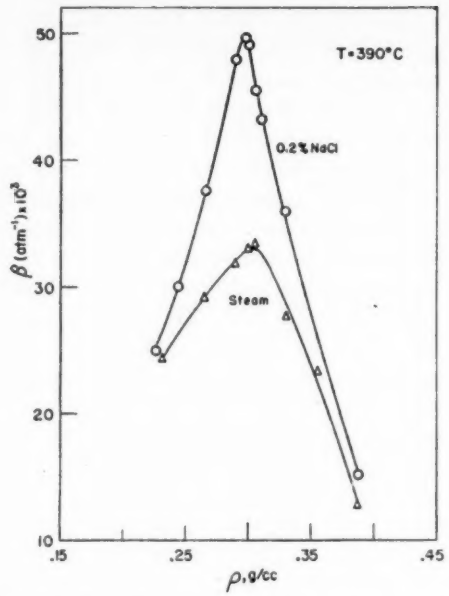

FIG. 4. The coefficient of compressibility-density curves for steam and for a 0.2 percent by weight solution of NaCl in steam.

Now $(dP/dX_2')_T$, at least at temperatures above 380°C, appears to be positive down to the vapor pressure of saturated liquid solution.[1,5] If we accept that $(\partial\mu_2'/\partial X_2')>0$, then the numerator of Eq. (3) is negative because the ratio of the mole fraction of NaCl to that of water is much greater in the liquid phase than in the vapor phase. The term $(V'/n_1' - V''/n_1'')$ is positive

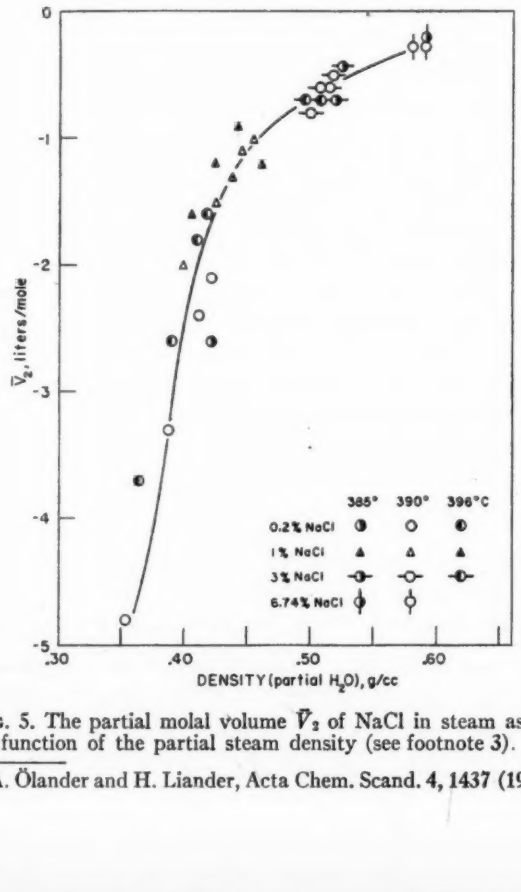

FIG. 5. The partial molal volume $\bar{V}_2$ of NaCl in steam as a function of the partial steam density (see footnote 3).

[5] A. Ölander and H. Liander, Acta Chem. Scand. 4, 1437 (1950).

because of the lower density of the vapor phase compared with the liquid phase. Therefore, if $(dP/dX_2')_T>0$, it follows that the partial molal volume of NaCl in steam, $\bar{V}_2'$, is negative.

Obviously, the partial molal volume of NaCl must be more negative than the value which makes the denominator of Eq. (3) zero. This limiting value is

$$\bar{V}_2'(\text{lim})=-\frac{\left(\frac{V'}{n_1'}-\frac{V''}{n_1''}\right)}{\left(\frac{X_2''}{X_1''}-\frac{X_2'}{X_1'}\right)}, \qquad (4)$$

and to estimate it we require only a knowledge of the densities and compositions of the two phases. Table III gives the limiting values of $\bar{V}_2'$ for NaCl in steam in equilibrium with saturated liquid solution. Under these conditions the mole ratio NaCl to water in the vapor phase is negligible compared to the ratio for the liquid phase and V'/n_1' is practically $18/\rho'$. If, instead of the pressures for saturated liquid solutions given by Keevil,[6] we use the pressures reported by Ölander and Liander,[5] which are some 12 atmos higher in this temperature range, the values of $\bar{V}_2'(\text{lim})$ are about 10 percent smaller numerically.

The values in Table III of $\bar{V}_2'(\text{lim})$ are, in order of magnitude, consistent with the partial molal volumes shown in Fig. 5 and are not inconsistent with the suggestion already made that the partial molal volume of NaCl goes through a minimum with decreasing solution density.

Some conclusions can also be drawn with regard to the partial molal volume of NaCl in the liquid phase. In Fig. 6 is shown the 396°C isotherm of the volume of liquid solution containlng 1 mole of water against the mole ratio of NaCl to water. This curve is based on densities estimated from a density-composition isotherm.[1] The density (~1.08 g/cc) used for the saturated liquid solution was that obtained in this laboratory by D. W. Fisher.[7] Three series of density determinations made by Fisher showed a maximum deviation of about 4 percent in the range 380–400°C. For the isotherm of Fig. 6 to become horizontal with increasing composition would require about a 12 percent increase in density over that used, so we feel that the final positive slope of the isotherm is significant. At compositions approaching saturation we would expect the liquid to be considerably less compressible than at lower compositions. It would be expected then that the curves of constant temperature and pressure in the homogeneous region below the liquid phase isotherm (see Fig. 6) would crowd together with increasing composition and become close and approximately parallel to the liquid isotherm. We thus conclude that at higher compositions the partial molal volume of NaCl (the slope of the constant temperature-

[6] N. B. Keevil, J. Am. Chem. Soc. 64, 841 (1942).
[7] D. W. Fisher (unpublished).

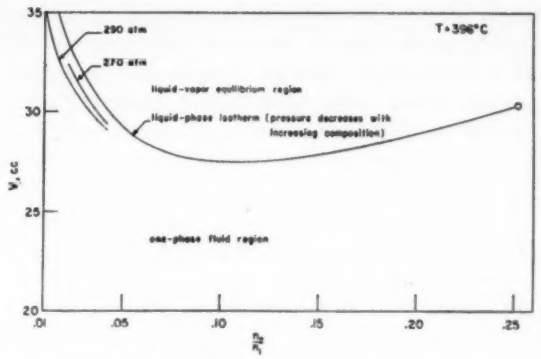

FIG. 6. Volume of solution containing 1 mole of water, V, as a function of the mole ratio of NaCl to water, n_2/n_1.

pressure curve) becomes zero and then positive. To the extent that the constant temperature-pressure curves parallel the liquid isotherm, we would expect the partial molal volume of NaCl to become zero at around 0.1 mole ratio NaCl to water (approximately 25 percent by weight NaCl) and to attain finally a value of the order of +25 cc/mole, a not at all unreasonable value.

DISCUSSION

It appears from Fig. 5 that, over the range of compositions and densities employed, the partial molal volume of NaCl is primarily dependent upon the solvent density. This is not too surprising. The large negative partial molal volumes must certainly indicate the collapse of the steam owing to a strong interaction between the NaCl and the steam. As long as there is no pronounced NaCl−NaCl interaction, at steam densities permitting ready collapse, we would anticipate the partial molal volume of the NaCl to be independent of composition.[8] Since at densities above 0.35 g/cc the compressibility of steam does not change much over the temperature range 385–396°C (Fig. 1), it is reasonable that the partial molal volumes not be very dependent on temperature. In line with the variation of the compressibility of steam with temperature, we would expect the partial molal volumes to decrease with increasing tem-

TABLE III. Limiting values of the partial molal volume of NaCl in steam in equilibrium with saturated liquid solution.

T °C	P[a] atmos	ρ'[b] g/cc	$\frac{V'}{n_1'}$ cc	$\frac{V''}{n_1''}$[c] cc	$\frac{n_2''}{n_1''}$[a]	$\bar{V}_2'$ (lim) liters/mole
385	144.5	0.066	273	30	0.254	−0.96
390	151	0.069	261	31	0.259	−0.89
396	159	0.072	250	31	0.264	−0.83

[a] Based on data of N. B. Keevil (see reference 6).
[b] Based on densities estimated from steam table data (reference 2) and the pressures in the second column.
[c] Based on densities of saturated liquid solutions, D. W. Fisher, unpublished data, this laboratory, and compositions of saturated liquid solutions given by N. B. Keevil (reference 6).

[8] It may be pointed out that at the highest composition and density indicated in Fig. 5 the concentration of NaCl is about 0.7 mole/liter.

perature. This seems to be borne out in general by the results shown in Fig. 5. At lower densities we would expect a considerably greater temperature dependence, the partial molal volumes becoming more negative as the critical temperature of water is approached.

At lower solution densities and at low compositions it appears probable that the partial molal volume of NaCl goes through a minimum with decreasing solution density. This conclusion results from a consideration of the isobars of Fig. 7, which is a plot at 390°C of the volume containing one mole of steam *vs* the mole ratio of NaCl to steam. The slope at any point of such an isobar in the homogeneous region is the partial molal volume of NaCl at that point. It seems reasonably evident that at a mole ratio of 6.17×10^{-4} (0.2 percent NaCl) or less, the slopes become first more negative and then less negative, with decreasing pressure and, hence, with decreasing density.

The variation of the coefficient of compressibility with density shown in Fig. 1, which is characteristic of all supercritical vapors, suggests that a kind of condensation still occurs above the critical temperature.[9] Since there is no phase separation, this must be interpreted as a continuous, short-range condensation (i.e., higher-order transition). As would be anticipated, this condensation becomes less significant as the temperature is increased.

In terms of a physical picture we would imagine that, at the minimum in the $\beta-\rho$ isotherm, molecular clusters start forming in the fluid (a process similar to that which must occur in supersaturated vapors below the critical temperature). As the volume of the system is decreased further, these must continue to grow until the maximum in the curve is reached and, on further compression, β decreases. Thus in this density region we pass continuously from a gas-like fluid with little or no short-range order to a liquid-like fluid in which short-range order must predominate. For gases considerably above their critical temperatures we must of course go to rather large pressures to reach the densities characteristic of this transition region.

In the density range over which this continuous, short-range condensation occurs, we would expect the

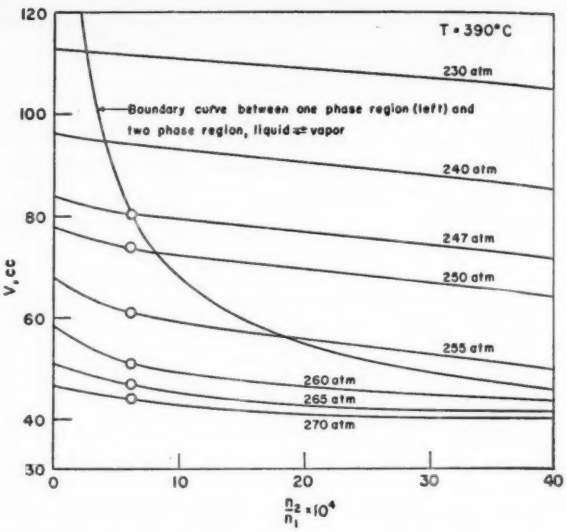

FIG. 7. The volume of solution, V, containing one mole of steam as a function of the mole ratio n_2/n_1 of NaCl to steam. Diagram, except for 0.2 percent points O based on our previously obtained data (see reference 1).

system to be very sensitive to the presence of even small amounts of a solute capable of strong interaction with the solvent. The introduction of NaCl markedly enhances the continuous condensation, probably through electrostatic interaction between water dipoles and solute ions and ion pairs.[10] The addition of one mole of NaCl to approximately 1600 moles of steam (0.2 percent NaCl) at 390°C and a constant pressure of 260 atmos cause about a 14 percent increase in density (see Fig. 2). The corresponding density increase is approximately 4 percent at 250 atmos and 6 percent at 270 atmos. Sufficient NaCl causes a true condensation, a liquid phase relatively rich in salt separating.[1]

The interesting behavior of the $NaCl-H_2O$ system in the critical region of the solvent should be duplicated by other solvent-solute systems. The use of other polar solvents, such as acetonitrile, is now being undertaken in this laboratory. If suitable solutes can be found, the relatively low critical temperatures and pressures of these solvents compared with water should permit a more precise examination of the critical region than has so far been possible with water.

The authors wish to express their appreciation to the U. S. Office of Naval Research for its support of this work.

[9] It is rather odd that this rather obvious property of critical fluids has escaped investigation or even detailed comment. From the point of view of physical continuity it is clear that the coefficient of compressibility β, which becomes infinite at the critical point, should show some remnant of this infinity in the form of maxima above the critical temperature, and such behavior is predicted for β by all the well-known equations of state. (Some authors have gone so far in neglecting these maxima as to smooth out experimental data which include one or two points from this region.)

[10] Unpublished electrical conductivity data taken in this laboratory by Mr. James K. Fogo indicate that NaCl in supercritical steam is partially dissociated.

Lifetime of the $^3\Sigma_u^+$ State of Nitrogen

E. E. MUSCHLITZ, JR.* AND L. GOODMAN†
Department of Chemistry, Cornell University, Ithaca, New York
(Received July 7, 1953)

A new method is proposed for the measurement of the "free space" lifetimes of particles in metastable states. An average lifetime of 2.3×10^{-4} second is obtained for nitrogen molecules in the $A\ ^3\Sigma_u^+$ state. The method also gives the collision diameter for collisions between metastable and normal N_2 molecules as 3.8A. Measurements of the appearance potential for molecules in the A state are presented.

INTRODUCTION

METASTABLE states of electronic excitation have long been known as energy carriers in photochemical processes, in combustion, and in gaseous discharges. The $A\ ^3\Sigma_u^+$ state of molecular nitrogen, in particular, is the upper state for the well known Vegard-Kaplan bands observed in the emission spectrum of the earth's upper atmosphere; it plays an important role in postulated mechanisms for the afterglow phenomenon of active nitrogen.

The most direct method of measuring the lifetime of an excited state is the molecular-beam method first attempted by Dunoyer.[1] In this method, particles in a molecular beam passing through a good vacuum are excited at one point in the beam path. The decrease in intensity of the excited particles is then observed as a function of distance along the path from the point of excitation. Since the velocity of particles in molecular beams is in the range 10^4 to 10^5 cm/sec, the method is limited to the range of lifetime for which the intensity decrease can be conveniently measured, 10^{-6} to perhaps 10^{-2} second.

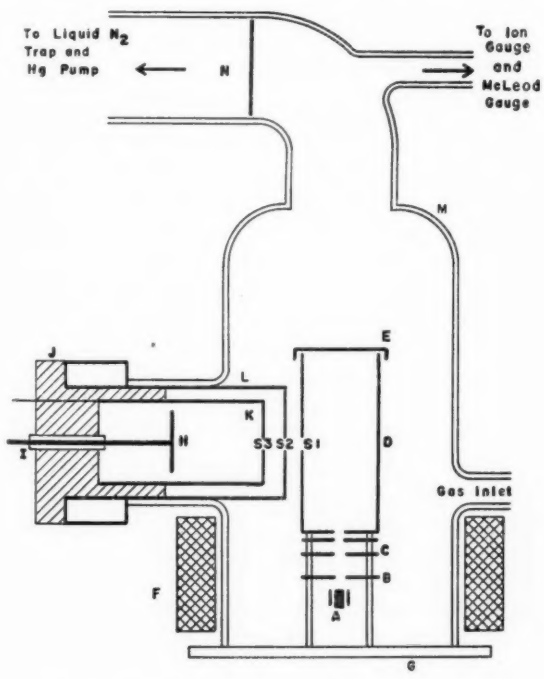

FIG. 1. Apparatus for measurement of metastable molecule lifetimes.

The method has not had wide application because of the inherent difficulties of the molecular-beam technique. The intensity of a molecular beam is low at best, and this difficulty is coupled with the fact that the excitation probability for the excited state may be low, so that the number of excited particles produced in the beam may not be measurable. Very few instances of the use of this method may be found and atomic beams were used in all cases.[2,3]

In the present work, a modification of the Dunoyer method is used. The molecules of a gas maintained at a pressure of from 2 to 40×10^{-4} mm are excited by electron impact. A system of three large slits is used to limit the direction of the particles which arrive at a detecting device placed at a known distance from the excitation region. The intensity of the excited molecules as measured by the detector is then determined as a function of the pressure and the slope of this curve at zero pressure obtained. This procedure is repeated with the detecting device at a different distance from the excitation region. The lifetime may be calculated, as shown below, from the ratio of the two slopes at zero pressure, the detector distances, and the average velocity of the gas molecules at the temperature of the experiment. The slopes so obtained are independent of molecular collisions, and hence, this method retains the primary advantage of the Dunoyer method; namely, no assumption is necessary as to the probability of deactivation of the excited molecules on collision with other molecules or with the walls of the apparatus. The lifetime obtained is the "free space" lifetime.

The intensity of the metastable molecules is measured by utilizing a detector first used by Webb.[4] The method is based on the fact that a metastable particle striking a metal surface is capable of ejecting an electron, provided the excitation energy of the particle is greater than the work function of the metal. This detector has been used

* Present location: College of Engineering, University of Florida, Gainesville, Florida.
† Present location: Department of Chemistry, Iowa State College, Ames, Iowa.
[1] L. Dunoyer, Compt. rend. **178**, 1475 (1924).
[2] H. D. Koenig and A. Ellet, Phys. Rev. **39**, 576 (1932).
[3] P. Soleillet, Compt. rend. **195**, 372 (1932).
[4] W. A. Webb, Phys. Rev. **24**, 113 (1924).

previously for metastable mercury,[4] helium,[5] and hydrogen[6] atoms.

APPARATUS

The essential features of the apparatus are shown in Fig. 1. An electron beam originates at the oxide-coated, end-fire, cathode A and is accelerated to the nickel anode B by a potential of 11 volts. The beam passes upward through a 2-mm hole in the anode and 1-mm holes in the defining plates C into the cylinder D. A magnetic field of approximately 600 gauss, produced by the solenoid F, is used to confine the electron beam. Elements C, D, and E are usually operated at the same potential, which could be readily varied from cathode potential to +45 volts. The electron gun assembly is mounted on a brass plate G which is sealed to the outer glass envelope M with Apiezon "W" wax.

The slit system S_1 (1.3 mm), S_2 (1.7 mm), and S_3 (1.7×2.5 mm) limits the direction of the metastable particles arriving at the detector H. This is a heavily copper-plated brass disk soldered to the end of a $\frac{1}{8}$-in. brass rod which passes out of the vacuum system through a glass sleeve I. Electrons released from the detector are collected on the cylinder K which is shielded by a larger cylinder L, and insulated from it by a Lucite plug J. Both K and L are operated at cathode potential, and H is 22.5 volts more negative than the cathode. The metal to glass and metal to Lucite connections are made vacuum tight with Apiezon "W" and the detector assembly sealed into a side arm on M. With potentials on the various elements as given above, electrons originating at the cathode cannot reach H, K, or L. However, nitrogen positive ions interfere with the measurements if the potential on C, D, and E is greater than the ionization potential, 15.58 volts.

Water-pumped nitrogen (99.6 percent) supplied by Mathieson Company was used. The gas was passed through a liquid-nitrogen trap and over phosphorus pentoxide before entering the apparatus through a capillary leak. A relatively constant pressure of nitrogen was obtained as follows: The apparatus was first pumped out through a large liquid-nitrogen trap by a single-stage, 50 liter/sec, mercury-vapor pump with the butterfly valve N open. A vacuum of 5×10^{-6} mm or less (as read on an RCA 1949 ion gauge) could be obtained after one or two hours of pumping. The valve was then closed and the capillary leak opened with the pump still operating. The pressure reached an equilibrium value in about 5 minutes. A range of pressures could readily be obtained by changing the pressure back of the capillary leak. Pressure measurements were made with an accurately calibrated McLeod gauge. Mercury levels in the gauge were read to 0.01 mm and corrections made for capillarity. A trap was placed between the gauge and the apparatus. Both this trap and the pump trap were maintained at liquid-nitrogen temperature while the apparatus was in operation.

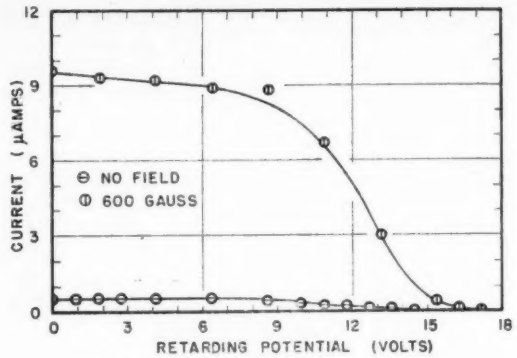

FIG. 2. Energy analysis of electron beam.

Current to the collector K was measured by an FP 54 amplifier.[7] Operating conditions were such that the sensitivity, with a control-grid resistance of 1000 megohms, ranged from 0.5 to 1×10^{-13} amp/cm deflection of the galvanometer used in the plate circuit.

All of the metal elements inside the apparatus, with the exception of the cathode and anode, were made of brass, heavily copper-plated, polished, and finally cleaned with reagent grade benzene before assembly. Between runs, the entire apparatus was filled to atmospheric pressure with dry nitrogen. Under these conditions, no significant change in the efficiency of the detector was found in successive runs.

PRELIMINARY EXPERIMENTAL PROCEDURE

Figure 2 shows the effect of a retarding potential applied to D and E on the electron beam current to E. At zero retarding potential, elements C, D, and E were plus 19.9 volts with respect to the cathode. The increased beam current in the presence of the magnetic field is clearly shown. When the apparatus was disassembled, a spot in the center of the lid E having a diameter of 3 mm was observed. This fact may be taken as evidence for good definition of the electron beam.

From the figure it may also be seen that the energy spread of the electron beam was ±3 volts and that the contact potential difference between the cathode and E was about 3 volts. The latter figure is a reasonable one, since the difference between the work functions of an oxide-coated cathode surface (0.8–2.2 ev) and a copper surface (4.5 ev) gives a range of from 2.3 to 3.7 electron volts.

In order to find and characterize the proper excited state in nitrogen, appearance potential measurements were made. Figure 3 shows a typical plot of electron current released from the target by metastable nitrogen molecules *versus* the applied potential accelerating the electron beam. Since the $A\ ^3\Sigma_u^+$ state is the lowest excited state in nitrogen, it is evident that the initial rise in current is due to metastable molecules in this state. The

[5] R. Dorresstein, Physica **9**, 433, 447 (1942).
[6] W. Lamb and R. Retherford, Phys. Rev. **79**, 549 (1950).
[7] L. A. Dubridge and H. Brown, Rev. Sci. Instr. **4**, 532 (1933).

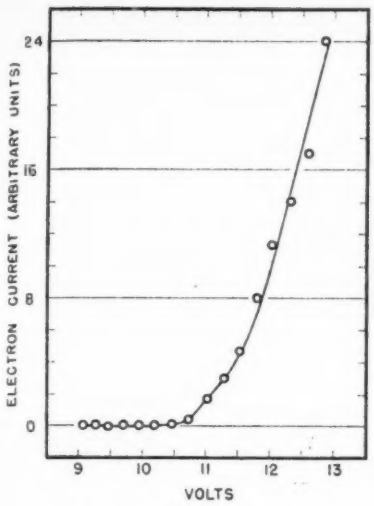

FIG. 3. Relation between collector current (proportional to metastable N_2) and applied voltage accelerating electron beam.

next excited state in nitrogen is also a triplet, $B\,^3\Pi_g$, and is 1.18 ev above the A state. The lowest singlet excited state, $a\,^1\Pi_g$, is 2.38 ev above the A state.[8] The lifetime measurements given below were taken at an applied potential of 12.70 v, approximately 2.1 v higher than the appearance potential. This was done in order to avoid appreciable production of molecules in the $a\,^1\Pi_g$ state which is also metastable. The B state does not interfere, since the transition $B \rightarrow A$ is short-lived. The irregularities in the curve of Fig. 3 may indicate the appearance of higher states, however, sufficient data was not taken to establish this with certainty.

Three determinations of the appearance potential are shown in Table I. In all cases an energy analysis of the electron beam was made as described above. In the table, V is the applied accelerating potential on the electrons, V_0 the energy of the fastest electrons, and V' the average energy of the electrons. The results for V' are reasonably close to the spectroscopic value for the ν_{00} transition (both states in the lowest vibrational level). The measurement of the appearance potential is subject to the same difficulties as those found in the mass spectrometric determination of ionization potentials.[9] Accuracy is difficult to achieve because of uncertainty in the contact potential difference and the energy distribution of the electrons, so that a gas of known ionization potential is usually used for calibration. The method used here avoids the first difficulty to a considerable extent, but not the second. A new absolute method of measurement of ionization potentials which could also be applied for a more accurate determination of metastable state energies has recently been proposed.[10]

Figure 4 is an extension of the previous figure to higher electron energies. The curve passes through a maximum at an applied potential of about 18 volts. Beyond 19 volts the formation of N_2^+ ions rapidly reduces the current to the electron collector K and eventually the current assumes large positive values. In preliminary experiments with 2^3S_1 He (19.73 volts above the ground state), which were made in order to check the detector, it was necessary to remove positive ions arising from impurities in the gas before measurements of the metastable atom intensity could be made. The applied potential at which the measurements in nitrogen were taken, however, was below the ionization potential of possible impurities.

In order to check the effect of electric and magnetic fields on the lifetime, the potential between D and L was increased from 0 to 90 volts negative with respect to cathode and the magnetic field varied from 200–800 gauss. No effect was found in the collector current, indicating that under these conditions the metastable particles were not appreciably quenched.

RESULTS

Equations showing the behavior of the electron current to K as a function of the pressure p and the target distance from the electron beam l may readily be derived. Consider a beam of metastable particles defined by the slit system. If n_0 is the intensity of the beam at the point of excitation, n the intensity of the beam at the target, and J the electron current to K,

$$n_0 = kp \quad \text{and} \quad J = \eta n, \tag{1}$$

where k and η are proportionality constants. The loss in beam intensity in the infinitesimal distance dx is given by

$$dn = -\alpha n p dx - k' n dx, \tag{2}$$

where α is the effective cross section (in cm²/cm³ of gas at unit pressure) for collisions between metastable and normal nitrogen molecules, and k' is a proportionality constant. In this equation the first term gives the loss of

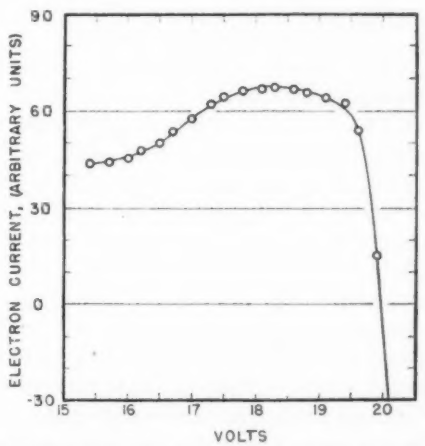

FIG. 4. Relation between collector current and applied voltage at higher voltages. The curve illustrates the formation of N_2^+ ions at higher electron energies.

[8] G. Herzberg, *Molecular Spectra and Molecular Structure* (D. Van Nostrand Company, Inc., New York, 1950), second edition, Vol. 1, pp. 449, 552–53.

[9] J. D. Morrison, J. Chem. Phys. **19**, 1305 (1951).

[10] Fox, Hickam, Kjeldaas, and Grove, Phys. Rev. **84**, 859 (1951).

intensity resulting from collisions, and the second gives the loss resulting from the decay of metastable particles by radiative processes. Integration of (2) between the limits 0 and l on x gives

$$n(l)=n_0e^{-(\alpha p+k')l}, \tag{3}$$

and, using Eq. (1),

$$J(l)=k\eta pe^{-(\alpha p+k')l}. \tag{4}$$

From (4) it may readily be seen that for a fixed target distance l the collector current $J(l)$ passes through a maximum as p is increased. The pressure at which this maximum occurs may be obtained by differentiating (4) with respect to pressure and equating to zero, giving

$$\alpha l p_{\max}=1. \tag{5}$$

The value of the derivative of (4) at $p=0$ is

$$\left(\frac{dJ(l)}{dp}\right)_{p=0}=k\eta e^{-k'l}. \tag{6}$$

The ratio of two such derivatives at two target distances, l and l', is

$$R=e^{-k'(l-l')}, \tag{7}$$

which gives

$$k'=\frac{-2.301\log R}{l-l'}. \tag{8}$$

The loss dn in the number of metastable particles due to radiative processes only is

$$dn=-k'ndx, \tag{9}$$

or

$$dn=-k'n\bar{v}dt, \tag{10}$$

where $\bar{v}$ is the average velocity of the metastable particles. The average lifetime $\bar{\tau}$ is given by

$$\bar{\tau}=\frac{1}{n_0}\int_0^{n_0}tdn=\frac{1}{k'\bar{v}}, \tag{11}$$

using Eq. (10) for the relation between n and t. It is assumed here, for the purpose of simplification, that all of the metastable particles in the beam have the same velocity $\bar{v}$. The average lifetime may then be obtained from the experimentally determined quantities l, l', and R, using Eqs. (8) and (11). The half-life may also be calculated using the relation, $\tau_{\frac{1}{2}}=\bar{\tau}\ln 2$.

The experimental results conform to Eq. (4) as shown in Fig. 5, in which the collector current J corrected for variations in the electron-beam current, is plotted against pressure. From the position of the maximum in the upper curve and the use of Eq. (5), $\alpha=156$ cm^2/cm^3 at one mm Hg pressure. Sufficient data was not obtained to locate the maximum for the lower curve, however, essentially the same value of α is obtained by fitting Eq. (4) to the data shown. The collision diameter d is 3.8A, using the relation $\alpha=N\pi d^2$, in which N is the

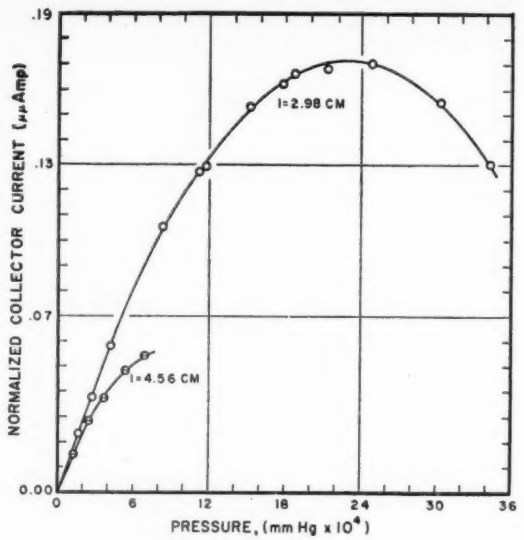

FIG. 5. Curves showing the relation between collector current and pressure. The upper curve is for a target distance of 2.98 cm, the lower for 4.56 cm.

number of molecules per cm^3 at 0°C and 1 mm pressure (3.536×10^{16}). The calculated value for d might be compared with the kinetic theory diameter of the nitrogen molecule, 3.75A.[11] However, a strict comparison would not be legitimate for several reasons. Since the kinetic theory value was obtained from viscosity measurements, its magnitude would be particularly dependent upon the number of collisions at angles near 90°. Also, the collisions considered here are between metastable nitrogen molecules and normal nitrogen molecules. The observed cross section is actually the sum of cross sections for elastic scattering and inelastic processes involving transfer or loss of the excitation energy. A thorough discussion of these points has been given by Massey and Burhop.[12]

Similar experiments have been carried out by Dorrestein and Smit[13] for collisions of helium atoms in the long-lived 2^3S_1 state with helium atoms in the ground state. They find a cross section approximately equal to the gas kinetic; however, the resolution of their apparatus was poor. The resolution of the present apparatus is considerably better, since the defining slit in front of the target intercepts an average angle of 6° at the point of excitation. It is probable that this is still not sufficient resolution for an accurate determination of the total cross section because of the large number of collisions taking place at small angles.[12]

It can be seen from Fig. 5 that the initial slopes of the two curves are not the same, indicating a finite lifetime for the metastable state. The average lifetime of the

[11] E. H. Kennard, *Kinetic Theory of Gases* (McGraw-Hill Book Company, Inc., New York, 1938).

[12] H. S. W. Massey and E. H. S. Burhop, *Electronic and Ionic Impact Phenomena* (Oxford University Press, London, 1952), Chapter VII.

[13] R. Dorrestein and J. A. Smit, Proc. Acad. Sci. Amsterdam 41, 725 (1938). See also p. 416 of reference 12.

TABLE I. Appearance potential measurements for $A\ ^3\Sigma_u^+ N_2$.

Run	V^a	$V_0{}^b$	V'^c	Spectroscopic values
1	10.70	7.90	5.8	
2	10.56	8.08	5.3	6.16 ev[d]
3	10.10	8.08	5.5	7.16 ev[e]
Av.		8.02	5.5	

[a] Applied electron accelerating potential, volts.
[b] Energy of the fastest electrons, ev.
[c] Average energy of the electrons, ev.
[d] Calculated from the frequency given for the ν_{00} $(X\rightarrow A)$ transition in reference 8.
[e] Calculated for the most probable transition according to the Franck-Condon principle, ν_{06} $(X\rightarrow A)$, from data given in reference 8.

$A\ ^3\Sigma_u^+$ state is calculated to be 2.3×10^{-4} second, using the equations given above with $\bar{v}=47.5\times10^3$ cm/sec at 25°C.[11] It is difficult to estimate the probable error of this result. Because of the nature of the method, a lifetime as long as 10^{-3} second could be reconciled with the experimental data, but one shorter than 10^{-4} second could not. The results are most accurate when conditions obtain which give the maximum possible difference between the initial slopes. It would seem, therefore, that data should be taken for both as long and as short a target distance as practicable. However, a longer target distance than that used here would necessitate accurate measurements of smaller pressures and collector currents. Further refinements of the method and apparatus are possible and should lead to measurements of greater accuracy. The value obtained for the lifetime must therefore be considered as a tentative one.

DISCUSSION

Since the first positive bands of nitrogen ($B\rightarrow A$ transition) are the predominant feature of the Lewis-Rayleigh afterglow in nitrogen, the presence of molecules in the B and A states in the afterglow is well established. An explanation of the long life of the afterglow must provide a mechanism for the continuous formation of molecules in the B state. Two theories have recently been proposed. Mitra[14] postulates the slow preassociation of N atoms giving molecules in the B state with $v\sim13$. Oldenburg[15] suggests that the slow process is a recombination of two normal N atoms in a three body collision, producing excited particles, particularly molecules in the A state. Molecules in the B state are then produced in a subsequent process involving the collision of $N_2(A)$ with a metastable atom.

A feature of the afterglow which is difficult to understand is the absence of the Vegard-Kaplan bands $(A\rightarrow X)$. The relatively short lifetime of the A state determined here makes an explanation more urgent. Molecules in the A state must be removed rapidly by inelastic impacts in the gas or by collisions with the walls. In particular, inelastic impacts of A molecules with atoms in the metastable ^2D or ^2P states may occur with high probability, as suggested in Oldenburg's mechanism. If the latent energy in the afterglow is considered to reside in dissociated nitrogen molecules, there must be a large initial concentration of atoms. It is therefore possible that many collisions occur between molecules in the A state and excited atoms. Furthermore, it is not unreasonable to suppose that, while recombination of N atoms on the walls of the discharge tube is a slow process, a conclusion which is necessary for a long-lived afterglow, deactivation of A molecules by collisions with the walls may be a highly probable process. In any case, it would seem that an explanation of the afterglow phenomenon cannot be tenable, if it presumes a relatively long lifetime for molecules in the A state.

The method for the determination of lifetimes of metastable particles presented here is generally applicable, provided the energy of the excited particles is large enough to permit the use of electron emission from a metal surface as a method of detection, and provided the lifetime is in the range 10^{-2} to 10^{-6} second. Within the range of its utility, the same method of detection can be employed for measurements of appearance potentials for molecular or atomic metastable states.

[14] S. K. Mitra, Phys. Rev. **90**, 516 (1953).
[15] O. Oldenburg, Phys. Rev. **90**, 727 (1953).

Primary Photochemical Process in Bromine

G. B. KISTIAKOWSKY AND JAMES C. STERNBERG*
Gibbs Chemical Laboratory, Harvard University, Cambridge, Massachusetts
(Received July 10, 1953)

A kinetic investigation of the photobromination of ethylene has led to results which are in general consistent with the earlier work of Schumacher *et al.* The existence of an induced oxidation reaction was demonstrated in mixtures containing traces of oxygen, which is a very strong inhibitor of the ethylene-bromine chain reaction.

The relative quantum yields of the photobromination reaction were measured at six wavelengths using narrow pass Baird interference filters. The quantum yields were shown to be independent of wavelength between the limits of 4800 and 6800A. Radiation of 7150A wavelength is absorbed but is totally ineffective photochemically. These results were interpreted with the aid of spectroscopic information to mean that the photochemically effective transitions of bromine molecules in radiation of wavelengths longer than the convergence limit, 5107A, lead to the continuum of the $^3\pi_{1u}$ state, which then dissociates in one elementary act to form two normal atoms. It is unnecessary to invoke the assumption of collisional dissociation of excited bromine molecules to explain their photochemical reactivity below the convergence limit.

WHILE no doubts have existed for a long time concerning the nature of the primary photochemical process following the absorption by bromine of wavelengths shorter than the convergence limit 5107A, the understanding of the processes following the absorption at longer wavelengths is by no means complete. Several photochemical investigations[1–7] have demonstrated that bromine molecules are dissociated on irradiation at the longer wavelengths and that the quantum yield is the same in the banded region, at 5460A, as in the continuum. These results were interpreted in terms of collisional dissociation of excited bromine molecules.[1,4] Spectroscopic investigations of the bromine spectrum have demonstrated, however, that in addition to that state which is responsible for most of the absorption in the continuum, there exist other low-lying excited states of the bromine molecule,[8–10] which contribute to absorption both below and above the convergence limit.

The hypothesis that every bromine molecule is dissociated on collision after excitation to a stable vibrational level of the main upper state is not very plausible. Hence it appears necessary to include the other excited states of bromine molecules to obtain a satisfactory interpretation of the photochemical reactivity below the convergence limit. Unfortunately, however, the potential energy diagrams constructed on the basis of spectroscopic evidence are not sufficiently conclusive, and the information on the photochemical reactivity of bromine after absorption of longer waves is too limited to permit a definitive correlation of these two sets of data.

The experiments described in this paper do permit such a correlation to be made, and they eliminate rather definitely the collisional dissociation of stable excited molecules as the prime source of photochemical reactivity of bromine in the longer wavelength region. The gas phase bromination of ethylene was chosen for this study because its very long chain length serves as a useful amplification factor of the primary photochemical process, and because its kinetics appeared to be rather well understood.[7] The present measurements have revealed some complicating features of the reaction, previously not reported, but, nonetheless, it was found useful for the main purpose outlined above.

EXPERIMENTAL DETAILS

The apparatus consisted of the usual all-glass vacuum system with provisions for the purification, storage, and mixing of the reagents. Connected to it was a cylindrical Pyrex cell, 5 cm long, with plane Pyrex windows. A capillary connection led from the cell to a modified Bodenstein quartz spiral manometer, used as a direct reading instrument. The thermostat containing the reaction cell was mounted on an optical bench, which supported also the optical system for the illumination of the cell and the measurement of the absorbed radiation.

The quartz spiral of the manometer was sealed into a Pyrex envelope connected to a large ballast flask with ample thermal lagging, a mercury manometer and, through suitable stopcocks, to vacuum and to atmospheric pressure. Light from a straight filament lamp was focused on two photocells after reflection from a small mirror attached to the free end of the spiral. The photocells were electrically bucking each other so that their net output was zero when they received equal

* Present address: Department of Chemistry, Michigan State College, East Lansing, Michigan.

[1] W. Jost, Z. physik. Chem. **134**, 92 (1928); **B3**, 95 (1929).
[2] J. Urmston and R. M. Badger, J. Am. Chem. Soc. **56**, 343 (1934).
[3] J. W. T. Spinks and J. M. Porter, J. Am. Chem. Soc. **56**, 264 (1934).
[4] A. G. Brown and J. W. T. Spinks, Can. J. Research **B15**, 113 (1937).
[5] J. W. T. Spinks and R. Mungen, Can. J. Research **B18**, 363 (1940).
[6] K. L. Müller and H. J. Schumacher, Z. physik. Chem. **B42**, 327 (1939); **B37**, 365 (1937).
[7] Schmitz, Schumacher, and Jäger, Z. physik. Chem. **B51**, 281 (1942).
[8] W. G. Brown, Phys. Rev. **38**, 1179 (1931); **39**, 777 (1932).
[9] O. Darbyshire, Proc. Roy. Soc. (London) **A159**, 93 (1937).
[10] O. Darbyshire, J. Chem. Phys. **4**, 747 (1936).

radiation intensities. The output was amplified by an FP-54 electrometer tube in a Du Bridge-Brown[11] circuit with a mirror galvanometer in the output. The manometer could be used as a null point instrument by adjusting pressure in the ballast flask until the differential output of the photocells was zero. It could also be used as a direct reading instrument by holding the pressure in the ballast flask constant and moving the photocells until balance was attained. To accomplish this the photocells were mounted on the carriage of a comparator, one turn of the screw of which corresponded to approximately 1-mm pressure difference between the interior and the exterior of the quartz spiral. The sensitivity of the system was 0.001 mm and its stability over longer periods of time somewhat better than 0.01-mm mercury. The calibration of the instrument was obtained by plotting the setting of the comparator screw against the pressure difference read on the mercury manometer. It gave an almost linear relationship and therefore pressure differences could be read directly to 0.01 mm or 0.2 percent, whichever was larger, over a range of -100 to $+100$ mm.

The photochemical radiation source was a 200-watt projection lamp run from a Sola transformer at a lower than normal voltage. The light from the lamp was focused on a small aperture, provided with an electrically operated shutter, so that exposure times of a few seconds could be accurately reproduced. A second lens, following the aperture, converted the light into a parallel beam. Here was inserted one of several Baird interference filters[12] together with auxiliary absorption filters to isolate the desired transmission band of the interference filter. The radiation then passed through a plane Pyrex plate set at a 45° angle to the beam, the reaction cell, and another Pyrex plate set at a 45° angle.

The radiation reflected by the Pyrex plates fell on two RCA 926 photocells, electrically bucking one another. Their differential output was fed into a FP-54 tube in a Du Bridge-Brown circuit with a mirror galvanometer in the output. The grid resistor, 10^9 ohms, instead of being grounded as in the usual Du Bridge-Brown circuit, was connected to one of the "emf" binding posts of an *L* and *N* Type *K* potentiometer, whose galvanometer circuit was shorted. The other emf post of the potentiometer and the center tap of the batteries driving the photocells were grounded. The potentiometer thus could be used to cancel whatever emf was set up across the grid resistor by the unbalance of the photocell currents. In operation, the amplifier was first balanced (for photocell dark current) with the photocells dark and a zero setting on the potentiometer. Then the photocell behind the reaction cell was exposed to radiation, and the amplifier was brought to balance by changing the setting of the potentiometer. Next the photocell before the reaction cell was also exposed to the radiation, the potentiometer reset to zero, and the amplifier balanced by adjusting a diaphragm placed in front of that photocell. Finally, bromine vapor was introduced into the reaction cell, and the potentiometer was adjusted to re-establish balance of the amplifier. The ratio of the two potentiometer readings was taken to be the fraction of the light energy absorbed by the bromine. This comparatively simple arrangement permits the measurement of very small fractional light absorption because it is virtually insensitive to incident intensity fluctuations, and because it uses the amplifier only at the balance point. The linearity of its readings in the incident light intensity is as good as the output of the photocells at constant imposed potential.

The incident light intensity was kept constant in experiments made at a fixed wavelength by making slight adjustments of the lamp current to bring the potentiometer reading to the chosen value with only the second photocell illuminated. Since the manufacturer supplies a spectral sensitivity curve for the 926 photocell, the potentiometer readings, being proportional to the photocell current, gave the relative incident light intensities at the several wavelengths employed when different filter combinations were used. The manufacturer's sensitivity curve was checked by placing a radiation thermopile† directly into the light beam, behind the second reflecting Pyrex plate, and comparing the readings of the thermopile with those of the potentiometer at several wavelengths. To get a measurable output of the thermopile, the lamp was run on a higher voltage than normal and the thermopile output was amplified by a Perkin Elmer DC breaker amplifier. After correcting for the infrared radiation transmitted by the filters, to which the photocells are insensitive but the thermopile responds, satisfactory agreement with the manufacturer's curve was obtained in the 5000–6300A region. At longer wavelengths our measurements gave relative sensitivities of the photocell lower by as much as 50 percent than the manufacturer's specifications. This introduced an uncertainty in the calculated quantum yields which will be mentioned later.

The reagents used were bromine, ethylene, and sulfur hexafluoride. Merck's Reagent Grade bromine was stored for a few days over potassium bromide and then repeatedly distilled in vacuum through phosphorus pentoxide tubes, while pumping off permanent gases. The bromine was then fractionally distilled, retaining only the middle third, which was kept at dry ice temperature when not in use. This stored bromine was periodically subjected to a repetition of the entire purification process.

Ethylene and sulfur hexafluoride of Mathieson cp grade were subjected to a similar purification procedure and stored as gases in large storage flasks.

In making an experimental run, the reagents were first introduced into a mixing flask where their partial

[11] J. Strong, *Procedures in Experimental Physics* (Prentice-Hall, Inc., New York, 1938), p. 418.

[12] B. H. Billings, Phot. Eng. **2**, 45 (1951).

† This was kindly loaned to us by Professor G. S. Forbes.

pressures were measured, and the contents of the flask were then mixed by a magnetically driven all-glass stirrer before admission to the reaction cells. The mixing process was deemed advisable because of some irreproducibility encountered in earlier experiments. Perhaps because of the use of ordinary stopcock grease (Apiezon N) in all stopcocks, a measurable dark reaction took place and had to be corrected for in the photochemical experiments. The latter therefore consisted of alternating dark and light periods, with frequent readings of the pressure. It was assumed that the rate of the photochemical reaction was the total rate on illumination, less the average of the dark rates before and after the light period.

RESULTS AND CONCLUSIONS

The present experiments investigating the dependence of the photochemical rate upon the light intensity and upon the composition and total pressure of the reaction mixture largely confirm the earlier results of Schumacher, Schmitz, and Jager.[7] In the low-pressure region (below *ca* 200 mm), the rate was found to increase linearly with light intensity, approximately linearly with the partial pressure of ethylene, and somewhat less than linearly with the partial pressure of bromine. A nearly linear increase of the rate with total pressure resulted upon the addition of an inert gas (sulfur hexafluoride). In the high-pressure region (200 to 400 mm) the rate became proportional to the square root of the incident light intensity and was found to decrease with added pressure of the inert gas. To account for their similar findings, Schumacher *et al.* proposed the following reaction mechanism:

$$\mathrm{Br_2}+h\nu\rightarrow 2\mathrm{Br},$$

$$\mathrm{Br}+\mathrm{C_2H_4}\rightleftarrows\mathrm{C_2H_4Br},$$

$$\mathrm{C_2H_4Br}+\mathrm{Br_2}\rightarrow\mathrm{C_2H_4Br_2}+\mathrm{Br},$$

$$\mathrm{Br}\xrightarrow{\text{wall}}\tfrac{1}{2}\mathrm{Br_2},$$

$$\mathrm{Br}+\mathrm{Br}+\mathrm{M}\rightarrow\mathrm{Br_2}+\mathrm{M}.$$

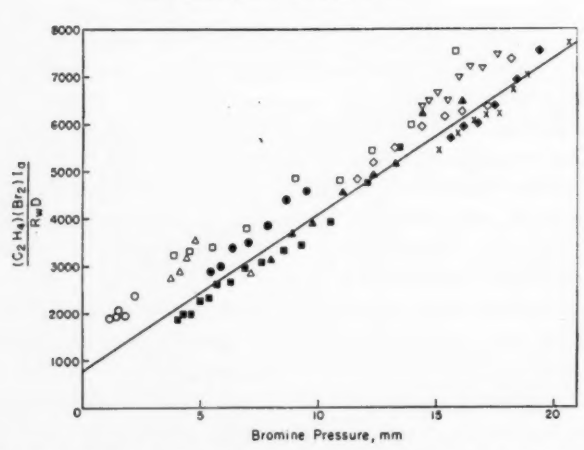

FIG. 1. Plot of photochemical results according to $[(C_2H_4)(Br_2)I_a]/R_wD=K(Br_2)+K'$. Each type of symbol refers to one run.

This leads to the following rate expressions:

$$\text{(low-pressure range)}\quad R=K_{\mathrm{I}}\frac{(\mathrm{C_2H_4})(\mathrm{Br_2})I_a\cdot P}{(\mathrm{Br_2})+K'}, \tag{1}$$

$$\text{(high-pressure range)}\quad R=K_{\mathrm{II}}\frac{(\mathrm{C_2H_4})(\mathrm{Br_2})}{(\mathrm{Br_2})+K'}(I_a/P)^{\frac{1}{2}}. \tag{2}$$

In the low-pressure range, where the chain breaking process is the diffusion of bromine atoms to the walls, the total pressure P in the rate expression accounts for the suppression of this diffusion with increasing pressure; this approximation is justified only if the diffusion coefficient of bromine atoms is independent of the composition of the reaction mixture—a situation which does not hold over a wide variation of the ethylene to bromine ratio. The present experiments fit Schumacher's Eq. (1) better when the factor P is replaced by $1/D$, where the diffusion coefficient D is calculated from the molecular constants of the three gases used in these experiments. The resulting extent of agreement is shown in Fig. 1.

In neither of the investigations did results agree quantitatively with Eq. (2) at higher pressures. The observed decrease of the rate with rising pressure is more rapid than predicted by that equation. This effect can be explained by introducing an additional chain-breaking reaction:

$$\mathrm{C_2H_4Br}+X\rightarrow\text{inactive products}$$

if it be further assumed that X is proportional to the total pressure. With this modification the complete rate expression, displayed in a form emphasizing the total pressure effect becomes

$$1/R=A/P+BP+RP/C, \tag{3}$$

where R is the rate, P the total pressure, and A, B, and C are coefficients involving the rate constants and the reactant concentrations. Figure 2 shows the fit obtainable by this equation for Schumacher's experimental data, which offer a more critical test because of the wider pressure range studied. The dotted line shows the behavior of the unmodified mechanism, for which the pressure dependence is expressed by

$$1/R=A/P+RP/C. \tag{4}$$

Schumacher *et al.* had noted that oxygen strongly inhibits the rate of bromination of ethylene, but they concluded that oxygen does not cause an induced oxidation. We have found that oxygen is indeed an extremely effective inhibitor; the addition of only 10^{-4} percent of oxygen to 200 mm of reaction mixture was found to decrease the rate by more than an order of magnitude. When minute amounts of oxygen were added intentionally to the reaction mixture, an induction period could be observed in the photochemical reaction. When shorter than normal illumination periods

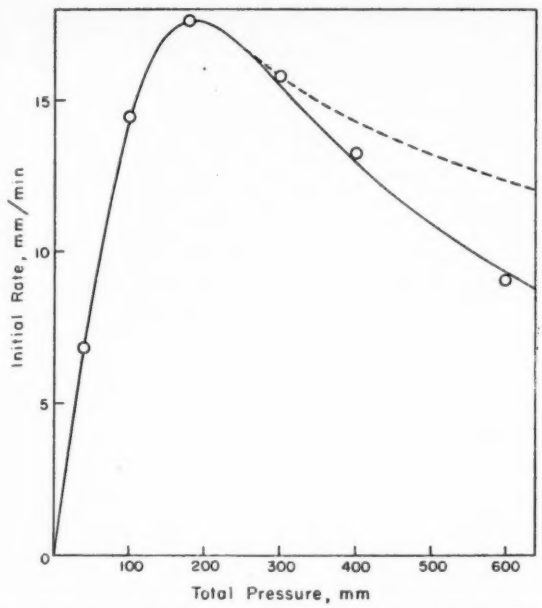

FIG. 2. Pressure dependence of rate of ethylene-bromine photochemical reaction. Solid curve: Results obtained by Schumacher *et al.*, using 20-mm ethylene, 20-mm bromine, and freon (CF_2Cl_2) as inert gas to give total pressure. Dotted curve: calculated for fall-off of rate with square root of total pressure (unmodified mechanism). Circles: calculated points using modified mechanism.

were used (two seconds instead of the usual ten seconds), an induction period could be found even when no oxygen was intentionally added, showing that the "pure" reagents contained small amounts of oxygen impurity, as shown in Fig. 3. The induction period suggested that oxygen does in fact participate in an induced oxidation reaction, and the existence of such a reaction was clearly demonstrated by strongly irradiating mixtures of purified ethylene and bromine containing added oxygen and isolating the products of the reaction. Some of these products were not sufficiently volatile to be distilled in vacuum at 200°C without decomposition. The infrared spectrum of the more volatile fractions was taken with the Baird infrared spectrometer. The lowest boiling fraction was largely ethylene dibromide, the only compound shown by infrared analysis to result from the photochemical reaction between pure ethylene and bromine. The higher boiling fraction showed strong carbonyl and less intense ester oxygen bands. Elementary analysis of this sample gave an empirical formula of $C_3H_7OBr_2$, indicating a mixture; the infrared spectrum suggested that bromoethyl bromoacetate might be the main ingredient.

The study of the effect of wavelength upon the quantum yield of the ethylene-bromine reaction was complicated by the existence of the induction period and the slight irreproducibility of the rate in supposedly identical mixtures; both effects can be largely attributed to the strong inhibition by residual traces of oxygen in the reagents. In experiments designed to study the effect of wavelength, therefore, the same mixture was alternately exposed to light in the continuum and to longer wavelength illumination. These experiments were carried out with mixtures of ethylene and bromine at pressures sufficiently low (*ca* 30 mm) that the rate was strictly proportional to incident light intensity. This facilitated the correction for the inequality of radiation intensities transmitted by the different filters in making comparison of quantum yields at various wavelengths.

Table I shows the absorption coefficients of bromine determined at the several wavelengths used in the photochemical experiments. They must be considered as averages over the widths of the transmission bands of the several filters used, and the half-widths for each filter are therefore included in the table, as well as the wavelengths of maximum transmission.

The results of rate measurements with these filters are presented in Table II. The quantum yields reported are relative to those observed with radiation of 4820A wavelength; two values are reported for each wavelength, the first calculated using the manufacturer's spectral sensitivity curve for the photocell, and the second using the response determined by the thermopile method. The absolute magnitude of the quantum yield of the reaction at both 4360A and 5460A with the reactant pressures used in these experiments is about

TABLE I. Absorption coefficients of bromine vapor at various wavelengths and at 35°C.

Wavelength of max transmission (A), and auxiliary filter	Transmitted band width, A	Bromine pressure (mm)	Percent absorbed	$\beta = \frac{1}{P}\log\frac{I}{I_0}$
4820 Corning Blue	150	4.91	25.1	2.56×10^{-2}
		10.28	44.3	2.48×10^{-2}
		20.27	68.3	2.46×10^{-2}
		29.4	82.6	2.58×10^{-2}
			average	$2.52\times10^{-2}\pm0.05\times10^{-2}$
5435 Corning Green	145	3.93	7.42	8.52×10^{-3}
		9.69	16.62	8.15×10^{-3}
		16.33	25.23	7.60×10^{-3}
		29.40	43.40	8.41×10^{-3}
			average	$8.17\times10^{-3}\pm0.30\times10^{-3}$
5940 Corning Yellow	95	4.18	1.32	1.38×10^{-3}
		9.66	3.31	1.51×10^{-3}
		12.83	4.45	1.54×10^{-3}
		17.35	5.81	1.50×10^{-3}
		29.40	11.00	1.72×10^{-3}
			average	$1.52\times10^{-3}\pm0.08\times10^{-3}$
6140 Corning Yellow	180	4.20	0.973	9.05×10^{-4}
		10.29	2.184	9.33×10^{-4}
		15.57	3.35	9.51×10^{-4}
		19.50	4.27	9.72×10^{-4}
		29.40	6.45	9.87×10^{-4}
			average	$9.58\times10^{-4}\pm0.26\times10^{-4}$
6800 Wratten Red	80	3.62	0.052	6.36×10^{-5}
		8.30	0.057	2.89×10^{-5}
		11.28	0.081	3.11×10^{-5}
		15.90	0.169	4.66×10^{-5}
		22.97	0.245	4.62×10^{-5}
		29.90	0.289	4.22×10^{-5}
			average	$4.31\times10^{-5}\pm1.08\times10^{-5}$
7150 Wratten Red	150	29.7 mm	0.097	1.41×10^{-5}

10^5, according to the measurements of Schumacher *et al.*[7]

Within the accuracy of these measurements the quantum yield is seen to be independent of wavelength from 4820 to 6800A; hence, throughout this spectral range, every bromine molecule absorbing a quantum of radiation must be eventually dissociated into atoms. Radiation of 7150A appears to be totally ineffective photochemically; the quantum energy at this wavelength corresponds to only 39.98 kcal/mole, as contrasted to the dissociation energy of bromine molecules into two normal atoms, 45.46 kcal/mole. However, radiation at 6800A corresponds to a quantum energy of only 42.04 kcal/mole, also below the dissociation energy of bromine

TABLE II. Reaction rates at various wavelengths at 35°C.

Wavelength, A	Rate, mm/min	Bromine pressure, mm	Corrected incident intensity[a] (a)	(b)	Percent absorbed by bromine	Relative quantum yield[a] (a)	(b)
4820	1.61	12.1	31.0	31.0	50.0	1.27	1.02
5435	1.37		51.4	62.6	20.4		
4820	0.99	9.9	31.0	31.0	43.6	1.37	1.12
5435	0.88		51.4	62.6	17.0		
4820	2.65	12.7	30.6	30.6	52.2	1.08	1.08
5940	0.49		63.8	63.8	4.35		
4820	1.41	9.3	30.6	30.6	41.7	1.33	1.33
5940	0.30		63.8	63.8	3.20		
4820	0.84	12.4	31.3	31.3	51.4	1.08	1.08
5940	0.16		66.6	66.6	4.25		
4820	1.52	12.3	29.8	29.8	51.0	1.09	1.28
6140	0.15		52.4	44.5	2.66		
4820	4.55	10.6	35.4	35.4	46.0	1.17	1.81
6800	0.067		300.7	194.0	0.105		
5940	0.29	14.6	66.6	66.6	4.96	1.70	2.63
6800	0.036		273.5	176.7	$0.086(\phi_{6800}/\phi_{5940})$		
4820	12.0	10.0	80	80	44.0		
7150	<0.01		1400	850		<0.1	

[a] The incident intensities and relative quantum yields in column (a) were calculated using the manufacturer's photocell spectral sensitivity curve. Column (b) was calculated from the experimentally determined sensitivity curve.

into two normal atoms. That the deficit could be supplied to *every* excited molecule by inelastic collisions of the first kind is very unlikely indeed. Hence it appeared probable that the light absorption at longer wavelengths may be largely due to bromine molecules already possessing some vibrational energy due to thermal excitation. This possibility was tested by measuring the light absorption coefficients for bromine at two different temperatures. The results, reported in Table III, clearly show that thermally excited bromine molecules are indeed responsible for all—or at least the major part—of absorption from the continuum of an incandescent filament source at longer wavelengths. Thus with the filter which has its maximum transmission at 6800A, the vibrational excitation of the absorbing molecules, coupled with a likelihood that the

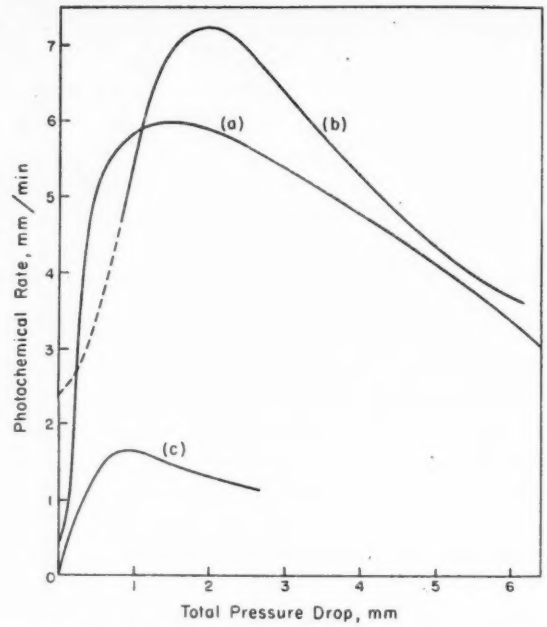

FIG. 3. Induction period. (a) Short illumination periods, "pure" reagents. (b) Oxygen added, 5×10^{-4} mm. (c) Oxygen added, 9×10^{-3} mm. Reactant pressures: Bromine and ethylene, 20 mm each; sulfur hexafluoride, 150 mm.

short wavelength tail of the filter-transmission band may account for most of the absorption with this filter, enables the excited molecules to have sufficient energy for direct dissociation.

The photochemical results may be summarized as showing that bromine is dissociated with undiminished quantum yield, as long as sufficient energy per quantum of radiation is present to dissociate bromine molecules into two normal atoms. The photochemical results alone do not permit distinction between dissociation resulting from continuous absorption, occurring in one elementary act, and dissociation following discrete absorption, leading to stable excited states of the bromine molecule which are subsequently dissociated into atoms only after undergoing collision. For such an interpretation of the mechanism of the dissociation, it is necessary to appeal to the available spectroscopic evidence.

Brown[8] worked out the quantum numbering of the vibrational levels of the main upper state, $^3\pi_{0^+u}$, the continuum of which starts at 5107A, with $^2P_{\frac{3}{2}}$ and $^2P_{\frac{1}{2}}$ atoms as products of dissociation. He also detected

TABLE III. The effect of temperature upon the absorption coefficient of bromine.

Filter wavelength (A)	Percent absorption at 35°C	Percent absorption at 149°C	Thermal excitation energy in cm^{-1}	Estimated v''
4820	82.6	82.5	0	0
5140	63.0	64.9	20	0
5435	43.4	48.4	89	0–1
5940	11.0	12.0	71	0–1
6140	6.45	10.94	424	1–2
6800	0.289	1.00	989	3–4
7150	0.097	0.214	632	2–3

bands due to another upper state dissociating into two normal, $^2P_{\frac{1}{2}}$, atoms. Darbyshire[9,10] further studied this state, $^3\pi_{1u}$, and gave a vibrational assignment which he estimated to be accurate to ± 2 units. The quantitative absorption measurements of Acton, Aickin, and Bayliss[13] demonstrated the complexity of the continuum in the bromine spectrum and suggested the existence of at least two, and possibly even three, low-lying excited states. Mulliken[14] discussed this spectroscopic evidence and suggested two alternative assignments (see Table IV), without making a definite selection.

TABLE IV.

Maximum[a]	Relative intensity	Assignment I	Assignment II
A (4150A)	2	$^1\Sigma_g^+ \rightarrow {}^1\pi_u$	$^1\Sigma_g^+ \rightarrow {}^1\pi_u$
B (4900A)	1	$^1\Sigma_g^+ \rightarrow {}^3\pi_{0^+u}$	$^1\Sigma_g^+ \rightarrow {}^3\pi_{1u}$
C (not observed)	?	$^1\Sigma_g^+ \rightarrow {}^3\pi_{1u}$	$^1\Sigma_g^+ \rightarrow {}^3\pi_{0^+u}$
		Calculated max at about 4500A and about equal in intensity to $^3\pi_{1u}$.	Calculated max at about 5350A and much weaker.

[a] Two maxima were observed by Acton, Aickin, and Bayliss in the continuum.

Rees[15] made use of the experimental data of Brown and of Darbyshire to construct potential energy curves for two of these states. His $^3\pi_{0^+u}$ curve extends to $v'=22$ and his $^3\pi_{1u}$ also extends to $v'=22$, accepting Darbyshire's numbering. The $^3\pi_{0^+u}$ curve extrapolates very well to the continuum evaluated by Bayliss;[16] the continuum of the $^3\pi_{1u}$ was only suspected by Brown[8] because of background absorption overlapping the bands due to the $^3\pi_{0^+u}$ state, and was entirely lacking in quantitative data. The $^1\pi_u$ state is expected to be repulsive, according to Mulliken,[17] and has not been directly observed.

These results as embodied in the Rees diagram have been reproduced in Fig. 4. The six ellipses also drawn in this figure indicate the states reached by the bromine molecules after absorption of the radiation transmitted by each of the six filters used in the present experiments. In drawing the ordinates of these ellipses, allowance was made for the width of the transmission bands of the filters; in drawing the abscissas, use was made of the Franck-Condon principle and of the information on the vibrational state of the absorbing molecules presented in Table III.

Figure 4 demonstrates very clearly that while the absorption at 4820A leads to the continuum of the $^3\pi_{0^+u}$ state, absorption at 5435, 5940, 6140, and 6800A leads to the continuum of the $^3\pi_{1u}$ state and therefore results in the formation of two normal atoms in one elementary act, without participation of molecular collisions. This explains the unchanging quantum yield in this entire region. The absence of any photochemical reaction with radiation of 7150A wavelength is also readily understandable, since in this region stable excited molecules are formed; evidently they are rarely if ever dissociated into atoms by collisions of the first kind.

Figure 4 leaves open the possibility that radiation of 5435A wavelength (and of 5460A used in other work) causes transitions to the discrete part of the $^3\pi_{0^+u}$ state. This possibility is made especially plausible by the fairly high intensity of the bands belonging to this state in this wavelength region. However, the continuous nature of the radiation source used in the present ex-

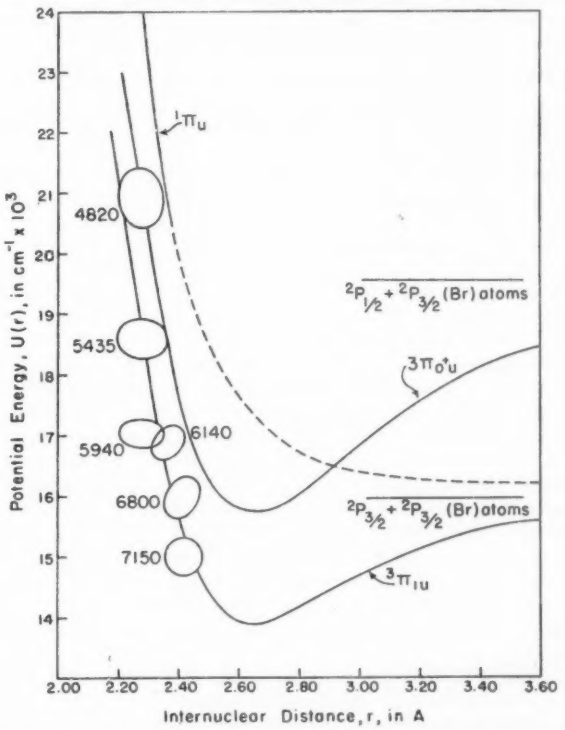

FIG. 4. The potential energy diagram and the photochemically observed transitions of the bromine molecule.

periments would suggest that by far the greater fraction of the absorption should lead to the $^3\pi_{1u}$ continuum. A predissociation process from the $^3\pi_{0^+u}$ to the $^1\pi_u$ appears less likely because the multiplicity change involved would probably make the transition sufficiently improbable so that many excited molecules would either radiate their energy as fluorescence or lose it in inelastic collisions, with an attendant decrease in the photochemical quantum yield.

ACKNOWLEDGMENTS

We wish to thank Baird Associates, Inc., and particularly Dr. David Z. Robinson for the loan of the interference filters. One of us (JCS) wishes to thank Monsanto Chemical Company for a predoctoral fellowship.

[13] Acton, Aickin, and Bayliss, J. Chem. Phys. **4**, 234 (1938).
[14] R. S. Mulliken, Phys. Rev. **57**, 500 (1940).
[15] A. L. G. Rees, Proc. Phys. Soc. (London) **59**, 998, 1008 (1947).
[16] N. S. Bayliss, Proc. Roy. Soc. (London) **A158**, 551 (1937).
[17] R. S. Mulliken, Phys. Rev. **46**, 549 (1934).

Letters to the Editor

THIS section will accept reports of new work, provided these are terse and contain few figures, and especially few half-tone cuts. The Editorial Board will not hold itself responsible for opinions expressed by the correspondents. Contributions to this section should not exceed 600 words in length and must reach the office of the Editor not later than the 15th of the second month preceding that of the issue in which the Letter is to appear. No proof will be sent to the authors. A publication charge of $15.00 per Letter is made which, when honored, will entitle the Institution to 100 free reprints.

Sintering of a Water Gas Shift Catalyst

J. HOOGSCHAGEN AND P. ZWIETERING
Central Laboratory of Staatsmijnen in Limburg, Geleen, The Netherlands
(Received September 8, 1953)

IF a porous catalyst possessing a large internal surface area is kept at a sufficiently high temperature, the surface area will gradually diminish due to sintering. We investigated this phenomenon quantatively.

Supposing that the rate at which the internal surface area decreases is proportional to the $(n+1)$th power of the existing area and further that the sintering process requires an energy of activation E, the following relation will express the surface area A as a function of the sintering time τ and the sintering temperature T:

$$1/A^n - 1/A_0^n = k\tau \exp(-E/RT), \quad (1)$$

where A_0 is the original surface area.

Equation (1) has been verified experimentally with a water gas shift catalyst (type $Fe_2O_3-Cr_2O_3$). After the reduction, the samples were heated in reactors controlled within 1°C. The sintering temperatures were 510, 530, and 550°C and the sintering times 3, 8, 24, 72, 216, and 648 hours, so in all, 18 samples were heated. Into the reactors a gas mixture was fed corresponding to water gas converted to equilibrium (about 8 percent CO, 17 percent CO_2, 50 percent H_2, and 25 percent H_2O), so that no temperature gradients due to reaction heat could occur. After being sintered, the samples were rapidly cooled down in a nitrogen stream and their surface areas measured according to the B.E.T. method, after a precautionary reduction in CO_2+H_2.

In Fig. 1 the B.E.T.-surface area is plotted against the sintering time both on a logarithmic scale. $\tau+\tau_0$ has been plotted as the abscissa, in order to obtain straight parallel lines also for short sintering times. $\tau_0=1/kA_0^n \exp(E/RT)$ is found by trial and error. All points lie along three parallel lines within the accuracy of the area measurement (5 percent). So Eq. (1) adequately represents the sintering of the surface area. An energy

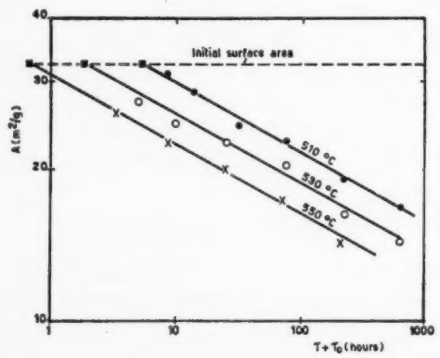

FIG. 1. Surface area of a water gas shift catalyst as a function of sintering time and sintering temperature.

of activation $E=65\,000$ cal/mole follows from the horizontal distances between the lines. The slope corresponds to a value of $n=7.3$. (Another catalyst with a higher Cr_2O_3 content yielded a value of $n=6.2$.) This high value of n points to a rapid sintering of the surface area at the beginning (during a time of the order of τ_0), while later on the area reaches a nearly constant limit.

Next, the catalytic first-order activity constant[1] at 350°C was measured on the sintered samples and plotted against the surface area in Fig. 2. (The high activities were slightly corrected for in-

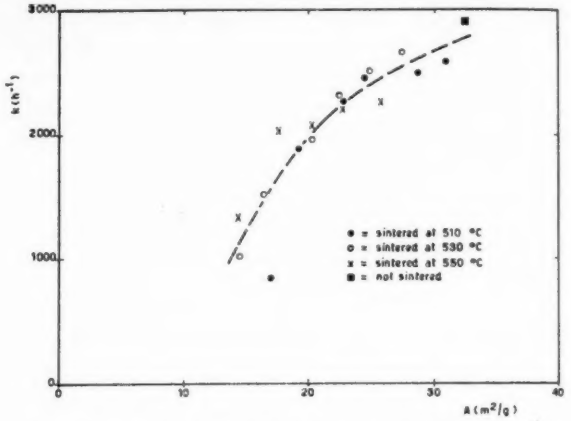

FIG. 2. True activity at 350°C as a function of the surface area.

ternal diffusion effects.[2]) Points corresponding to different sintering conditions T and τ are correlated reasonably well. This is to be expected on the basis of the hypothesis of the one-dimensional series of sinter states.[3] The activity seems to decrease more rapidly than the surface area, so the activity per unit surface area is not quite constant.

After a process time long in comparison with τ_0, the surface area will be $A=k^{-1/n}\tau^{-1/n}\exp(E/nRT)$. Therefore the surface area reaches a quasi-constant limit that for a *given* process time decreases with increasing temperature by a factor with a negative apparent energy of activation of $E/n=9000$ cal/mole. The catalytic water gas shift reaction itself requires the much higher energy of activation of 24 000 cal/mole.

In view of the relation between activity and surface area, it may therefore be expected that, notwithstanding the sintering, the mean activity for a given process time will continue to increase with temperature, at least if the area reached is not too low.

[1] Atwood, Arnold, and Appel, Ind. Eng. Chem. **42**, 1600 (1950).
[2] C. Bokhoven and J. Hoogschagen, J. Chem. Phys. **21**, 159 (1953).
[3] G. F. Hüttig, Z. Elektrochemie, **54**, 89 (1950).

Electron Configuration in 8-Coordinated and Other Complexes

BRYAN HIGMAN
University College of the Gold Coast, Achimota, Gold Coast, British West Africa
(Received June 25, 1953)

IN a review of the applications of group theory to molecular orbital calculations, the writer has had occasion to check the results given by G. E. Kimball[1] on atoms forming eight bonds. It would appear that the widely accepted[2] result that the dodecahedral arrangement of eight bonds can be based on d^4sp^3 is in error, and that in fact one f orbital must be brought into use. The position of molybdenum in the periodic table is not such as to make it unreasonable to assume that this happens in the ion $Mo(CN)_8^{-4}$.

The "reduction tables" in Kimball's paper contain a number of errors, mostly the substitution of 0 for 1 which can easily be detected by checking that the dimensions of the irreducible repre-

sentations do add up to those of the representation being analyzed. But in Table XXII, a 1 in the second line has strayed out of its column. The table, supplemented by an f line, should read

V_d	A_1	A_2	B_1	B_2	E
s	1	0	0	0	0
p	0	1	0	0	1
d	1	0	1	1	1
f	0	1	1	1	2
σ	2	0	0	2	2
π	2	2	2	2	4

and the eight σ bonds can be built up from sp^2d^4f.

It is also believed that there are other errors in Kimball's conclusions arising from a more deeply lying cause. If the Hamiltonian of a system is invariant under a group, the orbitals conform to the representations of that group. The Hamiltonian of the free atom is invariant under the orthogonal group. Algebraic functions of the coordinates, $\psi(x, y, z)$, provide the representations of the rotation group, but these are only one-half of the representations of the orthogonal group, namely $s_g\ p_u\ d_g\ f_u \cdots$. The other representations, $s_u\ p_g \cdots$, can only be provided by adding a fourth variable, η, of absolute value 1, which changes sign on an improper rotation. Then the two wave functions

$$\phi_1(x, y, z, \eta)=\psi(x, y, z) \quad \phi_2(x, y, z, \eta)=\eta\cdot\psi(x, y, z)$$

are orthogonal and belong to different representations of the orthogonal group. The variable η concerns the spin of the electron, and the wave functions ϕ_1 and ϕ_2 are those of two "paired" electrons.

In bond formation it does not matter which of two oppositely spinning electrons came from the central atom. In consequence, if P is a representation of the operative symmetry group, and $\bar{P}$ is the representation whose character differs from that of P only in that its sign is reversed for all improper rotations, then wave functions conforming to either P or $\bar{P}$ are equivalently available for bond formation. Had the errant "1" above strayed from the A_1 column, for example, Kimball's conclusion would have stood, because in V_d we have $\bar{B}_2=A_1$. The application of this principle is trivial for proper symmetry groups and for symmetry groups containing the inversion, but in other cases it relaxes somewhat the restrictions apparently imposed by Kimball's tables.

A fuller report is being prepared for publication elsewhere.

[1] G. E. Kimball, J. Chem. Phys. **8**, 188 (1940).
[2] E. g., R. S. Nyholm, Quart. Rev. Chem. Soc. **3**, 325 (1949).

$BaTiO_3-KF$ Phase Diagram

CLARENCE KARAN AND BERNARD J. SKINNER
Engineering Laboratory, International Business Machines Corporation, Poughkeepsie, New York
(Received September 21, 1953)

THE partial phase diagram for the $BaTiO_3-KF$ system, Fig. 1, has been determined in connection with a study of the growth of barium titanate crystals.

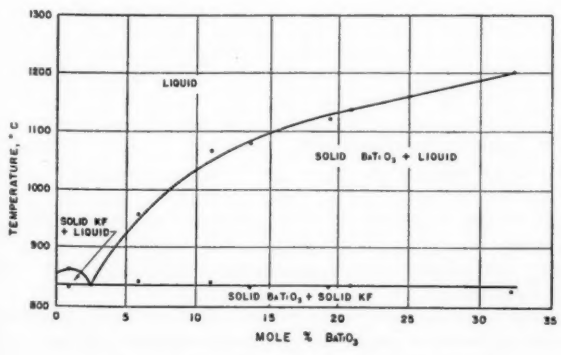

FIG. 1. Phase diagram, $KF-BaTiO_3$ system.

The phase diagram was obtained using the technique of differential thermal analysis. A Leeds and Northrup X−Y Recorder automatically plotted the temperature of the $BaTiO_3-KF$ melt on the x axis, and the difference temperature on the Y axis (Fig. 2). The heating rate of the furnace used for the analysis was

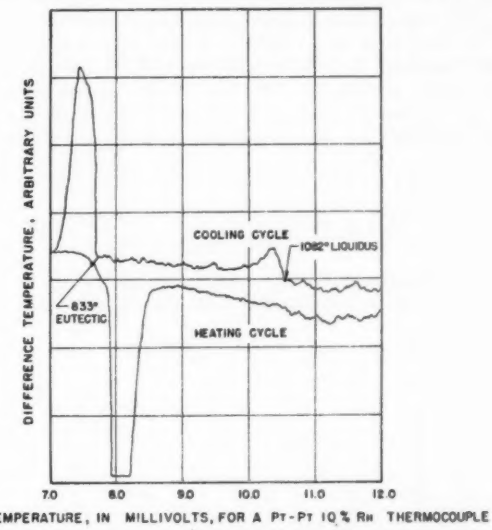

FIG. 2. Differential thermal analysis plot.

arbitrarily set but the cooling rate was kept fairly constant and was between 3° and 4°C per minute.

A "soak" at the upper temperature extreme was employed to make certain that a completely liquid phase had been attained but an unduly long "soak" was avoided in order to minimize the evaporation of KF. Tightly capped crucibles were used, for the same reason. Nevertheless, some KF did evaporate. The amount evaporated was determined by the loss of weight and the percentage composition of the $BaTiO_3-KF$ melt corrected accordingly.

There was no evidence of compound formation during the differential thermal analysis runs but we have found that BaF_2 is formed if the melt is maintained at elevated temperatures for long periods of time.

Internal Rotation in Sulfur Monochloride

N. W. LUFT AND K. H. TODHUNTER
Research Department, Simon-Carves Ltd., Cheadle Heath, Stockport, Cheshire, England
(Received September 21, 1953)

THE problem of internal rotation in sulfur monochloride, ClS·SCl, has not yet been solved satisfactorily. The C_{2h} structure is excluded because of the dipole moment of sulfur monochloride; but with the spectral data available it is impossible to make a decision between the other two configurations, *viz.* C_{2v} or C_2. Palmer,[1] however, gives the dihedral angle between the two SCl bonds as 90°, from electron diffraction experiments. The assumption of a twofold potential barrier with (approximately) equidistant and equivalent minima ($n=2$) seems to be in agreement with electrostatic considerations since the repulsive interactions between the lone electron pairs of the sulfur atoms would tend to favor a dihedral angle of 90°.

The Raman shift at about 106 cm^{-1} [2-5] is commonly looked upon as the torsional mode, although it was reported to be depolarized. With $n=2$ equivalent minima and the reduced moment of inertia $I_r=110.7\times10^{-40}$ gcm^2, the foregoing frequency corresponds to the barrier height $V_0=32$ kcal/mole. This result is unreasonably high from the point of electrostatic interactions and in view of the fact that the average barrier in HO·OH is only about $\bar{V}\sim\frac{1}{2}(12+4)=8$ kcal/mole.[6] The difficulties can be resolved by regarding the

Raman shift at 106 cm^{-1} as the first overtone of an unknown torsional fundamental $\delta_t \sim 53\ cm^{-1}$. Then $V_0 = 8.0$ kcal/mole is obtained for the internal rotational barrier in ClS−SCl and the weak Raman shift at 141 cm^{-1} observed[4] in solid S_2Cl_2 at −170°C may be interpreted as the second overtone of δ_t. The actual barrier is probably even smaller than 8 kcal and the apparent height may be partly due to deviations from a simple twofold cosine potential.

The other structural data[1] and fundamental frequencies[2–5,7] are readily available in the literature, *viz.*, $r(SCl) = 1.99$, $r(SS) = 2.05$A, $ClSS = 103°$. $\omega = 208, 242, 438, 446, 536\ cm^{-1}$. Frequencies of about 200 and 500 cm^{-1} have been observed in the ultraviolet absorption spectrum,[8] but they are probably due to upper electronic states.

From the structural data the principal moments of inertia are calculated for an azimuthal angle of $\phi = 90°$:

$$I_s = 588.6, \quad I_1 = 648.2, \quad I_2 = 150.6 \times 10^{-40}\ gcm^2,$$
$$I_1 I_2 I_s = 5.3965 \times 10^{-113}.$$

All individual moments, and especially I_s, change considerably with ϕ but the product of the three does not alter much (Fig. 1).

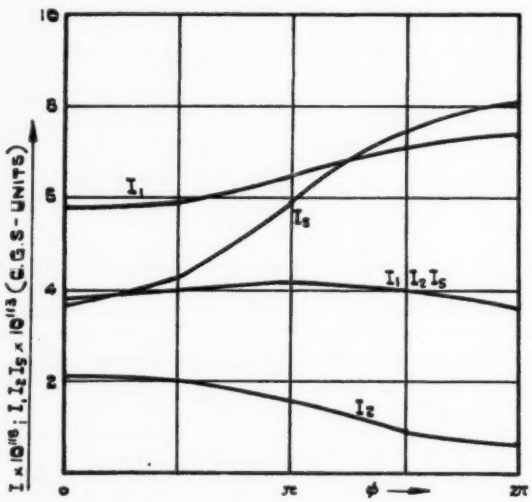

FIG. 1. Dependence of moments of inertia of ClS·SCl on dihedral angle ϕ.

These data have been used to calculate the thermodynamic functions to the harmonic oscillator and rigid rotator approximation for an ideal gas of S_2Cl_2 at a pressure of 1 atmos (Table I). As

TABLE I.

T°K	$-(F^0-H_0^0)/T$	S^0	$(H^0-H_0^0)/T$	C_p^0
298.16	65.55	79.24	13.69	17.57
300	65.63	79.34	13.71	17.59
400	69.76	84.57	14.81	18.57
500	73.14	88.77	15.63	19.12
600	76.05	92.28	16.23	19.47
700	78.60	95.29	16.70	19.68
800	81.02	98.11	17.09	19.81
900	82.88	100.27	17.39	19.87
1000	84.74	102.39	17.65	19.91

with C_{2v} and C_{2h} symmetries the product of external and internal symmetry numbers for ClS·SCl of point group C_2 is $ss_i = 2$. If the external symmetry number is taken as $s = 2$, then $s_i = n/f = 1$, i.e., the contribution $(-R \ln n)$ to S^0 and $-(F^0-H_0^0)/T$ is cancelled by the increment $(R \ln f)$, with $f = 2$, for optical isomerism.

[1] K. J. Palmer, J. Am. Chem. Soc. **60**, 2360 (1938).
[2] H. Gerding and R. Westrik, Rec. trav. chim. **60**, 702 (1941).
[3] R. Vogel-Högler, Acta. Phys. Austriaca, **1**, 311 (1947–48).
[4] N. C. Majundar, J. Sci. Ind. Research (India) **8B**(2), 25 (1949).
[5] H. J. Bernstein & J. Powling, J. Chem. Phys. **18**, 1018 (1950).
[6] N. W. Luft, J. Chem. Phys. **21**, 179 (1953).
[7] M. Goehring, Ber. deut. chem. Ges. **80**, 219 (1947).
[8] N. W. Luft and K. H. Todhunter (to be published).

Chlorine Quadrupole Resonances in Solids

P. J. BRAY AND P. J. RING
Rensselaer Polytechnic Institute, Troy, New York

(Received September 28, 1953)

A SELF–QUENCHING super-regenerative spectrometer[1] has been employed to investigate Cl^{35} nuclear quadrupole resonances in a number of polycrystalline solids. The compounds and their resonance frequencies at liquid nitrogen temperature are given in Table I.

TABLE I. Cl^{35} quadrupole resonance frequencies at liquid nitrogen temperature.

Compound		Frequency (Mc)	Strength[a]
p-$CH_2ClC_6H_4NO_2$	p-nitrobenzyl chloride	34.311	3
$Cl_2C_6H_3NH_2$	2,5-dichloroaniline	34.530	4
		34.413	3
$ClC_6H_3(NO_2)_2$	2,4-dinitrochloro-benzene	37.796	5
p-$ClC_6H_4SO_2Cl$	p-chlorobenzene-sulfonyl chloride	35.967	3
		32.832	VW
m-$NO_2C_6H_4SO_2Cl$	m-nitrobenzene-sulfonyl chloride	34.337	3
p-$NO_2C_6H_4SO_2Cl$	p-nitrobenzene-sulfonyl chloride	33.438	4
p-$BrC_6H_4SO_2Cl$	p-bromobenzene-sulfonyl chloride	32.895	3
$CCl_3CHOH(OC_2H_5)$	chloral alcoholate	39.140	4
		38.705	2½
		38.516	3
CCl:CClCCl$_2$CCl:CClC:O	hexachlorophenol	40.100	VW
		39.997	W
		38.157	5
		37.865	3
		37.553	3
$C_{10}H_8$-1,2,3,4-Cl_4	tetrachlorotetra-hydronaphthalene	37.055	VW
		36.783	W
		36.100	VW
		35.262	VW
$Ba(ClO_3)_2 \cdot H_2O$	barium chlorate	29.922	5

[a] W = weak. VW = very weak. Numbers give signal-to-noise amplitude ratio.

The frequency measurements employed an external oscillator (General Radio 605), a General Radio 1213-A Unit Crystal Oscillator, and a National Corporation HRO 60 receiver. An oscilloscope and audio oscillator were used for interpolation between 10-kc harmonics. Agreement was obtained within 1 kc among the measurements made on any individual resonance frequency. This limit of accuracy arises from the necessity for judgment in setting the nuclear signal pips and external oscillator pips in coincidence.

Comparison of signal-to-noise amplitude ratio measurements with previously reported values[2] indicates comparable sensitivity for the self-quenched and externally-quenched spectrometer.

The p-nitrobenzyl chloride resonance frequency of Table I should be compared with the p-chlorobenzyl chloride and benzyl chloride data of Meal;[3] the 2,5-dichloroaniline value with his p-chloroaniline data, and the 2,4-dinitrochlorobenzene frequency with the o-nitrochlorobenzene and m-nitrochlorobenzene values of the same paper.

The resonance frequencies of the particular sulfonyl chlorides given in Table I all occur higher than the frequencies for benzenesulfonyl chloride and p-toluenesulfonyl chloride reported by McCall and Gutowsky.[4] Assignment of the higher frequency in p-chlorobenzenesulfonyl chloride to the chlorine on the ring is made on the basis of the chlorobenzene derivatives data of Meal[3] and the two values of McCall and Gutowsky.[4]

The triplet structure reported by Allen[5] for chloral hydrate also occurs in chloral alcoholate at approximately the same frequency but within a narrower frequency region and with quite different spacing.

Generally weak lines were encountered in hexachlorophenol and tetrachlorotetrahydronaphthalene. The investigation of these compounds will be continued with an externally-quenched spectrom-

eter now under construction, since the resolution of the present apparatus is limited by a spectrum of response apparently more complex in shape than that of the externally-quenched variety. Any gain in sensitivity will also be valuable.

The barium chlorate resonance frequency of Table I lies between the values reported for sodium chlorate[6,7] and potassium chlorate.[7]

Temperature dependence studies of these chlorine quadrupole resonance frequencies are now in progress in this laboratory.

We wish to thank the Rensselaer Polytechnic Institute Research Fund for a grant in aid which helped make this work possible.

[1] C. Dean, thesis, Harvard University (1952).
[2] H. G. Dehmelt and H. Kruger, Z. Physik **130**, 385 (1951).
[3] H. C. Meal, J. Am. Chem. Soc. **74**, 6121 (1952).
[4] D. W. McCall and H. S. Gutowsky, J. Chem. Phys. **21**, 1300 (1953).
[5] H. C. Allen, J. Am. Chem. Soc. **74**, 6074 (1952).
[6] R. Livingston, Science **118**, 61 (1953).
[7] Wang, Townes, Schawlow, and Holden, Phys. Rev. **86**, 809 (1952).

A Note on the Kinetics of Unitary Processes

STUART A. RICE*,†
Gibbs Memorial Laboratory, Harvard University, Cambridge, Massachusetts
(Received August 6, 1953)

BECAUSE of the physically significant relationships to which it leads, the theory described in this note is of interest. While it is logically complete, it is in reality only a statistical framework within which the elementary mechanisms remain unspecified. The detailed specification of a mechanism leads to an equation describing the individual process being investigated. As developed, the theory is general enough to include all unitary or stepwise processes. It is then possible to regard each unitary process as a special case of a more general phenomenon. The approach presented here emphasizes the fundamental physical similarities and clearly shows the assumptions inherent in each individual treatment.

In all the systems considered, the primary process is assumed to consist of the transition of a particle or particles from one set of states to another, i.e., the addition or loss of single molecules.

The time scale is defined such that only one transition occurs between two adjacent states during a unit-time interval. That is, the probability of one transition is proportional to Δt, while that of two transitions is proportional to $(\Delta t)^2$ and hence negligible. A system is said to be in state E_s, the exact meaning of which varies from problem to problem. For example, in adsorption we take the state E_s as that state of the system when s atoms (molecules) have been adsorbed. We postulate the following:

(1) Only transitions to adjacent states are allowed. (2) The probability that the system in state E_s undergoes the transition $E_s \rightarrow E_{s+1}$ in the time interval Δt is $k_s \Delta t$. (3) The probability that the system in the state E_s undergoes the transition, $E_s \rightarrow E_{s-1}$, in the time interval Δt is $l_s \Delta t$.

At the time $t+\Delta t$, the system can be in state E_s only if (1) the system was in E_s at time t and no transition occurred in Δt, (2) the system was in E_{s-1} at time t and the transition $E_{s-1} \rightarrow E_s$ occurred in Δt, and (3) the system was in E_{s+1} at time t and the transition $E_{s+1} \rightarrow E_s$ occurred in Δt.

These are mutually exclusive, so the probabilities are additive,

$$C_s(t+\Delta t) = \{1 - k_s \Delta t - l_s \Delta t\} C_s + k_{s-1} \Delta t C_{s-1} + l_{s+1} \Delta t C_{s+1} \quad (1)$$

$$\lim_{\Delta t \to 0} \frac{C_s(t+\Delta t) - C_s(t)}{\Delta t} = \frac{\partial C_s}{\partial t} = -(k_s + l_s) C_s + k_{s-1} C_{s-1} + l_{s+1} C_{s+1}, \quad (2)$$

where the C_s, C_{s-1}, C_{s+1} are the probabilities of finding states E_s, E_{s-1}, E_{s+1}. This is the basic expression from which all the kinetic equations can be derived.

To show that this equation yields familiar results in the mean we will treat two simple cases.

(a) Kinetics of monolayer adsorption at gas/solid interfaces.

Let the state E_s refer to the physical situation when there are s adsorbed atoms (molecules), and let there be a total of N sites for adsorption. Then, neglecting interactions between particles,

$$k_s = (N-s)k_0; \quad l_s = s l_0,$$

where the k_0 contains a concentration term. Equation (2) now reads

$$\frac{\partial C_s}{\partial t} = -\{(N-s)k_0 + s l_0\} C_s + k_0 (N-s+1) C_{s-1} + (s+1) l_0 C_{s+1},$$

giving for the mean

$$\frac{d\langle s \rangle}{dt} = \Sigma [N k_0 - (k_0 + l_0) s] C_s; \quad \langle s \rangle = \frac{N k_0}{k_0 + l_0} (1 - e^{-(k_0 + l_0)t}),$$

when $k_0 = k_0' n$ is treated as a constant. Dole[1] has fitted the rate of adsorption of phosgene and chloropicrin to the equation

$$\frac{\partial n}{\partial t} = kc(N-n).$$

This is identical with the equation obtained if l_s and l_{s+1} are zero. Using this assumption,

$$\frac{d\langle s \rangle}{dt} = \Sigma (N k_0 - k_0 s) C_s = k_0' n (N - \langle s \rangle).$$

Using similar assumptions ($k_s = k_{s-1} = 0$) for the rate of desorption

$$\frac{d\langle s \rangle}{dt} = -l_0 \langle s \rangle.$$

This is known to fit the data over a reasonably wide range.[2]

(b) Rate of uptake of dyes by proteins.

Neglecting the rate of loss of dye from the protein and assuming that there is a great excess of dye in the solution,

$$\frac{\partial C_s}{\partial t} = -k_s C_s + k_{s-1} C_{s-1}; \quad k_s = k_0,$$

and

$$C_s = \frac{(k_0 t)^{s-1}}{(s-1)!} e^{-k_0 t}.$$

The mean is

$$\langle s \rangle = e^{k_0 t} - 1.$$

This example is formally identical with ethylene oxide-dibasic acid polymerizations and has been verified in that case.[3]

By suitable choice of the propagative and degradative constants, many other systems can be treated, i.e., adsorption at liquid/liquid interfaces, plastic deformation, etc.

The author wishes to thank Professor W. E. Moffitt and Dr. M. Goldstein for many valuable discussions and Professor P. M. Doty for reading the manuscript.

* Supported in part by a fellowship from the Carbide and Carbon Corporation.
† National Science Foundation Fellow, 1952–1953.
[1] M. Dole, J. Chem. Phys. **15**, 447 (1947).
[2] See, for example, D. D. Eley, Trans. Faraday Soc. **49**, 643 (1953).
[3] H. Mark, *The Chemistry of Large Molecules* (Interscience Publishers, Inc., New York, 1943).

Hyperfine Splittings in the Paramagnetic Resonances of Free Radicals*

S. I. WEISSMAN, J. TOWNSEND, DONALD E. PAUL, AND G. E. PAKE
Washington University, St. Louis, Missouri
(Received September 23, 1953)

WE record here several instances, not yet described in the literature, of hyperfine splitting in the paramagnetic resonances of free radicals. The resonances were observed in liquid solutions at concentrations of less than 10^{-3} molar. The observations were made at 9000 mc at fields close to 3200 oersteds.

TABLE I. Hyperfine patterns of free radicals.

Radical	Solvent	Number of components	Interval, oersteds
Naphthalene negative ion	Tetrahydrofuran	19	1.6
Difluorenyl nitrogen	Benzene	10	0.9
Wurster's blue ion	Water (heavy or light)	33	7.4 between centers of triplets; 2.1 between members of each triplet
Sodium trimesitylboron	Tetrahydrofuran	4	14

* Assisted by the joint program of the U. S. Office of Naval Research and U. S. Atomic Energy Commission.

The compounds, solvents, number of resolved hyperfine components, and the intervals, in oersteds, between components are given in Table I.

Reproductions of the spectra of Wurster's blue ion, naphthalene negative ion, and trimesitylboron negative ion are shown in Fig. 1.

We give no interpretation of the results at this time except to remark that the splittings in the cases of naphthalene negative ion and difluorenyl nitrogen require that the wave function of the odd electron must not vanish at the positions of some of the protons. In strictly planar, rigid molecules, this could occur only through admixture of highly excited configurations. It is possible that the zero-point vibrations of the protons are large enough to yield the observed effects.

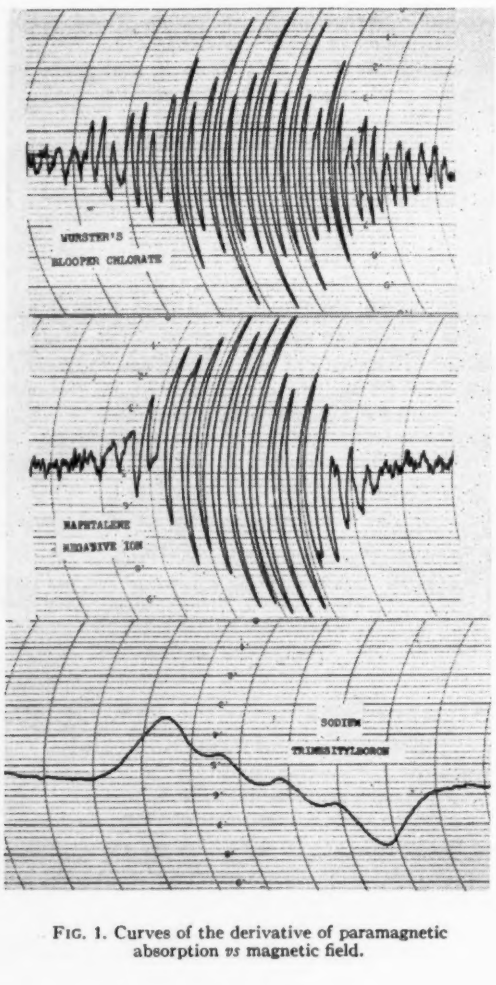

FIG. 1. Curves of the derivative of paramagnetic absorption *vs* magnetic field.

In the case of the boron free radical, the four peaks unquestionably arise from the interaction of the unpaired electron with the B^{11}, spin $\frac{3}{2}$ nucleus. Only a small admixture ($\sim$1 percent) of boron 2*s* wave function into the odd-electron function is required.

We are indebted to Professor H. C. Brown for the suggestion that the trimesitylboron negative ion would be a free radical and for furnishing us with a supply of trimesitylboron.

On the Theory of Reaction Rates

PETER T. LANDSBERG

*Randal Morgan Laboratory of Physics, University of Pennsylvania, Philadelphia, Pennsylvania.**

(Received September 28, 1953)

IN a recent paper[1] Eyring and Wallenstein dealt with some saturation phenomena in physics and chemistry by considerations which are based on reaction rate theory. We wish to point out that an amendment of their argument enables one to put their basic result into a form which is very similar to (but possibly more flexible than) a theory, based on phase-space considerations, which was put forward many years ago by Brillouin.[2] Indeed, where the two theories overlap they can yield formally identical results. It may be of interest to demonstrate this.

Eyring and Wallenstein considered a group of ω_i sites which contain n_i distinguishable units (atoms or molecules, etc.), while there are n_s free units which are in a gas-like state in a volume V. A site is saturated by d units, and the probability of a site being saturated is p. If a site contains ν units ($\nu<d$) it is assumed† that it presents $1+\nu$ "points of attachment" for a free unit; if $\nu=d$, it offers no such points. If K_i be the specific rate constant for the dissociation of a site and an adsorbed unit, and if K_s be the corresponding constant for the reverse process, then Eyring and Wallenstein showed that for equilibrium

$$K_i n_i=[\omega_i+n_i-\rho\omega_i(d+1)]K_s n_s. \tag{1}$$

Some cases of interest are specified by (*i*) $d=1$, $p=n_i/\omega_i$; (*ii*) $d=\infty$, $\rho=0$; and (*iii*) $\omega_i\gg n_i-\rho\omega_i(d+1)$, and were shown by these authors to lead to adsorption isotherms, quantum statistical distribution laws and the like.

(It should be observed that the term in p cannot be supposed to disappear in case (*ii*), as assumed by Eyring and Wallenstein, unless p behaves like $d^{-\alpha}(\alpha>1)$ for large d, or a similar assumption is made.)

One may replace the assumption that a site can saturate, and that a unit in a site can generate new sites, by a more general requirement. If a unit does not react at all with a site on which it is "adsorbed," then it will neither use up a site nor generate a new one, and (1) assumes the form which it has in case (iii), i.e., $K_i n_i=\omega_i K_s n_s$. The effect of interaction may be expressed by substituting for the ω_i sites, which are available to the free units in the absence of interaction, a quantity $\omega_i-F_i(\omega_i, n_i)$, where the function F_i may be positive or negative. This result is quite general. If one assumes

$$F_i(\omega_i, n_i)=B_i(\omega_i)n_i, \tag{2}$$

one finds

$$n_i=\omega_i/(a_i+B_i), \tag{3}$$

where $a_i\equiv K_i/K_s n_s$. Eyring and Wallenstein showed that a_i can be interpreted as $\exp[(\epsilon_i-\mu)/KT]$ for a Fermi-Dirac or a Bose-Einstein gas, where μ is the chemical potential per unit, and ϵ_i is the energy of the process (1).

On the other hand, with the notation (3), Brillouin's results may be written as

$$n_i=\omega_i/(a_i+b_i), \tag{4}$$

where b_i is defined by the requirement that the ratio of the volume of phase space available to the rth particle in the ω_i states to that available to the $(r+1)$th particle is $[\omega_i-(r-1)b_i]/$

$[\omega_i - rb_i]$. Thus the interaction characteristics B_i and b_i play analogous roles in both treatments. To appreciate their physical significance, it is essential to realize that if they are positive, there is an effective repulsion between the units condensed on the ith group of sites and the free units, while there is an effective attraction if they are negative.

Suppose now that the interaction function $F_i(\omega_i, n_i)$ is no longer given by (2), but is kept general, so that the parameter B_i disappears. Suppose also that the number of different ways of introducing n_i particles into the ω_i states of the ith group of energy levels is, in a generalization of Brillouin's treatment, $\omega_i^{n_i} - f_i(\omega_i, n_i)$ where f_i is the interaction term and is kept general. The function f_i, is then no longer expressed in terms of the additional parameter b_i, which also disappears. It is now easy to show that both treatments (reaction rate theory and statistical mechanics) give the same results for the equilibrium distributions, whatever the detailed mode of interaction, provided only $n_i \gg 1$, and the functions F_i, f_i are related by

$$\log[\omega_i^{n_i} - f_i(\omega_i, n_i)] = \int_0^{n_i} \log[\omega_i - F_i(\omega_i, x)]dx. \qquad (5)$$

Thus, if $F_i \equiv 0$, then $f_i \equiv 0$; but if F_i is nonzero and independent of n_i, then f_i has the same sign as F_i, though it may depend on n_i according to the equation

$$f_i(\omega_i, n_i) = \omega_i^{n_i}\{1 - \exp[-n_i F_i(\omega_i)]\}.$$

* On leave of absence from the University of Aberdeen, Scotland.
[1] H. Eyring and M. Wallenstein, Proc. Nat. Acad. Sci. **39**, 138 (1953).
[2] L. Brillouin, Compt rend. **184**, 589 (1927); Ann. Phys. **7**, 315 (1927); *Die Quantenstatiskik* (Springer, Berlin, 1931), p. 165 *ff.*
† Eyring and Wallenstein attempt to establish this result, but it appears preferable to us to regard it as an additional assumption.

A Method for Determining the Quantum Yields of Reactions Initiated by Mercury-6($^1P_1$)-Atoms*

R. A. Uphaus and H. E. Gunning
Department of Chemistry, Illinois Institute of Technology, Chicago, Illinois
(Received September 23, 1953)

If a mixture of mercury vapor and a foreign gas is exposed to the radiation of a quartz mercury resonance tube, Hg 6($^1P_1$) and Hg 6($^3P_1$) atoms are formed, respectively, by the 1849A and 2537A resonance lines present in the incident beam. A major experimental difficulty in the study of reactions photosensitized by Hg 6($^1P_1$) atoms alone is the prevention of simultaneous excitation of the mercury to the 6($^3P_1$) state. The present communication outlines one preliminary approach to the problem wherein advantage is taken of the fact that mercury vapor has a much higher absorption coefficient for the 1849A line than for the 2537A line.

The U-shaped immersion source has been previously described.[1] The 45/50 male joint of the lamp fitted into the matching female joint of the test-tube shaped Pyrex reaction cell. One stopcock connected the reactor to the high-vacuum manifold, while another led to a finger trap containing liquid mercury.

Propane was chosen as the foreign gas since its reaction with Hg 6($^3P_1$) atoms is quite well understood.[2,3] In each run the cell was filled with 100 mm of Phillips Research Grade Propane. The partial pressure of mercury vapor in the cell was varied by changing the temperature, T_{Hg}, of the liquid mercury in the finger trap.

The fraction of 1849A radiation, A_1 and of 2537A radiation, A_3, absorbed in a path length of l cm by a given concentration of mercury atoms in the presence of a known pressure of foreign gas can be calculated by familiar methods, provided the effective cross section for Lorentz broadening, σ_L^2, of the foreign gas is known.[4]

For our system, $l = 0.85$ cm, $\sigma_L^2 = 73.5 \times 10^{-16}$ cm^2 from reference 4, and X, the ratio of emission to absorption line breadths was taken as 1.5. The integrations were performed graphically. Some of the calculated values of A_1 and A_3 obtained are given in Table I,

Table I.

T_{Hg} °C	A_1	A_3
−20	0.18	0
−10	0.43	0.07
0	1.00	0.20
10	1.00	0.47
20	1.00	0.77
30	1.00	0.97

expressed as functions of the temperature T_{Hg} of the finger trap which controlled the partial pressure of mercury in the absorbing system. It is seen that for T_{Hg} values from 0°C to 30°C the 1849A line is completely absorbed, whereas 2537A absorption varies from 20 percent to 97 percent.

In each run the average rate of hydrogen production, R_{H_2}, was determined. Under our conditions the following relation should apply:

$$R_{H_2} = A_1 \cdot I_1 \cdot Q_1 + A_3 \cdot I_3 \cdot Q_3,$$

where I_1 and I_3 represent, respectively, the total emitted intensities of the 1849A and 2537A radiation, from the lamp, and the Q's the quantum yields of hydrogen formation in the Hg 6($^1P_1$) and Hg 6($^3P_1$) reactions.

R_{H_2} was measured for T_{Hg} values from 0°C to 30°C. A plot of R_{H_2} *vs* A_3 yielded, by linear extrapolation, $A_1 I_1 Q_1 = 3.8 \times 10^{-6}$ moles/min, at $A_3 = 0$. Whence, since $A_1 = 1$, $I_1 \cdot Q_1 = 3.8 \times 10^{-6}$ moles/min. The 1849A output of the lamp, I_1, was determined on a separate system using the ammonia photolysis[5] as an actinometer. A value of I_1 of 1.0×10^{-5} einsteins/min was obtained. From the foregoing data, Q_1, the quantum yield of hydrogen formation in the reaction of propane with Hg 6($^1P_1$) atoms, is 0.38. For the corresponding reaction with Hg 6($^3P_1$) atoms Bywater and Steacie found Q_3 to be 0.46.[3]

The present communication was intended to illustrate our approach to the problem. A more detailed report of our experimental findings will be published at a later date.

* This work was supported by contract with the U. S. Atomic Energy Commission.
[1] A. Kahn and H. E. Gunning, J. Chem. Phys. **18**, 392 (1950).
[2] E. W. R. Steacie and D. J. Dewar, J. Chem. Phys. **8**, 571 (1940).
[3] S. Bywater and E. W. R. Steacie, J. Chem. Phys. **19**, 319 (1951).
[4] For details of the calculation see: A. C. G. Mitchell and M. W. Zemansky, *Resonance Radiation and Excited Atoms* (Cambridge University Press, Cambridge, 1934), Chap. IV. The symbolism of these authors is followed here.
[5] D. L. Kantro and H. E. Gunning (unpublished).

The Crystal Structure of the Normal Paraffin Hydrocarbons*

A. E. Smith
Shell Development Company, Emeryville, California
(Received October 1, 1953)

In the course of an electron diffraction examination of a series of pure-n-paraffin hydrocarbons, reflections were observed from a single crystal of n-$C_{23}H_{48}$ which are forbidden by the space group ($V_h^{16} = P_{nam}$), reported[1,2] for the low-temperature form of normal hydrocarbons with an odd number of carbon atoms. Since a series of very carefully purified n-hydrocarbons in the range n-$C_{18}H_{38}$ to n-$C_{30}H_{62}$ prepared by A. Schaerer and C. J. Busso[3] were available, it appeared worth while to re-examine their structures.

Single crystals of all the normal hydrocarbons with an odd number of carbon atoms from n-$C_{21}H_{44}$ to n-$C_{29}H_{60}$ were grown slowly from toluene solutions. Most of the crystals were thin plates; however, several acicular-shaped crystals of n-$C_{24}H_{50}$ suitable for complete structure determination were obtained. Mass spectrometric analysis[4] showed that all of these hydrocarbons except n-$C_{27}H_{56}$ (99.0 percent pure) were better than 99.5 percent pure. Single crystal rotation and 0–4th level Weissenberg patterns as well as precession patterns were taken with n-$C_{23}H_{48}$. Precession patterns alone were taken for n-$C_{21}H_{44}$, n-$C_{25}H_{52}$, n-$C_{27}H_{56}$, and

n-$C_{29}H_{60}$. Powder patterns were also taken in a long-spacing vacuum camera. The following extinctions (hkl) and (hko) present in all orders, (hol) only with $1=2n$, (okl) only with $k=2n$ lead to the space groups $P_{bcm}-D_2^{11}h$ or $Pbc2_1-C_{2v}^5$. Previous work of Müller[1] has fairly well established that the hydrocarbon molecules in the orthorhombic form are parallel to the c-axes. For normal hydrocarbons containing an odd number of carbon atoms the assumption that the molecules are parallel to the c-axis leads to symmetry elements consistent only with P_{bcm}.

A satisfactory structure was determined on the basis of P_{bcm} by trial and error using (hko) and (hol) data. Approximate x and y parameters were determined from the (hko) data using Bragg and Lipson charts.[5]

Since the mirror planes present in P_{bcm} at $c/4$ and $3(c/4)$ must pass through the centers of 12th carbon atoms of the n-$C_{23}H_{48}$ molecules, the Z coordinates of these atoms are fixed at these coordinates. The only other Z parameter, Z_1 is one-half the distance between alternate carbon atoms. From the measured value of $C_0=62.31$A and the observed intensities and those calculated for the (ool) reflections as a function of Z_1, the distance between the alternate carbon atoms can be quite accurately determined,[1] assuming all $c-c$ distances are alike. The magnitude of the (ool) structure factors were calculated from the Fourier transform of the n-tricosane molecule. From the ratio of the magnitude of the structure factors (F_{0050}/F_{0048}) and (F_{0046}/F_{0048}) calculated as a function of Z_1 and the observed intensities a value $Z_1=1.274_5$ is obtained. This gives a value of 2.549×0.004A for the distance between alternate carbon atoms in the hydrocarbon chain in good agreement with the value obtained by Müller.[1] It was necessary to include the contributions of the hydrogen atoms in the calculation of the structure factors. For some of the reflections the contributions of the hydrogen were as large or larger than those of the carbon atoms. Although (hol) reflections with 1 indexes up to 78 were observed, it was possible because of symmetry to make a Fourier projection on the basis of a pseudo-cell of length $C/2$. The (hol) electron density projection (Fig. 1) was evaluated at intervals of 1/120 and 1/60 of the cell edges in the $C_0/2$ and a dimensions, respectively. Within the limit of experimental error the $c-c$ bond distances appear to be equal. The projection gives a value 2.55_1A for the mean alternate carbon-carbon distance in agreement with that obtained from the high-order reflections. A decline in maximum electron density of the carbon atoms and an increasing overlapping of electron density between chains is indicated in the electron density projection. This may possibly be a vibrational effect but further refinement will be required to determine if the effect is real.

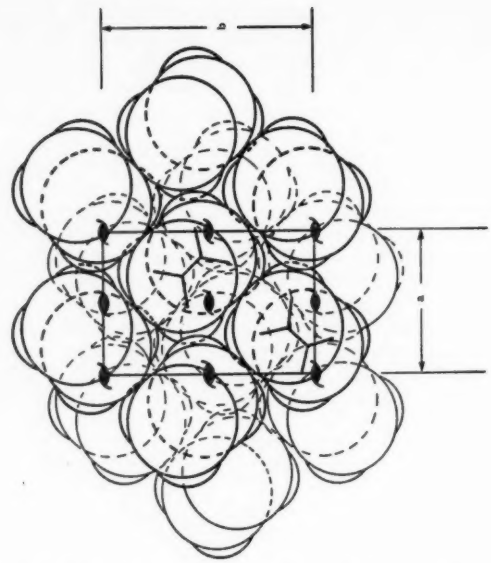

FIG. 2. Packing arrangement in n-$C_{23}H_{48}$ projection onto ab plane.

The packing arrangement for the n-hydrocarbons containing an odd number of carbon atoms is shown in Figs. 2 and 3(a) and (b). In Fig. 2 the hydrocarbon molecules are projected perpendicular to their long axis onto the ab plane. The lower layer of molecules are indicated by the lightly dotted outlines. In Figs. 3(a) and 3(b) the molecules are projected onto the ac and bc planes, respectively. The packing arrangement differs from that described by Müller[1] mainly in the relative translation of the upper and lower layers.

The approximate parameters and lattice constants are listed in Table I.

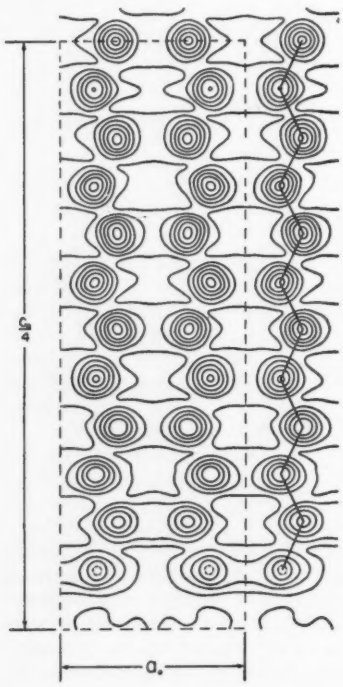

FIG. 1. n-$C_{23}H_{48}$ Fourier projection onto (010) plane contours at arbitrary intervals.

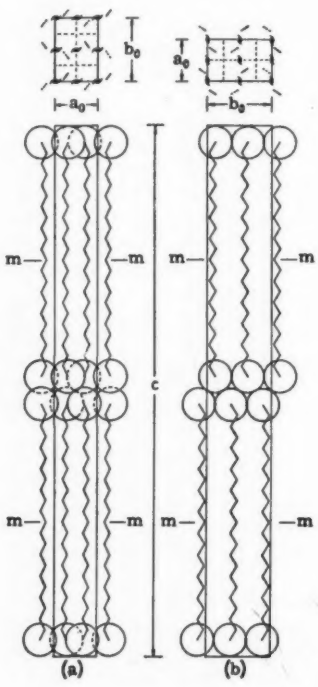

FIG. 3. Packing arrangement in n-tricosane (a) ac projection, (b) bc projection.

TABLE I.

n-$C_{23}H_{48}$	Space Group Pb cm	
$a_0=4.970\pm0.005$A	$b_0=7.478\pm0.005$A	$C_0=62.31\pm0.10$A
$x=0.250$	$Y_1=0.082$	$Z_1=\dfrac{1.275}{C_0}$

$=48°\pm5°$ = angle of inclination of plane of molecule to a axis.
Alternate carbon-carbon distance $=2.54_9$A.

	c_0
n-$C_{21}H_{44}$	57.30 ± 0.08A
n-$C_{25}H_{52}$	67.41 ± 0.10
n-$C_{27}H_{56}$	72.59 ± 0.10
n-$C_{29}H_{60}$	77.70 ± 0.18

Within the limit of experimental error these hydrocarbons have the same a_0 and b_0 dimensions.

Recently Müller and Lonsdale[6] and Mazee[7] have reported a triclinic form for n-$C_{18}H_{38}$ and n-$C_{24}H_{50}$ as the stable form at room temperature. Single crystals of the even numbered n-alkanes between n-$C_{18}H_{38}$ and n-$C_{30}H_{62}$ have been prepared and examined with x-rays. Normal $C_{20}H_{42}$ and n-$C_{22}H_{46}$ are also triclinic. Both a triclinic and a monoclinic form were observed with n-$C_{26}H_{54}$. The stable forms of n-$C_{28}H_{58}$ and n-$C_{30}H_{62}$ at room temperature are monoclinic, space group $P2_1/a$. The structure of the monoclinic form will be the subject of a separate note. The addition of a few percent of neighboring homologs to the triclinic and monoclinic forms observed with even numbered alkanes, converts them to an orthorhombic form. The presence of impurities undoubtedly accounts for some of the earlier reports[8,9] that even numbered n-alkanes in the range n-$C_{24}H_{46}$ to n-$C_{30}H_{62}$ were orthorhombic at room temperature.

A more detailed account of the structure of the n-hydrocarbons will appear later.

The author is indebted to Dr. A. Schaerer and C. J. Busso for supplying the very pure hydrocarbons and for many helpful discussions. He is also indebted to Miss L. B. Skinner and Mr. W. L. Birka for the preparation and measurement of most of the powder patterns.

* A preliminary account of this work was presented at the American Crystallographic Association Meeting at Camp Taminent, Pennsylvania, June, 1952.

[1] A. Müller, Proc. Roy. Soc. (London) **120**, 455 (1928).
[2] Wyckoff, *Crystal Structures* (Interscience Publishers, Inc., New York, 1951), Vol. II, XIIIc.
[3] A publication on the physical properties of these hydrocarbons is in press.
[4] M. J. O'Neal, Jr. and T. P. Wier, Jr., Anal. Chem. **23**, 880 (1951).
[5] W. L. Bragg and H. Lipson, Z. Kryst. **95**, 323 (1936).
[6] A. Müller and K. Lonsdale, Acta Cryst. **1**, 129–131 (1948).
[7] W. M. Mazee, Rec. trav. chim. **67**, 197–213 (1948).
[8] A. Müller, Proc. Roy. Soc. (London) **138**, 514–530 (1932).
[9] R. Kohlhass and K. H. Soremba, Z. Krist. **100**, 47 (1938).

Preliminary Work on the Microwave Spectrum of Acetic Acid

J. H. N. LOUBSER
National Physical Laboratory, Pretoria, Union of South Africa
(Received October 12, 1953)

THE absorption spectrum of acetic acid vapour at a pressure of 0.01 mm has been studied in the frequency range from 22 000 to 25 500 Mc/sec using a Stark modulation spectrometer with a 100 kc/s sine wave modulation. In Table I only the more intense observed lines are given together with an approximate estimate of their intensities. A limit to the complexity introduced into the observed spectra by excited vibrational states is set only by the available sensitivity of the spectrometer.

A resonator calibrated against the ammonia inversion lines was used for the frequency measurements, and the estimated accuracy of the listed frequencies is ±10 Mc/sec.

In an attempt to identify the lines in the observed spectrum the theoretical spectrum was calculated by assuming a probable structure of the molecule. The structure of the COOH radical is known from the infrared work done by Bauer and Badger[1,2] and Thompson[3] on formic acid. The structure determined by them

TABLE I. Measured spectrum.

Frequency Mc/sec	Relative intensity	Frequency Mc/sec	Relative intensity
		23 820	very weak
22 330	medium	23 870	medium
22 350	medium	24 010	weak
22 540	medium	24 330	very strong
22 610	medium	24 375	strong
22 695	strong	24 575	medium
22 970	medium	24 765	medium
23 130	weak	24 775	medium
23 135	weak	24 840	very weak
23 160	medium	24 875	very weak
23 175	weak	24 910	very weak
23 325	medium	24 945	strong
23 415	medium	24 970	medium
23 460	weak	25 190	weak
23 470	strong	25 325	weak
23 525	medium	25 400	weak
23 560	medium	25 445	weak

gives the following distances and angles of the planar COOH radical:

$$C=O=1.25\text{ A},\quad C-O=1.40\text{ A},\quad O-H=0.96\text{ A},$$
$$\text{Angle } O=C-O=123 \text{ and Angle } C-O-H=105.$$

Assuming for the C–C distance the usual value of 1.54 A and using the accepted CH_3 configuration, the calculated moments of inertia and rotational constants of CH_3COOH are:

$$I_A=75.83\times10^{-40}\text{ gm cm}^2 \qquad A=0.3691\text{ cm}^{-1}$$
$$I_B=96.36\times10^{-40}\text{ gm cm}^2 \qquad B=0.2904\text{ cm}^{-1}$$
$$I_C=166.95\times10^{-40}\text{ gm cm}^2 \qquad C=0.1676\text{ cm}^{-1}$$

and hence the asymmetry parameter $K=0.2192$ and $(A-C)/2=0.10175$ cm^{-1}. Since there is no component of dipole moment along the I_C axis, type "C" transitions are ruled out but both "A" and "C" type transitions are allowed as the molecule has no axis of symmetry. Calculations based on bond-moment considerations show that the component of the dipolement that lies in the axis of least moment of inertia (a axis) is equal to the component that lies in the axis of intermediate moment of inertia (b axis) within the accuracy of this rather approximate method. All the "strong" calculated lines given in Table II are, however, type "B" transitions so that if the aforementioned calculations are in error, their relative intensities are not affected. The calculated spectrum up to $J=10$, above which there seems very little likelihood of any further transitions occurring in this limited frequency range, consists of ten strong and medium lines and about nine very much weaker lines.

A reasonable fit of the four most intense calculated lines[4] which are all due to transitions with $\Delta J=0$, to the four strongest observed lines in their neighbourhood in the observed spectrum could be obtained by adjusting K to $K=0.22$ and $(A-C)/2$ to $(A-C)/2=0.1036$ cm^{-1}.

Thus assuming that the calculated rotational constants are not too far wrong a tentative assignment of four "strong" lines, one "medium," and one "weak" line could be made.

In Table II this very tentative assignment is given as well as observed and calculated relative intensities.[5]

$$K=0.22 \quad \text{and} \quad (A-C)/2=0.1036\text{ cm}^{-1}.$$

It was found impossible to fit the weaker calculated lines due to the $\Delta J=1$ transitions which fall in or near this region with any

TABLE II. Tentative assignment of strongest observed lines.

Observed frequency	Observed relative intensity	Transition	Calculated frequency	Calculated relative intensity
22 695 Mc/sec	strong	$3_0\rightarrow3_2$	22 725 Mc/sec	22
23 325	medium	$4_2\rightarrow4_4$	23 320	30
23 470	strong	$7_1\rightarrow7_3$	23 475	84
24 330	very strong	$8_0\rightarrow8_2$	24 335	100
24 375	strong	$7_{-1}\rightarrow7_1$	24 365	85
25 445	weak	$3_{-2}\rightarrow3_0$	25 460	20

reasonable certainty. They are the

$$1_0 \rightarrow 2_{-2}, \quad 1_0 \rightarrow 2_{-1}, \quad 1_{-1} \rightarrow 2_{-2}, \quad \text{and} \quad 1_{-1} \rightarrow 2_{-1}$$

lines in order of ascending relative intensity, from 20 to 33. Then there are still the much weaker (at least 100 times weaker than the above $\Delta J = 1$ lines) so-called "forbidden" lines $5_3 \rightarrow 6_{-4}$, $5_2 \rightarrow 6_{-3}$, $5_2 \rightarrow 6_{-4}$, and similar lines with higher values of J.

If, however, the observed strong line at 24 945 Mc/sec is assigned to the $1_{-1} \rightarrow 2_{-1}$ transition, which seems the most reasonable assignment, then the line at 22 540 Mc/sec of medium intensity is due to the $1_0 \rightarrow 2_{-1}$ transition, while the other two transitions fall below and above this frequency range. The calculated values of the rotational constants then assume the following values:

$$A = 0.3635 \text{ cm}^{-1}, \quad B = 0.2825 \text{ cm}^{-1}, \quad \text{and} \quad C = 0.1562 \text{ cm}^{-1}.$$

In order to check the accuracy of the rotational constants of formic acid and hence the configuration assigned to formic acid by Bauer and Badger, the theoretical microwave spectrum of formic acid was calculated using their constants and compared with the six known lines between 22 000 Mc/sec and 31 000 Mc/sec due to formic acid.[6] Six strong lines were found in and near this region but no accurate fit to the measured lines could be obtained even when each of the three rotational constants were alternately adjusted in steps up to and even above the 1 percent which they claim for the accuracy of their constants. This also proves that the configuration assigned to the HCOOH molecule must be out by a considerable amount.

Further work involving the Stark splitting of the strong lines in the acetic acid spectrum is to be undertaken together with a re-examination of the formic acid spectrum.

The author wishes to thank the Council for Scientific and Industrial Research of South Africa for permission to publish these results and to express his appreciation for the help of the members of the Electronics Section, Dr. J. C. R. Heydenrych, Mr. R. Holshausen, and Mr. W. W. Schroeder, who assisted him in the construction of the spectrometer.

Note added in proof.—It has subsequently come to the author's notice that the spectrum of formic acid has been re-examined [J. D. Rogers and D. Williams, Phys. Rev. **83**, 210 (1951)] and that the values found for the rotational constants A, B, and C differ by more than 5 percent in each case from the values determined by Bauer and Badger from the infrared data.

[1] S. H. Bauer and R. M. Badger, J. Chem. Phys. **5**, 825 (1937).
[2] G. Herzberg, *Infrared and Raman Spectra* (D. Van Nostrand Company, Inc., New York, 1945) pp. 321 and 437.
[3] H. W. Thompson, J. Chem. Phys. **7**, 453 (1939).
[4] King, Hainer, and Cross, J. Chem. Phys. **11**, 27 (1943).
[5] Cross, Hainer, and King, J. Chem. Phys. **12**, 210 (1944).
[6] Pietenpol, Rogers, and Williams, Phys. Rev. **78**, 480 (1950).

Carbon-14 Isotope Effect in the Exchange Reaction between Carbon Monoxide and Phosgene

D. R. STRANKS
Chemistry Department, University of Melbourne, Melbourne, Australia
(Received October 12, 1953)

EXPERIMENTAL values for C^{14} isotope effects in some unidirectional reactions appear to be larger than those predicted from statistical mechanical theory.[1] Whether this is due to experimental error, a shortcoming in the theoretical treatment, or to an inherent property of carbon-14 molecules is as yet undecided. To further investigate the position, work in this laboratory has been undertaken on the measurement of C^{14} exchange-equilibrium constants which have already been predicted from statistical mechanical calculations.[2] The theory of such exchange systems is rather more certain than the corresponding treatment of unidirectional reactions which requires a knowledge of the properties of activated complexes. Accordingly it is desired to report preliminary results for the exchange system:

$$C^{14}O + COCl_2 \rightleftharpoons C^{14}OCl_2 + CO.$$

C^{14}-labelled carbon monoxide was prepared by heating active barium carbonate with lead chloride at 400°C and then reducing the generated CO_2 with hot zinc at 410°C. Traces of CO_2 and oxygen (0.5 percent) were removed with solid potassium hydroxide and sodium mirrors, respectively. Phosgene was prepared by UV illumination of a carbon monoxide/chlorine mixture and purified by treatment with copper amalgam and repeated vacuum fractional distillation. Rates of exchange were measured by mixing $C^{14}O$ with inactive $COCl_2$, at known times freezing out the phosgene with liquid air and then measuring either the rate of disappearance of activity in the CO fraction or the rate of appearance of activity in the $COCl_2$ fraction. Identical rates of exchange have been found for the two alternative methods. To ensure that systematic instrumental errors were absent, the isotopic assays were performed by two independent techniques. In the first, both fractions were measured as CO in a quartz ionization chamber with an associated valve electrometer (the $COCl_2$ fraction being completely pyrolyzed to CO). In the second, after complete conversion of the CO fraction to $COCl_2$, the two fractions, as $COCl_2$, were frozen into CO_2-free sodium hydroxide, the resultant carbonate samples precipitated as barium carbonate and assayed with an end-window GM counter assembly.

At 10.0 C, a mixture of $C^{14}O$ (20 mm Hg), $COCl_2$ (88 mm) contained in a quartz vessel illuminated with a low-pressure Hg 2537 arc exhibits a half-time of exchange of 40 minutes. At 405°C in the dark, a mixture of $C^{14}O$ (14.5 mm), $COCl_2$ (15.0 mm), Cl_2 (24.5 mm) in a Pyrex vessel has a half-time of exchange of 360 minutes. Hence isotopic equilibrium concentrations have been measured under these experimental conditions after 10 half-times

TABLE I.

Temp. °C	Values of K IC	GC	Theoretical
10.0	1.118±0.015	1.120±0.012	1.116
405	1.010±0.016	1.007±0.014	1.011

have elapsed. Table I summarizes experimental values of the exchange equilibrium constant

$$K = \frac{[C^{14}OCl_2]}{[COCl_2]} \Big/ \frac{[C^{14}O]}{[CO]},$$

obtained by the ion-chamber (IC) and Geiger counter (GC) techniques compared to the theoretical statistical mechanical values. The "theoretical values" of K were calculated from isotopic partition function ratios already published.[2] [A computational error in these values was detected for the $\nu_6{}^{14}$ frequency of phosgene. The correct values of Q_{14}/Q_{12} for phosgene are: 1.3715 (273.16K), 1.3322 (293.16K), 1.2995 (313.16K).]

It is seen from Table I that the preliminary experimental values are in good agreement with the calculated values. More detailed experiments are now being conducted on the effect of such variables as temperature, radiation dose, and reactant concentrations on the value of K. The kinetics of both the photochemical and thermal exchanges are also under study.

The award of an I.C.I.A.N.Z. Research Fellowship by the University of Melbourne is gratefully acknowledged by the author.

[1] Yankwich, Stivers, and Nystrom, J. Chem. Phys. **20**, 344 (1952); Stevens, Pepper, and Lounsberry, J. Chem. Phys. **20**, 192 (1952); P. E. Yankwich and E. C. Stivers, J. Chem. Phys. **21**, 61 (1953).
[2] D. R. Stranks and G. M. Harris, J. Am. Chem. Soc. **75**, 2015 (1953).

Errata: Paramagnetism in a Thermochromic Compound

[J. Chem. Phys. **21**, 1619 (1953)]

WALTER G. NILSEN AND GEORGE K. FRAENKEL
Department of Chemistry, Columbia University, New York, New York

"Walter G. Nielsen" should be changed to "Walter G. Nilsen."

The word "energy" which appears as the eighth word in the next to the last line of the first paragraph should be deleted.

Production of Joshi Effect under High-Frequency Electric Discharge in Iodine Vapor

N. SUBRAHMANYAM AND N. A. RAMAIAH
Department of Chemistry, University of Delhi, Delhi, India
(Received October 13, 1953)

OCCURRENCE of positive and negative Joshi effects ($\pm\Delta i$) in a low-frequency (50 cycles/sec) electric discharge in H_2O or I_2 vapor, has been reported previously.[1] The present communication describes the studies of $\pm\Delta i$ in iodine vapor excited by potentials (V) of radio frequencies (0.1–10 megacycles/sec), on which no information exists in the literature. Iodine vapor was excited in cylindrical glass vessels fitted with external sleeve electrodes. Specially constructed Hartley type oscillators gave V of undamped oscillations; damped oscillatory potentials were obtained by spark circuits similar to those employed by Thomson and co-workers.[2] The structure of the discharge current was investigated by a cathode-ray oscillograph, and the rms value of the conductivity (i), measured by a sensitive galvanometer actuated by a diode. One typical series of results on potential variation of i and Δi is returned in Fig. 1. The range of potentials over which the studies were made in the self-maintained discharge,[3] could be divided into three regions: (a) the region in which the current in dark (i_D) increased markedly rapidly; (b) that in which i_D decreased initially; and (c) that in which i_D increased once more, with continuous raise of V (Fig. 1). This kind of variation of i with V, as mentioned elsewhere,[1] appeared to be a characteristic of low-pressure discharge and was noticed in air, Hg, and H_2O vapor $p<0.1$ mm Hg. In agreement with the observations of Knipp[4] and others,[5] the glow in the system at V corresponding to (a), was faint and intermittent occurring presumably when an avalanche was developed by an electron produced by any of the allowed secondary mechanisms[6] especially due to bombardment on the cathode by positive ions (γ) and photons ($\eta\theta g$ process).[3,6] In (b), the luminosity was intense and continuous, while in (c), it existed in the form of bright rings. The discharge in (a) was maintained[4,5] chiefly by γ and $\eta\theta g$ processes which were controlled by the applied electrostatic field. The region (c) was governed primarily by the self-magnetic field produced by ion currents; that is, the maintenance of the discharge in (c), as pointed out by Thomson,[2] did "not need the regenerative processes to renew the supply of electrons." The intermediate region (b) was controlled by both electrostatic and electromagnetic fields. It was interesting to note that negative Joshi effect, $-\Delta i$, corresponding to 55- to 60-percent current suppression (per curve marked $-\%\Delta i$, Fig. 1) was detected in (a); this was followed by marked inhibition of large numbers of *pulses* forming the current trace (Fig. 2) which was distinct from that noticed in low-frequency electric discharge in I_2 vapor;[3] the frequency of the *pulses* which remained under light corresponded to 80 kilocycles/sec. $-\Delta i$ decreased progressively with V in (b) and was little in (c). Under damped oscillatory discharge which was chiefly electromagnetic in character,[2,4] $-\Delta i$ was negligible; only $+\Delta i$ could be observed. These results suggested, for the first time in this field of research, that $-\Delta i$ occurred preferentially in electrostatic and $+\Delta i$, in electromagnetic regions of a self-maintained discharge. Remarkably enough, when the ion current responsible for the electromagnetic field was reduced, $+\Delta i$ decreased and changed its sign to give negative effect, $-\Delta i$.

FIG. 2. Oscillograms representing the current structure in a high-frequency electric discharge in iodine vapor. (25 volts of 3.20 megacycles/sec.)

The details of this investigation will appear elsewhere.

Grateful thanks are due Professor Joshi for suggesting the problem and for his kind interest in our work.

[1] Ramaiah, Bhatawdekar, and Subrahmanyam, J. Chem. Phys. **21**, 1160 (1953).
[2] Thomson, *Conduction of Electricity through Gases* (Cambridge University Press, Cambridge, 1933), vol. 2; Phil. Mag. **4**, 1128 (1927); Proc. Phys. Soc. (London) **40**, 79 (1928).
[3] Saxena, Bhatawdekar, and Ramaiah, J. Chem. Phys. **21**, 365 (1953); Dogra, Bhatawdekar, and Ramaiah, Proc. Phys. Soc. (London) **66**, 431 (1953).
[4] Kipp, Phys. Rev. **37**, 756 (1931).
[5] Varnold, Phil. Mag. **13**, 1179 (1932); **15**, 294 (1933); Roig, Compt. rend. **204**, 961 (1937); Townsend and Gill, Phil. Mag., **26**, 290 (1938).
[6] Loeb, *Fundamental Processes of Electrical Discharge in Gases* (John Wiley and Sons, Inc., New York, 1939); Revs. Modern Phys. **8**, 267 (1936); Phys. Rev. **76**, 255 (1949).

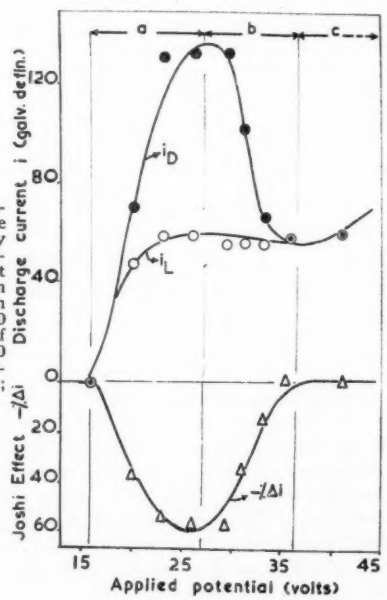

FIG. 1. Potential variation of Joshi effect in iodine vapor under high-frequency electric discharge. (i_D = current in dark; i_L = current when the excited system was exposed to light from 200 watt bulb; $-\%\Delta i = 100(i_D - i_L)/i_D$; frequency of exciting potential = 3.20 Mc/sec of undamped nature; $p_{I_2} = 0.04$ mm·Hg; 28°C).

Mass Spectral Investigation of "Active" Nitrogen

D. S. JACKSON AND H. I. SCHIFF
Department of Chemistry, McGill University, Montreal, Canada
(Received October 12, 1953)

ALTHOUGH much speculation has been made regarding the composition of "active" nitrogen, no experimental determination has yet been reported. A study of the nitrogen afterglow was therefore undertaken with the aid of a mass spectrometer. Purified nitrogen was passed through a discharge tube at a pressure of approximately 1 mm Hg and at a flow rate of 1.03×10^{-5} moles/sec. The walls of the discharge tube and the glass tubing leading to the mass spectrometer were "poisoned" with metaphosphoric acid. The nitrogen was subjected to a condensed discharge by means of an electrical circuit similar to that described by Greenblatt and Winkler.[1] From the discharge tube the gas was pumped through a conventional diffusion and rotary pump assembly. At a distance of 50 cm from the discharge tube a small central portion of the gas stream was continuously sampled into the mass spectrometer through a leak, 30 microns in diameter and 10 microns in length, made in a quartz thimble. The leak and sampling system were similar to those used by Tickner and Lossing in the detection of free radicals.[2] An electron energy of 50 electron volts was used in the ion source of the mass spectrometer.

When the discharge tube was excited the ion intensity corresponding to mass 28 was found to decrease while the intensity for mass 14 increased, suggesting the presence of atomic nitrogen. Values of the ratios of the ion intensities for mass 28 and 14 are shown in Table I for various values of nitrogen pressure and elec-

TABLE I.

Pressure mm Hg	Electron energy ev	Mass 28/14 ratio no discharge	Mass 28/14 ratio discharge on
1.03	70	24.5	18.5
1.03	50	26.0	23.8
1.03	40	38.9	26.8
1.03	30	44.5	31.1
1.03	20	168.8	81.0
0.64	50	27.5	24.6
1.09	50	25.9	23.6
1.45	50	24.2	22.2
1.70	50	23.3	22.0
2.24	50	21.4	19.8

tron energy. No additional peaks were found when the discharge tube was excited (such as 42 corresponding to N_3).

Preliminary measurements were made of the ion intensities as a function of electron energy both with and without the discharge. The normalized curves for mass 28 were superimposed thus giving no indication of the presence of excited nitrogen molecules. The curve obtained for mass 14 when the discharge tube was excited was displaced toward lower electron energies relative to the curve obtained without discharge. This again suggests the presence of atomic nitrogen although the actual value of the appearance potential for the mass 14 peak must first be made before positive identification can be made. Work along this line is now in progress and a full report will be published shortly.

The authors would like to thank the Canadian Industries Limited for the granting of an award to one of us (D. S. J.).

[1] J. Greenblatt and C. A. Winkler, Can. J. Research **B27**, 721 (1949).
[2] A. W. Tickner and F. P. Lossing, J. Chem. Phys. **20**, 907 (1952).

An Additive Function of Critical Constants

SHASHANKA SHEKHAR MITRA
Department of Physics, Allahabad University, Allahabad, India
(Received September 28, 1953)

IF T_c and P_c be the critical temperature and pressure, in °K and in atmospheres, respectively, it is found that the function

$$K=\frac{100n}{\log(T_c^2/P_c)},$$

where n is the number of carbon atoms in a normal paraffin, is additive for the homologous series. The observed data[1] are well fitted in the formula

$$K_n=32.77+20.06n.$$

The observed and calculated values of K are given in Table I. The agreement is fairly good (in most of the cases error is <1 per cent) except for the first few members, which is usually the case with the normal hydrocarbons. The mean value of K for the addition of a (CH_2) group is found to be 20.06. Substituting van der Waals' values of T_c, P_c in the K function we notice that $n/[\log(64/27R^2a)]$ is additive for the successive members.

TABLE I.

No. of C atoms	Paraffins	T_c in °K	P_c in atmos	K obs.	K calc.
1	Methane	190.7	45.8	34.48	52.83
2	Ethane	305.3	48.8	60.96	72.89
3	Propane	368.8	43.0	85.71	92.95
4	Butane	426.2	36.0	108.04	113.01
5	Pentane	470.4	33.04	130.70	133.07
6	Hexane	508.0	29.63	152.28	153.13
7	Heptane	540.0	26.89	173.46	173.19
8	Octane	569.4	24.66	194.24	193.25
9	Nonane	595.4	22.86	214.83	213.31
10	Decane	619.3	21.24	234.90	233.37
11	Undecane	642.6	19.92	254.87	253.43
12	Dodecane	663.8	18.59	274.20	273.49
13	Tridecane	683.2	17.55	293.67	293.55
14	Tetradecane	701.0	16.56	313.04	313.61
15	Pentadecane	717.6	15.75	332.25	333.67
16	Hexadecane	734.3	15.10	351.52	353.73
17	Heptadecane	749.3	14.41	370.43	373.79
18	Octadecane	763.2	13.83	389.34	393.85
19	Nonadecane	776.0	13.43	408.50	413.91

The author thanks Dr. K. Mazumdar for his guidance.

[1] Data are taken from Landolt-Bornstein, Taballen, and Hodgman's *Handbook of Chemistry and Physics.*

The Electronic Structure and Polarity of the Water Molecule

J. A. POPLE
Department of Theoretical Chemistry, University of Cambridge, England
(Received September 29, 1953)

EARLY theories of the structure of the water molecule[1,2] supposed that one lone pair of electrons occupied the $2s$ atomic orbital of oxygen and the other the $2p$ orbital with a node in the nuclear plane. The polarity of the molecule was then interpreted as arising from the unequal sharing of bonding electrons between the hydrogen $1s$ and other oxygen $2p$ functions. Later work[3-6] has indicated, however, that the lone pairs may be better described by hybridized atomic orbitals, forced to project out at the back of the molecule by the operation of the exclusion principle. Electrons in such directed lone pair orbitals will make a large and possibly dominant contribution to the dipole moment. Recently, Ellison and Shull[7] have obtained a set of self-consistent molecular orbitals for H_2O, expressed as linear combinations of given atomic orbitals. The purpose of the present note is to find out whether this more refined calculation supports the concept of directed lone pairs.

Ellison and Shull[7] have obtained the molecular orbitals given in Table I. The positive z axis bisects the H—O—H angle and the x axis is perpendicular to the nuclear plane. Although these orbitals are important in any discussion of spectroscopic processes such as ionization,[8] they are not altogether suitable for a discussion of the electronic structure of the ground state. As is well known,[9] an equivalent description is given by any set of orbitals obtained by a unitary transformation of the molecular orbitals. These degrees of freedom may be used to localize two of the a_1 orbitals on the oxygen atom. The set of localized symmetry orbitals given in Table II is deduced in this way.

TABLE I. Molecular orbitals for the ground state of H_2O.

$$1a_1=-0.0024[h_1(1s)+h_2(1s)]+1.0002(1s)+0.0163(2s)+0.0024(2pz)$$
$$2a_1=0.125[h_1(1s)+h_2(1s)]-0.029(1s)+0.845(2s)+0.133(2pz)$$
$$3a_1=0.237[h_1(1s)+h_2(1s)]-0.026(1s)-0.461(2s)+0.827(2pz)$$
$$1b_2=0.548[h_1(1s)-h_2(1s)]+0.533(2py)$$
$$1b_1=(2px)$$

TABLE II. Localized symmetry orbitals for the ground state of H_2O.

$1a_1'=$	$1.000(1s)+0.016(2s)+0.009(2pz)$	inner shell
$2a_1'=$	$-0.013(1s)+0.962(2s)-0.269(2pz)$	lone pair
$3a_1'=0.269[h_1(1s)+h_2(1s)]$	$-0.046(1s)-0.012(2s)+0.793(2pz)$	bonding
$1b_2=0.548[h_1(1s)-h_2(1s)]+0.543(2py)$		bonding
$1b_1=(2px)$		lone pair

The advantage of the second set of orbitals over those of Table I is that the orbitals $1a_1'$, $2a_1'$, $3a_1'$, may be said to represent the inner shell, the a_1 lone pair and the a_1 bonding orbital, respectively, whereas both $2a_1$ and $3a_1$ appear to be partly bonding. It is evident that the lone-pair orbital $2a_1'$ is mainly s-like in character, but the coefficient of $(2pz)$ is large enough for the hybrid to be appreciably directed in the negative z direction. The dipole moment (about the O nucleus) of two electrons in this orbital is $1.67D$. As the other lone-pair orbital $(1b_1)$ has no moment, this represents

the contribution of lone-pair electrons to the total dipole moment. It is rather smaller than the previous estimate of Duncan and Pople,[6] but is still greater than the calculated total moment of the molecule (1.51D). The bonding orbitals $3a_1'$ and $1b_2$ are formed mainly from $2p$ and $h(1s)$ orbitals and give rise to a dipole moment about the oxygen nucleus which is almost exactly cancelled by the contribution of the protons.

[1] J. H. Van Vleck and P. C. Cross, J. Chem. Phys. **1**, 357 (1934).
[2] L. Pauling, *The Nature of the Chemical Bond* (Cornell University Press, Ithaca, 1939).
[3] J. E. Lennard-Jones and J. A. Pople, Proc. Roy. Soc. (London) **A202**, 166 (1950).
[4] J. A. Pople, Proc. Roy. Soc. (London) **A202**, 323 (1950).
[5] C. A. Coulson, Proc. Roy. Soc. (London) **A207**, 63 (1951).
[6] A. B. F. Duncan and J. A. Pople, Trans. Faraday Soc. **49**, 217 (1953).
[7] F. O. Ellison and H. Shull, J. Chem. Phys. **21**, 1420 (1953).
[8] G. G. Hall and J. E. Lennard-Jones, Proc. Roy. Soc. (London) **A202**, 155 (1950).
[9] J. E. Lennard-Jones, Proc. Roy. Soc. (London) **A198**, 1 (1949).

Critical Temperature and Boiling Point of Normal Paraffins

YATENDRA PAL VARSHNI
Department of Physics, Allahabad University, Allahabad, India
(Received September 28, 1953)

SEVERAL relations have been suggested connecting the critical temperature (T_c) and boiling point (T_b). Perhaps the best known among them is the Guldberg-Guye rule[1] which states:

$$T_b=\tfrac{2}{3}T_c. \tag{1}$$

The rule is only approximate. Even in homologous series T_b/T_c may vary from 0.58 for the initial to 0.70 for the final members. There are other relations due to Prud'homme,[2] Livingstone,[3] Jatkar and Lakshminarayanan,[4] and others.

It is found that for the normal paraffins, a linear relation holds between the reciprocals of T_c and T_b, which may be expressed as

$$\frac{1}{T_c}=\frac{0.5405}{T_b}+0.0003937. \tag{2}$$

If either T_c or T_b is known, the other can be calculated. For T_c the equation becomes

$$T_c=\frac{T_b}{0.5405+0.0003937T_b}. \tag{3}$$

The observed and the calculated values of T_c are given in Table I.

The differences between the observed and the calculated values are less than 1 percent, in the majority of the cases less than 0.5 percent. These deviations can be due to the experimental errors in either T_c or T_b or both of them. Methane is known to depart from the regular behavior of the higher members.[5] However, for this relation there is excellent agreement between the observed and the calculated value, as if the anomalous factors "cancel out."

TABLE I.

No. of C atoms	Paraffin	T_b obs.	T_c obs.	T_c calc.
1	Methane	111.5	190.7	190.7
2	Ethane	184.7	305.3	301.1
3	Propane	230.9	368.8	365.6
4	Butane	272.6	426.2	420.9
5	Pentane	309.1	470.4	466.6
6	Hexane	342	508	506.5
7	Heptane	371.5	540	541.1
8	Octane	398.8	569.4	571.6
9	Nonane	423.8	595.4	599.1
10	Decane	447	619.3	623.5
11	Undecane	468.9	642.6	646.4
12	Dodecane	489.3	663.8	667
13	Tridecane	507	683.2	684.9
14	Tetradecane	525.5	701	702.8
15	Pentadecane	543.5	717.6	720.3
16	Hexadecane	560.5	734.3	736.3
17	Heptadecane	576	749.3	750.5
18	Octadecane	590	763.2	763.7
19	Nonadecane	603	776	775

The ratio T_b/T_c for the normal paraffins has been studied by Chen and Hu[6] and Corner.[7] Equation (2) yields

$$T_b/T_c=0.5405+0.0003937T_b. \tag{4}$$

The author is thankful to Dr. K. Majumdar and Dr. R. D. Tewari for their interest in the work.

[1] Guldberg, Z. physik. Chem. **5**, 374 (1890); Guye, Bull. soc. chim. **4**, 262 (1890); Stephenson, Chem. News **143**, 135 (1931).
[2] Prud'homme, J. chim. phys. **18**, 94 (1920).
[3] Livingstone, J. Phys. Chem. **46**, 340 (1942).
[4] Jatkar and Lakshminarayanan, J. Indian Inst. Sci. **A28**, 1 (1946).
[5] Egloff, Sherman, and Dull, J. Phys. Chem. **44**, 730 (1940); Varshni, J. Indian Chem. Soc. **28**, 535 (1951).
[6] Chen and Hu, J. Chinese Chem. Soc. **10**, 208, 212 (1943).
[7] Corner, Trans. Faraday Soc. **41**, 617 (1945); Proc. Cambridge Phil. Soc. **42**, 328 (1946).

Rates of Chemical Reactions Near Equilibrium

BRUNO J. ZWOLINSKI, *Stanford Research Institute, Menlo Park, California*
AND
RUDOLPH J. MARCUS, *University of Utah, Salt Lake City, Utah*
(Received September 28, 1953)

GILKERSON, Jones, and Gallup[1] have attempted to derive a relationship between kinetic and thermodynamic free energies for a chemical system approaching equilibrium based on the methodology of the theory of absolute rates of reaction. The following derivation is offered in the hope of clarifying the concepts of the attendant equilibria of the activated and final states of a chemical reacting system.

Assuming equilibria[2] for the activated states of the forward and reverse reactions in a nonideal bimolecular system,[3] the velocity of the forward reaction is

$$v_f=k_f^0c_Ac_B(\gamma_A\gamma_B/\gamma^{\pm}),$$

with a similar expression for the reverse reaction. For simplicity of the analysis, all chemical species are assumed to participate in the reactions to the first order. Invoking the principle of detailed balancing, the same activated state must be surmounted in both forward and reverse reactions. The over-all velocity of the kinetic system in its approach to thermodynamic equilibrium is given by

$$v=k_f^0c_Ac_B\frac{\gamma_A\gamma_B}{\gamma^{\pm}}-k_r^0c_Mc_N\frac{\gamma_M\gamma_N}{\gamma^{\pm}}.$$

Defining the activity quotient as

$$Q_a=\frac{a_Ma_N}{a_Aa_B}=\exp\left(\frac{\Delta F-\Delta F^0}{RT}\right),$$

and recalling that

$$k_f^0=k_r^0\exp\left(-\frac{\Delta F^0}{RT}\right),$$

our expression for the over-all velocity simplifies to

$$v=(a_Aa_B/\gamma^{\pm})k_f^0[1-\exp(\Delta F/RT)].$$

Near equilibrium where $\Delta F/RT\ll1$,

$$v\simeq-(a_Aa_B/\gamma^{\pm})k_f^0(\Delta F/RT),$$

and, since

$$k_f^0=k\frac{kT}{h}K_0^{\pm}=k\frac{kT}{h}\frac{a^{\pm}}{a_Aa_B},$$

the over-all velocity near equilibrium is given by

$$v\simeq-\frac{a^{\pm}k\Delta F}{\gamma^{\pm}hN}=-kc^{\pm}\frac{\Delta F}{hN}.$$

This is the basis for the statement usually made that this particular relationship between velocity and free energy will only hold very close to true equilibrium.

[1] Gilkerson, Jones, and Gallup, J. Chem. Phys. **20**, 1182 (1952).
[2] B. J. Zwolinski and H. Eyring, J. Am. Chem. Soc. **69**, 2702 (1947).
[3] K. J. Laidler and H. Eyring, Ann. N. Y. Acad. Sci. **39**, 303 (1940).

Electrical Conductivity of Chromia-Alumina Dehydrogenation Catalyst

P. B. Weisz, C. D. Prater, and K. D. Rittenhouse
Socony-Vacuum Laboratories, Paulsboro, New Jersey
(Received October 5, 1953)

RELATIONSHIPS may exist between catalytic and semiconductive properties of a solid catalyst.[1] In any event, the measurement of electrical properties must be considered a valuable tool in seeking an understanding[2] of its electronic or ionic structure.

We have studied the electrical properties of co-gelled chromia-alumina (30/70 percent) catalyst. Conductivities were measured by the four-electrode potential probe method to eliminate electrode contact resistance. (These were later found to be between one and two orders of magnitude larger than the bulk resistances.) The sign of the thermoelectric voltage was measured by two electrodes, introducing additional cooling on one and observing the resulting potential variation. We have succeeded in making electrical measurements and simultaneously measuring the reaction rate of the atmospheric pressure reaction: cyclohexane→benzene +hydrogen.

At a standard temperature of 480°C a stable, reproducible conductivity of about 3×10^{-6} ohm^{-1} cm^{-1} is obtained in oxygen (1 atmos), varying with temperature with a 1.8 ev activation energy.

The conductivity is dependent on oxygen partial pressure in the manner expected from a *P*-type stoichiometric semiconductor, as seen by the results of Fig. 1, curves *A* to *D*. Thermoelectric

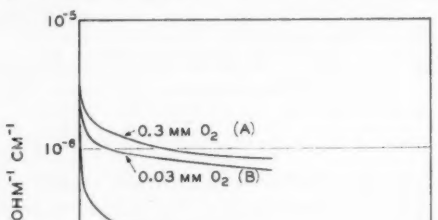

FIG. 1. Effect of oxygen partial pressure and of hydrogen and butane on electrical conductivity of chromia-alumina catalyst.

voltage measurements confirm *P*-typeness. This is in agreement with observations on Cr_2O_3 alone by Bevan, Shelton, and Anderson.[3]

The effect on conductivity of exposure of (oxygen-equilibriated) catalyst to hydrogen (curve *E*) and to butane (curve *F*) is shown in Fig. 1. The conductivity inversion obtained with butane suggests transition, through an intrinsic conductivity state, to *N*-typeness. Such conductivity inversion, apparently slow in hydrogen and faster with butane, becomes nearly instantaneous in contact with a hydrocarbon subject to high rates of catalytic dehydrogenation on the catalyst. The course of conductivity was measured before and during contact with cyclohexane at 1 atmos pressure (480°C). In Fig. 2 curve *A* shows the immeasurably rapid inversion on admission of cyclohexane followed by subsequent slow rise of electrical conductivity during the reaction cycle. Observation of thermoelectric voltage indicates *P*-typeness before and *N*-typeness immediately after contact with reactant, confirming the suspected transition.

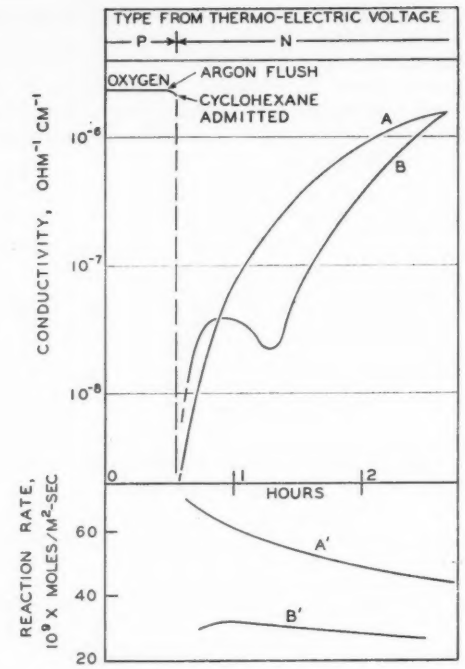

FIG. 2. Sign of thermoelectric voltage, electrical conductivity, and catalytic reaction rate of chromia-alumina during dehydrogenation of cyclohexane.

Simultaneously measured catalytic rate is shown in curve *A'* (Fig. 2). In many instances due to circumstances yet to be clarified, the conductivity has described a double "wiggle" as shown in *B*. In every such case the rate of reaction showed a maximum coinciding in time with the peak in conductivity.

The measurements demonstrate the importance of extending electrical measurements on semiconducting catalysts to include their actual chemical environment as catalysts. We conclude that chromia-alumina catalyst, ordinarily an oxygen excess semiconductor, has a finite concentration of Cr in the Cr^{4+} state. After contact with dehydrogenation reactant Cr^{2+} sites are formed in excess of any Cr^{4+} sites still existing. We propose that Cr^{4+} sites are changed to Cr^{3+} in the process of H_2 chemisorption and Cr^{2+} sites created on desorption of water.

In an article recently received, Chaplin, Chapman, and Griffith[4] report chromia-alumina catalyst to be an *N*-type semiconductor after 50 hours of hydrogen reduction at 500°C.

This work will be reported in greater detail at a later date.

[1] D. A. Dowden, J. Chem. Soc., 242 (1950).
[2] Garner, Gray, and Stone, Discussions Faraday Soc. **8**, 246 (1950).
[3] Bevan, Shelton, and Anderson, J. Chem. Soc., 1729 (1948).
[4] Chaplin, Chapman, and Griffith, Nature **172**, 77 (1953).

Electrical Conductivity of Hydrocarbon Cracking Catalyst

P. B. Weisz, C. D. Prater, and K. D. Rittenhouse
Socony-Vacuum Laboratories, Paulsboro, New Jersey
(Received October 5, 1953)

ELECTRICAL properties of silica-alumina and some other hydrocarbon cracking catalysts have been measured using techniques mentioned in the preceding letter.[1]

A thermoelectric voltage, positive for the cold electrode, was obtained at 500°C for all cracking catalysts tested. They included various laboratory prepared alumina- or magnesia-promoted silica bases and commercial synthetic silica-alumina (Socony-Vacuum Oil Company, Inc.) and natural clay-derived cracking catalyst (SR-Clay Catalyst, Filtrol Corporation).

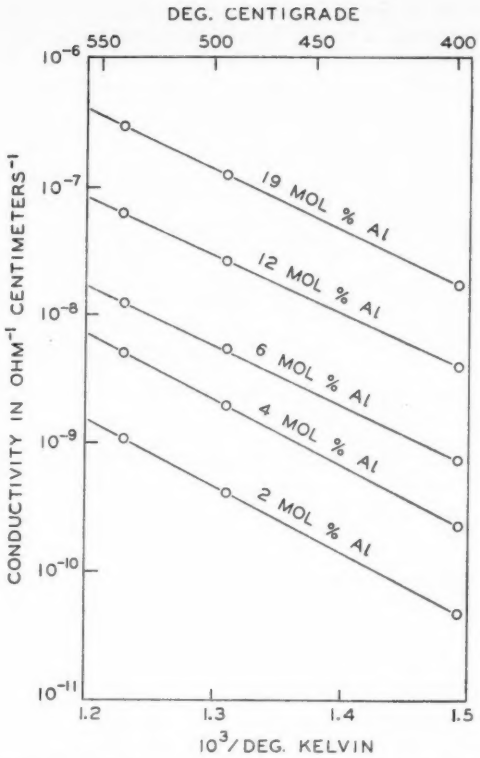

FIG. 1. Electrical conductivity *vs* temperature of a series of silica-alumina cracking catalysts.

At 420°C the electrical conductivity measured with the dc potential probe method is of the order of 10^{-6} to 10^{-11} ohms^{-1} cm^{-1} for typical catalyst samples. The conductivity was found to remain unchanged in air, hydrogen, or upon evacuation.

A series of silica-aluminas of varying promotor content (aluminum) was produced by co-gelation of sodium silicate and sodium aluminate. Figure 1 shows temperature plots of conductivity obtained on samples of this series. The conductivities increase—and have slopes corresponding to from about 1.1 ev to 0.88 ev activation energy—for samples of increasing Al content. Some polarization of the current electrodes has been observed; from a study of the decay of this potential, it is found that the charge responsible for this polarization is a small fraction only ($\sim 10^{-2}$) of the total current passed through the sample. No definite correlation of conductivity with concentration of impurities Fe, Ti, Mg, Cu, Na, and other minor impurities as analyzed by emission spectrography could be found. A sample of silica-alumina catalyst to which Cr was added in preparation to give 0.1 percent concentration (Cr_2O_3) had a conductivity by a factor of about 0.7 *lower* than that of catalyst without Cr addition. In an attempt to test for protons as charge carriers, we have base exchanged catalyst with aqueous NaCl to replace protons by Na ions. No appreciable change of conductivity was obtained after drying and calcining this catalyst.

Silica-alumina cracking catalyst is thus found to exhibit the behavior of an impurity semiconductor of the electron acceptor (*P*-) type. This behavior may arise from the incorporation of trivalent aluminum in the tetrahedral silica lattice—long presumed to be responsible for the "acidity" of the solid—creating the electron acceptor levels. Semiconductivity may then arise if the electron deficiency can be mobilized. The activation energy for ionizing the electron deficiency in a medium of dielectric constant $D=3.75$ (silica, International Critical Tables) calculates to $13.4/D^2=0.97$ ev, in good agreement with the experimental activation energy for conductivity. Studies of the bond structure of silica have indicated near or more than 50 percent valence (homopolar) bonding.[2-4] This allows us considerable freedom of speculation in qualitatively comparing the effect of the Al as "promotor" in SiO_2 with that of the Al in case of silicon or germanium. On the other hand, considering silica to be purely ionic for the moment, we wish to point to the fact that it has an electrically overlapping anion network. Anion-anion distances are smaller than twice the ionic oxygen radius. It is suggested that production of a mobile electron deficiency on an anion may be possible on this structure.

It is worth noting that the oxides best known to be cracking catalyst bases, namely SiO_2, Al_2O_3, and ZrO_2, are all characterized by an exceptional degree of anion-anion contact.

This work will be reported in greater detail at a later date.

[1] Weisz, Prater, and Rittenhouse, (previous letter).
[2] L. Pauling, *Nature of the Chemical Bond* (Cornell University Press, Ithaca, 1940), pp. 70 *ff* and 368 *ff*.
[3] A. F. Wells, *Structural Inorganic Chemistry* (Clarendon Press, Oxford, 1945), p. 39.
[4] F. Seitz, *Modern Theory of Solids* (McGraw-Hill Book Company, Inc., New York, 1940), p. 61.

Nuclear Quadrupole Resonance of Iodine in Molecular Solids

S. KOJIMA, K. TSUKADA, S. OGAWA, AND A. SHIMAUCHI
Department of Physics, Tokyo University of Education, Otsuka, Tokyo, Japan
(Received October 5, 1953)

PURE quadrupole spectra of chlorine and bromine isotopes in many solid halides are known. Because of spin 3/2 these isotopes are not suitable for the determination of the deviation of the field gradient from rotational symmetry. The iodine nuclei, I^{127}, of spin 5/2 have two resonance frequencies, ν_1 and ν_2, which are given by the formulas[1]

$$\nu_1=\frac{3}{20}eQq\left(1+\frac{59}{54}\eta^2\right) \quad \text{and} \quad \nu_2=\frac{3}{10}eQq\left(1-\frac{11}{54}\eta^2\right),$$

where eQq is the coupling constant and η is the asymmetry parameter of the field gradient. Therefore eQq and η are determined through the measurement of ν_1 and ν_2.

The resonance frequencies of the iodine nuclei in seven solid compounds have been measured with two super-regenerative detectors, one working in the frequency range between 150 Mc/sec and 350 Mc/sec and the other between 300 Mc/sec and 700 Mc/sec. The observed resonance frequencies, coupling constants and asymmetry parameters at the liquid air temperature are summarized in Table I.

On some of the alkyl iodides the coupling constants which were computed from the lower iodine frequencies with the assumption of symmetric field gradient were reported by Zeldes and Livingston[2] and by the authors[3] at almost the same time. The agreement between these results was excellent if the temperature dependency was considered. The values given in Table I take into account the asymmetry of the field gradient. The coupling constant of methyl iodide was already measured by Dehmelt[4] as 1753 Mc/sec, which is slightly different from the present result.

The study on four alkyl iodides shows that those with odd carbon number have a strong coupling, a large asymmetry, and high melting point and those with even carbon number a weak coupling, a small asymmetry, and low melting point.[5] The previous study[3] on alkyl bromides suggested that there was a correlation between the coupling constant and the melting point. This situation is seen to be a reality for alkyl iodides.

The spectrum of monoiode acetic acid has a doublet structure. On both components eQq and η were determined as shown in Table I.

On arsenic iodide the resonance frequencies were measured at temperatures ranging from the liquid air temperature to 107°C. The lower-resonance frequency was almost constant in the range from the liquid air temperature to −22°C giving a very small temperature coefficient, $(1/\nu_1)(d\nu_1/dt)=-9.3\times10^{-6}$/°C. The eQq increased from 1328 Mc/sec to 1345 Mc/sec and η decreased from

TABLE I. Quadrupole resonance frequencies, coupling constants, and asymmetry parameters at the liquid air temperature.

Compound	ν_1 (Mc/sec)	ν_2 (Mc/sec)	η (%)	eQq (Mc/sec)
CH_3I	264.973 ±0.01	529.515 ±0.01	2.5	1765.3
C_2H_5I	247.115 ±0.01	494.058 ±0.01	1.6	1647.0
n-C_3H_7I	250.810 ±0.02	499.810 ±0.01	5.2	1666.9
n-C_4H_9I	249.062 ±0.02	497.539 ±0.03	3.0	1658.8
CH_2ICOOH	298.87 ±0.10	596.12 ±0.20	4.6	1988
	297.86 ±0.10	592.79 ±0.20	6.1	1978
AsI_3	207.011 ±0.01	395.777 ±0.02	18.4	1328.2

18.4 percent to 14.5 percent when the temperature was changed from the liquid air temperature to the room temperature, 27°C. The large asymmetry parameter of this molecule seems to indicate double bonding between arsenic and iodine atoms. Above about 90°C the absorption lines split into triplets, whose frequencies at 110°C were 206.2, 208.5, and 211.7 Mc/sec for the lower lines and 403.2, 407.0, and 412.5 for the higher lines.

The spectrum of stannic iodide was also measured in the temperature range between the liquid air temperature and 69°C. The mean coupling constant of the doublet was changed continuously from 1389 Mc/sec to 1355 Mc/sec, when the temperature was raised through this range. This spectrum was first studied by Dehmelt[4] at room temperature and recently by Livingston and Zeldes[6] at 20°K and 70°K. The obtained results agreed well with that of Dehmelt and were consistent with those of Livingston and Zeldes.

[1] H. Krüger, Z. Physik **130**, 371 (1951); C. H. Townes and B. P. Dailey, J. Chem. Phys. **20**, 35 (1952).
[2] H. Zeldes and R. Livingston, J. Chem. Phys. **21**, 1418 (1953).
[3] Kojima, Tsukada, Ogawa, and Shimauchi, J. Chem. Phys. **21**, 1415 (1953).
[4] H. G. Dehmelt, Z. Physik **130**, 356 (1951).
[5] The melting points of methyl iodide, ethyl iodide, n-propyl iodide, and n-butyl iodide are −66.45, −111.1, −101.3, and −103.0°C, respectively. (Shiba "Table of Physical Constant." Iwanami, Tokyo).
[6] R. Livingston and H. Zeldes, Phys. Rev. **90**, 609 (1953).

Band Structure of Graphite

J. L. CARTER* AND J. A. KRUMHANSL
Cornell University, Ithaca, New York
(Received October 5, 1953)

SEVERAL workers have studied the electronic properties of graphite.[1] Theoretical interpretations of the results have been based on the Wallace theory.[2] Two conclusions from his theory are: (a) the P_z valence and conduction bands touch at the zone corner. (b) energy *vs* K curves are symmetric about the touching energy. From (b) one concludes that the Hall coefficient of normal graphite should be zero, in disagreement with experiments,[1] which invariably yield a sizeable negative value (electron conduction).

This disagreement led us to examine the lattice symmetry restrictions on band structure in greater detail. One of us[3] has applied group theoretical methods and among other results has concluded that neither (a) nor (b) is required. Any particular characteristic of the energy bands which is a consequence of lattice symmetry will appear regardless of the approximation method used for band calculations. That (b) is not required is noted in the discussion by Coulson and Taylor,[4] where inclusion of overlap integrals destroys the symmetry (b); however, near the zone corner the effect is negligible, so that this is insufficient to explain the anomalous electronic behaviors observed. Mrozowski[5] notes that Polder also has concluded that (a) and (b) are accidental.

Although an extensive cellular calculation would show these features in their proper form the labor involved seemed prohibitive. Rather we have attempted to modify the Wallace tight-binding calculation in a plausible manner to show how the more general features appear in this approximation. Of the several possible modifications of Wallace's assumptions we believe the most significant for the electronic properties near the zone corner is the inadequacy of his Eq. (4.5). Of the four atoms in the graphite unit cell two have nearest neighbors in adjacent planes (1 and 3) while two do not (2 and 4); thus it is more realistic to assume

$$H_{11}=H_{33}<H_{22}=H_{44}. \tag{1}$$

The difference is small (we estimate it from Coulomb penetration integrals to be $\gtrsim 0.01$ ev), but since the energy-level structure varies rapidly over a few tenths of a volt near the zone corner the effect is significant in this energy range. Appropriately modifying Wallace's Hermitean secular determinant to read

$$\begin{vmatrix} H_{11}-E, & -\gamma_0 S, & \gamma_1\Gamma, & \gamma_1'\Gamma S^* \\ & H_{22}-E, & \gamma_1'\Gamma S^*, & \gamma_1'\Gamma S \\ & & H_{11}-E, & -\gamma_0 S^* \\ & & & H_{22}-E \end{vmatrix} =0, \tag{2}$$

we find near the zone corner (by neglecting $\gamma_1' S$ as a small quantity of second order) the four roots

$$E=H_{22}+\left(\frac{H_{11}-H_{22}\mp\gamma_1\Gamma}{2}\right)+\left[(\gamma_0 S)^2+\left(\frac{H_{11}-H_{22}\mp\gamma_1\Gamma}{2}\right)^2\right]^{\frac{1}{2}}$$

$$E=H_{22}+\left(\frac{H_{11}-H_{22}\mp\gamma_1\Gamma}{2}\right)-\left[(\gamma_0 S)^2+\left(\frac{H_{11}-H_{22}\mp\gamma_1\Gamma}{2}\right)^2\right]^{\frac{1}{2}}. \tag{3}$$

The resulting modified band structure replacing Wallace's Figs. 10 and 11 is shown in Fig. 1, drawn with assumption that $H_{22}-H_{11}$

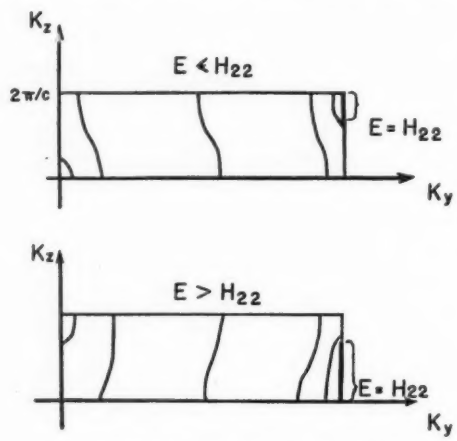

FIG. 1. Modified zone structure in graphite.

$<2\gamma_1$ (if this is not so, the bands do not touch at all). Similarly the densities of states are compared in Fig. 2 with Wallace's results; the sensitivity to the modification (1) is striking. For example, assuming $H_{22}-H_{11}=\frac{1}{2}\gamma_1$ the density of electron states at the lower edge of the upper band is ≈ 2.5 times that of the "hole"

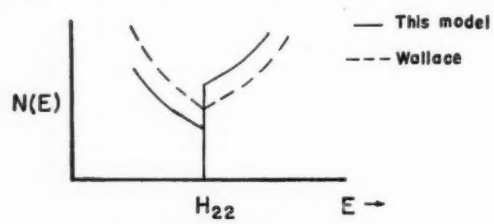

FIG. 2. Modified density of states.

states at the top of the lower band. One would expect similar asymmetry in the Hall coefficient, and the resistance changes with chemical additives.

In view of the uncertainties in relaxation times, polycrystalline effects, etc., in current experiments we have not exploited this model further. Indeed, one would not expect great precision from the tight binding approximation. Nonetheless, the above model is

in agreement with the more general group theoretical requirements and is probably more representative of the actual band structure near the zone corner than is Wallace's. Finally, it must be noted[4] that as soon as the Fermi level is moved a few tenths of a volt from the zone corner the system is essentially two dimensional and our modifications play a minor role. The authors would like to acknowledge discussions of these topics with W. W. Tyler, W. P. Eatherly, and members of the Knolls Atomic Power Laboratory.

* Present address, General Electric Company, West Lynn, Massachusetts.
[1] G. Hennig, J. Chem. Phys. **20**, 1438 (1952); W. W. Tyler and A. C. Wilson, Jr., Phys. Rev. **89**, 870 (1953).
[2] P. R. Wallace, Phys. Rev. **71**, 622 (1947).
[3] J. L. Carter, Ph.D. thesis, Cornell University, February, 1953.
[4] C. A. Coulson and R. Taylor, Proc. Phys. Soc. (London) **A65**, 815 (1952).
[5] S. Mrozowski, J. Chem. Phys. **21**, 492 (1953).

The Rate of Combination of Methyl Radicals

K. U. INGOLD,† I. H. S. HENDERSON,† AND F. P. LOSSING
Division of Pure Chemistry, National Research Council, Ottawa, Canada
(Received September 21, 1953)

FURTHER work on the combination of methyl radicals using the techniques described previously[1] has shown that while the contact time at 9 mm pressure of helium carrier gas was almost correct, there was a considerable error in its measurement at 4.8 mm and to a lesser extent at 18.5 mm. An improved method of measuring the contact time has shown that a factor of about 2 was involved over this pressure range, the longer contact time corresponding to the lower pressure. The effect of pressure on the rate of combination has therefore been re-determined over a range from 3.4 mm to 15.0 mm of helium at 1000°C. Relative rates are plotted in Fig. 1 against the helium pressure. It can be seen that the pressure has a considerable influence on the rate. Previously this effect was masked by the error in the contact time measurements at the different pressures. The finite intercept in the figure is due both to the first-order wall reaction which, at the methyl concentrations used is negligible except at low pressures, and to the third-body effects of the products themselves.

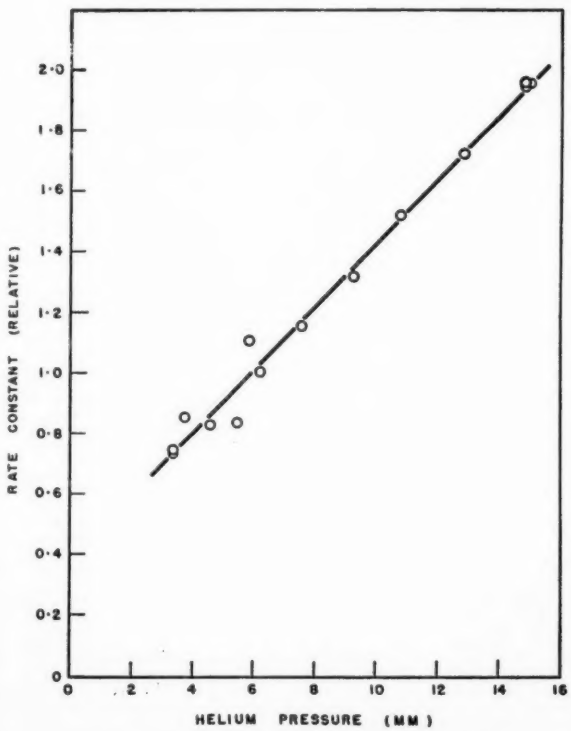

FIG. 1. The rate of combination of methyl radicals.

Since the pressure of the carrier gas is found to have an important effect on the rate of combination, our results are now in agreement with recent work on this subject.[2] Moreover, since kinetic theory predicts a negative temperature coefficient for the combination rate in the region of pressure dependence[3] it is no longer necessary to attribute this effect entirely to a variation in the collision cross section with temperature.

The collision efficiencies reported earlier[1] are unaffected by this error but refer, of course, only to the conditions stated, *viz.*, 9 mm of helium and the corresponding temperature. However, at constant temperature the rate is proportional to the helium pressure at around 9 mm. Therefore, using the same nomenclature as before, the values reported for the rate (i.e., the values of k_1) are really values of $k_1k_3[M]/k_2$. In this expression the powers of temperature involved in the collision numbers and the concentration term cancel so,

$$\ln(\text{rate}) = \ln(\text{constant}) - (E_1 + E_3 - E_2)/RT.$$

E_1 and E_2 are, respectively, the activation energies of the methyl-methyl collision process and its reverse. E_3 is the activation energy of the helium-ethane* collision. For this reason it is not necessary, when obtaining the over-all activation energy of the reaction, to multiply the rates by a factor of $T^{-\frac{1}{2}}$ as was done previously. This change lowers the activation energy $(E_1+E_3-E_2)$ to -1.5 kcal. Since it is generally assumed that E_1 and E_3 are close to zero, the negative temperature coefficient can be attributed to the in-increase of k_2 with temperature. That is, the lifetime of the complex C_2H_6* and therefore the over-all rate of reaction decrease with increasing temperature.

A point of considerable interest is the relative deactivating efficiency of various third bodies, i.e., the relative values of k_3. Unfortunately there are considerable experimental difficulties in replacing helium by some other gas with larger molecules in which a much greater efficiency of deactivation would be expected. We are therefore indebted to Dr. R. E. Dodd for permission to use his unpublished values of k_2/k_3 for acetone as the third body. By using Gomer and Kistiakowsky's value[4] for k_1, the value of k_2/k_3 for helium may be obtained from our previously published results.[1] In this way a comparison can be made of the deactivating efficiencies of helium and acetone:

	450°K	521°K
$\left(\frac{k_2}{k_3}\right)_{He}$	68.4×10^{16}	75.0×10^{16} molecules/cc
$\left(\frac{k_2}{k_3}\right)_{Ac}$	4.0×10^{16}	6.4×10^{16} molecules/cc.

Since k_2 is independent of the third body

$\frac{(k_3)_{He}}{(k_3)_{Ac}}$	0.059	0.085.

That is, acetone is some 12–17 times as efficient as helium in removing excess energy from the activated complex C_2H_6*.[5]

† National Research Council Postdoctorate Fellow.
[1] K. U. Ingold and F. P. Lossing, J. Chem. Phys. **21**, 1135 (1953).
[2] R. E. Dodd (private communication).
[3] S. W. Benson, J. Chem. Phys. **20**, 1064 (1952).
[4] R. Gomer and B. G. Kistiakowsky, J. Chem. Phys. **19**, 85 (1951).
[5] For a comparison of the efficiencies of third bodies in the iodine atom recombination see K. E. Russell and J. Simons, Proc. Roy. Soc. (London) **A217**, 271 (1953).

Erratum: The Use of Radioactive Alpha-Recoil in the Study of Soluble Ionized Surface Layers

[J. Chem. Phys. **21**, 1299–1300 (1953)]

GUNNAR ANIANSSON AND NAFTALI H. STEIGER
Division of Physical Chemistry, Royal Institute of Technology, Stockholm, Sweden

10^{-3} $CHNO_3$ should be changed to read $10^{-3}M$ HNO_3.

The Dissociation Energy of Oxygen*

P. BRIX† AND G. HERZBERG
Division of Physics, National Research Council, Ottawa, Canada
(Received October 14, 1953)

IT was pointed out some time ago by one of us[1] that a small but definite discrepancy exists between the value of the dissociation energy of oxygen obtained from the near ultraviolet absorption bands ($^3\Sigma_u^+ \leftarrow {}^3\Sigma_g^-$) and the value obtained from the Schumann-Runge bands ($^3\Sigma_u^- \leftarrow {}^3\Sigma_g^-$). Watanabe, Inn, and Zelikoff[2] have recently measured the absorption coefficients of oxygen under low resolution and have suggested a revised value for the dissociation limit of the Schumann-Runge system. Independently during the past year we have reinvestigated the fine structure of the Schumann-Runge bands under high resolution (0.65A/mm) right up to the convergence limit. The earlier determinations were based on the work of Knauss and Ballard,[3] who analyzed the bands only up to the 15–0 band. On the basis of the new measurements of bands up to 21–0, a much more precise value for the dissociation limit can be given. This value is 57127.5 ± 5 cm^{-1}. It differs from the (recalculated) dissociation limit of the near ultraviolet bands (41259 cm^{-1}) by 15868.$_5$ cm^{-1} which agrees within 1 cm^{-1} with the excitation energy of the ^1D state of the O atom. This agreement makes it very unlikely that there is an appreciable potential maximum in either potential energy curve. Therefore, the resulting value $D(O_2) = 41261 \pm 15$ cm^{-1} or $5.114_8 \pm 0.002$ ev or 117.96 ± 0.04 kcal/mole$_{chem}$ must be considered as definitive. The error quoted is considered to be a very conservative estimate taking account of all conceivable sources of error.

Complete details about the analysis of the Schumann-Runge bands and the determination of $D(O_2)$ may be found in a paper scheduled to appear in the January issue of the Canadian Journal of Physics.

* Contribution No. 0000 from the National Research Council of Canada.
† National Research Laboratories Postdoctorate Fellow.
[1] G. Herzberg, Can. J. Phys. **30**, 185 (1952).
[2] Watanabe, Inn, and Zelikoff, J. Chem. Phys. **21**, 1026 (1953).
[3] H. P. Knauss and S. S. Ballard, Phys. Rev. **48**, 796 (1935).

The Decomposition of Ozone on the Surface of Glass Wool

P. HARTECK AND S. DONDES
Rensselaer Polytechnic Institute, Troy, New York
(Received October 7, 1953)

IN connection with another research problem, an interim investigation was made of the decomposition velocity of ozone at 100°C on pure pyrex glass wool (as originally packaged by the manufacturer). Since the reaction velocity constants for this heterogeneous reaction indicated first order, over a wide range of concentrations used, we were prompted to include the results in a brief note.

Chapman[1] and co-workers, in studying the normal decomposition of ozone, showed it to be a second-order, homogeneous reaction when dealing with ordinary concentrations of ozone, whereas Riesenfeld[2] found that at very low concentrations (a few millimeters), the order of the reaction is influenced by the surface, to the extent of becoming heterogeneous and first order. These results were conclusively indicated in the exhaustive experimentation conducted by Glissmann and Schumacher.[3]

Experimentally, 21.95 grams of new pyrex glass wool were placed in a 1½-liter pyrex glass flask, and evenly dispersed throughout the volume. A known pressure of oxygen and ozone at slightly greater than one atmosphere was introduced into the flask, previously heated to 100°C, and after various time intervals, the concentration of ozone was measured.

With the introduction of the wool, the surface area within the flask was increased from 7×10^2 cm^2 to 6.7×10^4 cm^2. This approximate 100-fold increase, resulted in the surface reaction predominating over the decomposition in the gas phase. To date, the kinetics of the thermal decomposition of ozone molecules in the homogeneous gas phase has not been completely elucidated. A possible explanation for the heterogeneous decomposition of ozone on the surface of glass wool which follows a first-order reaction (Fig. 1) over a large range of concentrations, may be

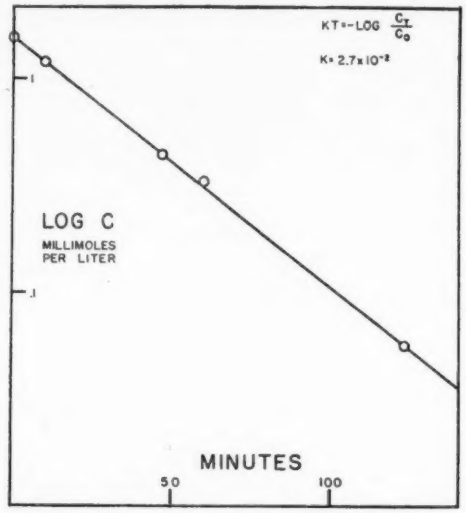

FIG. 1. Decomposition of ozone on the surface of glass wool ($T = 100$°C).

that the oxygen atoms, which are in thermal equilibrium with the ozone, diffuse to the surface of the glass and are there destroyed. This mechanism would lead to a first-order reaction over a large range of concentrations.

$$O_3 \rightleftarrows O_2 + O$$

The equilibrium constant, K_p, in the equation,

$$K_p = \frac{[O][O_2]}{[O_3]}$$

can be calculated by approximation methods to be 5.6×10^{-9} for 100°C. Since the $[O_2]$ concentration is at one atmosphere, the ratio $[O]/[O_3]$ becomes equal to 5.6×10^{-9}.

The number of collisions on a surface, N_z, per cm^2 per second, can be calculated from: $N_z = \frac{1}{4} N_i \omega$ where N_i is the number of particles per cm^3 and ω is the average particle velocity.

The number of collisions of oxygen atoms $N_{z(\text{O-atoms})}$ on a surface per cm^2 per second, is given by:

$$N_{z(\text{O-atoms})} = \tfrac{1}{4} N_i \omega [O],$$

where $[O]$ is the partial pressure of the oxygen atoms. Since $[O] = K_p[O_3]$, therefore $N_{z(\text{O-atoms})} = N_i \omega K_p [O_3]$.

The number of oxygen atoms colliding with the total surface within the flask Ω is obtained from

$$\Omega N_{z(\text{O-atoms})} = \tfrac{1}{4} N_i \omega K_p [O_3] \Omega.$$

The number of ozone molecules, $N_{[O_3]}$, in the volume of the flask V is $N_{[O_3]} = V N_i [O_3]$ where $[O_3]$ refers to the partial pressure of ozone.

The value α, which gives the ratio of the number of oxygen atoms which strike the total surface per second to the number of ozone molecules included in the volume V, is obtained from

$$\alpha = \frac{\frac{1}{4} N_i \omega [O_3] K_p \Omega}{V N_i [O_3]} = \frac{\frac{1}{4} \omega K_p \Omega}{V},$$

and calculated as

$$\alpha = \frac{\frac{1}{4} \times 7 \times 10^4 \times 5.6 \times 10^{-9} \times 6.7 \times 10^4}{1.5 \times 10^8} = 4.3 \times 10^{-3}.$$

The reciprocal $1/\alpha$ is the time in which as many oxygen atoms collide with the surface, as there are ozone molecules present in the volume V and equal to 230 seconds. (Note: The gradient

of the concentration of the oxygen atoms near the glass surface was not considered in these calculations.)

Since the time in which the ozone concentration drops to $1/e$ is about 2300 seconds, it follows that of the 10 collisions of oxygen atoms that take place on the pyrex glass surface, one leads to recombination. This result is in rather good agreement with the fraction of oxygen atoms recombining on a dry glass wall at 100°C obtained from other data involving gas discharge and combustion experiments. This experimental method, which we are not in a position to continue, makes the investigation of surface catalysis for the recombination of oxygen atoms rather simple, when there is no direct thermal decomposition of the ozone molecules.

Acknowledgment is made to the U. S. Atomic Energy Commission for financial assistance.

[1] D. L. Chapman and H. E. Clarke, J. Chem. Soc. **93**, 1638 (1908). D. L. Chapman and H. E. Jones, J. Chem. Soc. **97**, 2463, (1910).
[2] E. H. Riesenfeld and W. Bohnholtzer, Z. physik. Chem. **130**, 241 (1927). E. H. Riesenfeld and H. J. Schumacher, Z. physik. Chem. **138**, 268 (1928).
[3] A. Glissmann and H. J. Schumacher, Z. physik. Chem. **B21**, 323 (1933).

Comments on the Thermal Decomposition of Ozone

P. Harteck and S. Dondes
Rensselaer Polytechnic Institute, Troy, New York
(Received October 7, 1953)

THE thermal decomposition of ozone has been carefully investigated both theoretically and experimentally by Schumacher and co-workers.[1] Theoretical considerations indicate that when a small amount of ozone is in a large quantity of oxygen, a homogeneous second-order decomposition of ozone should occur. However, the observed results and theory are at slight variance. Thus, Laidler[2] states that "the details of the thermal decomposition of ozone are by no means understood." Since this reaction has many applications in kinetics, we were prompted to comment on the possible mechanism to explain the variance. Our comments are based on experimental work carried out at Rensselaer Polytechnic Institute.

Our experiments differed from those of Schumacher in the concentrations of ozone investigated, and in surface area within the reaction vessel. Schumacher started with ten millimoles of ozone per liter and concluded with less than one. We began with 1.6 millimoles per liter and concluded with less than 0.06. We increased the surface area within the glass vessel 100-fold by the addition of glass wool, and obtained a heterogeneous reaction of the first order over the entire range of concentrations used. With the 100-fold increase in the surface area, our initial reaction ran 3 to 4 times faster than his and was practically a wall-catalysis, due to the recombination of oxygen atoms on the surface of the glass wool. Thus, it became apparent that his increase in reaction velocity constants, at the end of the reaction, could not be due to the wall catalysis of the ozone, but of the oxygen atoms in thermal equilibrium with the ozone. From this, the increased effect at lower pressures can also be readily understood. This presumes that the surface of the glass utilized by Schumacher had the same behavior as the surface of our newly manufactured glass wool.

In addition, Schumacher should have made another correction to obtain greater correlation. This involves the amount of heat set free by the decomposition of ozone in the initial stages of the reaction in the same experiment, which would raise the temperature of the gas within the vessel a few degrees above the temperature of the bath in which the reaction vessel was immersed. This fact was noted by us on a thermometer placed in the reaction vessel. This condition leads to a complicated sequence of events. Initially, the reaction may run slightly faster, due to the higher temperature, and towards the end of the reaction the cooling of the gas will affect the decrease in pressure, which in turn may mask an increasing reaction velocity constant, due to the oxygen atom catalysis on the wall.

Thus, if the surface of the vessel is ideally clean, there is practically no ozone catalysis on the wall, but only an oxygen atom recombination. In addition, if the necessary temperature and pressure changes occurring during the reaction are considered, then there is a quantitative agreement between theory and experiment over the entire concentration range in Schumacher's work.

[1] A. Glissmann and H. J. Schumacher Z. physik. Chem. **B21**, 323 (1933). H. J. Schumacher *Chemische Gasreaktionen* (Verlag von Theodor Steinkopff, 1938), p. 433.
[2] K. J. Laidler *Chemical Kinetics* (McGraw-Hill Book Company, Inc., New York, 1950), p. 244.

Isotope Effect on the Dipole Moments of Diatomic Molecules

Aubrey P. Altshuller
1911 Clover Avenue, Cleveland, Ohio
(Received October 9, 1953)

A SIMPLE electrostatic treatment has been given[1] of the effect of isotopic substitution upon the dipole moments of diatomic molecules. Differences in vibrational amplitudes of the isotopic molecules result in small differences, $\langle\Delta\mu\rangle_{Av}$ in the dipole moments. The equation derived[1] has the form

$$\langle\Delta\mu\rangle_{Av}=\frac{3e\alpha b_1^2}{2a^4}[1-(m_1/m_2)^{\frac{1}{2}}], \quad (1)$$

where b_1 is the vibrational amplitude of one of the isotopic molecules, m_1 and m_2 are the masses of the isotopic atoms of the two molecules, a is the internuclear distance, and e is the electronic charge. One ion is assumed to be a point charge while the other has a polarizability α.

A few modifications should be made in this equation. First, both ions will usually be polarizable having polarizabilities α_1 and α_2. Second, instead of the masses of the isotopic atoms, the reduced masses μ_1 and μ_2 of the two isotopic molecules should be employed. A more general equation will be as follows:

$$\langle\Delta\mu\rangle_{Av}=\frac{3eb_1^2(\alpha_1+\alpha_2)}{2a^4}[1-(\mu_1/\mu_2)^{\frac{1}{2}}]. \quad (2)$$

In Eq. (2) higher-order terms in the induced moments[2] are neglected. This is justified by the fact that principally only the order of magnitude of the values of $\langle\Delta\mu\rangle_{Av}$ will be of interest.

Equation (1) was originally applied[1] to H_2 and HD with a $\Delta\mu$ of 0.01 to 0.05D predicted. Since the equation should apply only to ionic molecules, this example is a poor one. The equation may not be applied to the hydrogen, deuterium, and tritium halides because they are largely covalent and their total moments when calculated by this type of an electrostatic treatment are negative.[3] Unfortunately, this type of treatment also may not be used with the alkali metal hydrides, deuterides, and/or tritides because the method fails with this series of compounds also, i.e., their moments calculated by this method are negative.[4] Such an electrostatic treatment as is usually employed[2-4] fails when the radius of one of the ions, R, is greater than a, the internuclear distance.[2] Both the hydrogen halides and the alkali metal hydrides fail to meet the condition $a>R$. Although these compounds are generally unsatisfactory for this type of calculation, it is of some interest to indicate the magnitude of $\Delta\mu$ in the cases of the two compounds of these series, CsH and HF, which fail the condition $a>R$ to the least extent and which are, of course, the most ionic members of their series. For the two isotopic molecules CsH^1 and CsH^2, $\Delta\mu$ would be about 0.10D while for the molecules H^1F and H^2F the difference in moments would be to about 0.07D, if the treatment did apply.

The electrostatic treatment is applicable to the highly ionic alkali halides.[2] Small differences in dipole moments may be expected between such molecules as Li^6Cl and Li^7Cl or $NaCl^{35}$ and $NaCl^{37}$, etc. Owing to the small differences in reduced masses, the differences in dipole moment, $\Delta\mu$, for the isotopic alkali halied

molecules will naturally be considerably less than would be the case if molecules containing H^1, H^2, or H^3 could be considered.

The vibrational frequencies, ω, employed in the calculation of the values of b_1 as well as the internuclear distances for the alkali halides used are those given by Rittner.[2] The polarizabilities employed are those calculated by Pauling.[5]

TABLE I. Differences in dipole moments for some isotopic alkali halides.

Molecular species	$1-(\mu_1/\mu_2)^{\frac{1}{2}}$	$\langle\Delta\mu\rangle_{Av}\times10^{-21}$ (milliDebyes)
Li^6F, Li^7F	0.056	1.5
Li^6Cl, Li^7Cl	0.063	1.8
Li^6I, Li^7I	0.071	2.6
$NaCl^{35}$, $NaCl^{37}$	0.011	0.09
$K^{39}I$, $K^{41}I$	0.019	0.12
$RbCl^{85}$, $RbCl^{87}$	0.019	0.11
$CsCl^{35}$, $CsCl^{37}$	0.022	0.12

The values of $\langle\Delta\mu\rangle_{Av}$ calculated for isotopic alkali halides excepting the lithium halides are of the order of 10^{-4}D and these differences are considerably smaller than the uncertainties at the present time in the dipole moments calculated by means of data obtainable from microwave spectroscopy.[6] The dipole moments of a few molecules have been determined with good accuracy in the third decimal place.[6] These uncertainties are of the same magnitude as the values of $\langle\Delta\mu\rangle_{Av}$ found for the isotopic lithium halides. It is true that at present the dipole moments of the alkali halides which have been determined from microwave techniques have been uncertain in the second decimal place, but improved experimental methods and instrumental techniques may make values of $\langle\Delta\mu\rangle_{Av}$ of the magnitude predicted theoretically for the alkali halides, experimentally detectable.

[1] R. P. Bell, Trans. Faraday Soc. **31**, 1345 (1935).
[2] E. S. Rittner, J. Chem. Phys. **19**, 1030 (1951).
[3] P. Debye, *Polar Molecules* (Chemical Catalog Company, New York, 1929).
[4] A. P. Altshuller, J. Chem. Phys. (to be published).
[5] L. Pauling, Proc. Roy. Soc. (London) **A114**, 181 (1927).
[6] Gordy, Smith, and Trambarulo, *Microwave Spectroscopy* (John Wiley and Sons, Inc., New York, 1953).

Errata: Adsorption on Proteins and Interactions between Protein Molecules in Solution

[J. Chem. Phys. **21**, 1395 (1953)]

TERRELL L. HILL
Naval Medical Research Institute, Bethesda, Maryland

EQUATION (20) of this paper should read in general

$$\rho^{(n)}(\{n\})=\sum_{(B+1)^n}\rho\mathbf{n}(\{\mathbf{n}\}),\qquad(20)$$

where the sum is over the $(B+1)^n$ possible assignments of the $B+1$ different species to the n positions in space, $\{n\}$. The terms can be collected as indicated in the original Eq. (20) only after integration over $d\{n\}$ or when $n=1$ or 2. Only the $n=2$ case was applied in the original paper so no additional changes are necessary.

In Eq. (19), read $(m_s-n_s)!$ for $m_s!$

We take this opportunity to mention that, by a change of notation, the equations of this paper are actually still valid in the general case when the protein-protein interactions are assumed to depend on the detailed assignment of the adsorbed molecules on the various sites and on the orientations and internal molecular configurations of the protein molecules. With this generalization, for example, the potential of mean force between two isolated protein molecules,[1] averaged over assignments, orientations, and configurations (see above), is obtained as a special case [Eq. (21)]. The general theory, using the MacMillan-Mayer solution theory as a starting point, will be published later.

[1] Investigated recently by J. G. Kirkwood and J. B. Shumaker, Proc. Natl. Acad. Sci. **38**, 863 (1952).

The Volumes of Mixing of Some Nonpolar Liquids

R. THACKER AND J. S. ROWLINSON
Department of Chemistry, The University of Manchester, England

(Received October 9, 1953)

THE cell theory of pure liquids[1] has recently been extended to solutions, and expressions have been obtained relating the excess thermodynamic properties to the molecular interactions. If the molecules are spherical and of closely similar sizes and interaction energies, then this theory requires that the excess free energy, enthalpy, entropy, and volume are all of the same sign.[2] Longuet-Higgins[3] has shown, by more rigorous arguments which avoid the use of the cell model, that this must necessarily be so for solutions in which all but the first-order differences in molecular energy and size can be neglected. He quoted sixteen liquid solutions which show this behavior. Prigogine and others[2,4] have used the cell model to predict the properties of solutions in which the molecules have less similar energies and sizes. The most remarkable of their predictions is that solutions of nonpolar molecules of almost equal sizes but of very unequal energies of interaction will have a positive excess free energy and excess enthalpy and a negative excess volume. As the cell model gives quantitatively poor values of the first-order deviations from ideality,[5] we would place little reliance on these predictions based upon the second-order deviations unless they are supported by experimental evidence. Mathot and Desmyter[6] have recently found three systems which have a positive excess free energy (and presumably a positive excess enthalpy) but negative excess volumes. We have therefore tested further Prigogine's conclusions by measuring the volume of mixing at 25°C of four hydrocarbon solutions which conform closely to his criteria. Our results, those of Mathot and Desmyter, of Schulze,[7] and some of those quoted by Longuet-Higgins are shown in Fig. 1. The maximum volume change is

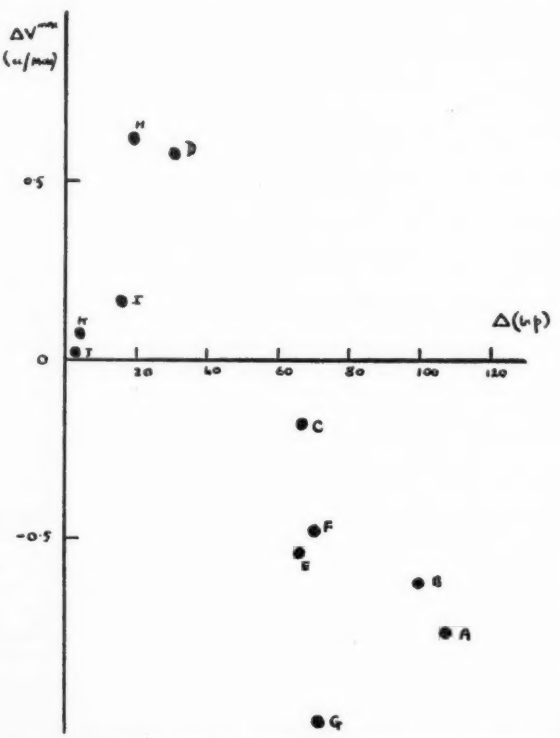

FIG. 1. Maximum volumes of mixing, *A*, *n*-pentane and *o*-xylene (this work); *B*, *n*-pentane and ethylbenzene (this work); *C*, *n*-hexane and ethylbenzene (this work); *D*, *c*-hexane and toluene (this work); *E*, neopentane and carbon tetrachloride (see reference 6); *F*, neo-pentane and benzene (see reference 6); *G*, neopentane and *c*-hexane (see reference 6); *H*, benzene and chloroform (see reference 7); *I*, carbon tetrachloride and chloroform (see reference 3); *J*, carbon tetrachloride and benzene (see reference 3); *K*, carbon tetrachloride and *c*-hexane (see reference 3).

plotted against the difference in the boiling points of the two components. This difference is a crude measure of the difference between their energies of interaction. All our solutions have positive heats of mixing. It is seen that our results confirm those of Mathot and Desmyter, and show that a difference in the boiling points of greater than 50°C can lead to negative volumes of mixing for substances of similar molar volume, as Prigogine's treatment predicts.

[1] J. E. Lennard-Jones and A. F. Devonshire, Proc. Roy. Soc. (London) **A163**, 53 (1937).
[2] I. Prigogine and V. Mathot, J. Chem. Phys. **20**, 49 (1952): J. S. Rowlinson, Proc. Roy. Soc. (London) **A214**, 192 (1952).
[3] H. C. Longuet-Higgins, Proc. Roy. Soc. (London), **A205**, 247 (1951).
[4] I. Prigogine and A. Bellemans, J. Chem. Phys. **21**, 561 (1953); Discussions Faraday Soc. (to be published).
[5] J. S. Rowlinson, Discussions Faraday Soc. (to be published).
[6] V. Mathot and A. Desmyter, J. Chem. Phys. **21**, 782 (1953).
[7] A. Schulze, Z. physik. Chem. **97**, 388 (1921).

The Kinetics of the Heterogeneous Parahydrogen Conversion*

Y. L. SANDLER
Laboratory for Insulation Research, Massachusetts Institute of Technology, Cambridge, Massachusetts
(Received October 13, 1953)

THE parahydrogen conversion, and similarly the H_2+D_2 reaction, has frequently been used as a model reaction in fundamental catalytic studies. Because of the kinetic simplicity of the reaction, certain strict relations exist between the observed kinetics and measurable equilibrium-adsorption properties which are independent of the particular reaction and adsorption mechanism. These relations have so far not been utilized or have been incorrectly stated. In particular, a simple relation exists between the observed activation energy E and the "true" activation energy E_s of the surface reaction; it is only the latter quantity which is of interest for a comparison with solid state properties. E_s is obtained from the observed temperature dependence by eliminating the change in the fraction of gas adsorbed and in the surface coverage.

It will be assumed that the conversion follows a strict first-order decay law. The observed rate r can be written as

$$r=kN=k_sN_s, \tag{1}$$

where N is the total number of molecules present in the reaction vessel and N_s is the number of adsorbed molecules. The "true" rate constant k_s is defined by Eq. (1). Like k, it generally will be a function of temperature and pressure (or coverage).

From Eq. (1) we obtain

$$\left(\frac{\partial \ln k}{\partial T}\right)_p=\left(\frac{\partial \ln k_s}{\partial T}\right)_p+\left(\frac{\partial \ln N_s}{\partial T}\right)_p-\left(\frac{\partial \ln N}{\partial T}\right)_p. \tag{2}$$

Since

$$d\ln p=\left(\frac{\partial \ln p}{\partial T}\right)_{N_s}dT+\left(\frac{\partial \ln p}{\partial \ln N_s}\right)_T d(\ln N_s)=0,$$

$$\left(\frac{\partial \ln N_s}{\partial T}\right)_p=-\left(\frac{\partial \ln p}{\partial T}\right)_{N_s}\cdot\left(\frac{\partial \ln N_s}{\partial \ln p}\right)_T$$

$$=-Q/RT^2\times n. \tag{3}$$

Here Q is the isosteric heat; it is equal to the partial molal enthalpy of desorption $H_{\text{gas}}-\bar{H}_{\text{ads}}$. n is defined by the relation

$$n=(\partial \log N_s/\partial \log p)_{T,A}, \tag{4}$$

where A = surface area, assumed constant throughout; n will be called the "adsorption order."

Substituting Eq. (3) into Eq. (2), we find

$$\left(\frac{\partial \ln k}{\partial T}\right)_p=\left(\frac{\partial \ln k_s}{\partial T}\right)_p-n\frac{Q}{RT^2}-\left(\frac{\partial \ln N}{\partial T}\right)_p. \tag{5}$$

We define the apparent kinetic order n_k by the equation

$$n_k=(\partial \log r/\partial \log p)_T. \tag{6}$$

The order of the surface reaction ("true order") we define by

$$n_s=(\partial \log r/\partial \log N_s)_T. \tag{7}$$

Then from Eqs. (4), (6), and (7) we find the simple relation connecting kinetic and adsorption orders.

$$n_k=n_s\times n. \tag{8}$$

Writing

$$d\ln k_s=\left(\frac{\partial \ln k_s}{\partial T}\right)_{N_s}dT+\left(\frac{\partial \ln k_s}{\partial \ln N_s}\right)_T d\ln N_s,$$

and using the definitions of n_s and n, given in Eqs. (7) and (4), we obtain

$$\left(\frac{\partial \ln k_s}{\partial T}\right)_p=\left(\frac{\partial \ln k_s}{\partial T}\right)_{N_s}+(n_s-1)\left(\frac{\partial \ln N_s}{\partial T}\right)_p.$$

Using relation (3) we find

$$\left(\frac{\partial \ln k_s}{\partial T}\right)_p=\left(\frac{\partial \ln k_s}{\partial T}\right)_{N_s}+(1-n_s)\frac{Q}{RT^2}\cdot n. \tag{9}$$

If we now substitute this expression in Eq. (5), using relation (8), we obtain

$$\left(\frac{\partial \ln k}{\partial T}\right)_p=\left(\frac{\partial \ln k_s}{\partial T}\right)_{N_s}-n_k\frac{Q}{RT^2}-\left(\frac{\partial \ln N}{\partial T}\right)_p. \tag{10}$$

Multiplying by RT^2, the desired relationship between E and E_s is obtained:

$$E=E_s-n_kQ-RT^2(\partial \ln N/\partial T)_p. \tag{11}$$

The following special experimental conditions generally are of interest: (a) If N is kept independent of temperature, the last term in Eq. (11) vanishes; then

$$E=E_s-n_kQ. \tag{11a}$$

(b) If the gas volume (V) is kept constant and if the relative amount of gas adsorbed is small ($N_s/N\ll 1$), then $N=N_{\text{gas}}$ and $-(\partial \ln N/\partial T)_{p,V}=1/T$; therefore

$$E=E_s-(n_kQ-RT). \tag{11b}$$

(c) If most of the gas is adsorbed $N_s/N\simeq 1$, then from Eq. (3) $(\partial \ln N/\partial T)_p=-nQ/RT^2$; therefore

$$E=E_s-(n_k-n)Q. \tag{11c}$$

The validity of Eqs. (11) to (11c) is completely unrestricted with regard to coverage or the nature of the surface. From (11b), setting $Q-RT=\lambda$, we obtain Hinshelwood's equation,[1] $E=E_s-\lambda$, as a special case if $n_k=1$. It is seen that the reaction order n_k takes care of the change of Q with coverage in a very simple manner.[2]

The equations may, for example, be applied to the conversion of parahydrogen on tungsten surfaces, which recently has been the subject of much discussion.[2-8] If we assume that the conversion rate is equal to the rate of desorption of chemisorbed hydrogen from the surface in accordance with the Bonhoeffer-Farkas mechanism,[9] then k_s will be the desorption rate constant and E_s will be the activation energy of desorption. Rideal and Trapnell[4,5] determined the isotherms for hydrogen on tungsten films and compared them with the kinetics of the parahydrogen conversion observed with tungsten filaments.[3,4] If one assumes (as do these authors) that, in absence of an appreciable activation energy of adsorption, the true heat of activation should be equal to the isosteric heat of adsorption, then no further assumptions concerning the adsorbed phase are required for a comparison between the observed activation energies and isosteric heats. In any case one may then assume that $E_s+RT\geq Q$.

As Eq. (11b) is applicable to the kinetic experiments,[4] one obtains $E_s=E+n_kQ-RT\geq Q-RT$, or

$$n_k\geq 1-E/Q. \tag{12}$$

The experimental data to be compared are $E=2000$ cal for $T=110°$ to 280°K and $Q=7000$ to 11 000 cal; n_k is between 0 and 0.3. Equation (12), however, leads to $n_k>0.7$. The large difference between E and Q is inconsistent with the low experimental reaction order. An attempt[8] to reconcile the low reaction

orders with the adsorption data thus seems futile. More recent kinetic experiments[7] with tungsten wires have shown that E is considerably higher in some cases. Therefore no conclusions should be drawn from the above discrepancy before kinetic and adsorption experiments have been carried out on the same surface.

* Sponsored by the U. S. Office of Naval Research, the U. S. Army Signal Corps, and the U. S. Air Force.
[1] C. N. Hinshelwood, *The Kinetics of Chemical Change* (Oxford University Press, London, 1940), Chap. VIII.
[2] E. K. Rideal and B. M. W. Trapnell, Discussions Faraday Soc. **8**, 114 (1950).
[3] A. Farkas, Z. physik. Chem. **B14**, 371 (1931).
[4] D. D. Eley and E. K. Rideal, Proc. Roy. Soc. (London) **A178**, 429 (1941).
[5] B. M. W. Trapnell, Proc. Roy. Soc. (London) **A206**, 39 (1951).
[6] G. D. Halsey, Trans. Faraday Soc. **47**, 649 (1951).
[7] A. Couper and D. D. Eley, Proc. Roy. Soc. (London) **A211**, 536 (1952).
[8] K. J. Laidler, J. Phys. Chem. **57**, 320 (1953).
[9] K. F. Bonhoeffer and A. Farkas, Z. physik. Chem. **B12**, 231 (1931).

A Method for Studying Gaseous Disproportionation Reactions of the Type $nA=mB+(n-m)C$†

ALAN W. SEARCY
Department of Chemistry, Purdue University, Lafayette, Indiana
(Received October 14, 1953)

ONE of the commonest and most convenient ways to determine the degree of association or disproportionation of molecules in the gas phase is to measure the vapor density under conditions of known total pressure. This method, however, is not applicable to studies of equilibria of the type $nA_{(g)}=mB_{(g)}+(n-m)C_{(g)}$ because here disproportionation of n molecules of A produces a total of n molecules of B and C and the vapor density is independent of the degree of disproportionation.

A number of very interesting disproportionation reactions belong to this class. The degree of disproportionation of mixed halides such as GeF_2Cl_2 and PF_2Br, for example, cannot be determined from vapor density measurements because a mixture of the disproportionation products would have the same vapor density as the original mixed halides. Determination of the degree of disproportionation of the indium dihalides to indium monohalides and trihalides as well as the disproportionation of sulfur dichloride to sulfur monochloride (S_2Cl_2) and to chlorine are among unsettled problems for which vapor density measurements cannot be used.

The purpose of this note is to show that a Knudsen effusion[1] or a Langmuir[2] determination of the weight loss of a sample in conjunction with an independent determination of the total vapor pressure P_T would allow calculation of the degree of disproportionation in a reaction of this type.

The total pressure is the sum of the partial pressures of the gaseous species $P_A+P_B+P_C$. The total number of moles effusing (for a Knudsen determination) or vaporizing (for a Langmuir determination) per unit time per unit area may be called Z_T. For reactions of this type, Z_T is independent of the degree of disproportionation. The number of moles of B effusing per unit area per unit time Z_B, is related to the number of moles of A and of C effusing by

$$Z_C=(n-m)Z_B/m \quad \text{and} \quad Z_A=Z_T-nZ_B/m.$$

According to the Knudsen and Langmuir equations the partial pressure of B is $P_B=Z_B(2\pi RM_BT)^{\frac{1}{2}}$ where M_B is the molecular weight of B gas. The partial pressures of A and C are given by similar equations. Solving the equations for P_B we obtain,

$$P_B=mM_B^{\frac{1}{2}}[P_T-Z_T(2\pi RM_AT)^{\frac{1}{2}}]/[mM_B^{\frac{1}{2}}+(n-m)M_C^{\frac{1}{2}}-nM_A^{\frac{1}{2}}].$$

The pressure of P_C is expressed by an equation similar in form to that for P_B and the pressure of

$$P_A=M_A^{\frac{1}{2}}[nP_T-Z_T(2\pi RT)^{\frac{1}{2}}\{mM_B^{\frac{1}{2}}+(n-m)M_C^{\frac{1}{2}}\}]/[nM_A^{\frac{1}{2}}-mM_B^{\frac{1}{2}}-(n-m)M_C^{\frac{1}{2}}].$$

Thus at a given temperature the partial pressure of a substance and of its gaseous disproportion products can each be expressed in terms of the total weight loss of a sample per unit area per unit time, the total pressure of the three gas species, and known constants for the reaction.

For the method to be valid, the concentrations of gas species other than A, B, and C must be negligible. For the method to be practical, the molecular weights of the disproportionation products should differ appreciably. The existence or nonexistence of OF gas for example would be very difficult to decide by this method because the probable decomposition products, O_2 and F_2, differ so little in molecular weight.

† Work supported by the U. S. Office of Naval Research.
[1] M. Knudsen, Ann. Physik. (4)**28**, 999 (1909).
[2] I. Langmuir, Phys. Rev. **2**, 329 (1913).

Some Properties of Sodium and Potassium Near Their Melting Points

L. G. CARPENTER
Royal Aircraft Establishment, Farnborough, Hants., England
(Received October 5, 1953)

MACDONALD[1] has recently published some measurements of the electrical resistance of Li, Na, and K over a wide range of temperature. As the melting point (T_m) is approached, he observes an "anomalous" rise in the resistance, which he attributes to the formation of vacant lattice sites. He deduces the activation energies for the process as 9.3 ± 0.35, 9.1 ± 0.1, and 9.1 ± 0.1 kcal/mole^{-1} for the three elements, which he compares with the values of 9.8 ± 1 and 9.5 ± 1.5 kcal/mole^{-1} given by Gutowsky and McGarvey[2] for the activation energies of self-diffusion in Li and Na. Nachtrieb, Catalano, and Weil[3] have measured the self-diffusion coefficient in Na, and obtain an activation energy of 10.45 ± 0.30 kcal/mole^{-1}.

Some years ago the author and his co-workers[4,5] observed an anomalous rise in the specific heat of Li, Na, and K, setting in about 100 degrees below T_m.

The purpose of the present note is to examine how far the resistance, diffusion, and specific heat phenomena can be interpreted in terms of a common model.

In calculating the effect of the formation of vacant lattice sites on specific heat, consider a gram atom of metal. The number (n) of Frenkel or Schottky defects is given[6] by

$$n\propto\exp-U/kT, \tag{1}$$

where U is, in the Frenkel case, half the energy required to take an atom from a normal lattice site and place it in an interstitial position some distance away, and, in the Schottky case, the energy required to move an atom from a normal lattice site to a position on the surface of the crystal.

The excess specific heat, ΔC, associated with the formation of vacant sites, will be given by

$$\Delta C\propto\frac{d}{d_T}(U\exp-U/kT), \tag{2}$$

i.e.,

$$T^2\Delta C\propto\frac{U^2}{k}\exp-U/kT,$$

or

$$\ln T^2\Delta C=\text{const}-U/kT. \tag{3}$$

Hence, if we know ΔC as a function of T, a logarithmic plot gives U.

The fraction (f) of the total number of sites which are vacant at T_m is given, in the Frenkel case, by

$$f=\frac{\int_{T_0}^{T_m}\Delta C dT}{2UN_0}, \tag{4}$$

or by

$$\frac{\int_{T_0}^{T_m}\Delta C dT}{UN_0}$$

in the Schottky case, where T_0 is the temperature below which the number of vacant sites is negligible, and N_0 is Avogadro's number.

Reference 4 shows that, because of its high Debye temperature, the specific heat of Li at (say) 100° below T_m is still far from approaching a constant asymptotic value. Hence it is not possible by inspection of the curve quantitatively to estimate the magnitude of an anomalous rise setting in as T_m is approached.

Figure 1 shows the specific heats of Na and K derived from references 4 and 5. For K both C_p and C_v are available; for Na only C_p. The dotted lines give the course of the specific heats estimated from the low-temperature parts of the curves.

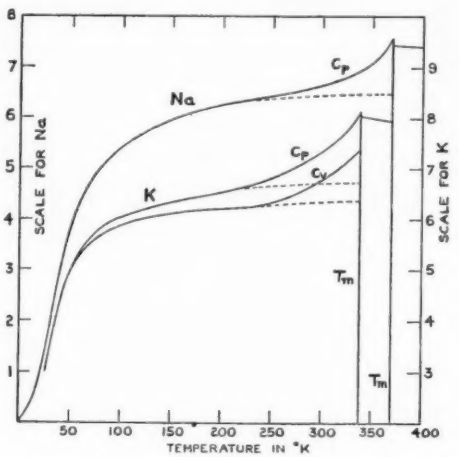

FIG. 1. The atomic heats of K and Na in cal deg^{-1} mole^{-1}.

Figure 2 shows plots of Eq. (3). There is about 10 percent difference between the activation energies derived from the two specific heats of K.

In order to determine the sensitivity of the deduced activation energies to the particular way in which the dotted curves, defining the excess specific heat, were drawn, Mr. F. J. Bradshaw kindly undertook to make entirely independent computations, starting from the data of references 3 and 4. He obtained values of U agreeing within 14 percent with those given on Fig. 2.

It may therefore be concluded that, if the vacancy model be accepted, the specific heat data for Na and K lead to a value of U of about 6 kcal/mole^{-1} with an uncertainty of about 20 percent.

The values of $\int_{T_0}^{T_m}\Delta C_p dT$ for Na and K are roughly 45 and 30 cal, respectively. Equation (4) with $U=6$ kcal/mole^{-1} gives values for f of 3.8×10^{-3} and 2.4×10^{-3} if Frenkel defects are postulated, the figures being doubled for Schottky defects.

Bearing in mind the crudeness of the treatment, all that can be safely concluded is that, at T_m, concentrations of defects of the order $\frac{1}{10}$ atomic percent are not inconsistent with the specific heat data.

An estimate of the concentration of vacancies in Na may be made from MacDonald's data, if we take Jongenburger's calculation[7] of "excess" specific resistance in Cu caused by 1 atomic percent of vacancies as applicable as regards order of magnitude. At T_m MacDonald[1] gives ΔR as about 10 percent of R, i.e., about 0.5×10^{-6} ohm cm, while $\frac{1}{10}$ atomic percent vacancies should give $\sim10^{-7}$ ohm cm. This agreement is perhaps as good as could be expected.

The energy deduced from specific heat data for the formation of defects in Na and K (*viz.*, ~6 kcal/mole^{-1}) is quite compatible with that found for diffusion (~10 kcal/mole^{-1}) since 4 kcal/mole^{-1} is a reasonable activation energy for movement.

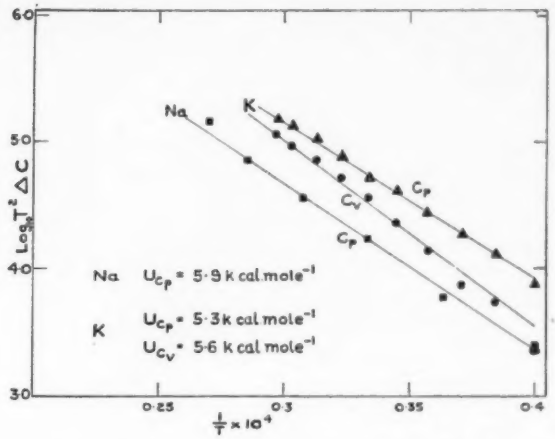

FIG. 2. Derivation of activation energies for Na and K.

It is interesting that Paneth's theoretical calculations[8] for sodium give ~7 kcal/mole^{-1} for the formation of a "crowdion" and about the same for its movement.

Miss D. M. Leggett gave valuable assistance with the computational work. Acknowledgment is also made to the Chief Scientist, Ministry of Supply, for permission to publish this note.

[1] D. K. C. MacDonald, J. Chem. Phys. **21**, 177 (1953).
[2] H. S. Gutowsky and B. R. McGarvey, J. Chem. Phys. **20**, 1472 (1952).
[3] Nachtrieb, Catalano, and Weil, J. Chem. Phys. **20**, 1185 (1952).
[4] Carpenter, Harle, and Steward, Nature **141**, 1015 (1938).
[5] L. G. Carpenter and C. J. Steward, Phil. Mag. **27**, 551 (1939).
[6] N. F. Mott and R. W. Gurney, *Electronic Processes in Ionic Crystals* (1948), second edition, pp. 28–9.
[7] P. Jongenburger, Phys. Rev. **90**, 710 (1953).
[8] H. R. Paneth, Phys. Rev. **80**, 708 (1950).

Negative Cluster Concentrations and Association Constants

HARVEY WINSTON
Research and Development Laboratories, Hughes Aircraft Company, Culver City, California
(Received October 5, 1953)

KILPATRICK[1] has called attention to the possible occurrence of negative partial pressures of certain clusters in connection with Woolley's[2] association constant method of representing gas properties. He reconciles the anomaly by showing that the necessary equations can be derived from the grand-partition function in a way which ascribes no physical significance to m_j, the number of clusters containing j particles. The purpose of this note is to point out that these numbers, positive or negative, do possess a physical significance.

According to Mayer and Mayer,[3] the set of numbers m_j describes a distribution in which "m_1 molecules are randomly distributed throughout the volume of the system, m_2 pairs of molecules are close together in excess over the number which would be expected from the random distribution of the m_1 unbound molecules, and m_3 clusters of three molecules each exist in excess of the random expectation from the given values of m_1 and m_2, etc." A negative m_j indicates that the gas contains fewer j clusters than expected from random aggregation of m_1 singlets, m_2 excess doublets, $\cdots m_{j-1}$ excess $(j-1)$ clusters.

It is instructive to show that Woolley's and Kilpatrick's[4] expression for the association constant,

$$P_j/P_1{}^j=K_j=(g_j/g_1{}^j)(kT)^{1-j}, \qquad (1)$$

is consistent with this point of view. Kilpatrick expressed surprise that K_j was not given by $Z_j/Z_1{}^j$. The usual relation between equilibrium constants and partition functions is obeyed, however, when we work with the actual numbers of j clusters, including the contribution from random aggregation of smaller clusters, rather

than with just the excess number. If P_j' is the sum of P_j^0, a partial pressure corresponding to the number of j clusters expected from aggregation of smaller clusters, and P_j, corresponding to the excess, we have

$$P_j'/P_1^j=(V/kT)^{j-1}Z_j/Z_1^j=K_j'. \quad (2)$$

K_j', involving as it does the total pressure of j clusters, is a conventional equilibrium constant, which K_j is not. The essential agreement between Eqs. (1) and (2) may be seen from the following direct calculation for clusters up to four. V/kT is abbreviated as α; then αP gives the number of molecules in volume V at pressure P and is the appropriate quantity to use with the number equilibrium constant given by the ratio of partition functions.

$$(\alpha P_2^0)/(\alpha P_1)^2=\tfrac{1}{2},$$

$$(\alpha P_2)/(\alpha P_1)^2=(Z_2/Z_1^2)-\tfrac{1}{2}=(Z_2-\tfrac{1}{2}Z_1^2)/Z_1^2; \quad (3)$$

$$\alpha P_3^0=(1/3!)(\alpha P_1)^3+(\alpha P_1)(\alpha P_2)$$
$$=[(1/3!)+(\alpha P_2)/(\alpha P_1)^2](\alpha P_1)^3,$$

$$(\alpha P_3)/(\alpha P_1)^3=(Z_3-Z_2Z_1+\tfrac{1}{3}Z_1^3)/Z_1^3; \quad (4)$$

$$\alpha P_4^0=[(1/4!)+(\alpha P_2)/2!(\alpha P_1)^2$$
$$+(\alpha P_2)^2/2!(\alpha P_1)^4+(\alpha P_3)/(\alpha P_1)^3](\alpha P_1)^4,$$

$$(\alpha P_4)/(\alpha P_1)^4=[Z_4-(\tfrac{1}{2}Z_2^2+Z_1Z_3)+Z_1^2Z_2-\tfrac{1}{4}Z_1^4]/Z_1^4; \quad (5)$$

etc.

Equations (3), (4), and (5) are of the same form as Eq. (1), and comparison with the expressions given by Kilpatrick[5] for g's in terms of Z's shows that they are identical to Eq. (1).

Since Kilpatrick has mentioned the pedagogical value of the association-constant method, it seems worth while to emphasize that this method is consistent with the conventional elementary definition of equilibrium constant K_j' of Eq. (2) as well as with the rather special "excess" equilibrium constant K_j of Eq. (1).

It is a pleasure to acknowledge helpful discussions with T. O. Woodruff.

[1] J. E. Kilpatrick, J. Chem. Phys. **21**, 1366 (1953).
[2] H. W. Woolley, J. Chem. Phys. **21**, 236 (1953).
[3] J. E. Mayer and M. C. Mayer, *Statistical Mechanics* (John Wiley and Sons, Inc., New York, 1940), p. 283.
[4] Equation 5 of reference 1 appears to have $(kT)^{j-1}$ in the numerator instead of the denominator.
[5] J. E. Kilpatrick, J. Chem. Phys. **21**, 274 (1953), Eq. (11).

Crystalline Chlorophyll and Bacteriochlorophyll

EARL E. JACOBS, ALBERT E. VATTER, AND A. STANLEY HOLT
Photosynthesis Research Project, Department of Botany, University of Illinois, Urbana, Illinois
(Received August 3, 1953)

SOLID chlorophyll is described in the literature as waxy and amorphous, implying the absence of ordered structure extending over more than a few molecular diameters. Hanson[1] published in 1939 an x-ray diffraction pattern of solid chlorophyll, prepared by evaporating an ethereal solution of the pigment to dryness. No well-defined diffraction lines were evident in this pattern, supporting the generally accepted concept that chlorophyll is an amorphous solid.

In our experiments with ethyl chlorophyllide, a relatively easily crystallizable derivative of chlorophyll, we observed[2] a shift of the red absorption band from its 660 mμ position in pure acetone to 740 mμ in microcrystalline suspensions. This shift was attributed to resonance interaction between identical chromophores in a regular array. During similar experiments with chlorophyll, certain conditions of condensation have been found to lead to an even wider shift of the red band. This suggested true crystallization. Subsequently, factors essential for obtaining the crystalline form could be elucidated.

When an acetonic solution of pure chlorophyll *a* is diluted with distilled water, a colloidal suspension consisting of pigment-water-solvent droplets is formed. The absence of recognizable crystals in the product of this procedure distinguishes phytyl chlorophyllide (chlorophyll) *a* from ethyl (or methyl) chlorophyllide *a*. The red absorption maximum of colloidal chlorophyll suspensions of this type lies between 670 and 675 mμ. We found that the addition of Ca^{++} ions to the water, either before or after dilution, leads to crystallization in the form of triangular sheets. Figure 1 shows these sheets as they appear under an electron

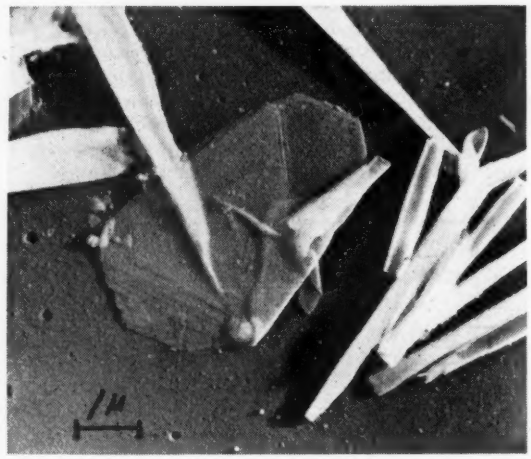

FIG. 1. Crystalline sheets of chlorophyll *a* as seen under an electron microscope (10 000×).

microscope. Their red absorption band is located between 735 and 770 mμ. Their tendency to roll up indicates that rigidity is confined to one or perhaps a few crystalline planes. X-ray diffraction (using chromium K radiation) gives a Debye powder diagram shown in the upper strip in Fig. 2. The most intense lines occur at D_{hkl} values of 44.0, 22.0, 14.6, and 7.6A (the 44A line is the one closest to the beam stop). The simplicity of the pattern indicates a true, but low-order symmetry in the orientation of the molecules. Electron-optical and spectroscopic evidence favors a model consisting of stacked bimolecular layers.

The Ca^{++} ions probably neutralize the dipole layers on the surface of the colloidal droplets, permitting their coalescence and subsequent "two dimensional crystallization." Spectroscopic evidence indicates the absence of Ca^{++} ions in the crystals. The effect of Ca^{++} ions is quite specific in the case of the acetone-water dilution technique. Crystallization, however, may be achieved also by two other procedures, not involving Ca^{++} ions at all.

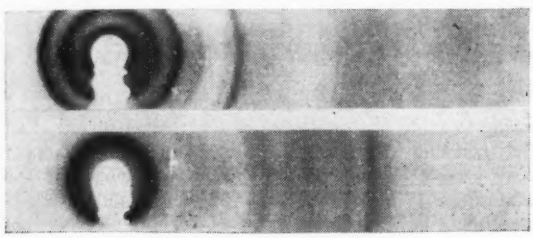

FIG. 2. X-ray powder diffraction patterns of chlorophyll *a* (upper strip) and bacteriochlorophyll (lower strip).

The first method consists in the evaporation of a concentrated chlorophyll solution in a 25 percent ether+75 percent petroleum ether ("Skelly B") solvent placed on top of a layer of water. After the evaporation of the organic solvents is completed, a crystalline flocculate is found in the water. The second method consists in the evaporation of acetone from a concentrated pigment solution in acetone, containing 1 percent water. Chlorophyll

a and chlorophyll *a*+*b* (3:1) prepared by any of these three techniques show indistinguishable x-ray patterns. We have not yet found the proper conditions for the crystallization of chlorophyll *b*.

Condensation by evaporation of anhydrous organic solvents—ether, ether+petroleum ether, or acetone—does not produce the above described extended ordered structures. This explains Hanson's failure to observe diffraction patterns and suggests that the presence of water molecules is a prerequisite for crystallization.

Bacteriochlorophyll crystallized from a concentrated 25 percent ether–75 percent petroleum-ether solution when the ether was slowly evaporated. The presence of water is not required. The crystals can be separated from the petroleum ether by filtration. X-ray diffraction gives the pattern shown in the lower strip in Fig. 2. One sees a remarkably intense band (*D hkl* of 23.6A), and a series of weaker bands which correspond to smaller spacings.

The above-described crystalline preparations are stable. Several months of storage in the dark at room temperature causes no measurable changes in their absorption spectra. The stability of crystalline chlorophyll *a* and bacteriochlorophyll seems to be not different from that of the crystalline alkyl chlorophyllides and bacteriochlorophyllides.

This work is to be reported in full at a later date. Our thanks are due to Dr. E. Rabinowitch and other members of the Photosynthesis Research Project for their assistance. We also wish to thank Dr. G. L. Clark of the x-ray laboratory of the University of Illinois for his kind advice. This work has been carried out with the assistance of the U. S. Office of Naval Research.

[1] E. A. Hanson, Rec. trav. botan. néerl. **36**, 180 (1939).
[2] E. E. Jacobs and A. S. Holt, J. Chem. Phys. **20**, 1326 (1952).
[3] Rabinowitch, Jacobs, Holt, and Kromhout, Z. Physik **133**, 261 (1952).

UNIVERSITY
OF MICHIGAN
FEB 12
PHYSICS
LIBRARY

THE JOURNAL OF CHEMICAL PHYSICS

VOLUME 21 NUMBER 12

DECEMBER, 1953

Published by the

AMERICAN INSTITUTE OF PHYSICS

Incorporated

Lancaster, Pa., and New York, N. Y.

THE JOURNAL OF CHEMICAL PHYSICS

BOARD OF EDITORS

CLYDE A. HUTCHISON, JR., *Editor*

Associate Editors

Term ending December 31, 1953	*Term ending December 31, 1954*	*Term ending December 31, 1955*
H. G. DRICKAMER	THEODORE H. BERLIN	RICHARD M. BADGER
H. E. GUNNING	B. P. DAILEY	DAVID M. DENNISON
J. O. HIRSCHFELDER	HARALD H. NIELSEN	JOHN G. KIRKWOOD
DONALD F. HORNIG	HARRISON SHULL	G. B. KISTIAKOWSKY
JOHN R. PLATT	CHARLES P. SMYTH	A. W. LAWSON
D. P. STEVENSON	FRANK H. WESTHEIMER	S. S. PENNER
ANTHONY TURKEVICH		ROBERT L. SCOTT

THE JOURNAL OF CHEMICAL PHYSICS is published monthly by the American Institute of Physics. Its purpose is to bridge a gap between journals of physics and journals of chemistry. The artificial boundary between physics and chemistry has now been in actual fact completely eliminated, and a large and active group is engaged in research which is as much the one as the other. It is to this group that the Journal is rendering its principal service and makes its greatest appeal, both as a prompt and efficient medium for publication of research and as a convenient and carefully edited assemblage of pertinent information.

Information for Contributors

Send **manuscripts** to Clyde A. Hutchison, Jr., Editor, *The Journal of Chemical Physics*, Institute for Nuclear Studies, University of Chicago, Chicago 37, Illinois. Unless otherwise stated submission of a manuscript is a representation that it has been neither copyrighted, published, nor submitted for publication elsewhere. Textual material (abstract, body of the paper, tabular material, references, and figure captions) must be in English, typewritten (except mathematical expressions) double spaced with wide margins on a durable, white paper, preferably letter size. The original copy, not the carbon, should be submitted. For general style, spellings, abbreviations, and form, consult recent issues of this journal. The authors' institutions are requested to pay a **publication charge** of $15.00 per page which, if honored, entitles them to 100 free reprints. Instructions will be sent with galley proofs.

An **abstract** must accompany each article. It should be adequate as an index and as a summary.

All but the simplest **mathematical expressions** should be carefully printed in by hand. Be sure to distinguish between capital and small letters. Indicate clearly superscripts and subscripts by inverted carets and carets, respectively. Avoid complicated superscripts and subscripts. Avoid repetition of a complicated expression by representing it by a symbol. Identify in the margin Greek letters and unusual symbols. Use fractional exponents instead of root signs. Use the solidus (/) for fractions wherever its use will save vertical space.

References should appear as footnotes, numbered consecutively. Literature citations of technical journals should be in the form indicated in the Style Manual of the American Institute of Physics and Chemical Abstracts (Chem. Abstracts 45, I-CCLV (1951)).

Tables may be typewritten on sheets separate from the running text. Each table must have a caption which will make the data in the table intelligible without reference to the text. Avoid complicated column headings.

Wherever possible **figures** should be planned for the width of a column (3 in.). A convenient reduction ratio is about 2:1 or 3:1. Lettering should be large enough on the original that when reduced it shall not be less than about $\frac{1}{16}$ in. (~1.5 mm). Line drawings must be in *india ink* on white paper or tracing cloth. Coordinate paper is not desirable but if used must be blue lined and the coordinate lines which are to show must be inked over. Photographs should have maximum black and white contrast. Identify each original drawing or photograph on the back with the author's name and the figure number. Figures should be numbered consecutively. Captions should be typed on a separate sheet of paper.

A limited number of **alterations** in proof are unavoidable, but the cost of making extensive alterations after the article has been set in type will be charged to the author.

Proof and all correspondence concerning papers in the process of publication should be addressed to the Publication Manager, American Institute of Physics, 57 East 55 Street, New York 22, New York.

Subscription Price

	U. S. and Canada	Elsewhere
To members of the American Institute of Physics and Affiliated Societies	$12.00	$13.00
To all others	15.00	16.00

Back Number Prices

Yearly rate when complete year is available: $17.00.
Single copies: $1.50 each.

Subscriptions, renewals, and orders for single copies should be addressed to the American Institute of Physics, 57 East 55 Street, New York 22, New York.

Changes of address should be sent to the American Institute of Physics.

The Journal of Chemical Physics is published monthly at Prince and Lemon Streets, Lancaster, Pennsylvania.

Entered as second-class matter December 30, 1932, at the Post Office at Lancaster, Pa., under the Act of August 24, 1912. Acceptance for mailing at special rate of postage provided for in paragraph (d-2), section 34.40, P. L. & R. of 1948, authorized February 8, 1933.